ADVISORY BOARD

I. Bertini
Università Degli Studi di Firenze
Florence, Italy

A. H. Cowley
University of Texas
Austin, Texas

H. B. Gray
California Institute of Technology
Pasadena, California

M. L. H. Green
University of Oxford
Oxford, United Kingdom

O. Kahn
Institut de Chimie de la Matière Condensée de Bordeaux (I.C.M.B.)
Pessac, France

A. Ludi
Universitat Bern
Bern, Switzerland

D. M. P. Mingos
Imperial College of Science, Technology, and Medicine
London, United Kingdom

J. Reedijk
Leiden University
Leiden, The Netherlands

A. M. Sargeson
The Australian National University
Canberra, Australia

Y. Sasaki
Hokkaido University
Sapporo, Japan

D. F. Shriver
Northwestern University
Evanston, Illinois

K. Wieghardt
Ruhr-Universität Bochum
Bochum, Germany

Advances in
INORGANIC CHEMISTRY

EDITED BY

A. G. Sykes

Department of Chemistry
The University
Newcastle upon Tyne
United Kingdom

VOLUME 42

ACADEMIC PRESS

San Diego New York Boston
London Sydney Tokyo Toronto

This book is printed on acid-free paper. ♾

Copyright © 1995 by ACADEMIC PRESS, INC.

All Rights Reserved.
No part of this publication may be reproduced or transmitted in any form or by any means, electronic or mechanical, including photocopy, recording, or any information storage and retrieval system, without permission in writing from the publisher.

Academic Press, Inc.
A Division of Harcourt Brace & Company
525 B Street, Suite 1900, San Diego, California 92101-4495

United Kingdom Edition published by
Academic Press Limited
24-28 Oval Road, London NW1 7DX

International Standard Serial Number: 0898-8838

International Standard Book Number: 0-12-023642-7

PRINTED IN THE UNITED STATES OF AMERICA
95 96 97 98 99 00 EB 9 8 7 6 5 4 3 2 1

ADVANCES IN INORGANIC CHEMISTRY, VOL. 42

SUBSTITUTION REACTIONS OF SOLVATED METAL IONS

STEPHEN F. LINCOLN and ANDRÉ E. MERBACH

Department of Chemistry, University of Adelaide, Australia; and Institut de Chimie Minérale et Analytique, Université de Lausanne, Switzerland

I. Introduction
  A. General Aspects
  B. The Formation of Metal Complexes
  C. The Classification of Mechanisms
  D. The Volume of Activation
II. Solvent Exchange and Ligand Substitution on Main Group Metal Ions
  A. General Characteristics
  B. Beryllium(II) and Magnesium(II)
  C. Aluminum(III), Gallium(III), Indium(III), and Scandium(III)
III. Solvent Exchange and Ligand Substitution on Transition Metal Ions
  A. General Characteristics
  B. Solvent Exchange on Divalent Octahedral First-Row Transition Metal Ions
  C. Ligand Substitution on Divalent Octahedral First-Row Transition Metal Ions
  D. The Influence of Nonleaving Ligands on Lability
  E. Solvent Exchange and Ligand Substitution on Hexaaquaruthenium(II) and Related Complexes
  F. Solvent Exchange on Octahedral Trivalent Transition Metal Ions
  G. Ligand Substitution on Octahedral Trivalent Transition Metal Ions
  H. Solvent Exchange and Ligand Substitution on Trivalent Transition Metal Aquapentaammine Complexes
  I. Solvent Exchange and Ligand Substitution on First-Row Transition Oxometal Ions
  J. Solvent Exchange and Ligand Substitution on Divalent Square-Planar Transition Metal Ions
IV. Solvent Exchange and Ligand Substitution on the Trivalent Lanthanides and Dioxouranium(VI)
  A. Aqueous Solution
  B. The Influence of Polyaminocarboxylate Ligands on Water Exchange
  C. Dimethylformamide Solution
  D. Lower Coordination Number Species
  E. Dioxouranium(VI)
V. Solvent Exchange and Ligand Substitution on Some Molybdenum and Tungsten Cluster Complexes
VI. Concluding Comments
VII. Appendix: Ligand Abbreviations, Formulae, and Structures
References

Copyright © 1995 by Academic Press, Inc.
All rights of reproduction in any form reserved.

I. Introduction

A. General Aspects

The most common ligand substitution on a solvated metal ion is the exchange of a water molecule in the first coordination sphere of a metal ion with a water molecule from the second coordination sphere. Water exchange on metal ions may also be viewed as being particularly fundamental, as it is through the intervention of another type of ligand in this process that the stoichiometry of the first coordination sphere is changed and a vast range of metal complexes is formed. Accordingly, it is appropriate to review the water exchange process and the 18 orders of magnitude variation in the water exchange rate constant, k_{H_2O}, and lability exhibited by metal ions towards this process. This is most effectively commenced through an inspection of Fig. 1, which in its evolving forms has been one of the most intellectually focusing compilations of information about ligand substitution since it was published by Eigen in 1963 (*1*). At one end of the lability scale it is seen that the mean lifetime of a water molecule in the first coordination sphere of $[Rh(H_2O)_6]^{3+}$, τ_{H_2O} ($= 1/k_{H_2O}$), is 14.4 years, whereas at the other extreme, that of a water molecule bound to Cs^+ is $\sim 2 \times 10^{-10}$ s, during which time light travels ~6 cm. Clearly the microscopic interpretation of the macroscopic kinetic and related observations of water exchange and its substitution in the first coordination sphere by other ligands, the ligand substitution mechanism, must account for this great variation in lability reflected in the range of k_{H_2O} characterizing the metal ions in Fig. 1.

The metal ions may be conveniently considered in three categories, the first of which is the main group metal ions which, for a given ionic charge, exhibit an increase in k_{H_2O} with an increase in ionic radius, r_M (*2*). Thus, the lability of the alkali metal ions increases by an order of magnitude as r_M increases from Li^+ to Cs^+, and in general terms these ions are particularly labile coincident with their low ionic charge-to-r_M ratio. In contrast, the lability of the alkaline earth metal ions spans approximately seven orders of magnitude, coincident with their higher charge and larger variation in r_M. At this point it is appropriate to note that the more labile of the metal ions in these two sets are particularly difficult to characterize in terms of their numbers of coordinated water molecules. Thus, the coordination number of Li^+ is variously quoted as 4 and 6, and that of Cs^+ as 9, while intermediate values are quoted for Na^+, K^+, and Rb^+. For Be^{2+} and Mg^{2+}, coordination numbers of 4 and 6, respectively, are well established, but a range from 6 to 10 is

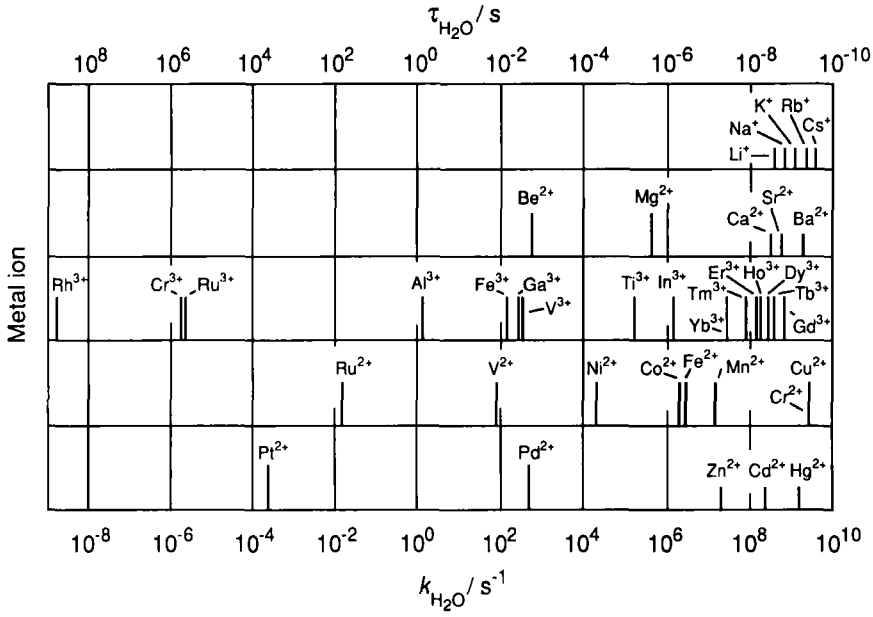

FIG. 1. Mean lifetimes of a single water molecule in the first coordination sphere of a given metal ion, τ_{H_2O}, and the corresponding water exchange rate constants, k_{H_2O}. The tall bars indicate directly determined values, and the short bars indicate values deduced from ligand substitution studies. References to the plotted values appear in the text.

quoted for Ca^{2+} and similar or greater values are anticipated for Sr^{2+} and Ba^{2+} (*3–5*). As r_M increases with coordination number, so the metal ion–water dipole interaction weakens and lability increases. The labilities exhibited by the six-coordinate sets—Zn^{2+}, Cd^{2+}, and Hg^{2+} (*1*) and Al^{3+}, Ga^{3+}, and In^{3+} (*6–8*)—vary over two and six orders of magnitude, respectively, and it is not surprising that the smallest of these ions, Al^{3+}, is the least labile in the light of the preceding discussion.

The second category is the transition metal ions, all of which in Fig. 1 are six-coordinate with the exception of Pt^{2+} and Pd^{2+}, which are square-planar four-coordinate (*6–9*). Their labilities are strongly influenced by the electronic occupancy of their *d* orbitals. This is illustrated by the divalent first-row transition metal ions, which should exhibit similar labilities to Zn^{2+} on the basis of their r_M; instead, however, their labilities encompass seven orders of magnitude. On a similar basis, the trivalent first-row transition metal ions might be expected to be of similar lability to Ga^{3+}, but instead they exhibit a lability variation of 11 orders of magnitude, with Cr^{3+} being at the

lower end of this lability scale. Second-row Ru^{3+} and Rh^{3+} are slightly more labile and three orders of magnitude less labile than Cr^{3+}, respectively.

The third category is the heavy eight-coordinate trivalent lanthanides, whose lability decreases with the progressive filling of the 4*f* orbitals and the resulting lanthanide contraction, and which are very labile as a consequence of their large r_M (*7, 10, 11*).

B. The Formation of Metal Complexes

It is generally considered that some orientation of water in the second coordination sphere of the archetypal aqua ion, $[M(H_2O)_n]^{m+}$, occurs (*4, 12*), but exchange of this water with bulk water appears to occur at close to diffusion-controlled rates. Hence, it is only in the case of the most labile metal ions that the rate of entry of a substituting ligand, L^{x-}, into the first coordination sphere is within an order of magnitude or so of its rate of entry into the second coordination sphere. Usually, the entry of L^{x-} into the first coordination sphere is preceded by the formation of an outer-sphere complex (*13*), in which L^{x-} resides in the second coordination sphere of $[M(H_2O)_n]^{m+}$. An impressive armory of kinetic techniques has facilitated the study of ligand substitution processes in solution, ranging from those occurring at close to diffusion-controlled rates to those taking place over extended times (*14–16*). However, it is seldom the case that more than one stage of the movement of a monodentate ligand from the bulk water environment into the first coordination sphere is observed, except in ultrasonic studies where as many as three steps have been detected. It is such studies which have provided the basis for most current discussion of the mechanisms of metal complexation. Thus, the formation of metal complexes has been conveniently formalized in a mechanism proposed by Eigen and Tamm (*17*), and illustrated by Eq. (1), where M^{m+} is the metal ion, L^{x-} is the substituting ligand, and only those water molecules interposed between M^{m+} and L^{x-} are shown. Initially, in a diffusion-controlled step, M^{m+} and L^{x-} form a species (1) in which they are separated by two layers of water molecules. This is followed by a fast step in which L^{x-} enters the second solvation sphere or second coordination sphere of M^{m+} to form an outer-sphere complex (2), and the inner-sphere complex (3) is formed in the final and slowest step characterized by k_{23}, which is frequently denoted k_i because it indicates the step in which L^{x-} interchanges between the second and first coordination spheres. By analogy, k_{32} is often denoted k_{-i}. The formation of (1) is seldom detected (*18*), and as a consequence, the simpler mechanism

shown in Eq. (2) is often discussed instead and is sometimes referred to as the Eigen–Wilkins mechanism (*19*).

$$\begin{array}{ccccc} (0) & & (1) & & (2) \\ M^{m+} + L^{x-} & \underset{k_{10}}{\overset{k_{01}}{\rightleftharpoons}} & M \cdot OH_2 \cdot OH_2 \cdot L^{(m-x)+} & \underset{k_{21}}{\overset{k_{12}}{\rightleftharpoons}} & M \cdot OH_2 \cdot L^{(m-x)+} \\ & & & & \underset{k_{23} = k_{32}}{\rightleftharpoons} \\ & & & & ML^{(m-x)+} \\ & & & & (3) \end{array} \quad (1)$$

$$M^{m+} + L^{x-} \underset{k_{21}}{\overset{k_{12}}{\rightleftharpoons}} M \cdot OH_2 \cdot L^{(m-x)+} \underset{k_{32}}{\overset{k_{23}}{\rightleftharpoons}} ML^{(m-x)+} \quad (2)$$

$$K_{12} = K_o = (4\pi NR^3/3000)\exp(-z_M z_L e_0^2/\varepsilon RkT) \quad (3)$$

$$M^{m+} + L^{x-} \underset{k_b}{\overset{k_f}{\rightleftharpoons}} ML^{(m-x)+} \quad (4)$$

$$k_{obs} = \frac{k_i K_O[L^{x-}]}{1 + K_O[L^{x-}]} + k_{-i} \quad (5)$$

The successive equilibria are characterized by K_{12} and K_{23}, respectively, and when K_{12} (often denoted K_o) cannot be directly determined, it may be estimated from the Fuoss equation (3), where R is the distance of closest approach of M^{z+} and L^{x-} (considered as spherical species) in $M \cdot OH_2 \cdot L^{(m-x)+}$, ε is the solvent dielectric constant, and z_M and z_L are the charges of M^{m+} and L^{x-}, respectively (*20*). Frequently, it is only possible to characterize kinetically the second equilibrium of Eq. (2), and the overall equilibrium is then expressed as in Eq. (4) (which is a general expression irrespective of mechanism). Here, the pseudo first-order rate constant for the approach to equilibrium, k_{obs}, is given by Eq. (5), in which the first and second terms equate to k_f and k_b, respectively, when $[L^{x-}]$ is in great excess over $[M^{m+}]$. When $K_o[L^{x-}] \ll 1$, $k_{obs} \approx k_i K_o[L^{x-}] + k_{-i}$, and when $K_o[L^{x-}] \gg 1$, $k_{obs} \approx k_i + k_{-i}$. Analogous expressions apply when $[M^{m+}]$ is in excess. When the entering ligand, L, is uncharged, the stability of the outer-sphere complex $M \cdot OH_2 \cdot L^{z+}$ may be so low that its concentration does not differ significantly from that arising from diffusive collisions between $M \cdot OH_2^{m+}$ and L. Under these conditions, entry of L into the

first coordination sphere may only occur if $M \cdot OH_2^{m+}$ has generated a reactive intermediate, or if the collision produces a reactive intermediate involving L. These two cases are akin to the **D** and **A** mechanisms, respectively, discussed in Section I,C, and although they are seldom unequivocally identified in water, there is strong evidence for their occurrence when other solvents exchange on metal ions in the presence of inert diluents, as is discussed in Section II,B and following sections.

It is the mechanisms through which L^{x-} and L interchange between the second and first coordination spheres which remain the subject of considerable debate (*4, 6–9, 15, 21–26*), and which constitute the central facet of the discussion which follows.

C. The Classification of Mechanisms

In this discussion, the simple transition-state theory is considered most convenient to describe ligand substitution processes, but it is acknowledged that in due course more sophisticated models may be adopted to describe the energetics of such rate processes (*27–31*). On this basis, a ligand substitution mechanism is a philosophical concept which seeks to explain the energetic and stereochemical changes which occur along the reaction coordinate as reactants progress through the transition state to the product. Kinetic measurements provide information about the stoichiometry of the transition state, but cannot directly provide details of its stereochemistry. However, the detection of products where retention of stereochemical configuration is retained, as in square-planar platinum(II) systems (*32, 33*), and the observation of changes in mechanism with variation in size and electronic configuration give structural clues which are considered in later sections (*7–9*). The mechanistic framework on which subsequent discussion is based is now considered.

The two extreme possibilities which arise for the entry of L^{x-} into the first coordination sphere of $[M(H_2O)_n]^{m+}$ are discussed employing the convenient nomenclature of Langford and Gray (*34*) in a somewhat different manner from its original usage. The first occurs when $[M(H_2O)_n]^{m+}$ loses H_2O to form a reactive intermediate of decreased coordination number, $[M(H_2O)_{n-1}]^{m+}$, which has normal vibrational modes and survives several molecular collisions prior to reacting with L^{x-} to form $[M(H_2O)_{n-1}L]^{(m-x)+}$ as shown in Eq. (6). Thus, the rate-determining step is the dissociation of an H_2O, the substitution rate is independent of L^{x-}, and the mechanism is said to be dissociatively (**d**) activated and the mechanism is classified as **D.** By the principle of microscopic reversibility, the loss of L^{x-} from $[M(H_2O)_{n-1}L]^{(m-x)+}$ to produce $[M(H_2O)_n]^{m+}$ will also proceed through a dissociative (**D**)

mechanism, and the rate will depend on the nature of L^{x-}. Formally, in the presence of excess $[L^{x-}]$, the expression for the pseudo first-order rate constant, k_{obs}, for the approach to equilibrium is given by Eq. (7), which predicts a dependence of k_{obs} on $[L^{x-}]$ and is deceptively similar to that predicted by Eq. (5). However, the tendency for oppositely charged reactants in particular to form outer-sphere complexes, as discussed earlier, usually precludes the observation of such a rate law for most systems so far studied. Nevertheless, this does not preclude the operation of a **D** mechanism through reaction of $[M(H_2O)_{n-1}]^{m+}$ and L^{x-} within an outer-sphere complex.

$$[M(H_2O)_n]^{m+} + L^{x-} \underset{k_{-1}}{\overset{k_1}{\rightleftharpoons}} [M(H_2O)_{n-1}]^{m+} + H_2O + L^{x-} \underset{k_{-2}}{\overset{k_2}{\rightleftharpoons}} [M(H_2O)_{n-1}L]^{(m-x)+} + H_2O \quad (6)$$

$$k_{obs} = \frac{k_1 k_2 [L^{x-}] + k_{-1} k_{-2}}{k_{-1} + k_2 [L^{x-}]} \quad (7)$$

At the other extreme is the associatively (**a**) activated associative (**A**) mechanism, in which the rate-determining step for substitution by L^{x-} proceeds through a reactive intermediate of increased coordination number, $[M(H_2O)_nL]^{(m-x)+}$, which has normal vibrational modes and survives several molecular collisions before losing H_2O to form $[M(H_2O)_{n-1}L]^{(m-x)+}$, as shown in Eq. (8). Equation (9) indicates the linear variation with excess $[L^{x-}]$ anticipated for k_{obs}, which is similar in form to that of Eq. (5) when $K_o[L^{x-}] \ll 1$ and $k_{obs} \approx k_i K_o [L^{x-}] + k_{-i}$. Thus, although the rate of substitution should be very dependent on the nature of L^{x-}, distinguishing the operation of an **A** mechanism according to Eq. (8) from ligand substitution proceeding through an outer-sphere complex on the basis of rate laws is usually not feasible. This does not, however, preclude the operation of an **A** mechanism within an outer-sphere complex.

$$[M(H_2O)_n]^{m+} + L^{x-} \underset{k_{-1}}{\overset{k_1}{\rightleftharpoons}} [M(H_2O)_nL]^{(m-x)+} \underset{k_{-2}}{\overset{k_2}{\rightleftharpoons}} [M(H_2O)_{n-1}L]^{(m-x)+} + H_2O \quad (8)$$

$$k_{obs} = k_2 [L^{x-}] + k_{-2} \quad (9)$$

In between these two extremes, there exists a continuum of mechanisms in which the leaving and entering ligands make varying contributions to the transition state energetics, and which are generally classified as interchange mechanisms. These mechanisms vary from the **d**-activated dissociative interchange ($\mathbf{I_d}$) mechanism, in which bond

breaking is of major importance, through the interchange (**I**) mechanism, where bond breaking and making are of similar importance, to the **a**-activated mechanism ($\mathbf{I}_a$), in which bond making is of major importance.

The question now arises as to how these mechanisms are to be distinguished. In principle a clear operational distinction should be possible between **d**- and **a**-activated mechanisms from a comparison of the rate of water exchange on $[M(H_2O)_n]^{m+}$ and the rate at which L^{x-} substitutes for H_2O in the first coordination sphere. For a **d**-activated mechanism, L^{x-} cannot substitute faster than the rate of water exchange, and when statistical factors (*35–38*) are taken into account, may substitute more slowly. Also, $\Delta H^{\ddagger}$ should be similar to that for the water exchange process. However, within the continuum of mechanisms, an $\mathbf{I}_d$ mechanism may incorporate some contribution from the entering L^{x-} so that a small selectivity for L^{x-} arises. For an **a**-activated mechanism, the rate of substitution by L^{x-} may range from being much less than to much greater than the rate of water exchange. However, these generalizations are subject to the provisos that the L^{x-} selectivity range in an **a**-activated mechanism may be substantially decreased for hard base L^{x-} species interacting with a hard acid M^{m+} (*22, 39, 40*), and that selectivity ranges are expected to decrease as the lability of M^{m+} increases, to the point at which no selectivity will be exhibited when water exchange approaches diffusion-controlled rates, where $k_{H_2O} \approx 3.6 \times 10^{11}\ s^{-1}$ and the frequency at which encounters between L^{x-} and $[M(H_2O)_n]^{m+}$ results in substitution becomes very high (*4*).

Clearly it is desirable to have additional criteria whereby ligand substitution mechanisms may be assigned, and because of the fundamental importance which an understanding of water exchange on $[M(H_2O)_n]^{m+}$ holds in such an assignment, it is also desirable to have a criterion through which the mechanism of this process, in particular, may be assigned with confidence. The variations of the enthalpy and entropy of activation within a series of similar ligand substitution systems do give a guide to mechanistic change. Thus, **d**-activated substitutions tend to have greater $\Delta H^{\ddagger}$ magnitudes than do **a**-activated substitutions, and $\Delta S^{\ddagger}$ tend to be positive and negative for **d**- and **a**-activated substitutions, respectively. However, it is often difficult to find a series of similar ligand substitutions from which mechanistic deductions may be made from $\Delta H^{\ddagger}$ and $\Delta S^{\ddagger}$. The magnitudes of the contributions to these two parameters arising from interactions occurring beyond the first coordination sphere can be uncertain, and determination of $\Delta S^{\ddagger}$ is particularly prone to error. Obviously, a further criterion to aid mechanistic deduction is very desirable. One such major

criterion has proved to be the volume of activation, $\Delta V^{\ddagger}$, which is now discussed in some detail.

D. The Volume of Activation

The volume of activation, $\Delta V^{\ddagger}$, is a potent tool for the identification of the mechanism of water and other solvent exchange reactions in particular and ligand substitution reactions in general, and to some extent has modified the criteria for assigning such mechanisms, as will become apparent later (*4, 6–9, 12, 41–45*). In general terms, $\Delta V^{\ddagger}$ is defined as the difference between the partial molar volume of the reactants and the transition state and is related to the pressure dependence of the ligand substitution rate constant through Eq. (10). Thus, the substitution reaction is respectively either slowed or accelerated by increasing pressure when $\Delta V^{\ddagger}$ is positive and negative, respectively. A convenient expression for the relationship between the substitution rate constant at a given applied pressure, k_P, and that at ambient pressure, k_0, is given in Eq. (11), where $\Delta\beta^{\ddagger}$ is the compressibility coefficient of activation, which is a measure of the pressure dependence of $\Delta V^{\ddagger}$. Usually, the $\Delta\beta^{\ddagger}$ term is small by comparison with the $\Delta V^{\ddagger}$ term for solvent exchange and for uncharged ligand substitution processes where little change in the tightness of binding of solvent in the second coordination sphere and beyond occurs on forming the transition state. As a consequence, the deviation from linearity of the pressure dependence of $\ln(k_P/k_0)$ may not be detected within the limits of experimental error. The $\Delta\beta^{\ddagger}$ term may become significant for ligand substitution processes which produce changes in charge distribution in the transition state, especially in nonaqueous solvents, and thereby changes in electrostriction.

$$(\delta \ln k/\delta P)_T = -\Delta V^{\ddagger}/RT \tag{10}$$

$$\ln k_P = \ln k_0 - \Delta V^{\ddagger}P/RT + \Delta\beta^{\ddagger}P^2/2RT \tag{11}$$

The interpretation of $\Delta V^{\ddagger}$ for ligand substitution on metal ions is based on a simplified version of the transition state theory, which does not take the dynamics of solvent interactions beyond the first coordination sphere into account. This simplification usually applies to slower than diffusion-controlled ligand substitution processes and is adopted throughout this review. Thus, $\Delta V^{\ddagger}$ is usually considered to be composed of two dominant components: an intrinsic contribution, $\Delta V^{\ddagger}_{int}$, arising from changes in the internuclear distances of the reactants during the formation of the transition state, and an electrostriction contribution, $\Delta V^{\ddagger}_{elec}$, which largely arises from changes in the

electrostriction of solvent in the second coordination sphere and beyond as distribution of charge changes when the reactants form the transition state. When charged reactants are involved, $\Delta V^{\ddagger}_{elec}$ may dominate $\Delta V^{\ddagger}$ so that $\Delta V^{\ddagger}_{int}$, which contains most of the mechanistic information, cannot be readily determined. Fortunately, solvent exchange on metal ions involves negligible differences in electrostriction between the reactants and the transition state such that $\Delta V^{\ddagger}_{elec} \approx 0$ cm^3 mol^{-1} and $\Delta V^{\ddagger} \approx \Delta V^{\ddagger}_{int}$. Thus, the variations in the slopes of $\ln(k_P/k_0)$ for water exchange on $[M(H_2O)_6]^{2+}$ in Fig. 2 and the derived $\Delta V^{\ddagger} = -4.1$, -5.4, $+3.8$, $+6.1$, and $+7.2$ cm^3 mol^{-1} when M = V, Mn, Fe, Co, and Ni, respectively, imply substantial mechanistic differences (*6, 46, 47*).

The model used to interpret variations in the magnitude of $\ln (k_P/k_0)$ with P assumes $\Delta V^{\ddagger}$ to be a direct measure of the degree of bond making and bond breaking occurring in the transition state and the concurrent lengthening or shortening of non-exchanging ligand to metal center distances. A continuous variation of transition state configurations may be envisaged, as shown for a solvent exchange or identical ligand exchange process in Fig. 3. At one extreme the **D** mechanism is characterized by a greatly expanded transition state in which the increase in volume resulting from the dissociation of the leaving ligand is only slightly compensated for by the contraction of the first coordination sphere volume, and $\Delta V^{\ddagger}$ is large and positive. At the other extreme, the **A** mechanism is characterized by a greatly contracted transition state in which the decrease in volume resulting from the entry of the entering ligand into the first coordination sphere is only partially offset by the expansion of the volume of the first coordination sphere, and

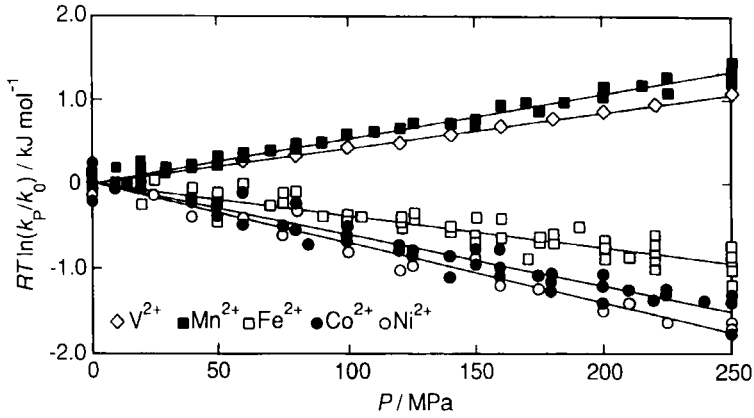

FIG. 2. The effect of applied pressure, P, on the ratio of the rate constants for water exchange on $[M(H_2O)_6]^{2+}$ observed at applied and ambient pressures, k_P/k_0 (*6*).

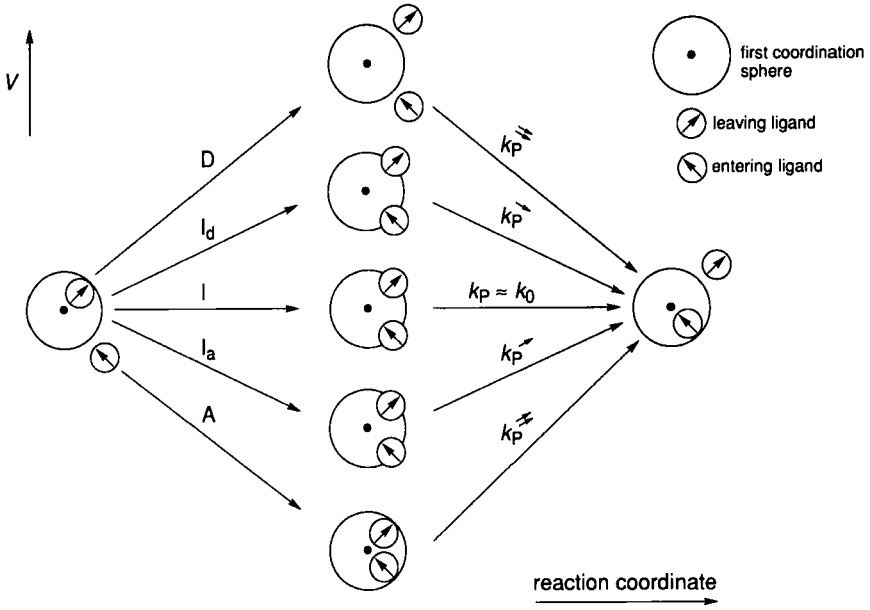

FIG. 3. Representations of the transition states for the spectrum of solvent or symmetrical ligand exchange processes (7).

$\Delta V^{\ddagger}$ is large and negative. In between these two mechanisms is the **I** mechanism, in which the equal amounts of bond breaking and bond making balance one another in their contributions to $\Delta V^{\ddagger}$ which, as a consequence, is zero. On either side of the **I** mechanism are the $\mathbf{I}_d$ and $\mathbf{I}_a$ mechanisms, in which the bond making contribution to the transition state is greater than the bond breaking contribution and vice versa, and which are characterized by positive and negative $\Delta V^{\ddagger}$ values, respectively. Thus, both the sign and magnitude of $\Delta V^{\ddagger}$ changes as the contributions of **d** and **a** activation to the transition state change.

The application of pressure to a **d**-activated exchange process produces a decrease in $\ln(k_P/k_0)$ because the approach to the transition state requires an increase in volume, as indicated qualitatively by the one or two descending superscript arrows on k_P in Fig. 3. The opposite is the case for an **a**-activated exchange process where the approach to the transition state requires a decrease in volume, indicated qualitatively by the one or two ascending superscript arrows on k_P in Fig. 3. On this basis, it is clear that when M = V and Mn, water exchange on $[M(H_2O)_6]^{2+}$ is **a**-activated, but when M = Fe, Co, and Ni, it is **d**-activated. The origins of these differences are considered in more detail in Section III,B.

As no method is available for the detection of the intermediate species of decreased or increased coordination numbers anticipated for **D** and **A** mechanisms, respectively, for water exchange on $[M(H_2O)_6]^{2+}$, the experimental distinction between these limiting mechanisms and the interchange mechanisms is not readily made. Accordingly, it is necessary to consider the magnitudes of $\Delta V^{\ddagger}$ in more detail. Simple geometric models have been used to predict $\Delta V^{\ddagger}$ values for **D** and **A** mechanisms (*12, 48*) and more recently Swaddle (*4, 41, 42*) has proposed a model based on the semiempirical Eq. (12) in which the absolute partial molar volume, V_{abs}^{0} ($cm^3\ mol^{-1}$), of a hydrated metal ion is related to its effective ionic radius r_M (pm) appropriate to its coordination number, n, and its charge, z. The first right-hand term of Eq. (12) gives the volume of $[M(H_2O)_n]^{z+}$ as that of a sphere of radius $(r_M + \Delta r)$, where $\Delta r = 238.7$ pm is the contribution made by first coordination sphere water molecules to the effective radius of $[M(H_2O)_n]^{z+}$. The second and third right-hand terms, respectively, represent the loss of the contribution of n water molecules to the volume of the free water, and the electrostrictive effect of $[M(H_2O)_n]^{z+}$ on water beyond the first coordination sphere treated as a continuous dielectric. The calculated $\overline{V}_{abs}^{0}$ are in good agreement with the observed V_{abs}^{0} for a wide range of hydrated metal ions. (Inevitably there are exceptions to this agreement; in this case low-spin t_{2g}^6 $[Rh(H_2O)_6]^{3+}$ appears more compacted than is anticipated from the crystallographic ionic radius.) Taking into account the change of r_M with n, V_{abs}^{0} may be calculated for $[M(H_2O)_n]^{z+}$ and $[M(H_2O)_{n\pm1}]^{z+}$, and the differences between the first and either of the second values are $\Delta V^{\ddagger}$ for the **D** and **A** mechanisms. (For the first row transition $[M(H_2O)_6]^{z+}$ r_M either increases or decreases by ~6 pm when n changes from 6 to either 7 or 5, respectively.) The $|\Delta V^{\ddagger}|$ calculated in this way shows little dependence on r_M so that it has about the same value, $13.5 \pm 1\ cm^3\ mol^{-1}$ for all of the first-row divalent and trivalent transition metal ions (*7, 48*). This important observation means that their $\Delta V^{\ddagger}$ may be directly compared when making mechanistic deductions.

$$\overline{V}_{abs}^{0} = 2.523 \times 10^{-6}(r_M + \Delta r)^3 - 18.07n - 417.5z/(r_M + \Delta r) \tag{12}$$

On the basis of the preceding discussion, the systematic trend in $\Delta V^{\ddagger}$ observed for water exchange on $[M(H_2O)_6]^{2+}$ may be rationalized through a More–O'Ferral type of diagram (*4, 7*) as shown in Fig. 4. The bond-making and bond-breaking contributions to $\Delta V^{\ddagger}$ are plotted on the two axes, which are scaled to $\Delta V^{\ddagger}$ for a **D** mechanism being

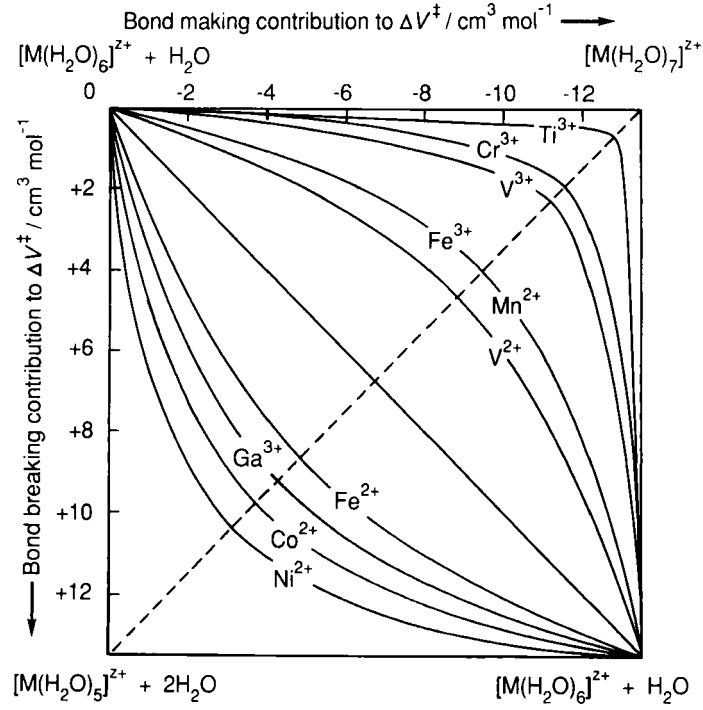

FIG. 4. Bond-making and bond-breaking contributions to the volumes of activation for water exchange on $[M(H_2O)_6]^{z+}$, $\Delta V^{\ddagger}$ (*7*).

+ 13.5 cm^3 mol^{-1} and that for an **A** mechanism being − 13.5 cm^3 mol^{-1}, the limiting values calculated from Eq. (12). Thus, for $[V(H_2O)_6]^{2+}$ (*47*), the sum of the coordinates of each point along the trajectory represents the change in volume reached at that point, and $\Delta V^{\ddagger}$ = −4.1 cm^3 mol^{-1} is reached at the intersection with the dashed diagonal; similar considerations apply to the other $[M(H_2O)_6]^{2+}$ (*46*) and $[M(H_2O)_6]^{3+}$ (*49–53*). It is clear that neither $[V(H_2O)_6]^{2+}$ nor $[Mn(H_2O)_6]^{2+}$ approaches an **A** exchange mechanism, as judged from a comparison of their observed $\Delta V^{\ddagger}$ with the calculated value of −13.5 cm^3 mol^{-1}. Consequently, both metal ions are assigned $\mathbf{I_a}$ mechanisms as bond making dominates bond breaking in the transition state. Similarly, $[Fe(H_2O)_6]^{2+}$, $[Co(H_2O)_6]^{2+}$, and $[Ni(H_2O)_6]^{2+}$ are assigned $\mathbf{I_d}$ mechanisms, although it should be noted that the degree of dominance of bond breaking varies as anticipated from the mechanistic continuum discussed in Section I,C. The $[M(H_2O)_6]^{3+}$ ions also exhibit mechanistic

variations, and it is seen that the $\Delta V^{\ddagger} = -12.5$ cm^3 mol^{-1} for $[Ti(H_2O)_6]^{3+}$ closely approaches -13.5 cm^3 mol^{-1} calculated for a **A** mechanism. Clearly, $\Delta V^{\ddagger}$ is a very important aid to the determination of mechanism, and its further application in this role and the factors causing mechanistic variation are discussed in following sections.

II. Solvent Exchange and Ligand Substitution on Main Group Metal Ions

A. General Characteristics

There are only five main group metal ions amenable to detailed mechanistic study of solvent exchange and simple ligand substitution processes: Be^{2+}, Mg^{2+}, Al^{3+}, Ga^{3+}, and In^{3+}. Nevertheless, they provide an opportunity to study the influence of size, charge, and stereochemistry on mechanism without the complicating effects of the variation of the electronic occupancy of the *d*-orbitals, which exerts a major influence on the labilities and mechanisms of the transition metal ions as discussed in Section III,A. As was noted earlier, all of the alkali ions and Ca^{2+}, Sr^{2+}, and Ba^{2+} are very labile as a consequence of their relatively low charge-to-r_M ratios, and their k_{H_2O} are within an order of magnitude or so of diffusion control. Thus, the kinetic characterization of the substitution of simple ligands into the first coordination spheres of these metal ions presents a major experimental challenge, and few data are available (*1*). Nevertheless, encapsulating ligands such as coronands, cryptands, and pendant-arm macrocyclic ligands have brought their alkali metal ion complexes in particular into more accessible time scales, and substantial mechanistic information has resulted (*54–58*). However, these fascinating systems are outside the scope of this review.

B. Beryllium(II) and Magnesium(II)

Beryllium(II) is the smallest metal ion, $r = 27$ pm (*2*), and as a consequence forms predominantly tetrahedral complexes. Solution ^{1}H NMR (nuclear magnetic resonance) (*59–61*) and x-ray diffraction studies (*62*) show $[Be(H_2O)_4]^{2+}$ to be the solvated species in water. In the solid state, x-ray diffraction studies show $[Be(H_2O)_4]^{2+}$ to be tetrahedral (*63*), as do neutron diffraction (*64*), infrared, and Raman scattering spectroscopic studies (*65*). Beryllium(II) is the only tetrahedral metal ion for which a significant quantity of both solvent-exchange and ligand-substitution data are available, and accordingly it occupies a

unique niche in mechanistic studies and is now discussed in some detail.[1]

A pressure-jump relaxation study of sulfate substitution on $[Be(H_2O)_4]^{2+}$, as shown in Eq. (13), is the origin of an early model of ligand substitution on $[Be(H_2O)_4]^{2+}$ (*16, 66*). This model is based on the premise that Be^{2+} is readily accommodated in the tetrahedral interstice formed by the oxygen donor atoms of the four bound waters, and that the entering sulfate positions itself on the trigonal face opposite to that of the leaving water such that these two ligands are on a common axis with Be^{2+} (Fig. 5). A concerted process then occurs whereby the three nonleaving waters move apart to accommodate Be^{2+} in the trigonal space between them to form a transition state, which is followed by

[1] The definition of solvent exchange rates has sometimes led to misunderstandings in the literature. In this review k_1/s^{-1} (or k_2[solvent]), sometimes also referred to as k_{ex}/s^{-1}, is *the rate constant for the exchange of a particular coordinated solvent molecule* in the first coordination sphere (for example, solvent molecule number 2, if the solvent molecules are numbered from 1 to n, where n is the coordination number for the solvated metal ion, $[MS_n]^{m+}$). Thus, the equation for solvent exchange may be written:

$$[MS_n]^{m+} + n{*}S \overset{k_{ex}}{\rightleftharpoons} [M{*}S_n]^{m+} + nS \qquad (S = \text{solvent})$$

As defined here, k_{ex} is also *the rate constant for the exchange of all n solvent molecules* because each particular solvent molecule (for example, solvent molecule number 2, if the solvent molecules are numbered from 1 to n) exchanges at the same rate. The mean lifetime of a particular solvent molecule in the first coordination sphere, $\tau_{ex} = 1/k_{ex}$, is the same for each of the n coordinated solvent molecules. Thus, the probability of exchange of each particular solvent molecule is the same as the probability of exchange for all n solvent molecules, but is n times smaller than the probability of exchange of one unspecified solvent molecule.

Alternatively, the solvent exchange equation may be written:

$$[MS_n]^{m+} + {*}S \overset{k}{\rightleftharpoons} [MS_{n-1}{*}S]^{m+} + S \qquad (S = \text{solvent})$$

where the rate constant, k, for the exchange of an unspecified solvent molecule (any of the n solvent molecules: 1, 2, . . . or n) is n times greater than k_{ex} such that $k = nk_{ex}$. It follows that the rate constant, k, for the exchange of an unspecified solvent molecule (any of the n solvent molecules: 1, 2, . . . or n) in the first coordination sphere is n times greater than the rate constant for a particular solvent molecule such that $k = nk_{ex}$. While k is the relevant rate constant in making comparisons with complex formation rate constants, for historical reasons, k_{ex} is systematically reported in the literature, as well as $\Delta H_{ex}^{\ddagger}$, $\Delta S_{ex}^{\ddagger}$, and $\Delta V_{ex}^{\ddagger}$. The enthalpies and volumes of activation are identical for k_{ex} and k, but the $\Delta S_{ex}^{\ddagger}$ and $\Delta S_{ex}^{\ddagger}$ values differ by $R \ln(n)$. The understanding of the difference between k_{ex} and k is essential when comparing these values with complex formation rate constants.

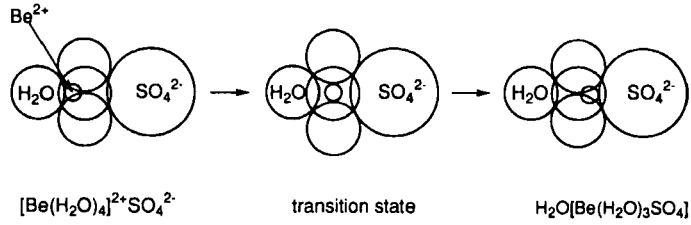

FIG. 5. A model for SO_4^{2-} substitution on $[Be(H_2O)_4]^{2+}$ proceeding from the outer-sphere complex on the left through the transition state at center to the inner-sphere complex at the right of the figure (*16, 66*).

the formation of the product ground state in which Be^{2+} occupies the tetrahedral interstice formed by the three nonleaving waters and the entering sulfate. Calculations based on hard sphere electrostatic calculations indicate that sulfate substitution is unlikely to occur through a **D** mechanism, and that both the leaving water and the entering sulfate make substantial contributions to the energetics of the transition state.

$$[Be(H_2O)_4]^{2+} + SO_4^{2-} \underset{k_{21} = 4 \times 10^8\ s^{-1}}{\overset{k_{12} = 4 \times 10^{10}\ dm^3\ mol^{-1}\ s^{-1}}{\rightleftharpoons}} [Be(H_2O)_4]^{2+}SO_4^{2-} \underset{k_{32} = 285\ s^{-1}}{\overset{k_{23} = 185\ s^{-1}}{\rightleftharpoons}} [Be(H_2O)_3(SO_4)] + H_2O \quad (13)$$

($\Delta H_{23}^{\ddagger} = 48$ kJ mol^{-1}, $\Delta S_{23}^{\ddagger} = -40$ J K^{-1} mol^{-1}, $K_{12} = 100$ dm^3 mol^{-1}, $K_{23} = 0.65$ dm^{3}mol^{-1}, $\Delta H_{12}^{0} = 6$ kJ mol^{-1}, $\Delta S_{12}^{0} = 60$ J K^{-1} mol^{-1}, $\Delta V_{12}^{0} = 10$ cm^3 mol^{-1}, $\Delta H_{23}^{0} = 4$ kJ mol^{-1}, $\Delta S_{23}^{0} = 10$ J K^{-1} mol^{-1}, $\Delta V_{23}^{0} = 3$ cm^3 mol^{-1}.)

Water exchange on $[Be(H_2O)_4]^{2+}$ is characterized by $\Delta V^{\ddagger} = -13.6$ cm^3 mol^{-1}, which is the most negative value observed for a water exchange process and compares with the molar volume of pure H_2O, $\Delta V_s^{0} = 18.0$ cm^3 mol^{-1} and a calculated limiting $\Delta V^{\ddagger} = -12.9$ cm^3 mol^{-1} for an **A** mechanism (*59*). This is strong evidence for the operation of an **A** mechanism for water exchange on $[Be(H_2O)_4]^{2+}$ and is in general agreement with the mechanism proposed for sulfate substitution (*16, 66*). The limiting $\Delta V^{\ddagger}$ value was estimated from the difference between the absolute partial molar volumes, V_{abs}^{0}, for $[Be(H_2O)_4]^{2+}$ and $[Be(H_2O)_5]^{2+}$ calculated through Eq. (12), using $r_M = 27$ pm and 36 pm as the ionic radii of four- and five-coordinate Be^{2+}, respectively, and $\Delta r = 238.7$ pm (*59*).

In nonaqueous solvents, the bulk of the solvent molecule becomes an important parameter determining the solvent exchange mechanism (*59, 67–71*). Overall, the data in Table I indicate that solvent exchange on $[Be(solvent)_4]^{2+}$ occurs according to a general rate law as expressed in Eq. (14), where k_1 and k_2 typify **d**- and **a**-activated exchange paths, respectively. Thus, for DMSO, TMP, DMMP, and MMPP, the k_2 term dominates and either an **A** or an $\mathbf{I}_a$ mechanism operates, as is also indicated by the negative $\Delta V^{\ddagger}$ values. Both the k_1 and k_2 terms apply for DMF, NMA, DMA, and DEA, consistent with the parallel operation of **d**- and **a**-activated mechanisms, and for the most sterically hindering solvents, DMADMP, TMU, and DMPU, a **D** mechanism dominates and only the k_1 term applies. This conclusion is supported by the corresponding positive $\Delta V^{\ddagger}$ values. For $[Be(H_2O)_r]^{2+}$, it is only possible to study the exchange process in neat solvent, and so no rate dependence on water concentration was determined. However, the negative $\Delta V^{\ddagger}$ is consistent with the operation of an **A** mechanism for $[Be(H_2O)_4]^{2+}$.

$$\text{rate} = 4(k_1 + k_2[\text{solvent}])[Be(\text{solvent})_4{}^{2+}] \qquad (14)$$

The sterically controlled exchange mechanism crossover from **a**- to **d**-activation as the steric hindrance at the Be^{2+} center increases with increasing size of the solvent is also observed in six-coordinate systems, as is discussed in Sections II, C and III, B. The **A** and **D** mechanisms call for incipient five- and three-coordinate transition states, and the simple model in Fig. 5 provides for this when the leaving and entering solvent to Be^{2+} distances, respectively, allow significant and insignificant bonding interactions. However, the steric characteristics of the nonleaving solvent molecules also affect the energetics of the transition state, and consequently some solvent exchange processes may progress along a reaction coordinate similar to that in Fig. 5, but others may not. Ab initio molecular orbital calculations show that although local energy minima exists for $[Be(H_2O)_4]^{2+}$, $[Be(H_2O)_5]^{2+}$, and $[Be(H_2O)_6]^{2+}$, in each case only four water molecules occupy the first coordination sphere, and any other water molecules reside in the second coordination sphere (*72*). Such calculations do not appear to have been extended to the water exchange process itself.

The only reported study in which $\Delta V^{\ddagger}$ data are available for ligand substitution on $[Be(H_2O)_4{}^{2+}$ is that involving substitution by bidentate oxygen-donor 4-isopropyltropolone (Hipt) to form $[Be(H_2O)_2(ipt)]^+$ (*73*). The observed reaction volume is $+5.3$ cm^3 mol^{-1} (Fig. 6), and the reaction volume for Hipt deprotonation is -8.2 cm^3 mol^{-1}, from which it is estimated that the reaction volume for the substitution of $[Be(H_2O)_4]^{2+}$ by ipt^- to form $[Be(H_2O)_2(ipt)]^+$ is $+13.5$ cm^3 mol^{-1}. This

TABLE I

PARAMETERS FOR SOLVENT EXCHANGE ON $[Be(solvent)_4]^{2+}$ AND $[Mg(solvent)_6]^{2+}$ IN d_3-NITROMETHANE DILUENT

Solvent	k_1(298.2 K)[a]/s^{-1}	k_2 (298.2 K)[a]/ $dm^3\ mol^{-1}\ s^{-1}$	$\Delta H^{\ddagger}$/ kJ mol^{-1}	$\Delta S^{\ddagger}$ J $K^{-1}\ mol^{-1}$	$\Delta V^{\ddagger}$/ $cm^{-1}\ mol^{-1}$	Mechanism	Ref.
			$[Be(solvent)_4]^{2+}$				
H_2O[b]	730	13.2[c]	59.2	+8.4	−13.6	**A**	*59*
DMSO		213	35.0	−83.0	−2.5	**A, I_a**	*59*
		140	51.1	−32.3		**A, I_a**	*67*
TMP		4.2	43.5	−87.1	−4.1	**A, I_a**	*59*
		1.5	56.0	−54.0		**A, I_a**	*68*
DMMP		0.81	60.2	−44.4		**A, I_a**	*68*
MMPP		0.22	68.7	−26.1		**A, I_a**	*69*
DMF		16	52.0	−47.5	−3.1	**A, I_a**	*59*
	0.2		74.9	−7.3		**D**	*59*
		8.5	58.1	−32.0		**A, I_a**	*70*
	0.1		83.6	+16.3		**D**	*70*
NMA		0.32	76.8	+3.1		**A, I_a**	*70*
	0.23		71.5	−17.3		**D**	*70*

DMA		0.34	66.7	−30.1		**A, I_a**	*70*
	0.38		56.9	−62.1		**D**	*70*
DEA		0.59	68.5	−19.6		**A, I_a**	*71*
	0.044		76.4	−14.6		**D**	*71*
DMADMP	0.0073		89.1	+12.6		**D**	*68*
TMU	1.0		79.6	+22.3	+10.5	**D**	*59*
	1.4		77.1	+16.4		**D**	*67*
DMPU	0.1		92.6	+47.5	+10.3	**D**	*59*
			$[Mg(solvent)_6]^{2+}$				
H_2O[b]	6.6×10^5		49.4	+32.3	+6.0	**D, I_d**	*76*
H_2O[b]	5.3×10^5		42.7	+8		**D, I_d**	*37*
MeOH[b]	4.7×10^3		69.9	+59		**D, I_d**	*80*
EtOH[b]	2.8×10^6		74.1	+126		**D, I_d**	*81*
DMF	4.3×10^5		54.8	+46.8	+8.5	**D, I_d**	*77*
DMF[d]	6.2×10^6		77.8	+146		**D, I_d**	*78*
TMP[d]	7.4×10^5		51.3	+39.5		**D, I_d**	*79*

[a] Rate constant for the exchange of a particular coordinated solvent molecule.
[b] Neat solvent.
[c] kg mol^{-1} s^{-1}, 730 s^{-1}/55.5 mol kg^{-1}.
[d] d_2-Dichloromethane diluent.

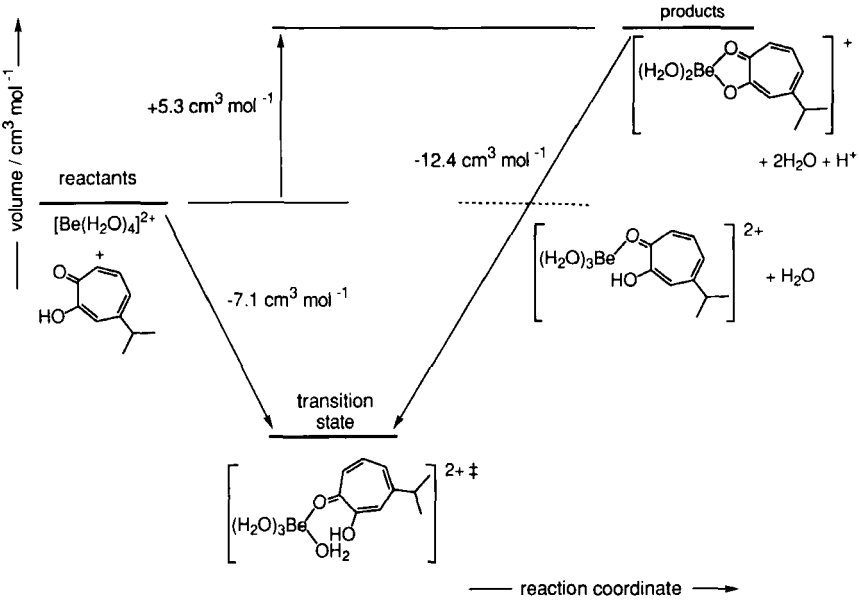

FIG. 6. A volume profile for the substitution of Hipt on $[Be(H_2O)_4]^{2+}$ to form $[Be(H_2O)_2ipt]^{+}$ (*73*).

substitution reaction volume arises mainly from the change in electrostriction caused by the changes in charge. Thus, the decrease in charge of the Be^{2+} species from 2+ to 1+ and the cancellation of charge of ipt^- on complexation contribute +8.7 and +2.8 $cm^3\ mol^{-1}$, respectively. These, when subtracted from +13.5 $cm^3\ mol^{-1}$, leave +4.8 $cm^3\ mol^{-1}$, which is thought to arise from changes in bond lengths and the change in volume of ipt^- when it becomes chelated (*74*).

When $[Be(H_2O)_4{}^{2+}]$ is in excess, the observed pseudo first-order rate constant for the approach to equilibrium, k_{obs}, is given by Eq. (15). The rate-determining complexation step is the formation of the first Hipt bond to Be^{2+} to form $[Be(H_2O)_3(Hipt)]^{2+}$, for which k_f (298.2 K) = 58.1 $dm^3\ mol^{-1}\ s^{-1}$, $\Delta H_f^{\ddagger}$ = 38.1 kJ mol^{-1}, $\Delta S_f^{\ddagger}$ = −83.5 J $K^{-1}\ mol^{-1}$ and $\Delta V_f^{\ddagger}$ = −7.1 $cm^3\ mol^{-1}$, as shown in Fig. 6. Because Hipt is uncharged there is unlikely to be any change in electrostriction on forming the transition state, and the negative $\Delta V_f^{\ddagger}$ therefore indicates that an a-activated mechanism is operating. The subsequent chelation step to form $[Be(H_2O)_2(ipt)]^{+}$, during which Hipt loses a proton, is rapid. The decomplexation reaction is characterized by k_r (298.2 K) = 49.8 $dm^3\ mol^{-1}\ s^{-1}$, $\Delta H_b^{\ddagger}$ = 35.7 kJ mol^{-1}, $\Delta S_b^{\ddagger}$ = 92.7 J $K^{-1}\ mol^{-1}$, and $\Delta V_b^{\ddagger}$ = −12.4 $cm^3\ mol^{-1}$. As there is no formal charge on Hipt, its

complexation by $[Be(H_2O)_4]^{2+}$ to form $[Be(H_2O)_3(Hipt)]^{2+}$ is likely to result in a reaction volume of zero (as indicated by the dashed line in Fig. 6), from which it is seen that $\Delta V^{\ddagger}$ for the displacement of Hipt from $[Be(H_2O)_3(Hipt)]^{2+}$ must be negative, consistent with the operation of an **a**-activated mechanism.

$$k_{obs} = k_f[Be(H_2O)_4{}^{2+}] + k_b[H^+] \tag{15}$$

The formation rate constant for Hipt at 298.2 K, $k_f = 58.1$ dm^3 mol^{-1} s^{-1}, compares with $k_f = 73$ dm^3 mol^{-1} s^{-1} for HF substitution (*75*) and $k_f = k_{12}k_{23}/k_{21} = 1.85 \times 10^4$ dm^3 mol^{-1} s^{-1} for $SO_4{}^{2-}$ substitution (*16, 66*). This illustrates the accelerating effect of the 2− sulfate charge, which probably arises from the strong electrostatic interaction lending a high stability to the outer-sphere complex. By comparison, the water exchange rate constant for $[Be(H_2O)_4]^{2+}$ is 13.2 kg mol^{-1} s^{-1} (*59*).

The increase in ionic radius from 27 pm for beryllium(II) to 72 pm (*2*) for magnesium(II) is accompanied by an increase in coordination number from 4 to 6, a substantial increase in lability, and a greater tendency towards a **d**-activation mode. Positive $\Delta V^{\ddagger}$ values (Table I) for solvent exchange on $[Mg(H_2O)_6]^{2+}$ and $[Mg(DMF)_6]^{2+}$, and the rate independence of free DMF concentration exhibited for $[Mg(DMF)_6]^{2+}$ in d_3-nitromethane diluent, indicate the operation of **d**-activated mechanisms (*76, 77*). Similar rate independences of free DMF concentration for exchange on $[Mg(DMF)_6]^{2+}$ and of free TMP concentration for exchange on $[Mg(TMP)_6]^{2+}$ in $d_2$dichloromethane and acetone diluents are also consistent with a **D** mechanistic assignment (*78, 79*). For the exchange of methanol and ethanol (*37, 80, 81*), solvent exchange rate laws and $\Delta V^{\ddagger}$ are not available, and so mechanistic assignment is less certain. Nevertheless, exchange of all five solvents is characterized by substantial positive $\Delta S^{\ddagger}$ values which are consistent with **d**-activated exchange processes.

Ligand substitution data for the substitution of water on $[Mg(H_2O)_6]^{2+}$ are scarce, but the early ultrasonic studies of substitution by sulfate and chromate are illuminating (*17*). The three-stage Eigen–Tamm mechanism was found to operate, and the third stage in which the entering ligand moves from the second to the first coordination sphere was characterized by $k_{23} = 1 \times 10^5$ s^{-1} for $SO_4{}^{2-}$ and $CrO_4{}^{2-}$ at 298.2 K, which is quite close to $k_{H_2O} = 6.6 \times 10^5$ s^{-1} (*76*). In the same study $k_{23} = 2 \times 10^7$ s^{-1} was reported for the substitution of $CrO_4{}^{2-}$ on $[Ca(H_2O)_n]^{2+}$, consistent with a further labilization of water in the first coordination sphere with increase in ionic radius.

C. Aluminum(III), Gallium(III), Indium(III), and Scandium(III)

The Al^{3+}, Ga^{3+}, and In^{3+} ions may be conveniently discussed simultaneously with the Sc^{3+} ion, as the first and last of these ions have d^0 electronic configurations and the other two possess d^{10} configurations. Together, they provide a basis for assessing the influence of metal ion size on ligand substitution on six-coordinate trivalent metal ions. Water exchange on $[Al(H_2O)_6]^{3+}$ and $[Ga(H_2O)_6]^{3+}$ are characterized by positive $\Delta V^{\ddagger}$ which are substantially less than anticipated for a **D** mechanism, and it is probable that an $\mathbf{I}_d$ mechanism operates (Table II) (*6, 53, 82–91*). However, as the steric crowding about the Al^{3+} and Ga^{3+} centers increases with increasing solvent size, it appears that a **D** mechanism becomes operative for TMP exchange. This deduction is based on the comparison of $\Delta V^{\ddagger}$ for TMP exchange on these centers with the reaction volume change, $\Delta V^0 = 23.8$ cm^3 mol^{-1}, for the loss of TMP from $[Nd(TMP)_7]^{3+}$ to form $[Nd(TMP)_6]^{3+}$ (*92*). Thus, it appears that the transition states for TMP exchange on $[Al(TMP)_6]^{3+}$ and $[Ga(TMP)_6]^{3+}$ closely approach five-coordination. It may be similarly reasoned, from their substantial negative $\Delta V^{\ddagger}$ magnitudes, that $[Sc(TMP)_6]^{3+}$ and $[In(TMP)_6]^{3+}$ closely approach an **A** mechanism for TMP exchange. The positive $\Delta V^{\ddagger}$ magnitudes observed for DMF exchange on $[Al(DMF)_6]^{3+}$ and $[Ga(DMF)_6]^{3+}$ are, respectively, greater than and similar to $\Delta V^0 = 9.1$ cm^3 mol^{-1} (*93*), for the loss of DMF from $[Nd(DMF)_9]^{3+}$ to form $[Nd(DMF)_8]^{3+}$. It may be argued that these exchange processes also approach the **D** mechanism. The exchange of TMP and DMF on Al^{3+} and Ga^{3+} in inert CD_3NO_2 diluent is independent of exchanging solvent concentration, also consistent with the operation of **D** mechanisms. It is on the basis of the $\Delta V^{\ddagger}$ sign and magnitude and the solvent exchange rate law observed in d_3-nitromethane diluent that the mechanistic assignments in Table II are made.

Two general trends emerge from the data in Table II. The first is that as the size of the $[M(solvent)_6]^{3+}$ metal center increases the lability of the solvent increases through a **d**-activated mechanism, which changes to an **a**-activated mechanism as the center size increases to the point at which bond making with the entering solvent becomes a dominant factor in the transition state energetics. In parallel with this, $\Delta H^{\ddagger}$ tends to decrease markedly and $\Delta S^{\ddagger}$ to change from positive to negative as the mechanism changes from **d**- to **a**-activation. The second trend is that as solvent size increases, so the tendency towards **d**-activation increases. This is well illustrated by $[Sc(TMU)_6]^{3+}$, which exchanges TMU through a **D** mechanism, in contrast to the other $[Sc(solvent)_6]^{3+}$ ions, which exchange solvent through $\mathbf{I}_a$ or **A** mecha-

TABLE II

PARAMETERS FOR SOLVENT EXCHANGE ON DIAMAGNETIC $[M(solvent)_6]^{3+}$ IN d_3-NITROMETHANE DILUENT

$[M(solvent)_6]^{3+}$	r_M[a]/pm	k_1(298 K)[b]/s^{-1}	k_2(298 K)[b]/ $dm^3\ mol^{-1}\ s^{-1}$	$\Delta H^{\ddagger}$/ kJ mol^{-1}	$\Delta S^{\ddagger}$ J K^{-1} mol^{-1}	$\Delta V^{\ddagger}$/ $cm^3\ mol^{-1}$	$\Delta V^{\ddagger}/V_s^0$	Mechanism	Ref.
$[Al(H_2O)_6]^{3+}$[c]	54	1.29		84.7	+41.6	+5.7	+0.32	I_d	*82*
$[Al(DMSO)_6]^{3+}$		0.30		82.6	+22.3	+15.6	+0.22	D	*83, 84*
$[Al(DMF)_6]^{3+}$		0.05		88.3	+28.4	+13.7	+0.18	D	*83, 84*
$[Al(TMP)_6]^{3+}$		0.78		85.1	+38.2	+22.5	+0.20	D	*6*
$[Al(TMP)_6]^{3+}$		0.38		98.3	+76.1			D	*85*
$[Al(DMMP)_6]^{3+}$		5.1		79.5	+33.0			D	*85*
$[Al(HMPA)_4]^{3+}$			4800	32.2	−42.7			A	*85*
$[Ga(H_2O)_6]^{3+}$[c]	62	400		67.1	+30.1	+5.0	+0.29	I_d	*53*
$[Ga(DMSO)_6]^{3+}$		1.87		72.5	+3.5	+13.1	+0.18	D	*83, 84*
$[Ga(DMF)_6]^{3+}$		1.72		85.1	+45.1	+7.9	+0.10	D	*83, 84*
$[Ga(TMP)_6]^{3+}$		6.4		76.5	+27.0	+20.7	+0.18	D	*6*
$[Ga(TMP)_6]^{3+}$		5.0		87.9	+63.2			D	*86*
$[Sc(TMP)_6]^{3+}$[c]	75		1200	37.4	−60.5	−20.1	−0.21	A, I_a	*87*
$[Sc(TMP)_6]^{3+}$			38.4	21.2	−143.5	−18.7	−0.16	A, I_a	*6*
$[Sc(TMP)_6]^{3+}$			45.3	26.0	−126			A, I_a	*88*
$[Sc(DMMP)_6]^{3+}$			13.2	29.7	−124			A, I_a	*89*
$[Sc(TMU)_6]^{3+}$		0.21		91.2	+47.8			D	*90*
$[In(H_2O)_6]^{3+}$[c]	80	40000		19.2	−96			A, I_a	*91*
$[In(TMP)_6]^{3+}$			7.6	32.8	−118	−21.4	−0.19	A, I_a	*6*
$[In(TMP)_6]^{3+}$			7.2	35.6	−109			A, I_a	*86*

[a] Ref. (*2*).

[b] Rate constant for the exchange of a particular coordinated solvent molecule.

[c] In neat solvent.

nisms. An extreme example of the influence of solvent size is the decreased coordination number of $[Al(HMPA)_4]^{3+}$, which exchanges HMPA through an **A** mechanism, in contrast to the $[Al(solvent)_6]^{3+}$ ions for which **d**-activated mechanisms operate.

It is now appropriate to consider the ratios $\Delta V^{\ddagger}/\Delta V_s^0$ in Table II, where ΔV_s^0 is the partial molar volume of the free exchanging solvent. When a magnitude of $|13.5|$ cm^3 mol^{-1} assumed for either a **D** or an **A** water exchange mechanism, a $\Delta V^{\ddagger}/\Delta V_s^0$ magnitude of 0.75 cm^3 mol^{-1} is anticipated. These magnitudes for $[Al(H_2O)_6]^{3+}$ and $[Ga(H_2O)_6]^{3+}$ are substantially less than this, consistent with the operation of $\mathbf{I}_d$ mechanisms. In contrast, the $\Delta V^{\ddagger}/\Delta V_s^0$ magnitudes for $[Al(TMP)_6]^{3+}$ and its Ga^{3+}, Sc^{3+}, and In^{3+} analogues are much smaller, and yet the evidence for the close approach of the first and last pairs of these species to **D** and **A** TMP exchange mechanisms, respectively, is compelling, as discussed above. This indicates that the exchange of small solvent molecules such as water may exhibit large $\Delta V^{\ddagger}/\Delta V_s^0$ magnitudes for **D** and **A** mechanisms, whereas the exchange of larger solvents such as TMP and DMF are likely to exhibit smaller $\Delta V^{\ddagger}/\Delta V_s^0$ magnitudes. (ΔV_s^0 = 18.0, 40.5, 52.2, 77.4, 85.9, and 118 cm^3 mol^{-1} for H_2O, MeOH, MeCN, DMF, DMSO, and TMP, respectively.)

Ligand substitution studies on $[Al(H_2O)_6]^{3+}$ are complicated by the formation of $[Al(H_2O)_5(OH)]^{2+}$ even at low pH, and also by the so-called "proton ambiguity" which arises when the substitution of the conjugate base form of a ligand on the first species and the substitution of the conjugate acid form of a ligand on the second species become experimentally indistinguishable. Additionally, it appears that in some $[Al(H_2O)_6]^{3+}$ ligand substitution studies, significant amounts of $[Al(H_2O)_5(OH)]^{2+}$ may not have been accounted for in the kinetic analysis. However, a study of the substitution of $[Al(H_2O)_6]^{3+}$ by five hydroxamic acids {$R_1C(O)N(OH)R_2$ where R_1 and R_2 are H, alkyl or aryl groups}, at acid concentrations where these ligands only exist as the conjugate acid, yield k_i in the range 2.0 to 3.1 s^{-1} at 298.2 K through the relationship $k_f = k_i S K_o$, where the statistical factor S = 0.75 and a calculated K_o = 0.1 dm^3 mol^{-1} (*35*). The close similarity between these k_i and k_{H_2O} = 1.29 s^{-1} suggests that an $\mathbf{I}_d$ ligand substitution mechanism is operative, but it should be noted that the estimation of S and K_o is critical in the derivation of k_i, as is also the case in a range of other $[Al(H_2O)_6]^{3+}$ ligand substitution studies in which k_i varying over an order of magnitude on either side of k_{H_2O} have been reported (*82*). The hydroxamic acids substitute 10^4 times faster on $[Al(H_2O)_5(OH)]^{2+}$ than on $[Al(H_2O)_6]^{3+}$, consistent with the directly determined labilization of coordinated water by hydroxo ligands on other trivalent metal ions as discussed in Sections III,F and G.

A proton ambiguity frequently complicates the interpretation of $[Ga(H_2O)_6]^{3+}$ ligand substitution studies, which when analyzed in a similar manner to the $[Al(H_2O)_6]^{3+}$ studies yield k_i values ranging over an order of magnitude on either side of k_{H_2O} for $[Ga(H_2O)_6]^{3+}$ (*53, 94*). The variations of k_i for $[Al(H_2O)_6]^{3+}$ and $[Ga(H_2O)_6]^{3+}$ may be generated more by the kinetic analyses through which k_i is derived than the ligand substitution process itself. However, the range of k_i is quite small by comparison with $[Cr(H_2O)_6]^{3+}$ and $[Fe(H_2O)_6]^{3+}$ ligand substitution processes, where an **a**-activation mode operates (*51, 95*). In contrast, the derivation of $\Delta V^{\ddagger}$ for a neutral substituting ligand is less subjective, and the report that $\Delta V^{\ddagger} = +4.0$ cm^3 mol^{-1} for the substitution of tropolone on $[Ga(H_2O)_6]^{3+}$ is strong evidence for a **d**-activated substitution mechanism in this case (*96*).

III. Solvent Exchange and Ligand Substitution on Transition Metal Ions

A. General Characteristics

The labilities and solvent exchange and ligand substitution mechanisms of the transition metal ions are profoundly affected by the electronic occupancy of their *d*-orbitals. Thus, the sequence of reactivity of the first-row metal ions ($Cu^{2+} > Mn^{2+} > Fe^{2+} > Co^{2+} > Ni^{2+} > V^{2+}$) is largely independent of mechanism and semiquantitatively coincides with predictions based on ligand field activation energies (LFAE) (*97*) and molecular orbital calculations (*98*). The variations of $\Delta G^{\ddagger}$ and $\Delta V^{\ddagger}$ (*46, 47, 50–53, 95, 99–101*), and the LFAE for water exchange on $[M(H_2O)_6]^{2+/3+}$ through **D** and **A** mechanisms are shown in Fig. 7. Most of the $\Delta G^{\ddagger}$ values are directly determined, but in the case of $[Cr(H_2O)_6]^{2+}$ a value similar to that of $[Cu(H_2O)_6]^{2+}$ is assumed as an upper limit from a comparison of directly determined values for their methanol analogues (*102, 103*). In the case of $[Zn(H_2O)_6]^{2+}$, an upper limit for $\Delta G^{\ddagger}$ is estimated from ligand substitution studies (*100*). The LFAE values are calculated for the high-spin divalent and low-spin trivalent species as the differences in ligand field energies between octahedral ground states and square pyramidal and pentagonal bipyramidal transition states for the **D** and **A** mechanisms, respectively (*104–106*), using a one-electron formula (*107*). The variations of LFAE in each case reflect the variation of $\Delta G^{\ddagger}$ such that a small LFAE coincides with a high lability and a large LFAE coincides with a lesser lability. Thus, no distinction between the operation of either **D** or **A** mechanisms seems possible on the basis of the LFAE contribution to the energetics of water exchange. Although the magnitudes of LFAE

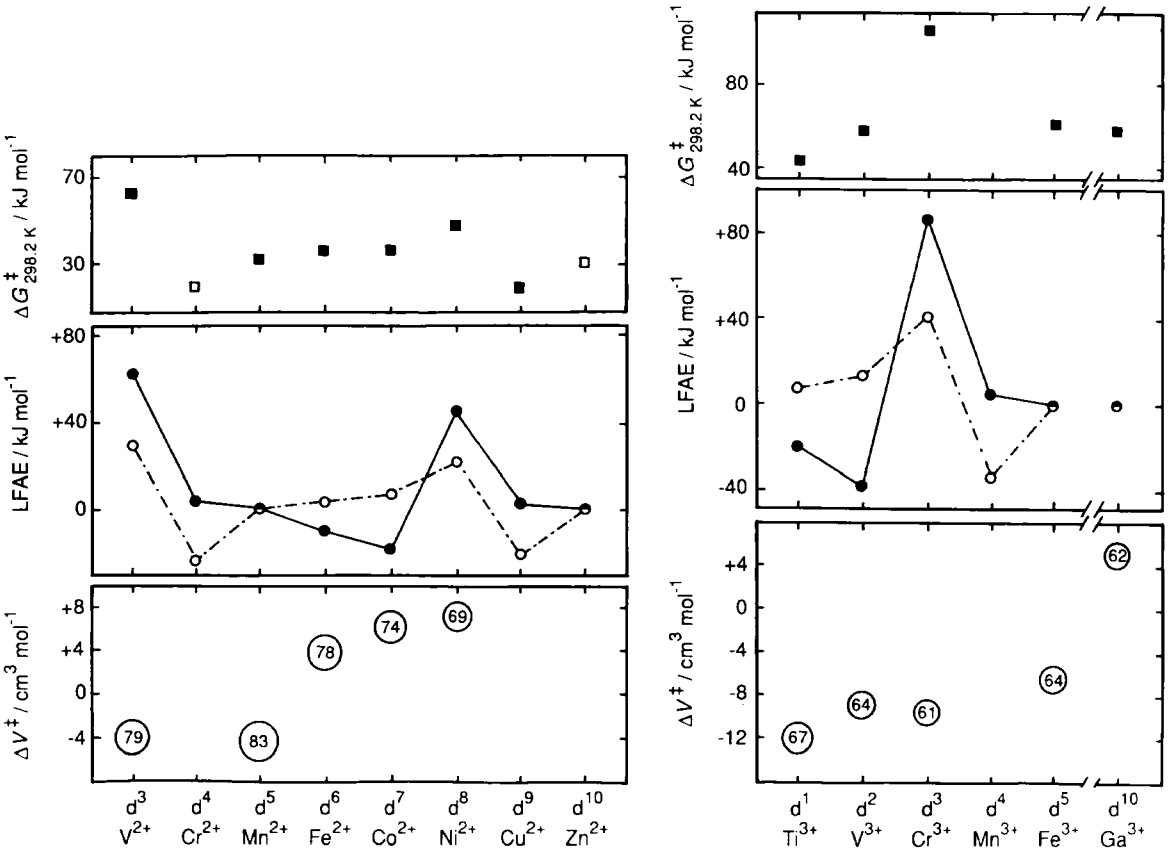
$\Delta G^{\ddagger}_{298.2\,K}$ / kJ mol^{-1}
70
30
LFAE / kJ mol^{-1}
+80
+40
0
$\Delta V^{\ddagger}$ / cm^3 mol^{-1}
+8
+4
0
-4
79
83
78
74
69
d^3 V^{2+}
d^4 Cr^{2+}
d^5 Mn^{2+}
d^6 Fe^{2+}
d^7 Co^{2+}
d^8 Ni^{2+}
d^9 Cu^{2+}
d^{10} Zn^{2+}
$\Delta G^{\ddagger}_{298.2\,K}$ / kJ mol^{-1}
80
40
LFAE / kJ mol^{-1}
+80
+40
0
-40
$\Delta V^{\ddagger}$ / cm^3 mol^{-1}
+4
0
-4
-8
-12
67
64
61
64
62
d^1 Ti^{3+}
d^2 V^{3+}
d^3 Cr^{3+}
d^4 Mn^{3+}
d^5 Fe^{3+}
d^{10} Ga^{3+}

are dependent on the ligand field exerted by the solvent, and therefore vary with the nature of the solvent, the relative labilities predicted for $[M(solvent)_6]^{2+/3+}$ are similar for all solvents.

Generally the magnitudes of solvent exchange rate constants increase in the sequence $NH_3 > H_2O > DMF > MeCN > MeOH$, which is largely independent of the nature of the metal ion (*108, 109*). This sequence cannot be readily identified with specific characteristics such as dielectric constant, donor number, electric dipole moment, or stereochemistry, and it appears to reflect the overall solvent characteristic. There may be a correlation between the $\Delta H^{\ddagger}$ for solvent exchange on $[M(solvent)_6]^{2+}$ and the heat of dissociation of solvent from this species (*110*).

While the influence of *d*-orbital electronic occupancy is most strikingly illustrated through the variation of reactivity of the first-row transition metal ions with LFAE, it will be seen later that this occupancy also has a significant correlation with activation mode. Given the relatively small number of second- and third-row metal ions kinetically characterized, the pattern of *d*-orbital occupancy effects is less apparent. However, their mechanistic differences from the first-row metal ions can be interpreted in terms of the *d*-orbitals becoming more diffuse (*48*), the metal center becoming more polarizable, and larger ligand field stabilization energies (*104*). Some examples of these effects are considered next.

B. Solvent Exchange on Divalent Octahedral First-Row Transition Metal Ions

Solvent exchange on the first-row transition metal $[M(solvent)_6]^{2+}$ species has been subjected to extensive study, as is exemplified by Table III, which contains data for four solvent systems which have been particularly intensively studied (*46, 47, 97, 99, 103, 110–117*). The solvent exchange mechanism progressively changes from $\mathbf{I}_a$ to $\mathbf{I}_d$ as the number of *d*-electrons increases and r_M decreases for H_2O, MeOH, and MeCN solvents, as judged from the changes in sign of $\Delta V^{\ddagger}$. It is also seen that lability decreases with increase in $\Delta H^{\ddagger}$ substantially, as

FIG. 7. The variation of $\Delta G^{\ddagger}$ for water exchange on high-spin $[M(H_2O)_6]^{2+}$ and low-spin $[M(H_2O)_6]^{2+/3+}$ at 298.2 K with d^n, where the closed squares represent directly determined values, and the open squares represent estimated values. The LFAE calculated for **D** and **A** mechanisms are indicated by open and closed circles, respectively. The $\Delta V^{\ddagger}$ are indicated by circles enclosing the r_M of the metal ions in picometers.

TABLE III

PARAMETERS FOR SOLVENT EXCHANGE ON DIVALENT TRANSITION-METAL IONS

$[M(solvent)_6]^{3+}$	r_M[a]/pm	*d*-electronic configuration	k_{ex} (298 K)[b]/s^{-1}	$\Delta H^{\ddagger}$/ kJ mol^{-1}	$\Delta S^{\ddagger}$/ J K^{-1} mol^{-1}	$\Delta V^{\ddagger}$/ cm^3 mol^{-1}	Mechanism	Ref.
$[V(H_2O)_6]^{2+}$	79	t_{2g}^3	8.7×10^1	61.8	−0.4	−4.1	I_a	*47*
$[Mn(H_2O)_6]^{2+}$	83	$t_{2g}^3e_g^2$	2.1×10^7	32.9	+5.7	−5.4	I_a	*46*
$[Fe(H_2O)_6]^{2+}$	78	$t_{2g}^4e_g^2$	4.39×10^6	41.4	+21.2	+3.8	I_d	*46*
$[Co(H_2O)_6]^{2+}$	74	$t_{2g}^5e_g^2$	3.18×10^6	46.9	+37.2	+6.1	I_d	*46*
$[Ni(H_2O)_6]^{2+}$	69	$t_{2g}^6e_g^2$	3.15×10^4	56.9	+32.0	+7.2	I_d	*46*
$[Cu(H_2O)_6]^{2+}$	73	$t_{2g}^6e_g^{3c}$	4.4×10^9	11.5	−21.8		I_d[d]	*99*
$[Cr(MeOH)_6]^{2+}$	80	$t_{2g}^3e_g^{1c}$	1.2×10^8	31.6	+16.6		I_d[d]	*102*
$[Mn(MeOH)_6]^{2+}$	83	$t_{2g}^3e_g^2$	3.7×10^5	25.9	−50.2	−5.0	I_a	*97, 111*
$[Fe(MeOH)_6]^{2+}$	78	$t_{2g}^4e_g^2$	5.0×10^4	50.2	+12.6	+0.4	I	*97, 111*
$[Co(MeOH)_6]^{2+}$	74	$t_{2g}^5e_g^2$	1.8×10^4	57.7	+30.1	+8.9	I_d	*112, 113*
$[Ni(MeOH)_6]^{2+}$	69	$t_{2g}^6e_g^2$	1.0×10^3	66.1	+33.5	+11.4	I_d	*112, 113*
$[Cu(MeOH)_6]^{2+}$	73	$t_{2g}^6e_g^{3c}$	3.1×10^7	17.2	−44.0	+8.3	I_d[d]	*103*
$[Mn(MeCN)_6]^{2+}$	83	$t_{2g}^3e_g^2$	1.4×10^7	29.6	−8.9	−7.0	I_a	*114*
$[Fe(MeCN)_6]^{2+}$	78	$t_{2g}^4e_g^2$	6.6×10^5	41.4	+5.3	+3.0	I_d	*114*
$[Co(MeCN)_6]^{2+}$	74	$t_{2g}^5e_g^2$	3.4×10^5	49.5	+27.1	+8.1[e]	I_d	*113, 115, 116*
$[Ni(MeCN)_6]^{2+}$	69	$t_{2g}^6e_g^2$	2.8×10^3	64.3	+37	+8.5	I_d	*113, 115*
$[Mn(DMF)_6]^{2+}$	83	$t_{2g}^3e_g^2$	2.2×10^6	34.6	−7.4	+2.4	I_d	*109*
$[Fe(DMF)_6]^{2+}$	78	$t_{2g}^4e_g^2$	9.7×10^5	43.0	+13.8	+8.5	I_d	*109*
$[Co(DMF)_6]^{2+}$	74	$t_{2g}^5e_g^2$	3.9×10^5	56.9	+52.7	+6.7	I_d	*113, 117*
$[Ni(DMF)_6]^{2+}$	69	$t_{2g}^6e_g^2$	3.8×10^3	62.8	+33.5	+9.1	I_d	*112, 117*

[a] Ref. (*2*).

[b] Rate constant for the exchange of a particular coordinated solvent molecule.

[c] Tetragonal distortion.

[d] Labilized through a tetragonal distortion.

[e] Average of +9.9, +6.7, and 7.7 cm^3 mol^{-1}.

predicted from the variation of LFAE, and consistent with the *d*-electronic rearrangement accompanying the activation process making a substantial contribution to $\Delta H^{\ddagger}$ for $[V(solvent)_6]^{2+}$ and $[Ni(solvent)_6]^{2+}$ and no contribution for $[Mn(solvent)_6]^{2+}$. The variation in mechanism may be explained through a combination of an increase in steric crowding with decrease in r_M favoring **d**-activation, and an increase in t_{2g} electronic occupancy increasing the electronic repulsion between an entering solvent molecule approaching a trigonal face of $[M(solvent)_6]^{2+}$ in an **a**-activated mechanism (*46, 97*). Thus, $[V(solvent)_6]^{2+}$ and $[Mn(solvent)_6]^{2+}$ exchange solvent through **a**-activated mechanisms, while **d**-activated mechanisms operate for their Fe^{2+}, Co^{2+}, and Ni^{2+} analogues. However, as the size of the solvent molecule increases, the tendency towards **d**-activation increases, as is illustrated by $[M(DMF)_6]^{2+}$ for which $\Delta V^{\ddagger}$ is positive in all cases including that for $[Mn(DMF)_6]^{2+}$ (*109, 118, 119*). This change towards a **d**-activation mode for $[Mn(solvent)_6]^{2+}$ has also been observed when the solvent is acetic acid (*120*) and dimethylthioformamide (*119*). In contrast to the change of activation mode exhibited by $[Mn(solvent)_6]^{2+}$, its Ni^{2+} analogue invariably undergoes exchange through a **d**-activated mechanism, as indicated by $\Delta V^{\ddagger} = +5.9, +11.4, +13.7, +13.1, +12.4, +14.4$, and $+13.1$ cm^3 mol^{-1} when the solvent is ammonia (*121*), 1,2-diaminopropane (*122*), propionitrile, butyronitrile, isobutyronitrile, valeronitrile, and benzonitrile, respectively (*123*). This is further demonstrated by the independence of free DMF concentration of the exchange rate of $[Ni(DMF)_6]^{2+}$ in nitromethane dilute (*124*), and evidence for lower coordination number species found in solvent exchange studies of $[Ni(DEF)_6]^{2+}$ and $[Ni(DMA)_6]^{2+}$ (*125*).

The high lability of d^9 $[Cu(H_2O)_6]^{2+}$ is coincident with the operation of a dynamic Jahn–Teller effect which causes its tetragonal distortion to randomly reorientate, or invert, about the *x*, *y*, and *z* axes very rapidly (Fig. 8) so that the lifetime of a given distortion, τ_i, is much less than the lifetime of a given coordinated H_2O molecule, τ_{H_2O} (*99,*

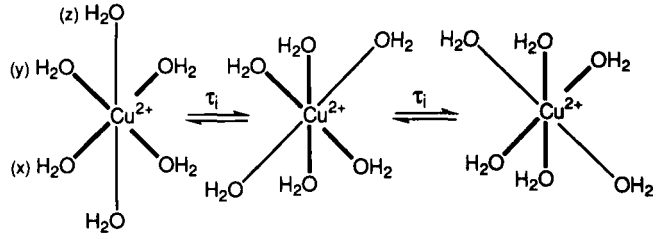

FIG. 8. An illustration of the inversion of the tetragonal distortion in $[Cu(H_2O)_6]^{2+}$.

126, 127). Thus, an axial H_2O site in $[Cu(H_2O)_6]^{2+}$ converts to an equatorial site with each inversion, and an equatorial site converts to an axial site every second inversion on average, such that each H_2O in $[Cu(H_2O)_6]^{2+}$ experiences all orientations of the tetragonal distortion many times before it undergoes exchange with free H_2O, rendering the six-coordinated H_2O kinetically indistinguishable. It is reasonable to assume that the longer axial bonds in $[Cu(H_2O)_6]^{2+}$ should facilitate solvent exchange through a **d**-activation mode. Solution x-ray diffraction (*128–132*) and neutron diffraction studies (*133*) show a tetragonal distortion of $[Cu(H_2O)_6]^{2+}$ with four equatorial H_2O at a mean Cu–O distance of between 196 and 200 pm with the two axial H_2O at a greater, but less well defined, Cu–O distance. An ^{17}O NMR study (*99*) is consistent with a rapid inversion of the tetragonal distortion occurring in $[Cu(H_2O)_6]^{2+}$ characterized by $\tau_i = 5.1 \times 10^{-12}$ s at 298.2 K. The same study yields $\tau_{H_2O} = 2.3 \times 10^{-10}$ s at 298.2 K and the kinetic parameters in Table III for H_2O exchange on $[Cu(H_2O)_6]^{2+}$ (*99*). Thus, each H_2O in $[Cu(H_2O)_6]^{2+}$ experiences 45 inversions of the tetragonal distortion orientation for each exchange with free H_2O. Similar studies of $[Cu(MeOH)_6]^{2+}$ (*103, 127*) yield $\tau_i = 1.2 \times 10^{-11}$ s and $\tau_{MeOH} = 3.2 \times 10^{-8}$ s at 298.2 K and the kinetic parameters in Table III for MeOH exchange. The positive $\Delta V^{\ddagger}$ for $[Cu(MeOH)_6]^{2+}$ is consistent with the operation of a **d**-activated methanol exchange process, although the negative $\Delta S^{\ddagger}$ is unexpected for this mode of activation, but this may reflect an aspect of the tetragonal distortion (*103*). The high lability of $[Cr(MeOH)_6]^{2+}$ is also anticipated from its $t_{2g}^3 e_g^1$ electronic configuration. However, it appears that the rate of inversion of the tetragonal distortion is slow by comparison to the rate of methanol exchange, which consequently occurs predominantly at the two kinetically distinct axial sites (*102*).

C. Ligand Substitution on Divalent Octahedral First-Row Transition Metal Ions

Ligand substitution on the $[M(H_2O_6]^{2+}$ first-row transition metal ions generally shows little rate dependence on the nature of the substituting ligand, L^{x-}, for a particular M^{2+}, beyond that anticipated for the influence of the ligand charge x- on the magnitude of K_o for Eq. (3) which characterizes the outer-sphere complex in an interchange mechanism, as is discussed in Section I, B. This, together with the observation that the trends in ligand substitution rate closely follow those in water exchange rates as M^{2+} varies, led to the early conclusion that ligand substitution proceeded through an I_d mechanism for all $[M(H_2O)_6]^{2+}$ (*1, 19, 134*). As it was anticipated that ligand substitution rates should

reflect the selectivity of M^{2+} for L^{x-} in **a**-activated mechanisms, this assignment of an I_d mechanism was reasonable, especially in view of the emphasis placed on the absence and presence of ligand selectivity in the original definitions of **d**- and **a**-activated mechanisms by Langford and Gray (*34*). On this basis, little selectivity would be anticipated in ligand substitution on $[M(H_2O)_6]^{2+}$ other than when M^{2+} is either V^{2+} or Mn^{2+}, as it is only for these species that an **a**-activated mechanism operates for water exchange, as indicated by their negative $\Delta V^{\ddagger}$ values (Table III).

There are few ligand substitution data available for $[V(H_2O)_6]^{2+}$, and while there are more data available for $[Mn(H_2O)_6]^{2+}$, no clear selectivity pattern emerges (*46, 135*). It may be that because the borderline hard acid nature of Mn^{2+} restricts its formation of stable complexes to ligands with hard base donor atoms, the range of polarizability, and therefore nucleophilicity, is too small in the substituting ligands so far studied for a selectivity pattern to emerge. However, $\Delta V^{\ddagger}$ for ligand substitution on $[M(H_2O)_6]^{2+}$ shows a strong correlation with $\Delta V^{\ddagger}$ for water exchange, consistent with **a**-activated mechanisms operating for both water exchange and ligand substitution on $[V(H_2O)_6]^{2+}$ and $[Mn(H_2O)_6]^{2+}$, and **d**-activated mechanisms operating for the other $[M(H_2O)_6]^{2+}$, as seen from Table IV (*46, 47, 136–146*). In contrast

TABLE IV

ACTIVATION VOLUMES, $\Delta V_i^{\ddagger}$, FOR WATER EXCHANGE AND LIGAND SUBSTITUTION[a] ON $[M(H_2O)_6]^{2+}$

Ligand	V^{2+}	Mn^{2+}	Fe^{2+}	Co^{2+}	Ni^{2+}	Cu^{2+}	Zn^{2+}	Ref.
H_2O	−4.1	−5.4	+3.8	+6.1	+7.2			*46. 47*
NH_3				+4.8	+6.0			*136*
Imidazole					+11.0			*137*
Isoquinoline					+7.4			*138*
Pada[b]				+7.9[c]	+7.1[c]			*136, 139, 140*
Bpy		−1.2		+5.9[c]	+5.3[c]		+7.1	*141–143*
Tpy		−3.4	+3.6	+4.1	+5.6			*135, 142*
SCN^-	−5.3							*144*
Glycinate (−1)				+5	+7	+9	+4	*145*
Murexide (−1)					+8.7			*146*

[a] $\Delta V_i^{\ddagger} = \Delta V_f^{\ddagger} - \Delta V_o^0 = 0$ cm^3 mol^{-1} for neutral ligands, $\Delta V_o^0 = +3.2$ cm^3 mol^{-1} for uninegative ligands, where $\Delta V_i^{\ddagger}$, $\Delta V_f^{\ddagger}$, and ΔV_o^0 correspond to the activation volumes associated with k_i and k_f in Eqs. (4) and (5), and the volume change associated with K_o in Eq. (3).

[b] Pyridine-2-azo-(*p*-dimethylanaline).

[c] Average value.

to the $\Delta V^{\ddagger} = +7.1$ and $+3.6$ cm^3 mol^{-1} for substitution of bpy on $[Zn(H_2O)_6]^{2+}$ and the reverse reaction, respectively, consistent with **d**-activated mechanisms operating, $\Delta V^{\ddagger} = -5.5$ and -6.9 cm^3 mol^{-1} for substitution of bpy on $[Cd(H_2O)_6]^{2+}$ and the reverse reaction, respectively, are consistent with **a**-activated mechanisms operating (*143*). This is another demonstration of the effect of r_M on mechanism, whereby Zn^{2+} ($r_M = 74$ pm) is too small to increase its coordination number in the transition state, while the larger Cd^{2+} ($r_M = 95$ pm) is able to do so and substitutes through an **a**-activated mechanism.

The change to **d**-activation mode for DMF exchange on $[Mn(DMF)_6]^{2+}$ is also reflected in $\Delta V_i^{\ddagger} = +7.2$ cm^3 mol^{-1} for the first step in the substitution of bidentate diethyldithiocarbamate on this species, and for the corresponding Fe^{2+}, Co^{2+}, and Ni^{2+} species $\Delta V_i^{\ddagger} = +9.7$, $+9.5$, and $+7.4$ cm^3 mol^{-1}, respectively (*147, 148*). A complete reaction volume profile for the **d**-activated substitution of bidentate pada on $[Fe(DMF)_6]^{2+}$ is shown in Fig. 9.

D. The Influence of Nonleaving Ligands on Lability

Although this review is primarily concerned with the solvent exchange and single ligand substitution on fully solvated metal ions, it is nevertheless appropriate to note that substitution of coordinated solvent in $[M(solvent)_6]^{2+}$ by other ligands can substantially alter the lability of the remaining solvent. This is illustrated for a range of

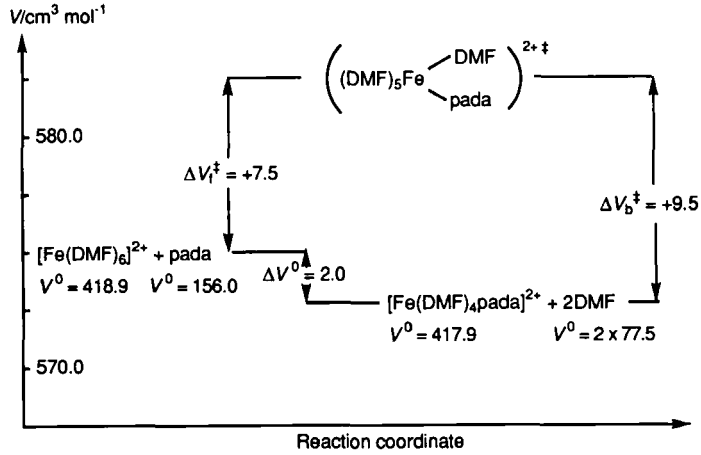

FIG. 9. Reaction volume profile for the substitution of $[Fe(DMF)_6]^{2+}$ by *trans*-pyridine-2-azo(*p*-dimethylaniline), pada (*147*).

nickel(II) complexes in Table V (*46, 149–159*). Substitution by ammonia and polyamines labilizes the remaining waters roughly in proportion to the number of coordinating nitrogen atoms. This suggests that greater electron donation through the σ-bonding system to the metal center is the source of the labilization (*159*). However, it appears that although bpy and tpy may also donate electron density to the metal center through σ-bonding, electron withdrawal through the π-bonding systems of these ligands results in only modest changes in lability. The origin of the labilization found for the last four complexes in Table V probably arises from a variety of sources, but it appears that a decrease in strength of the water dipole–Ni^{2+} interaction resulting from the decrease in overall positive charge of the complex ions may be a contributing factor. It has also been observed that five-coordinate $[Cu(tren)(H_2O)]^{2+}$ is characterized by $k_{H_2O} = 2.5 \times 10^5\ s^{-1}$ at 298.2 K (*151*), which is some four orders of magnitude less than that for $[Cu(H_2O)_6]^{2+}$, presumably because a combination of the constraining effect of tren and the change to five-coordination removes the dynamic Jahn–Teller effect as a labilizing force. A similar interpretation has been placed on the decreased lability of $[Cu(tren)(MeCN)]^{2+}$, for which $k_{ex}(298.2\ K) = 1.7 \times 10^6\ s^{-1}$ for MeCN exchange (*160*). The effect of stereochemically constraining ligands such as 2,2′,2″-tri(*N*,*N*-dimethylamino)triethylamine (Me_6tren) can have substantial effects

TABLE V

THE VARIATION OF THE LABILITY OF COORDINATED WATER IN NICKEL(II) COMPLEXES AT 298.2 K

Complex	$10^{-4}k_{H_2O}{}^{a}/s^{-1}$	Ref.	Complex	$10^{-4}k_{H_2O}{}^{a}/s^{-1}$	Ref.
$[Ni(H_2O)_6]^{2+}$	3.15	*46*	$[Ni(cyclen)(H_2O)_2]^{2+}$	2100	*152*
$[Ni(NH_3)(H_2O)_5]^{2+}$	25	*149*	$[Ni(Me_4cyclam)(H_2O)_2]^{2+b}$	1600	*153*
$[Ni(NH_3)_2(H_2O)_4]^{2+}$	61	*149*	$[Ni(Me_4cyclam)(H_2O)]^{2+c}$	160	*153*
$[Ni(NH_3)_3(H_2O)_3]^{2+}$	250	*149*	$[Ni(bpy)(H_2O)_4]^{2+}$	4.9	*154*
$[Ni(en)(H_2O_4]^{2+}$	44	*150*	$[Ni(bpy)_2(H_2O)_2]^{2+}$	6.6	*154*
$[Ni(en)_2(H_2O)_2]^{3+}$	540	*150*	$[Ni(tpy)(H_2O)_3]^{2+}$	5.2	*155*
$[Ni(dien)(H_2O)_3]^{2+}$	120	*159*	$[Ni(H_2O)_5Cl]^{+}$	14	*156*
$[Ni(trien)(H_2O)_2]^{2+}$	290	*159*	$[Ni(H_2O)_2(NCS)_4]^{2-}$	110	*157*
$[Ni(tren)(H_2O)_2]^{2+d}$	82	*151*	$[Ni(H_2O)(EDTA)]^{2-}$	70	*158*
	900		$[Ni(H_2O)(HEDTA)]^{-e}$	20	*158*

[a] Rate constant for the exchange of a particular coordinated water molecule.
[b] *RRSS* form of macrocycle.
[c] Five-coordinate *RSRS* form of macrocycle.
[d] The two inequivalent H_2O exchange at different rates.
[e] Monoprotonated $EDTA^{4-}$.

on stereochemistry, lability, and mechanism. This is exemplified by five-coordinate $[Mn(Me_6tren)DMF]^{2+}$ and its Co^{2+} and Cu^{2+} analogues, for which DMF exchange is characterized by k_{ex} (198.2 K) = 2.7×10^6, 51.4, and 555 s^{-1}, and $\Delta V^{\ddagger} = -6$, -2.7, and $+6.5$ cm^3 mol^{-1}, respectively, with I_a mechanisms operating for the first two complexes and an I_d mechanism operating for the last (*161*). It has been similarly shown that Me_6tren and other nonleaving ligands can substantially modify the solvent exchange process on a variety of metal ions (*109, 162–164*). The effects of nonleaving ligands on the labilities of metal ions are also considered in Sections III,E and IV,B.

E. Solvent Exchange and Ligand Substitution on Hexaaquaruthenium(II) and Related Complexes

Studies of low-spin t_{2g}^6 $[Ru(H_2O)_6]^{2+}$ and $[Ru(MeCN)_6]^{2+}$ provide the most comprehensive solvent exchange and ligand substitution data for a divalent second-row transition metal ion (*165, 166*). A comparison of the solvent exchange data for the first two species (Table VI) (*165, 167, 168*) with that for the analogous high-spin $t_{2g}^4e_g^2$ iron(II) species (Table III) show $[Ru(H_2O)_6]^{2+}$ and $[Ru(MeCN)_6]^{2+}$ to be many orders of magnitude less labile, largely as a consequence of their much larger $\Delta H^{\ddagger}$ values. These effects arise from their larger ligand fields and low-spin states generating larger LFAE values and also a smaller r_M = 73 pm (*169*) which compares with r_M = 78 pm for high-spin Fe^{2+} (*2*). The lability of $[Ru(MeCN)_6]^{2+}$ is eight orders of magnitude less than that of $[Ru(H_2O)_6]^{2+}$. This is largely a consequence of the larger $\Delta H^{\ddagger}$ of the

TABLE VI

Parameters for Solvent Exchange on Ruthenium(II)[a] Complexes

Complex	k_{ex}(298 2K)[b]/s^{-1}	$\Delta H^{\ddagger}$/ kJ mol^{-1}	$\Delta S^{\ddagger}$/ J K^{-1} mol^{-1}	$\Delta V^{\ddagger}$/ cm^3 mol^{-1}
$[Ru(H_2O)_6]^{2+}$	1.8×10^{-2}	87.8	+16.1	−0.4
$[Ru(\eta^6\text{-}C_6H_6)(H_2O)_3]^{2+}$[c]	11.5	75.9	+29.9	+1.5
$[Ru(MeCN)_6]^{2+}$	8.9×10^{-11}	140.3	+33.3	+0.4
$[Ru(\eta^6\text{-}C_6H_6)(MeCN)_3]^{2+}$[c]	4.07×10^{-5}	102.5	+15.0	+2.4
$[Ru(\eta^5\text{-}C_5H_5)(MeCN)_3]^{+}$[c]	5.6	86.5	+59.6	+11.1

Adapted from Refs. (*165–168*).

[a] Electronic configuration = t_{2g}^6. Six-coordinate ionic radius = 73 pm (*169*).

[b] Rate constant for the exchange of a particular coordinated solvent molecule.

[c] All three H_2O and MeCN are equivalent.

first species, which probably arises from the very strong back-bonding from the electron-rich t_{2g}^6 Ru^{2+} into the acetonitrile π^* orbital (*170, 171*). Such back-bonding does not exist in $[Ru(H_2O_6]^{2+}$. In contrast, $[Fe(H_2O)_6]^{2+}$ is less than an order of magnitude more labile than $[FeMeCN)_6]^{2+}$, and the change in the lability difference between the two systems reflects the relatively minor importance of π back-bonding in $[Fe(MeCN)_6]^{2+}$.

Both H_2O and MeCN are greatly labilized by nonleaving π-bonding ligands, as is seen from Table VI. The increase in lability by 6.3×10^{10}-fold along the sequence $[Ru(MeCN)_6]^{2+} < [Ru(\eta^6\text{-}C_6H_6)(MeCN)_3]^{2+} < [Ru(\eta^5\text{-}C_5H_5)(MeCN)_3]^{+}$ is a consequence of a corresponding decrease in $\Delta H^{\ddagger}$ and the last complex having the largest $\Delta S^{\ddagger}$. It is also accompanied by an increase in the Ru–N distances in the sequence 203, 206, and 209 pm (*167*), and an increasingly strong **d**-activation mode as indicated by $\Delta V^{\ddagger}$ increasing in the sequence +0.4, +2.4, and +11.1 $cm^3\ mol^{-1}$. Thus, the kinetic *trans* effect correlates with the structural *trans* influence. For $[Ru(H_2O)_6]^{2+}$ and $[Ru(\eta^6\text{-}C_6H_6)(H_2O)_3]^{2+}$, the 640-fold greater lability of the latter complex arises from its smaller $\Delta H^{\ddagger}$ and more positive $\Delta S^{\ddagger}$. This is accompanied by a more positive $\Delta V^{\ddagger}$, consistent with a strengthened **d**-activation mode. The labilization of H_2O in $[Ru(\eta^6\text{-}C_6H_6)(H_2O)_3]^{2+}$ is also attributed to the *trans* labilizing effect of the π-acid $\eta^6\text{-}C_6H_6$, but there is no corresponding structural effect reflected in the Ru–O distances, which are 212 pm in both complexes. Thus, the overall range of lability is 12 orders of magnitude within a series of t_{2g}^6 ruthenium(II) complexes in which H_2O, MeCN, C_6H_6, and $C_5H_5^-$ are coordinated.

The deduction of the reaction mechanism from solvent exchange and ligand substitution on low-spin t_{2g}^6 $[Ru(H_2O)_6]^{2+}$ provides a cautionary tale. For the mono substitution of ligands of different charge and donor atom on $[Ru(H_2O)_6]^{2+}$, k_i (Table VII) (*165, 172–175*) shows only a small variation consistent with the operation of an $\mathbf{I}_d$ mechanism (*174*), whereas water exchange was initially assigned an **I** mechanism on the basis of $\Delta V^{\ddagger} = -0.4\ cm^3\ mol^{-1}$ (*165*). The donor atoms in the substituting ligands include Cl, Br, I, N, O, and S; maleic acid, fumaric acid, and 2,5-dihydrofuran are η^2-coordinated to Ru^{2+} through their π-bonds (*175*); and the ligand charge varies through +1, 0, and −1. Thus, the approximately sixfold variation in k_i observed for this wide range of ligand type is smaller than anticipated for substitution on the borderline soft acid Ru^{2+} center and is strong evidence that water dissociation from $[Ru(H_2O)_6]^{2+}$ makes the major contribution to the transition state energetics and the operation of an $\mathbf{I}_d$ mechanism. For water exchange, $\Delta V^{\ddagger}$ is expected to be significantly positive for an $\mathbf{I}_d$

TABLE VII

PARAMETERS FOR THE MONOCOMPLEX FORMATION REACTIONS OF $[Ru(H_2O)_6]^{2+}$ WITH DIFFERENT LIGANDS, L, IN AQUEOUS SOLUTION

L	k_f (298.2 K)/ kg mol^{-1} s^{-1}	$\Delta H_f^{\ddagger}$/ kJ mol^{-1}	$\Delta S_f^{\ddagger}$/ J K^{-1} mol^{-1}	K_o[a]/ kg mol^{-1}	k_i[b] (298.2 K)/s^{-1}	Ref.
Cl^-	0.0085	84.4	−2	1	0.009	*172*
Br^-	0.0102	82.8	−5	1	0.010	*172*
I^-	0.0098	81.5	−10	1	0.010	*172*
$O_2CCO_2H^-$	0.026[c]	101.1	+65	2	0.013	*173*
H_2O		87.8	+16.1		0.018[d]	*165*
MeCN[e]	0.00207	81.1	−24	0.16	0.013	*174*
Me_2SO[e]	0.00131	87.3	−7	0.16	0.008	*174*
1,4-Thioxane[e]	0.0022	82.4	−2	0.16	0.014	*174*
4H-thiophene	0.0024			0.16	0.015	*174*
Maleic acid[e]	0.00218[c]	84	−15	0.16	0.014	*175*
Fumaric acid[e]	0.00172[c]	128	+133	0.16	0.011	*175*
2,5-Dihydrofuran	0.00106[c]	126	+120	0.16	0.007	*175*
NMP^+[f]	0.00073	77.7	−44	0.02	0.040	*174*

[a] K_o calculated using Eq. (3).
[b] Calculated from $k_f = k_i K_o$.
[c] dm^3 mol^{-1} s^{-1}.
[d] Rate constant for the exchange of a particular coordinated water molecule.
[e] In D_2O.
[f] *N*-methylpyrazinium cation.

mechanism, and it therefore appears that the model used to interpret $\Delta V^{\ddagger}$ for the main group metal ions and the high-spin divalent first-row transition metal ions may not apply for low-spin t_{2g}^6 $[Ru(H_2O)_6]^{2+}$. It is possible that the $[Ru(H_2O)_6]^{2+}$ transition state contracts to a substantially greater extent than is the case for the larger high-spin $t_{2g}^4 e_g^2$ $[Fe(H_2O)_6]^{2+}$, for which $\Delta V^{\ddagger} = +3.8$ cm^3 mol^{-1}. Swaddle has reported that his Eq. (12) underestimates ΔV_{abs}^0 for low-spin t_{2g}^6 $[Rh(H_2O)_6]^{3+}$ (*4, 42*), and it may be that a related ligand field effect is reflected in the small $\Delta V^{\ddagger} = -0.4$ cm^3 mol^{-1} observed for water exchange on low-spin t_{2g}^6 $[Ru(H_2O)_6]^{2+}$.

In a study of the aquation reactions of low-spin t_{2g}^6 $[Co(NH_3)_5L]^{n+}$, it was estimated that the difference in molar volumes $\{V_c([Co(NH_3)_6]^{3+}) - V_c([Co(NH_3)_5]^{3+})\} = 17$–$20$ cm^3 mol^{-1} (*176*). Assuming similar differences in V_c, $\Delta V^{\ddagger}$ for water exchange on $[Ru(H_2O)_6]^{2+} - V_c([Ru(H_2O)_5]^{2+})\} = 17$–$20$ cm^3 mol^{-1} and $V_c(H_2O) = 18$ cm^3 mol^{-1}, $\Delta V^{\ddagger} \approx 0$ cm^3 mol^{-1} for a **D** mechanism. For an $\mathbf{I}_d$ mechanism, the volume difference between $[Ru(H_2O)_6]^{2+}$ and the transition

state is likely to be less as the degree of bond breaking is less, and the $V_c(H_2O)$ contribution will be correspondingly decreased, such that $\Delta V^{\ddagger} \approx 0$ cm^3 mol^{-1} is also possible (*174*). Thus, the observed $\Delta V^{\ddagger} = -0.4$ cm^3 mol^{-1} may be attributable to a negative contribution from the contraction of the $[Ru(H_2O_6]^{2+}$ transition state and a positive one from the partial loss of a water molecule.

$$\Delta V^{\ddagger} = V_c([Ru(H_2O)_6]^{2+}) + V_c(H_2O) - V_c[Ru(H_2O)_5]^{2+}) \quad (16)$$

The $\mathbf{I_d}$ mechanism proposed for ligand substitution on $[Ru(H_2O)_6]^{2+}$, which is in accord with the predictions of **a**-activation being disfavored for ligand substitution on metal ions with high electronic t_{2g} orbital occupancies (Section III,B), is also thought to operate for $[Ru(NH_3)_5H_2O]^{2+}$, which is an order of magnitude more reactive (*166*). This probably explains why $[Ru(NH_3)_5N_2]^{2+}$ (*177*) was observed long before $[Ru(H_2O)_5N_2]^{2+}$ (*178*); the latter species forms much more slowly, unless a high N_2 pressure is used to increase aqueous solubility.

F. Solvent Exchange on Octahedral Trivalent Transition Metal Ions

Solvent exchange on the $[M(solvent)_6]^{3+}$ ions shows a similar variation in lability and mechanism with *d*-electronic configuration to that of their divalent analogues. It is seen from Table VIII (*49–53, 87, 165, 179–185*) that $[Cr(solvent)_6]^{3+}$ is the least labile of the first transition species as a consequence of its large LFAE, which is reflected in its large $\Delta H^{\ddagger}$ values. In contrast, the smaller LFAE of t_{2g}^2 $[V(H_2O)_6]^{3+}$ renders it more labile than t_{2g}^3 $[V(H_2O)_6]^{2+}$ (see Table III) despite the smaller formal charge of the latter species. [In d_3-nitromethane diluent, DMSO exchange on $[V(DMSO)_6]^{3+}$ is linearly dependent on the concentration of free DMSO, and a second-order rate constant $= 37.4 \times 10^{-3}$ kg mol^{-1} s^{-1} at 240.3 K is consistent with the operation of an **A** or $\mathbf{I_a}$ mechanism (*180*). A change from **a**-activation to **d**-activation occurs for $[M(H_2O)_6]^{3+}$ as the series is traversed from left to right. The $\Delta V^{\ddagger}$ for $[Ti(H_2O)_6]^{3+}$ approaches the limiting value of -13.5 cm^3 mol^{-1} for an **A** mechanism (see Section I,D), and this mechanism may well operate for water exchange in this case. However, $\Delta V^{\ddagger}$ becomes less negative as both the t_{2g} electronic occupancy and the consequent electronic repulsion towards an entering ligand increase, until for $[Ga(H_2O)_6]^{3+}$ $\Delta V^{\ddagger} = +5.0$ cm^3 mol^{-1}, which indicates the operation of an $\mathbf{I_d}$ mechanism. Similar trends are discerned in the less com-

TABLE VIII

PARAMETERS FOR SOLVENT EXCHANGE ON TRIVALENT OCTAHEDRAL TRANSITION METAL SPECIES AND RELATED SPECIES

Species	r_M[a]/pm	*d*-electronic configuration	k_{ex}(298 K)[b]/s^{-1}	$\Delta H^{\ddagger}$/ kJ mol^{-1}	$\Delta S^{\ddagger}$/ J K^{-1} mol^{-1}	$\Delta V^{\ddagger}$/ cm^3 mol^{-1}	pK_a	Mechanism	Ref.
$[Sc(TMP)_6]^{3+}$	75	t_{2g}^0	1.21×10^3	37.4	−60.5	−20.1		I_a	*87*
$[Ti(H_2O)_6]^{3+}$	67	t_{2g}^1	1.8×10^5	43.4	+1.2	−12.1		A, I_a	*49*
$[Ti(DMF)_6]^{3+}$			6.6×10^4	23.6	−73.6	−5.7		I_a	*179*
$[V(H_2O)_6]^{3+}$	64	t_{2g}^2	5.0×10^2	49.4	−27.8	−8.9		I_a	*52*
$[V(DMSO)_6]^{3+}$			1.31×10^1	38.5	−94.5	−10.1		I_a	*180*
$[Cr(H_2O)_6]^{3+}$	61	t_{2g}^3	2.4×10^{-6}	108.6	+11.6	−9.6	2.9	I_a	*51*
$[Cr(H_2O)_5OH]^{2+}$			1.8×10^{-4}	111.0	+55.6	+2.7		I	*51*
$[Cr(DMSO)_6]^{3+}$			3.1×10^{-8}	96.7	−64.5	−11.3		I_a	*181*
$[Cr(DMF)_6]^{3+}$			3.3×10^{-7}	97.1	−43.5	−6.3		I_a	*182*
$[Fe(H_2O)_6]^{3+}$	64	$t_{2g}^3 e_g^2$	1.6×10^2	64.0	+12.1	−5.4	4.1	I_a	*50, 95*
$[Fe(H_2O)_5OH]^{2+}$			1.2×10^5	42.4	+5.3	+7.0		I_d	*50,95*
$[Fe(DMSO)_6]^{3+}$			9.3	62.5	−16.7	−3.1		I_a	*183*
$[Fe(DMF)_6]^{3+}$			6.1×10^1	42.3	−69.0	−0.9		I	*183*
$[Ga(H_2O)_6]^{3+}$	62	$t_{2g}^6 e_g^4$	4.0×10^2	67.1	+30.1	+5.0	3.9	I_d	*53*
$[Ga(H_2O)_5OH]^{2+}$			1.1×10^5	58.9	—	+6.2		I_d	*53*
$[Ga(DMSO)_6]^{3+}$			1.87	72.5	+3.5	+13.1		D	*83*
$[Ga(DMF)_6]^{3+}$			1.72	85.1	+45.1	+7.9		D	*83*
$[Ga(TMP)_6]^{3+}$			6.4	76.5	+27	+20.7		D	*6*
$[Ru(H_2O)_6]^{3+}$	68	t_{2g}^5	3.5×10^{-6}	89.8	−48.3	−8.3	2.7	I_a	*165*
$[Ru(H_2O)_5OH]^{2+}$			5.9×10^{-4}	95.8	+14.9	+0.9		I	*165*
$[Rh(H_2O)_6]^{3+}$	69[c]	t_{2g}^6	2.2×10^{-9}	131	+29	−4.2	3.5	I_a	*184*
$[Rh(H_2O)_5OH]^{2+}$			4.2×10^{-5}	103	—	+1.5		I	*184*

[a] Ref. (*2*).

[b] Rate constant for the exchange of a particular coordinated solvent molecule.

[c] Ref. (*185*).

plete data for the other solvents where the lability of $[M(solvent)_6]^{3+}$ increases with change in solvent in the sequence TMP > H_2O > DMF > DMSO.

The second-row transition low-spin $t_{2g}^5[Ru(H_2O)_6]^{3+}$ and $t_{2g}^6[Rh(H_2O)_6]^{3+}$ also exhibit the considerable influence of LFAE magnitudes on lability. The lower LFAE of $[Ru(H_2O)_6]^{3+}$ contributes to it being three orders of magnitude more labile than $[Rh(H_2O)_6]^{3+}$, for which a high $\Delta H^{\ddagger}$ demonstrates the retarding influence of the large LFAE arising from a t_{2g}^6 configuration. In both cases, the negative $\Delta V^{\ddagger}$ values suggest the operation of **a**-activated exchange mechanisms. Although no directly determined water exchange data are available, it appears that third-row t_{2g}^6 $[Ir(H_2O)_6]^{3+}$ may be even less labile than $[Rh(H_2O)_6]^{3+}$ (*186*). The lability of t_{2g}^6 $[Ru(H_2O)_6]^{2+}$ is four orders of magnitude greater than that of t_{2g}^5 $[Ru(H_2O)_6]^{3+}$ in water, and it appears that the lower charge of the former species, and differences in mechanisms, are largely accountable for this difference. It was the knowledge of this difference in lability which lead to the unequivocal identification of an outer-sphere mechanism operating in the electron exchange between $[Ru(H_2O)_6]^{2+}$ and $[Ru(H_2O)_6]^{3+}$ (*187*, *188*).

An interesting aspect of the data in Table VIII is the influence of the deprotonation of a coordinated water to produce the conjugate base species, $[M(H_2O)_5OH]^{2+}$, on the lability and mechanism of water exchange. In all five cases, the lability of coordinated water is greatly increased in the conjugate base, which is characterized by a more positive $\Delta V^{\ddagger}$, consistent with donation of electron density from the hydroxo ligand to the metal center, weakening its bonds to water and inducing a greater tendency towards a **d**-activation mode. Thus, the $\mathbf{I}_a$ exchange mechanism for $[Fe(H_2O)_6]^{3+}$ changes to $\mathbf{I}_d$ for $[Fe(H_2O)_5OH]^{2+}$. Similar trends are observed in the analogous chromium(III), ruthenium(III), and rhodium(III) systems, although the less negative $\Delta V^{\ddagger}$ values observed for their conjugate bases suggest that **d**-activation is less important, and an **I** mechanism is assigned.

G. Ligand Substitution on Octahedral Trivalent Transition Metal Ions

The interpretation of ligand substitution data for $[M(H_2O)_6]^{3+}$ transition metal ions involves all of the considerations discussed in Sections III,C and D. In addition, it has to accommodate the added complication of the occurrence of the conjugate base species, $[M(H_2O)_5OH]^{2+}$, at quite low pH values, which can present substantial experimental and intellectual challenges in determining the relative contributions made

to the rate process in which both $[M(H_2O)_6]^{3+}$ and $[M(H_2O)_5OH]^{2+}$ undergo substitution, particularly if the substituting ligand exists in conjugate acid and base forms also. Nevertheless, some illuminating studies have been made, as exemplified by that of ligand substitution on $[Ti(H_2O)_6]^{3+}$, for which the rate constants, k_f, are presented in Table IX (*189–192*). Generally, k_f increases with increasing ligand basicity, as anticipated for an **a**-activated mechanism, and covers greater than three orders of magnitude (*188*). This in agreement with the deduction that water exchange occurs through an **A** or $\mathbf{I}_a$ mechanism. Similar arguments has been presented in support of an **a**-activated mechanism operating for ligand substitution on $[V(H_2O)_6]^{3+}$ (*52, 193*).

The rate constants for ligand substitution, k_f, on $[M(H_2O)_6]^{3+}$ and $[M(H_2O)_5OH]^{2+}$, where M is either Fe or Cr, are presented in Table X (*51, 194–198*). It is seen that the relative labilities of the four species towards ligand substitution qualitatively reflect their relative labilities towards water exchange (Table VIII) in accord with the generalization that lability towards simple ligand substitution processes is largely determined by the nature of the metal center. Thus, the labilization of water exchange observed in $[M(H_2O)_5OH]^{2+}$ species, by comparison with that of $[M(H_2O)_6]^{3+}$, is reflected in their greater labilities towards ligand substitution. Superimposed on this is the effect of differences in mechanism, which is well illustrated by the Cr^{3+} data. A comparison of the k_f values for the monoanions shows 938- and 15-fold variations for $[Fe(H_2O)_6]^{3+}$ and $[Fe(H_2O)_5OH]^{2+}$, consistent with the operation of $\mathbf{I}_a$ and $\mathbf{I}_d$ mechanisms, respectively, as was also deduced from their $\Delta V^{\ddagger}$ values for water exchange (Section III,E). Similarly, k_f for $[Cr(H_2O)_6]^{3+}$ and $[Cr(H_2O)_5OH]^{2+}$ exhibit 2050- and 21-fold variations, consistent

TABLE IX

RATE CONSTANTS FOR THE SUBSTITUTION OF A LIGAND, L, ON $[Ti(H_2O)_6]^{3+}$ IN AQUEOUS SOLUTION

L	$10^{-2}k_f$/dm^3 mol^{-1} s^{-1}	T/K	Ref.
$ClCH_2COOH$	7	288.2	*189*
CH_3COOH	10	288.2	*189*
NCS^-	80	281–289	*190*
$Cl_2CHCO_2^-$	1100	288.2	*189*
$ClCH_2CO_2^-$	2100	288.2	*189*
Methylmalonate(1−)	3200	288.2	*191*
$HC_2O_4^-$	3900	283.2	*192*
Malonate(1−)	4200	288.2	*191*
$CH_3CO_2^-$	18,000	288.2	*189*

with the operation of $\mathbf{I}_a$ and **I** mechanisms, respectively, also in accord with the deductions made from their $\Delta V^{\ddagger}$ values for water exchange.

The factors affecting the magnitude of the variation of k_f, or more generally the degree of selectivity exhibited by a metal center for entering ligands seem destined to remain the subject of debate until a substantially more extensive range of entering ligands and metal centers have been studied (*4, 6–9, 15, 21–26*). In the meantime, the ratio $k_{fNCS^-}/k_{fCl^-} = R$ for ligand substitution by NCS^- and Cl^- provides an estimate of the selectivity exercised by a metal center, and thereby qualitative comparisons of the amount of **a**-activated character present in ligand substitution processes (*198*). The good correlation between the sign of $\Delta V^{\ddagger}$ and R in assigning the dominance of either **d**- or **a**-activation modes for five of the aquaions in Table XI (*199*), as discussed earlier, adds confidence to the assignment of **a**-activated mechanisms to $[Co(H_2O)_6]^{3+}$ and $[Mo(H_2O)_6]^{3+}$ and a **d**-activated mechanism to $[Co(H_2O)_5OH]^{2+}$, for which $\Delta V^{\ddagger}$ for water exchange is not available. This is reinforced by the determination of $\Delta V_f^{\ddagger} = -11.4$ cm^3 mol^{-1} for substitution of $[Mo(H_2O)_6]^{3+}$ by NCS^-, from which $\Delta V_i^{\ddagger} \approx -17$ cm^3 mol^{-1} is calculated for the interchange step in an $\mathbf{I}_a$ mechanism after changes in electrostriction are allowed for (*200*). Similarly, the $\Delta V_f^{\ddagger}$ values observed for the substitution of NCS^- on $[V(H_2O)_6]^{3+}$,

TABLE X

RATE CONSTANTS (298.2 K) FOR LIGAND SUBSTITUTION ON $[M(H_2O)_6]^{3+}$ AND $[M(H_2O)_5OH]^{2+}$

L	k_f/dm^3 mol^{-1} s^{-1}	k_f/dm^3 mol^{-1} s^{-1}	Ref.
	$[Fe(H_2O)_6]^{3+}$	$[Fe(H_2O)_5OH]^{2+}$	
SO_4^{2-}	2.3×10^3	1.1×10^5	*194*
*N*CS$^-$	9.0×10^1	5.0×10^3	*195*
Cl^-	4.8	5.5×10^3	*196*
Br^-	1.6	2.8×10^3	*197*
$Cl_3CCO_2^-$	6.3×10^1	7.8×10^3	*198*
$Cl_2CHCO_2^-$	1.18×10^2	1.9×10^4	*198*
$ClCH_2CO_2^-$	1.5×10^3	4.1×10^4	*198*
	$[Cr(H_2O)_6]^{3+}$	$[Cr(H_2O)_5OH]^{2+}$	
SO_4^{2-}	1.1×10^{-5}	6.1×10^{-4}	*51*
*N*CS$^-$	1.7×10^{-6}	9.7×10^{-5}	*51*
NO_3^-	7.1×10^{-7}	1.5×10^{-4}	*51*
Cl^-	3.0×10^{-8}	4.2×10^{-5}	*51*
Br^-	8.7×10^{-9}	2.7×10^{-5}	*51*
*S*CN$^-$	9.8×10^{-9}	2.1×10^{-5}	*51*
I^-	8.3×10^{-10}	4.6×10^{-6}	*51*

TABLE XI

R VALUES FOR THE SUBSTITUTION OF WATER IN SEVERAL AQUAIONS

Aquaion	*R*	Aquaion	*R*
$[V(H_2O)_6]^{3+}$	≥36	$[Cr(H_2O)_5OH]^{2+}$	2.3[a]
$[Cr(H_2O)_6]^{3+}$	57[a]	$[Fe(H_2O)_5OH]^{2+}$	0.9[a]
$[Fe(H_2O)_6]^{3+}$	19[a]	$[Co(H_2O)_5OH]^{2+}$	2.0
$[Co(H_2O)_6]^{3+}$	≥43	$[Mo(H_2O)_6]^{3+}$	62

Adapted from Ref. (*199*).
[a] Calculated from data in Table X.

$[Fe(H_2O)_6]^{3+}$ (*201, 202*), and their DMF analogues are consistent with the operation of $\mathbf{I}_a$ mechanisms (*180, 203*). In the accessible pH range, $[Ti(H_2O)_6]^{3+}$, $[V(H_2O)_6]^{3+}$, and $[Mo(H_2O)_6]^{3+}$ do not exhibit ligand substitution rate terms dependent on $[H^+]^{-1}$, indicative of substitution occurring on $[M(H_2O)_5OH]^{2+}$, which probably indicates how favorable the $\mathbf{I}_a$ reaction path is for these hexaaqua ions.

A rare opportunity to compare aquaions of the same electronic configuration (t_{2g}^3) in different periods is afforded by $[Cr(H_2O)_6]^{3+}$ and $[Mo(H_2O)_6]^{3+}$. It is the latter which is the more labile towards substitution by several orders of magnitude. [For $[Mo(H_2O)_6]^{3+}$, k_{fCl^-} and (k_{fNCS^-} are 0.0046 and 0.27 $dm^3\ mol^{-1}\ s^{-1}$ at 298.2 K, respectively (*200*). This largely arises from the lower $\Delta H^{\ddagger}$ values characterizing the $[Mo(H_2O)_6]^{3+}$ substitutions, which are a little unexpected in view of the larger LFAE anticipated for a second-row transition metal ion. It has been suggested that the greater lability of $[Mo(H_2O)_6]^{3+}$ is a consequence of a greater degree of **a**-activation in its substitution mechanism (*199*). The lability of $[Co(H_2O)_6]^{3+}$ towards ligand substitution (k_{fCl^-} and k_{fNCS^-} are ≤2 and 86.5 $dm^3\ mol^{-1}\ s^{-1}$ at 298.2 K, respectively) (*204–206*) is high compared with that of $[Cr(H_2O)_6]^{3+}$, and its large *R* value, suggesting an **a**-activated mechanism, is unexpected for its t_{2g}^6 electronic configuration (*207*), which should produce a large LFAE and a resistance towards **a**-activation. However, it appears that the $t_{2g}^4 e_g^2$ state may be accessible at excitation energies comparable to those encountered during ligand substitution (*4*). If ligand substitution occurs through this high-spin state, the lack of a significant LFAE and the decreased t_{2g} electronic occupancy should enhance both lability and the probability of an **a**-activated ligand sutstitution occurring. For $[Co(H_2O)_5OH]^{2+}$, the decrease in *R* to 2 mirrors the chromium(III) and iron(III) systems and, as in their cases, suggests a change towards a **d**-activated mechanism.

A classic example of the operation of an $\mathbf{I}_a$ mechanism arises in the substitution of L^{x-} on $[Cr(DMF)_6]^{3+}$, for which the $10^5 k_i$ (344.5 K) = 0.65, 7.53, 17.3, and 424 s^{-1} for $L^{x-} = Br^-, Cl^-, NCS^-$, and N_3^-, respectively, which compare with $10^5 k_{ex}$ (344.5 K) = 7.37 s^{-1} (*208*). The increase of k_i in the same order in which nucleophilicity increases and the 59-fold greater magnitude of k_i for N_3^- by comparison with that of k_{ex}, together with the direct determination of K_o values, are convincing evidence for the operation of an $\mathbf{I}_a$ mechanism. The lesser magnitude of k_{ex} than of k_i is observed in this case because DMF is not as effective a competitor for the Cr^{3+} center as is water.

H. Solvent Exchange and Ligand Substitution on Trivalent Transition Metal Aquapentaammine Complexes

Ligand substitution, or anation, on the trivalent transition metal aquapentammine complexes and its reverse or aquation reaction, as shown in Eq. (17), has been the most studied of all ligand substitutions, but nevertheless remains the subject of robust debate (*4, 9, 21–26*). In principle, the aquapentaammines form ideal prototypes to test mechanistic ideas, as only the coordinated water undergoes substitution under mild conditions, and the pentaammine moiety is largely inert towards substitution. Thus, substitution at a single site may be conveniently studied, as is exemplified by the water exchange data for some aquapentammine complexes [and some of their aquapentakis(methylamine) analogues] in Table XII (*209–213*). The LFAE for either a

TABLE XII

Parameters for Water Exchange on $[M(NH_3)_5H_2O]^{3+}$ and $[M(CH_3NH_3)_5H_2O]^{3+}$

M^{3+}	r_M[a]/ pm	*d*-electronic configuration	k_{H_2O}(298.2 K)/ s^{-1}	$\Delta H^{\ddagger}$/ kJ mol^{-1}	$\Delta S^{\ddagger}$/ J K^{-1} mol^{-1}	$\Delta V^{\ddagger}$/ cm^3 mol^{-1}
			$[M(NH_3)_5H_2O]^{3+}$ (*209–212*)			
Cr^{3+}	61	t_{2g}^3	5.2×10^{-5}	97	0	−5.8
Co^{3+}	54	t_{2g}^6	5.7×10^{-6}	111	+28	+1.2
Ru^{3+}	68	t_{2g}^5	2.30×10^{-4}	91.5	−7.7	−4.0
Rh^{3+}	66	t_{2g}^6	8.4×10^{-6}	103	+3	−4.1
Ir^{3+}	68	t_{2g}^6	6.1×10^{-8}	118	+11	−3.2
			$[M(CH_3NH_3)_5H_2O]^{3+}$ (*213*)			
Cr^{3+}	61	t_{2g}^3	4.1×10^{-6}	98.5	−17.5	−3.8
Co^{3+}	54	t_{2g}^6	7.0×10^{-4}	99.0	+26.7	+5.7
Rh^{3+}	66	t_{2g}^6	1.06×10^{-5}	112.7	+37.8	+1.2

[a] Ref. (*2*).

d- or an **a**-activated water exchange mechanism is smallest for t_{2g}^3 $[Ru(NH_3)_5H_2O]^{3+}$, and this may explain its greater lability compared with that of t_{2g}^3 $[Cr(NH_3)_5H_2O]^{3+}$ and those of the three t_{2g}^6 complexes whose larger LFAE values render them less labile. These LFAE variations are qualitatively reflected in the $\Delta H^{\ddagger}$ values. Generally, the greater water dipole–metal center interaction arising from the 3+ charge of $[M(NH_3)_5H_2O]^{3+}$ is likely to further decrease the rate of water exchange by comparison with those of the divalent metal ions discussed in preceding sections.

$$[M(NH_3)_5H_2O]^{3+} + L^{x-} \underset{k_b}{\overset{k_f}{\rightleftharpoons}} [M(NH_3)_5L]^{(3-x)+} + H_2O \qquad (17)$$

The positive $\Delta V^{\ddagger}$ value observed for $[Co(NH_3)_5H_2O]^{3+}$ implies the operation of an $\mathbf{I}_d$ mechanism, while the negative values for the other three complexes suggest the operation of $\mathbf{I}_a$ mechanisms. An $\mathbf{I}_a$ mechanism is more likely to operate for $[Cr(NH_3)_5H_2O]^{3+}$ on the basis of its larger r_M and t_{2g}^3 configuration than is the case for t_{2g}^6 $[Co(NH_3)_5H_2O]^{3+}$, which has a smaller r_M and for which an $\mathbf{I}_d$ mechanism operates. This difference in sign of $\Delta V^{\ddagger}$, and the implied mechanistic difference, has been observed for the substitution of L = $OSMe_2$, $OCHNH_2$, $OC(NH_2)_2$, $OC(NHMe)_2$, and $OCMeNMe_2$, and several other uncharged oxygen donor ligands by water in $[Cr(NH_3)_5L]^{3+}$ and $[Co(NH_3)_5L]^{3+}$ (*214, 215*). Thus, there seems little doubt that there is a significant mechanistic difference for ligand substitution on the two metal centers. The operation of $\mathbf{I}_a$ mechanisms for $[Ru(NH_3)_5H_2O]^{3+}$, $[Ru(NH_3)_5H_2O]^{3+}$, and $[Ir(NH_3)_5H_2O]^{3+}$, despite their high t_{2g} electronic occupancies, is explicable in terms of a combination of their *d*-orbitals being more diffuse and their greater r_M allowing more interaction with the entering water than is possible for $[Co(NH_3)_5H_2O]^{3+}$.

When steric crowding of the metal center is increased on going from $[M(NH_3)_5H_2O]^{3+}$ to $[M(CH_3NH_2)_5H_2O]^{3+}$, the rate of water exchange (298.2 K) is decreased, increased, and almost unchanged when M = Cr, Co, and Rh, respectively (Table XII) (*213*). These rate changes are consistent with **a**- and **d**-activated mechanisms operating when M = Cr and Co, respectively, but the change is too small for mechanistic interpretation when M = Rh. The $\Delta V^{\ddagger}$ for water exchange becomes more positive as steric crowding increases for all three M, and indicates a change to either a more dissociative or a less associative mode of activation. Such mechanistic changes with variation of the occupancy of the first coordination sphere are not unusual, as observed for both

main group and transition metal ions, for which an increase in crowding caused by increased ligand size favors a change towards the dominance of **d**-activation (Sections II,B and C, and III,B).

The aquation of $[M(NH_3)_5L]^{(3-x)+}$, characterized by k_b in Eq. (17), has featured strongly in mechanistic debate (*4, 9, 21–26*). A linear free energy relationship (LFER) with a slope of unity exists between log k_b and $\log(k_b/k_f)$ for a $[Co(NH_3)_5L]^{2+}$ series, where L^{x-} is a uninegative ligand (*216*). Thus, although the nature of L^{x-} determines the variation of k_b, it is implied that it has little effect on k_f, and therefore little participation in the transition state for substitution of H_2O in $[Co(NH_3)_5H_2O]^{3+}$ during the formation of $[Co(NH_3)_5L]^{2+}$. Consequently, the transition state for reaction (17) in either direction is thought to resemble five-coordinate $[Co(NH_3)_5]^{3+}$, and a **d**-activated mechanism operates. However, Eq. (17) does not include the diffusion-controlled formation of the outer-sphere complex, as shown in Eq. (18). Hence, as $k_f = k_i K_o$, the observed LFER implies the unexceptional requirement that K_o should be similar for simple monoanions (*217*). A parallel LFER exists for dianions. Such LFERs may be expressed in terms of free energy, as in Eq. (19), which also implies the existence of a volume relationship as in Eq. (20), where α is the slope in both cases (*22*). Substitution on $[Co(NH_3)_5H_2O]^{3+}$ by several anions yield $\alpha = 1$ for Eq. (20) (*218*). On these grounds, the assignment of an $\mathbf{I}_d$ mechanism ligand substitution on $[Co(NH_3)_5H_2O]^{3+}$ seems well justified, and consistent with $R = 0.5$ (*4*). [A LFER between log k_b and $\log(k_b/k_f)$ with a slope of 0.56 exists for the aquation of $[Cr(H_2O)_5L]^{2+}$ (*219*). This implies that L^{x-} does play a significant role in the transition state for substitution on $[Cr(H_2O)_6]^{3+}$ to form $[Cr(H_2O)_5L]^{2+}$ through an $\mathbf{I}_a$ mechanism, consistent with a similar deduction made in Section III,G.]

$$[M(NH_3)_5H_2O]^{3+} + L^{x-} \overset{K_o}{\rightleftharpoons} [M(NH_3)_5H_2O]^{3+} \ldots L^{x-} \overset{k_i}{\underset{k_{-i}}{\rightleftharpoons}} [M(NH_3)_5L]^{(3-x)} + H_2O \qquad (18)$$

$$\delta\Delta G^{\ddagger} = \alpha\delta\Delta G^{0} \qquad (19)$$

$$\delta\Delta V^{\ddagger} = \alpha\delta\Delta V^{0} \qquad (20)$$

The mechanism of substitution of anionic ligands on $[Cr(NH_3)_5H_2O]^{3+}$ has received both $\mathbf{I}_d$ and $\mathbf{I}_a$ assignments from various authors (*23*). This dichotomy of viewpoint comes about substantially

because of the negative $\Delta V^{\ddagger}$ for water exchange on $[Cr(NH_3)_5H_2O]^{3+}$, and $\alpha = 0.69$ from a LFER (*218*) for the aquation of $[Cr(NH_3)_5L]^{2+}$ are consistent with I_a mechanisms, but the small selectivity of $[Cr(NH_3)_5H_2O]^{3+}$ towards L^{x-} in substitution reactions, reflected in $R = 6$ (*4*), has been taken as evidence for the operation of an I_d mechanism (*220, 221*). The question is how to resolve these apparently conflicting mechanistic assignments.

The replacement of five waters in $[Cr(H_2O)_6]^{3+}$ by NH_3 in $[Cr(NH_3)_5H_2O]^{3+}$ causes a 20-fold increase in the lability of the single remaining water (which is quite small by comparison with such replacement in $[Ni(H_2O)_6]^{2+}$, as seen from Table V) and appears to decrease the importance of the **a**-activation mode in the approach to the transition state (see Section III,G). Assuming that the free radii (*222*) of H_2O (138 pm) and NH_3 (169 pm) reflect their relative electrostricted coordinated radii, it is anticipated that the first coordination sphere of $[Cr(H_2O)_6]^{3+}$ will be less crowded than that of $[Cr(NH_3)_5H_2O]^{3+}$ and that the extent of **a**-activation character in the substitution of water in the latter species will decrease.

Mechanistic interpretation now hinges on the degree to which **a**-activation needs to be dominant in an interchange mechanism before significant selectivity for L^{x-} is apparent. It seems likely that a combination of the decreased importance of **a**-activation and the hardness of Cr^{3+} decreases selectivity amongst the L^{x-} studied to a low level, and that in consequence L^{x-} competes poorly with small hard base H_2O which is present as the solvent in large excess concentration over competing L^{x-}. [It is possible that the hard bases F^-, NO_3^-, and SO_4^{2-} might compete effectively, but its Brønsted basicity complicates F^- ligand substitution studies (*223*), and substitution by the other two ligands causes loss of NH_3 (*224, 225*).] If these suppositions are correct, the absence of selectivity is not diagnostic of mechanism for $[Cr(NH_3)_5H_2O]^{3+}$, and the negative $\Delta V^{\ddagger}$ for water exchange remains as the more reliable indicator of mechanism. The few ligand substitution data for $[Rh(NH_3)_5H_2O]^{3+}$ and $[Ir(NH_3)_5H_2O]^{3+}$ yield LFERs with $\alpha = 0.72$ and 0.85, respectively (*226*), and in ligand substitution on both species, L^{x-} appears to compete more effectively with water. This has been interpreted in terms of the operation of an **a**-activated mechanism (*227–230*), in agreement with the deductions made from the negative $\Delta V^{\ddagger}$ values for water exchange. A linear relationship exists between α from the LFERs at 298.2 K for the aquation of $[Cr(H_2O)_5L]^{2+}$, $[Cr(NH_3)_5L]^{2+}$, $[Rh(NH_3)_5L]^{2+}$, $[Ir(NH_3)_5L]^{2+}$, and $[Co(NH_3)_5L]^{2+}$ and $\Delta V^{\ddagger}$ for water exchange on the corresponding $[M(NH_3)_5H_2O)^{3+}$. This suggests that the importance of **a**-activation diminishes as the series

is traversed from left to right such that **d**-activation dominates the $[Co(NH_3)_5L]^{2+}$ and $[Co(NH_3)_5H_2O]^{3+}$ systems (*226*).

I. Solvent Exchange and Ligand Substitution on First-Row Transition Oxometal Ions

The uncommon monomeric first-row transition oxometal ions are of substantial interest for solvent exchange and ligand substitution studies, as they provide an opportunity to examine the effect of the oxo ligand charge on the lability of the metal center towards ligand substitution, and also the effect of the variation of lability of the axial and equatorial ligand substitution sites. At present, oxotitanium(IV) (*231–233*) and oxovanadium(IV) (*234–247*) are the only species of this type for which solvent exchange and ligand substitution studies have been reported. Oxovanadium(IV) has been characterized by electronic absorption spectroscopy (*248*), electron double resonance (ENDOR) spectroscopy (*249*), and x-ray studies (*250, 251*) and is the most readily available of the monomeric first-row transition oxometal ions. The V(IV) center lies 10–30 pm above the plane delineated by the four equatorial coordination sites, and the ligand in the axial site is farther from the metal center than are the equatorial ligands. By comparison, oxotitanium(IV) complexes with a monomeric TiO^{2+} core are quite rare and are exemplified by [TiO(porphyrin)] (*252*), [TiO(phthalocyanine)] (*253, 254*), $[TiOCl_4]^{2-}$ (*255*), and $[TiOF_5]^{3-}$ (*256*).

Solvent exchange has been studied on several $[VO(solvent)_5]^{2+}$ species, as indicated in Table XIII (*231, 234–241*). Exchange of equatorial water on $[VO(H_2O)_5]^{2+}$ occurs slowly by comparison with axial water, as anticipated on the basis of the greater axial water–vanadium center distance. The oxo ligand exchange is characterized by $k_{ex} = 2.4 \times 10^{-5}\ s^{-1}$ at 298.2 K (*246, 247*), which is much slower than the exchange of the oxo ligand of $[TiO(H_2O)_5]^{2+}$ ($k_{ex} = 1.6 \times 10^4\ s^{-1}$ at 298.2 K). The difference is attributed to the oxo ligand of the latter species being relatively readily protonated and thereby labilized (*231, 232*). In $[VO(DMF)_5]^{2+}$, the axial DMF is seen to be much more labile than an equatorial DMF, but in the other solvents only exchange at the equatorial sites is observed. It is appropriate to note that the d^1 $[VO(solvent)_5]^{2+}$ species are paramagnetic, and as a consequence their solvent exchange rates are derived from observations of the relaxation and chemical shift variations of the bulk solvent NMR following Swift and Connick (*257*). It should also be noted that it is not always possible to observe contributions to these variations arising from each inequivalent exchanging site using this method (*151, 162*).

TABLE XIII

PARAMETERS FOR AXIAL AND EQUATORIAL SOLVENT EXCHANGE ON $[TiO(solvent)_5]^{2+}$ AND $[VO(solvent)_5]^{2+}$

Solvent	k_{ex}(298.2 K)[a]/ s^{-1}	$\Delta H^{\ddagger}$/ kJ mol^{-1}	$\Delta S^{\ddagger}$/ J K^{-1} mol^{-1}	$\Delta V^{\ddagger}$/ cm^3 mol^{-1}	Ref.
		$[TiO(solvent)_5]^{2+}$[b]			
DMSO	161 (eq)	57.5	−9.9	+4.8	*231*
	6100 (ax)	59.8	+28.3	+1.6	*231*
		$[VO(solvent)_5]^{2+}$			
H_2O	500 (eq)	57.3	−2.4	+1.9	*234, 235*
	$\approx 10^9$ (ax)				*234*
MeOH	565 (eq)	39.6	−59.4		*236*
MeCN	2850 (eq)	29.5	−83.7		*237*
DMSO	1760 (eq)	60.1	+18.5	−5.3	*238, 239*
DMF	575 (eq)	30.3	−87.7		*240*
	200 (eq)	54.8	−17.2		*241*
	46,000 (ax)	64	+58.0		*241*
DMA	4700 (eq)	42.3	−33.1		*241*

[a] Rate constant for the exchange of a particular coordinated solvent molecule.
[b] Studied in d_3-nitromethane diluent.

The rate of axial DMSO exchange is much greater than that of equatorial DMSO in diamagnetic d^0 $[TiO(DMSO)_5]^{2+}$ (for which both exchange processes are separately discerned by ^1H NMR spectroscopy). Also, the rates of both processes are independent of the concentration of free DMSO in d_3-nitromethane diluent, consistent with the operation of **d**-activated exchange mechanisms, as are the positive $\Delta V^{\ddagger}$ values (*231*). Although no crystal structures have been reported for $[TiO(solvent)_5]^{2+}$ ions, it is probable that the structure of $[TiO(DMSO)_5]^{2+}$ is similar to that of $[VO(solvent)_5]^{2+}$, and that the greater lability of the axial DMSO is due to the longer and consequently weaker axial bond. Thus, the smaller size of the positive $\Delta V^{\ddagger}$ for the exchange of axial DMSO may reflect the lesser extension required of the axial bond to reach the transition state by comparison with the shorter equatorial bonds. It is clear that in both $[TiO(solvent)_5]^{2+}$ and $[VO(solvent)_5]^{2+}$, the oxo ligand exerts a strong labilizing effect on the axial site.

Rate constants for ligand substitution (k_i) at the equatorial sites in $[VO(H_2O)_5]^{2+}$ and $[TiO(H_2O)_5]^{2+}$ (*242*) and for solvent exchange on $[VO(solvent)_5]^{2+}$ and $[TiO(solvent)_5]^{2+}$ are mostly in the range 10^2–10^3 s^{-1} (Table XIII). However, ligand substitution of the equatorial H_2O in [VO(*N*-(2-pyridylmethyl)iminodiacetato)(H_2O)] (*241*) and [VO(nitrilotriacetato)(H_2O)]$^-$ (*242*), in which the axial site is taken up

by a tertiary amino group of the chelating ligands, proceeds more slowly. It has been suggested that this indicates that k_i for direct substitution at an equatorial site is $\approx 0.1\ s^{-1}$, and that the larger values observed for k_{ex} and k_i characterizing $[VO(H_2O)_5]^{2+}$ arise through a rapid migration between axial and equatorial sites characterized by $k_{migration} \approx 10^3\ s^{-1}$, as shown in approximate terms in Fig. 10. Such a mechanism may also operate for equatorial DMSO exchange on $[TiO(DMSO)_5]^{2+}$, whereby a concerted migration of the axial DMSO to an equatorial site and loss of the equatorial DMSO occurs (*231*). A similar mechanism involving axial equatorial migration appears to operate for ligand substitution at the equatorial sites of $[Mo_2(H_2O)_{10}]^{4+}$ and $[Rh_2(H_2O)_{10}]^{4+}$ (*258, 259*).

J. Solvent Exchange and Ligand Substitution on Divalent Square-Planar Transition Metal Ions

Square-planar stereochemistry is largely confined to the d^8 transition metal ions, rhodium(I), iridium(I), nickel(II), paladium(II), platinum(II), and gold(III). Some of the most investigated ligand substitutions are those on Pd^{2+} and Pt^{2+} centers, which have generated an impressive degree of mehanistic understanding (*32, 33*). The vast majority of such systems so far studied undergo ligand substitution through a-activated mechanisms, probably as a consequence of the coordinatively unsaturated four-coordinate 16 outer-shell electron complex achieving a noble gas configuration in five-coordinate transition states or reactive intermediates. It is well established that the lability

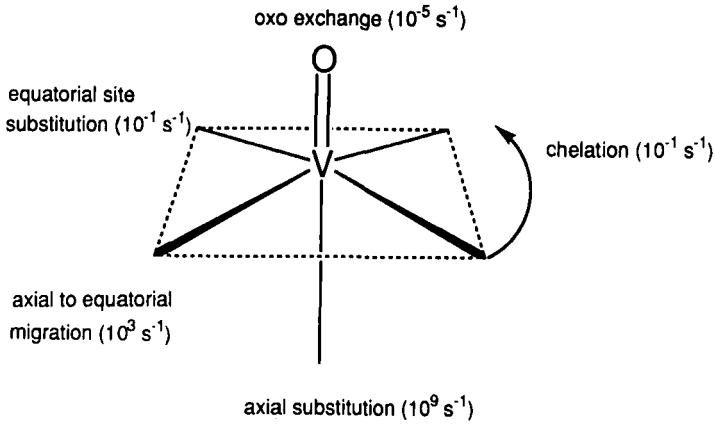

FIG. 10. Approximate magnitudes of first-order rate constants for exchange or substitution of $[VO(H_2O)_5]^{2+}$ at 298.2 K.

of a leaving ligand is strongly affected by the nature of the nonleaving ligand in the *trans* position. This kinetic "*trans* effect" is generally considered to arise from a combination of ground state and transition state influences. The ground state *trans* influence arises from the weakening of the bond to the leaving ligand by a strong σ-donor ligand in the *trans* position, with an order of effectiveness $H^- > PR_3 > SCN^- > I^- > CH_3^- > CO > CN^- > Br^- > Cl^- > NH_3 > OH^-$. The transition state is expected to approximate to a trigonal bipyramid, and the *trans* effect arises through its stabilization by a strong π-acceptor ligand in the equatorial plane with an order of effectiveness C_2H_4, $CO > CN^- > NO_2^- > SCN^- > I^- > Br^- > Cl^- > NH_3 > OH^-$. The combination of these two sequences may be used to rationalize the order of effectiveness of nonleaving ligands in the kinetic *trans* effect, which is C_2H_4, CO, $CN^- > PR_3$, $H^- > CH_3^- > C_6H_5^-$, NO_2^-, $SCN^- > I^- > Br^-$, Cl^- > pyridine, NH_3, OH^-, H_2O (*32–34, 104, 260*).

The order of increasing reactivity of the entering ligand toward Pd^{2+} and Pt^{2+} is similar to that of the *trans* effect, with the soft base ligands being more reactive. In contrast, the order of increasing lability of leaving ligands is almost the reverse of the *trans* effect. This is not surprising when it is recalled that the *trans* effect is substantially a measure of the strength of bonding of the *trans* directing ligand. Ligands *cis* to the leaving ligand have relatively small effects on reaction rates. Usually ligand substitution occurs with stereoretention. This is in accord with an $\mathbf{I_a}$ or **A** mechanism occurring through a trigonal bipyramidal transition state or reactive intermediate in which the *trans* directing ligand and the entering and leaving ligands share the equatorial plane. As five-coordinate complexes of Pt^{2+} and other d^8 metal ions have been found to approximate to both trigonal-bipyramidal (*261–263*) and square-pyramidal geometry (*264, 265*), and the energy differences between the two geometries appear to be small (*266*), it has been suggested that stereoretentive **a**-activated ligand substitution on square-planar complexes proceeds through a series of five-coordinate transition states and reactive intermediates, as shown schematically in Fig. 11. This brief synopsis of some aspects of square planar ligand substitution chemistry provides the framework for the mechanistic discussion which follows, and which is primarily concerned with ligand substitution on solvated Pd^{2+} and Pt^{2+}.

Direct kinetic studies of water exchange on $[Pd(H_2O)_4]^{2+}$ and $[Pt(H_2O)_4]^{2+}$, the parameters for which appear in Table XIV (*267–274*), were first reported well after the chemistry outlined in the preceding paragraph had become established. Solvent and ligand exchange on

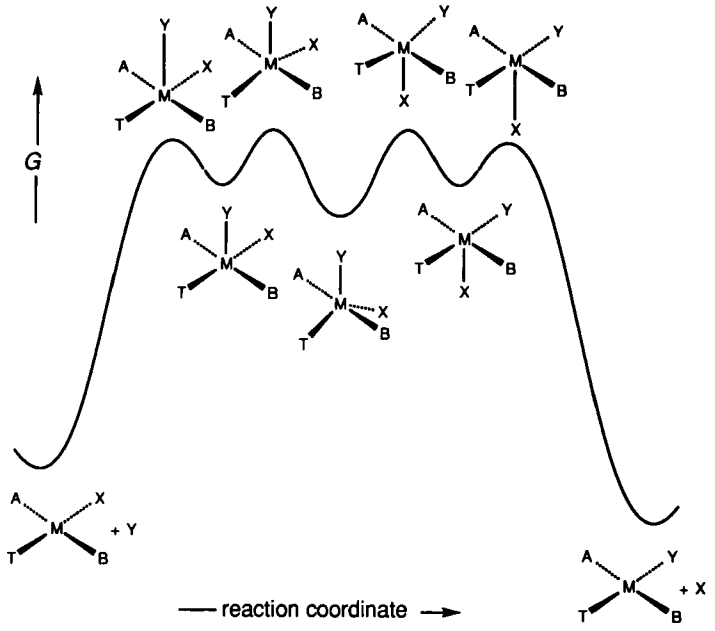

FIG. 11. A proposed reaction coordinate for the substitution of Y on square-planar [MABTX] to produce square-planar [MABTY], where T is the *trans* directing ligand and Y and X are the entering and leaving ligands, respectively (*32, 33*).

the Pd^{2+} and Pt^{2+} complexes in Table XIV exhibit a variation in lability encompassing almost 16 orders of magnitude and are characterized by either negative or near-zero $\Delta V^{\ddagger}$ values. With the exception of $[Pd(H_2O)_4]^{2+}$ and $[Pt(H_2O)_4]^{2+}$, the exchange processes have been studied in inert diluents and are found to have a first-order rate dependence on free solvent or ligand concentration, according to Eq. (21). The effect of ligand size on lability is demonstrated by the less sterically hindered $[Pd(Me_2S)_4]^{2+}$ undergoing ligand exchange 430 times more rapidly than does $[Pd(Et_2S)_4]^{2+}$, even though the soft ligands Me_2S and Et_2S are of similar basicity. It is clear that in these cases, a combination of the steric characteristics of the complex and the entering ligand dominate the relative labilities. Another example of such dominance is provided by $[Pd(DMA)_4]^{2+}$, which is less labile than $[Pd(DMF)_4]^{2+}$, despite DMA (Gutmann donor number = D_N = 27.8) (*275*) being a stronger nucleophile than DMF (D_N = 27.0). It appears that the extra methyl group of DMA creates sufficient steric hindrance to reverse the order of reactivity expected on the basis of relative nucleophilicity. Such steric

TABLE XIV

PARAMETERS FOR SOLVENT AND LIGAND EXCHANGE ON Pd^{2+} AND Pt^{2+} COMPLEXES

Complex	k_{ex}(298.2 K)[a]/ kg mol^{-1} s^{-1}	$\Delta H^{\ddagger}$/ kJ mol^{-1}	$\Delta S^{\ddagger}$/ J K^{-1} mol^{-1}	$\Delta V^{\ddagger}$/ cm^3 mol^{-1}	Ref.
$[Pd(NH_3)_4]^{2+}$[b]	0.016	67.3	−54.1		*267*
$[Pd(Et_2S)_4]^{2+}$[c]	5.0	50.4	−62.8	−11.6	*268*
$[Pd(H_2O)_4]^{2+}$[b]	10.2[d]	49.5	−60	−2.2	*269*
	560[e]	49.5	−26	−2.2	
$[Pd(DMA)_4]^{2+}$[c]	34.8	43.2	−76.2	−2.8	*268*
$[Pd(MeCN)_4]^{2+}$[c]	48.8	45.4	−60.1	−0.1	*268*
$[Pd(CN)_4]^{2-}$[f]	124	17	−147		*270*
$[Pd(DMF)_4]^{2+}$[c]	153	41.9	−62.3	−0.2	*268*
$[Pd(Me_2S)_4]^{2+}$[c]	2140	31.9	−74.3[g]	−9.4	*268*
$[Pd(1,4\text{-dithiane})_2]^{2+}$[c]	9780	22.9	−91.6	−9.8	*271*
$[Pd(MeNC)_4]^{2+}$[h]	1.06×10^6	16.4	−74.5	−3.1	*268*
$[Pt(NH_3)_4]^{2+}$[b]	9.5×10^{-10}[d]	125	+4		*272*
$[Pt(H_2O)_4]^{2+}$[b]	7.1×10^{-6}[d]	89.7	−43	−4.6	*273*
	3.9×10^{-4}[e]	89.7	−9	−4.6	
$[Pt(Me_2S)_4]^{2+}$[c]	1.54	42.1	−100.2	−22.0	*271*
cis$[Pt(Me_2SO)_2(Me_2SO)_2]^{2+}$[c,i]	2	47	−74	−5	*274*
cis$[Pt(Me_2SO)_2(Me_2SO)_2]^{2+}$[c,j]	3200	32.8	−62.0	−2.5	*274*
$[Pt(CN)_4]^{2-}$[f]	25	24	−137		*270*
$[Pt(1,4\text{-dithiane})_2]^{2+}$[c]	28.8	32.9	−106	−12.6	*271*
$[Pt(MeNC)_4]^{2+}$[h]	6.2×10^5	13.8	−87.9	−3.7	*268*

[a] Second-order rate constant for the exchange of a particular solvent molecule.
[b] In aqueous solution.
[c] Diluent = d_3-nitromethane.
[d] Units are dm^3 mol^{-1} s^{-1}.
[e] First-order rate constant for the exchange of a particular water molecule.
[f] In ethanol.
[g] Misprint in Ref. (*268*) corrected in Ref. (*271*).
[h] Diluent = d_3-acetonitrile.
[i] Sulfur bonded.
[j] Oxygen bonded.

retardation of exchange is consistent with the operation of an **a**-activated mechanism.

$$\text{Rate} = 4k_{ex}[\text{Pt(ligand)}_4^{2+}][\text{ligand}]_{free} \qquad (21)$$

Ligands such as H_2O, MeCN, DMF, and DMA with hard donor atoms have exchange rates on Pd^{2+} within a factor of 15 of each other. The much softer Me_2S and MeNC ligands undergo ligand exchange more rapidly, consistent with ligand nucleophilicity and the *trans* effect de-

termining relative reactivity in the absence of significant steric hindrance. The very high reactivity of the MeNC complexes may be a consequence of the formation of a five-coordinated intermediate stabilized by π back-bonding from the metal center to MeNC. [A five-coordinate intermediate has been isolated in the substitution of MeNC by I^- in $[Pt(PPh_3)_2(MeNC)_2]^{2+}$ (*276*).] An interesting example of ambidentate DMSO acting as a hard and a soft donor in its respective *O*- and *S*-bonding forms is provided by *cis*$[Pt(Me_2SO)(Me_2SO)_2]^{2+}$ (*274*). Thus, the soft donor Me_2SO exerts a strong *trans* effect on the hard donor Me_2SO, which is a good leaving ligand, and vice versa, with the consequence that Me_2SO exchanges much more rapidly than Me_2SO.

The relative labilities of Pd^{2+} and Pt^{2+} vary considerably with the nature of the ligand. With a hard ligand such as H_2O, $[Pd(H_2O)_4]^{2+}$ undergoes exchange 10^6 times more rapidly than $[Pt(H_2O)_4]^{2+}$, while with soft ligands such as CN^-, MeNC, and olefins (*277*), the exchange rates are similar. However, $[Pd(1,4\text{-dithiane})_2]^{2+}$ and $[Pd(Me_2S)_4]^{2+}$ are much more labile than their Pt^{2+} analogues, despite the soft S donor atoms. This demonstrates the difficulty of distinguishing between the factors determining lability such as the *trans* and *cis* effects, and the influences of the entering and leaving ligands in the complexes in Table XIV, as a change from one complex to another alters all of these factors simultaneously. However, the greater sensitivity of Pt^{2+} to the nature of the exchanging ligand is consistent with it being a softer metal center than is Pd^{2+}.

The mechanistic interpretation of the $\Delta V^{\ddagger}$ data in Table XIV is complicated by the square-planar geometry of the exchanging complexes. The less crowded complexes may have loosely bound solvent molecules occupying the axial sites. Their loss, in concert with the formation of a new bond when a five-coordinate transition state forms, may result in compensatory volume change contributions which render the overall volume change quite small. It is therefore difficult to distinguish between $\mathbf{I}_a$ or **A** mechanisms, but the tendency towards $\Delta V^{\ddagger}$ being negative together with the observed second-order exchange rate law of Eq. (21) is consistent with a predominance of **a**-activation.

Single ligand substitution on $[Pd(H_2O)_4]^{2+}$, as shown in Eq. (22), and a similar substitution on $[Pt(H_2O)_4]^{2+}$, maintains *cis, trans,* and leaving-ligand effects constant and thereby allows a clearer assessment of the effect of the entering ligand. Thus, for $[Pd(H_2O)_4]^{2+}$ at 298.2 K, when L^{x-} = DMSO, $k_f = 2.45\ dm^3\ mol^{-1}$, $k_b = 0.24\ s^{-1}$, and $\Delta V_f^{\ddagger}$, $\Delta V_b^{\ddagger}$, and $\Delta V^0 = -9.2, -1.7$, and $-7.5\ cm^3\ mol^{-1}$, respectively. When L^{x-} = MeCN, $k_f = 309\ dm^3\ mol^{-1}$, $k_b = 16\ s^{-1}$, and $\Delta V_f^{\ddagger}$, $\Delta V_b^{\ddagger}$, and $\Delta V^0 = -4.0, -1.5$, and $-2.5\ cm^3\ mol^{-1}$, respectively (*278, 279*). (N.B.

When $L^{x-} = H_2O$, $k_f = 4k_{ex}/55 = 41$ dm^3 mol^{-1} s^{-1}, which is the k_{ex} per coordination site recalculated to second-order units, and $k_b = k_{ex} = 560$ s^{-1}.) The large variation of k_f with the nature of L^{x-} for the Pd^{2+} and Pt^{2+} centers is indicative of the dominance of the **a**-activation mode in reactions of the type shown in Eq. (22), as is the lesser variation of k_b (Table XV) (*269, 273, 278, 280–285*). There is a trend for k_{fPd}/k_{fPt} to vary from $\sim 10^6$ for hard nucleophiles such as H_2O and Cl^- to $\sim 5 \times 10^4$ for the soft thioethers. This is consistent with Pt^{2+} showing a wide range of selectivity for L^{x-} and being a softer center than Pd^{2+}, as was also deduced from the data in Table XIV.

$$[Pd(H_2O)_4]^{2+} + L^{x-} \underset{k_b}{\overset{k_f}{\rightleftharpoons}} [Pd(H_2O)_3L]^{(2-x)+} + H_2O \qquad (22)$$

The volume profiles for the ligand substitutions on $[Pd(H_2O)_4]^{2+}$, shown in Fig. 12, exhibit an overall contraction in the transition state ($\Delta V_f^{\ddagger}$) as DMSO substitutes for H_2O, a smaller one as MeCN substitutes, and a yet smaller one as water substitutes. The three negative $\Delta V_b^{\ddagger}$ values are identical within experimental error and also indicate a contraction to the transition state. It is particularly interesting that the difference in volume between the transition state and the reactants is independent of the leaving ligand when the entering ligand is water. Release of either DMSO or MeCN into bulk solution would produce a

TABLE XV

RATE CONSTANTS FOR THE SINGLE SUBSTITUTION OF L^{x-} IN $[Pd(H_2O)_4]^{2+}$ AND $[Pt(H_2O)_4]^{2+}$ AT 298 K

L^{x-}	k_{fPd}/ dm^3 mol^{-1} s^{-1}	k_{fPt}/ dm^3 mol^{-1} s^{-1}	k_{fPd}/k_{fPt}	Ref.
H_2O	41[a]	2.8×10^{-5}[a]	1.5×10^6	*269, 273*
Cl^-	1.8×10^4	2.66×10^{-2}	6.8×10^5	*281, 282*
Br^-	9.2×10^4	2.11×10^{-1}	4.4×10^5	*281, 282*
SCN^-	4.4×10^5	1.33	3.3×10^5	*282, 283*
I^-	1.14×10^6	7.7	1.4×10^5	*284*
DMSO	2.45	8.4×10^{-5}	2.9×10^4	*278, 285*
Me_2S	1.51×10^5	3.6	4.2×10^4	*280*
Et_2S	8.3×10^4	1.92	4.3×10^4	*280*

[a] Where k_f is the rate constant for the exchange of an unspecified one of the four coordinated water molecules recalculated to second-order units [k_{ex} is the first-order rate constant (s^{-1}) for the exchange of a particular coordinated solvent molecule].

large expansion. This suggests that these two ligands remain tightly bound to the Pd^{2+} center in the transition state, and it follows that an **A** mechanism probably operates despite the small $\Delta V_b^{\ddagger}$ values. When steric crowding of the Pd^{2+} center is increased, the lability of coordinated water is decreased and the mechanism of exchange remains **a**-activated. This is shown by $[Pd(dien)H_2O]^{2+}$, $[Pd(Me_5dien)H_2O]^{2+}$, and $[Pd(Et_5dien)H_2O]^{2+}$, for which k_{H_2O} (298.1 K) = 5100, 187, and 2.9 s^{-1} and $\Delta V^{\ddagger}$ = −2.8, −7.2, and −7.7 $cm^3\ mol^{-1}$, respectively (*286*). Substitution of H_2O in the pentamethyl and pentaethyl complexes by thiourea, dimethylthiourea, and tetramethylthiourea is characterized by decreasing substitution rates with increasing size of the entering ligand. For pentamethyl complexes, $\Delta V^{\ddagger}$ = −9.3, −9.1, and −13.4 $cm^3\ mol^{-1}$, respectively; for pentaethyl complexes, it is −8.3, −10.2 and −12.7 $cm^3\ mol^{-1}$, respectively. This is consistent with the operation of **a**-activated mechanisms. Similar studies of the substitution of anionic ligands are also consistent with **a**-activation (*287*).

In contrast to the **a**-activated mechanisms discussed so far, strong σ-donor ligands such as phenyl and methyl encourage the operation of *d*-activated mechanisms proceeding through a three-coordinate, 14 outer-shell electron configuration intermediate (*288*). Thus, the rate of exchange of DMSO on *cis*-$[PtPh_2(DMSO)_2]^{2+}$ is almost independent of

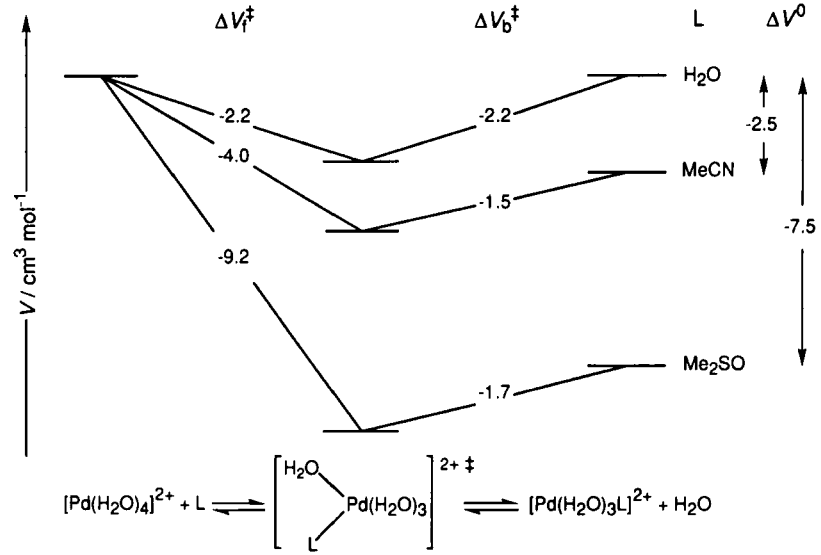

FIG. 12. Volume changes in the formation of $[Pd(H_2O)_3L]^{2+}$ from $[Pd(H_2O)_4]^{2+}$ and vice versa (*279*).

free DMSO concentration in $CDCl_3$ diluent, consistent with the operation of a **D** exchange mechanism. In the same diluent, the substitution of the first DMSO of *cis*-$[PtPh_2(DMSO)_2]^{2+}$ by bpy is rate-determining, and the substitution rate law indicates competition between bpy and DMSO for an intermediate of decreased coordination number. Other ligand substitution studies on this and similar complexes indicate the generation of intermediates of reduced coordination numbers through **D** mechanisms (*289–293*). Variable pressure studies of the exchange of L, shown in Eq. (23) (where k_{ex}' refers to the exchange of a particular coordinated ligand), also yield positive $\Delta V^{\ddagger}$ in accord with the operation of a **d**-activated mechanism (*293*). When R = Ph and L = Me_2S, k_{ex} (342.1 K) = 0.47 s^{-1} and $\Delta V^{\ddagger}$ = +4.7 $cm^3\ mol^{-1}$ in benzene. When R = Ph and L = DMSO, k_{ex} (330.8 K) = 0.91 s^{-1} and $\Delta V^{\ddagger}$ = +5.5 $cm^3\ mol^{-1}$ in chloroform. When R = Me and L = DMSO, k_{ex} (337.1 K) = 0.50 s^{-1} and $\Delta V^{\ddagger}$ = +4.9 $cm^3\ mol^{-1}$ in benzene. Extended Huckel theory and molecular electrostatic potential calculations indicate that the **d**-activation in these and similar complexes is a consequence of the destabilization of the ground state, concurrent with an increase of electron density at the Pt^{2+} center, which substantially hinders the approach of nucleophilic ligands to the four-coordinate complex (*294*).

$$cis\text{-}[PtR_2L_2]^{2+} + 2{*}L \overset{k_{ex}'}{\rightleftharpoons} cis\text{-}[PtR_2{*}L_2]^{2+} + 2L \qquad (23)$$

IV. Solvent Exchange and Ligand Substitution on the Trivalent Lanthanides and Dioxouranium(VI)

A. Aqueous Solution

The 15 trivalent lanthanide, or *f*-block, ions La^{3+}, Ce^{3+}, Pr^{3+}, Nd^{3+}, Pm^{3+}, Sm^{3+}, Eu^{3+}, Gd^{3+}, Tb^{3+}, Dy^{3+}, Ho^{3+}, Er^{3+}, Tm^{3+}, Yb^{3+}, and Lu^{3+}, which may be collectively denoted Ln^{3+}, represent the most extended series of chemically similar metal ions. The progressive filling of the 4*f* orbitals from La^{3+} to Lu^{3+} is accompanied by a smooth decrease in r_M with increase in atomic number as a consequence of the increasingly strong nuclear attraction for the electrons in the diffuse *f* orbitals (the lanthanide contraction). Thus, the nine-coordinate r_M decrease from 121.6 to 103.2 pm from La^{3+} to Lu^{3+}, and the eight-coordinate ionic radii decrease from 116.0 to 97.7 pm from La^{3+} to Lu^{3+} (*2*). Ligand field effects are small by comparison with those observed for the first-

row transition metal ions as a consequence of the shielding of the 4*f* orbitals by the filled 5*s* and 5*p* orbitals. Hence, the stereochemistry of Ln^{3+} complexes is little affected by directional effects emanating from the metal center and, together with the coordination number, is substantially influenced by the nature of the ligand.

The coordination numbers of the Ln^{3+} ions in water have been the subject of substantial debate (*4, 10, 11*), but it is now well established from neutron scattering (*295, 296*), x-ray scattering (*297–299*), extended x-ray absorption fine structure (EXAFS) (*300*), density (*301*) and spectrophotometric (*302*) techniques that the lighter La^{3+}–Nd^{3+} ions are predominantly nine-coordinate, Pm^{3+}–Eu^{3+} exist in equilibria between eight- and nine-coordinate states, and the heavier Gd^{3+}–Lu^{3+} ions are predominantly eight-coordinate. [This makes an interesting contrast with the solid state, where x-ray diffraction studies have shown tricapped trigonal prismatic $[Ln(H_2O)_9]^{3+}$ to be the hydrated ion when Ln^{3+} = La^{3+}, Pr^{3+}, Sm^{3+}, Gd^{3+}, Ho^{3+}, Er^{3+}, Yb^{3+}, and Lu^{3+} in the presence of $CF_3SO_3^-$, $EtOSO_3^-$ and BrO_3^- counterions (*302–308*) but octahedral $[Ln(H_2O)_6]^{3+}$ to be the hydrated ion when Ln^{3+} = La^{3+}, Tb^{3+}, and Er^{3+} in the presence of ClO_4^- counterions (*309*). This change in coordination number is also reflected in the absolute partial molar volumes, V_{abs}^0, of several Ln^{3+} ions determined in aqueous $LnCl_3$ solution (*301*). These are plotted in Fig. 13 together with $\overline{V}_{abs}^0$ calculated from Eq. (12), and the agreement between the experimental and calculated values is good (*4, 41, 42*). This coordination number change has substantial implications for the interpretation of ligand substitution data, which are now discussed.

The rate constants, k_i, for the substitution of SO_4^{2-} on Ln^{3+} in aqueous solution determined by ultrasonic methods are plotted in Fig. 13 (*310*). It is striking that k_i reaches a maximum for Sm^{3+}, Eu^{3+}, and Gd^{3+}, for which an equilibrium between $[Ln(H_2O)_8]^{3+}$ and $[Ln(H_2O)_9]^{3+}$ is well established. For these species, interconversion between the eight- and nine-coordinate states requires relatively little energy, and Sm^{3+}, Eu^{3+}, and Gd^{3+} should accordingly have the fastest water exchange rates and ligand substitution rates. The mechanistic inference to be drawn from a combination of these observations is that water exchange on $[Ln(H_2O)_8]^{3+}$ will be **a**-activated, and that on $[Ln(H_2O)_9]^{3+}$ will be **d**-activated. Water exchange rate constants are only available for the heavier lanthanides, $[Ln(H_2O)_8]^{3+}$, but they exhibit a similar correlation with the r_M of Ln^{3+} as does k_i for SO_4^{2-} substitution which has a similar magnitude to that of k_{H_2O}, as seen from Fig. 13 and Table XVI. The latter observation may be fortuitous, but it is surprising for an **a**-activated process where some effect of the different natures of the

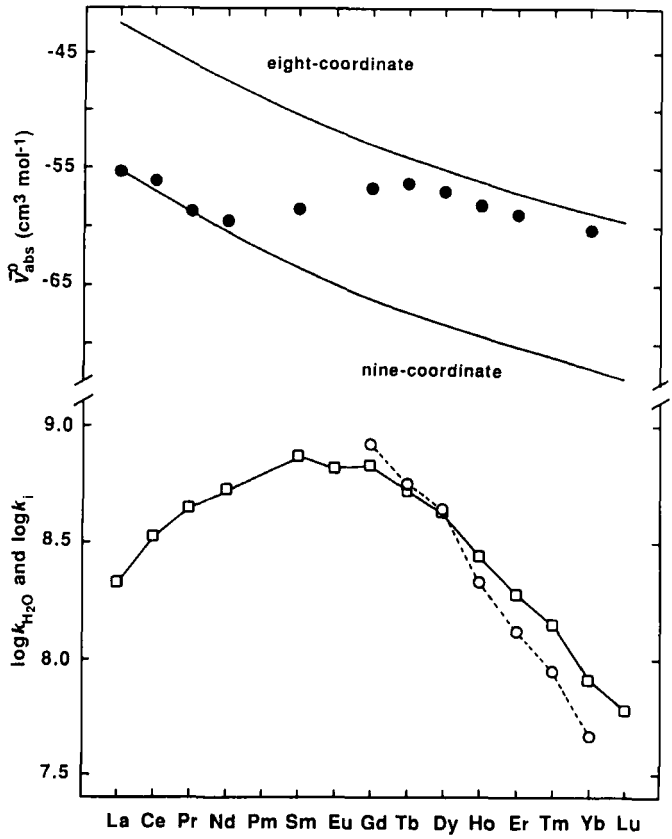

FIG. 13. Absolute partial molar volumes, $V_{abs}{}^0$, of $[Ln(H_2O)_n]^{3+}$ in aqueous $LnCl_3$ solutions (*301*) (closed circles), compared with the calculated $\bar{V}_{abs}{}^0$ values (*4, 42*) for $[Ln(H_2O)_8]^{3+}$ and $[Ln(H_2O)_9]^{3+}$ indicated by the upper and lower solid curves, respectively. Interchange rate constants, k_i (298 K) (*310*), for the substitution of $SO_4{}^{2-}$ on $[Ln(H_2O)_n]^{3+}$ are shown as open squares, and water exchange rate constants, k_{H_2O} (298 K) (*311, 312*), for $[Ln(H_2O)_8]^{3+}$ are shown as open circles.

entering ligand might be anticipated. However, the lability of $[Ln(H_2O)_8]^{3+}$ towards ligand substitution is very high, and it may be that under these circumstances the selectivity of $[Ln(H_2O)_8]^{3+}$ is not great, particularly as the interaction between hard acid Ln^{3+} and hard base $SO_4{}^{2-}$ is mainly electrostatic.

Water exchange on $[Ln(H_2O)_8]^{3+}$ for the heavier lanthanides Gd^{3+}–Yb^{3+} is characterized by a systematic decrease in k_{H_2O} and an increase in $\Delta H^{\ddagger}$ as the ionic radius decreases from Tb^{3+} to Yb^{3+}, and both $\Delta S^{\ddagger}$ and $\Delta V^{\ddagger}$ are negative (*311–313*). The $\Delta V^{\ddagger}$ are significantly less than either the value of -12.9 cm^3 mol^{-1} calculated for water

TABLE XVI

PARAMETERS FOR WATER EXCHANGE ON $[Ln(H_2O)_8]^{3+}$ (*311, 312*)

Ln^{3+}	r_M[a]/ pm	$10^{-7}k_{H_2O}$(298 K)[b]/ s^{-1}	$\Delta H^{\ddagger}$/ kJ mol^{-1}	$^{\Delta}S^{\ddagger}$/ J K^{-1} mol^{-1}	$\Delta V^{\ddagger}$/ cm^3 mol^{-1}
Gd^{3+}	105.3	83.0	14.9	−24.1	−3.3
Tb^{3+}	104.0	55.8	12.1	−36.9	−5.7
Dy^{3+}	102.7	43.4	16.6	−24.0	−6.0
Ho^{3+}	101.5	21.4	16.4	−30.5	−6.6
Er^{3+}	100.4	13.3	18.4	−27.8	−6.9
Tm^{3+}	99.4	9.1	22.7	−16.4	−6.0
Yb^{3+}	98.5	4.7	23.3	−21.0	

Adapted from Refs. (*311, 312*).

[a] Eight-coordinate ionic radii from Ref. (*2*).

[b] Rate constant for the exchange of a particular coordinated water molecule.

exchange on $[Ln(H_2O)_8]^{3+}$ through an **A** mechanism (*4, 41, 312*), or the reaction volume of -11 cm^3 mol^{-1} determined for the nine- to eight-coordination change (*314*) in the equilibrium shown in Eq. (24),

$$[Ce(H_2O)_8]^{3+} + H_2O \rightleftharpoons [Ce(H_2O)_9]^{3+} \qquad (24)$$

which should be similar to $\Delta V^{\ddagger}$ for water exchange on $[Ln(H_2O)_8]^{3+}$ proceeding through a nine-coordinate transition state in an **A** mechanism. On this basis an $\mathbf{I}_a$ mechanism is assigned to water exchange on the $[Ln(H_2O)_8]^{3+}$ listed in Table XVI, an assignment which is also in accord with the negative $\Delta S^{\ddagger}$. The systematic decrease in k_{H_2O} as the ionic radius decreases from Gd^{3+} to Yb^{3+} is consistent with increasing steric crowding hindering the entry of the incoming water dominating the variation of k_{H_2O}. The corresponding increase in surface charge density might be expected to provide an increased electrostatic attraction between the entering water and Ln^{3+} and thereby accelerate the water exchange rate, but this is evidently not of major significance here. It should be noted that $[Gd(H_2O)_8]^{3+}$ is adjacent to the region in which the coordination number change occurs (Fig. 13), and it may be that the presence of a small proportion of $[Gd(H_2O)_9]^{3+}$ makes a contribution to the derived kinetic parameters.

Possible stereochemistries for eight-coordinate $[Ln(H_2O)_8]^{3+}$ are the dodecahedron, the square antiprism, and the cube, although the last seems less likely (*295*). The proposed nine-coordinate $[Ln(H_2O)_9]^{3+}$ tricapped trigonal prism transition state is similar to the $[Ln(H_2O)_9]^{3+}$ structures observed in the solid state. Thus, the possible water exchange

paths for $[Ln(H_2O)_8]^{3+}$ may be envisaged as in Fig. 14. Monte Carlo simulations predict an **a**-activated water exchange process for $[Ln(H_2O)_8]^{3+}$ and a **d**-activated process for $[Ln(H_2O)_9]^{3+}$, and also predict a change from nine- to eight-coordination with the lanthanide contraction (*315*).

B. The Influence of Polyaminocarboxylate Ligands on Water Exchange

Polyaminocarboxylate complexes of Gd^{3+} are used as contrast agents in medical magnetic resonance imaging. The contrast produced by these agents depends on their ability to induce NMR relaxation in the protons of surrounding water, which in turn depends on the water proton exchange rate. Until recently it was assumed that the rate of water exchange on these complexes was as rapid as that on $[Gd(H_2O)_8]^{3+}$. The influence of non-exchanging polyaminocarboxylate ligands on the parameters for water exchange on Gd^{3+} has now been shown to be substantial, as is seen from the data in Table XVII, and is largely attributable to a combination of a change in the constraining effect of the polyaminocarboxylate ligands and a change in coordination number (*311, 316, 317*). Thus, the decrease in lability and in negative $\Delta V^{\ddagger}$ magnitude observed on going from eight-coordinate $[Gd(H_2O)_8]^{3+}$ to eight-coordinate $[Gd(PDTA)(H_2O)_2]^{-}$ is probably a consequence of $PDTA^{4-}$ decreasing the stereochemical flexibility of the first coordination sphere. This decreases the ability to accommodate the incoming water molecule to form an **a**-activated transition state so that the exchange mechanism becomes less associative in character. The change in coordination number to nine for $[Gd(DTPA)H_2O]^{2-}$,

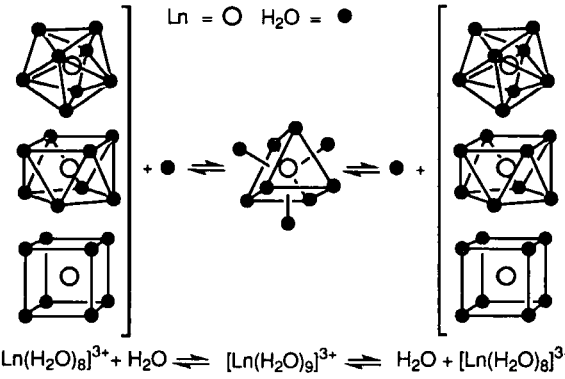

FIG. 14. Possible mechanistic paths for water exchange on $[Ln(H_2O)_8]^{3+}$.

TABLE XVII

PARAMETERS FOR WATER EXCHANGE ON Gd(III) COMPLEXES (*311, 316, 317*)

Complex	$10^{-5}k_{H_2O}$(298 K)[a]/ s^{-1}	$\Delta H^{\ddagger}$/ kJ mol^{-1}	$\Delta S^{\ddagger}$/ J K^{-1} mol^{-1}	$\Delta V^{\ddagger}$/ cm^3 mol^{-1}
$[Gd(H_2O)_8]^{3+}$	8300	14.9	−24.1	−3.3
$[Gd(PDTA)(H_2O)_2]^-$	1020	11.0	−54.6	−1.5
$[Gd(DTPA)H_2O]^{2-}$	41	52.0	+56.2	+12.5
$[Gd(DOTA)H_2O]^-$	48	48.8	+46.6	+10.5
$[Gd(DTPA\text{-}BMA)H_2O]$	4.3	46.6	+18.9	+7.3

Adapted from Refs (*311, 316, 317*).

[a] Rate constant for the exchange of a particular coordinated water molecule.

$[Gd(DOTA)H_2O]^-$, and $[Gd(DTPA\text{-}BMA)H_2O]^-$ results in a change to a **d**-activated mechanism, as indicated by the large positive $\Delta V^{\ddagger}$ values, which are similar to $\Delta V^0 = +11$ cm^3 mol^{-1} for the nine- to eight-coordination number change observed for $[Ce(H_2O)_8]^{3+}$ (*314*), for the first two complexes and indicate the operation of a **D** mechanism for water exchange. Without the participation of the entering water molecule, more energy is required to break the bond between the leaving water molecule and the highly charged Gd^{3+}, leading to the relatively very low water exchange rates. The increased $\Delta H^{\ddagger}$ and positive $\Delta S^{\ddagger}$ values are also consistent with this interpretation. The three complexes have similar $\Delta H^{\ddagger}$ values, and so the decreased lability of $[Gd(DTPA\text{-}BMA)H_2O]^-$ results from its smaller $\Delta S^{\ddagger}$. All of the polyaminocarboxylate complexes in Table XIV are either actual or potential contrast agents for biomedical magnetic resonance imaging (MRI), and thus a knowledge of their water exchange rates is important in understanding the factors affecting their proton relaxivity profiles (*316–320*).

C. DIMETHYLFORMAMIDE SOLUTION

As in aqueous solution, the lanthanide contraction favors a change from nine-coordination for the light lanthanides to eight-coordination for the light lanthanides such that $[Ln(DMF)_8]^{3+}$ is the major species when $Ln^{3+} = Ce^{3+}–Nd^{3+}$, and that this becomes the only detected species when $Ln^{3+} = Tb^{3+}–Lu^{3+}$ in dimethylformamide perchlorate solution (*11, 92, 93, 321–323*). Thus, Nd^{3+} is characterized by $\Delta H^0 = -14.9$ kJ mol^{-1}, $\Delta S^0 = -69.1$ J K^{-1} mol^{-1}, and $\Delta V^0 = -9.8$ cm^3 mol^{-1} for the equilibrium shown in Eq. (25) (*93*). The molar volume of DMF is 72 cm^3 mol^{-1}, and it therefore appears that the substantially smaller magnitude of ΔV^0 is a consequence of significant

lengthening of the other eight Nd^{3+}–DMF bonds upon formation of $[Nd(DMF)_9]^{3+}$.

$$[Nd(DMF)_8]^{3+} + DMF \rightleftharpoons [Nd(DMF)_9]^{3+} \quad (25)$$

The exchange of DMF on $[Ln(DMF)_8]^{3+}$ for the heavier lanthanides, as shown in Eq. (26), is characterized by positive $\Delta V^{\ddagger}$ values, a systematic increase in $\Delta H^{\ddagger}$, and a change from negative to positive $\Delta S^{\ddagger}$ values as the ionic radius decreases from Tb^{3+} to Yb^{3+} (Table XVIII). The increase in $\Delta H^{\ddagger}$ may be explained on the basis of a **d**-activated exchange process where the increasing surface charge density of the metal center generates an increasing electrostatic attraction between it and DMF. The concomitant increase in steric crowding resulting from the lanthanide contraction causes the mechanism to closely approach a **D** mechanism for the heavier lanthanides. (A $\Delta V^{\ddagger} \geq +9.8$ cm^3 mol^{-1} observed for the ΔV^0 for the loss of a DMF from $[Nd(DMF)_9]^{3+}$ might be anticipated for a **D** mechanism for the heavier $[Ln(DMF)_8]^{3+}$.)

$$[Ln(DMF)_8]^{3+} + 8{*}DMF \overset{k_{ex}}{\rightleftharpoons} [Ln(*DMF)_8]^{3+} + 8DMF \quad (26)$$

The origin of the change in sign of $\Delta S^{\ddagger}$ is revealed when the $[Ln(DMF)_8]^{3+}$ exchange process is studied in inert d_3-nitromethane diluent (*11, 93*). For $Ln^{3+} = Tb^{3+}, Er^{3+}, Tm^{3+}$, the general form of the DMF exchange rate equation is as in Eq. (27). When $Ln^{3+} = Tb^{3+}$, the second term on the right-hand side dominates. Both terms are im-

TABLE XVIII

PARAMETERS FOR DIMETHYLFORMAMIDE EXCHANGE ON $[Ln(DMF)_8]^{3+}$

Ln^{3+}	r_M[a]/ pm	$10^{-5}k_{ex}$(298 K)[b]/ s^{-1}	$\Delta H^{\ddagger}$/ kJ mol^{-1}	$\Delta S^{\ddagger}$/ J K^{-1} mol^{-1}	$\Delta V^{\ddagger}$/ cm^3 mol^{-1}	Mechanism
Tb^{3+}	104.0	190	14.1	−58	+5.2	I_d
Dy^{3+}	102.7	63	13.8	−69	+6.1	I_d
Ho^{3+}	101.5	36	15.3	−68	+5.2	I_d
Er^{3+}	100.4	130	23.6	−30	+5.4	**D** and I_d
Tm^{3+}	99.4	310	33.2	+10	+7.4	**D**
Yb^{3+}	98.5	990	39.3	+40	+11.8	**D**

Adapted from Ref. (*93*).

[a] Eight-coordinate ionic radii from Ref. (*2*).

[b] Rate constant for the exchange of a particular coordinated solvent molecule.

portant when $Ln^{3+} = Er^{3+}$, and the first term dominates when $Ln^{3+} = Tm^{3+}$. This is consistent with the $\mathbf{I}_d$ transition state being favored for Tb^{3+}, the $\mathbf{I}_d$ and **D** transition states being similarly favored for Er^{3+}, and the **D** transition state becoming dominantly favoured for Tm^{3+} as the r_M of these ions decrease with the lanthanide contraction. Thus, the variation in the magnitude and sign of $\Delta S^{\ddagger}$ for DMF exchange may be rationalized in terms of a decrease in the degrees of freedom accompanying the involvement of the incoming DMF in an $\mathbf{I}_d$ transition state resulting in a negative $\Delta S^{\ddagger}$, whereas the accompanying positive $\Delta V^{\ddagger}$ arises from a combination of an increase in volume accompanying bond lengthening for the leaving DMF, a lesser increase in volume as the bond distances of the non-exchanging DMF increase, and a decrease in volume accompanying the penetration of the incoming DMF into the first coordination sphere. In contrast, $\Delta S^{\ddagger}$ and $\Delta V^{\ddagger}$ are both positive for the **D** transition state as the departure of a DMF increases the degrees of freedom and results in an increase in volume.

$$\text{rate} = 8k_{ex}[Ln(DMF)_8^{3+}] = \{k_D + k_i K_o[DMF]/(1 + K_o[DMF])\}[Ln(DMF)_8^{3+}] \quad (27)$$

D. Lower Coordination Number Species

As the size of monodentate ligands bound to Ln^{3+} increases, so the coordination number decreases. Thus, in trimethylphosphate, $[Ln(TMP)_7]^{3+}$ is the dominant species for the light lanthanides, whereas $[Ln(TMP)_6]^{3+}$ is the dominant species for the heavy lanthanides (*92*). The equilibrium shown in Eq. (28) is characterized by $\Delta H^0 = -32.7$ kJ mol^{-1}, $\Delta S^0 = -114$ J K^{-1} mol^{-1}, and $\Delta V^0 = -23.8$ cm^3 mol^{-1}, and it is the last value which was used for comparison with $\Delta V^{\ddagger}$ observed for TMP exchange on $[M(TMP)_6]^{3+}$ in Section II,C. The greater magnitudes of ΔH^0 and ΔS^0 observed for this system by comparison with those for the higher coordination number DMF system [Eq. (25)] are consistent with an increase in Ln^{3+}–ligand bonding strength, with the decrease in coordination number and the tighter binding producing a greater decrease in entropy. It also appears that a decrease in coordination number results in a decrease in lability, as evidenced by the data in Table XIX (*324–327*) for the exchange of TMU on $[Ln(TMU)_6]^{3+}$ when compared with the rate constants in Tables XVI and XVIII. These data were obtained in d_3-acetonitrile diluent, and k_{ex} was found to be independent of reactant concentration, consistent with the operation of a **D** mechanism or an $\mathbf{I}_d$ mechanism characterized by a high K_o, except in the case of $[Tb(TMU)_6]^{3+}$ and its Dy^{3+} and Ho^{3+} analogues, where the rate law was not reliably determined. The de-

TABLE XIX

PARAMETERS FOR TETRAMETHYLUREA EXCHANGE ON $[M(TMU)_6]^{3+}$ IN CD_3CN DILUENT

M^{3+}	r_M[a]/ pm	k_{ex}(298.2 K)[b]/ s^{-1}	$\Delta H^{\ddagger}$/ kJ mol^{-1}	$\Delta S^{\ddagger}$/ J K^{-1} mol^{-1}	Mechanism
Tb^{3+}	92.3	1380	38.2	−56.7	—
Dy^{3+}	91.2	1290	38.6	−56.0	—
Ho^{3+}	90.1	510	40.9	−55.9	—
Y^{3+}	90.0	253	27.1	−108	**D**, I_d
Er^{3+}	89.0	214	35.5	−81.3	**D**, I_d
Tm^{3+}	88.0	145	29.3	−105	**D**, I_d
Yb^{3+}	86.8	65.5	38.3	−81.8	**D**, I_d
Lu^{3+}	86.1	41.9	41.7	−74	**D**, I_d
Sc^{3+}	74.5	0.90	68.6	−15.7	**D**, I_d

Adapted from Ref. (*324–327*).

[a] Six-coordinate ionic radii from Ref. (*2*).

[b] Rate constant for the exchange of a particular coordinated TMU molecule.

crease in k_{ex} and increase in $\Delta H^{\ddagger}$ from $[Er(TMU)_6]^{3+}$ to $[Lu(TMU)_6]^{3+}$ with decrease in r_M is consistent with the increasing strength of Ln^{3+}–TMU bonding being the dominant factor in a **d**-activated exchange mechanism. It is seen that the pseudo-lanthanides Y^{3+} and Sc^{3+}, whose r_M bracket those of Er^{3+} and Lu^{3+}, fit the trend in k_{ex} and $\Delta H^{\ddagger}$ magnitudes and lend support to the deduction that relative lability is strongly influenced by r_M.

$$[Nd(TMP)_6]^{3+} + TMP \rightleftharpoons [Nd(TMP)_7]^{3+} \tag{28}$$

$$[M(TMU)_6]^{3+} + 6{*}TMU \overset{k_{ex}}{\rightleftharpoons} [M(*TMU)_6]^{3+} + 6TMU \tag{29}$$

E. DIOXOURANIUM(VI)

Although the number of actinides is the same as that of the lanthanides, their availability and chemical characteristics have so far largely restricted the study of their ligand substitution mechanisms to dioxouranium(VI), which is the ionic form of uranium most amenable to such studies in solution. In the solid state, the oxo ligands occupy axial sites above and below the U(VI) center, and four (*328*), five (*329, 330*), and six (*331, 332*) oxygen donor atoms have been reported to occupy equatorial positions. From a mechanistic point of view, this variability of the occupancy of the equatorial plane suggests the possibility of both **d**- and **a**-activated ligand substitution pro-

cesses occurring. The most commonly observed solvated species have the stoichiometry $[UO_2(solvent)_5]^{2+}$, and it is probable that the U–O axial and equatorial distances of 176(4) pm and 238(4) pm, respectively, observed for $[UO_2(DMSO)_5]^{2+}$ in the solid state (*329*), apply to solvated species of the same stoichiometry in solution. Similar distances are observed in the solid state for $[UO_2(H_2O)_5]^{2+}$, which is characterized by U–O axial and equatorial distances of 171(7) pm and 245(6) pm, respectively (*330*). However, a contraction in the equatorial distances occurs in the lower coordination number $[UO_2(HMPA)_4]^{2+}$, which has U–O axial and equatorial distances of 174(4) pm and 227(5) pm, respectively (*328*).

While protolysis and oligomerization have so far precluded a direct study of water exchange of $[UO_2(H_2O)_5]^{2+}$, the exchange of several other solvents has been studied in inert diluents using ^1H NMR methods. Thus, the HMPA exchange rate law for $[UO_2(HMPA)_4]^{2+}$ has two terms in d_2-methylenechloride diluent, as shown in Eq. (30), where the k_2 term is dominant and is characterized by k_2 (298 K) = 251 kg mol^{-1} s^{-1}, $\Delta H^{\ddagger}$ = 47.1 kJ mol^{-1}, $\Delta S^{\ddagger}$ = −41.7 J K^{-1} mol^{-1}, and $\Delta V^{\ddagger}$ = −11.3 cm^3 mol^{-1} (*333*). This is consistent with the dominance of an **A** mechanism in which a fifth HMPA enters the equatorial plane in the transition state. The negative $\Delta V^{\ddagger}$ for the k_2 path is only a small fraction of the molar volume of pure HMPA, ΔV_s° = 175.0 cm^3 mol^{-1}. This is consistent with an outward movement of the four bound HMPA to contribute a substantial positive component to $\Delta V^{\ddagger}$, which partially counterbalances the negative contribution to $\Delta V^{\ddagger}$ as a fifth HMPA enters the equatorial plane. It is anticipated from solid state data that the average equatorial U–O bond distances of 227 pm and 90° O–U–O equatorial angles observed in six-coordinated $[UO_2(HMPA)_4]^{2+}$ will increase to 238–245 pm and decrease to 72°, respectively, in seven-coordinated $[UO_2(HMPA)_5]^{2+}$. Although the ligand substitution processes of $[UO_2(HMPA)_4]^{2+}$ are restricted to the equatorial plane, space-filling models based on crystal structures indicate that there is substantial freedom of movement for bond rotation of the $-P(NMe_2)_3$ moieties above and below the equatorial plane, which may make significant contributions to $\Delta V^{\ddagger}$.

$$\text{rate} = 4[UO_2(HMPA)_4{}^{2+}](k_1 + k_2[HMPA]) \qquad (30)$$

In contrast, the rate law for TMP exchange on $[UO_2(TMP)_5]^{2+}$ is as shown in Eq. (31), which indicates the operation of a **D** mechanism in which a TMP is almost lost from the equatorial plane in the transition state. This is characterized by k_1 (298 K) =

873 s^{-1}, $\Delta H^{\ddagger}$ = 44.1 kJ mol^{-1}, $\Delta S^{\ddagger}$ = −40.7 J K^{-1} mol^{-1}, and $\Delta V^{\ddagger}$ = +2.1 cm^3 mol^{-1}. The $\Delta V^{\ddagger}$ is very small by comparison with ΔV_s° = 118 cm^3 mol^{-1} for pure TMP. This probably arises from the counterbalancing respective positive and negative contributions made to $\Delta V^{\ddagger}$ as the leaving TMP moves out of the equatorial plane, while the remaining four TMP shorten their U–O bond distances. Several other seven-coordinate $[UO_2(solvent)_5]^{2+}$ species (*334–336*) are characterized by an exchange rate law of the form of Eq. (31) which is interpreted in terms of the operation of a **D** mechanism.

$$\text{rate} = 5[UO_2(TMP)_5{}^{2+}](k_1[TMP]) \tag{31}$$

V. Solvent Exchange and Ligand Substitution on Some Molybdenum and Tungsten Cluster Complexes

The preceding sections of this chapter amply demonstrate the impressive understanding of ligand substitution processes at single metal centers which has now accrued. As a consequence, it seems particularly appropriate that the penultimate section of this review should explore some of the recent results of ligand substitution studies of multinuclear metal clusters. Such clusters have biological significance, as exemplified by the iron clusters encountered in the ferredoxins (*337*) and the iron/molybdenum cluster found in nitrogenase (*338*). In addition, they bring to the fore some of the additional considerations which arise because more than one metal center is available for substitution.

The trinuclear molybdenum and tungsten clusters $[M_3X_4(H_2O)_9]^{4+}$ (I), the tetranuclear molybdenum cluster $[Mo_4S_4(H_2O)_{12}]^{4+/5+/6+}$ (II), the trinuclear molybdenum and tungsten clusters $[M_3(\mu_3\text{-}O)_2(\mu_2\text{-}CH_3CO_2)_6(H_2O)_3]^{2+}$ (III), and the trinuclear cluster $[W_3(\mu_3\text{-}O)(\mu_2\text{-}CH_3CO_2)_6(H_2O)_3]^{2+}$ (IV), whose structures are shown schematically in Fig. 15, may be used as examples to illustrate some of the intricacies of ligand substitution on metal clusters. The octahedrally coordinated Mo's in Mo_4S_4 and related incomplete Mo_3S_4 clusters have the advantage of being stable in acidic aqueous media, unlike the tetrahedrally coordinated Fe–S clusters. Moreover, it has not been possible to synthesize analogues of the Fe_3S_4 clusters identified in some 20 proteins, the synthetic approach yielding only a linearized $Fe(\mu\text{-}S)_2Fe(\mu\text{-}S)_2Fe$ form. The most intensively studied cluster ligand substitution processes are those reported for the trinuclear molybdenum(IV) (*339–348*) and tungsten(IV) (*349–351*) clusters, $[M_3X_4(H_2O)_9]^{4+}$, which incorporate μ-oxo,

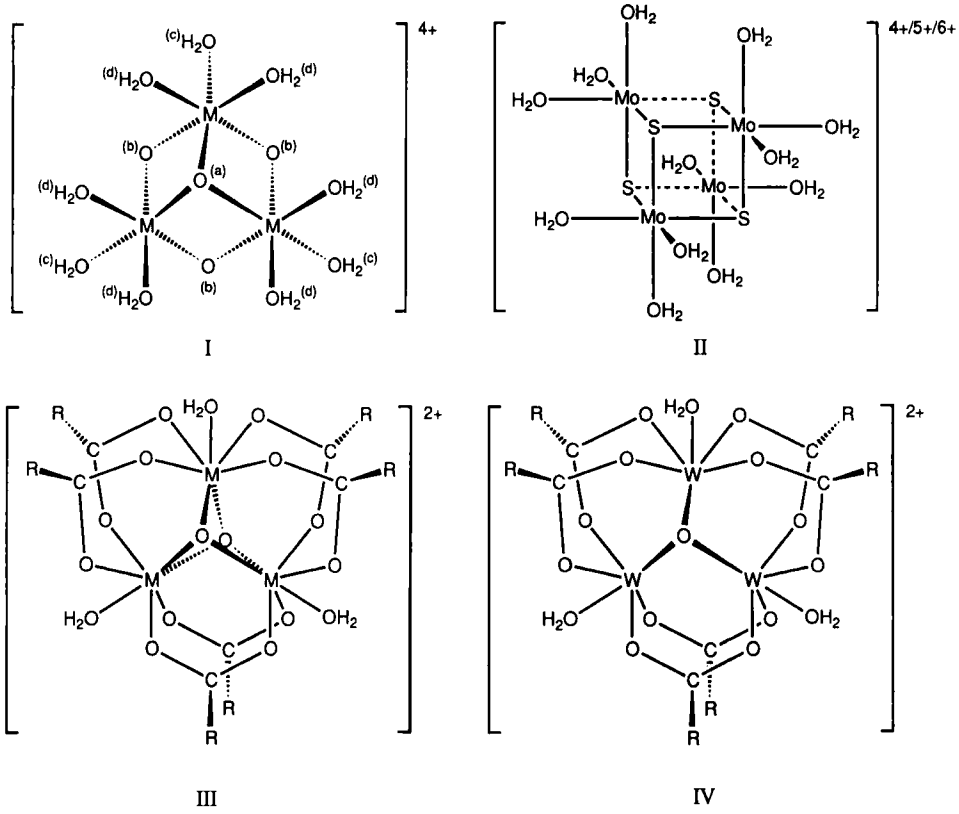

FIG. 15. The structures of some molybdenum and tungsten cluster complexes.

μ-sulfido, and μ-selenido ligands (X) in the incomplete cuboidal structures shown in Fig. 15. In the solid state, M_3X_4 core atoms delineate an incomplete cube with one μ_3-X, three equivalent μ_2-X ligands, and three octahedral M centers, to each of which are bound one water (c) *trans* to μ_3-X (a) and two waters (d) *trans* to μ_2-X (b) with identical M-c-OH_2 and M-d-OH_2 bond distances in each cluster (*346, 352, 353*). Studies in water are consistent with this structure persisting in solution. The M_3X_4 core is long-lived, as exemplified by $[Mo_3O_4(H_2O)_9]^{4+}$, which is the dominant form in which Mo^{4+} is encountered in water. Its half-life for exchange of μ_3-O and μ_2-O is ~10 years at 298 K, while the coordinated water is substantially more labile (*346, 348*). The approach to equilibrium for the substitution of a water of $[M_3X_4(H_2O)_9]^{4+}$ by a ligand, L^-, in excess $[L^-]$ is characterized by the pseudo first-order equilibration rate constant k_{eq}, as in Eq. (32), where

k_f is the forward rate constant, k_{aq} is the aquation rate constant, and the statistical factor of 3 is a consequence of there being three equivalent M sites for substitution (*348*). The pH dependence of k_{eq} shows that k_f is of the form of Eq. (33), where K_a characterizes the deprotonation of a d-H_2O and k_l and k_{OH} characterize substitution of a H_2O in $[M_3X_4(H_2O)_9]^{4+}$ and $[M_3X_4(H_2O)_8(d\text{-}OH)]^{3+}$, respectively, as shown in Eqs. (34)–(40), which also show the water exchange processes. k_{1d}*, k_{1OHd}*, k_{1c}*, and k_{1OHc}* represent the rate constants for exchange of a particular water molecule.

$$k_{eq} = (k_f[L^-]/3) + k_{aq} = k_f[M_3X_4(H_2O)_9{}^{4+}] + k_{aq} \tag{32}$$

$$k_f = \frac{k_l[H^+] + k_{OH}K_a}{[H^+] + K_a} \tag{33}$$

$$[M_3X_4(H_2O)_9]^{4+} \overset{K_a}{\rightleftharpoons} [M_3X_4(H_2O)_8(d\text{-}OH)]^{3+} + H^+ \tag{34}$$

$$[M_3X_4(H_2O)_9]^{4+} + L^- \underset{k_{-l}}{\overset{k_l}{\rightleftharpoons}} [M_3X_4(H_2O)_8L]^{3+} + H_2O \tag{35}$$

$$[M_3X_4(H_2O)_9(OH)]^{3+} + L^- \underset{k_{-OH}}{\overset{k_{OH}}{\rightleftharpoons}} [M_3X_4(H_2O)_8(OH)L]^{2+} + H_2O \tag{36}$$

$$[M_3X_4(H_2O)_9]^{4+} + H_2O^* \overset{6k_{1d}^*}{\rightleftharpoons} [M_3X_4(H_2O)_8(d\text{-}H_2O^*)]^{4+} + H_2O \tag{37}$$

$$[M_3X_4(H_2O)_8(OH)]^{3+} + H_2O^* \overset{6k_{OHd}^*}{\rightleftharpoons} [M_3X_4(H_2O)_7(d\text{-}H_2O^*)(OH)]^{3+} + H_2O \tag{38}$$

$$[M_3X_4(H_2O)_9]^{4+} + H_2O^* \overset{3k_{1c}^*}{\rightleftharpoons} [M_3X_4(H_2O)_8(c\text{-}H_2O^*)]^{4+} + H_2O \tag{39}$$

$$[M_3X_4(H_2O)_8(OH)]^{3+} + H_2O^* \overset{3k_{OHc}^*}{\rightleftharpoons} [M_3X_4(H_2O)_7(c\text{-}H_2O^*)(OH)]^{3+} + H_2O \tag{40}$$

The water exchange rate constant k_{H_2O} for both c-H_2O and d-H_2O of $[Mo_3O_4(H_2O)_9]^{4+}$ is of the form of Eq. (41).

$$k_{H_2O} = K_a k_{OH}^*/(K_a + [H^+]) \tag{41}$$

This is consistent with the conjugate base species, $[Mo_3O_4(H_2O)_8(d\text{-}OH)]^{3+}$, in which one of the d-$H_2O$ is deprotonated (K_a = 0.31 dm^3 mol^{-1}), providing the predominant path for water exchange on

$[Mo_3O_4(H_2O)_9]^{4+}$ as shown in Eqs. (37) to (40). Thus, exchange of a d-H_2O, characterized by k_{OHd}* (298 K) = 1.6×10^2 s^{-1} for a particular water molecule, $\Delta H^{\ddagger}$ = 71.0 kJ mol^{-1} and $\Delta S^{\ddagger}$ = 35.2 J K^{-1} mol^{-1}, is much faster than that of a c-H_2O, for which k_{OHc}* (298 K) = 1.5×10^{-3} s^{-1} for a particular water molecule (*346*). The labilization of an adjacent d-H_2O, but not an adjacent c-H_2O, infers a charge transfer through a molecular orbital common only to the d-H_2O sites (*348, 354–356*). Ligand substitution of a d-H_2O also proceeds through $[Mo_3O_4(H_2O)_8(d\text{-}OH)]^{3+}$ such that the k_1 term in Eq. (33) is negligible, and k_f = 4.8 and 3.3 dm^3 mol^{-1} for NCS^- and $HC_2O_4^-$, respectively (*343*). On the assumption of the operation of an interchange mechanism such that $k_f = k_i K_o$, and a value of K_o within the range 0.5–10 dm^3 mol^{-1}, k_i values within the range 0.4–8 s^{-1} are estimated for NCS^- and $HC_2O_4^-$. These k_i are substantially smaller than k_{OHd}*, and together with the positive $\Delta S^{\ddagger}$ for d-H_2O exchange and the similarities of k_f for NCS^- and $HC_2O_4^-$, are compatible with the operation of an I_d mechanism.

The $[Mo_3S_4(H_2O)_9]^{4+}$ cluster is substantially more labile towards ligand substitution by comparison with $[Mo_3O_4(H_2O)_9]^{4+}$, and both the conjugate acid and base species undergo ligand substitution through the paths indicated by Eqs. (35) and (36). This is consistent with the observation that k_f is of the form of Eq. (33) (*344, 345, 348*). Substitutions by NCS^- and Cl^- on $[Mo_3S_4(H_2O)_9]^{4+}$ are characterized by k_1 = 108 and 91 dm^3 mol^{-1} s^{-1}, respectively. If an interchange mechanism and K_o = 0.2 dm^3 mol^{-1} are assumed, k_i = 540 and 455 s^{-1} are obtained, which compare with k_{1d}* = <10 s^{-1} and k_{1c}* = 0.02 s^{-1}, consistent with the operation of an I_a mechanism. Ligand substitution on $[Mo_3S_4(H_2O)_8(OH)]^{3+}$ is characterized by k_{OH} = 1120 and 790 dm^3 mol^{-1} s^{-1} for NCS^- and Cl^-, respectively, from which k_i = 5600 and 3975 s^{-1} are calculated using K_o = 0.2 dm^3 mol^{-1}, and compare with k_{OHd}* = 7500, which is accompanied by $\Delta H^{\ddagger}$ = 83.0 kJ mol^{-1} and $\Delta S^{\ddagger}$ = 107.6 J K^{-1} mol^{-1}. The k_i magnitudes do not exceed k_{OHd}*, which is consistent with the possible operation of an I_d mechanism, as is the positive $\Delta S^{\ddagger}$ for water exchange. If these deductions that I_a and I_d mechanisms operate for ligand substitution on $[Mo_3S_4(H_2O)_9]^{4+}$ and $[Mo_3S_4(H_2O)_8(OH)]^{3+}$, respectively, are correct, this mechanistic change may be likened to the change from an I_d to an I_d mechanism for $[Fe(H_2O)_6]^{3+}$ and $[Fe(H_2O)_5(OH)]^{2+}$, respectively (Section III,G).

The replacement of μ_3-O in $[Mo_3O_4(H_2O)_9]^{4+}$ by μ_3-S and μ_3-Se causes 14- and sixfold decreases in the lability of the d-H_2O towards substitution by NCS^-, respectively (a *cis* retarding effect). In contrast, the subsequent progressive replacement of μ_2-O by μ_2-S and μ_2-Se shows

these μ_2-ligands to labilize d-H_2O (a *trans* labilizing effect) in the sequence μ_2-O < μ_2-S < μ_2-Se (*344–347*). Similar changes in lability are observed as μ_3-O and μ_2-O are replaced by μ_2-S in $[W_3O_4(H_2O_9)]^{4+}$ (*350, 351*). The influence of the nature of M and X on the lability of d-H_2O towards substitution by NCS^- is considerable, as is seen from Table XX. Thus, when M = either Mo or W, only the k_{OH} path is detected when X = O, but when X = S or Se (only when M = Mo), the k_1 path becomes important, consistent with the electron rich μ-S and μ-Se ligands labilizing d-H_2O, possibly as a consequence of S and Se *d*-orbitals becoming involved in bonding (*345*). The k_{-1} and k_{-OH} paths are similarly labilized. When Mo is replaced by W, an approximate 10-fold decrease in lability occurs. This decrease has been attributed to the greater participation of 5*d* orbitals than of 4*d* orbitals in bonding due to a relativistic expansion effect which causes the W–OH_2 bonds to be stronger than the Mo–OH_2 bonds (*357, 358*).

Substitutions of the waters on the tetranuclear cuboidal $[Mo_4S_4(H_2O)_{12}]^{4+/5+/6+}$ clusters by NCS^- are subject to statistical factors which reveal a significant degree of independence of the molybdenum centers towards ligand substitution. Thus, a statistical factor of 4 applies for substitution by NCS^- on $[Mo_4S_4(H_2O)_{12}]^{4+}$ when $[NCS^-]$ is in excess, whereas a statistical factor of unity applies when $[Mo_4S_4(H_2O)_{12}{}^{4+}]$ is in excess, as shown in Eq. (42), because there are four Mo(III) centers available for substitution (*359*). However, substitution by NCS^- on the mixed valence state $[Mo_4S_4(H_2O)_{12}]^{5+}$ occurs through two parallel paths, the faster of which is characterized by a statistical factor of 3 when $[NCS^-]$ is in excess and a statistical factor of one when $[Mo_4S_4(H_2O)_{12}{}^{5+}]$ is in excess. This is shown in Eq. (43) and is consistent with substitution occurring at the three Mo(III) centers. For the slower path, a statistical factor of unity applies in the

TABLE XX

RATE CONSTANTS FOR NCS^- SUBSTITUTION OF A d-H_2O IN $[M_3X_4(H_2O)_9]^{4+}$ IN WATER AT I = 2.00 mol dm^{-3} ($LiClO_4$) AND 298.2K

$[M_3X_4(H_2O)_9]^{4+}$	k_1/ $dm^3\ mol^{-1}\ s^{-1}$	k_{OH}/ $dm^3\ mol^{-1}\ s^{-1}$	k_{-1}/ s^{-1}	k_{-OH}/ s^{-1}	Ref.
$[Mo_3O_4(H_2O)_9]^{4+}$	—	4.8[a]	—	0.0172[a]	*343*
$[Mo_3S_4(H_2O)_9]^{4+}$	108	1120	~0.07	>1	*345*
$[Mo_3Se_4(H_2O)_9]^{4+}$	237	2000	—	—	*347*
$[W_3O_4(H_2O)_9]^{4+}$	—	1.2	—	0.00106	*349*
$[W_3S_4(H_2O)_9]^{4+}$	11.9	192	0.015	0.244	*351*

[a] I = 2.00 mol dm^{-3} (Li *p*-toluenesulfonate). Substitution by NCS^- at I = 2.00 mol dm^{-3} ($LiClO_4$) is approximately two times faster (*338*).

presence of either excess [NCS^-] or excess [$Mo_4S_4(H_2O)_{12}^{5+}$], as shown in Eq. (44), consistent with substitution occurring at the single Mo(IV) center. [In the solid state, x-ray diffraction studies of [$Mo_4S_4(H_2O)_{12}$](*p*-toluenesulfonate)$_5$ show the four Mo centers to be stereochemically equivalent (*360*), but it has been suggested that this may be a consequence of random packing such that the effect of averaging results in four apparently equivalent Mo centers (*361*). For substitution of NCS^- on [$Mo_4S_4(H_2O)_{12}$]$^{6+}$, a single pH-dependent rate process is observed, to which a statistical factor of two applies, as shown in Eq. (45) (*361*). The pH dependence is consistent with the operation of a conjugate base mechanism similar to that observed for the [$M_3X_4(H_2O)_9$]$^{4+}$ clusters, and the statistical factor of 2 is thought to arise either because substitution occurs at the two equivalent Mo(IV) centers, or because [$Mo_4S_4(H_2O)_{12}$]$^{6+}$ behaves as two mixed-valence Mo(IV)Mo(III) pairs in its substitution reactions.

$$k_{eq} = (k_f[NCS^-]/4) + k_{aq} = k_f[Mo_4S_4(H_2O)_{12}^{4+}] + k_{aq} \quad (42)$$
$$(k_f = 1.95\ dm^3\ mol^{-1}\ s^{-1};\ k_{aq} = 1.44 \times 10^{-3}\ s^{-1})$$

$$k_{eq1} = (k_{f1}[NCS^-]/3) + k_{aq1} = k_{f1}[Mo_4S_4(H_2O)_{12}^{5+}] + k_{aq1} \quad (43)$$
$$(k_{f1} = 0.116\ dm^3\ mol^{-1}\ s^{-1};\ k_{aq1} = 4.3 \times 10^{-5}\ s^{-1})$$

$$k_{eq2} = (k_{f2}[NCS^-]) + k_{aq2} = k_{f2}[Mo_4S_4(H_2O)_{12}^{5+}] + k_{aq2} \quad (44)$$
$$(k_{f2} = 1.66 \times 10^{-2}\ dm^3\ mol^{-1}\ s^{-1};\ k_{aq2} = 5.0 \times 10^{-6}\ s^{-1})$$

$$k_{eq} = (k_f + k_{fOH}[H]^{-1})([NCS^-]/2) + (k_{aq} + k_{aqOH}[H]^{-1}) \quad (45)$$
$$(k_f = 13.3\ dm^3\ mol^{-1}\ s^{-1};\ k_{fOH} = 5.13\ s^{-1};\ k_{aq} = 2.53 \times 10^{-3}\ s^{-1};\ k_{aqOH} = 1.08 \times 10^{-3}\ s^{-1})$$

The assignment of k_f to substitution at a Mo(III) center in [$Mo_4S_4(H_2O)_{12}$]$^{4+}$ is clear-cut, but comparison with the mixed-valence [$Mo_4S_4(H_2O)_{12}$]$^{5+}$ and [$Mo_4S_4(H_2O)_{12}$]$^{6+}$ is not simple, as a degree of electron delocalization between the formally Mo(III) and Mo(IV) states may substantially change labilities. The lifetime of ion-pairing at a Mo(III) or Mo(IV) center as compared with the exchange between Mo(III) and Mo(IV) sites is thought to be a controlling factor in the slow (~1 day) substitution processes of the 5+ cluster. It is anticipated that the K_o characterizing the 4+, 5+, and 6+ clusters will increase substantially with increase in charge. However, for NCS^- substitution of d-H_2O on [$Mo_3S_4(H_2O)_9$]$^{4+}$, k_f = 108 $dm^3\ mol^{-1}\ s^{-1}$ and k_{fOH} = 248 s^{-1}. By comparison with the analogous data for [$Mo_4S_4(H_2O)_{12}$]$^{4+/5+/6+}$ [Eqs. (42)–(45)], this is in accord with the greater *trans* labilizing effect of the μ_2-S ligand on d-H_2O by comparison with that of μ_3-S discussed earlier.

The trinuclear acetato-bridged dioxo-capped clusters (III in Fig. 15) $[Mo_3(\mu_3\text{-}O)_2(\mu_2\text{-}CH_3CO_2)_6(H_2O)_3]^{2+}$ [k_{H_2O} (298 K) = 5.6×10^{-6} s^{-1}, $\Delta H^{\ddagger}$ = 126 kJ mol^{-1}, and $\Delta S^{\ddagger}$ = 77 J K^{-1} mol^{-1}] and $[W_3(\mu_3\text{-}O)_2(\mu_2\text{-}CH_3CO_2)_6(H_2O)_3]^{2+}$ [k_{H_2O} (298 K) = 1.02×10^{-6} s^{-1}, $\Delta H^{\ddagger}$ = 58 kJ mol^{-1}, and $\Delta S^{\ddagger}$ = -164 J K^{-1} mol^{-1}] and the monooxo-capped $[W_3(\mu_3\text{-}O)(\mu_2\text{-}CH_3CO_2)_6(H_2O)_3]^{2+}$ (IV in Fig. 15) [k_{H_2O} (298 K) = 5.3×10^{-4} s^{-1} and $\Delta H^{\ddagger}$ = 53 kJ mol^{-1} and $\Delta S^{\ddagger}$ = -131 J K^{-1} mol^{-1}] are substantially less labile towards water exchange and ligand substitution than are the $[M_3X_4(H_2O)_9]^{4+}$ clusters (*362*). Thus, water exchange of d-H_2O in $[M_3O_4(H_2O)_9]^{4+}$ is $\sim 10^8$ times more rapid than water exchange on $[Mo_3(\mu_3\text{-}O)_2(\mu_2\text{-}CH_3CO_2)_6(H_2O)_3]^{2+}$, and substitution by NCS^- on the latter cluster is also slower. These differences may be attributed to conjugate base labilization of d-H_2O in $[M_3O_4(H_2O)_9]^{4+}$. Saturation kinetics are observed for the substitution of NCS^- on $[Mo_3(\mu_3\text{-}O)_2(\mu_2\text{-}CH_3CO_2)_6(H_2O)_3]^{2+}$ in excess [NCS^-], consistent with the operation of an interchange mechanism, and the $k_i = 9.4 \times 10^{-6}$ s^{-1} value is comparable to $k_{H_2O} = 5.6 \times 10^{-6}$ s^{-1} for water exchange at 298 K. This, in combination with the similar large $\Delta H^{\ddagger}$ and positive $\Delta S^{\ddagger}$ for water exchange and NCS^- substitution, is probably indicative of an $\mathbf{I}_d$ mechanism. Substitution by $C_2O_2^{2-}$ may similarly be interpreted in terms of an $\mathbf{I}_d$ mechanism. However, substitution by $HC_2O_2^-$ is characterized by a smaller $\Delta H^{\ddagger}$ and negative $\Delta S^{\ddagger}$, which probably indicates a change to a concerted mechanism whereby the oxygen from the substituted water and the entering $HC_2O_2^-$ are interchanged during the substitution process. The k_{H_2O} and ligand substitution data for $[W_3(\mu_3\text{-}O)_2(\mu_2\text{-}CH_3CO_2)_6(H_2O)_3]^{2+}$ and $[W_3(\mu_3\text{-}O)(\mu_2\text{-}CH_3CO_2)_6(H_2O)_3]^{2+}$ and NCS^- substitution data for the latter cluster have been interpreted in terms of an $\mathbf{I}_a$ mechanism, whereas the substitution of CD_3OD on the latter cluster has been interpreted in terms of a **d**-activated mechanism (*363*). Relative to ligand substitution studies at single metal centers, studies of these and other clusters are at an early stage. It is to be expected that they will provide a rewarding area for continuing mechanistic study.

VI. Concluding Comments

It is salutary to read the comment, "At the time when I became interested in the reactions of coordination compounds the formula of not a single aquo complex was known with certainty," made by Taube in a recent review (*364*). In marked contrast, this review is predominantly concerned with the intimate detail of the mechanisms of sol-

vent exchange and ligand substitution on solvated metal ions of well-established stoichiometry. This illustrates the remarkable acquisition of knowledge which has occurred over a few decades, during which exciting advances in the mechanistic interpretation of the process of ligand substitution occurred in parallel with the development of new methods for the study of ligand substitution. A few of these advances and developments are now discussed. It is probable that Garrick's paper on a conjugate base mechanism for labilizing complexes such as $[Co(NH_3)_5Br]^{2+}$ was the first concerning the intimate mechanism of ligand substitution at a metal center (*365*). This was the precursor to the lively debate on the role of hydroxide in accelerating the aquation of acidopentamminecobalt(III) complexes (*366–368*). In its turn, this was probably a major stimulus for the publication of the first edition of *Mechanisms of Inorganic Reactions* by Basolo and Pearson (*104*), which generated great interest in the mechanisms of ligand substitution amongst those of other inorganic reactions. The development of techniques for studying fast reactions by Eigen (*1*) and his colleagues, together with the development of an NMR method for the direct determination of water exchange on labile paramagnetic metal ions by Swift and Connick (*257*), opened the door to the study of the wide range of metal ions discussed in this review. Subsequently, this facilitated the variable-pressure studies (*6–9*) which have provided major new mechanistic insight, and which feature strongly in this review.

Despite the stimulus these intellectual and technological advances provided to mechanistic study of an extensive range of metal ions, for a long time the discussion of ligand substitution mechanisms centered largely on the relatively slow ligand substitutions occurring in amminecobalt(III) and platinum(II) complexes. This was probably because access to equipment for studying rapid reactions was largely restricted to those with the resources to build it. Nevertheless, this period gave rise to the **D**, **I**, and **A** terminologies used in this review, which replaced the S_{N1} and S_{N2} classifications borrowed from organic chemistry (*34*). With the increase in the commercial availability of rapid reaction technology in this and the preceding decade, it is now a normal expectation that reports of ligand substitution studies encompassing metal centers ranging from Li^+ to UO_2^{2+} will be found in the current chemical literature.

This very truncated survey of the history of the study of ligand substitution studies brings us to the present and the question of future directions. Although this review predominantly deals with solvent exchange and monodentate ligand substitution processes, the ideas ex-

plored also apply to the fascinating chemistry of substitution by multidentate ligands and their complexes, as the reader will discover in the several excellent sources available (*15, 369, 370*). A cursory inspection of the current journal shelf in a chemical library quickly reveals that the mechanistic approach to ligand substitution has been extended into the burgeoning area of bioinorganic chemistry. It is fascinating to see that in a recent review, Williams has classified aspects of metal ion involvement in life processes on a reaction time scale of fast exchange, slow exchange, and no exchange, which is largely based on metal ion lability (*371*). There seems little doubt that an understanding of ligand substitution processes will prove to be very important in bioinorganic chemistry. Despite this broadening of the scope of ligand substitution studies, it is apparent from this review that there remain significant questions still to be answered concerning ligand substitution processes on the solvated metal ion. Not least among these is the question of the role played by solvent beyond the first coordination sphere in the ligand substitution process. It seems probable that a substantial aid in the search for an answer to this and other mechanistic questions will prove to be computer modeling (*315, 372*).

VII. Appendix: Ligand Abbreviations, Formulae, and Structures

bpy = 2,2′-bipyridine =

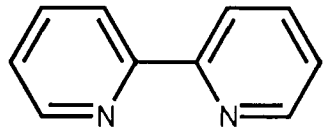

cyclen = 1,4,7,10-tetraazacyclododecane =

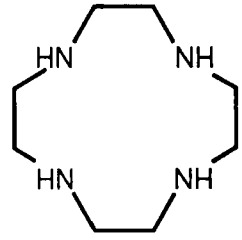

DEA = *N,N*-diethylacetamide = $OC(Me)N(Et)_2$

dien = diethylenetriamine =

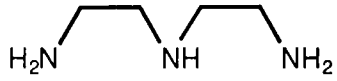

$DOTA^{4-}$ = 1,4,7,10-tetraazacyclododecane-*N*,*N*′,*N*″,*N*‴-tetraacetate =

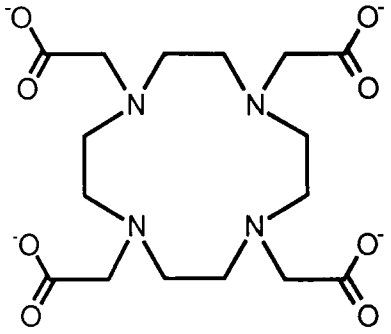

$DTPA^{5-}$ = diethylenetriamine-*N*,*N*,*N*′,*N*″,*N*″-pentaacetate =

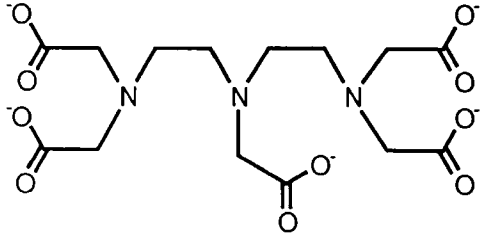

DMA = *N*,*N*-dimethylacetamide = $OC(Me)(NMe_2)$
DMADMP = *O*,*O*′-dimethyl-*N*,*N*-dimethylphosphoramidate = $OP(Me)_2(NMe_2)$
DMF = *N*,*N*-dimethylformamide = $OC(H)(NMe_2)$
DMMP = dimethyl methylphosponate = $OP(OMe)_2(Me)$
DMPU = dimethypropyleneurea =

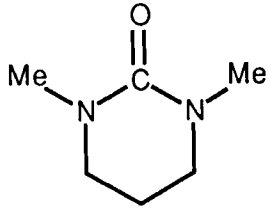

DMSO = dimethylsulfoxide = $OSMe_2$
DTPA-BMA^{3-} = *N*,*N*′-bis[(*N*-methylcabamoyl)methyl]-3-azapentane-1,5-diamine-3,*N*,*N*′-triacetate =

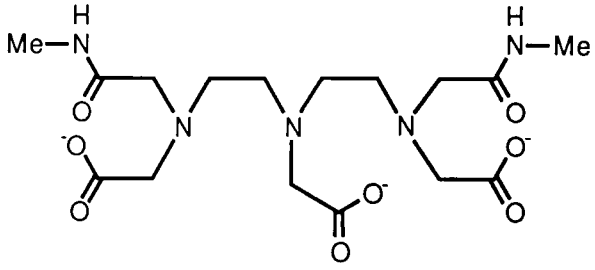

EDTA^{4-} = 1,2-diaminoethane-*N*,*N*,*N*′,*N*′-tetraacetate =

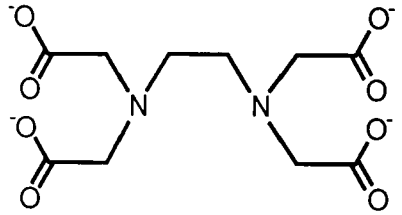

en = 1,2-diaminoethane =

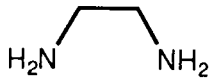

Et_5dien = *N*,*N*,*N*′,*N*″,*N*″-pentaethyldiethylenetriamine =

Hipt = 4-isopropyltropolone =

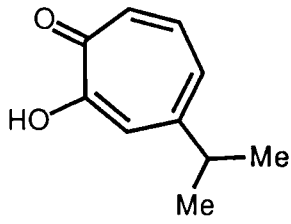

HMPA = hexamethylphosphoramide = $OP(NMe_2)_3$
Me_4cyclam = *N,N',N'',N'''*-tetramethyl- = 1,4,8,11-tetraazacyclotetradecane =

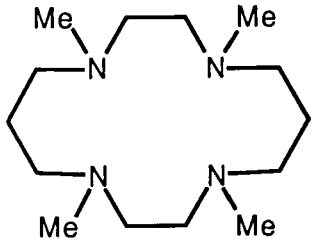

Me_5dien = *N,N,N',N'',N''*-pentamethyldiethylenetriamine =

Me_6tren = 2,2',2''-tri(*N,N*-dimethylamino)triethylamine =

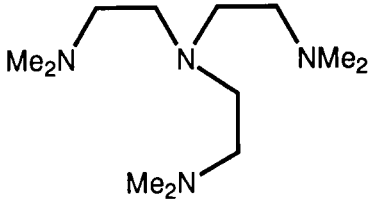

MMPP = methyl methylphenylphosphinate = OP(OMe)(Me)(Ph)
NMA = *N*-methylacetamide = OC(Me)N(H)(Me)
NMP^+ = *N*-methylpyrazinium cation =

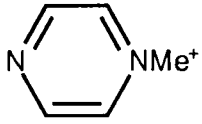

pada = *trans*-pyridine-2-azo(*p*-dimethylaniline) =

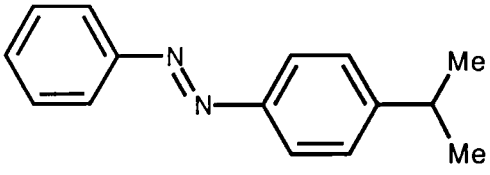

$PDTA^{4-}$ = 1,3-propylenediaminetetraacetate =

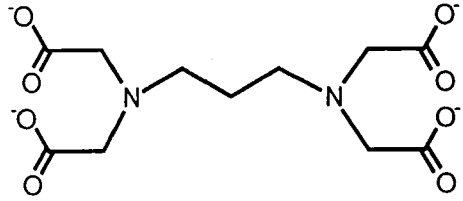

TMP = trimethylphosphate = $OP(OMe)_3$
TMU = *N,N,N',N'*-tetramethylurea = $OC(NMe_2)_2$
tren = 2,2',2''-triaminotriethylamine =

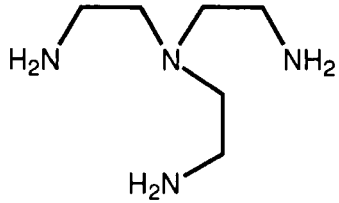

trien = triethylenetetramine =

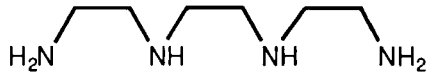

tpy = 2,2',2''-terpyridine =

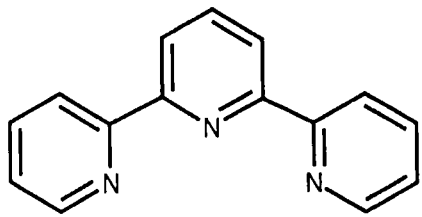

References

1. Eigen, M., *Pure Appl. Chem.* **6,** 97 (1963).
2. Shannon, R. D., *Acta Crystallogr., Sect. A: Cryst. Phys., Diffr., Theor. Gen. Crystallogr.* **A32,** 751 (1976).
3. Neilson, G. W., and Enderby, J. E., *Adv. Inorg. Chem.* **34,** 195 (1989).
4. Swaddle, T. W., *Adv. Inorg. Bioinorg. Mech.* **2,** 95 (1983).
5. Lincoln, S. F., *Coord. Chem. Rev.* **6,** 309 (1971).
6. Merbach, A. E., *Pure Appl. Chem.* **54,** 1479 (1982).
7. Merbach, A. E., *Pure Appl. Chem.* **59,** 161 (1987).
8. Merbach, A. E., and Akitt, J. W., *NMR: Basic Princ. Prog.* **24,** 189 (1990).

9. van Eldik, R., and Merbach, A. E., *Comments Inorg. Chem.* **12,** 341 (1992).
10. Lincoln, S. F., *Adv. Inorg. Bioinorg. Mech.* **4,** 217 (1986).
11. Cossy, C., and Merbach, A. E., *Pure Appl. Chem.* **60,** 1785 (1988).
12. Stranks, D. R., *Pure Appl. Chem.* **38,** 303 (1974).
13. Beck, M. T., *Coord. Chem. Rev.* **3,** 91 (1968).
14. Wilkins, R. G., *Adv. Inorg. Bioinorg. Mech.* **2,** 139 (1983).
15. Wilkins, R. G., "Kinetics and Mechanisms of Reactions of Transition Metal Complexes." VCH, Weinheim, 1991.
16. Strehlow, H., "Rapid Reactions in Solution." VCH, Weinheim, 1992.
17. Eigen, M., and Tamm, K., *Z. Elektrochem.* **66,** 93, 107 (1962).
18. Bechtler, A., Breitschwerdt, K. G., and Tamm, K., *J. Chem. Phys.* **52,** 2975 (1970).
19. Eigen, M., and Wilkins, R. G., *Adv. Chem. Ser.* **49,** 55 (1965).
20. Fuoss, R. M., *J. Am. Chem. Soc.* **80,** 5059 (1958).
21. Swaddle, T. W., *Rev. Phys. Chem. Jpn.* **50,** 230 (1980).
22. Swaddle, T. W., *Coord. Chem. Rev.* **14,** 217 (1974).
23. Mønsted, L., and Mønsted, O., *Coord. Chem. Rev.* **94,** 109 (1989).
24. Lay, P. A., *Coord. Chem. Rev.* **110,** 213 (1991).
25. Lay, P. A., *Comments Inorg. Chem.* **11,** 235 (1991).
26. Swaddle, T. W., *Comments Inorg. Chem.* **12,** 237 (1991).
27. Schroeder, J., and Troe, J., *Annu. Rev. Phys. Chem.* **38,** 163 (1987).
28. Troe, J., *J. Phys. Chem.* **90,** 357 (1986).
29. Troe, J., *High Pressure Res.* **5,** 625 (1990).
30. Frauenfelder, H., and Wolynes, P. G., *Science* **229,** 337 (1985).
31. Jonas, J., *Acc. Chem. Res.* **17,** 74 (1984).
32. Cross, R. J., *Chem. Soc. Rev.* **14,** 197 (1985).
33. Cross, R. J., *Adv. Inorg. Chem.* **34,** 219 (1989).
34. Langford, C. H., and Gray, H. B., "Ligand Substitution Dynamics." Benjamin, New York, 1965.
35. Garrison, J. M., and Crumbliss, A. L., *Inorg. Chem.* **26,** 3660 (1987).
36. Nichols, P. J., and Grant, M. W., *Aust. J. Chem.* **31,** 2581 (1978).
37. Neely, J., and Connick, R. E., *J. Am. Chem. Soc.* **92,** 3476 (1970).
38. Langford, C. H., and Muir, W. R., *J. Am. Chem. Soc.* **89,** 3141 (1967).
39. Pearson, R. G., *J. Am. Chem. Soc.* **85,** 3533 (1963).
40. Pearson, R. G., *Coord. Chem. Rev.* **100,** 403 (1990).
41. Swaddle, T. W., *Inorg. Chem.* **22,** 2663 (1983).
42. Swaddle, T. W., and Mak, M. K. S., *Can. J. Chem.* **61,** 473 (1983).
43. Ducommun, Y., and Merbach, A. E., *in* "Inorganic High Pressure Chemistry" (R. van Eldik, ed.), p. 69. Elsevier, Amsterdam, 1986.
44. Merbach, A. E., *in* "High Pressure Chemistry and Biochemistry" (R. van Eldik and J. Jonas, eds.), p. 311. Reidel, Dordrecht, The Netherlands, 1987.
45. van Eldik, R., *in* "High Pressure Chemistry and Biochemistry" (R. van Eldik and J. Jonas, eds.), p. 333. Reidel, Dordrecht, The Netherlands, 1987.
46. Ducommun, Y., Newman, K. E., and Merbach, A. E., *Inorg. Chem.* **19,** 3696 (1980).
47. Ducommun, Y., Zbinden, D., and Merbach, A. E., *Helv. Chim. Acta* **65,** 1385 (1982).
48. Swaddle, T. W., *Inorg. Chem.* **19,** 3203 (1980).
49. Hugi, A. D., Helm, L., and Merbach, A. E., *Inorg. Chem.* **26,** 1763 (1987).
50. Swaddle, T. W., and Merbach, A. E., *Inorg. Chem.* **20,** 4212 (1981).
51. Xu, F.-C., Krouse, H. R., and Swaddle, T. W., *Inorg. Chem.* **24,** 267 (1985).
52. Hugi, A. D., Helm, L., and Merbach, A. E., *Helv. Chim. Acta* **68,** 508 (1985).
53. Hugi-Cleary, D., Helm, L., and Merbach, A. E., *J. Am. Chem. Soc.* **109,** 4444 (1987).

54. Lehn, J.-M., *Pure Appl. Chem.* **51,** 979 (1979).
55. Gokel, G. W., "Crown Ethers and Cryptands." Royal Society of Chemistry, Cambridge, UK, 1991.
56. Lincoln, S. F., Brereton, I. M., and Spotswood, T. M., *J. Am. Chem. Soc.* **108,** 8134 (1986).
57. Stephens, A. K. W., and Lincoln, S. F., *Inorg. Chem.* **30,** 3529 (1991).
58. Stephens, A. K. W., and Lincoln, S. F., *J. Chem. Soc., Dalton Trans.*, 2123 (1993).
59. Pittet, P.-A., Elbaze, G., Helm, L., and Merbach, A. E., *Inorg. Chem.* **29,** 1936 (1990).
60. Alei, M., and Jackson, J. A., *J. Chem. Phys.* **41,** 3402 (1964).
61. Frahm, J., and Füldner, H.-H., *Ber. Bunsenges. Phys. Chem.* **84,** 173 (1980).
62. Yamaguchi, T., Ohtaki, H., Spohr, E., Pálinkás, G., Heinzinger, K., and Probst, M. M., *Z. Naturforsch., A* **41A,** 1175 (1986).
63. Dance, I. G., and Freeman, H. C., *Acta Crystallogr., Sect. B: Struct. Crystallogr. Cryst. Chem.* **B25,** 304 (1969).
64. Sikka, S. K., and Chidambaram, R., *Acta Crystallogr., Sect. B: Struct. Crystallogr. Cryst. Chem.* **B25,** 310 (1969).
65. Piganet, C., *J. Raman Spectrosc.* **13,** 66 (1982).
66. Strehlow, H., and Knocke, W., *Ber. Bunsenges. Phys. Chem.* **73,** 427 (1969).
67. Lincoln, S. F., and Tkaczuk, M. N., *Ber. Bunsenges. Phys. Chem.* **85,** 433 (1981).
68. Delpuech, J. J., Peguy, A., Rubini, P., and Steinmetz, J., *Nouv. J. Chim.*, 133 (1977).
69. Tkaczuk, M. N., and Lincoln, S. F., *Ber. Bunsenges. Phys. Chem.* **86,** 147 (1982).
70. Lincoln, S. F., and Tkaczuk, M. N., *Ber. Bunsenges. Phys. Chem.* **86,** 221 (1982).
71. Tkaczuk, M. N., and Lincoln, S. F., *Aust. J. Chem.* **35,** 1555 (1982).
72. Bock, C. W., and Glusker, J. P., *Inorg. Chem.* **32,** 1242 (1993).
73. Inamo, M., Ishihara, K., Funahashi, S., Ducommun, Y., and Merbach, A. E., *Inorg. Chem.* **30,** 1580 (1991).
74. Amari, T., Funahashi, S., and Tanaka, M., *Inorg. Chem.* **27,** 3368 (1988).
75. Baldwin, W. G., and Stranks, D. R., *Aust. J. Chem.* **21,** 2161 (1968).
76. Pittet, P.-A., Université de Lausanne, private communication.
77. Furrer, P., Frey, U., Helm, L., and Merbach, A. E., *High Pressure Res.* **7,** 144 (1991).
78. Pisaniello, D., and Lincoln, S. F., *Aust. J. Chem.* **32,** 715 (1979).
79. Pisaniello, D., Lincoln, S. F., and Williams, E. H., *Inorg. Chim. Acta* **31,** 237 (1978).
80. Nakumura, S., and Meiboom, S., *J. Am. Chem. Soc.* **89,** 1765 (1967).
81. Alger, T. D., *J. Am. Chem. Soc.* **91,** 2220 (1969).
82. Hugi-Cleary, D., Helm, L., and Merbach, A. E., *Helv. Chim. Acta* **68,** 545 (1985).
83. Amman, C., Moore, P., Merbach, A. E., and McAteer, C. H., *Helv. Chim. Acta* **63,** 268 (1980).
84. Merbach, A. E., Moore, P., Howarth, O. W., and McAteer, C. H., *Inorg. Chim. Acta* **39,** 129 (1980).
85. Delpuech, J.-J., Khaddar, M. R., Peguy, A. A., and Rubini, P. R., *J. Am. Chem. Soc.* **97,** 3377 (1975).
86. Roderhüser, L., Rubini, P. R., and Delpuech, J.-J., *Inorg. Chem.* **16,** 2837 (1977).
87. Helm, L., Amman, C., and Merbach, A. E., *Z. Phys. Chem. (Wiesbaden)* [N.S.] **155,** 145 (1987).
88. Pisaniello, D. L., Lincoln, S. F., and Williams, E. H., *J. Chem. Soc., Dalton Trans.*, 1473 (1979).
89. Pisaniello, D. L., and Lincoln, S. F., *Inorg. Chim. Acta* **36,** 85 (1979).
90. Pisaniello, D. L., and Lincoln, S. F., *J. Chem. Soc., Dalton Trans.*, 699 (1980).
91. Glass, G. E., Schwabacher, W. B., and Tobias, R. S., *Inorg. Chem.* **7,** 2471 (1968).

92. Pisaniello, D. L., Nichols, P. J., Ducommun, Y., and Merbach, A. E., *Helv. Chim. Acta* **65,** 1025 (1982).
93. Pisaniello, D. L., Helm, L., Meier, P., and Merbach, A. E., *J. Am. Chem. Soc.* **105,** 4528 (1983).
94. Campisi, A., and Tregloan, P. A., *Inorg. Chim. Acta* **100,** 251 (1985).
95. Grant, M., and Jordan, R. B., *Inorg. Chem.* **20,** 55 (1981).
96. Yamada, S., Iwanagawa, A., Funahashi, S., and Tanaka, M., *Inorg. Chem.* **23,** 3528 (1984).
97. Meyer, F. K., Newman, K. E., and Merbach, A. E., *J. Am. Chem. Soc.* **101,** 5588 (1979).
98. Rode, B. M., Reibnegger, G. J., and Fujiwara, S., *J. Chem. Soc., Faraday Trans. 2* **76,** 1268 (1980).
99. Powell, D. H., Helm, L., and Merbach, A. E., *J. Chem. Phys.* **95,** 9258 (1991).
100. Laurenczy, G., Ducommun, Y., and Merbach, A. E., *Inorg. Chem.* **28,** 3024 (1989).
101. Hugi-Cleary, D., Helm, L., and Merbach, A. E., *Inorg. Chem.* **26,** 1763 (1987).
102. Li, C., and Jordan, R. B., *Inorg. Chem.* **26,** 3855 (1987).
103. Helm, L., Lincoln, S. F., Merbach, A. E., and Zbinden, D., *Inorg. Chem.* **25,** 2550 (1986).
104. Basolo, F., and Pearson, R. G., "Mechanisms of Inorganic Rections." Wiley, New York, 1967.
105. Companion, A., *J. Phys. Chem.* **73,** 739 (1969).
106. Krishnamurthy, R., and Schaap, W. B., *J. Chem. Educ.* **46,** 799 (1969).
107. Spees, S. T., Perumareddi, J. R., and Adamson, A. W., *J. Phys. Chem.* **72,** 1822 (1968).
108. Rusnak, L. L., Yang, E. S., and Jordan, R. B., *Inorg. Chem.* **17,** 1810 (1978).
109. Cossy, C., Helm, L., and Merbach, A. E., *Helv. Chim. Acta* **70,** 1516 (1987).
110. Hioki, A., Funahashi, S., Ishi, M., and Tanaka, M., *Inorg. Chem.* **25,** 1360 (1986).
111. Breivogel, F. W., *J. Chem. Phys.* **51,** 445 (1969).
112. Luz, Z., and Meiboom, S., *J. Chem. Phys.* **40,** 2686 (1964).
113. Meyer, F. K., Newman, K. E., and Merbach, A. E., *Inorg. Chem.* **18,** 2142 (1979).
114. Sisley, M. J., Yano, Y., and Swaddle, T. W., *Inorg. Chem.* **21,** 1141 (1982).
115. Yano, Y., Fairhurst, M., and Swaddle, T. W., *Inorg. Chem.* **19,** 3267 (1980).
116. Monnerat, A., Moore, P., Newman, K. E., and Merbach, A. E., *Inorg. Chim. Acta* **47,** 139 (1981).
117. Matwiyoff, N., *Inorg. Chem.* **5,** 788 (1966).
118. Ishii, M., Funahashi, S., and Tanaka, M., *Chem. Lett.,* 871 (1987).
119. Fielding, L., and Moore, P., *J. Chem. Soc., Chem. Commun.,* 49 (1988).
120. Ishii, M., Funahashi, S., and Tanaka, M., *Inorg. Chem.* **27,** 3192 (1988).
121. Batstone-Cunningham, R. L., Dodgen, W. H., and Hunt, J. P., *Inorg. Chem.* **21,** 3831 (1982).
122. Soyama, S., Ishii, M., Funahashi, S., and Tanaka, M., *Inorg. Chem.* **31,** 536 (1992).
123. Ishii, M., Funahashi, S., Ishihara, K., and Tanaka, M., *Bull. Chem. Soc. Jpn.* **62,** 1852 (1989).
124. Frankel, L. S., *Inorg. Chem.* **10,** 2360 (1971).
125. Lincoln, S. F., Hounslow, A. M., and Boffa, A. N., *Inorg. Chem.* **25,** 1038 (1986).
126. West, R. J., and Lincoln, S. F., *J. Chem. Soc., Dalton Trans.,* 281 (1974).
127. Poupko, R., and Luz, Z., *J. Chem. Phys.* **57,** 3311 (1972).
128. Licheri, G., Musinu, A., Pashina, G., Piccaluga, G., Pinna, G., and Sedda, A. F., *J. Chem. Phys.* **80,** 5308 (1984).
129. Sham, T. K., Hastings, J. B., and Perlman, M. L., *Chem. Phys. Lett.* **83,** 391 (1981).

130. Tajiri, Y., and Wakita, H., *Bull. Chem. Soc. Jpn.* **59,** 2285 (1986).
131. Onori, G., Santucci, A., Scafati, A., Belli, M., and Della Lonza, S., *Chem. Phys. Lett.* **149,** 289 (1988).
132. Magini, M., *Inorg. Chem.* **21,** 1535 (1982).
133. Salmon, P. S., and Neilson, G. W., *J. Phys.: Condens. Matter* **1,** 5291 (1989).
134. Wilkins, R. G., *Acc. Chem. Res.* **3,** 408 (1970).
135. Mohr, R., Mietta, L. A., Ducommun, Y., and van Eldik, R., *Inorg. Chem.* **24,** 757 (1985).
136. Caldin, E. F., Grant, M. W., and Hasinoff, B. B., *J. Chem. Soc., Faraday Trans. 1* **68,** 2247 (1972).
137. Yu, A. D., Waissbluth, M. D., and Greiger, R. A., *Rev. Sci. Instrum.* **44,** 1390 (1973).
138. Ishihara, K., Funahashi, S., and Tanaka, M., *Inorg. Chem.* **22,** 2564 (1983).
139. Caldin, E. F., and Greenwood, R. C., *J. Chem. Soc., Faraday Trans. 1* **77,** 773 (1981).
140. Doss, R., van Eldik, R., and Kelm, H., *Rev. Sci. Instrum.* **53,** 1592 (1982).
141. Doss, R., and van Eldik, R., *Inorg. Chem.* **21,** 4108 (1982).
142. Mohr, R., and van Eldik, R., *Inorg. Chem.* **24,** 3396 (1985).
143. Ducommun, Y., Laurenczy, G., and Merbach, A. E., *Inorg. Chem.* **27,** 1148 (1988).
144. Nichols, P. J., Ducommun, Y., and Merbach, A. E., *Inorg. Chem.* **22,** 3993 (1983).
145. Grant, M. W., *J. Chem. Soc., Faraday Trans. 1* **69,** 560 (1973).
146. Jost, A., *Ber. Bunsenges. Phys. Chem.* **79,** 850 (1975).
147. Ducommun, Y., Nichols, P. J., and Merbach, A. E., *Inorg. Chem.* **28,** 2643 (1989).
148. Nichols, P. J., Frésard, Y., Ducommun, Y., and Merbach, A. E., *Inorg. Chem.* **23,** 4341 (1984).
149. Desai, A. G., Dodgen, H. W., and Hunt, J. P., *J. Am. Chem. Soc.* **92,** 798 (1970).
150. Desai, A. G., Dodgen, H. W., and Hunt, J. P., *J. Am. Chem. Soc.* **91,** 5001 (1969).
151. Rablen, D. P., Dodgen, H. W., and Hunt, J. P., *J. Am. Chem. Soc.* **94,** 1771 (1972).
152. Coates, J. H., Hadi, D. A., Lincoln, S. F., Dodgen, H. W., and Hunt, J. P., *Inorg. Chem.* **20,** 707 (1981).
153. Moore, P., *Pure Appl. Chem.* **57,** 347 (1985).
154. Grant, M., Dodgen, H. W., and Hunt, J. P., *J. Am. Chem. Soc.* **92,** 2321 (1970).
155. Rablen, D. P., and Gordon, G., *Inorg. Chem.* **8,** 395 (1969).
156. Lincoln, S. F., Aprile, F., Dodgen, H. W., and Hunt, J. P., *Inorg. Chem.* **7,** 929 (1968).
157. Jordan, R. B., Dodgen, H. W., and Hunt, J. P., *Inorg. Chem.* **5,** 1906 (1966).
158. Grant, M., Dodgen, H. W., and Hunt, J. P., *Chem. Commun.*, 1446 (1970).
159. Hunt, J. P., *Coord. Chem. Rev.* **7,** 1 (1971).
160. West, R. J., and Lincoln, S. F., *J. Chem. Soc., Dalton Trans.*, 282 (1974).
161. Lincoln, S. F., Hounslow, A. M., Doddridge, B. G., Pisaniello, D. L., Coates, J. H., Merbach, A. E., and Zbinden, D., *Inorg. Chem.* **23,** 1090 (1984).
162. West, R. J., and Lincoln, S. F., *Inorg. Chem.* **12,** 494 (1973).
163. Lincoln, S. F., Hounslow, A. M., and Coates, J. H., *Inorg. Chim. Acta* **77,** L7 (1983).
164. Lincoln, S. F., and West, R. J., *J. Am. Chem. Soc.* **96,** 400 (1974).
165. Rapaport, I., Helm, L., Merbach, A. E., Bernhard, P., and Ludi, A., *Inorg. Chem.* **27,** 873 (1988).
166. Ojo, J. F., Olubuyide, O., and Oyetunji, O., *J. Chem. Soc., Dalton Trans.*, 957 (1987).
167. Luginbühl, W., Zbinden, P., Pittet, P.-A., Armbruster, T., Bürgi, H.-B., Merbach, A. E., and Ludi, A., *Inorg. Chem.* **30,** 2350 (1991).
168. Stebler-Röthlisberger, M., Hummel, W., Pittet, P.-A., Bürgi, H.-B., Ludi, A., and Merbach, A. E., *Inorg. Chem.* **27,** 1358 (1988).
169. Bernhard, P., Bürgi, H.-B., Hauser, J., Lehmann, H., and Ludi, A., *Inorg. Chem.* **21,** 3936 (1982).

170. Gress, M. E., Creutz, C., and Quicksall, C. O., *J. Am. Chem. Soc.* **103,** 981 (1981).
171. Lehmann, H., Schenk, K. J., Chapuis, G., and Ludi, A., *J. Am. Chem. Soc.* **101,** 6197 (1979).
172. Kallen, T. W., and Earley, J. E., *Inorg. Chem.* **10,** 1149 (1971).
173. Patel, A., Leitch, P., and Richens, D. T., *J. Chem. Soc., Dalton Trans.,* 1029 (1991).
174. Aebischer, N., Laurenczy, G., Ludi, A., and Merbach, A. E., *Inorg. Chem.* **32,** 2810 (1993).
175. Karlen, T., University of Bern, private communication (1993).
176. Sisley, M. J., and Swaddle, T. W., *Inorg. Chem.* **20,** 2799 (1981).
177. Allen, A. D., and Senoff, C. V., *Chem. Commun.,* 621 (1965).
178. Laurenczy, G., Helm, L., Ludi, A., and Merbach, A. E., *Inorg. Chim. Acta* **189,** 131 (1991).
179. Dellavia, I., Helm, L., and Merbach, A. E., *Inorg. Chem.* **31,** 2230 (1992).
180. Dellavia, I., Sauvageat, P.-Y., Helm, L., Ducommun, Y., and Merbach, A. E., *Inorg. Chem.* **31,** 792 (1992).
181. Carle, D. L., and Swaddle, T. W., *Can. J. Chem.* **51,** 3795 (1973).
182. Lo, S. T. D., and Swaddle, T. W., *Inorg. Chem.* **14,** 1878 (1975).
183. Meyer, F. K., Monnerat, A. R., Newman, K. E., and Merbach, A. E., *Inorg. Chem.* **21,** 774 (1982).
184. Laurenczy, G., Rapaport, I., Zbinden, D., and Merbach, A. E., *Magn. Reson. Chem.* **29,** S45 (1991).
185. Armstrong, R. S., Beattie, J. K., Best, S. P., Skelton, B. W., and White, A. H., *J. Chem. Soc., Dalton Trans.,* 1973 (1983).
186. Castillo-Blum, S. E., Sykes, A. G., and Gamsjäger, H., *Polyhedron* **6,** 101 (1987).
187. Bernhard, P., Helm, L., Rapaport, I., Ludi, A., and Merbach, A. E., *J. Chem. Soc., Chem. Commun.,* 302 (1984).
188. Bernhard, P., Helm, L., Ludi, A., and Merbach, A. E., *Inorg. Chem.* **107,** 312 (1985).
189. Chaudhuri, P., and Diebler, H., *Z. Phys. Chem. (Wiesbaden)* [N.S.] **139,** 191 (1984).
190. Diebler, H., *Z. Phys. Chem. (Wiesbaden)* [N.S.] **68,** 64 (1969).
191. Chaudhuri, P., and Diebler, H., *J. Chem. Soc., Dalton Trans.,* 1693 (1986).
192. Chaudhuri, P., and Diebler, H., *J. Chem. Soc., Dalton Trans.,* 596 (1977).
193. Perlmutter-Hayman, B., and Tapuhi, E., *Inorg. Chem.* **18,** 2872 (1979).
194. Cavasino, F. P., *J. Phys. Chem.* **72,** 1378 (1968).
195. Funahashi, S., Adachi, S., and Tanaka, M., *Bull. Chem. Soc. Jpn.* **46,** 479 (1973).
196. Hasinoff, B. B., *Can. J. Chem.* **54,** 1820 (1976).
197. Hasinoff, B. B., *Can. J. Chem.* **57,** 77 (1979).
198. Perlmutter-Hayman, B., and Tapuhi, E., *J. Coord. Chem.* **6,** 31 (1976).
199. Sasaki, Y., and Sykes, A. G., *J. Chem. Soc., Dalton Trans.,* 1048 (1975).
200. Richens, D. T., Ducommun, Y., and Merbach, A. E., *J. Am. Chem. Soc.* **109,** 603 (1987).
201. Sauvageat, P.-Y., Ducommun, Y., and Merbach, A. E., *Helv. Chim. Acta* **72,** 1801 (1989).
202. Funahashi, S., Ishihara, K., and Tanaka, M., *Inorg. Chem.* **22,** 2070 (1983).
203. Ishihara, K., Funahashi, S., and Tanaka, M., *Inorg. Chem.* **22,** 3589 (1983).
204. Conocchioli, T. J., Nancollas, G. H., and Sutin, N., *Inorg. Chem.* **5,** 1 (1971).
205. Davies, G., and Watkins, K. O., *J. Phys. Chem.* **74,** 3388 (1970).
206. McAuley, A., Malik, M. N., and Hill, J., *J. Chem. Soc.* A, 2461 (1970).
207. Navon, G., *J. Phys. Chem.* **85,** 3547 (1981).
208. Lo, S. T. D., and Swaddle, T. W., *Inorg. Chem.* **15,** 1881 (1976).
209. Swaddle, T. W., and Stranks, D. R., *J. Am Chem. Soc.* **94,** 8357 (1972).
210. Hunt, H. R., and Taube, H., *J Am Chem. Soc.* **80,** 2642 (1958).

211. Tong, S. B., and Swaddle, T. W., *Inorg. Chem.* **13,** 1538 (1974).
212. Doine, H., Ishihara, K., Krouse, H. R., and Swaddle, T. W., *Inorg. Chem.* **26,** 3240 (1987).
213. González, G., Moullet, B., Martinez, M., and Merbach, A. E., *Inorg. Chem.* **33,** 2330 (1994).
214. Lawrence, G. A., *Inorg. Chem.* **21,** 3687 (1982).
215. Curtis, N. J., Lawrence, G. A., and van Eldik, R., *Inorg. Chem.* **28,** 329 (1989).
216. Langford, C. H., *Inorg. Chem.* **4,** 265 (1965).
217. Haim, A., *Inorg. Chem.* **9,** 426 (1970).
218. Jones, W. E., Carey, L. R., and Swaddle, T. W., *Can. J. Chem.* **50,** 2739 (1972).
219. Swaddle, T. W., and Guastalla, G., *Inorg. Chem.* **7,** 1915 (1968).
220. Gaswick, D. C., and Malinak, S. M., *Inorg. Chem.* **32,** 175 (1993).
221. Ramasami, T., and Sykes, A. G., *Inorg. Chem.* **15,** 2885 (1976).
222. Arnau, C., Ferrer, M., Martinez, M., and Sánchez, A., *J. Chem. Soc., Dalton Trans.,* 1839 (1986).
223. Swaddle, T. W., and King, E. L., *Inorg. Chem.* **4,** 532 (1965).
224. Guastalla, G., and Swaddle, T. W., *J. Chem. Soc., Chem. Commun.,* 61 (1973).
225. Guastalla, G., and Swaddle, T. W., *Can. J. Chem.* **52,** 527 (1974).
226. Mønsted, L., *Acta Chem. Scand., Ser. A* **A32,** 377 (1978).
227. Monacelli, F., *Inorg. Chim. Acta* **2,** 263 (1968).
228. Bott, H. L., Pöe, A. J., and Shaw, K., *Chem. Commun.,* 793 (1968).
229. Bott, H. L., Pöe, A. J., and Shaw, K., *J. Chem. Soc. A,* 1745 (1970).
230. Borghi, E., Monacelli, F., and Prosperi, T., *Inorg. Nucl. Chem. Lett.* **6,** 667 (1970).
231. Dellavia, I., Helm, L., and Merbach, A. E., *Inorg. Chem.* **31,** 4151 (1992).
232. Comba, P., and Merbach, A. E., *Inorg. Chem.* **26,** 1315 (1987).
233. Thompson, G. A. K., Taylor, R. S., and Sykes, A. G., *Inorg. Chem.* **16,** 2880 (1977)
234. Wüthrich, K., and Connick, R. E., *Inorg. Chem.* **6,** 583 (1967).
235. Kuroia, Y., Harada, M., Tomiyasu, H., and Fukutomi, H., *Inorg. Chim. Acta* **146,** 7 (1988).
236. Angerman, N. S., and Jordan, R. B., *Inorg. Chem.* **8,** 1824 (1969).
237. Angerman, N. S., and Jordan, R. B., *Inorg. Chem.* **8,** 65 (1969).
238. Kaya, K., Ikeda, Y., and Fukotomi, H., *Bull. Chem. Soc. Jpn.* **58,** 2648 (1985).
239. Harada, M., Ikeda, Y., Tomiyasu, H., and Fukutomi, H., *Chem. Lett.,* 1195 (1984).
240. Jordan, R. B., and Angerman, N. S., *J. Chem. Phys.* **48,** 3983 (1968).
241. Miller, G. A., and McClung, R. E. D., *J. Chem. Phys.* **58,** 4358 (1973).
242. Saito, K., and Sasaki, Y., *Adv. Inorg. Bioinorg. Mech.* **1,** 179 (1982).
243. Gamsjäger, H., and Murmann, R. K., *Adv. Inorg. Bioinorg. Mech.* **2,** 317 (1983).
244. Nishizawa, M., and Saito, K., *Inorg. Chem.* **17,** 3676 (1978).
245. Nishizawa, M., and Saito, K., *Inorg. Chem.* **19,** 2284 (1980).
246. Murmann, R. K., *Inorg. Chim. Acta* **25,** L43 (1977).
247. Johnson, M. D., and Murmann, R. K., *Inorg. Chem.* **22,** 1068 (1983).
248. Ballhausen, C. J., and Gray, H. B., *Inorg. Chem.* **1,** 111 (1962).
249. Mustafi, D., and Makinen, M., *Inorg. Chem.* **27,** 3360 (1988).
250. Khodashova, T., Porai Koshits, M., Sergienko, V., Butman, L., Buslaev, Y., Kovalev, V., and Kusnetsova, A., *Sov. J. Coord. Chem.* (*Engl. Transl.*) **4,** 1473 (1978).
251. Théobald F., and Tachez, M., *Acta Crystallogr., Sect. B: Struct. Crystallogr. Cryst. Chem.* **B36,** 1757 (1980).
252. Dwyer, P. N., Puppe, L., Buchler, J. W., and Scheidt, W. R., *Inorg. Chem.* **14,** 1782 (1975).
253. Taube, R. *Z. Chem.* **3,** 194 (1963).

254. Block, B. P., and Meloni, E. G., *Inorg. Chem.* **4,** 111 (1965).
255. Felz, A., *Z. Chem.* **7,** 158 (1967).
256. Dehnicke, K., Pausewang, G., and Rüdorff, W., *Z. Anorg. Allg. Chem.* **366,** 64 (1969).
257. Swift, T. J., and Connick, R. E., *J. Chem. Phys.* **37,** 307 (1962).
258. Finholt, J. E., Leupin, P., and Sykes, A. G., *Inorg. Chem.* **22,** 3315 (1983).
259. Pittet, P.-A., Dadci, L., Zbinden, D., Abou-Hamdan, A., and Merbach, A. E., *Inorg. Chim. Acta* **206,** 135 (1993).
260. Lin, Z., and Hall, M. B., *Inorg. Chem.* **30,** 646 (1991).
261. Lukosius, E. J., and Coskran, K. J., *Inorg. Chem.* **14,** 1922 (1975).
262. Stalick, J. K., and Ibers, J. A., *Inorg. Chem.* **8,** 1090 (1969).
263. Favez, R., and Roulet, R., *Inorg. Chem.* **20,** 1598 (1981).
264. Roberts, N. K., and Wild, S. B., *Inorg. Chem.* **20,** 1892, 1900 (1981).
265. Albinati, A., Pregosin, P. S., and Ruegger, H., *Angew. Chem., Int. Ed. Engl.* **23,** 78 (1984).
266. Muetterties, E. L., and Guggenberger, L. J., *J. Am. Chem. Soc.* **96,** 1748 (1974).
267. Brønnum, B., Johansen, H. S., and Skibsted, L. H., *Acta Chem. Scand.* **43,** 975 (1989).
268. Hallinan, N., Besançon, V., Forster, M., Elbaze, G., Ducommun, Y., and Merbach, A. E., *Inorg. Chem.* **30,** 1112 (1991).
269. Helm, L., Elding, L. I., and Merbach, A. E., *Helv. Chim. Acta* **67,** 1453 (1984).
270. Pesek, J. J., and Mason, W. R., *Inorg. Chem.* **22,** 2958 (1983) (activation parameters recalculated as described in Ref. *269*).
271. Frey, U., Elmroth, S., Moullet, B., Elding, L. I., and Merbach, A. E., *Inorg. Chem.* **30,** 5033 (1991).
272. Brønnum, B., Johansen, H. S., and Skibsted, L. H., *Inorg. Chem.* **31,** 3023 (1992).
273. Helm, L., Elding, L. I., and Merbach, A. E., *Inorg. Chem.* **24,** 1719 (1985).
274. Ducommun, Y., Helm, L., Merbach, A. E., Hellquist, B., and Elding, L. I., *Inorg. Chem.* **28,** 377 (1989).
275. Gutmann, V., "The Donor-Acceptor Approach to Molecular Interactions." Plenum, New York, 1968.
276. Treichel, P. M., and Hess, R. W., *J. Chem. Soc., Chem. Commun.*, 1626 (1970).
277. Olsson, A., and Kofod, P., *Inorg. Chem.* **31,** 183 (1992).
278. Ducommun, Y., Merbach, A. E., Hellquist, B., and Elding, L. I., *Inorg. Chem.* **26,** 1759 (1987).
279. Hellquist, B., Elding, L. I., and Ducommun, Y., *Inorg. Chem.* **27,** 3620 (1988).
280. Elmroth S., Bugaric, Z., and Elding, L. I., *Inorg. Chem.* **31,** 3551 (1992).
281. Elding, L. I., *Inorg. Chim. Acta* **6,** 683 (1972).
282. Elding, L. I., *Inorg. Chim. Acta* **28,** 255 (1978).
283. Bugarcic, Z., Ph.D. Thesis, Kragujevac University (1989).
284. Elding, L. I., and Olsson, L. F., *Inorg. Chim. Acta* **117,** 9 (1986).
285. Elding, L. I., and Gröning, A.-B., *Inorg. Chim. Acta* **27,** 3620 (1978).
286. Berger, J., Kotowski, M., van Eldik, R., Frey, U., Helm, L., Merbach, A. E., *Inorg. Chem.* **28,** 3759 (1989).
287. Pienaar, J. J., Kotowski, M., and van Eldik, R., *Inorg. Chem.* **28,** 373 (1989).
288. Romeo, R., *Comments Inorg. Chem.* **11,** 21 (1990).
289. Lanza, S., Minniti, D., Moore, P., Sachinidis, J., Romeo, R., and Tobe, M. L., *Inorg. Chem.* **23,** 4428 (1984).
290. Alibrandi, G., Bruno, G., Lanza, S., Minniti, D., Romeo, R., and Tobe, M. L., *Inorg. Chem.* **26,** 185 (1987).

291. Minniti, D., Alibrandi, G., Tobe, M. L., and Romeo, R., *Inorg. Chem.* **26,** 3956 (1987).
292. Alibrandi, G., Minniti, D., Scolaro, M., and Romeo, R., *Inorg. Chem.* **28,** 1939 (1989).
293. Frey, U., Helm, L., Merbach, A. E., and Romeo, R., *J. Am. Chem. Soc.* **111,** 8161 (1989).
294. Romeo, R., Grassi, A., and Scolaro, L. M., *Inorg. Chem.* **31,** 4383 (1992).
295. Cossy, C., Barnes, A. C., Enderby, J. E., and Merbach, A. E., *J. Chem. Phys.* **90,** 3254 (1989).
296. Helm, L., and Merbach, A. E., *Eur. J. Solid State Inorg. Chem.* **28,** 245 (1991).
297. Habenschuss, A., and Spedding, F. H., *J. Chem. Phys.* **70,** 2797 (1979).
298. Habenschuss, A., and Spedding, F. H., *J. Chem. Phys.* **70,** 3758 (1979).
299. Habenschuss, A., and Spedding, F. H., *J. Chem. Phys.* **73,** 442 (1980).
300. Yamaguchi, T., Nomura, M., Wakita, H., and Ohtaki, H., *J. Chem. Phys.* **89,** 5153 (1988).
301. Spedding, F. H., Shiers, L. E., Brown, M. A., Derer, J. L., Swanson, D. L., and Habenschuss, A. J., *J. Chem. Eng. Data.* **20,** 81 (1975).
302. Miyakawa, K., Kaizu, Y., and Kobayashi, H., *J. Chem. Soc., Faraday Trans. 1* **84,** 1517 (1988).
303. Harrowfield, J. McB., Kepert, D. L., Patrick, J. M., and White, A. H., *Aust. J. Chem.* **36,** 483 (1983).
304. Albertsson, J., and Elding, I., *Acta Crystallogr., Sect. B: Struct. Crystallogr. Cryst. Chem.* **B33,** 1460 (1977).
305. Hubbard, C. R., Quicksall, C. O., and Jacobson, R. A., *Acta Crystallogr., Sect. B: Struct. Crystallogr. Cryst. Chem.* **B30,** 2613 (1974).
306. Fitzwater, D. R., and Rundle, R. E., *Z. Kristallogr., Kristallgeom., Kristallphys., Kristallchem.* **112,** 362 (1959).
307. Broach, R. W., Williams, J. M., Felcher, G. P., and Hinks, D. G., *Acta Crystallogr., Sect. B: Struct. Crystallogr. Cryst. Chem.* **B35,** 2317 (1979).
308. Sikka, S. K., *Acta Crystallogr., Sect. A: Cryst. Phys., Diffr., Theor. Gen. Crystallogr.* **A25,** 621 (1969).
309. Glaser, J., and Johansson, G., *Acta Chem. Scand., Ser. A* **A35,** 639 (1981).
310. Fay, D. P., Litchinsky, D., and Purdie, N., *J. Chem. Phys.* **73,** 544 (1969).
311. Micskei, K., Powell, D. H., Helm, L., Brücher, E., and Merbach, A. E., *Magn. Reson. Chem.* **31,** 1011 (1993).
312. Cossy, C., Helm, L., and Merbach, A. E., *Inorg. Chem.* **28,** 2699 (1989).
313. Cossy, C., Helm, L., and Merbach, A. E., *Inorg. Chem.* **27,** 1973 (1988).
314. Laurenczy, G., and Merbach, A. E., *Helv. Chim. Acta* **71,** 1971 (1988).
315. Galera, S., Lluch, J. M., Oliva, A., Betrán, J., Foglia, F., Helm, L., and Merbach, A. E., *New J. Chem.* **17,** 773 (1993).
316. Micskei, K., Helm, L., Brücher, E., and Merbach, A. E., *Inorg. Chem.* **32,** 3844 (1993).
317. González G., Powell, D. H., Tissières, V., and Merbach, A. E., *J. Phys. Chem.* **98,** 53 (1994).
318. Lauffer, R. B., *Chem. Rev.* **87,** 901 (1987).
319. Koenig, S. H., Brown, R. D., III, *Prog. NMR Spectrosc.* **22,** 487 (1990).
320. Geraldes, C. F. G. C., Brown, R. D., III, Brücher, E., Koenig, S. H., Sherry, A. D., and Spiller, M., *Magn. Reson. Med.* **27,** 284 (1992).
321. Pisaniello, D. L., and Merbach, A. E., *Helv. Chim. Acta* **65,** 573 (1982).
322. Bunzli, J.-C. G., and Yersin, J. R., *Helv. Chim. Acta* **65,** 2498 (1982).
323. Pisaniello, D. L., Helm, L., Zbinden, D., and Merbach, A. E., *Helv. Chim. Acta* **66,** 1872 (1983).

324. Lincoln, S. F., and White, A., *Inorg. Chim. Acta* **168,** 265 (1990).
325. Pisaniello, D. L., Lincoln, S. F., Williams, E. H., and Jones, A. J., *Aust. J. Chem.* **34,** 495 (1981).
326. Lincoln, S. F., Hounslow, A. M., and Jones, A. J., *Aust. J. Chem.* **35,** 2393 (1982).
327. Pisaniello, D. L., and Lincoln, S. F., *J. Chem. Soc., Dalton Trans.,* 699 (1980).
328. Nassimbeni, L. R., and Rodgers, A. L., *Cryst. Struct. Commun.* **5,** 301 (1976).
329. Harrowfield, J. M., Kepert, D. L., Patrick, J. M., White, A. H., and Lincoln, S. F., *J. Chem. Soc., Dalton Trans.,* 393 (1983).
330. Alcock, N. W., and Esperas, S., *J. Chem. Soc., Dalton Trans.,* 893 (1977).
331. Alcock, N. W., *J. Chem. Soc., Dalton Trans.,* 1616 (1973).
332. Dalley, N. K., Mueller, M. H., and Simonsen, S. H., *Inorg. Chem.* **10,** 323 (1971).
333. Abou-Hamdan, A., Burki, N., Lincoln, S. F., Merbach, S. F., and Vincent, S. J. F., *Inorg. Chim. Acta* **207,** 27 (1993).
334. Bowen, P. R., Lincoln, S. F., and Williams, E. H., *Inorg. Chem.* **15,** 2126 (1976).
335. Honan, J. H., Lincoln, S. F., Spotswood, T. M., and Williams, E. H., *Inorg. Chim Acta* **33,** 235 (1979).
336. Honan, J. H., Lincoln, S. F., and Williams, E. H., *J. Chem. Soc., Dalton Trans.,* 320 (1979).
337. Holm, R. H., *Adv. Inorg. Chem.* **38,** 528 (1992).
338. Kim, J., and Rees, D. C., *Science* **257,** 1677 (1992).
339. Souchay, P., Cadiot, M., and Duhameau, M., *C. R. Hebd. Seances Acad. Sci.* **262,** 1524 (1966).
340. Ojo, J. F., Sasaki, Y., Taylor, R. S., and Sykes, A. G., *Inorg. Chem.* **15,** 1006 (1976).
341. Rodgers, K. R., Murmann, R. K., Schlemper, E. O., and Shelton, M. E., *Inorg. Chem.* **24,** 1313 (1985).
342. Kathirgamanathan, P., Soares, A. B., Richens, D. T., and Sykes, A. G., *Inorg. Chem.* **24,** 2950 (1985).
343. Ooi, B.-L., and Sykes, A. G., *Inorg. Chem.* **27,** 310 (1988).
344. Ooi, B.-L., Martinez, M., and Sykes, A. G., *J. Chem. Soc., Chem Commun.,* 1324 (1988).
345. Ooi, B.-L., and Sykes, A. G., *Inorg. Chem.* **28,** 3799 (1989).
346. Richens, D. T., Helm, L., Pittet, P.-A., Merbach, A. E., Nicolò, F., and Chapuis, G., *Inorg. Chem.* **28,** 1394 (1989).
347. Lamprecht, G. J., Martinez, M., Nasreldin, M., Routledge, C. A., Najat A.-S., and Sykes A. G., *J. Chem. Soc., Dalton Trans.,* 747 (1993).
348. Richens, D. T., Pittet, P.-A., Merbach, A. E., Humanes, M., Lamprecht, G. J., Ooi, B.-L., and Sykes A. G., *J. Chem. Soc., Dalton Trans.,* 2305 (1993).
349. Ooi, B.-L., Petrou, A. L., and Sykes A. G., *Inorg. Chem.* **27,** 3626 (1988).
350. Li, Y.-J., Routledge, C. A., and Sykes A. G., *Inorg. Chem.* **30,** 5043 (1991).
351. Nasreldin, M., Olatuji, A., Dimmock, P. W., and Sykes A. G., *J. Chem. Soc., Dalton Trans.,* 1765 (1990).
352. Akashi, T., Shibahara, T., and Kuroya, H., *Polyhedron* **9,** 1671 (1990).
353. Shibahara, T., Takeuchi, T., Ohtsuji, A., Kohda, K., and Kuroya, H., *Inorg. Chim. Acta* **127,** L45 (1987).
354. Bursten, B. E., Cotton, F. A., Hall, M. B., and Najjar, R. C., *Inorg. Chem.* **21,** 302 (1982).
355. Wendan, C., Qianer, Z., Jinshun, H., and Jiaxi, L., *Polyhedron* **8,** 2785 (1989).
356. Harris, S., *Polyhedron* **8,** 2843 (1989).
357. Pitzer, K. S., *Acc. Chem. Res.* **12,** 271 (1979).
358. McKelvey, D. R., *J. Chem. Educ.* **60,** 112 (1983).

359. Li, Y.-J., Nasreldin, M., Humanes, M., and Sykes A. G., *Inorg. Chem.* **31,** 3011 (1992).
360. Akashi, H., Shibahara, T., Narabara, T., Tsuru, H., and Kuroya, H., *Chem. Lett.,* 129 (1989).
361. Hong, M.-C., Li, Y.-J., Lu, J., Nasreldin, M., and Sykes A. G., *J. Chem. Soc., Dalton Trans.,* 2613 (1993).
362. Powell, G., and Richens, D. T., *Inorg. Chem.* **32,** 4021 (1993).
363. Nakata, K., Nagasawa, A., Soyama, N., Sasaki, Y., and Ito, T., *Inorg. Chem.* **30,** 1575 (1991).
364. Taube, H., *J. Chem. Soc., Dalton Trans.,* 547 (1991).
365. Garrick, F. J., *Nature (London)* **139,** 507 (1937).
366. Pearson, R. G., and Basolo, F., *J. Am. Chem. Soc.* **78,** 4878 (1956).
367. Ingold, C. K., Nyholm, R. S., and Tobe, M. L., *J. Chem. Soc.,* 1691, 1707 (1956).
368. Basolo, F., Schmidke, H. H., and Pearson, R. G., *J. Am. Chem. Soc.* **79,** 4055 (1957).
369. Jordan, R. B., "Reaction Mechanisms of Inorganic and Organometallic Systems." Oxford Univ. Press, Oxford, 1991.
370. Margerum, D. W., Cayley, G. R., Weatherburn, D. C., and Pagenkopf, G. W., *in* "Coordination Chemistry" (A. E. Martell, ed.), Vol. 2, pp. 1–194, Am. Chem. Soc., Washington, DC, 1978.
371. Williams, R. J. P., *Coord. Chem. Rev.* **100,** 573 (1990).
372. Connick, R. E., and Alder, B. J., *J. Phys. Chem.* **87,** 2764 (1983).

LEWIS ACID–BASE BEHAVIOR IN AQUEOUS SOLUTION: SOME IMPLICATIONS FOR METAL IONS IN BIOLOGY

ROBERT D. HANCOCK* and ARTHUR E. MARTELL†

*Department of Chemistry, University of the Witwatersrand, Johannesburg, South Africa, and †Department of Chemistry, Texas A&M University, College Station, Texas

I. Introduction
II. Lewis Acid–Base Interactions in Gas Phase
III. Comparison of Behavior of Lewis Acids and Bases in Aqueous Solution and in the Gas Phase
IV. Significance of HSAB Ideas for Zinc-Containing Metalloenzymes
V. Chelate Ring Size and Metal Ion Selectivity
VI. The Neutral Oxygen Donor
VII. The Negative Oxygen Donor
VIII. The Nitrogen Donor
IX. Sulfur Donors
X. Systems Containing More Than One Metal Ion — The Reverse Chelate Effect
References

I. Introduction

In previous reviews (*1, 2*) the design of ligands for selective complexation of metal ions was discussed for use in areas such as medicine (*3*), extraction metallurgy, and the environment. The use of molecular mechanics (MM) calculations in understanding steric effects in such applications has been described (*4*). There is clearly a need to examine factors that control strength of metal–ligand interactions as these might relate to metal ions in biology. One could not in a review of the present length make this an exhaustive account of selectivity for metal ions in biological systems. Rather, an attempt is made to give the reader an overview of factors that have been identified (*1*) as being important in metal ion selectivity, and examples of where these principles may apply in biology. In order to understand the interaction between metal ions and complex ligands of biological interest, one must

Copyright © 1995 by Academic Press, Inc.
All rights of reproduction in any form reserved.

first understand the interaction between a metal ion and a simple unidentate ligand in aqueous solution:

$$[M(H_2O)_m]^{n+}(aq) + L(aq) = [M(H_2O)_{(m-1)}L]^{n+}(aq) + H_2O. \quad (1)$$

Lewis acid–base interactions between metal ions and ligands in the gas phase are essential to an understanding of Lewis acid interactions in solution. Gas-phase and aqueous-phase results together offer insights into hard and soft acid–base (*5, 5a*) (HSAB) behavior in aqueous solution. The strength with which particular unidentate ligands bind a metal ion is a guide to choice of donor atoms for that metal ion, and preference of donor atoms for different metal ions is considered. An understanding of factors that control Lewis acid–base interactions in aqueous solution is important in understanding the functioning of metal ions in biology.

Nature uses only a few metal ions from the first-row transition metal ions in the periodic table in catalytic roles, chiefly Zn, Fe, Cu, Co, Mn, and Ni (*6*). In contrast, the elegant catalyses of organometallic chemistry have tended to involve complexes of metals from the second and third rows of transition elements of the periodic table, in low oxidation states. Nature appears to have significant access only to Mo from the heavier transition elements (*6*), and metal ions are usually not in very low oxidation states. With limitations of pH close to 7.4 and temperature of 37°C, Nature can effect remarkable catalytic results, and one should try to see how Lewis acid–base behavior of metal ions has been altered to achieve this. An example of such altered Lewis acidity is that iron as Fe^{2+} or Fe^{3+} aqua ions cannot complex dinitrogen, but it appears that iron in nitrogenase may be able to (*7*). How donor atoms already attached to metal ions can alter Lewis acid–base interactions of a metal ion with additional ligands is also discussed. Finally, it is clearly important to analyze how selectivity for metal ions in biological systems in more complex multidentate ligands is controlled in terms of principles of ligand design (*1*), based on both choice of donor atom and on ligand architecture, as this might relate to metal ions in biology.

II. Lewis Acid–Base Interactions in the Gas Phase

Present understanding of Lewis acidity and basicity is based mainly on the "A" and "B" type classification of metal ions of Ahrland, Chatt,

and Davies (*8*), and the HSAB classification of Pearson (*5*, *5a*). The HSAB classification is based largely on studies in aqueous solution, although Pearson has suggested how gas-phase results might yield orders of hardness and softness (*5a*). Behavior in the gas phase may be quite different to that in solution. First, the metal ion to which, typically, one or two ligands may be coordinated in the gas phase is not solvated, and so effects that occur in aqueous solution because of interaction between coordinating ligands and the solvation sphere of the metal ion are absent. Figure 1 shows energies of complex formation

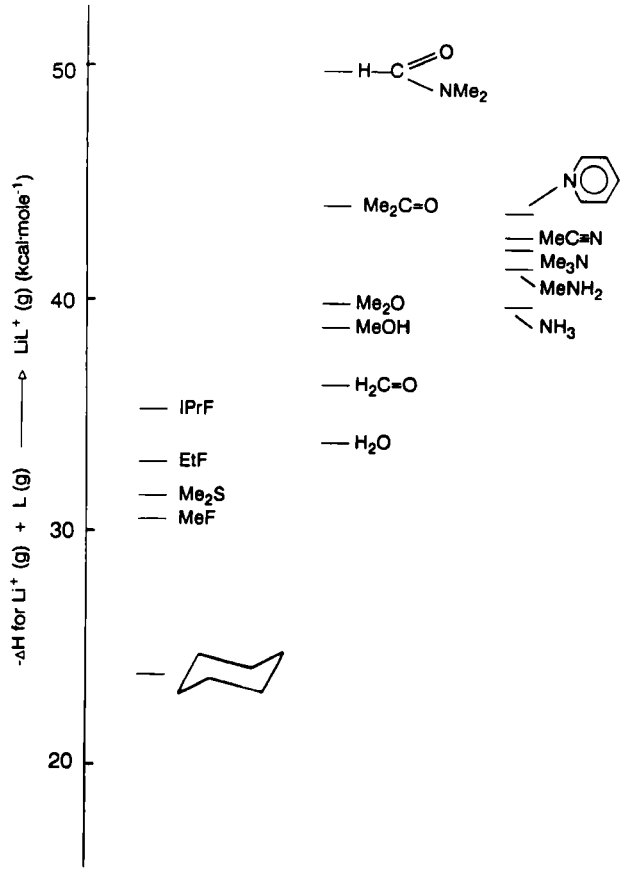

FIG. 1. Energies of complex formation for complexes of lithium(I) in the gas phase with a variety of ligands. Data from Ref. (*9*).

for lithium(I) with unidentate bases in the gas phase (*9*). What is noteworthy about metal ions in the gas phase is the order of complex stability with amines of $NH_3 < N(CH_3)_3$. Similarly, dimethyl ether is a stronger base than water. In aqueous solution neither trimethylamine nor dimethyl ether is a good Lewis base for metal ions. Calculations by Woodin and Beauchamp (*9*) show that stability of the Li(I) complexes with the methylamines would increase linearly with increasing methyl substitution if only electronic effects such as inductive effects are considered. However, when adverse steric effects of methyl groups are included (Fig. 2), a maximum in complex stability at dimethylamine occurs as more methyl groups are added. Figure 2 shows various contributions to complex stability of Li(I) complexes with *N*-methyl amines. Trimethylamine is a slightly weaker ligand than dimethylamine because the inductive effects of the methyl groups of trimethylamine are overwhelmed by adverse steric effects. That this occurs with a bare Li(I) ion in the gas phase coordinating a single trimethylamine is remarkable. The steric effects of the methyl groups must be much worse when the metal ion has an inner and outer sphere of coordinated solvent waters attached to it. Steric interaction between coordinated ligands and water coordinated to metal ions in aqueous solution is considered to be important in determining Lewis acid character of metal ions (*1, 2*). Thus, only metal ions of low coordination number and long M–N bonds such as Ag(I) are able (*10*) to form complexes of any stability (*11*) whatever with ligands such as triethylamine in aqueous solution. The Ag(I) ion has a low coordination number, usually two, and long M–L bonds, leading to weak solvation, making it rather like a metal ion in the gas phase (*10*). We shall return to this theme, particularly in relation to the nature of HSAB behavior.

Figure 3 shows the variation of heats of protonation in the gas phase of bases with different donor atoms as a function of number of methyl groups on the donor atom (*12*). In the gas phase, bases containing heavy donor atoms, such as dimethylthioether or trimethyl phosphine, are stronger proton bases than respective analogues such as dimethylether and trimethylamine. How can things be so different in aqueous solution? Part of the answer must lie in steric crowding effects of water coordinated to the proton, as discussed earlier, but a second important effect is the role of hydrogen bonding in dispersing charge from the cation into the solvent. Thus, the proton in water is stabilized by several water molecules coordinated to it via their oxygen atoms. These waters, in turn, because of distribution of positive charge out from the proton, organize several more spheres of structured water until the water is

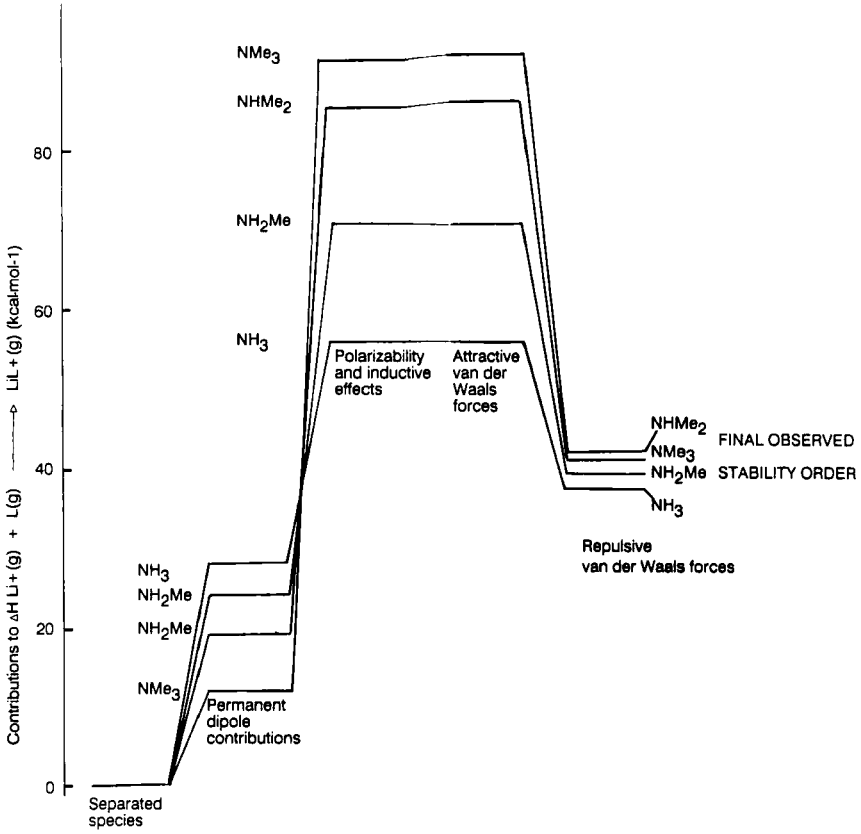

FIG. 2. Components of Li^+ enthalpies of complexation with methylamines. Successive steps indicate the effect on energy of interaction between Li^+ and the amine of inclusion of additional components of the binding energy. The diagram shows that the permanent dipoles on amines (the charge on the nitrogen of the isolated amine) favor ammonia over trimethylamine complexation, but that polarizability and inductive effects (shift of negative charge onto the nitrogen in the complex) cause a massive turnaround in favor of complexation with trimethylamine rather than ammonia. Of particular importance is the near inversion of order caused by the addition of repulsive van der Waals terms. Modified after Ref. (*9*).

no longer distinguishable from bulk solvent. Hydrogens attached to donor atoms such as sulfur or phosphorus are, like those on a hydrocarbon, virtually incapable of hydrogen bonding. The cascade of dispersion of charge to the solvent by layers of coordinated solvent molecules is thus interrupted by ligands that cannot hydrogen-bond to the solvent, so complexes are greatly destabilized (*12*). One can thus account for

protonation constants of methyl-substituted amines and phosphines in water in terms of these ideas:

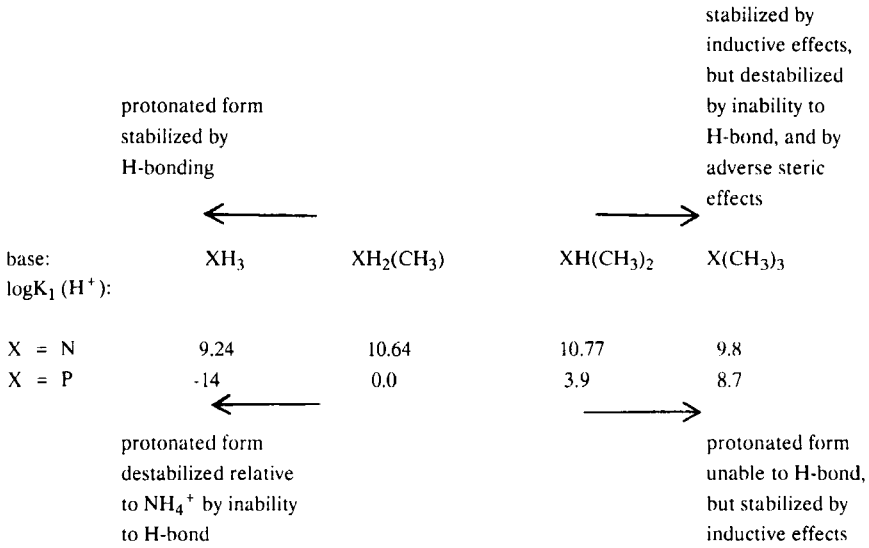

Energies of complex formation by Lewis acids of bases in the gas phase may be used to analyze HSAB ideas (*9, 13–15*). Figure 4 shows the energies of complex formation for the $NiCp^+$ ion (Cp = cyclopentadienyl) versus those for the Mn^+ ion (*14*). There is a linear relationship for oxygen donor ligands, and a second correlation offset from this, for "soft" ligands, which in this case contain N and S rather than O donors. Figure 5 contains a similar diagram for Li^+ versus the Mn^+ ion. Figure 5 resembles Fig. 4, except that offset of soft ligands is towards the $NiCp^+$ ion in Fig. 4, and towards the Mn^+ ion in Fig. 5. The order of preference for soft relative to hard ligands is thus $NiCp^+ > Mn^+ > Li^+$, which is what might be expected as an order of softness for these Lewis acids (*14*). Using such diagrams (*13–15*), the order of softness $Al^+ < K^+ < Li^+ < Mn^+ < Co^+ < NiCp^+ < H^+ < Ni^+ < Cu^+$ is obtained (*16*) in the gas phase. The position of H^+ in this order is somewhat ambiguous. The proton has a high relative affinity for soft ligands such as thioethers in the gas phase, which suggests that it is soft (*13–15*). However, the bonding of H^+ to nitriles in the gas phase is anomalously weak compared to other Lewis acids, which, if nitriles are regarded as soft, suggests that the proton is harder than indicated by the foregoing order. It seems likely that bonding of metal ions to nitriles in the gas phase involves some factor such as edge-on

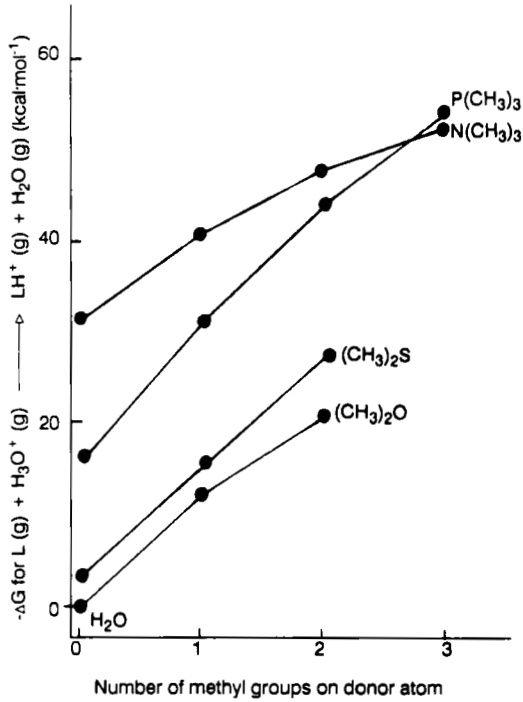

FIG. 3. Variation of heats of protonation in the gas phase of bases with N, O, P, and S donor atoms as hydrogens are replaced by methyl groups as substituents on the donor atoms. Data from Ref. (*12*).

bonding to both the C and the N of the cyano group, which is not possible for the proton.

III. Comparison of Behavior of Lewis Acids and Bases in Aqueous Solution and in the Gas Phase

The approach used (*13–15*) to order Lewis acids in the gas phase according to hardness can be extended to aqueous solution (*17*). Figure 6 shows log K_1 for Ag(I) complexes in aqueous solution plotted against log K_1 for analogous CH_3Hg^+ complexes. As for the gas-phase studies (*13–15*), ligands are ordered as indicated in Fig. 6 as expected if Ag^+ is softer than CH_3Hg^+. In Fig. 7, where log K_1 values for Bi^{3+} are plotted against log K_1 for CH_3Hg^+ complexes, ligands are ordered as expected if Bi^{3+} were harder than CH_3Hg^+. Figures 6 and 7 indicate also that the order of softness for ligands is F^- < O-donors < N-donors < Cl^- < Br^- < I^-, S, P, and C-donors. Similar behavior for all

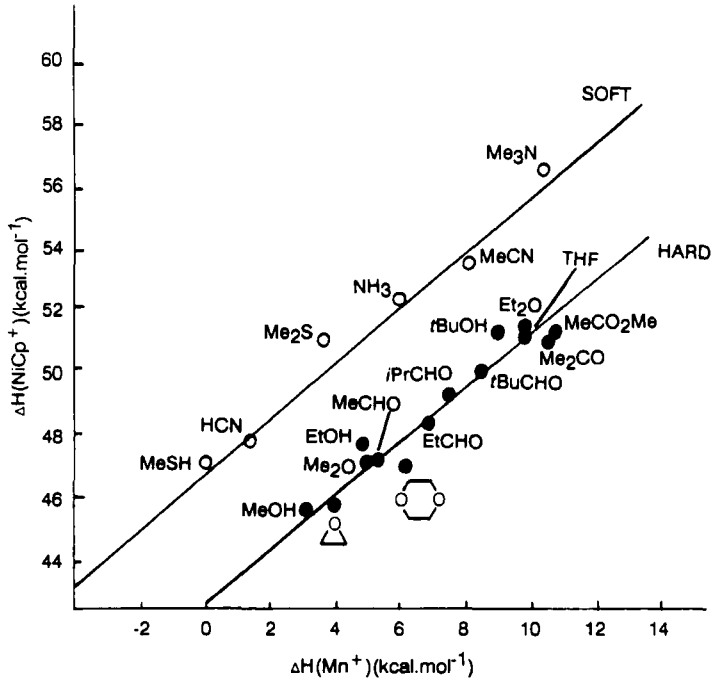

FIG. 4. Plot of enthalpies of complex formation in the gas phase of $CpNi^+$ complexes (Cp = cyclopentadienyl) vs those for the corresponding Mn^+ complexes. The ligands are segregated into correlations for "soft" (○) (N and S donors) and "hard" (oxygen donors) (●). Energies are in kcal mol^{-1}. Redrawn after Ref. (*14*).

other pairs of metal ions, with ligands ordered according to hardness and softness, is observed. Behavior like that seen in Figs. 6 and 7, for example, can be modeled for all metal ions using a dual basicity equation:

$$\log K_1 = E_A^{aq} \cdot E_B^{aq} + C_A^{aq} \cdot C_B^{aq}. \tag{2}$$

E^{aq} and C^{aq} are the tendency of acid A and base B to undergo ionic and covalent bonding, respectively. Equation (2) resembles that proposed by Drago *et al.* (*18*) to model heats of complex formation of acids and bases in solvents of low dielectric constant. Only Lewis acids of ionic radius greater than 1.0 Å obey Eq. (2). For all smaller Lewis acids, a third pair of parameters has to be introduced:

$$\log K_1 = E_A^{aq} \cdot E_B^{aq} + C_A^{aq} \cdot C_B^{aq} - D_A \cdot D_B. \tag{3}$$

The D parameters are thought to account for adverse steric effects on complex formation, and possibly also inability of the ligand to transfer

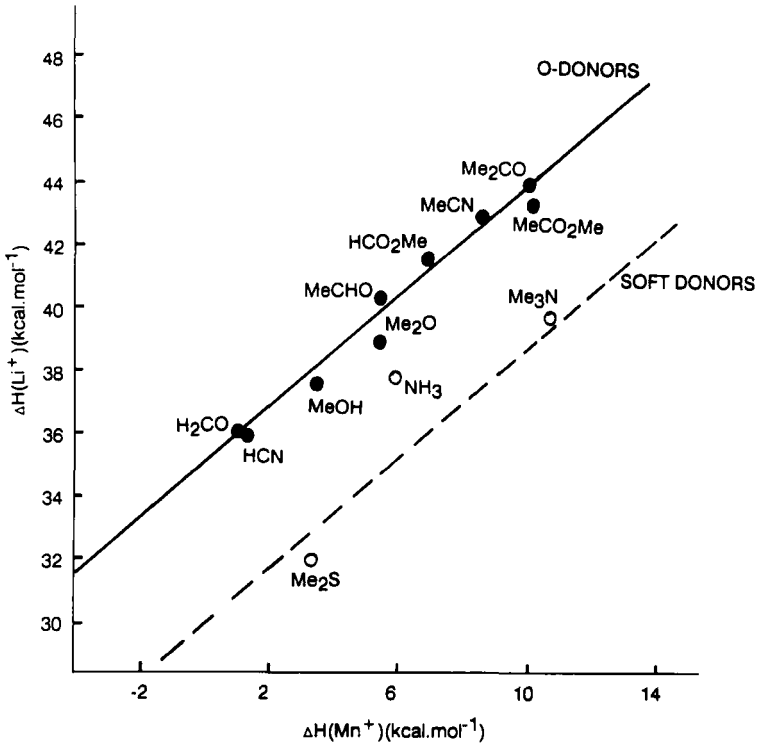

FIG. 5. Plot of enthalpies of complex formation in the gas phase for formation of Li^+ complexes versus those for the corresponding Mn^+ complexes. Ligands are segregated into correlations for hard (●) and soft (○) donors. Energies in kcal mol^{-1}. Redrawn after Ref. (*14*).

charge from the Lewis acid to solvent via hydrogen bonding (*17*). Adverse steric effects arise chiefly from clashes with coordinated water molecules also present on the Lewis acid, which can be brought about by (1) a donor atom that is significantly larger than the water molecule displaced from the Lewis acid by an incoming ligand, or (2) large substituents on a donor atom, such as alkyl groups. These two similar effects cause ligands with large donor atoms such as I^-, or large alkyl substituents such as trimethylamine, to form much weaker complexes with small metal ions than might otherwise be anticipated. Since many soft ligands have large donor atoms, small metal ions such as Cu^{2+} or Co^{3+} *may thus form weak complexes with these ligands, and appear hard for reasons of steric crowding rather than electronic factors.*

Equation (3) predicts $\log K_1$ values for metal ions in aqueous solution with considerable accuracy. Some E_A, C_A, and D_A parameters for Lewis acids are shown in Table I, and for bases in Table II. When Eq. (3)

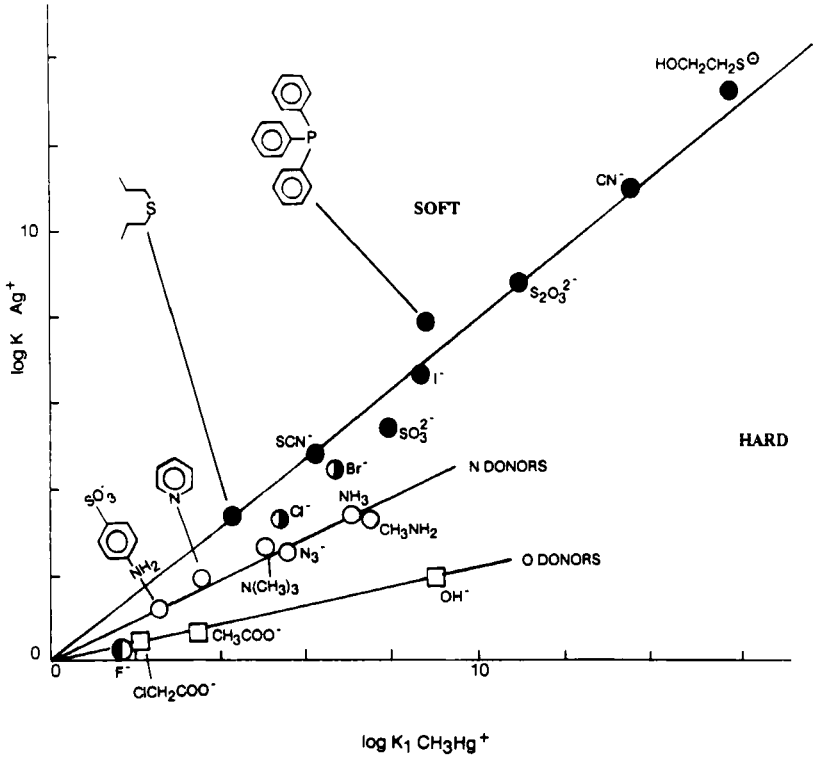

FIG. 6. Plot of log K_1 values for Ag^+ complexes with unidentate ligands vs log K_1 values for corresponding complexes with CH_3Hg^+. Data at 25°C and ionic strength zero in aqueous solution, from Ref. (*11*). Ligands are classified as soft (●); intermediate (◑); hard, N-donors (○); hard, O-donors (□), or F^- (◐). Formation constant data from Ref. (*11*).

was published (*17*), log K_1 values for some azide complexes were not available, although predicted values were listed (*17*). Since then, values for some of these azide constants have been published (*11*), and these can be compared with predicted values (*17*):

Metal ion:	GaIII	In(III)	UO_2^{2+}	La(III)
log K_1(azide),				
Predicted (*17*):	4.28[a]	4.31	2.10	1.33
Reported (*11*):	4.4	4.09	2.14	1.52

[a] The E and C parameters for Ga(III) have been revised from the original paper, as seen in Table I, and originally gave a predicted log K_1 with azide of 3.84.

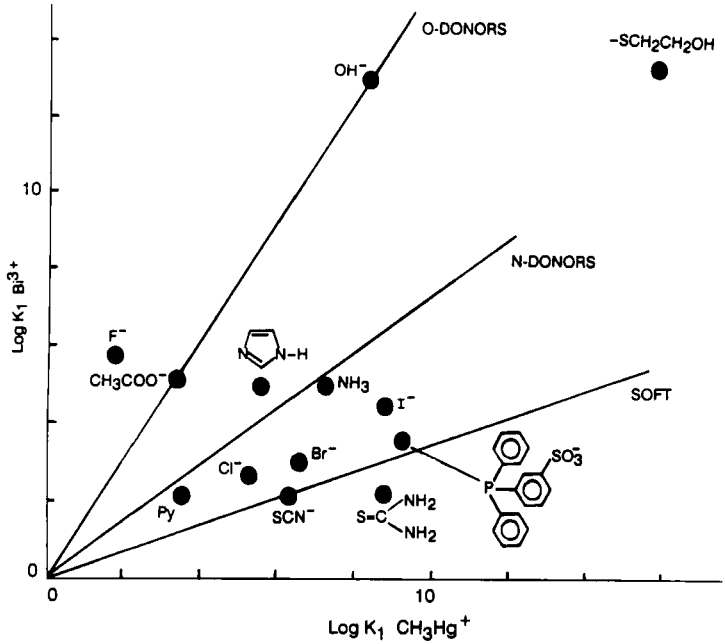

FIG. 7. Plot of log K_1 values for Bi^{3+} complexes with unidentate ligands vs log K_1 values for corresponding complexes with CH_3Hg^+. Data at 25°C and corrected to ionic strength zero, from Ref. (*11*).

Equation (3) has good quantitative predictive power and is a successful extra-thermodynamic relationship like the Hammett sigma function. No other approach to modeling complex formation equilibria, including HSAB itself, can predict log K_1 values for unidentate ligands so accurately.

The E_A/C_A ratio was proposed as a measure of hardness of the Lewis acid, and E_B/C_B as hardness of the Lewis base *in aqueous solution* (*17*). It now seems that the E/C ratio is not a measure of hardness in the sense in which Pearson (*5, 5a*) defined hardness. Rather, the E/C ratio for a Lewis acid or base is a measure of the tendency to ionicity in the M–L bonds formed. The E_A/C_A ratio should rather be called I_A, and the E_B/C_B ratio I_B, the tendency to ionic bonding in forming the M–L bond. Acids and bases in Tables I and II are placed in order of increasing tendency towards ionicity in the M–L bond, according to the E/C ratios I_A and I_B. A justification for this interpretation is that the order of I_A values for metal ions in aqueous solution strongly resembles the order of hardness derived by Pearson (*19*) from enthalpies of complex forma-

TABLE I

IONICITY PARAMETER, I_A, AND C_A, E_A, AND D_A PARAMETERS FOR USE IN EQ. (3), FOR SELECTED LEWIS ACIDS IN AQUEOUS SOLUTION[a]

Lewis acid	I_A	C_A	E_A	D_A	R^+ (Å)[b]	HSAB[c]
Ag^+	−10.6	0.190	−1.53	0.0	1.13	S
Cu^+	−1.30	0.43	−0.55	2.5	0.96	S
Hg^{2+}	1.63	0.826	1.35	0.0	1.10	S
Tl^+	1.77	0.056	0.1	0.0	1.51	S
$[Cu(tetb)]^{2+}$	2.07	0.193	0.40	0.3	—	(S)
CH_3Hg^+	2.50	0.640	1.60	0.0	—	S
Cu^{2+}	2.68	0.466	1.25	6.0	0.57	I
Zn(II) in carbonic anhydrase	2.7	0.33	0.9	1.4	—	(S)
H^+	3.04	1.009	3.07	20.0	—	H
Cd^{2+}	3.31	0.300	0.99	0.6	0.95	S
Ni^{2+d}	3.37	0.300	1.01	4.5	0.69	I
Co^{3+e}	3.77	0.875	3.30	7.0	0.50	H
Zn^{2+}	4.26	0.312	1.33	4.0	0.74	I
Co^{2+d}	4.34	0.276	1.20	3.0	0.72	I
Fe^{2+d}	5.94	0.256	1.52	2.0	0.76	I
In^{3+}	6.30	0.714	4.49	0.5	0.81	H
Bi^{3+}	6.39	0.926	5.92	0.0	1.03	I
Pb^{2+}	6.69	0.413	2.76	0.0	1.18	I
VO^{2+}	6.71	0.593	3.98	3.5	—	H
Ga^{3+}	7.07	0.809	5.72	1.5	0.62	H
Mn^{2+}	7.09	0.223	1.58	1.0	0.80	H
Cr^{3+}	7.14	0.721	5.15	1.5	0.53	H
Fe^{3+d}	7.22	0.841	6.07	1.5	0.55	H
Be^{2+}	8.47	0.614	5.20	8.0	0.31	H
La^{3+}	10.30	0.379	3.90	0.0	1.03	H
Mg^{2+}	10.46	0.178	1.86	1.5	0.72	H
Al^{3+}	10.50	0.657	6.90	2.0	0.50	H
Ba^{2+}	10.67	0.03	0.32	0.0	1.36	H
Ca^{2+}	12.16	0.081	0.98	0.0	1.00	H
Li^+	22.11	0.026	0.58	1.0	0.60	H

Adapted from Ref. (*17*).

[a] Arranged in order of increasing I_A, or ionicity on the M–L band. Also shown are ionic radii and HSAB classification (*5*) of the Lewis acids.

[b] In Å, from Ref. (*20*), for six coordination, except for Be^{2+} and Cu^{2+}, which are four-coordinate.

[c] The HSAB classification of the Lewis acid, from Pearson (*5*, *5a*): H = hard, I = intermediate, S = soft. Classifications given in parentheses are from this work.

[d] High-spin ions. Low- or intermediate-spin ions are expected to be softer than high-spin ions.

[e] Low-spin ion.

TABLE II

I_B, E_B, C_B, AND D_B PARAMETERS FOR LEWIS BASES IN AQUEOUS SOLUTION[a]

Ligand	I_B	E_B	C_B	D_B	r(vdw)[b]
F^-	inf	1.00	0	0	1.35
CH_3COO^-	0	0.0	4.76	0	1.40
OH^-	0	0.0	14.00	0	1.40
N_3^-	−0.064	−0.067	10.4	0.2	1.50
SCN^-	−0.082	−0.76	9.3	0.2	1.50
NH_3	−0.088	−1.08	12.34	0.0	1.50
Imidazole	−0.09	−1.1	12.3	0.1	1.50
$HOCH_2CH_2S^-$	−0.097	−3.78	39.1	0.9	1.85
C_5H_5N	−0.102	−0.74	7.0	0.1	1.50
Cl^-	−0.100	−1.04	10.4	0.6	1.80
SO_3^{2-}	−0.107	−1.94	18.2	0.4	1.85
Br^-	−0.108	−1.54	14.2	1.0	1.95
$S_2O_3^{2-}$	−0.119	−3.15	26.5	1.1	1.85
I^-	−0.122	−2.43	20.0	1.7	2.15
NCS^-	−0.128	−1.83	14.3	1.0	1.85
$(HOCH_2CH_2)_2S$	−0.135	−1.36	10.1	0.6	1.85
$PPh_2(3\text{-}C_6H_4SO_3^-)$	−0.132	−3.03	23.0	0.7	1.9
$As(3\text{-}C_6H_4SO3^-)_3$	−0.135	−1.93	14.3	1.2	2.0
$(NH_2)_2C{=}S$	−0.135	−2.46	18.2	0.6	1.85
$HOCH_2CH_2PEt_2$	−0.141	−4.89	34.7	0.6	1.9
CN^-	−0.148	−4.43	30.0	0.38	1.7

[a] From Ref. (*17*).

[b] The van der Waals radii of the donor atoms of the ligand, in angstroms, from L. Pauling, "The Nature of the Chemical Bond," 3rd ed., p. 260. Cornell Univ. Press, Ithaca, NY, 1960.

tion of cationic Lewis acids with halide ions in the gas phase. Pearson (*19*) suggested that the ratio $\Delta H(F^-)/[\Delta H(F^-) - \Delta H(I^-)]$, here called I_P, would provide a measure of hardness of metal ions. Pearson has not pursued this measure of hardness, possibly because I_P does not conform to ideas of hardness derived from aqueous solution behavior. However, Fig. 8 shows a remarkable correlation between I_A and I_P, with cations falling on separate relationships according to charge. Equation (3) shows that Lewis acids can display what Pearson would call hardness, i.e., an order of stability with halide ions that is $F^- > Cl^- > Br^- > I^-$ in aqueous solution, for two very different reasons. The proton is hard, not because it cannot form covalent bonds—the C–H bond is very covalent. Rather, with ligands with large donor atoms such as I, S, or P, complexes with the proton are destabilized by adverse steric effects, and inability of the ligand to disperse charge to the solvent by H-

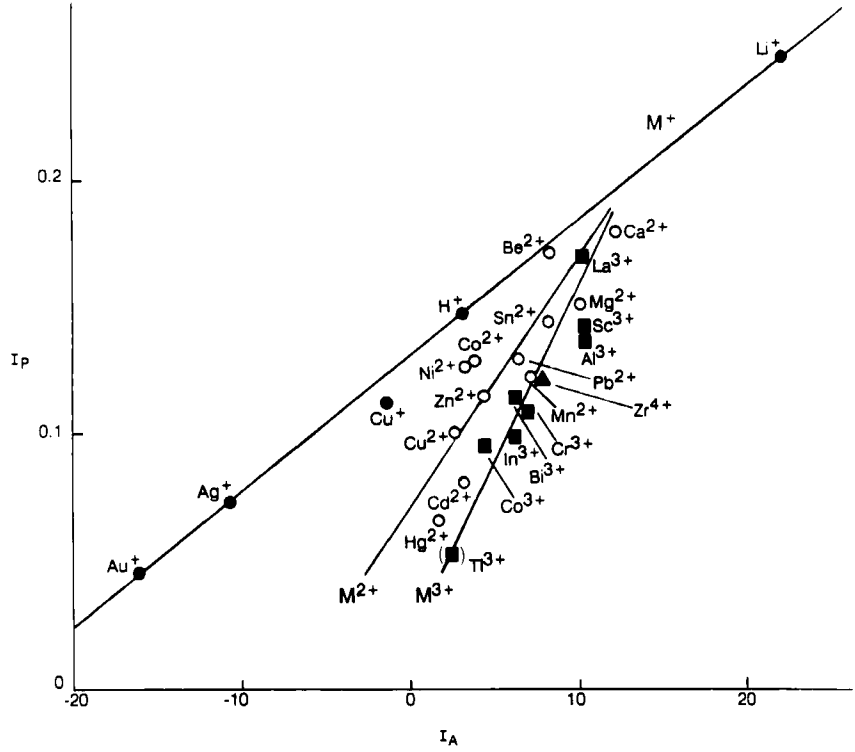

FIG. 8. Correlation between Pearson's hardness parameter (I_P) derived from gas-phase enthalpies of formation of halide compounds of Lewis acids (*19*), and the hardness parameter in aqueous solution (I_A), derived from formation constants of fluoride and hydroxide complexes in aqueous solution (*17*). The Lewis acids are segregated by charge into separate correlations for monopositive (●), dipositive (○), and tripositive (■) cations, with a single tetrapositive ion (Zr^{4+}, ▲). The I_P value for Tl^{3+} was not reported, but the point is included in parentheses to show the relative ionicity of Tl(III) to ligand bonds.

bonding. This is hardness that arises in the D parameters in Eq. (3). The second kind of hardness occurs in Lewis acids such as La^{3+}. This ion has a radius in excess of 1.0 Å, and so should not experience steric destabilization of its complexes (*20*). La^{3+} is hard because it is not able to form very covalent bonds, which is hardness arising in the E and C parameters of Eq. (3). Phillips and Williams (*21*) have suggested that hardness can arise in these two ways, without actually translating their ideas into a quantitative model. Table I shows that all metal ions of ionic radius in excess of 1 Å have a D_A of zero, suggesting that large ions have little difficulty in packing large donor atoms around themselves, and may have less need of dispersing charge to the solvent via H-bonding.

IV. Significance of HSAB Ideas for Zinc-Containing Metalloenzymes

As noted, biological processes use only metals such as Mg, Ca, Zn, Fe, Cu, Co, Ni, and Mn, with Mo being the only metal used from the second row of transition elements. How, then, is the chemistry of these metal ions altered to give the required bonding properties? For example, Zn^{2+} as the aquo ion has a modest affinity for hydroxide ion, with $\log K_1(OH^-)$ being only 4.6 (*11*). It occurs in many metalloenzymes such as carbonic anhydrase or alcohol dehydrogenase (*22*), where Zn(II) has a log K_1 with hydroxide ion of over 6.0. This increase in acidity of Zn(II) is important for it to function at biological pH. Replacement of Zn(II) with less acidic Cd(II) [$\log K_1(OH^-) = 3.8$] produces enzymes that function, but only at higher pH (*22*). A further alteration of ligand binding properties of Zn(II) in metalloenzymes is that, whereas Zn^{2+} aquo ion is classified as borderline (*5, 5a*) in HSAB classification and has log K_1 values as shown below, in carbonic anydrase (*23*) the order is reversed to $F^- < Cl^- < Br^- < I^-$, so that Zn(II) in this metalloenzyme would be classified as a soft Lewis acid:

$\log K_1$:	F^-	Cl^-	Br^-	I^-	OH^-
$Zn^{2+}(aq)$:[a]	1.15	0.43	0.03	−0.9	4.6
Zn(II) in carbonic anhydrase:[b]	−0.07	0.72	1.19	2.07	6.2

[a] Ref. (*11*).

[b] For bovine carbonic anhydrase, from Ref. (*23*).

Binding in the metalloenzyme has altered the Lewis acid properties of Zn(II) so that it is a stronger acid, and has become soft instead of intermediate in HSAB. This seems to relate to the coordination geometry and coordination number forced on Zn(II) by the enzyme binding site, since these properties have been replicated in simple model Zn(II) complexes (*24, 25*), such as 12-aneN_3. There may also be a contribution from the hydrophobic cavity in which the Zn(II) occurs in these metalloenzymes to the "soft" behavior of the Zn(II), since this would make the Zn(II) more like a metal ion in the gas phase (*6*). However, duplication of the soft behavior in model compounds with no hydrophobic cavities (*24, 25*) indicates that it must be largely a function of the bonding properties of the Zn(II) itself. Also important is that Zn(II) in alcohol dehydrogenases appears to bind alcohols (*26*). Ordinarily, metal ions bind alcohols only weakly in aqueous solution, so how does Zn(II) bind alcohols in these metalloenzymes?

An insight into metalloenzyme action is provided (*1*) by the work of Chung in studies (*27–29*) of binding of ligands to Cu(II) complexes of the macrocycle tetb (Fig. 9). As with $Zn^{2+}(aq)$, $Cu^{2+}(aq)$ has low affinity (*11*) for halide ions and is classified (*5, 5a*) as intermediate in HSAB. On incorporation into tetb, binding constants for simple unidentate ligands at the axial site of the complex change enormously, and Cu(II) in tetb is soft in HSAB (*1*):

log K_1 for	Cl^-	Br^-	I^-	NH_3	$CH_3CH_2NH_2$	$NH(CH_3)_2$
$Cu^{2+}(aq)$:[a]	0.4	−0.03	< -1	4.04	3.2[b]	no complex
$[Cu(tetb)]^{2+}$:[c]	1.19	1.26	1.35	1.95	2.84	2.69

[a] From Ref. (*11*).
[b] Estimated by comparison with Ni^{2+} complex.
[c] From Refs. (*27–29*).

The change of Lewis acidity of $[Cu(tetb)]^{2+}$ relative to $Cu^{2+}(aq)$ resembles the change in Lewis acidity observed for passing from $Zn^{2+}(aq)$ to Zn(II) in carbonic anhydrase. In parallel with the bonding order $Cl^- < Br^- < I^-$ for binding to the axial coordination site of $[Cu(tetb)]^{2+}$, there is a major alteration in tolerance of $[Cu(tetb)]^{2+}$ to steric effects of large bulky substituents. $[Cu(tetb)]^{2+}$ is unusual in aqueous solution in forming a complex with dimethylamine that is more stable than that formed with ammonia (*28*). *This is what would be expected from the physical model behind Eq. (3).* The *D* parameters in Eq. (3) have been interpreted (*17*) as steric effects on ligands with large donor atoms in tight coordination spheres of metal ions such as $Cu^{2+}(aq)$. If the steric problems of Cu(II) are overcome by placing it in the ligand tetb, then one should expect, in parallel with this, that $[Cu(tetb)]^{2+}$ should show increased tolerance to bulky alkyl substituents on the donor atoms of ligands such as amines. *The change of HSAB behavior from* Cu^{2+} *to* $[Cu(tetb)]^{2+}$ *that causes a reversal of complex stability from* $Cl^- > Br^- > I^-$ *(hard Lewis acid) to* $Cl^- < Br^- < I^-$ *(soft Lewis acid) is paralleled by a greatly increased tolerance toward sterically bulky alkyl groups on donor atoms, as expected if a contribution to "hard" behavior can arise in steric effects.*

An observation regarding HSAB theory here is that metal ions that are soft in aqueous solution must not only be able to form covalent M–L bonds, but also must have a loose enough coordination sphere to tolerate potentially adverse steric effects such as bulky donor atoms or substituents on a ligand. For a soft Zn(II) ion to be produced in zinc metalloenzymes, its coordination number must drop from six in the

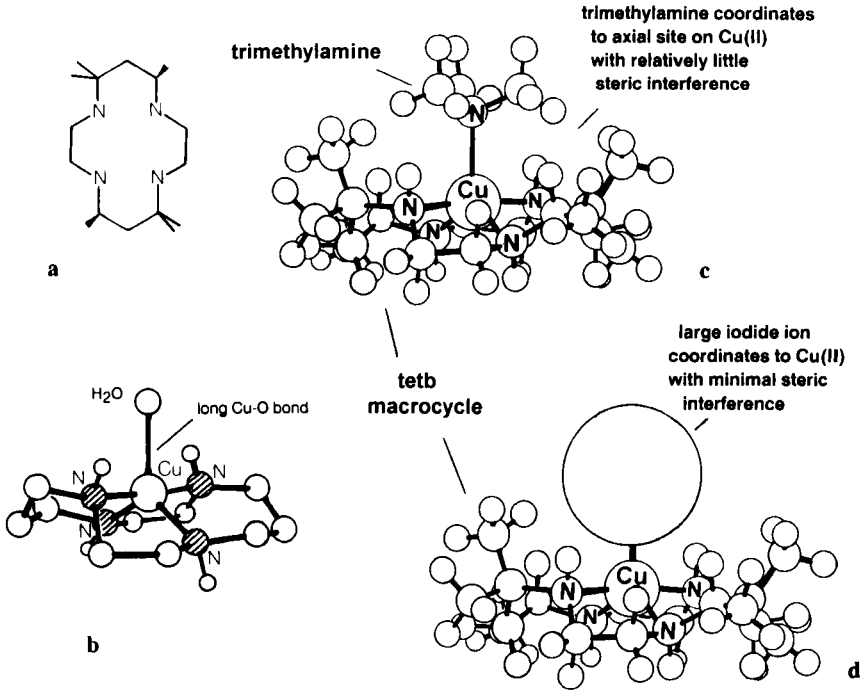

FIG. 9. The relationship between the steric situation at the coordination site and the observation of softness in Lewis acids. In addition to a covalent M–L bond, a low potential for steric hindrance of the coordinated unidentate ligand is required. (a) The ligand tetb (the ligand is the racemic form, only one enantiomer of the racemic pair is shown). (b) The crystal structure of blue $[Cu(tetb)H_2O]^{2+}$, showing the approximately trigonal bipyramidal coordination around the Cu(II), which leaves the coordinated unidentate ligand (in this case water) in a uniquely low-strain situation. Structure redrawn from Ref. (*27*). For clarity, all hydrogens except N–H hydrogens and the C-methyl groups on the ligand have been omitted. (c) The $[Cu(tetb)]^{2+}$ complex of trimethylamine, and (d) the same structure with an iodide in place of the axial trimethylamine molecule, showing how little steric contact there is between the iodide or trimethylamine and the $[Cu(tetb)]^{2+}$ complex. For clarity all the atoms in (c) and (d) were drawn with one-third van der Waals radii, except for iodide, which was drawn with full van der Waals radius. Structures in (c) and (d) were generated by MM calculation using the program SYBYL (Tripos Associates, St. Louis, Mo.).

aquo ion (*30*) to four in alcohol dehydrogenase or carbonic anhydrase. Lowered coordination number first decreases steric crowding around the metal ion and makes way for bulky donors such as I^-. Also, tolerance for bulky substituents, such as the ethyl group on ethanol, is increased. This could be an important aspect of increasing strength of binding of alcohols, whether as neutral molecules or alkoxides, to Zn(II)

in alcohol dehydrogenase. Figure 1 shows that in the gas phase, alcohols are stronger Lewis bases than the water molecule. In water, they are weaker bases than water itself, because bulky alkyl groups cause steric problems with most Lewis acids. By adopting tetrahedral geometry in metalloenzymes, Zn(II) can coordinate more effectively with alcohols, and other bulky substrates, than most ordinary metal aquo ions. This is because of lowered steric crowding. Also, as a second contribution, the ability for form covalent bonds should be somewhat higher for four-coordinate than six-coordinate zinc.

The structure of $[Cu(tetb)H_2O]^{2+}$ in Fig. 9 suggests how soft behavior arises sterically. Trigonal bipyramidal coordination geometry around the copper, coupled with a long Cu–O bond of 2.25 Å means that a bulky ligand that replaces the coordinated water will have minimal steric interaction with the tetb ligand. Equation (3) predicts that large metal ions that show a soft stability order with halides of $Cl^- < Br^- < I^-$ will also show unusual tolerance for bulky alkyl substituents on, for example, amines. Thus, Pb(II) has very long Pb–N bonds, as seen in the Pb–N of 2.53 Å in a complex (*31*) with ethylenediamine. These long Pb–N bonds should lead to high tolerance to steric effects of *N*-alkyl substituents. This is found for $R–N(CH_2CH(OH)CH_3)_2$ complexes of Pb(II) (*10*). Unlike the small $Cu^{2+}(aq)$ ion, there is a strong increase in log K_1 for Pb(II) as inductive effects increase along this series, R = $CH_3–$, $CH_3CH_2–$, $(CH_3)_2CH–$, $(CH_3)_3C–$. The $Pb^{2+}(aq)$ ion also forms (*32*) complexes with triethylamine that are much more stable than those with ammonia (*32*), as expected from Eq. (3).

Equation (3) usually models formation constants for Lewis acids with unidentate ligands well, as shown for log K_1 values for $[Cu(tetb)]^{2+}$ with unidentate ligands:

Ligand:	OH^-	NH_3	Cl^-	Br^-	I^-	N_3^-	NCS^-	CH_3COO^-	CN^-
log K_1 for $[Cu(tetb)]^{2+}$,									
Calculated:[a]	2.70	1.95	1.05	1.22	1.36	1.56	1.53[b]	0.93	3.65
Observed:[c]	2.71	1.95	1.19	1.26	1.35	1.93	2.16	0.26	3.45

[a] Calculated from Eq. (3) using parameters in Table I for $[Cu(tetb)]^{2+}$, and in Table II for Lewis bases.

[b] Calculated for bonding as a mixture of N and S bonded forms. Value of log K_1 for bonding through S is 1.13 and through N is slightly higher at 1.31. The crystal structure (*29*) of $[Cu(tetb)(SCN)]^+$ shows bonding to Cu through S.

[c] Observed log K_1 values from Refs. (*27–29*), ionic strength 0.1.

Change of Cu(II) from intermediate in $Cu^{2+}(aq)$ to soft in $[Cu(tetb)]^{2+}$ is due (Table I) mainly to a drop in D_A parameter from 6.0 in

$Cu^{2+}(aq)$ to 0.9 in $[Cu(tetb)]^{2+}$. There is also a modest increase in softness due to changes in E_A and C_A parameters, which can be interpreted in terms of the "symbiosis" proposed by Jorgensen (*33*). The low D_A parameter for $[Cu(tetb)]^{2+}$ suggests that the main effect in transforming Cu(II) to a soft Lewis acid in $[Cu(tetb)]^{2+}$ is the altered steric situation in coordination of bulky donor atoms to the metal ion.

Vallee and Williams (*34*) proposed that in the "entatic state," metal ions are forced to adopt unusual coordination numbers and geometries to produce properties required for specific functions of enzymes in which they occur. This appears to be particularly true for Zn(II). There are several examples (*22*) where Zn(II) ions are forced into low coordination numbers where they occur in metalloenzymes, with geometries approximating to tetrahedral, or trigonal bipyramidal, rather than octahedral. Achievement of stronger Lewis acidity, as well as softer acid character, and hence reduction in steric hindrance at the coordination site on the metal, may be important in binding bulky organic substrates. Some examples of this type of entatic state are shown in Fig. 10. These include Zn(II) in alcohol dehydrogenase, carbonic anhydrase, and in various peptidases, ribonucleases, and snake venoms (see Table III). This type of entatic state may be more difficult to achieve for other metal ions, possibly accounting for how often Zn(II) occurs in metalloenzymes. In addition, the fact that octahedral Zn(II) is a weaker and harder Lewis acid than tetrahedral Zn(II) means that the Lewis acid Zn(II) in alcohol dehydrogenase can be "switched off" (*35*) when the required coenzyme NAD^+ is not bound to the protein. Binding of NAD^+ to the protein causes a conformational change that promotes the octahedral–tetrahedral transition for Zn(II) in the metalloenzyme.

It is not clear how important assumption of low coordination number is for other metal ions in metalloenzymes in order to promote catalytic reactions. In nitrogenase (*7*) there are iron atoms that appear to be only three-coordinate, which one expects should lead to unusual Lewis acidity (Fig. 11), leading to an ability to coordinate the extremely weak ligand dintrogen. The binding of dioxygen by copper hemocyanin (*36*) has been successfully modelled by Kitajima *et al.* (*37*) from Cu(II) tris(1,3-di-*i*-propylpyrazolyl)borate (TPB) complexes (see Chart 1 for key to ligand abbreviations). Two coppers from two Cu(II) TPB complexes bind to oxygen in an edge-on fashion (Fig. 11), as deduced for hemocyanin itself (*36*). The Cu(II) ion appears extremely reluctant to adopt a tetrahedral environment (*37*). Thus, one might have expected the tripodal tris(pyrazolyl)borate ligand to promote tetrahedral coordination to Cu(II). However, the tetrahedral structure of [Cu(II)(TPB)Cl] is maintained only in the solid state or solvents of low dielectric constant (*37*). In a polar solvent such as DMF, a five-coordinate square

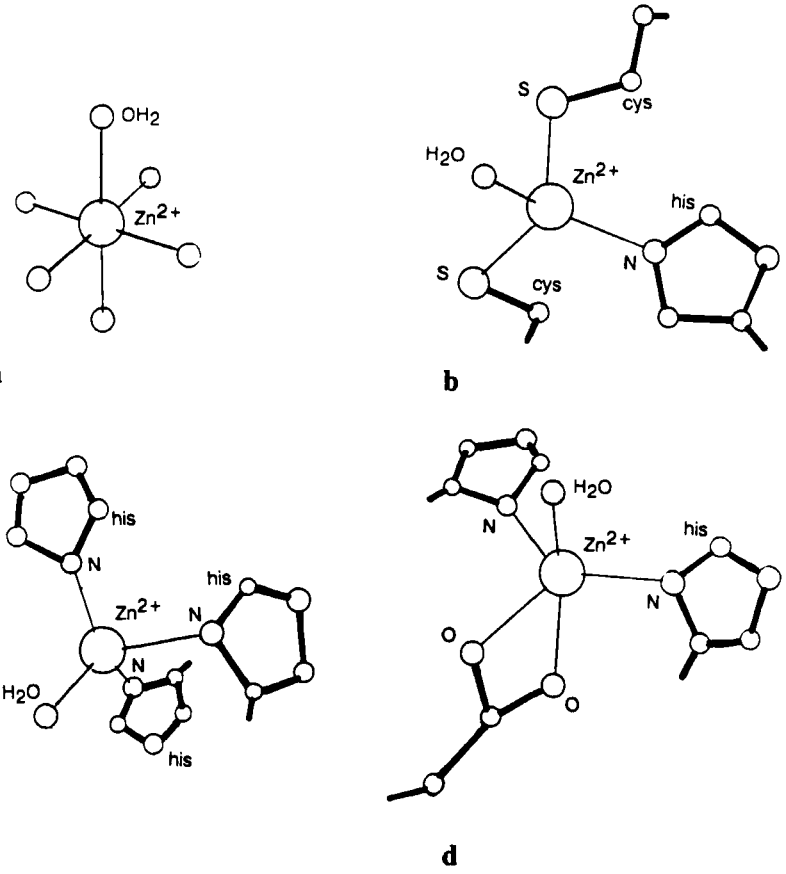

FIG. 10. Examples of coordination geometry in the entatic state (*34*) where the Lewis acidity of Zn(II) in its metalloprotein is considerably altered as compared with that for (a) the Zn^{2+} aquo ion (*30*), (b) Zn(II) in alcohol dehydrogenase, (c) Zn(II) in carbonic anhydrase, and (d) Zn(II) in carboxypeptidase. Redrawn after Ref. (*22*).

pyramidal structure is assumed. This may be one reason why Cu(II) is not as widely used in a strong Lewis acid role as is Zn(II). Thus, where one might have expected the tripodal TPB ligand to force Cu(II) to adopt a tetrahedral structure, the Cu(II) manages to form a distorted square pyramidal structure (Fig. 11), with the edge-on oxygen occupying two of the coordination sites in the plane. The structure of the nitrogen binding site of nitrogenase shows some three-coordinate irons that are nearly planar (*7*) (Fig. 11), and it seems possible that this is aimed at coordination of the very weak ligand dintrogen. The structure shown in Fig. 11 for nitrogen bound to nitrogenase is a highly specula-

TABLE III

OCCURRENCE, COORDINATION GEOMETRY, COORDINATING GROUPS, AND FUNCTION OF ZINC(II) IN SOME METALLOENZYMES

Enzyme	Coordination geometry	Coordinating groups
Carbonic anhydrase	tetrahedral	3 N (his), 1 O (water)
Alcohol dehydrogenase	tetrahedral	1 N (his), 2 S (cys), 1 O (H_2O)
Carboxypeptidase	5-coordinate	2 N (his), 3 O (bidentate acetate, H_2O)
Alkaline phosphatase		
site A	5-coordinate	2 N (his), 3 O (H_2O?)
site B	4-coordinate	N (his), 3 O (2 asp, ser)

tive one where the nitrogen is bound within a cage of six irons. Other possibilities (*7*) may involve sideways binding of the nitrogen to four of the irons on the outside of the cluster, perhaps indeed to the Mo, which is not yet excluded from consideration.

V. Chelate Ring Size and Metal Ion Selectivity

Chelate ring size and metal ion selectivity have been analyzed (*1*, *38*) and are discussed only briefly here. The geometry of chelate rings (Fig. 12) is such that five-membered chelate rings incorporate larger metal ions (M–L length ~ 2.5 Å) with small L–M–L angles (~70°) with least steric strain, while six-membered chelate rings best incorporate small metal ions (M–L ~ 1.6 Å) with large (~109.5°) L–M–L angles. As coordination geometry deviates from the requirements of these two different-sized chelate rings, so steric strain rises, and complexes are destabilized. This leads to a principle (*38*) of ligand design: *increase of chelate ring size leads to decrease in stability of complexes of larger relative to smaller metal ions.* This is seen (Table IV) in changes that occur in formation constants (*11*) for EDTA and TMDTA with metal ions of different sizes. EDTA forms five-membered chelate rings, and TMDTA forms six-membered chelate rings (Table IV), using the two nitrogen donors of these ligands.

Figure 12 also shows ideal geometry for symmetrical four-membered chelate rings involving phosphate and carboxylate. (By symmetrical is meant chelate rings having equal M–O distances to both coordinated oxygen donor atoms.) Four-membered chelate rings require very large metal ions, with even higher coordination numbers to produce the small

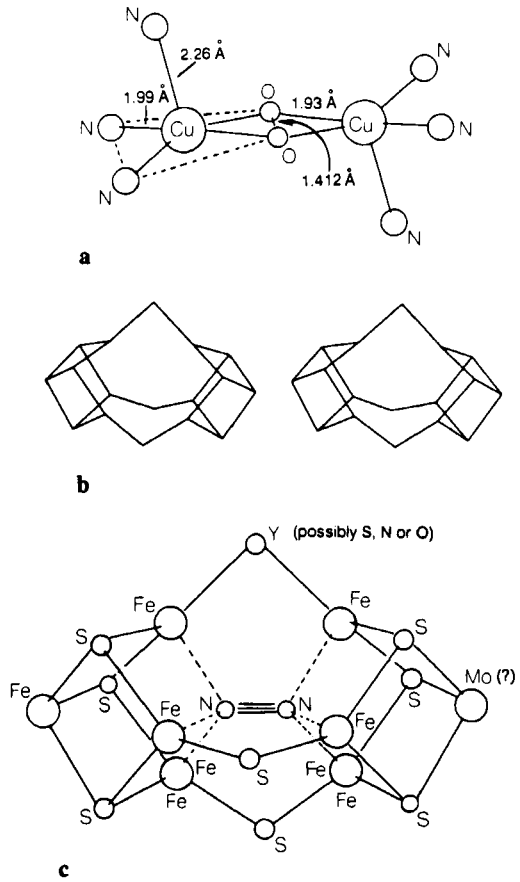

FIG. 11. (a) Structure of the bis[copper(II) tris-pyrazolyl borane] dioxygen complex of Kitajima *et al.* (*37*), which appears to be a good model for the coordination of dioxygen in hemocyanin. The coppers manage to adopt a square-pyramidal coordination geometry, which avoids the tetrahedral geometry that might have been expected with the tripodal TPB ligand. (b) A stereoview of the proposed (*7*) FeMo binding site for dinitrogen in nitrogenase. (c) The binding site for nitrogen in nitrogenase, suggesting how a nitrogen might be bound within the cavity. The highly speculative structure shown was generated by placing a nitrogen molecule within the iron–sulfur cluster, generated using the molecular mechanics program SYBYL (Tripos Associates, St Louis, Mo.). The drawing of the hemocyanin model of Kitajima *et al.* was executed using coordinates available in the Cambridge Crystallographic database, and the program SYBYL.

O–M–O bond angles required. One can relate bite sizes (distances between the donor atoms) of strain-free chelate rings of different sizes to the dimensions of the chair form of the cyclohexane ring (*39*), which has the minimum steric strain possible for a cycloalkane. The bite size of strain-free four- and six-membered chelate rings both correspond to

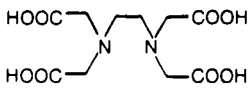

EDTA

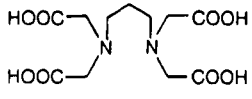

TMDTA

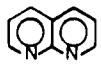

1,8-naphthyridine

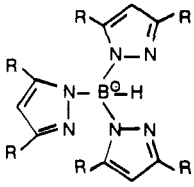

TPB R = 

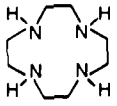

12-ane N_4

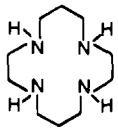

14-ane N_4

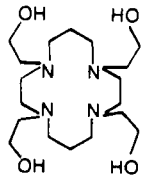

THEC

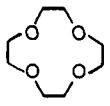

12-crown-4

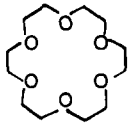

18-crown-6

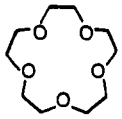

15-crown-5

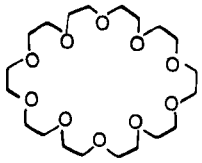

30-crown-10

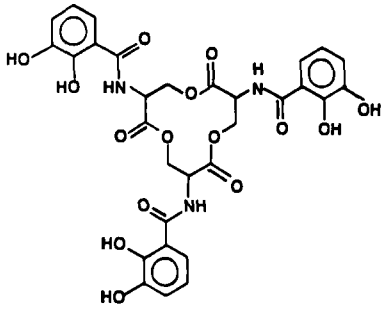

Enterobactin

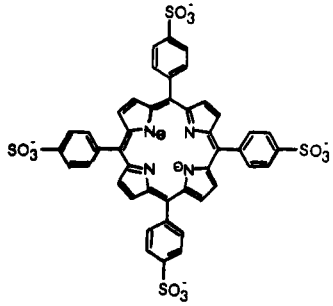

TSPP

CHART 1

the 1,3 distance across a cyclohexane ring. These distances are not greatly altered if, as is the case in chelate rings, sp^3 carbons are replaced with nitrogen or oxygen donor atoms. If larger atoms such as sulfur or phosphorus are part of the chelate ring, distances become greater, but the overall argument remains the same.

Structures of coordination compounds suggest that smaller chelate rings promote higher coordination numbers. Twelve coordination

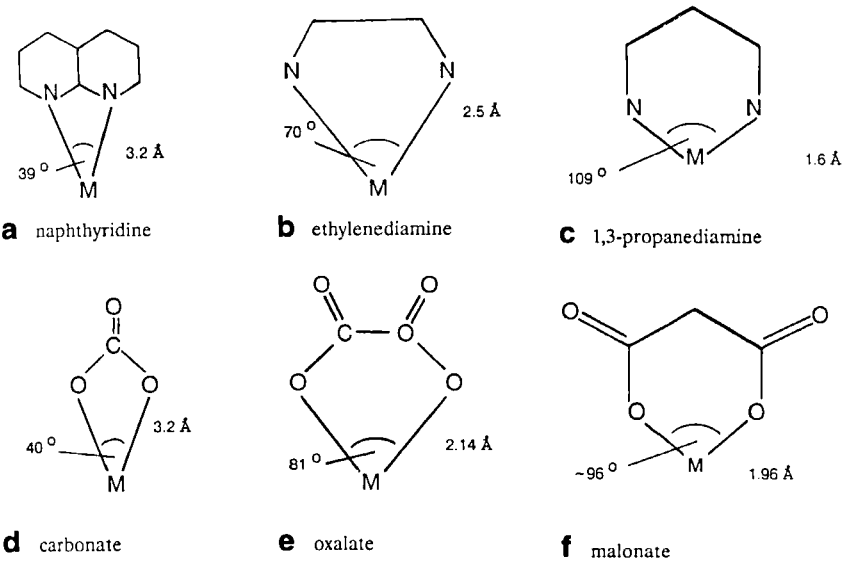

FIG. 12. The geometric origin of chelate ring size preference for metal ions of different sizes. (a) The four-membered ring, as exemplified for nitrogen donors with naphthyridine, requires the largest metal ions, and very small N–M–N angles. (b) The five-membered chelate ring of ethylenediamine has a preferred M–N length of 2.5 Å, and small N–M–N angle of 69°. (c) The six-membered chelate ring has a preferred M–N length of 1.6 Å and large N–M–N angle of 109.5°. In carboxylates, similar trends are observed for chelate rings of different sizes as exemplified by (d) carbonate, (e) oxalate, and (f) malonate. Minimum strain geometries calculated by Molecular Mechanics calculation (*4*).

TABLE IV

EFFECT OF CHELATE RING SIZE ON COMPLEX STABILITY: COMPARISON OF STABILITIES OF COMPLEXES OF EDTA (CHELATE RING SIZE FIVE INVOLVING THE TWO NITROGENS) AND TMDTA (ANALOGOUS CHELATE RING SIZE SIX)[a]

Metal ion	Ionic radius (Å)	log K_1		Difference in log K_1
		EDTA	TMDTA	
Be(II)	0.31	9.20	10.7	+1.5
Cu(II)	0.57	18.70	18.82	+0.12
Zn(II)	0.74	16.44	15.23	−1.21
Cd(II)	0.95	16.36	13.83	−2.53
Ca(II)	1.00	10.61	7.26	−3.35
La(III)	1.03	15.46	11.28	−4.18
Sr(II)	1.17	8.68	5.28	−3.40
Pb(II)	1.18	17.88	13.70	−4.18

[a] Data from Ref. (*11*). Ionic radii in Å from Ref. (*20*).

is always associated with four-membered chelate rings, as in the complexes $[Ce(NO_3)_6]^{2-}$ and $[Pr(napth)_6]^{3+}$, where naphth is 1,8-naphthyridine (*40*). Part of what determines coordination number may be the steric strain that would result from a mismatch between metal ion size and coordination number on the one hand, and chelate ring size on the other. With six-membered chelate rings, a metal ion should adopt its lower accessible coordination numbers, while with four-membered chelate rings, higher accessible coordination numbers should be preferred.

This may be discerned in biology with the Ca^{2+} ion. Selective binding of Ca^{2+} rather than Mg^{2+} may be essential in calcium proteins such as annexin (*41*), parvalbumin (*41a*), or calmodulin (*42*). In the binding sites in annexin and calmodulin (Fig. 13), Ca(II) is coordinated to several neutral oxygens, and a bidentate carboxylate from an aspartate. The Ca^{2+} occupying the "EF hand" site in parvalbumin is bound to two (*41, 41a*) bidentate carboxylates (Fig. 13). The four-membered ring in the bound carboxylate should favor binding of the large Ca^{2+} ion over the small Mg^{2+} ion. How neutral oxygen donors produce selectivity for large relative to small metal ions is discussed in Section E.

Proteins, as opposed to simple chelating ligands, are well suited to orient carboxylates to favor chelation. Carboxylates need long connecting chains to other donor atoms in a ligand if they are to twist around enough to be correctly oriented for binding in the symmetrical chelating mode. Ordinarily, long, flexible connecting chains lead to weak complexes, but proteins can provide rigid structures where carboxylates can be well spaced but correctly oriented. In simple chelating ligands, occurrence of carboxylate as part of a small chelate ring, e.g., carboxylates in EDTA, strongly favors only unidentate coordination of carboxylate.

An important aspect of how much chelate ring size can control metal ion selectivity is directional character of the bond to the donor atom. If a reasonably large force constant is associated with the Ca–O–C bond angle, then chelate ring size will have a strong effect on complex stability. If the M–O bond is so ionic that there is little tendency to keep the M–O–C bond at a well defined angle, then the chelate ring size principle will be weakly obeyed. This means that, as a rule, the more covalent the M–L bond, the more strongly the chelate ring size principles will be obeyed. One expects an increasing order of tendency to obey the chelate ring size principles of alkali metal ions < alkali earth metal ions < lanthanides < heavy post-transition metal ions [e.g., Pb(II), Cd(II)] ~ transition metal ions. Nitrogen donors form more covalent bonds than oxygen donors, so the principle should hold more

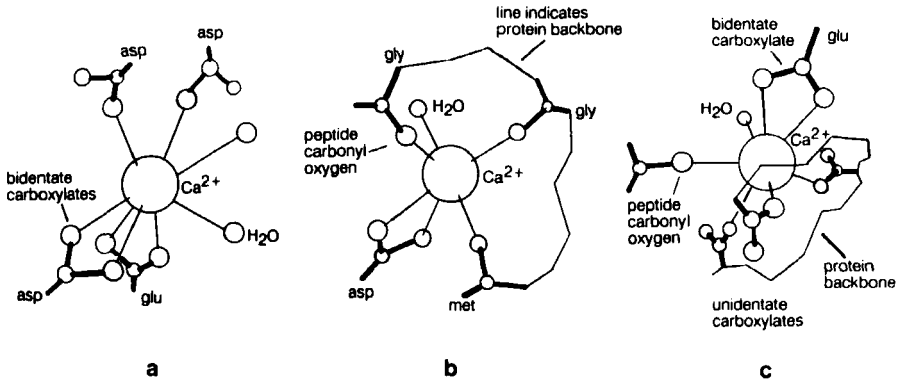

FIG. 13. The binding sites of calcium in (a) parvalbumin (*41a*), (b) annexin (*41*) and (c) calmodulin (*42*). The drawings show two bidentate carboxylates coordinated to Ca^{2+} in the "EF-hand" site of parvalbumin, and one bidentate carboxylate coordinated to Ca^{2+} in annexin and calmodulin. All the donor atoms coordinated to the calciums are oxygen donor atoms from carboxylates of asp = aspartate, or glu = glutamate, or else peptide carbonyl oxygens from gly = glycine or met = methionine. Redrawn after Refs. (*41–42*).

strongly with nitrogen donor ligands than oxygen donors. Table V shows stabilities of complexes formed by some metal ions with oxalate (five-membered chelate rings) and malonate (six-membered chelate rings). The large Cd(II) suffers a somewhat greater drop in log K_1 on increase of chelate ring size than does the slightly larger but more ionically bound Ca(II). However, Ca(II) shows (Table V) a reasonable decrease in log K_1 in passing from oxalate to malonate, suggesting considerable directional character in the Ca–O–C bond. Also, crystal structures (*43*) of calcium complexed to carboxylates show that even with unidentate coordination of the carboxylate, so that the ligand could in principle coordinate at any angle to the Ca(II), the Ca–O bond is located at a fairly specific angle relative to the C–O group involving the coordinated oxygen, indicating directional character in the Ca–O bond.

The chelate ring size principle can have structural effects as well as effects on thermodynamic stability in aqueous solution. An example is coordination of metal ions by sugars (*44*). The cyclic polyol *cis*-inositol can coordinate metal ions in two distinct ways (Fig. 14) (*45*). In *ax–ax–ax* bonding (Fig. 14), the metal ion is part of three fused six-membered chelate rings. Alternatively, in *ax–eq–ax* coordination, the metal ion is part of two fused five-membered and one six-membered chelate rings. Angyal has noted that metal ions of radius more than 0.8 Å adopt the *ax–eq–ax* structure (*44*), whereas with an ionic radius

TABLE V

EFFECT OF CHELATE RING SIZE ON COMPLEX STABILITY WITH METAL IONS OF DIFFERENT SIZES: OXALATE (RING SIZE FIVE) AND MALONATE (RING SIZE SIX)[a]

Metal ion	Ionic radius	log K_1		Difference
		Oxalate	Malonate	
Be(II)	0.31	4.96	6.18	+1.22
Cu(II)	0.57	6.23	5.80	−0.43
Mg(II)	0.72	3.43	2.85	−0.58
Cd(II)	0.95	3.89	3.22	−0.67
Ca(II)	1.00	3.00	2.35	−0.65
La(III)	1.03	6.03	4.94	−1.09
Pb(II)	1.18	4.91	3.68	−1.23

[a] Formation constant data from Ref. (*11*), ionic radii (Å) from Ref. (*20*).

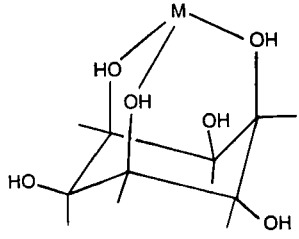

a ***ax-ax-ax***

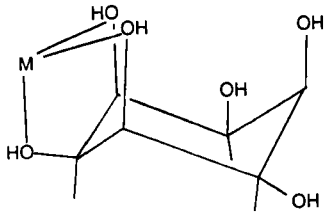

b ***ax-eq-ax***

FIG. 14. (a) The *ax–ax–ax* structure adopted by small metal ions, and (b) the *ax–eq–ax* type of structure adopted by large metal ions in their complexes with *cis*-inositol (*44*, *45*).

less than 0.8 Å the *ax–ax–ax* structure is adopted. The chelate ring size principle indicates why this should occur (*45*). Large metal ions chelate with least steric strain as part of five-membered chelate rings, and the *ax–eq–ax* structure maximizes the number of five-membered chelate rings of which the large metal ion is a part. Small metal ions adopt the *ax–ax–ax* structure, as this maximizes the number of six-membered chelate rings involving the metal ion. Other examples of the chelate ring size principle occur in structures of complexes of citrate ion (*46, 47*). Tridentate coordination of citrate (Fig. 15) with metal ions can lead to two six-membered chelate rings, or one five-membered and one six-membered chelate ring. The Cambridge crystallographic data base reveals that most metal ions adopt the structure that gives one five-membered and one six-membered chelate ring, shown for the large Bi(III) ion (*46*) in Fig. 15. Only very small Al(III) shows the structure with two six-membered chelate rings (*47*) (Fig. 15), in accord with the chelate ring size principle (*38*). Unpublished MM calculations by the present authors show that only metal ions of M–O bond length about 1.90 Å or less should favor the form of citrate complex with two six-membered chelate rings, compared to the structure with one five- and one six-membered chelate ring. The average Al–O bond length in the Al(III) citrate complex is 1.91 Å (*47*), and in the crystal lattice of the Al(III) citrate complex are present examples of coordination of Al(III) to citrate to give both six,six and five,six chelate ring sizes.

The enzyme aconitase (*48*) contains a Fe_4S_4 cluster which catalyzes the conversion of citrate to *iso*-citrate (*6*) via aconitic acid, as a part of the citric acid cycle. The crystal structure of aconitase (*48*) with *iso*-citrate bound to an Fe of the Fe_4S_4 cluster leads to the geometry around Fe shown in Fig. 15c. The *iso*-citrate binds in a bidentate fashion so as to form a five-membered chelate ring involving the hydroxyl and one carboxylate of *iso*-citrate. The Fe in aconitase has long Fe–O bonds to *iso*-citrate, averaging (*48*) approximately 2.3 Å in length, which is typical of the long Fe–O bonds found in Fe(II) complexes. A five-membered chelate ring would be preferred to a six-membered chelate ring with long Fe–O bonds of 2.3 Å. One might speculate on how the enzyme drives the switch from citrate to *iso*-citrate, and why a whole Fe_4S_4 cluster appears to be necessary, rather than a single Fe(II) ion held in a suitable donor atom environment. One possibility is a mechanism like the one we suggest in the following scheme, which involves the formation of a six-membered chelate ring in the transition state, with the transition state involving a more Fe(III)-like iron.

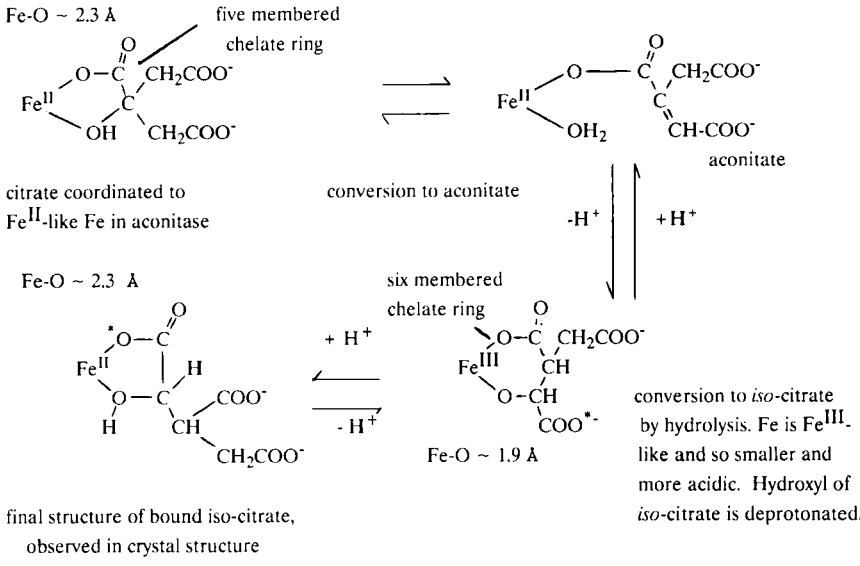

It might be that an electron shift within the Fe_4S_4 cluster occurs, which would decrease the Fe–O bond lengths and so favor the formation of a six-membered chelate ring. The electron shift within the Fe_4S_4 cluster would make the initial Fe(II)-like iron, with long Fe–O bonds, more Fe(III)-like, with short Fe–O bonds. What might cause the electron shift is coordination of the citrate. The driving force here might be tridentate coordination of the citrate (not shown), or deprotonation of either the alcoholic hydroxyl of the citrate or of a water coordinated to iron. The formation constant (*11*) (log K_1) for Fe(III) with citrate is 11.50, compared to 4.4 for Fe(II), so coordination of citrate in a tridentate fashion causes a shift of the Fe(III)/Fe(II) reduction potential of 120 mV in favor of FE(III). Deprotonation of the hydroxyl group of coordinated citrate causes a further shift in favor of Fe(III) at biological pH of about 100 mV. So either of these processes, tridentate coordination of the citrate or deprotonation of the coordinated hydroxyl of citrate, might trigger the electron shift within the Fe_4S_4 cluster. However, the coordination of citrate *iso*-citrate in a bidentate fashion without deprotonation of a hydroxyl would alter the Fe(III)/Fe(II) potential only slightly. Such bidentate coordination gives a glycolate-like ligand. The logK_1 value of Fe(III) with glycollic acid is only 2.9 (*11*), and of Fe(II) is 1.3, which would alter the Fe(III)/Fe(II) potential by only about 25 mV. The resemblance of bidentate coordinated citrate to glycolate is shown below:

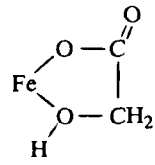

coordinated glycolate

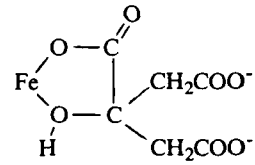

citrate bound in a bidentate fashion.

That the aconitase mechanism might involve an electron shift to give an Fe(III)-like iron in the transition state with the substrate bound to it suggests why a whole Fe_4S_4 cluster is needed. This mechanism would also explain how the substrate triggers the whole mechanism,

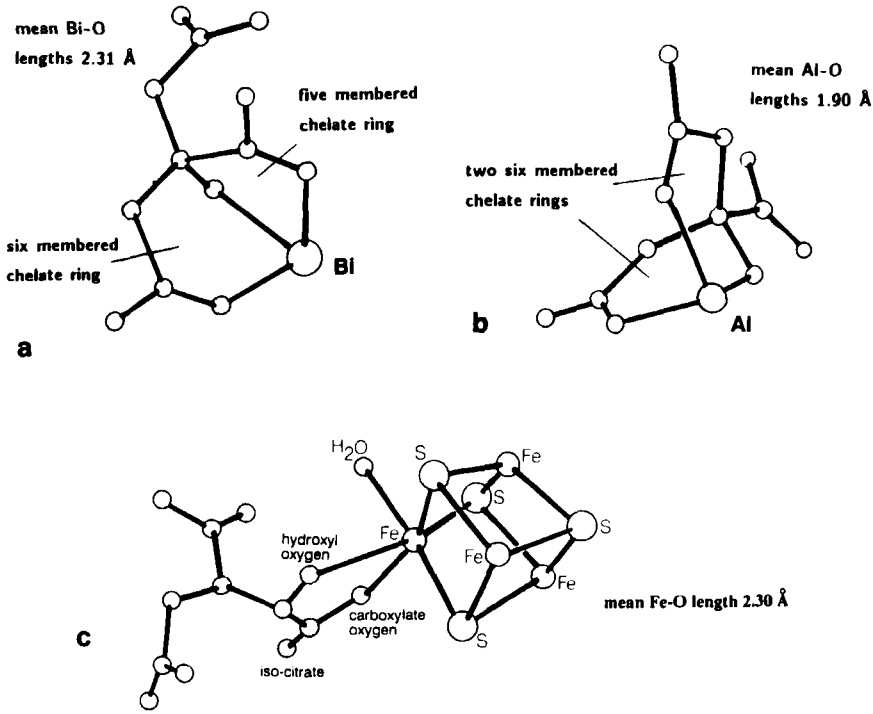

FIG. 15. Crystal structures of citric acid complexes of (a) Bi(III) (*46*) and (b) Al(III) (*47*), and of (c) *iso*-citrate bound to iron in the binding site of aconitase (*48*). The structures show (*45*) that, in accord with the chelate ring size ligand design principle (*38*), the large Bi(III) ion adopts the structure which gives one five-membered and one six-membered chelate ring, while the small Al(III) ion adopts a structure which gives it two six-membered chelate rings. The long Fe–O bonds in aconitase lead to *iso*-citrate bound so as to give a five-membered chelate ring. Redrawn after Refs. (*46–48*).

i.e., by deprotonation of the hydroxyl of the bound citrate, which makes the iron in the transition state more Fe(III)-like, and also more acidic. The greater acidity of the Fe(III)-like iron in the transition state would also promote proton transfer reactions to aconitase from waters coordinated to the Fe(III)-like iron.

The basis of the chelate ring size principle is that orientation of lone pairs on donor atoms is important. The entatic state hypothesis (*34*) proposes that the coordination geometry of metal ions may be distorted in metallo-enzymes to produce required properties. MM calculations suggest that bond length deformation by external steric factors is more difficult than bond angle deformation (*4*). The observation that bond lengths in carboxypeptidase A substituted with metal ions such as Co(II), Mn(II), Cd(II), or Cu(II) all appear normal for each metal ion is not surprising (*49*). For example, the M–O bond length to the same glutamate carboxylate oxygen donor in the carboxypeptidase A substituted with different metal ions varies from 2.17 to 2.61 Å with these different metal ions, depending on the bond lengths required by the metal ion. This shows how the metal ion can distort its immediate environment in the protein to suit its bond length needs. Conversely, all the metal ions studied have greatly distorted coordination geometry, showing that bond angles around metal ions are more easily distorted than bond lengths (*49*). This suggests that the entatic state should more readily involve distortion of bond angles around metal ions than bond lengths.

VI. The Neutral Oxygen Donor

Coordinating properties of neutral oxygen donors have been reviewed (*1, 50*) and are discussed only briefly, and then related to the occurrence of this donor group in systems of biological interest. The neutral oxygen donor is of particular interest, since it is the donor atom of water, the solvent in biological systems. Figure 1 shows that ligands containing neutral oxygen donors are not all of equal donor strength in the gas phase. Firstly, there is an increase in basicity as alkyl substitution increases along the series $H_2O < CH_3OH < (CH_3)_2O$. Ether oxygens, for example, are of considerable importance in monensin-type antiobiotics (*51*) (Fig. 16), which selectively complex Na^+. The other neutral oxygen donor of biological interest is the carbonyl group as found in esters or amides. The amide group is commonly found as a donor for binding calcium in proteins (*43*) and potassium in enniatin (*52*), while carbonyls of ester groups commonly occur in small biological molecules

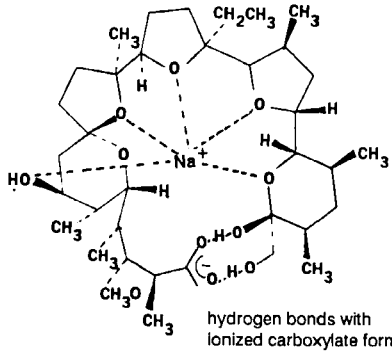

a MONENSIN

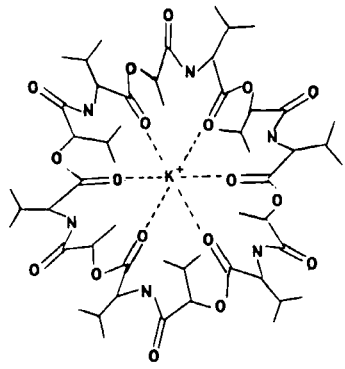

b VALINOMYCIN

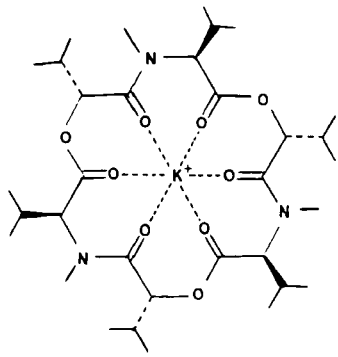

c ENNIATIN-B

FIG. 16. The antibiotic ligands (a) monensin, which binds Na^+ selectively, and (b) valinomycin and (c) enniatin-B, which bind K^+ selectively.

such as valinomycin (*52*) that bind K^+ (Fig. 16). Studies of crown ethers, and many ligands of biological interest, show that some metal ion types complex well with ligands containing neutral oxygen donors, while others do not. What determines whether a metal ion binds well with neutral oxygens? One widely accepted idea of what controls selectivity for metal ions, but which does not bear close inspection, is that of size-match selectivity (*53, 54*). In this idea, the metal ion forms its most stable complex with that member of a series of macrocycles where the size of the cavity in the macrocycle corresponds most closely to the size of the metal ion (*55*).

An indication of what controls selectivity with neutral oxygen donor ligands may be obtained from the stability of complexes of ligands with neutral oxygen donors on pendent donor groups. These donors are not part of macrocyclic rings, so that the neutral oxygen can be examined as a donor in its own right. For Li^+ (Fig. 1) and all other metal ions studied (*9, 13–15*), the order of stability with saturated neutral oxygen donors in the gas phase is $H_2O < MeOH < Me_2O$. One might therefore expect addition of pendent alcoholic donor groups to lead to an increase in complex stability compared to the unsubstituted ligand. For many metal ions this is true, as seen for the formation constants of complexes of the large Pb(II) ion with EN and THEEN (*11*):

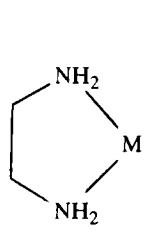

EN

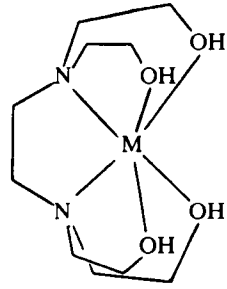

THEEN

$\log K_1$ [Pb(II)][11]	5.0	7.6
$\log K_1$ [Ni(II)][11]	7.3	6.5

For the small Ni(II) ion shown here, complex stability decreases on addition of neutral oxygens. Examination (*1, 50*) of relevant formation constant data (*11*) shows that the effect on complex stability of addition of neutral oxygen donors to ligands relates to metal ion size. This leads to a second ligand design principle: *Addition of groups containing neutral oxygen donors to a ligand leads to increase in selectivity for*

large metal ions over small metal ions. In the preceding example, Pb(II) is large, with an ionic radius (*20*) of 1.18 Å, while Ni(II) is small, with an ionic radius of 0.69 Å. As with the chelate ring size principle, the design principle concerning neutral oxygen donors holds with considerable accuracy. This can be seen in Fig. 17, where $\Delta\log K_1$, the change in $\log K_1$ produced on adding 2-hydroxyethyl groups to EN to give THEEN, is plotted against metal ion radius (*20*). Also in Fig. 17 is a plot of $\Delta\log K_1$ for PDTA-diamide versus EDDA. The C-methyl group on PDTA-diamide, not present on EDDA, should not cause significant changes in complex stability.

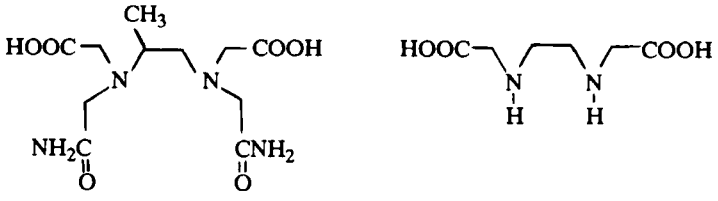

PDTA-diamide EDDA

Figure 17 shows how well metal ions follow the ligand design principle concerning neutral oxygen donor ligands and metal ion selectivity, whether the neutral donors are from alcohols or amides. Similar behavior (Fig. 18) is observed for macrocycles and cryptands. Addition of neutral oxygen donors so as to form macrocycles and cryptands (*1*) generally also obeys the principle on neutral oxygen donors and metal ion selection. However, the three-dimensional structure of cryptands gives the cavity in the ligand more rigidity than the cavity in simple macrocycles, and cryptands with smaller cavities may complex smaller metal ions more strongly than larger metal ions, displaying genuine size-match selectivity.

What may partly cause neutral oxygen donors to promote complex stability of larger metal ions, and destabilize complexes of smaller metal ions, is that in virtually all ligands where neutral oxygen donors are present, they are part of five-membered chelate rings (*50*). Thus, in accord with the idea that chelate ring size is a dominant factor in controlling metal ion size-based selectivity, even cryptands that form six-membered chelate rings (*56, 57*) show relatively greater complex destabilization with larger metal ions than do ordinary cryptands where all chelate rings formed are five-membered. Compared to usual

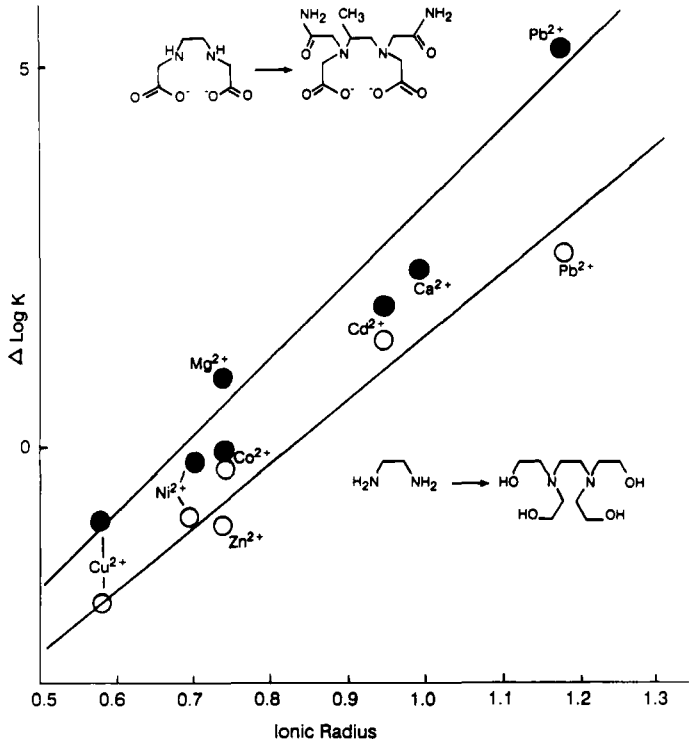

FIG. 17. Plot of change in complex stability, $\Delta\log K_1$, that occurs for the pairs of ligands THEEN and EN (○), and PDTA-amide and EDDA (●), as a function of metal ion radius (*20*). The diagram shows how netural oxygen donors stabilize the complexes of large metal ions relative to small metal ions. $\Delta\log K_1$ for THEEN and EN, for example, is log K_1 for the THEEN complex of the particular metal ions, minus log K_1 for the EN complex. Data from Ref. (*11*).

cryptands (*57, 58*), complex stability changes as would be expected for an increase in chelate ring size from five- to six-membered:

cryptand:

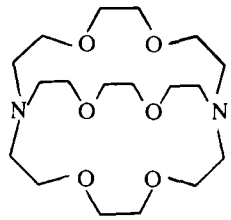

I

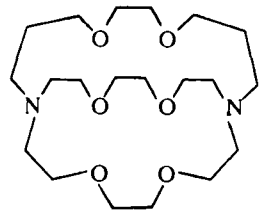

II

Metal ion	Ionic radius[a]	log K_1[b]	log K_1[b]	Change in log K_1
Na^+	0.98	4.11	1.3	2.8
K^+	1.33	5.58	1.2	4.4
Ca^{2+}	1.00	4.57	1.7	2.9
Ba^{2+}	1.36	9.7	4.4	5.3

[a] In Å, from Ref. (*20*).
[b] Refs. (*55–57*), 25°C, in water, ionic strength 0.1.

Almost counterintuitively, larger six-membered chelate rings have greatly destabilized complexes of large metal ions. Furthermore, complexes of the larger metal ions Ba^{2+} and K^+ have been destabilized more than those of the smaller metal ions Ca^{2+} and Na^+, in accord with the chelate ring size principle (*38*). Would the destabilization of complexes of even smaller metal ions such as Mg^{2+} or Li^+ be even less for the cryptand containing six-membered chelate rings? This might occur, although a further factor might outweigh the effect of chelate ring size. This is the denticity of the cryptand, which favors octadentate coordination to metal ions, which would be difficult for smaller metal ions. A ligand such as II contains conflicting ligand design features. The eight donor atoms require eight-coordination of the metal ion, which should therefore be large, while the six-membered chelate rings which it forms promote complexation of small metal ions.

Similarly, crown ethers that form six-membered chelate rings show strong selectivity for the very small Li^+ ion (*59*) over the larger Na^+ and K^+ ions. A further factor that may be important for neutral oxygen donors that are alcohols, ethers, or derived from carbonyl groups may be the reduced ability, compared with water, to hydrogen-bond with solvent water, and so disperse charge from the metal ion to the solvent, which should be more important for smaller, more highly charged metal ions. In keeping with both of these ideas, metal ions that complex well with crown ethers and other ligands containing neutral oxygen donors tend to be large, i.e., have an ionic radius of 1.0 Å or above.

Figure 19 shows the variation with metal ion radius of log K_1 for some crown ethers of differing macrocyclic ring size. The variation of log K_1 with size of metal ion and macrocyclic ring does not conform well with ideas of size match selectivity (*53*). In Fig. 19, a small crown ether such as 12-crown-4 shows almost no discrimination between the small Na^+ and the large Cs^+ ions. At the other end of the macrocyclic ring size range, a large macrocycle such as 30-crown-10 shows no strong preference for the very large Cs^+ ions over the smaller K^+ ion. MM

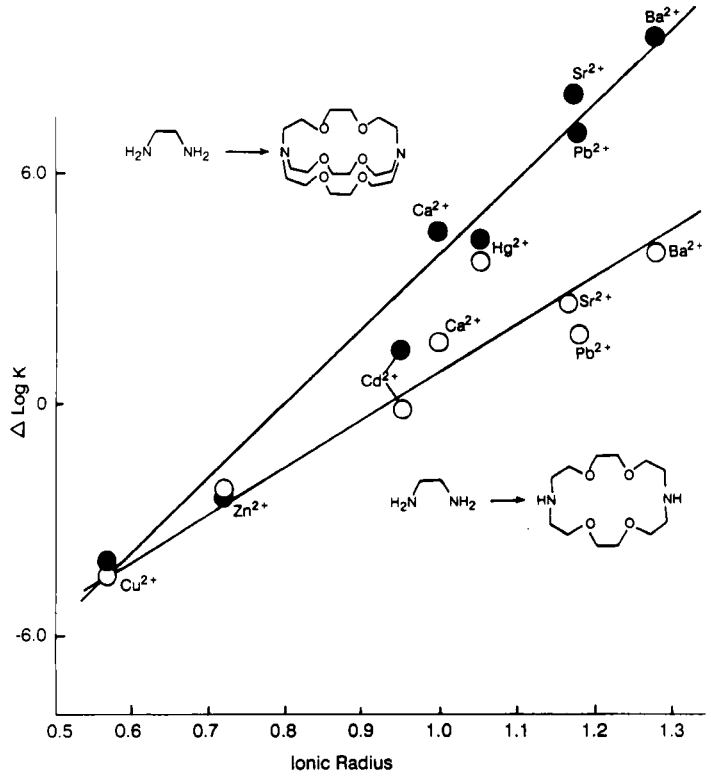

FIG. 18. Plot of change in complex stability, $\Delta\log K_1$, that occurs for the pairs of ligands cryptand-2,2,2 and EN (●), and 18-aneN_2O_4 and EN (○), as a function of metal ion radius (*20*). The diagram shows how neutral oxygen donors tend to stabilize the complexes of large relative to small metal ions in macrocyclic ligands. Data from Ref. (*11*).

calculations (*60*) suggest why this is so. A technique for evaluating which M–L bond length would produce the best fit with any particular ligand involves varying the ideal M–L bond length (*4, 61*) (for crown ethers, the M–O length) in the MM calculation, keeping all other parameters constant, and observing how strain energy varies with M–L length. A plot of strain energy as a function of M–O length (*4*) gives a minimum in strain energy which is the best-fit M–O length for coordinating with that ligand. The steepness of the curve indicates how strongly the ligand will select for the best-fit metal ions. Flatter curves suggest the ligand will not select strongly against metal ions of "incorrect" size. Where several conformers of the complex are energetically attainable, strain energy as a function of M–L length can be calculated for these conformers, and regions of M–L length where one

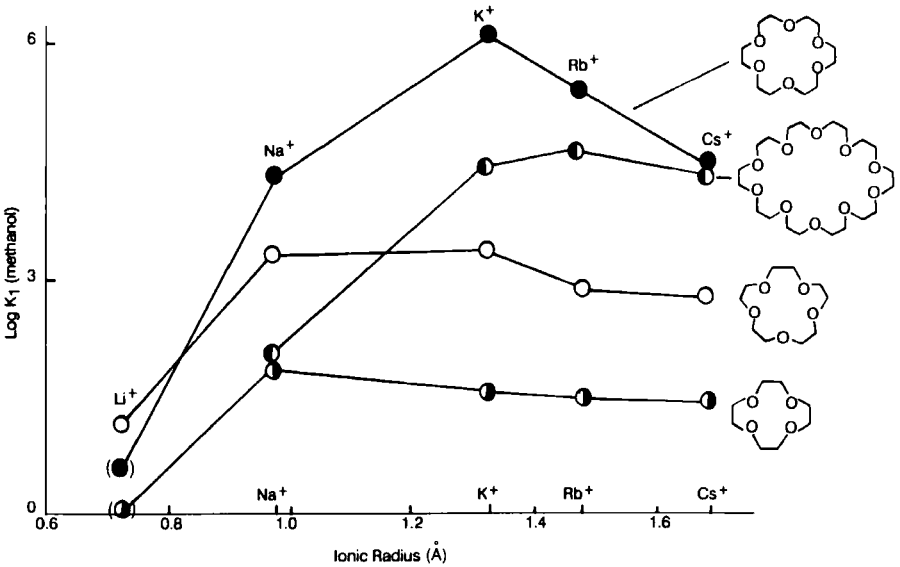

FIG. 19. The variation in $\log K_1$ for alkali metal ions with crown ethers 12-crown-4 (◑), 15-crown-5 (○), 18-crown-6 (●) and dibenzo-30-crown-10 (◐) as a function of metal ion radius. Metal ion radii in Å from Ref. (*20*). Formation constants in methanol from Refs. (*49* and *50*).

or other conformer is of lowest energy can be discerned. Figure 20 shows variation of strain energy with M–O bond length for what we shall term the buckled, the half-buckled, and planar (D_{3d}) form of 18-crown-6 complex (Fig. 21). The result is largely typical of what is observed for macrocyclic ligands. At M–O lengths above about 2.55 Å, the planar, or D_{3d}, conformer, is of lowest energy, and there is a minimum in strain energy for this conformer at an M–O length of about 2.9 Å. From 2.55 Å to about 2.3 Å, the half-buckled conformer is most stable. This agrees with adoption by the Na^+ ion, with a mean M–O bond length of 2.39 Å (*62*), of the half-buckled conformer in its complex with 18-crown-6. Below an M–O length of 2.3 Å, the buckled $+ + - + + -$ conformer is of lowest energy, and so is that observed in the complex of 18-crown-6 with Bi(III) (*63*), with its mean M–O length of 2.25 Å. The global minimum in strain energy for $[M(18\text{-crown-6})]^{n+}$ complexes at 2.9 Å accords with the complex of K^+, with 18-crown-6 being the most stable, since the mean K–O bond length in the complex of K^+ with 18-crown-6 is 2.88 Å (*64*). 18-crown-6 is unusual in that there is a range of M–O lengths where the D_{3d} conformer is of much lower energy than any of the other observed conformers in complexes

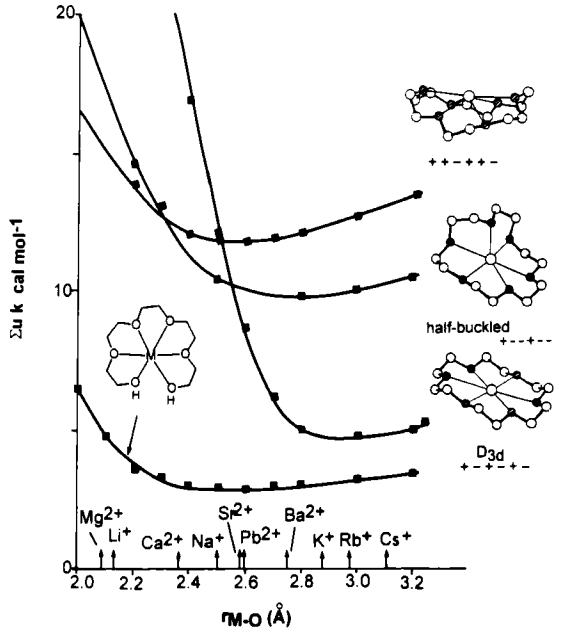

FIG. 20. The variation in strain energy, U, for various conformations of $[M(18\text{-crown-}6)]^{n+}$ complex, as a function of strain-free M–O bond length. The M–O bond lengths of various metal ions are indicated on the M–O bond length axis. The curves are for the planar D_{3d} (+-+-+-), half-buckled (+--+--), and buckled (++-++-) conformers shown in Fig. 21, and for the complex of the open chain complex of pentaethylene glycol. The calculations were carried as described in the text, and in Refs. (*4* and *60*). Redrawn after Ref. (*60*).

with metal ions. This accounts for the fairly sharp selectivity observed for K^+ with 18-crown-6 in Fig. 19.

Figure 22 shows variation in strain energy with M–O bond length of the + + + + conformer of 12-crown-4, and the conformer of 15-crown-5 observed in the benzo-15-crown-5 complex of Na^+ (*65*). Also included is variation in strain energy with M–O length of complexes of the open-chain ligands triethylene glycol and tetraethylene glycol. There is very little difference in steepness and shape of the curves for the complexes of the macrocycles 12-crown-4 and 15-crown-5 on the one hand, and their open-chain analogues triethyleneglycol and tetraethyleneglycol on the other. For most macrocycles, the ligand is too flexible to exert any real size-match selectivity. For macrocycles that are generally too small for the metal ion to lie in the cavity, such as the crown ether 12-crown-4 or the tetraaza macrocycle 12-aneN_4, metal ions are coordi-

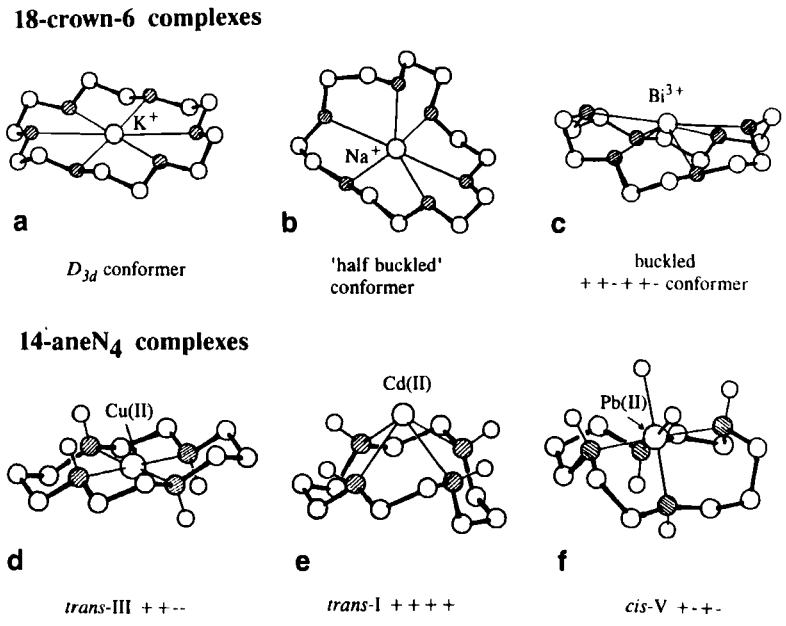

FIG. 21. (a) The D_{3d} (+-+-+-) conformer, and (b) The half-buckled (+--+--) and (c) + + -+ + - conformers of 18-crown-6. (d) The *trans*-III (+ + --), (e) the *trans*-I (+ + + +), and (f) the *cis*-V (+-+-) conformers of 14-aneN$_4$.

nated lying out of the plane formed by the donor atoms of the macrocycle, and steric factors that control metal-ion size-based selectivity tend to be the same as is found for open-chain ligands, namely size of the chelate rings formed. Only in a few situations, where the symmetry of the conformer formed by the macrocycle in its complex is such that the metal ion is to some extent constrained to lie in the plane of the donor atoms of the macrocycle, such as the D_{3d} conformer of 18-crown-6, or the trans-III + + − − conformer of 14-aneN$_4$ complexes (Fig. 21), is anything like size-match selectivity observed. Even so, the contribution of size-match selectivity to metal ion selectivity is not as great as might be expected, since for complexes of these ligands, where metal ions are too large for coordination in the cavity of the macrocycle, other conformers such as the half-buckled or buckled conformers of 18-crown-6 complex, or the folded *cis*-V and *trans*-I complex of 14-aneN$_4$ (Fig. 21), are of not too much higher energy for stable complexes to be formed.

Selectivity of ion channels for metal ions is of great current interest (*66*), as it relates to conduction of nerve signals, maintenance of the appropriate metal ion distribution in the intracellular and extracellular

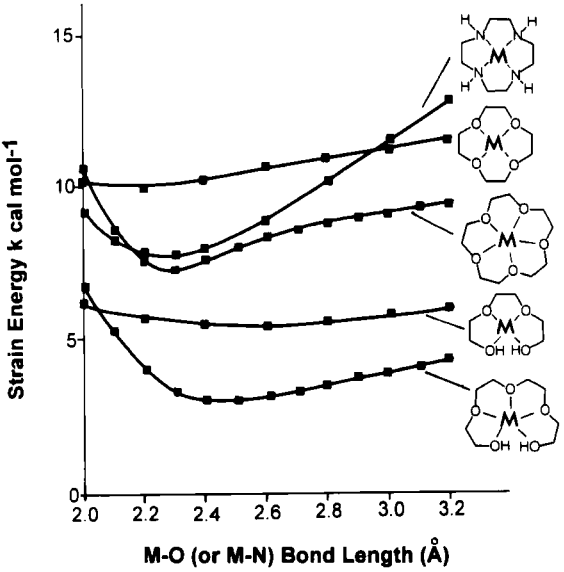

FIG. 22. Strain energy (U) as a function of strain-free M–O bond length for complexes of 12-crown-4 and 15-crown-5. Also shown are the curves of strain energy vs M–O bond length for the open-chain analogues triethylene glycol and tetraethylene glycol. The curve for the *trans*-I form of 12-aneN_4 complex shows how the more covalent M–N bonds lead to sharper size selectivity for metal ions. Redrawn after Ref. (*60*).

medium, and drug action. A puzzle is that proteins that act as potassium channels appear to contain few polar side groups (*67*). There is a conserved region in proteins that form potassium-selective channels, where several phenyl side groups are present in the region of the protein that appears to engender selectivity for K^+. The presence of these phenyl groups has led to the interesting suggestion (*67*) that π complexation of the K^+ is occurring and is responsible for the high selectivity for K^+ that K^+ channels display. The final word on potassium selectivity will have to await a crystal structure of a relevant channel-forming protein. However, some interesting insights can be obtained by considering K^+ ion channel permittivity (the rate at which ions pass through the channel) compared to the affinity of the same cations for a crown ether such as 18-crown-6. The ability of monovalent metal ions to permeate through potassium channels is shown as a function of log K_1 with 18-crown-6 in Fig. 23. Figure 23 suggests that the groups that metal ions might bind to in potassium channels have some resemblance to ethereal oxygens of 18-crown-6. However, the sequences of proteins that form potassium ion channels have few oxy-

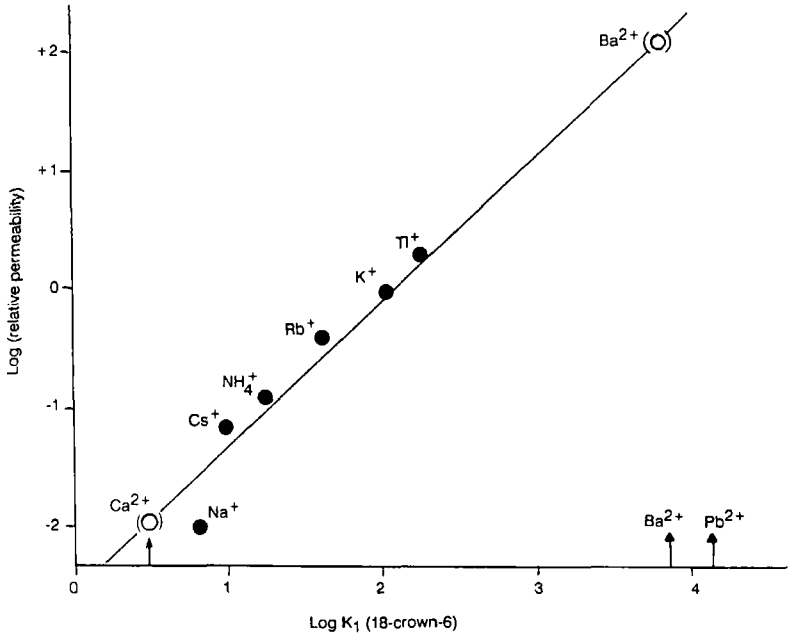

FIG. 23. Correlation between permeability of potassium ion channels to univalent metal ions and formation constant of the same metal ions with the crown ether 18-crown-6. Data for permeability of potassium ion channels for giant squid axon from Ref. (*66*), and formation constants for 18-crown-6 in water at ionic strength 0.1 and 25°C, from Ref. (*11*). The low formation constant for Ca(II) with 18-crown-6 may point towards the origin of the selectivity of the potassium ion channels against Ca^{2+}, while the high formation constant with Ba^{2+} suggests why Ba^{2+} is able to block potassium channels. The Pb^{2+} ion should also be able to block these channels.

gen donor side groups in the region thought to control metal ions selectivity (*67*). It seems possible that the neutral oxygen donors (*67*) in the ion channels derive from carbonyl oxygens of peptide amide groups, oriented into the channel so as to coordinate with ions passing through the channel. Amide oxygens are much stronger bases than ethereal or alcoholic oxygens (see Fig. 1 and Fig. 17), but are otherwise expected to show similar selectivity patterns (*1*). The correlation in Fig. 23 extends to explaining the selectivity against the divalent Ca^{2+} observed (*66*) in K^+ channels, which is expected from the low affinity of Ca^{2+} for 18-crown-6. One would say that Ca^{2+} is, like Na^+, too small [both have ionic radii (*20*) of about 1.0 Å] to coordinate well to the proposed amide oxygen donor groups of the K^+ channel. Figure 23 accounts for an interesting phenomenon observed with K^+ channels (*66*). For maximum rate of passage of ions from one aqueous phase,

through a membrane, and into a second aqueous phase, the ligand in the membrane has an optimal strength of binding to the cation. If the ligand binds the cation too weakly, as happens with Na+ and Ca^{2+} in K^+ ion channels, distribution from the first aqueous phase into the organic phase is too weak, and transfer is slow. Conversely, if the ligand binds the cation too strongly, it sticks in the organic phase, and transfer to the second aqueous phase is slow. Figure 23 indicates very strong binding of Ba^{2+} with 18-crown-6. It is found that Ba^{2+} sticks in K^+ ion channels (*67*). Although K^+ ions ordinarily pass through the K^+ channel on the time scale of nanoseconds, a single Ba^{2+} ion can block a K^+ channel to passage of K^+ ions for several seconds. This indicates very tight binding of Ba^{2+} by potassium ion channels, as would be expected from the correlation in Fig. 23. Figure 23 predicts that, if the binding of metal ions in K^+ channels resembles complexation with 18-crown-6, the Pb^{2+} ion should block K^+ channels even more strongly than does Ba^{2+}. It would be interesting to see whether this is so.

VII. The Negative Oxygen Donor

The negative oxygen donor occurs in a number of donor groups of biological interest, such as carboxylates, hydroxamates, phosphates, and phenolates. What controls thermodynamic stability of complexes of metal ions with ligands with negative oxygen donors (*1*) is affinity for the archetypal negative oxygen donor, hydroxide ion. Figure 24 shows the relationship between log K_1 for the siderophore DFB (desferriferrioxamine-B) and log K_1 (OH^-) for metal ions. Highest complex stability for DFB occurs with the most acidic metal ions. Acidity of metal ions is related to metal ion size and charge, and also covalence in the M–O bond (*68*). This is shown by the acidity of the trivalent group (III) metal ions Al(III) to Tl(III), where acidity varies inversely with ionic radius and appears to be controlled by covalence, which varies inversely with the ionicity parameter I_A (see Section B for significance of I_A parameters):

Metal ion:	Al(III)	Ga(III)	In(III)	Tl(III)
Ionic radius (Å)[a]	0.50	0.62	0.81	0.95
I_A[b]	10.50	7.07	6.30	2.66
log K_1 (OH^-)(*11*)	9.01	11.4	10.0	13.4

[a] From Ref. (*20*).

[b] Decreasing I_A indicates increasing covalence. From Table I.

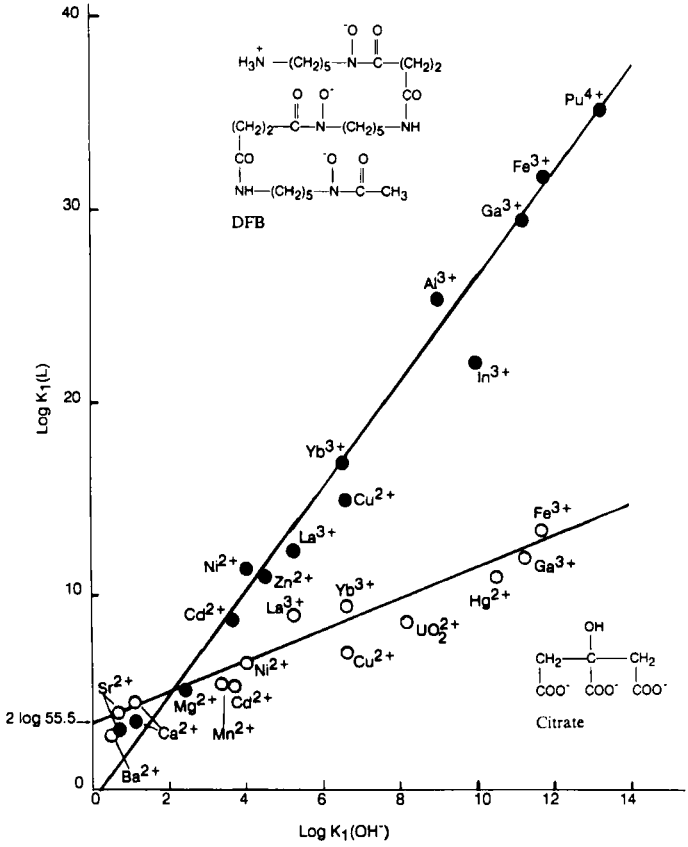

FIG. 24. Correlation between log K_1 for polydentate ligands containing negative oxygen donors, and log $K_1(OH^-)$ for the same metal ions. Ligands shown in the correlation are DFB (β-desferriferrioxamine-B) (●) and citrate (○). The sizes of the intercepts on the correlations are indicators of the level of preorganization of the polydentate ligand, as discussed. Formation constant data from Ref. (*11*).

Fe(III) is the ion of high charge and small size of importance in biological systems. Its covalence appears to be similar to that of Ga(III) (*17*).

Two important factors (*1*) control correlations such as Fig. 24. Firstly, more basic donor atoms on the ligand lead to steeper slopes for such correlations. Steeper slopes lead to higher selectivity for more acidic metal ions such as Fe(III) (*69*). Accordingly, donor atoms (*70*) in siderophores contain more basic negative oxygen donor groups such as hydroxamates and phenolic oxygens, which produce greater selectivity for Fe(III). Secondly, the size of the intercept in correlations such as Fig. 24 depends on the level of preorganization of the ligand. Analysis of

the chelate effect (*71*) suggests that the chelate effect should give a stabilization of $(n - 1)\log 55.5$, where n is the denticity of the multidentate ligand in Eq. (4):

$$\log K_1 \text{ (multidentate)} = \log \beta_n \text{ (unidentate)} + (n - 1)\log 55.5. \quad (4)$$

$\log \beta_n$ refers to the cumulative stability constant of the complex containing n unidentate analogues of the multidentate ligand bound to the metal ion. The $(n - 1)\log 55.5$ term is an entropy contribution to complex stability. More flexible ligands give smaller intercepts than expected from Eq. (4). Thus, a ligand such as DFB, with its long connecting bridges between the donor groups, is of low preorganization, and the intercept is smaller than the 5 log 55.5, or 8.7 log units, expected for a hexadentate ligand (*71*). For smaller ligands with short connecting bridges between donor groups, such as citric acid in Fig. 24, the intercept is close to the theoretical value of 2 log 55.5 for a tridentate ligand (*71*). The intercept on a correlation such as Fig. 24 is an indicator of the level of preorganization of the ligand.

Greater basicity favors complexation of more acidic metal ions, while a large number of highly preorganized donor groups will produce a large intercept on correlations such as Fig. 24. Thus, Fe(III) is complexed in flexible ligands with low levels of preorganization such as DFB and enterobactin (*70*). The high basicity of the hydroxamate or phenolate oxygens of these ligands favors more acidic Fe(III), while the flexibility of the ligand leads to low intercepts in correlations such as Fig. 24, and poor affinity for metal ions of low acidity such as Ca(II) or Zn(II). An additional factor here is that the low level of preorganization will lead to more rapid metallation reactions. The price of high preorganization is slow kinetics (*1*). In contrast, to complex ions of low acidity such as Ca(II), without the ligand being preferentially complexed by more acidic metal ions, the basicity of the negative oxygen donor must be low, and so in calcium binding proteins such as calmodulin (*42*) the negative oxygen donor atoms are low-basicity carboxylate groups. To maximize affinity of the ligand for the low-acidity Ca(II) ion, several well-preorganized carboxylates or other donor groups could be used, which would promote complex stability for the Ca(II) by maximizing the entropy contribution to the chelate effect.

VIII. The Nitrogen Donor

The nitrogen donor commonly found coordinated to metal ions in biology is the imidazole group from histidine. It is found coordinated

to metal ions such as Cu(II) in hemocyanin (*36*) and Zn(II) in carbonic anhydrase (*22*). These metal ions have a well-studied (*11*) aqueous chemistry with nitrogen donor ligands. However, transferrin has an imidazole coordinated to Fe(III), in addition to two phenolates (*72*). One expects negative oxygen donors to be used to complex the acidic Fe(III) ion (Section F), but what affinity does Fe(III) have for imidazole nitrogen? A variety of procedures have been used to estimate the formation constants of metal ions such as Fe(III) for nitrogen donor ligands such as ammonia (*1, 73*). The reason that Fe(III) does not form complexes with ligands such as NH_3 in water is not that the complex has a low formation constant, but that high acidity of Fe(III) leads to hydrolysis according to

$$Fe(NH_3)^{3+} + H_2O = FeOH^{2+} + NH_4^+. \quad (5)$$

The estimated (*73*) log $K_1(NH_3)$ for Fe(III) of 3.8 suggests that reaction (5) would have a reaction quotient of 3.2 log units, so $Fe(NH_3)^{3+}$ could not be detected in aqueous solution. In Table VI are values of log K_1 with imidazole for metal ions of interest in biology, both experimental (*11*) are predicted by Eq. (3). As expected from its high stability constant with ammonia, Fe(III) forms a strong complex with imidazole, accounting for its use in transferrin. Cobalt(III) has a very high affinity for nitrogen donor ligands, relating to its occurrence (*74*) in vitamin B_{12},

TABLE VI

STABILITY OF COMPLEXES OF IMIDAZOLE WITH METAL IONS OF BIOLOGICAL AND BIOMEDICAL INTEREST[a]

Metal ion	log K_1 imidazole	Metal ion	log K_1 imidazole
Metal ions of biological interest:			
Ca(II)	−0.1[b]	Mg(II)	0.0[b]
Zn(II)	2.56	Cu(II)	4.18
Cu(I)	6.8	Fe(II)	1.4
Mn(II)	0.8[b]	Ni(II)	3.02
Fe(III)	3.5[b]	Co(III)	6.4[b]
VO^{2+}	2.5[b]	H^+	7.03 (7.03[b])
Metal ions of biomedical interest:			
Gd(III)	0.5[b]	Y(III)	0.4[b]
Ga(III)	3.5[b]	In(III)	3.8[b]
Bi(III)	5.0[b]	Pb(II)	1.6
Cd(II)	2.80	Hg(II)	9.2

[a] Experimental data from Ref. (*11*).
[b] Estimated data from Eq. (3) and parameters in Tables I and II.

where it is held by four nitrogen donors. The log K_1 (imidazole) estimated is for high-spin Fe^{3+}, and bonds to low-spin Fe(III) should be considerably stronger.

The porphyrins (*75*) are among the most highly preorganized ligands. A recent study (*76*) of the formation constants of metal ions with TSPP (tetrasulfophenylporphyrin) in 80 : 20 DMSO/H_2O shows that even with metal ions such as Mg(II), which has only low affinity for nitrogen donor ligands (Table VI), the formation constant is extremely high. An advantage of the solvent used is that, unlike water, a high enough pH can be attained to measure the high first and second protonation constants of the free ligand. In water, these can only be estimated. The results in DMSO : water should otherwise not be too different from those in water. One can contrast (Table VII) formation constants of the porphyrin TSPP with the tetraaza macrocycles cyclam and THEC [tetrakis(2-hydroxyethyl)cyclam] for the same metal ions. Mg(II) has only a low affinity for THEC, but a high affinity for TSPP, showing the high preorganization of porphyrins. The high levels of preorganization of porphyrins lead to high kinetic inertness to metallation and demetallation, seen in the fact that equilibration of the Cu(II)/TSPP solutions with the proton took two years (*76*). Thus, the thermodynamic selectivity of porphyrins for metal ions based on size-match selectivity is perhaps not of direct significance in biology. Possibly more relevant is the effect of metal ion size on structure. MM can be used (*77*, *78*) to show that metal ions with M–N bond lengths of 2.035 Å fit best into

TABLE VII

STABILITY OF COMPLEXES OF THE PORPHYRIN TSPP COMPARED WITH THE NITROGEN DONOR MACROCYCLES CYCLAM AND THEC, WITH METAL IONS OF BIOLOGICAL INTEREST[a]

Metal ion	log K_1:[b]	$TSPP^{2-}$	Cyclam	THEC
Cu(II)		38.1	27.2	15.7
Zn(II)		34.6	15.5	6.4
Mg(II)		28.8	(~2?)	1.9
Protonation constants:				
$L + 2H^+ = LH_2$		32.8	22.0	17.0
$LH_2 + 2H^+ = LH_4$		3.6	3.9	3.9

[a] Abbreviations: $TSPP^{2-}$ = tetrakis(2-sulfophenyl)porphyrin, cyclam = 1,4,8,11-tetraazacyclotetradecane, THEC = *N,N′,N″,N‴*-tetrakis(2-hydroxyethyl)cyclam.

[b] Formation constants for TSPP (*76*) in 80:20 DMSO/water, for cyclam and THEC in water (*11*) at ionic strength 0.1.

the porphyrin cavity (*77*). Porphyrins can respond in several ways to a mismatch in size between the metal ion and the cavity:

a. The porphyrin remains planar, and the M–N bond lengths are stretched or compressed depending on whether the metal ion is too small or too large.

b. If the metal ion is too small for the cavity, the porphyrin may "ruffle," as seen in Fig. 25. The buckling of the porphyrin here leads to a smaller cavity.

c. If the metal ion is too large for the cavity, the porphyrin may dome, and the metal ion may rise up out of the cavity of the porphyrin, as found for Pb(II) (*79*).

The MM calculations show (*77*) that for a metal ion the size of five-coordinate high-spin Fe(II) in a porphyrin, there is a very small difference in energy between whether the Fe(II) rises up out of the plane or remains in the plane of the porphyrin. Thus, a small modification of the "bell-pull" mechanism (*80*) of hemoglobin may be that the high-spin Fe(II) with no oxygen coordinated to it does not rise out of the

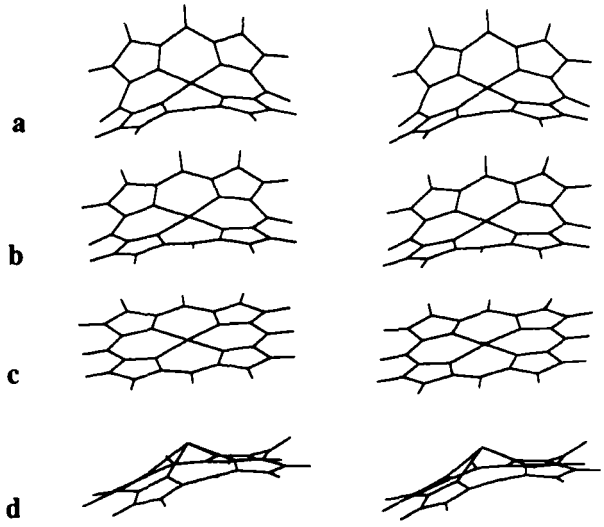

FIG. 25. The effect of metal ion size on porphyrin ruffling. Very small metal ions [P(V) with an ideal P–N bond length of 1.84 Å and low-spin Ni(II) with an ideal Ni–N length of 1.90 Å in (a) and (b)] cause extensive S_4 ruffling. Metal ions close to the right size (M–N = 2.035 Å) give planar structures [Zn(II) in (c)]. Metal ions that are too large [Pb(II) at (d) with ideal Pb–N of 2.39 Å] are extruded from the plane of the porphyrin and cause it to "dome." For clarity, substituents on the porphyrins such as phenyl or ethyl groups have been omitted. Modified after Ref. (*77*).

plane of the porphyrin in order to escape compression, but because square pyramidal coordination, with the iron sitting above the plane of the porphyrin donor atoms, is the preferred geometry.

IX. Sulfur Donors

The sulfur donor atom in biology occurs as mercapto groups from cysteine and complexes, for example, metal ions such as Zn(II) in metalloenzymes (*22*) where the Zn(II) has a catalytic role, and in "zinc fingers" where the Zn(II) has a structural role (*81*). Sulfur is also involved, both as cysteine groups and as actual sulfide (S^{2-}) ion, in complexing iron in numerous iron/sulfur proteins (*81*), where an important function is electron transfer. The metallothioneins (*82*) (MT) are a class of proteins containing an unusually high number of cysteines, which may protect against toxic levels of metal ions by binding Cu(I), Zn(II), Cd(II), Pb(II), and Hg(II). Our interest here is the affinity that the mercapto group has for different metal ions, as a guide to the distribution of metal ions on mercapto sites of proteins. As a start, the formation constants for metal ions of biological and biomedical interest with simple mercaptans such as mercaptoethanol (*11*) (ME) can serve as a guide to the relative affinity of metal ions for cysteine sites on proteins. Unfortunately, formation constants with ligands with mercapto groups are not known with many metal ions of biological interest (*11*), and in Table VIII many of the values have been estimated from Eq. (3) and parameters in Tables I and II. Until experimental values become available, some confidence in the estimated values can be derived from the good agreement between values predicted by Eq. (3) and observed values shown in Table VIII (*11*). Table II shows that the I_B value for ME corresponds to a ligand that is intermediate in HSAB, not soft. In agreement with this, it is found that metal ions such as Ga(III) or In(III), which are classified (*5, 5a*) as hard, form complexes of great stability with ligands with mercapto groups (*11, 83*), which they do not do with the truly soft cyanide ion. The fact that the hard high-spin Fe(III) ion forms complexes of great stability with mercapto groups is essential for the existence of iron/sulfur clusters and points again to the harder nature of the mercapto group. Even the very hard Al(III) ion, along with Ga(III) and In(III), forms complexes of considerable stability with MEA (2-mercaptoethylamine) (*84*). Mercapto sulfur can form bonds of great covalent strength to metal ions, but there is also an ability to form bonds of some ionicity. Table I suggests that the mercapto group is similar to Cl^- in hardness. Thus, Cd(II) is classi-

TABLE VIII

FORMATION CONSTANTS OF MERCAPTOETHANOL WITH METAL IONS OF MEDICAL AND BIOMEDICAL INTEREST[a]

Metal ions of biological interest:			
Ca(II)	−0.55[b]	Mg(II)	−1.42[b]
Zn(II)	5.7[b]	Cu(II)	8.1[b,c]
Cu(I)	16.7[b]	Ni(II)	3.9[b]
Mn(II)	1.8[b]	Fe(II)	2.5[b]
Fe(III)	8.6[b,c]	VO^{2+}	5.0[b]
H^+	9.72 (9.84[b])		
Metal ions of biomedical interest:			
Gd(III)	0.1[b]	Y(III)	−0.5[b]
Ga(III)	8.7[b]	In(III)	9.1 (9.6[b])
Bi(III)	13.8 (13.4[b])	Pb(II)	6.6 (5.7[b])
Cd(II)	6.1 (7.4[b])	CH_3Hg^+	15.9 (15.6[b])
Hg(II)	25.0[b]		

[a] From Ref. (*11*), ionic strength 0.1 and 25°C.

[b] Estimated from Eq. (3) and parameters in Tables I and II.

[c] These ions are reduced by thiols. Since Cu(II) forms less stable complexes with thiols than Cu(II), this will always occur in an environment of thiols alone. However, log K_1 for Fe(III) with thiols is larger than for Fe(II), and so log β_4 for Fe(III) with ME should be proportionately much larger than with Fe(II). Thus, coordination of four thiolate groups, as occurs in electron transfer proteins, will lead to a very stable Fe(III) complex, which is much less easily reduced to Fe(II) than when only a single thiolate is coordinated.

fied as soft, and Zn(II) and Pb(II) are classified as intermediate in HSAB, but, as seen in Table VIII, mercapto groups have similar formation constants with all three metal ions. Thus, use of RS^--type ligands for removal of Pb(II) and Cd(II) from the body produces very useful ligands (*85*), but it is unlikely that ligands of this type will display selectivity for the poisonous Pb(II) and Cd(II) ions over the essential Zn(II) ion.

Mammalian metallothioneins typically bind seven metal ions in cluster structures, with bridging sulfur groups, as seen in the x-ray structure of the Cd_5Zn_2MT complex (*86*). It is therefore difficult to develop a simple formation-constant description for the binding of metal ions to MT (*87*), considering that protonation–deprotonation equilibria of the free protein itself should also be taken into account. However, the usefulness of Table VIII as a guide to the affinity of metal ions for mercapto donor ligands is seen in that the ability of metal ions to

displace Zn(II) and Cd(II) from MT (*88, 89*) accords well with the affinities indicated in Table VIII. Thus, both Co(II) and Ni(II) in Table VIII have predicted log K_1 values with ME that are less than that for Zn(II), and accordingly cannot displace Zn(II) from MT (*88*). The Pb(II) ion has log K_1 with ME similar to that for Zn(II), and so only partially displaces Zn(II) and MT (*89*). The metal ions Bi(III), In(III), Cu(I), and Hg(II) all have log K_1 values with ME considerably higher than that with Cd(II) and Zn(II), and accordingly completely displace Cd(II) and Zn(II) from MT (*89*).

An important aspect of metal thiolate chemistry is that thiolate has a strong tendency to form bridges between two or even three metal ions in solution (*11*) or in the solid state. This is seen in the occurrence in aqueous solution of numerous cluster-type thiolate species with most metal ions studied. Thus, for Cd(II), species identified in aqueous solution (*11*) with ME were as complex as $[Cd_4(RS)_5]^{3+}$. Thus, in mammalian metallothioneins, two clusters are observed where typically seven metal ions in all are held in two complex clusters, one involving 11 cysteine mercapto groups and four metal ions, and the other cluster containing three metal ions and nine cysteine sulfurs. In these clusters, several mercapto sulfurs form bridges between the metal ions. In the case of iron/sulfur clusters, bridging sulfide groups are present which in Fe_4S_4 clusters bridge three irons. The sulfide ion is expected to show similar trends in its affinities for metal ions to those of the mercapto group. Thus, for divalent ions there is good agreement between the order of decreasing solubility products (*11*) for the solid metal sulfides, and log K_1 values for the metal ions with ME in Table VIII.

Metal ion:	Ca^{2+}	Mn^{2+}	Fe^{2+}	Co^{2+}	Ni^{2+}	Zn^{2+}	Cd^{2+}	Pb^{2+}	Cu^{2+}	Hg^{2+}
log K_1(ME):	−0.55	1.8	2.5	3.6	3.9	5.7	6.1	6.6	8.1	25.0
log K_{so} (S^{2-}):	soluble	−10.5	−18.1	−21.3	−23.6	−23.5	−25.8	−27.5	−36.1	−51.0

The position of Cu(II) in the predicted sequence of log K_1 values for ME is supported by the value of the solubility of CuS(s). This is support for Eq. (3) as a means of predicting unknown formation constants with unidentate ligands. The formation constant of Cu^{2+} (aq) with unidentate ligands containing mercapto groups is experimentally inaccessible because Cu^{2+} (aq) is reduced by mercapto groups to Cu(I). Why this should be so is seen (Table VIII) in the much higher log K_1 value of ME with Cu(I) (16.7) than Cu(II) (8.1), which greatly stabilizes the Cu(I) relative to the Cu(II) oxidation state.

X. Systems Containing More Than One Metal Ion—The Reverse Chelate Effect

As noted, metal ions used in biology are far from exotic, so that ways have to be found to produce unusual properties. In the chelate effect (*90*), more than one donor atom occurs on a single ligand that binds a single metal ion. The reverse effect may be employed, where more than one metal ion, all held together on a single ligand (which in biological systems is likely to be a protein), will bind a second ligand through bonding to all the metals simultaneously.

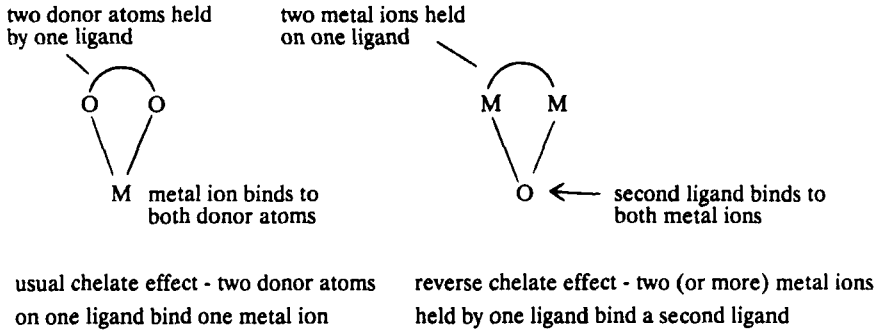

Examples of such systems are the binding of oxygen between the two coppers of hemocyanin (*36*), or possibly nitrogen to at least several of the six irons of nitrogenase (*7*). It is not yet clear that the nitrogen would bind within the cavity of six irons of nitrogenase as shown in Fig. 11, but it seems a lot of trouble to build such an unusual cavity if it serves no purpose. The aim here is to look at the thermodynamic advantages of the more preorganized arrangement of metal ions that occurs in such multinuclear systems.

The ligand O-BISTREN binds (*91–94*) two metal ions with a space between them for complexation of small ligands (Fig. 26).

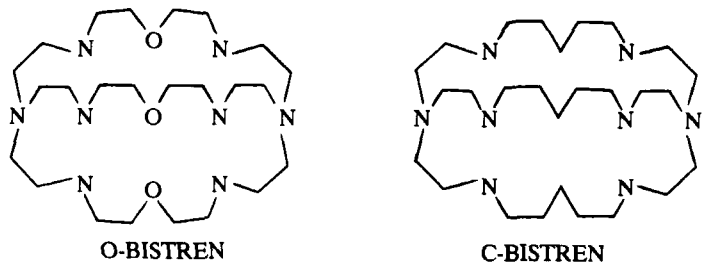

O-BISTREN C-BISTREN

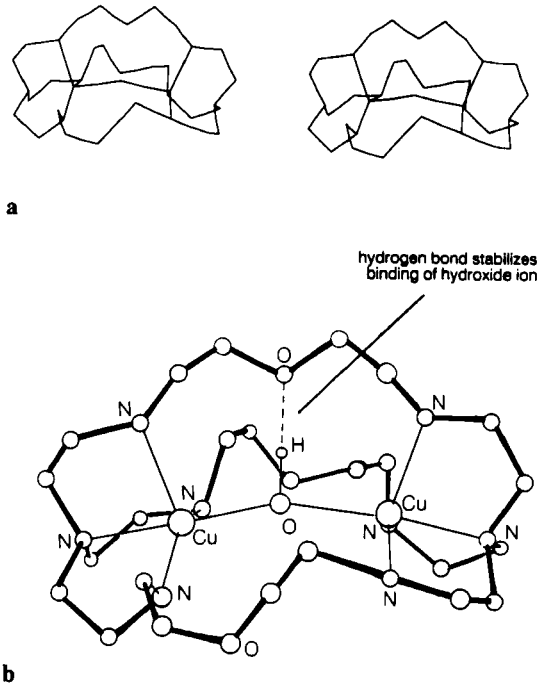

FIG. 26. (a) A stereoview of the hydroxide-bridged complex and (b) the crystal structure (*93*) of the complex cation Cu(II)(OH)(O-BISTREN), showing the hydrogen bonding that appears to promote formation of the bridged hydroxy complex.

The formation constants of simple ligands such as F^-, Cl^-, and OH^- with the O-BISTREN complex (*92*) with two Cu(II) ions in it can be compared with the situation where these ligands bind to the free Cu^{2+} ion.

log K_1 with:	Cu^{2+} [a]	$Cu(II)_2L$ [b]	$(Cu^{2+})_2$ [c]
OH^-	6.3	9.89	8.2
F^-	0.7	4.7	—
Cl^-	0.1	2.1	—

[a] Formation constants from Ref. (*11*) at 25°C and ionic strength 0.1.

[b] L is the ligand O-BISTREN; formation constants from Refs. (*92* and *94*), ionic strength 0.1 and 25°C. The equilibrium is $Cu_2L + X^-$ ($X^- = OH^-$, F^-, or Cl^-) = Cu_2LX.

[c] Formation constant from Ref. (*11*) for $2Cu^{2+} + OH^- = Cu_2OH)^+$, at 25°C and ionic strength 3.0.

The complex $Cu(II)_2$(O-BISTREN) is much more acidic than the free Cu^{2+} ion, by a factor of more than three log units. This is primarily due to the presence of two Cu(II) ions, because the formation constant of the $Cu_2(OH)^+$ complex is not much less than that for the Cu_2(O-BISTREN) complex with hydroxide. This is not a good indication of how well two free Cu^{2+} ions would bind hydroxide compared to the Cu_2(O-BISTREN) complex, however, since one must take into account the dilution effect operative in the chelate effect to make the comparison more realistic (*90*). Thus, the formation constant for the Cu_2OH^+ complex above applies for the standard reference state of 1 M Cu^{2+}. In contrast, in 10^{-6} M Cu^{2+}, for example, the pH at which $Cu_2(OH)^+$ would form is raised from pH 5.6 to 11.6, ignoring the fact that $Cu(OH)_2$(s) would precipitate out long before this pH as reached. By comparison, the acidity of the Cu_2(O-BISTREN) complex is not affected by dilution and would still form the hydroxide complex at pH 3.9 if present at a 10^{-6} M concentration.

The stability of the hydroxide complex Cu_2(OH)(O-BISTREN) is, even in the standard reference state of 1 M, somewhat higher than that of $Cu_2(OH)^+$. By analogy with Eq. (4), one would expect the "reverse chelate effect" discussed here to contribute to log 55.5., which is 1.74 log units, in extra stability to the "chelating" complex Cu_2(OH)(O-BISTREN) compared to $Cu_2(OH)^+$. This is almost exactly the difference found between log K_1 for Cu_2(OH)(O-BISTREN) and $Cu_2(OH)^+$, of $9.89 - 8.2 = 1.7$ log units. This difference should be an entropy effect if it derives from a chelate-effect type of contribution. However, the agreement between the expected and observed magnitude of the "reverse chelate effect" probably masks some cancelling effects, since the structure of the Cu_2(OH)(O-BISTREN) complex in Fig. 26 (*93*) shows that the hydroxide held between the two Cu(II) ions is hydrogen-bonded to an oxygen of the bridge of the O-BISTREN ligand. The ligand C-BISTREN lacks these bridge oxygens, and consequently binds hydroxide much more weakly (*92*), presumably because it cannot form the essential hydrogen bond. Thus, the strength of binding of unidentate ligands between two or more metal ions will have many more contributions than just a simple chelate-effect contribution, and factors that are likely to be important are the spacing between the metal ions and, by analogy with chelating ligands, the orientation of orbitals on the metal ions that must form bonds to the incoming ligand. Also of importance would be the ability to stabilize the complex by hydrogen bonding, and match-up of hydrophobic zones on the incoming ligand and the system holding the two or metal ions in place.

One sees that two metal ions held in a complex such as Cu_2(BISTREN)

can bind simple unidentate ligands three to four orders of magnitude more strongly than a single metal ion. Clearly, this type of effect must be important in the operation of metalloproteins such as hemocyanin and nitrogenase. One can see the potential importance of high levels of preorganization of the irons of nitrogenase, if one is to bind a very weak ligand such as dinitrogen.

The ideas presented here merely scratch the surface of factors that control metal ion selectivity in biological systems. It is hoped that in future the picture will become even clearer, enabling us to learn much more about ligand design and selective metal ion complexation.

ACKNOWLEDGMENTS

The authors acknowledge generous financial support (for R. D. H.) from the University of the Witwatersrand and the Foundation for Research Development. In addition, R. D. H. thanks A E. M. for hosting him as a Visiting Professor to Texas A&M, when this review was written. Support was provided by Grant No. CA-42925, National Cancer Institute, U. S. Public Health Service.

REFERENCES

1. Hancock, R. D., and Martell, A. E., *Chem. Rev.* **89,** 1875 (1989).
2. Hancock, R. D., and Martell, A. E., *Comments Inorg. Chem.* **6,** 237 (1988).
3. Jurisson, S., Berning, D., Jia, W., and Ma, D., *Chem. Rev.* **93,** 1137 (1993); Lauffer, R. B., *Chem. Rev.* **87,** 901 (1987); Gansow, O. A., *Nucl. Med. Biol.* **18,** 369 (1991); Bulman, R. A., *Struct. Bonding (Berlin)* **67,** 91 (1987).
4. Hancock, R. D., *Prog. Inorg. Chem.* **37,** 187 (1989).
5. Pearson, R. G., *J. Am. Chem. Soc.* **85,** 3533 (1963).
5a. Pearson, R. G., *Coord. Chem. Rev.* **100,** 403 (1990).
6. Frausto da Silva, J. J. R., and Williams, R. J. P., "The Biological Chemistry of the Elements." Oxford Univ. Press (Clarendon), Oxford, 1991.
7. Kim, J., and Rees, D. C., *Science* **257,** 1677 (1992); *Nature (London)* **360,** 553 (1992); Rees, D. C., Chan, M. K., and Kim, J., *Adv. Inorg. Chem.* **40,** 89 (1993).
8. Ahrland, S., Chatt, J., and Davies, N. R., *Q. Rev., Chem. Soc.* **12,** 265 (1958).
9. Woodin, R. L., and Beauchamp, J. L., *J. Am. Chem. Soc.* **100,** 501 (1978).
10. Damu, K., Maumela, H., Hancock, R. D., Boeyens, J. C. A., and Dobson, S. M., *J. Chem. Soc., Dalton Trans.,* 2717 (1991); Hancock, R. D., *J. Chem. Soc., Dalton Trans.* 416 (1980).
11. Martell, A. E., and Smith, R. M., "Critical Stability Constants," Vols. 1–6. Plenum, New York, 1974, 1975, 1976, 1977, 1982, 1989.
12. Taft, R. W., *in* "Kinetics of Ion-Molecule Reactions" (P. Ausloos, ed.), p. 271. Plenum, New York, 1979.
13. Staley, R. H., and Beauchamp, J. L., *J. Am. Chem. Soc.* **97,** 5920 (1975).
14. Uppal, J. S., and Staley, R. H., *J. Am. Chem. Soc.* **104,** 1235, 1238 (1982).
15. Kappes, M. M., and Staley, R. H., *J. Am. Chem. Soc.* **104,** 1813, 1819 (1982).

16. Hancock, R. D., *in* "Environmental Inorganic Chemistry" (K. J. Irgolic and A. E. Martell, eds.), p. 117. VCH Publishers, Deerfield Beach, FL, 1985.
17. Hancock, R. D., and Marsicano, F., *Inorg. Chem.* **17,** 560 (1978); **19,** 2709 (1980).
18. Drago, R. S., Vogel, G. C., and Needham, T. E., *J. Am. Chem. Soc.* **93,** 6014 (1971).
19. Pearson, R. G., and Mawby, R. J., *in* "Halogen Chemistry" (V. Gutmann, ed.), Vol. 3, p. 55. Academic Press, London and New York, 1967.
20. R. D. Shannon, *Acta Crystallogr., Sect. A: Cryst. Phys., Diffr., Theor. Gen. Crystallogr.* **A32,** 751 (1976).
21. C. S. G. Phillips and R. J. P. Williams, "Inorganic Chemistry," Vol. 2, p. 533. Oxford Univ. Press, Oxford, 1966.
22. Bertini, I., Luchinat, C., Maret, W., and Zeppezauer, M., eds., "Progress in Inorganic Biochemistry and Biophysics," Vol. 1. Birkhaeuser, Verlag, Basel, 1986.
23. Pocker, Y., and Stone, J. T., *Biochemistry* **7,** 2936 (1968).
24. Woolley, P., *Nature (London)* **258,** 677 (1975); Gellma, S. H., Petter, R., and Breslow, R. J., *J. Am. Chem. Soc.* **108,** 2388 (1986); Groves, J. T., and Chambers, R. R., *J. Am. Chem. Soc.* **106,** 630 (1984).
25. Kimura, E., Shiota, T., Koike, T., Shiro, M., and Kodama, M., *J. Am. Chem. Soc.* **112,** 5805 (1990).
26. Pettersen, G., and Kvassman, J., *Eur. J., Biochem.* **103,** 565 (1980).
27. Wu, S.-H., Lee, D.-S., and Chung, C.-S., *Inorg. Chem.* **23,** 2548 (1984).
28. Chang C.-C., and Chung, C.-S., *J. Chem. Soc., Dalton Trans.*, 1685 (1991).
29. Sheu, H.-R., Lee, T.-J., Lu, T.-H., Liang, B.-F., and Chung, C.-S., *Proc. Natl. Sci. Counc. Rebublic of China* **7,** 113 (1983).
30. Ohtaki, H., and Radnai, T., *Chem. Rev.* **93,** 1157 (1993).
31. Harrison, P. G., Begley, M. G., Kikabai, T. K., and Steel, A. T., *J. Chem. Soc., Dalton Trans.*, 2443 (1989).
32. Maumela, H., Darmesh, K., and Hancock, R. D., to be published.
33. Jorgensen, C. K., *Inorg. Chem.* **3,** 1201 (1964).
34. Vallee, B. L., and Williams, R. J. P., *Proc. Natl. Acad. Sci. U.S.A.* **59,** 498 (1968).
35. Cedergren-Zeppezauer, E. S., Samama, J.-P., and Eklund, H., *Biochemistry* **21,** 4895 (1982).
36. Loehr, T. M., *in* "Oxygen Complexes and Oxygen Activation" (A. E. Martell and D. T. Sawyer, eds.), p. 17, Plenum, New York, 1988, Magnus, K., and Hoa, T.-T. *J. Inorg. Biochem.* **47,** 20 (1992), Magnus, K. A., Hoa, T.-T., and Carpenter, J. E., *in* "Bioinorganic Chemistry of Copper" (K. D. Karlin and Z. Tyeklar, eds.), p. 143. Chapman & Hall, London, 1993.
37. Kitajima, N., Fujisawa, K., Fujimoto, C., Moro-oka, Y., Hashimoto, S., Kitagawa, T., Toriumi, K., Tatsumi, K., and Nakamura, A., *J. Am Chem. Soc.* **114,** 1277 (1992); Kitajima, N., Fujisawa, K., Tanaka, M., and Moro-oka, Y., *J. Am. Chem. Soc.* **114,** 9232 (1992). Kitajima, N., *Adv. Inorg. Chem.* **38,** 1 (1992).
38. Hancock, R. D., *J. Chem. Educ.* **69,** 615 (1992).
39. Hancock, R. D., *Acc. Chem. Res.* **23,** 253 (1990).
40. Drew, M. G. B., *Coord. Chem. Rev.* **24,** 179 (1977).
41. Huber, R., Schneider, M., Mayr, I., Romisch, J., and Paques, E.-P., *FEBS Lett.* **275,** 15 (1990).
41a. Moews, P. C., and Kretzinger, R. H., *J. Mol. Biol.* **91,** 201 (1975).
42. Babu, Y. S., Bugg, C. E., and Cook, W. J., *J. Mol. Biol.* **204,** 191 (1988).
43. Einspahr, H., and Bugg, C. E., *in* "Metal Ions in Biological Systems" (H. Sigel, ed.), p. 51. Dekker, New York, 1984.

44. Angyal, S. J., *Chem. Soc. Rev.*, **9,** 415 (1980); Burger, K., and Nagy, L., *in* "Biocoordination Chemistry" (K. Burger, ed.), p. 236. Ellis Horwood, New York, 1990.
45. Hancock, R. D., and Hegetschweiler, K., *J. Chem. Soc., Dalton Trans.*, 2137 (1993).
46. Herrman, W. A., Hedtweck, E., and Pajdla, L., *Inorg. Chem.* **30,** 2579 (1991).
47. Feng, T. L., Gurian, P. L., Healy, M. D., and Barron, A. R., *Inorg. Chem.* **29,** 408 (1990).
48. Lauble, H., Kennedy, M. C., Beinert, H., and Stout, C. D., *Biochemistry* **31,** 2735 (1992), Kennedy, M. C., and Stout, C. D., *Adv. Inorg. Chem.* **38,** 323 (1992).
49. Rees, D. C., Howard, J. B., Chakrabarti, P., Yeates, T., Hsu, B. T., Hardman, K. D., and Lipscomb, W. N., *Prog, Inorg. Biochem. Biophys.*, **1,** 155 (1986).
50. Hancock, R. D., *in* "Perspectives in Inorganic Chemistry" (A. P. Williams, C. Floriani, and A. E. Merbach, eds.), p. 129 VCH, Weinheim/Helv. Chim. Acta, Basel, 1992.
51. Westley, J. W., ed., "Polyether Antibiotics: Naturally Occuring Ionophores," Vols. 1 and 2. Dekker, New York, 1982.
52. Dobler, M., "Ionophores and Their Structures." Wiley, New York, 1981.
53. Gokel, G. W., "Crown Ethers and Cryptands." Royal Society of Chemistry, London, 1991.
54. Thom, V. J., Fox, C. C., Boeyens, J. C. A., and Hancock, R. D., *J. Am. Chem. Soc.* **106,** 5947 (1984).
55. Hendrick, K., Tasker, P. A., and Lindoy, L. F., *Prog. Inorg. Chem.* **33,** 1 (1985).
56. Krakowiak, K. E., Bradshaw, J. S., Kent Dalley, N., Zhu, C., Yi, G., Curtis, J. C., Li, D., and Izatt, R. M., *J. Org. Chem.* **57,** 3166 (1992).
57. An, H.-Y., Bradshaw, J. S., and Izatt, R. M., *Chem. Rev.* **92,** 543 (1992).
58. Izatt, R. M., Pawiak, K., Bradshaw, J. S., and Bruening, R. L., *Chem. Rev.* **91,** 1721 (1991).
59. Bartsch, R. A., Czech, B. P., Kang, S. I., Stewart, L. E., Wolkowiak, W., Charewicz, W. A., Heo, G. S., and Son, B., *J. Am. Chem. Soc.* **107,** 4997 (1985).
60. Hancock, R. D., *J. Inclusion Phenom Mol. Recognition* **17,** 63 (1994).
61. McDougall, G. J., and Hancock, R. D., *J. Chem. Soc., Dalton Trans.* 654 (1980).
62. Dobler, M., Dunitz, J. D., and Seiler, P., *Acta Crystallogr., Sect B: Struct. Crystallogr. Cryst. Chem.* **B30,** 2741 (1974).
63. Alcock, N. W., Ravindran, M., and Willey, G. R., *J. Chem. Soc., Chem. Commun.* 1063 (1989).
64. Seiler, P., Dobler, M., and Dunitz, J. D., *Acta Crystallorgr., Sect. B: Struct. Crystallogr. Cryst. Chem.* **B30,** 2744 (1974).
65. Bush, M. A., and Truter, M. R., *J. Chem. Soc., Perkin* 2, 341 (1972).
66. Hille, B., "Ionic Channels of Excitable Membranes," 2nd ed. Sinauer Assoc. Sunderland, MA, 1992.
67. Miller, C., *Science* **261,** 1692 (1993); Kumpf, R. A., and Dougherty, D. A., *Science,* **261,** 1708 (1993); Neyton, J., and Miller, C., *J. Gen. Physiol.* **92,** 549, 569 (1988); Miller, C., *Biophys. J.* **52,** 123 (1987).
68. Wulfsberg, G., "Principles of Descriptive Inorganic Chemistry." Brooks/Cole, Monterey, CA, 1987.
69. Evers, A., Hancock, R. D., Martell, A. E., and Motekaitis, R. J., *Inorg. Chem.* **28,** 2189 (1989).
70. Bergeron, R. J., and Brittenham, G. M., eds., "The Development of Iron Chelators for Clinical Use." CRC Press, Boca Raton, FL, 1994.
71. Hancock, R. D., and Marsicanco, F., *J. Chem. Soc., Dalton Trans.*, 1096 (1976).

72. Baker, E. N., and Blundell, T., *Proc. Natl. Acad. Sci. U.S.A.* **84,** 1769 (1987).
73. Mulla, F., Marsicano, F., Nakani, B. S., and Hancock, R. D., *Inorg. Chem.* **24,** 3076 (1985).
74. Pratt, J. M., "Inorganic Chemistry of Vitamin B12," Academic Press, New York, 1972, Dolphin, D., ed., "B12," Vols. 1 and 2. Wiley, New York, 1982.
75. Scheidt, W. R., and Reid, C. A., *Chem. Rev.* **81,** 543 (1981); Scheidt, W. R., and Lee, Y. J., *Struct. Bonding (Berlin)* **64,** 1 (1987).
76. Jimenez, H. R., Julve, M., and Faus, J., *J. Chem. Soc., Dalton Trans.,* 1945 (1991).
77. Munro, O. Q., Bradley, J. C., Hancock, R. D., Marques, H. M., Marsicano, F., and Wade, P. W., *J. Am. Chem. Soc.* **114,** 7230 (1992).
78. Hancock, R. D., Weaving, J. S., and Marques, H. M., *J. Chem. Soc., Chem. Commun.,* 1176 (1989).
79. Barkigia, K. M., Fajer, J., Adler, A. D., and Williams, G. J. B., *Inorg. Chem.* **19,** 2057 (1980).
80. Perutz, M. F., *Annu. Rev. Biochem.* **48,** 327 (1979).
81. Klug, A., and Rhodes, D., *Trends Biochem. Sci.* **12,** 464 (1987).
82. Sykes, A. G., ed., "Advances in Inorganic Chemistry," Vol. 38. Academic Press, San Diego, CA, 1992.
83. Tanaboylu, K., and Schwarzenbach, G., *Helv. Chim. Acta,* **55,** 2065 (1972).
84. Li, Y., and Martell, A. E., *Inorg. Chim. Acta* **231,** 159 (1995).
85. Casas, J. S., Sanchez, A., Bravo, J., Garcia-Fontan, S., Castellano, E. E., and Jones, M. M., *Inorg. Chim. Acta* **158,** 119 (1989).
86. Furey, W. F., Robbins, A. H., Clancy, L. L., Winge, D. R., Wang, B. C., and Stout, C. A., *Science* **231,** 704 (1986).
87. Vasak, M., and Kagi, J. H. R. *in* "'Metal Ions in Biology" (H. Sigel, ed.), Vol. 15. p. 213. Dekker, New York, 1983.
88. Vasak, M., Kagi, J. H. R., Holmquist, B., and Vallee, B. L., *Biochemistry* **20,** 6659 (1981).
89. Nielsen, K. B., Atkin, C. L., and Winger, D. P., *J. Biol. Chem.* **260,** 5342 (1985).
90. Martell, A. E., *in* "Essays in Coordination of Chemistry" (W. Schneider, G. Anderegg, and R. Gut, eds.), p. 52. Birkhaeuser, Basel, 1964.
91. Martell, A. E., *Adv. Supramol. Chem.* **1,** 145 (1990).
92. Motekaitis, R. J., Martell, A. E., Murase, I., Lehn, J. M., and Hosseini, M. W., *Inorg. Chem.* **27,** 3630 (1988).
93. Motekaitis, R. J., Martell, A. E., Rudolf, P., and Clearfield, A., *Inorg. Chem.* **28,** 112 (1989).
94. Motekaitis, R. J., Martell, A. E., Dietrich, B., and Lehn, J. M., *Inorg. Chem.* **24,** 1588 (1984).

ADVANCES IN INORGANIC CHEMISTRY, VOL. 42

THE SYNTHESIS AND STRUCTURE OF ORGANOSILANOLS

PAUL D. LICKISS

Chemistry Department, Imperial College of Science, Technology and Medicine, London SW7 2AY, United Kingdom

I. General Introduction
  A. Silica Surfaces
  B. Polysiloxanes, Silicones
  C. Sol–Gel Processes
II. General Synthetic Methods
  A. Introduction
  B. From Si–H Compounds
  C. From Halosilanes, Alkoxysilanes, Amides, etc.
  D. Hydrolysis of Si–N Functions
  E. Hydrolysis of Si–C Bonds
  F. From Silyl–Metal Compounds
  G. Addition of Water to Si Multiple Bonds
  H. Miscellaneous Preparative Methods
III. The Acidity and Basicity of the Silanol Group
  A. Acidity
  B. Basicity
IV. Structural Studies of Silanols
  A. Introduction
  B. Calculations on the Structures of Silanols
  C. Compounds Containing One Si–OH Group
  D. Compounds Containing Two Si–OH Groups
  E. Compounds Containing Three Si–OH Groups
  F. Compounds Containing Four Si–OH Groups
  G. Compounds Containing an $Si(OH)_2$ Group, Silanediols
  H. Compounds Containing Two $Si(OH)_2$ Groups
  I. Compounds Containing an $Si(OH)_3$ Group, Silanetriols
V. Summary and Conclusions
References

I. General Introduction

Organosilanols are analogous to alcohols; the most common are simple silanols of the type R_3SiOH, but compounds of the types $R_2Si(OH)_2$, silanediols, and $RSi(OH)_3$, silanetriols, are also well known. Between

Copyright © 1995 by Academic Press, Inc.
All rights of reproduction in any form reserved.

them, these three classes of compounds have been widely studied and are precursors to materials having a variety of important uses. The first compound containing an SiOH function to be prepared was Et_3SiOH, which was made in 1871 by Ladenburg (*1, 2*), who hydrolyzed Et_3SiCl with aqueous ammonia. He coined the term "silicole" for this new type of compound, by analogy with the organic name "carbinole." Today, although the term carbinol is in common use, the term silanol rather than silicol is usually used for the SiOH group. The Si–OH group is ubiquitous in nature because the aquatic environment contains very low levels of dissolved silicic acid $Si(OH)_4$ and the many varieties of silica, SiO_2, and silicate rocks have surface hydroxyl groups.

Compounds containing the silanol group are well known not only in nature, but also in industrial processes in which polymeric materials such as polydimethylsiloxanes (silicones) and sol–gels are produced by condensation reactions of the reactive R_3SiOH, $R_2Si(OH)_2$, $RSi(OH)_3$, and $Si(OH)_4$ species. Although the silanol functional groups are, therefore, to be found in a wide variety of situations, compounds containing such groups are relatively rarely isolated as discrete molecular species. This review will concentrate on well-defined monomeric species, a description of their structures, and the means by which they may be prepared. Some of the industrial situations in which silanols play an important role will, however, be considered briefly.

A. Silica Surfaces

Materials containing a high proportion of silicon and oxygen, such as quartz, silicate rocks, and glass, usually have OH groups attached to the surface in the form of Si–OH functions. These surface silanol groups interact via hydrogen bonding with other suitable species—especially, for example, water in the natural aqueous environment. Such bonding therefore plays an important role at the interface between the inorganic world and the biological world of aqueous solutions. The acidity of surface silanol groups has been the subject of numerous investigations that are beyond the scope of this review; a recent theoretical estimate of the acidity of such groups can be found in Ref. *3*. The silanol groups at a surface may also react with certain compounds to give surface modified materials in which useful chemical functions are tethered to the surface by covalent bonding. Such linking of a discrete molecular entity to a bulk surface is often carried out using a "silane coupling agent," which is frequently an alkoxysilane. The silane coupling reaction relies on the hydrolysis of the alkoxysilane, usually a trimethoxysilane derivative, to give a silanol, which then

reacts with a surface hydroxy group with the elimination of water to form a strong siloxane linkage. This method has been used to attach a very large variety of molecular functions to silica surfaces, and the materials so formed have many useful properties. The preparation and uses of silane coupling agents has been reviewed thoroughly (*4*), and they will not be discussed further in this article. Similarly, the surface reactions of Si–OH groups are outside the scope of this review.

The use of small polyhedral silsesquioxanes as molecular models of silica surfaces has been studied increasingly in recent years, because catalysts, etc., attached to such species are relatively easy to handle and characterize when compared to bulk silica. The preparation and structures of silsesquioxanes used in this type of work are described later in Sections II,C, IV,E, and IV,F. Further recent examples may be found in Ref. *5*.

B. Polysiloxanes, Silicones

A second industrially important field in which silanols play a vital role is in the preparation of polysiloxanes, often known as silicones. As in the case of silane coupling agents, there is a vast literature available on the topic of polysiloxanes, and only the most general discussion will be given here, concentrated on the reactions that involve silanols.

An important reaction of silicon compounds containing electronegative substituents, such as the halogens or a Group 15 or 16 element, is hydrolysis, which often occurs very readily even with atmospheric moisture. The primary reaction in silicone production is the hydrolysis of halosilanes, usually the readily available chlorosilanes, to give silanols, which then undergo acid-catalyzed condensation with loss of water, as shown in Scheme 1.

By careful choice of monomer ratios and reaction conditions, polymers with a wide range of molecular weights, degree of branching or cross-linking, and physical properties may be prepared, all of the reactions relying on the formation of silanol species at some point in the synthesis. The condensation reaction of silanol to siloxane is catalyzed by acids and bases and is also promoted by high temperatures. A discussion of the mechanisms of the reactions important in the formation of siloxanes from silanols is again outside the scope of this article, and further detailed information is given in several reviews (*6*). Recent detailed kinetic data on silanol condensation reactions may be found in Ref. *7*.

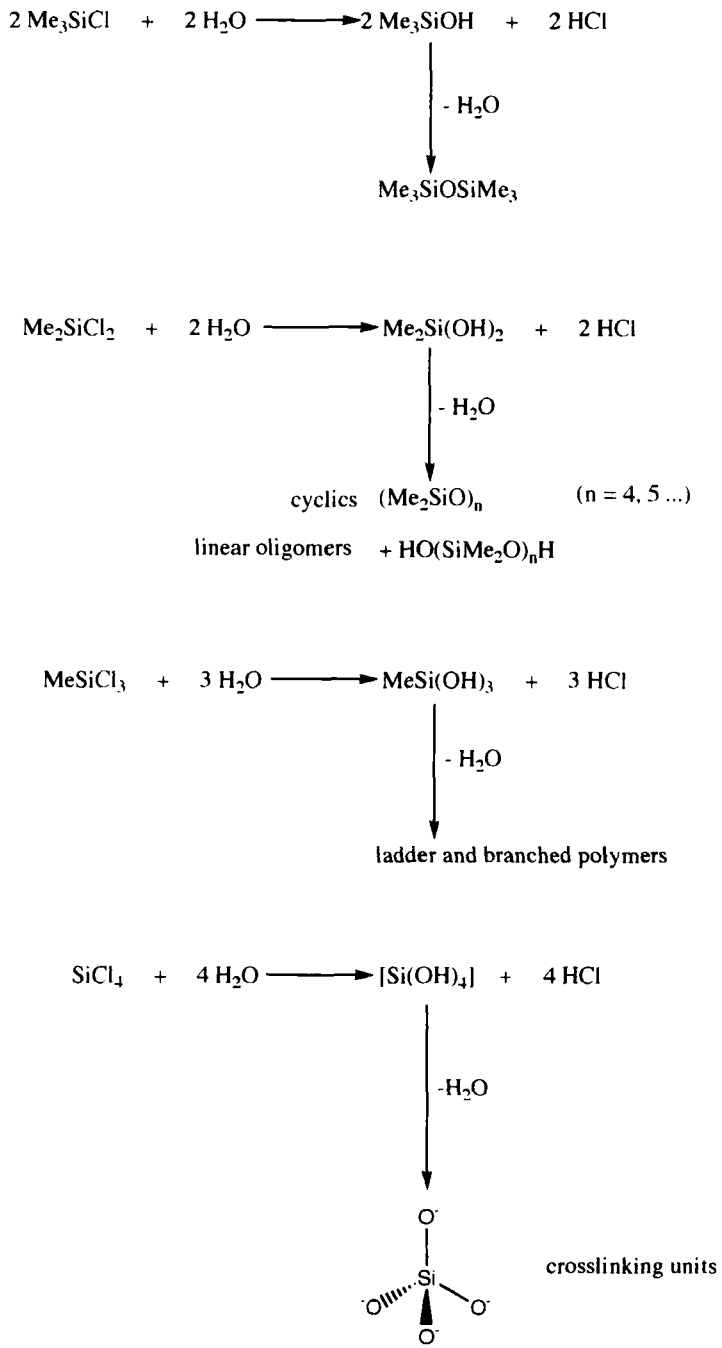

SCHEME 1. The hydrolysis of methylchlorosilanes.

$$(EtO)_4Si + H_2O \underset{\text{alcoholysis}}{\overset{\text{hydrolysis}}{\rightleftharpoons}} (EtO)_3SiOH + EtOH \text{ etc.}$$

$$(EtO)_3SiOH + (EtO)_4Si \rightleftharpoons (EtO)_3SiOSi(OEt)_3 + EtOH$$

condensation with alcohol formation

$$2\,(EtO)_3SiOH \rightleftharpoons (EtO)_3SiOSi(OEt)_3 + H_2O$$

condensation with water formation

SCHEME 2. Hydrolysis of alkoxysilanes.

C. SOL–GEL PROCESSES

The fabrication of colloidal silica and optical glasses by the sol–gel process has attracted a great deal of attention (*8*). The process relies on the hydrolytic polycondensation reactions of alkoxysilanes, usually $(EtO)_4Si$, in which the reactive silanols $(EtO)_{4-n}Si(OH)_n$ (n = 1–4) are formed. These then undergo acid- or base-catalyzed condensation with both water and alcohol formation, as shown in Scheme 2.

The formation of polymeric silica or a gel from this process is clearly complicated (*9*) and will not be discussed further in this article; for reviews of the sol–gel process, see Ref. *10*. The important point for this general discussion is that silanol species play a vital role in the formation of numerous industrially important materials.

II. General Synthetic Methods

A. INTRODUCTION

This section deals with the various types of synthetic routes that are most commonly used for the synthesis of silanols. Further specific examples of most of these types of synthesis can be found in the section on structures, where individual silanols are described in more detail.

As has been seen in the preceding section concerned with the industrial uses of silanols as intermediates, the most likely reaction that a silanol may undergo is that of self-condensation to form a siloxane. This can be a very serious problem, because silanols are sensitive to base, acid, and heat. The following points should therefore be considered when planning the synthesis and isolation of a silanol.

1. Because the condensation reactions are bimolecular in silanol, the use of dilute solutions will be beneficial.

2. Solvolytic systems that generate either an acid or a base should be avoided unless such products can be neutralized in some way as they are formed—for example, by the addition of an amine to give a hydrochloride salt in the case of HCl generation.

3. Reactions should be carried out at the lowest convenient temperature.

4. The presence of bulky substituents such as Bu^t on silicon greatly reduces the tendency towards siloxane formation, and with two or more such groups present the precautions suggested in points 1, 2, and 3 can often be relaxed. For example, the hydrolysis of highly sterically hindered halosilanes may require rather severe conditions.

B. From Si–H Compounds

1. Oxidation

Organosilanes containing small substituents and several Si–H bonds such as $RSiH_3$ (R = Me, Et or Bu^n) species are highly reactive towards oxygen. They may ignite in the presence of a metal (for example, mercury in a manometer) or under pressure (*11*). The photo-oxidation of Cl_3SiH by O_2 in $SiCl_4$ gives Cl_3SiOH in low concentration via a free radical pathway, but this is not a practical synthesis for many silanols (*12*). Larger substituents or fewer Si–H groups lead to compounds that are more stable and which may be distilled in air, for example, *c*-$C_6H_{11}SiH_3$ and $Bu^n{}_3SiH$ (*11*). Although Ph_3SiH is stable in air, it is oxidized by O_2 in benzene solution in the presence of benzoyl peroxide (*13*).

Oxidation may also be carried out with perbenzoic acid. For example, the reaction between Et_3SiH, $PhMe_2SiH$, or Ph_2MeSiH and perbenzoic acid in benzene gives the corresponding silanols in 70, 60, and 58% yields, respectively (*14*). This type of oxidation has been shown to proceed with retention of stereochemistry at silicon (*15*), Eq. (1). The powerful oxidizing agent potassium permanganate has also been used occasionally; for example the bulky silanol $(Me_3Si)_3CSiEt_2OH$ can be made readily by oxidation of $(Me_3Si)_3CSiEt_2H$ with $KMnO_4$ (*16*), and the vinyl compound **1** can also be oxidized in good yield, Eq. (2) (*17*).

$$\text{(-)-PhMe(1-naphthyl)SiH} + PhCO_3H \longrightarrow \text{(-)-PhMe(1-naphthyl)SiOH} + PhCO_2H \quad (1)$$

$$(Me_3Si)_2C(SiMe_2H)(SiMe_2CH{=}CH_2) \xrightarrow{KMnO_4} (Me_3Si)_2C(SiMe_2OH)(SiMe_2CH{=}CH_2)$$

1

(2)

The oxidation of sterically hindered silanes by $KMnO_4$ is improved by carrying out the reactions in the presence of ultrasound, which helps to break down the $KMnO_4$ in an organic solvent and aids solubility. For example, the hindered silanes Ph_3SiH, $(Me_3Si)_3CSiMe_2H$, and $(Me_3Si)_3CSiH_3$ are readily oxidized in THF to give good yields of Ph_3SiOH, $(Me_3Si)_3CSiMe_2OH$, and $(Me_3Si)_3CSi(OH)_3$, respectively, in an hour or less at room temperature (*18*). The dibutyl compound $Bu^t_2SiH_2$ tends to give a mixture of Bu^t_2SiHOH and $Bu^t_2Si(OH)_2$ under similar conditions, while the extremely bulky diphenyl compound $(Me_3Si)_3CSiPh_2H$ does not react at all (*18*). The silver salts $AgNO_3$ and $AgNO_2$ and the oxide AgO will also oxidize Si–H bonds cleanly, and generally in good yield [Eqs. (3)–(5)] (*19*). Diethylsilane is also reported to be oxidized by HgO (*20*).

$$Ph_3SiH + AgNO_2 \xrightarrow[14\ h]{Et_2O,\ reflux} \underset{95\ \%}{Ph_3SiOH} + NO + Ag \quad (3)$$

$$Bu^n_3SiH + AgNO_3 \xrightarrow[3\ h]{Et_2O} \underset{80\ \%}{Bu^n_3SiOH} + \text{N-oxides} + Ag \quad (4)$$

$$Et_3SiH + Ag_2O \xrightarrow[9\ h]{Et_2O} \underset{90\ \%}{Et_3SiOH} + 2\,Ag \quad (5)$$

Compounds containing Si–H bonds are rapidly oxidized by ozone in solution at low temperature to give good yields of silanols, which may be isolated if the substituents on silicon are large enough to prevent rapid condensation to the corresponding siloxane [Eq. (6)] (*21, 22*). Ozonolysis of the highly sterically hindered silane Bu^t_3SiH gave Bu^t_3SiOH as the only detectable product (*23*). In the case of Et_3SiH, the hydrotrioxide $Et_3SiOOOH$ is thought to be an intermediate, which decomposes to give the silanol and singlet oxygen (*24*). The oxidation of Si–H groups by ozone has been reviewed (*25*) as has the chemistry of organosilicon peroxides (*26*), which will not be covered in this discussion.

$$R_3SiH + O_3 \xrightarrow[<0\,^\circ C]{CH_2Cl_2} R_3SiOH + O_2 \quad (6)$$

$R_3 = Et_3$, $(c\text{-}C_6H_{11})_3$, $PhMe_2$, Ph_3 *etc.*

A more recent method for the formation of silanols by insertion of oxygen into an Si–H bond employs highly reactive dioxiranes. Thus, oxirane **2** oxidizes $PhMe_2SiH$ and Et_3SiH in less than 1 min at −20 to 0°C, giving almost quantitative yields, and oxirane **3** gives silanol **4** in excellent yield in 18 min under similar conditions [Eqs. (7) and (8)] (*27*). The dioxirane can also be used to oxidize Si–H bonds in good yields within the coordination sphere of a transition metal such as iron (*28*) [Eq. (9)] or tungsten where, for example, $Cp^*(CO)_2(PMe_3)WSiRH_2$ may be oxidized to $Cp^*(CO)_2(PMe_3)WSiR(OH)_2$ (R = Me or OH) (*29*). This extremely mild method, in which the only by-product is either acetone or $Me(CF_3)CO$, should be applicable in many syntheses where low temperatures and the absence of acids or bases are required for preparation of particularly sensitive compounds (see Section IV for further examples).

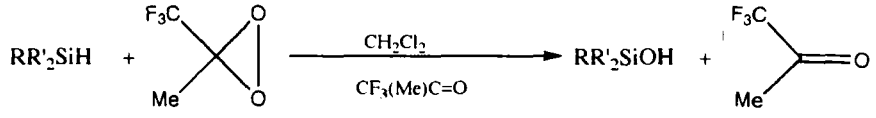

2 (7)

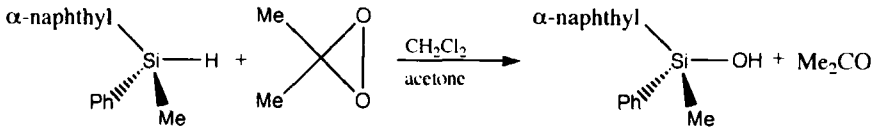

3 **4** (8)

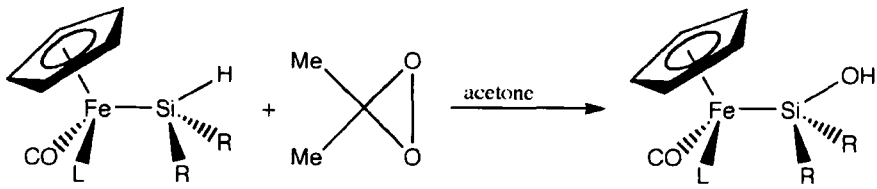

L = CO; R = Me, Bu^t, Ph, or *o*-tolyl
L = PPh_3; R = *o*-tolyl (9)

2. Hydrolysis

Although organosilanes appear to react slowly (if at all) with water alone, in the presence of acids or bases (e.g., alkali metal hydroxides), reactions to give a silanol and H_2 are rapid, with bases being particularly powerful catalysts. The evolution of H_2 in this type of reaction may be used as both a qualitative and a quantitative test for Si–H bonds, and the mechanism of the acid and the base hydrolysis has been discussed in detail (*30, 31*). This hydrolytic method is not very common for the preparation of silanols that are to be isolated, because both acids and bases catalyze the condensation of silanols to siloxanes, and therefore, only compounds containing large substituents are conveniently made in this way. If an anhydrous alkali metal salt is used, a metal siloxide may be isolated and subsequently hydrolyzed to give the silanol [Eq. (10)] (*32*).

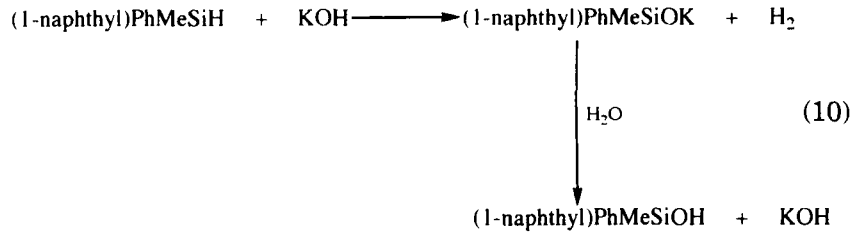

(10)

Excellent yields of silanols may also be obtained by transition metal–catalyzed reactions between Si–H compounds and a buffered aqueous solution of NaOH. Palladium, ruthenium, platinum, or rhodium on either charcoal or alumina as a support catalyze the hydrolysis of *p*-$(HMe_2Si)_2C_6H_4$, $(HMe_2Si)_2O$, Ph_3SiH, Et_3SiH, $(MeO)_2MeSiH$, etc., at room temperature or slightly above, the two palladium catalysts giving the best results. Nickel has also been found to catalyze the hydrolysis of $PhMe_2SiH$, although less effectively than the other metals (*33*).

Phenylmethylsilanediol can also be prepared by solvolysis of $PhMeSiH_2$ [Eq. (11)] and the *para*-disubstituted arene *p*-$(HMe_2Si)_2C_6H_4$ is also solvolyzed to give the corresponding compound containing two Si–OH groups (*34*).

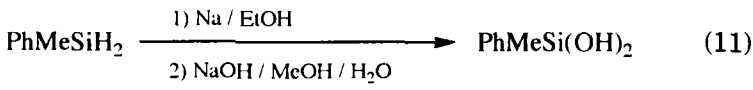

(11)

C. From Halosilanes, Alkoxysilanes, Amides, etc.

Silanols are most often produced by hydrolysis of a compound containing a bond between silicon and a more electronegative atom such as a halogen, O, S, N, or P. The silicone industry is based on the hydrolysis of chlorosilanes, as discussed earlier. The formation of silanols by the cleavage of Si–N and Si–O bonds in particular is becoming much more common, because silyl protecting groups such as Me_3Si, Bu^tMe_2Si, and Bu^tPh_2Si are increasingly used in organic synthesis. Removal of such groups usually leads to silanol formation, although in the case of the Me_3Si group, the final product is usually the siloxane $Me_3SiOSiMe_3$. Only a small number of examples representing the various types of compounds hydrolyzed will be given here; again, many specific examples are given later in the structures section.

A table of physical constants for more than 40 silanols is given in Ref. *35*, together with tabulated data on synthetic routes to silanols (*36, 37*).

1. Hydrolysis of Halosilanes

a. Fluorosilanes. The hydrolysis of silyl fluorides requires alkaline conditions; thus, Me_3SiF may be titrated to the neutral point with 1 N NaOH to give Me_3SiOH (*38*), and Pr^i_3SiF, $Pr^i_2SiF_2$, $Bu^i_2SiF_2$, and *o*-$tolyl_2SiF_2$ react with aqueous ethanolic sodium or potassium hydroxide solutions to give the corresponding silanols Pr^i_3SiOH and $R_2Si(OH)_2$ (R = Pr^i, Bu^i, or *o*-tolyl) in 50 to 80% yields (*39*). Hydrolysis of $Pr^i_2SiF_2$ using H_2O/KOH/dioxane also gives $Pr^i_2Si(OH)_2$ in 50% yield (*39*), which is somewhat lower than that obtained from the corresponding dibromide (see Section II,C,1,c). The hydrolysis of $Bu^t_2SiF_2$ gives a mixture of $Bu^t_2Si(OH)_2$ and Bu^t_2SiFOH (see also Section II,C,1,b) (*40*). Although it is not a hydrolytic reaction, it should also be noted here that sterically hindered fluorosilanes may react directly with KOH in the absence of water to give silanols. For example, Bu^t_2MeSiF reacts with an equimolar amount of KOH at reflux to give $Bu^t_2MeSiOH$ in 78% yield, and $(Bu^t_2MeSiO)_2SiF_2$ with KOH in refluxing hexane affords a 35% yield of $(Bu^t_2MeSiO)_2SiF(OH)$ (*41*).

b. Chlorosilanes. Chlorosilanes are probably the most widely used starting materials for silanol synthesis because of their ready availability and good reactivity. There are, however, problems associated with their use. For example, Section I,B gives an outline of the hydrolysis

of methylchlorosilanes, which normally gives siloxanes rather than silanols as the final products. [The acid- and the base-catalyzed condensation reactions of Me_3SiOH in aqueous dioxane and toluene/water have been studied (*42*).] If, however, precautions are taken to remove or neutralize the acid formed—e.g., by adding pyridine to the reaction mixture (so that the HCl formed is removed as a precipitate of pyridinium hydrochloride) or adding NaOH or KOH to the solution to maintain neutrality—then silanols may often be isolated (*36*). If larger groups are present, as for example in Ph_3SiOH or $Bu^t_2Si(OH)_2$, then formation of siloxanes is much less ready, and fewer precautions need to be taken. Thus, $PhSi(OH)_3$ [but not $MeSi(OH)_3$] may be obtained from $PhSiCl_3$ in the presence of aniline (*43*), and even the triols $(Me_3Si)_3CSi(OH)_3$ and $(Me_3Si)_3SiSi(OH)_3$ are remarkably thermally stable, decomposing only at their melting points of 285–290 and 210–213°C, respectively (*44*).

Although simple hydrolysis of Me_2SiCl_2 affords cyclic and linear siloxanes $(Me_2SiO)_n$ and $HOMe_2Si(OSiMe_2)_nOH$, if precautions are taken to neutralize the HCl formed, then low molecular-weight silanols may be isolated. The use of slightly different conditions (temperature, time, etc.) in the hydrolysis of Me_2SiCl_2 in a $(NH_4)_2CO_3/H_2O$ system can give $Me_2Si(OH)_2$, $(HOMe_2Si)_2O$, or a mixture of oligosiloxanes $HO(SiMe_2O)_nH$ (n = 3–5), which can be separated by fractional distillation under reduced pressure. The oligosiloxanes may be kept as pure liquids, but it is recommended that $Me_2Si(OH)_2$ be kept as a suspension in pentane at 0°C to minimize condensation reactions. Similarly, variations in the conditions used allow the hydrolysis of Ph_2SiCl_2 in $(NH_4)_2/H_2O/Et_2O$ to give $Ph_2Si(OH)_2$ or a mixture of $HO(SiPh_2O)_nH$ (n = 2 or 3) (*45*). Hydrolysis of Et_2SiCl_2 with aqueous NaOH also gives $Et_2Si(OH)_2$ in good yield (*46*), and rapid hydrolysis with stirring of Cl_4Si in dioxane does allow $Cl_nSi(OH)_{3-n}$ (n = 1, 2, or 3) species to be observed in solution by ^{29}Si NMR spectroscopy before condensation reactions and the formation of Si–O–Si linkages occur (*47*).

The presence of two bulky Bu^t groups at silicon gives compounds of much greater stability than those containing other simple alkyl groups, even resulting in the stabilization of the SiH(OH) functional group, so that $Bu^t_2SiH(OH)$, prepared by hydrolysis of Bu^t_2SiHCl with $NaOH/H_2O/Et_2O$, can be sublimed without decomposition (*48, 49*). If large R groups are present, then SiX(OH) functions (X = halogen) may be prepared which are relatively stable towards condensation to siloxanes [Eq. (12)] (*50*). (See also Scheme 4 for compounds containing SiH_2OH and SiH(OH)X groups.)

$$Bu^t_2Si(OH)_2 + PX_5 \xrightarrow[-\ POX_3]{-\ HX} Bu^t_2Si(X)OH \qquad (12)$$

X = Cl or Br

The aminosilanol $Bu^t_2Si(NH_2)OH$ is also stable towards self-reaction (Si–N bonds are normally very susceptible towards attack by protic species) and is prepared by treating $Bu^t_2SiCl(OH)$ [see Eq. (12)] with ammonia (*51*). The bulky diol $Bu^t_2Si(OH)_2$ is similarly reluctant to undergo condensation reactions, and it can be distilled at 210°C without decomposition and treated with concentrated HCl or with concentrated H_2SO_4 at 110°C without siloxane formation (*52*). This diol does, however, undergo condensation to give the disiloxane in the presence of *p*-toluenesulfonic acid in boiling heptane (*53*). The structures and preparations of a range of Bu^t_2SiXY species (X or Y = Cl, F, OH, OLi, NH_2, etc.) and the formation of siloxane and silazane rings from them have been reviewed (*54*).

Steric hindrance by a metal cluster also seems to prevent condensation of the silanols **5** formed by hydrolysis of the corresponding chlorides in the absence of a base, Eq. (13). Such reaction conditions would normally be expected to cause condensation to occur (particularly in the case of the triol), and even concentrated H_2SO_4 in Et_2O did not bring about siloxane formation (*55*). Compounds such as $Cp(CO)_2FeSiMe_n(OH)_{3-n}$ (n = 1 or 2) and $Cp^*(CO)_2FeSi(OH)_3$ may be obtained from the corresponding chlorides by hydrolysis using H_2O/Et_3N. Such compounds are also remarkably stable towards heat, base, or acid, the stability being attributed to the electron-donating nature of the iron fragment, which lowers the acidity of the silanol groups. Thus, even SiH(OH)-containing species such as $Cp^*(CO)_2FeSi(p\text{-tolyl})H(OH)$, $Cp(CO)_2FeSiPr^iH(OH)$, and $Cp^*(CO)_2(PMe_3)WSiMeH(OH)$ may be isolated in this way (*29*).

$$Me_nCl_{3-n}SiCCo_3(CO)_9 \xrightarrow[30\ \text{min reflux}]{C_6H_6\ /\ H_2O} Me_n(OH)_{3-n}SiCCo_3(CO)_9 \qquad (13)$$

5

The very large bulk of the $(Me_3Si)_3C$ group causes solvolytic reactions of chlorides $(Me_3Si)_3CSiR_2Cl$ (R = Me, Et, or Ph) to be severely inhibited. Even the trichloride $(Me_3Si)_3CSiCl_3$ is stable towards boiling MeOH or aqueous EtOH, even in the presence of silver nitrate (*56*). Use of more forcing conditions, such as refluxing 2 M NaOMe/MeOH, leads to fragmentation rather than simple substitution reactions (*57*).

The closely related silicon-centered chlorosilanes $(Me_3Si)_3SiSiCl_3$ and $(Me_3Si)_3SiSiPh_2Cl$, in which there are longer bonds around the central atom than in the carbon analogues, do react "normally." The trichloride reacts with aniline/H_2O/Et_2O to give $(Me_3Si)_3SiSi(OH)_3$ in 45 min at room temperature (*44*), and the phenyl compound gives $(Me_3Si)_3SiSiPh_2OH$ in good yield after 1 h reflux in aqueous THF (*58*). The solvolysis of the chlorofluoro compound $(Me_3Si)_2C(SiMe_2Cl)(SiMe_2F)$ in 0.5 vol. % H_2O in MeOH gives a mixture, 70% of which is the fluorohydroxide $(Me_3Si)_2C(SiMe_2F)(SiMe_2OH)$, which shows the difference in reactivity between chloro and fluoro substituents at silicon (*59*).

The particularly inert halides $(Me_3Si)_3CSiMe_2X$ (X = Cl or Br) react under phase transfer conditions in a three-phase system to give high yields of the silanol [Eq. (14)] (*60*). The bromide also reacts with KOCN in MeOH containing a very low concentration of water to give $(Me_3Si)_3CSiMe_2OH$ as the major product (*61*). This again shows the preference for hydrolysis over methanolysis in $(Me_3Si)_3CSiMe_2X$ species, because the perchlorate and cyanate also undergo similar reactions (see Sections II,C,2,c and II,C,2,e). The importance of steric factors can again be seen as the closely related silylchloride $(Me_3Si)_3CSiMe_2OSiMe_2Cl$, in which the Si–Cl group is now removed from the immediate effects of the very bulky $(Me_3Si)_3C$ group, is hydrolyzed readily to give $[(Me_3Si)_3CSiMe_2OSiMe_2]_2O$ via dimerization of the intermediate silanol (*62*). Another highly hindered chlorosilane, Bu^t_3SiCl, only forms the corresponding silanol when treated with KOH for two days in boiling ethanol (*63*).

$$(Me_3Si)_3CSiMe_2X + H_2O \xrightarrow[\text{heptane, 100 °C}]{Bu^n_4PCl\ /\ KCl} (Me_3Si)_3CSiMe_2OH \qquad (14)$$

2 - 4 days

X = Cl or Br

A series of 15 RMe_2SiOH silanols in which R is an *n*-alkyl group, e.g., Et, *n*-C_6H_{13}, or *n*-$C_{18}H_{37}$, or a polyether chain, e.g., $MeOCH_2CH_2O(CH_2)_4$ or $MeO(CH_2CH_2O)_4(CH_2)_4$, have been prepared in good yields by hydrolysis of RMe_2SiCl species in the presence of $NaHCO_3$, naphthylamine, or aniline (*64*). These authors report that these silanols have a "considerably increased stability on storage if they are first filtered through a short column of silica gel." Hydrolysis of trichlorosilanes containing long-chain ethers as substituents, $MeO(CH_2CH_2O)_n(CH_2)SiCl_3$ (n = 1, 2, 3, 6, or 7) gives analogous silanetriols, which even in the absence of HCl acceptors are remarkably stable in aqueous solution. This stability has been attributed to intra-

molecular hydrogen bonding to the ether oxygens, which gives rise to structures such as **6** (*65*).

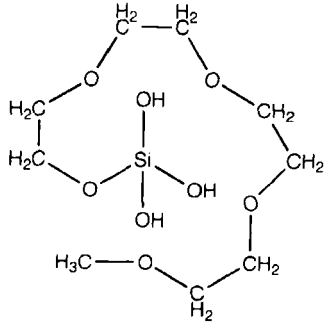

6

Unsymmetrical hydroxydisiloxanes are formed by treatment of $(ClMe_2Si)_2O$ with alkyllithium reagents followed by hydrolysis. Similar reactions may be carried out starting from $ClMe_2SiOSiMe_2OSiMe_2Cl$, but the alkylations are less specific and cyclic siloxanes are formed in significant amounts in the hydrolysis step, Eq. (15) (*66*). The Si–O bonds in the cyclic chlorosiloxane **7** are unaffected by KOH, so that the hydrolysis gives a 63% yield of **8** [Eq. (16)] (*67*).

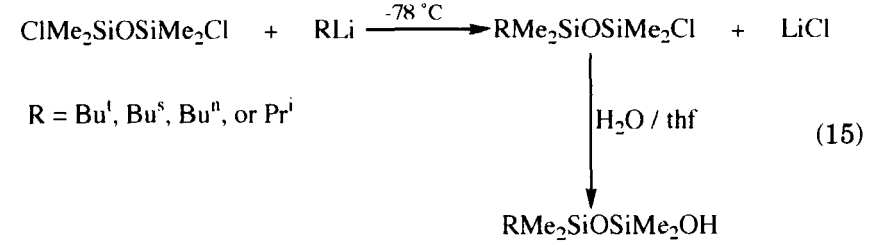

(15)

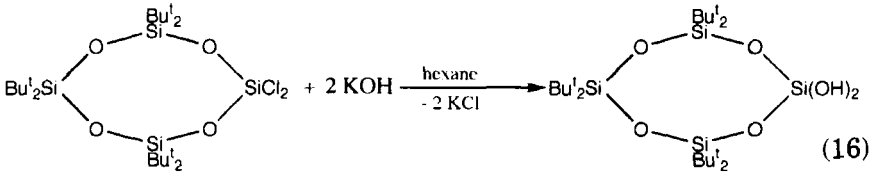

(16)

7 **8**

The benzylic silanols $(PhCHX)Me_2SiOH$ (X = Cl or Br) have been prepared by hydrolysis of the corresponding chlorosilanes with

$(NH_4)HCO_3/H_2O/Et_2O$ at 0°C, which gave 90–95% yields of the solid silanols (*68*). Diarylsilanediols $(X — C_6H_4)_2Si(OH)_2$ (X = H, *p*-F, or *p*-Cl) have been prepared as needle-like crystals by hydrolysis of the corresponding chlorosilanes under similar conditions (*69*).

A range of siloxysilanols, e.g., $(RMe_2SiO)_3SiOH$, $(PhMe_2SiO)_n(Me_3SiO)_{3-n}SiOH$, and $Me_{3-n}(RMe_2SiO)_nSiOH$ (n = 1–3; R = Me, Ph, $PhMe_2SiO$, or Me_3SiO), have been prepared by careful hydrolysis of the corresponding chlorides in H_2O/Et_2O with either $(NH_4)_2CO_3$ or pyridine present to remove the liberated HCl (*70*). The products obtained from the hydrolysis of $(Bu^tO)_2SiCl_2$ depend greatly on the conditions and on the ratio of chlorosilane to water used. Use of a large excess of water (in pyridine/Et_2O) allows $(Bu^tO)_2Si(OH)_2$ to be isolated. Use of a chlorosilane : water ratio of 2 : 1 surprisingly gives **9** (Scheme 3) (containing both an Si–Cl and an SiOH group) and **10**, while a 1 : 8 ratio gives **11**. Hydrolysis of **9** also gives **11**, and hydrolysis of a mixture of $(Bu^tO)_2Si(OH)_2$ and **10** gives the trisiloxane **12**. The silanols are all thermally unstable and give the cyclic trisiloxane $[(Bu^tO)_2SiO]_3$ on heating in solution (Scheme 3) (*71*). Further alkoxy and siloxysilanols—for example, $(RO)_nMe_{3-n}SiOH$ and $(RO)_n(Me_3SiO)_{3-n}SiOH$ (n = neo-pentyl, Pr^i, Bu^s, Bu^t, or cyclo-C_6H_{11})—are also obtained by hydrolysis of the corresponding chlorosilane in a two-phase mixture of Et_2O and aqueous $(NH_4)HCO_3$, or in the case of the less stable methylsilanols, with $(NH_4)HCO_3$/pyridine as HCl acceptors (*72*). Rapid hydrolysis of $Me_3SiO(SiMe_2O)_2SiMe_2Cl$ with ice water without added base to neutralize the HCl liberated does enable isolation of the silanol $Me_3SiO(SiMe_2O)_2SiMe_2OH$, but only in 20–30% yield (*73*).

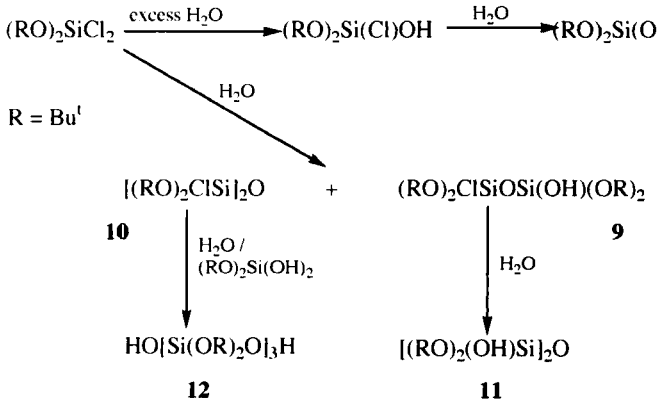

SCHEME 3. The hydrolysis of *tert*-butoxy silanes.

Hydrolysis of $RSiCl_3$ (R = cyclo-C_6H_{11}) in H_2O/acetone over a period of several months to three years gives a mixture of products as incompletely condensed silsesquioxanes, including **13, 14,** and **15,** which may be separated by fractional crystallization (*74, 75*). Hydrolysis of $RSiCl_3$ (R = Pr^i or Bu^t) with 1.5 equivalents of water gives good yields of $[RSiO_{1.5}]_4$ (*76*). (See Sections IV,H and IV,I for the products derived from hydrolysis of Bu^tSiCl_3 under different conditions.)

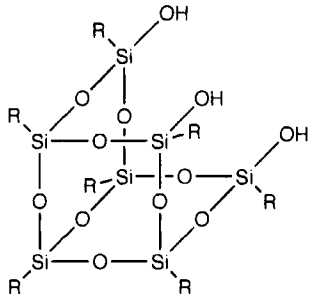

13

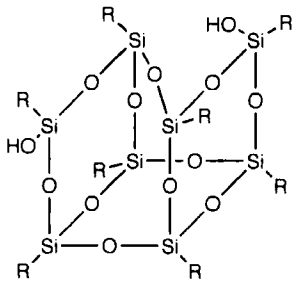

14

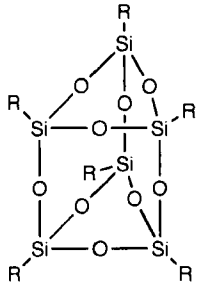

15

c. Bromosilanes. Silyl bromides are rarely used as starting materials for silanol synthesis, but they may be hydrolyzed in similar ways to chlorosilanes. Again, special care must be taken to ensure that the strongly acidic HBr formed on hydrolysis is not allowed to cause siloxane formation (or cleavage of Si–aryl bonds). Careful hydrolysis of Ph_2SiHBr in a medium containing $NH_4Cl/NH_3/H_2O/Et_2O$ has been reported to give $(Ph_2HSi)_2O$ as the usual product, but $Ph_2SiH(OH)$ in some experiments (two out of seven) as a crystalline solid (*77*). Hydrolysis of $Pr^i{}_2SiBr_2$ with aqueous ammonia gives $Pr^i{}_2Si(OH)_2$ in 90% yield, which is much better than the 50% obtained by hydrolysis of $Pr^i{}_2SiF_2$

(see Section II,C,1,a) (*39*). Hydrolysis of $(BrMe_2Si)_3CH$ with 0.5 M aqueous NaOH in Et_2O at 0°C gives the trisilanol $(HOMe_2Si)_3CH$ (*78*).

The $(Me_3Si)_3C$ group provides such a large degree of steric hindrance that the tribromide $(Me_3Si)_3CSiBr_3$ can be recovered unchanged after 72 h reflux in 1/1 v/v H_2O/EtOH (*79*). A small decrease in steric hindrance in tetrasilylmethanes increases reactivity greatly. $(HMe_2Si)_{4-n}C(SiMe_2Br)_n$ (n = 1 or 2) species react rapidly at room temperature in THF containing 5 vol% H_2O to give $(HMe_2Si)_{4-n}C(SiMe_2OH)_n$, whereas $(Me_3Si)_3CSiMe_2Br$, $(Me_3Si)_2C(SiMe_2Br)_2$, and $(BrMe_2Si)_4C$ are only hydrolyzed relatively slowly (*80*). Solvolysis of $(Me_3Si)_2C(SiMe_2Br)(SiMe_2OSO_2CF_3)$ in 20% H_2O in acetone gives $(Me_3Si)_2C(SiMe_2OH)_2$ exclusively after both bromide and triflate hydrolysis. It is likely that the triflate is hydrolyzed first, and then the solvolysis of the bromide is anchimerically assisted by the γ-OH group in $(Me_3Si)_2C(SiMe_2Br)(SiMe_2OH)$ (*59*). The reaction between $(Me_3Si)_2CCl(SiMe_2Br)$ and either Et_2NH in "dry" Et_2O or with "dry" Bu^tOH in both cases has led to the rapid formation of $(Me_3Si)_2CCl(SiMe_2OH)$, presumably as a result of hydrolysis by residual water in the solvents, showing how sensitive silyl bromides (and silyl amides) are towards hydrolysis (*59*).

d. Iodosilanes. Generally speaking, the hydrolysis of iodosilanes is very rapid, but the presence of very bulky substituents at silicon may not only give stable silanols but may also actually cause problems in their preparation. For example, the iodide $(Me_3Si)_3CSiMe_2I$ undergoes solvolytic reactions rather slowly, and conversion to the corresponding silanol is only readily achieved using the relatively harsh conditions of 16 h reflux in aqueous dioxane or 1 h heating at 130°C in wet DMSO (*81*). Similarly, the even more hindered iodides $(Me_3Si)_3CSiRR'I$ (R = R′ = Ph, R = R′ = Et, R = Ph, R′ = Me) are hydrolyzed very slowly. The diphenyl compound requires 60 days under reflux in 5 vol% H_2O/MeCN or 24 h under reflux in 20 vol% H_2O/DMSO. The diethyl compound requires 25 days reaction in 2 vol% H_2O/MeCN at 60°C, and $(Me_3Si)_3CSiPhMeI$ requires 2 h reflux in 1/2/7/v/v H_2O/MeCN/DMSO (*82, 83*). The relative rates of reactions of $(Me_3Si)_2C(SiMe_2CH{=}CH_2)(SiMe_2I)$ and $(Me_3Si)_3CSiMe_2I$ with water have been studied in various organic media. The vinyl compound reacts 1.2 to 2 times more rapidly than the all-methyl compound, the fastest reactions occurring in DMF and DMSO, although the most rapid reaction observed for $(Me_3Si)_3CSiMe_2I$ was that in 2% v/v H_2O/DMF, having a half-life of 19 min at 60°C. These reactions are still relatively very slow for the hydrolysis of a silyl iodide (*17*). As has been found

for related silicon-centered chlorosilanes, the less hindered iodide $(Me_3Si)_3SiSiMe_2I$ is hydrolyzed readily in wet CH_2Cl_2 in 10 min at room temperature (*58*).

The much lower degree of hindrance in $(Me_3Si)_3CSiH_2I$ is reflected in its ease of hydrolysis, because it reacts with 19/1 v/v H_2O/DMSO in 15 min at room temperature to give 82% of $(Me_3Si)_3CSiH_2OH$. This silanol reacts with iodine to give the remarkably stable iodohydroxysilane $(Me_3Si)_3CSiHIOH$, the steric hindrance provided by the $(Me_3Si)_3C$ group preventing bimolecular reactions between the normally incompatible OH and I groups; see Scheme 4 for an outline of the formation of sterically hindered silanols (*81*). The iodosilane $(Me_3Si)_3CSiHIOH$ reacts with $AgBF_4$ in dry Et_2O to give $(Me_3Si)_3CSiFH(OH)$. This can also be prepared from the fluoroiodosilane $(Me_3Si)_3CSiHFI$, which reacts with 1/1 v/v H_2O/acetone to give 88% $(Me_3Si)_3CSiHF(OH)$ in 2 h at room temperature, showing the relative ease of hydrolysis of I compared with both F and H (*79*). Treatment of $(Me_3Si)_3CSiHF(OH)$ with either Br_2 or ICl affords $(Me_3Si)_3CSiBrF(OH)$ and $(Me_3Si)_3CSiIF(OH)$, respectively, again demonstrating the effect of the bulk of the $(Me_3Si)_3C$ group, since OH groups and Si–Br or Si–I groups are usually incompatible; the iodide, however, is hydrolyzed to give $(Me_3Si)_3CSiF(OH)_2$ in aqueous acetone (*79*).

The iodosilane $(Me_3Si)_3CSiPhHI$ is hydrolyzed readily in 1/1 v/v H_2O/acetone or 6/1 v/v dioxane/water to give $(Me_3Si)_3CSiPhHOH$ (*84*),

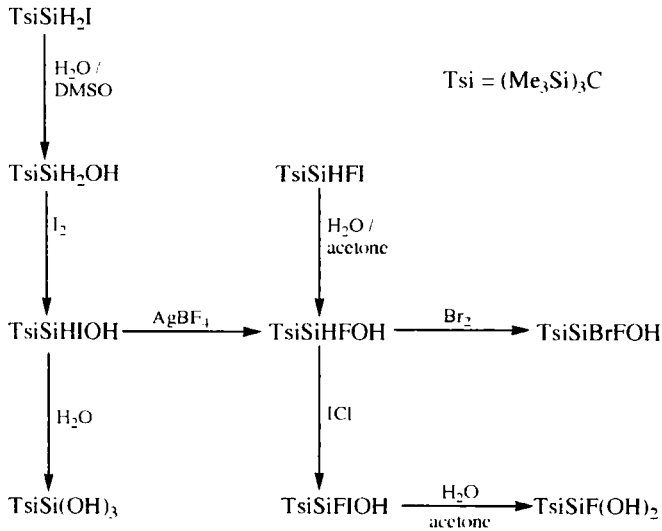

SCHEME 4. Preparative routes to silanols containing the bulky $(Me_3Si)_3C$ group.

which in turn reacts with ICl to give the stable iodosilanol $(Me_3Si)_3C$-SiPhIOH. This reacts further with a second equivalent of ICl to give the chlorosilanol $(Me_3Si)_3CSiPhClOH$ (*85*). Hydrolysis of $(Me_3Si)_3CSi$-MeHI in 1/1 v/v acetone/water gives a good yield of $(Me_3Si)_3CSi$-MeHOH, which reacts with I_2 in CCl_4 to give $(Me_3Si)_3CSiMeIOH$, which in turn reacts with ICl to give the chlorosilanol $(Me_3Si)_3CSiMeClOH$ (Scheme 5) (*86*).

The formation of silanols from severely sterically hindered silyl iodides may be greatly assisted by metachloroperbenzoic acid (mcpba). Thus, $(Me_3Si)_3CSiR_2I$ (R = Me or Ph) and Bu^t_3SiI react with wet mcpba in MeOH to give the silanols $(Me_3Si)_3CSiMe_2OH$, $(Me_3Si)_2C(SiMePh_2)$-$(SiMe_2OH)$, and Bu^t_3SiOH. The dimethyl compound reacts in 2.5 h at room temperature (13-fold excess of mcpba), the diphenyl compound undergoes 90% reaction in 10 h (15-fold excess of mcpba), and the Bu^t compound gives a 50% yield in 3.5 h (15-fold excess of mcpba). All of these processes are much faster than the simple hydrolyses mentioned earlier for this type of compound, and they presumably involve oxidation of the iodide ligand to a better leaving group such as IO_n (*87*). The bulky Bu^t_3SiOH is also formed by hydrolysis of Bu^t_3SiI and by hydrolysis of tri-*t*-butylsilylpyridiniumperchlorate (*88*).

Treatment of highly sterically hindered iodosilanes with a silver salt in a solvent containing water has also been used successfully to prepare bulky silanols (Scheme 6). The introduction of the OH group seems to occur not only by hydrolysis of the silyl perchlorates formed, but also by reaction of the bridged silicocationic species that are formed as intermediates in this type of reaction (*62*). The reaction

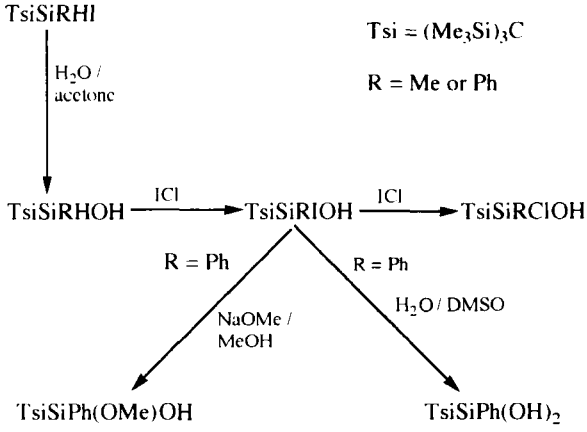

SCHEME 5. Preparative routes to highly sterically hindered silanols.

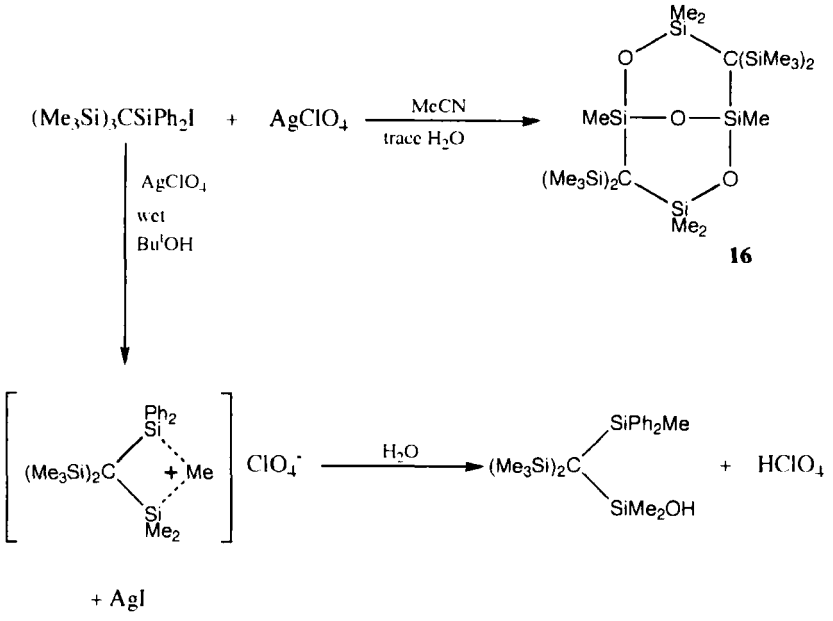

SCHEME 6. Reactions of $(Me_3Si)_3CSiPh_2I$ in the presence of different amounts of water.

between $(Me_3Si)_3CSiPh_2I$ and $AgOClO_3$ in dried MeCN containing very little water gives the bicyclic tetrasiloxane **16.** This presumably arises from the initial formation of $(Me_3Si)_2C(SiPh_2Me)(SiMe_2OH)$, which is then attacked by the strong acid $HClO_4$ formed in the reaction, which brings about Si–Ph bond cleavage. The trisilanol $(Me_3Si)_2C[SiMe(OH)_2](SiMe_2OH)$ may then be formed, and this can then dimerize. Alternatively, dimerization of the initial silanol may occur, and then Si–Ph cleavage, so that further Si–O–Si linkages are formed (*89*).

2. *Hydrolysis of Si–O and Si–S Functions*

a. Alkoxy and Siloxy Silanes. The hydrolysis of alkoxysilanes has been the subject of a considerable amount of research because of their use as coupling agents, in silicone manufacture, and in the treatment of surfaces. The details of the mechanisms of such reactions are complicated and have been the subject of several reviews (*2, 4, 6–10, 90, 91*); they will not be covered further here. The hydrolysis of alkoxysilanes is slowest at about pH 7. Changes in pH away from this to either higher or lower pH increase the rate of hydrolysis by a factor of 10 per pH unit. For example, at pH 4, hydrolysis is ca. 1000 times faster

than at pH 7. For a discussion of the relative stabilities of simple methylsilanols in aqueous solution, see Ref. *91*. The hydrolysis of an alkoxysilane provides one way of preparing sensitive silanols containing small substituents. For example, careful hydrolysis of $Me_2Si(OEt)_2$ gives crystalline $Me_2Si(OH)_2$, which is very sensitive towards both acids and bases and undergoes condensation reactions in contact with acid-washed glass (*92*). This type of synthesis has also been used to prepare other highly sensitive silanediols containing halogenated methyl groups from dimethoxysilanes (*93*). The success of these preparations depends on the formation of an alcohol as a by-product, rather than the mineral acid which would be formed if an analogous halosilane were hydrolyzed. Hydrolysis of $Me_3SiOMgI$ with saturated aqueous ammonium chloride solution also gives Me_3SiOH (*94*). Silanols may also be prepared by treatment of cyclic siloxanes, e.g., $(R_2SiO)_3$ (R = Me or Ph) with organolithium reagents R'Li to give $R'R_2SiOLi$ species, which may then be hydrolyzed with aqueous acid to give $R'R_2SiOH$ compounds [Eq. (17)]. For example, MeLi and $(Ph_2SiO)_3$ in hexane afford after workup a 93% yield of $Ph_2MeSiOH$, while Bu^tLi and $(Me_2SiO)_3$ in Et_2O afford Bu^tMe_2SiOH in 98% yield (*95*).

$$(Ph_2SiO)_3 + 3.3\ RLi \xrightarrow[2)\ H_3O^+]{1)\ \text{reflux}} 3\ RPh_2SiOH \qquad (17)$$

R = Me, Bu^n, Bu^s, or Bu^t

Hydrolysis of $(c\text{-}C_6H_{11})_3SiO(c\text{-}C_6H_{11})$ with hot concentrated HCl in ethanol gives $(c\text{-}C_6H_{11})_3SiOH$ in 70% yield, the three bulky cyclohexyl substituents preventing siloxane formation in the strongly acidic solution (*39*). The acid- and the base-catalyzed hydrolysis of R_3SiOPh compounds (R = Me, Et, Pr^n, Bu^n, or *n*-pentyl) in EtOH show that the R group has a significant role, the rates for acid hydrolysis being about 150 times greater for the methyl derivative than for the pentyl compound, and for base hydrolysis about 1100 times greater for the methyl compound (*96*).

A range of silicon analogues of drugs and fragrances containing SiOH groups have been prepared, and their properties and structures (see Section IV,C) compared with the corresponding carbon species. Acid- and base-catalyzed hydrolysis of methoxysilanes have been used to prepare the antimuscarinic agent **17**, both routes giving about 75% yield of the silanol [Eq. (18)] (*97*). The silicon derivative, **18**, of α-terpineol, with a fragrance of lily of the valley, has been made by hydrolysis of both an ethoxysilane and a chlorosilane precursor, the chlorosilane route giving the better yield [Eq. (19)] (*98*).

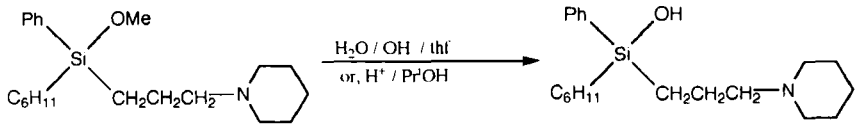

17 (18)

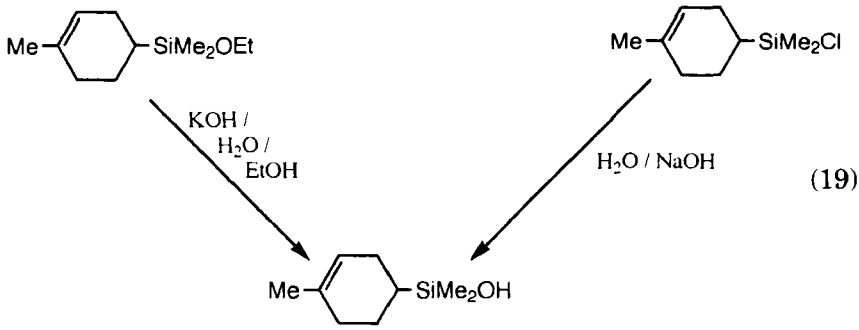

(19)

18

Various aryldisilanols, e.g., **19, 20,** and **21,** have been prepared by hydrolysis of the corresponding ethoxysilanes in a MeOH/EtOH/H_2O/NaOH reaction medium. It was found to be difficult to remove solvent of crystallization from some of these compounds, but stoichiometric complexes between silanol and solvent do not seem to be formed (*99*) as they are in the case of some other silanols (see Section IV,C). Hydrolysis of *p*-$(EtOMe_2Si)_2C_6H_4$ with NaOH/H_2O/MeOH gives 85% of *p*-$(HOMe_2Si)_2C_6H_4$ (*100*), and a similar method has also been used to prepare the analogous 4,4′-bis(hydroxydimethylsilyl)biphenyl (*101*). A wide range or arylsilanetriols X-$C_6H_4Si(OH)_3$ (X = *p*-NMe_2, *p*-OMe, *p*-

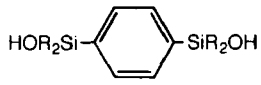

R = Me or Ph

19

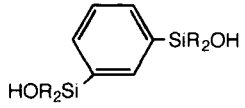

R = Me or Ph

20

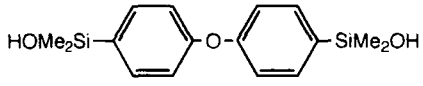

21

Me, *m*-OMe, *m*-Cl, *m*-CF_3, etc.) have been prepared by hydrolysis of the corresponding X-$C_6H_4Si(OMe)_3$ compounds in an H_2O/MeOH mixture. Again, the formation of an alcohol, MeOH, rather than a hydrogen halide is beneficial in the synthesis of such sensitive triols (*102*).

Unusual monosodium salts of ethyl- or phenylsilanetriol $RSi(OH)_2ONa.1.37H_2O$ (R = Et or Ph) are reported to be obtained by treating the polymers obtained from the simple hydrolysis of $RSiCl_3$ with 20% aqueous NaOH/EtOH (*103*). Relatively few silanols have been isolated from the cleavage of siloxanes, as the conditions required to carry out such reactions are likely to cause further reactions of any silanols formed.

The bulky disiloxane $(Me_3Si)_3CSiMe_2OSiMe_3$ is very resistant to Si–O bond cleavage, no reaction occurring, for example, with either 2.5 M HCl in MeOH for 24 h at room temperature or with 1 M NaOMe in MeOH under reflux for 3 h. The silanol $(Me_3Si)_3CSiMe_2OH$ is formed, however, if the disiloxane is treated with either anhydrous CF_3CO_2H (20 min room temperature, showing that the O–$SiMe_3$ bond and not the $(Me_3Si)_3CSi$–O bond is broken) or the strongly basic medium KOH/H_2O/Me_2SO (75°C, 4 h), although some Si–C bond cleavage occurs to give $(Me_3Si)_3CH$ in the latter case (*62*). The highly bulky silanols $Bu^t_2MeSiOH$ and Bu^t_3SiOH are formed in the reductions of 4-*tert*-butylcyclohexanone in the presence of CF_3CO_2H. First the ketone is silylated, and then the silanol is lost in the presence of the acid (*104*).

The preparation of α,ω-diols may also be achieved by the hydrolysis under various conditions (the best being use of $CaCO_3$ to neutralize AcOH) of α,ω-acetoxy compounds. Thus, $AcO(SiRR'O)_nAc$ compounds where R = R′ = Me (n = 2–6) or R = Me, R′ = $CF_3CH_2CH_2$ (n = 2–4) give $HO(SiRR'O)_nH$ species in good yields (*105*). The hydrolysis of $Cl_2C_6H_3Si(OAc)_3$ and $[Cl_2C_6H_3Si(OAc)_2]_2O$ in H_2O/Et_2O with no base present gives $Cl_2C_6H_3Si(OH)_3$ in 15–20% yield and $[Cl_2C_6H_3Si(OH)_2]_2O$, respectively. The addition of base to neutralize the acid formed in these hydrolyses would no doubt give increased yields (*106*). The hydrolysis of Me(1-naphthyl)$Si(OAc)_2$ with aqueous NaOH solution affords the diol Me(1-naphthyl)$Si(OH)_2$ in about 50% yield (*107*). The reaction between the acetate $(Me_3Si)_2C(SiMePh_2)(SiMe_2OAc)$ and $LiAlH_4$, followed by an aqueous workup, affords the silanol $(Me_3Si)_2C(SiMePh_2)(SiMe_2OH)$, rather than the expected Si–H compound $(Me_3Si)_2C(SiMePh_2)(SiMe_2H)$. This is presumably because of the reaction at the carbonyl group rather than at the silicon atom, which is severely sterically hindered, since the acetate itself is resistant towards hydrolysis under the workup conditions (*108*). The bulky carboxylates $(Me_3Si)_3CSiMe_2OC(O)R$ (R = Me, Ph, CF_3, $C_6H_4NO_2$-*p*,

etc.) and $Bu^t_3SiOC(O)CF_3$, in which nucleophilic attack at silicon is again severely sterically hindered, react with 0.2 M NaOMe/MeOH to give $(Me_3Si)_3CSiMe_2OH$ and Bu^t_3SiOH, respectively. The rate of reaction for the $(Me_3Si)_3C$ derivatives falls in the order R = CF_3 > $C_6H_4NO_2$-*p* > Me > Ph, and the products arise from O–C cleavage, rather than the O–Si cleavage which would be expected for less hindered molecules (*109*). Less hindered compounds such as $(Me_3Si)_3$-CSiPhHOC(O)Me react with 0.2 M NaOMe/MeOH to give $(Me_3Si)_3$-CSiPhHOH as the major product, together with about 5–10% of the methoxide $(Me_3Si)_3CSiPhHOMe$ (*109*), and $Bu^tMe_2SiOC(O)Me$ reacts with Bu^nONa/Bu^nOH to give Bu^tMe_2SiOH and $Bu^tMe_2SiOBu^n$ in a 1:4 ratio (*110*).

b. Silyl Triflates. The triflate group is displaced very readily from silicon, the hydrolysis of silyl triflates occurring rapidly even in crowded molecules. For example, the silyl triflates $(Me_3Si)_2C(SiMe_2CH=CH_2)(SiMe_2OSO_2CF_3)$ and $(Me_3Si)_3CSiMe_2OSO_2CF_3$ both react readily with 1% water in MeOH to give the corresponding silanols exclusively (*17*). The reaction between $(PhMe_2Si)_3CSiMe_2I$ and $AgOSO_2CF_3$ in 10/1 v/v Et_2O/H_2O affords $(PhMe_2Si)_3CSiMe_2OH$ in 87% yield, presumably via hydrolysis of the initially formed triflate $(PhMe_2Si)_3CSiMe_2$-OSO_2CF_3 (*111*). The hydrolysis of silyl triflates in the presence of Et_3N also gives silanols [Eq. (20)] (*112*).

$$\begin{array}{c} \text{tflOSiMeBu}^t\text{O(SiMePhO)}_2\text{SiMeBu}^t\text{Otfl} \\ \Big\downarrow \; 2\ \text{Et}_3\text{N} / \text{H}_2\text{O} \\ \text{HOSiMeBu}^t\text{O(SiMePhO)}_2\text{SiMeBu}^t\text{OH} \; + \; 2\ \text{NEt}_3\text{H.Otfl} \end{array} \qquad (20)$$

c. Silyl Perchlorates. As in the case of triflates, silyl perchlorates are very readily hydrolyzed even in severely sterically congested systems. The hydrolysis of $(Me_3Si)_3CSiMe_2OClO_3$ in MeOH containing 1% water gives $(Me_3Si)_3CSiMe_2OH$ with no detectable $(Me_3Si)_3CSiMe_2OMe$ (*113*). The hydrolysis of silyl perchlorates formed as intermediates in reactions between silyl iodides and $AgOClO_3$ have been discussed earlier (Scheme 6). The perchlorate $(Me_3Si)_2C(SiMePh_2)(SiMe_2OClO_3)$ reacts rapidly with wet MeCN at 50°C to give $(Me_3Si)_2C(SiMePh_2)(Si$-$Me_2OH)$. The products of the reactions between $(Me_3Si)_3CSiR_2I$ (R = Me or Ph) and $AgClO_4$ in wet MeCN are also silanols, $(Me_3Si)_3$-

$CSiMe_2OH$ and $(Me_3Si)_2C(SiMePh_2)(SiMe_2OH)$, respectively (*108*). Treatment of $Bu^t_2SiH(OClO_3)$ with Bu^tLi at $-78°C$ brings about rapid reduction of the perchlorate group, to give Bu^t_2SiHOH in good yield, rather than alkylation at silicon (*48*).

d. Silyl Sulfates. The sulfate group is also hydrolyzed readily from silicon, but silyl sulfates are rarely used deliberately as precursors to silanols, as they would normally be prepared from species that would also act as good hydrolytic precursors to silanols, and the formation of H_2SO_4 on hydrolysis is likely to cause condensation reactions. Ring-opening polymerization of cyclic oligosiloxanes may be effected by sulfuric acid by hydrolysis of the sulfates formed, giving rise to polysiloxanes. Triethylsilyl sulfate can be titrated with 1 N NaOH at 0°C to the neutral point to give Et_3SiOH in 75% yield (*38*). A further example of sulfate hydrolysis is involved in the synthesis of $(Me_3Si)_2C(SiMe_2OH)_2$ from $(Me_3Si)_2CSiMe_2OMe$ (*114*). In this case it is thought that anchimeric assistance by the OMe group first assists the loss of a methyl group as methane, and then the methoxy group is lost as methanol, giving the bis sulfate $(Me_3Si)_2C(SiMe_2OSO_3H)_2$, which undergoes rapid hydrolysis to give the disilanol.

e. Silyl Cyanates. The Si–OCN group is very uncommon, but the cyanate group has been found to be particularly readily removed from silicon by hydrolysis. In sterically hindered compounds, it has a leaving-group ability similar to that of triflate and somewhat greater than that of iodide (*115*). Thus, the cyanate $(Me_3Si)_3CSiMe_2OCN$ reacts with low concentrations of water in apparently "dry" solvents such as MeOH or MeCN to give $(Me_3Si)_3CSiMe_2OH$ (*115, 116*). A further example of cyanate hydrolysis in the preparation of $(HOMe_2Si)_4C$ can be found in Section IV,F.

f. Silanethiols and Silyl Sulfides. The silanethiol Ph_3SiSH is hydrolyzed in hot aqueous Bu^tOH over 10 h to give Ph_3SiOH in 96% yield (*117*), and triethylsilanol has been prepared by treating $(Et_3Si)_2S$ with aqueous dioxane (*118*).

D. Hydrolysis of Si–N Functions

Compounds containing an Si–N bond are usually susceptible to hydrolysis. In the same way that hydrolysis of a compound giving an acid requires a base to be present for neutralization, if the reaction yields a basic by-product, such as NH_3 in the hydrolysis of $(Me_3Si)_2NH$, then dilute aqueous HCl may be used for the hydrolysis, thus neutralizing

the base as it forms (*94*). Trimethylsilanol is formed by the hydrolysis of $Me_3SiNHC(O)Me$ (*65, 119*), and by hydrolysis of $(Me_3Si)_2NH$ in Et_2O, followed by neutralization with 2 M HCl, followed by vacuum distillation (*120*). Triethylsilanol has been prepared by treating Et_3SiNCS with aqueous dioxane, whereas Et_3SiX species (X = F, H, or NCO) did not react under the same conditions (*118*). It has also been found possible to remove by hydrolysis in cold water the NH_2 groups, but not the *tert*-alkoxy groups, in $(Bu^t_2O)_2Si(NH_2)_2$ to give $(Bu^tO)_2Si(OH)_2$ (*121*).

E. Hydrolysis of Si–C Bonds

1. Alkyl, Alkenyl, and Aryl Compounds

In compounds containing a carbon-centered substituent that can act as a relatively good leaving group, the cleavage of an Si–C bond may lead to silanol formation. Thus, base-catalyzed hydrolysis of $Cl_3SiCH_2CH{=}CH_2$ affords propene and presumably $Si(OH)_4$ (which would condense to give silica), as the three chloride substituents will also undergo hydrolysis (*122*). A similar reaction occurs if chloroalkyl substituents are present, an E2-type elimination occurring in the case of the presence of a β-Cl [Eqs. (21)–(23)] (*123–125*). This type of cleavage is, however, unlikely to be of synthetic use, because of the very specific requirements for the nature of the substituents and the presence of acids and bases in the reaction sequence.

$$Me_2(CH_2Cl)SiCl + H_2O / OH^- \longrightarrow Me_2Si(OH)_2 + MeCl + HCl \quad (21)$$

$$Me(CHCl_2)SiCl_2 + H_2O / OH^- \longrightarrow MeSi(OH)_3 + CH_2Cl_2 + HCl \quad (22)$$

$$Cl_3CSiCl_3 + H_2O \longrightarrow Si(OH)_4 + CHCl_3 + HCl \quad (23)$$

Although the steric bulk of the C_6Cl_5 groups protects $(C_6Cl_5)_2SiCl_2$ from rapid hydrolysis by atmospheric moisture, the compound is hydrolyzed rapidly under basic, acidic, or neutral conditions in solution to give C_6Cl_5H [and presumably $Si(OH)_4$] and not the expected diol $(C_6Cl_5)_2Si(OH)_2$. This is because $C_6Cl_5^-$ is a good leaving group (*126*). It has, however, been found possible to convert $(C_6Cl_5)_2SiCl_2$ to the diol by treatment with moist ether for 20 min followed by immediate removal of the volatiles under vacuum. The short reaction time and

rapid removal of acidic by-products evidently enables the successful isolation of the diol (*127*). Hydrolysis of $(C_6Cl_5)_nPh_{3-n}SiCl$ (n = 1 or 2) under basic conditions ($THF/H_2O/NaOH$) also leads to Si–C bond cleavage and formation of C_6Cl_5H, indicating, as has been found in other work, that the Si–pentahalophenyl bond is susceptible to cleavage by nucleophilic reagents (*128*). Under acidic conditions (THF/1 N HCl), only hydrolysis of the Si–Cl group occurs, giving the silanols $(C_6Cl_5)_nPh_{3-n}SiOH$ (*128*).

2. *Silyl Carboxylic Acids and Acylsilanes*

Triphenylsilanol is one of several products obtained in the thermally induced decarbonylation of Ph_3SiCO_2H (*129*). Acylsilanes react readily with aqueous base; for example, $Ph_3SiC(O)Ph$ affords Ph_3SiOH and PhC(O)H when treated with aqueous sodium hydroxide solution (*130*). Similarly, hydrolysis of the allenyl silane **22** leads to the formation of **23** via the acylsilane **24** [Eq. (24)] (*131*). (For further examples of acylsilane chemistry, see Refs. *132–134*.)

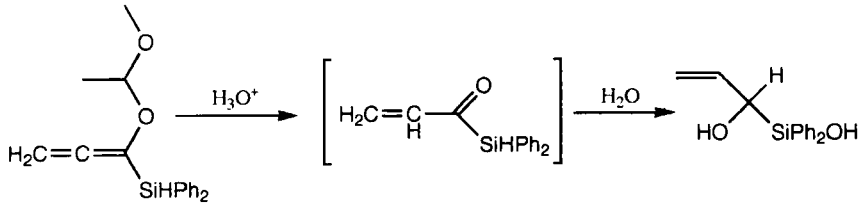

22 **24** **23** (24)

F. From Silyl–Metal Compounds

Although many compounds containing M–Si bonds have undoubtedly been hydrolyzed to give silanol or siloxane products, this is usually an unwanted or accidental reaction, and few syntheses of silanols using this method have been reported. Aqueous alkali is also reported to cleave the Si–Ti bond in $(Ph_3Si)_4Ti$ to give Ph_3SiOH, presumably arising from alkaline hydrolysis of the initially formed Ph_3SiH (*135*).

The isolated product obtained by the hydrolysis of Ph_3SiK is Ph_3SiOH. This presumably arises by the hydrolysis of the initially formed Ph_3SiH catalyzed by the KOH formed in the initial reaction (*136*). The reaction of Ph_3SiLi with O_2 proceeds by a free radical mechanism and gives Ph_3SiOH, together with Ph_3SiH and $Ph_3SiSiPh_3$ (*137*).

G. Addition of Water to Si Multiple Bonds

Compounds containing double bonds to silicon are almost without exception highly reactive towards addition across the multiple bond. Many studies have been carried out using methanol to trap reactive species, but water is used relatively rarely. The products are less easy to characterize (the presence of an OH group is less easy to determine than that of an OMe group by NMR spectroscopy). Also, the silanol group itself may undergo reactions subsequent to the initial addition. Consequently, only a few reactions of this type are described here. This method of synthesis is not likely to become of widespread use because of the difficulties associated with preparing the unsaturated precursors.

Photolytic generation of silene $Me_3Si(Me)C{=}SiMe_2$ in the presence of an excess of D_2O or a trace of H_2O affords disiloxanes **25,** presumably via condensation of the silanol **26** in the case of D_2O, or by reaction of the silanol **27** with further silene in the case of H_2O (Scheme 7) (*138, 139*).

Addition of a large excess of water to a silene gives the silanol, whereas addition of less than a stoichiometric amount of water leads to siloxane formation by addition of a second mole of silene to the initially formed silanol group (*140*). Addition of water to the stable silene $(Me_3Si)_2Si{=}C(OSiMe_3)(C_{10}H_{15})$ ($C_{10}H_{15}$ = 1-adamantyl), or addition of water as the silene is being generated, gives the expected addition product $(Me_3Si)_2Si(OH)CH(OSiMe_3)adam$ (*141*). Reaction of the stable silene $Me_3Si(SiMeBu^t_2)C{=}SiMe_2$ with water also gives the expected product $Me_3Si(SiMeBu^t_2)CHSiMe_2OH$ (*142*), but this also un-

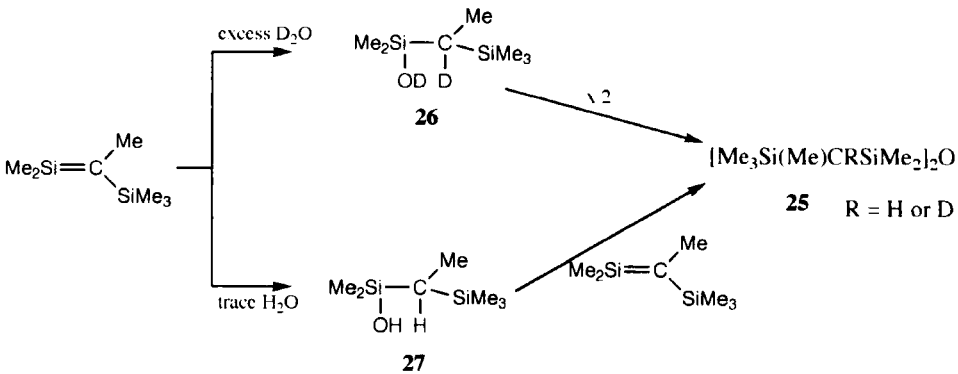

SCHEME 7. Silene reactions with water.

dergoes condensation to the siloxane unless the reaction with water is carried out slowly at 0°C (*143*). The crystalline silanol may alternatively be prepared by reaction of $Me_3Si(SiMeBu^t_2)CHSiMe_2Br$ with $NaOH/H_2O/Et_2O$ (*143*). Hydrolysis with H_2O/thf of the base-stabilized silene $(Me_3Si)_2C{=}SiMe_2 \cdot NMe_3$ affords $(Me_3Si)_2CHSiMe_2OH$ via addition of water across the reactive double bond (*144*).

The reaction of water with disilenes gives simple addition products containing an Si(H)–Si(OH) grouping. Thus addition of water to the bulky disilenes $mes_2Si{=}Simes_2$ (mes = 2,4,6-trimethylphenyl) and *trans*-$Bu^tmesSi{=}SiMesBu^t$ is rapid at 50°C but slow at 25°C, and it does not need catalysis as does alcohol addition to olefins. The products of hydrolysis are the expected $mes_2SiHSi(OH)mes_2$ and $Bu^tmesSiHSi(OH)mesBu^t$ (*145*). Water also adds across the Si=Si bond in the relatively stable disilene $R_2Si{=}SiR_2$ [R = $(Me_3Si)_2CH$] to give $R_2SiHSi(OH)R_2$ in 95% yield (*146*), and to the thermally unstable disilene $Bu^t_2Si{=}SiBu^t_2$ to give silanol $Bu^t_2SiHSi(OH)Bu^t_2$ (*147*). The apparent slower rate of addition of water to disilenes than to silenes may be associated with the fact that the Si=Si bond, in contrast to the Si=C bond, is unpolarized.

Addition of water to the Si=N multiple bond in silanimine $R_2Si{=}NSiBu^t_3$ gives the expected $R_2(HO)Si\text{-}NH(SiBu^t_3)$ (R = Me or Bu^t). Steric factors presumably prevent the rapid cleavage of the Si–N single bonds that remain in the product (*139, 148*).

H. Miscellaneous Preparative Methods

Alkoxysilanes can also be converted into silanol groups in the presence of H_2/Raney Ni at temperatures of 200–300°C and 150–200 atm pressure. For example, Et_3SiOH may be obtained from Et_3SiOR (R = Et, Bu, or CH_2Ph) and Pr^n_3SiOH from $Pr^n_3SiOCH_2Ph$. Unfortunately, the extreme conditions required for this transformation mean that much of the silanol formed in the reactions condenses to the corresponding disiloxane, so that this route is unlikely to be of great use (*149*). Hydrolysis of the products obtained from the thermolysis of $Et_2AlOSiPh_3$ at 250–300°C affords both $EtPh_2SiOH$ and $Et_2PhSiOH$, presumably by redistribution of ligands at high temperature and then hydrolysis of the Al–O bonds present (*150*).

Transition metal complexes containing Si–OH groups have been isolated in low yield after hydrolysis of the products formed in the reaction between $(Me_2N)_2SiCl_2$ and ferrocene under Friedel–Crafts conditions [Eq. (25)] (*151*).

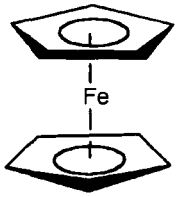

$$+ \quad (Me_2N)_2SiCl_2 \xrightarrow[2)\ H_2O]{1)\ AlCl_3} Fc_2Si(OH)_2 \quad + \quad Fc_3SiOH$$

Fc = ferrocenyl

(25)

III. The Acidity and Basicity of the Silanol Group

A. Acidity

The high reactivity and acidity of silanols was commented on in 1946 when it was found that Et_3SiOH reacted readily with sodium in xylene and that the silanolate Me_3SiONa was formed rapidly when the corresponding silanol was treated with 12 N NaOH solution (*38*). Many subsequent studies, mainly using IR spectroscopic monitoring and acid/base titration, have confirmed the relatively high acidity of silanols compared with carbinols. The effects of silicon on the acidity and basicity of a variety of other types of organosilicon compounds have been reviewed (*152*). The approximate proportionality between the change, $\Delta\nu$, in the O–H stretching frequency between a "free" SiOH and one involved in hydrogen bonding to a suitable base and ΔH for the hydrogen bonding interaction has been used for many years to give an estimate of the strength and relative acidity of OH groups (*153*). Such measurements indicate that silanols have a stronger hydrogen bonding interaction than carbinols, because $\Delta\nu$ is often nearly twice as large for silanols as for carbinols (*77*). For example, the change of O–H stretch for on going from free Ph_3SiOH to a complex with acetone is 226 cm^{-1}, while the change from free Ph_3COH to the acetone complex is only 120 cm^{-1}. A similar comparison has also been made for complexes of Ph_3SiOH or Ph_3COH with ethers such as Et_2O, $Bu^n{}_2O$, THF, or anisole, and again stronger interactions are found in the case of the silanol. For example, the shift on coordination of Ph_3COH with THF is 213 cm^{-1}, while with Ph_3SiOH the shift is 333 cm^{-1} (*154*). Infrared spectroscopic studies of the O–H band shifts on mixing silanols with the bases diethyl ether and mesitylene reveal the order of relative acidities to be arylsilanols > alkylsilanols > arylcarbinols > alkylcarbinols (*77*). Similar studies have also been carried out for thiols and silanethiols (*155*). The interaction of Ph_3SiOH and Ph_3COH with various ketones, e.g., acetone, acetophenone, and cyclohexanone, has

been studied by IR spectroscopy in solution; see selected data in Table I. The spectra show that Ph_3SiOH forms stronger associations with ketones. They also show that, apart from cyclohexanone, the spectral shifts $\Delta\nu$ on forming a silanol : ketone complex correspond well with nucleophilicity parameters of the ketones, but not with Taft's steric and polar factors, nor with dissociation constants pK_a of the ketones (*156*, *157*). Relative acidities of alkoxysilanols and siloxysilanols have also been estimated from IR spectroscopic measurements (*158*), and the OH band positions and their shifts on association with Et_2O have been measured for silanols RMe_2SiOH (R = Me, CH_2Cl, CH_2Br, CH_2I, $CHCl_2$, CH_2Ph, CHClPh, and CHBrPh) (see Table I) (*159*). The acidity of several *para*-substituted arylsilanes (p-XC_6H_4)Me_2SiOH (X = H, Cl, F, Me, OMe, OEt, OBu^t, and Bu^t) shows a good correlation with Hammett σ constants (*160*). The magnitude of the band shift of the OH group in the IR spectrum on association with a donor has also been measured for a range of substituted triarylsilanols (X-C_6H_4)$_3SiOH$ (X = H, p-F, m-F, p-Cl, m-Cl, p-CF_3, p-Me, and m-Me) (see Table I). Again it can be seen that the electron-withdrawing substituents cause greater acidity of the silanols, and hence a larger $\Delta\nu$ shift on coordination to a base (*161*). The O–H stretching frequencies in a range of arylsilanetriols X-$C_6H_4Si(OH)_3$ (X = p-NMe_2, p-OMe, p-Me, m-OMe, m-Cl, m-CF_3, etc.) also correlate well with Hammett σ constants. The frequency on coordination with DMSO is given by $\nu = 3285.5 - 31.91\sigma$ ($r = 0.996$) (*102*).

The intensities and frequencies of silanol O–H stretches have been measured for R_3SiOH (R = Me, Et, Pr^n, Bu^n, and Ph) and for $PhMe_2SiOH$ and $Ph_2MeSiOH$ in a variety of solvents. As the polarity of the solvent decreases on going from chloroform to cyclohexane, the free O–H group interaction with the solvent weakens and the stretching frequency increases (see Table II). At the same time, however, the relative intensity of the band decreases (*162*). An interesting comparison may be made between Ph_3SiOH and $Ph_3SiSiPh_2OH$, for which the $\Delta\nu$ values for the IR spectra with DMSO are about equal (see Table I), but the acidity of the pentaphenyl compound as measured by acid/base titration is about 2.67 pK_a units higher than that of Ph_3SiOH. The enhanced acidity of $Ph_3SiSiPh_2OH$ has been attributed to interaction of an oxygen lone pair with the LUMO of the Si–Si system (*163*). This study brings into focus the potential discrepancies possible when relating acidity solely to hydrogen bonding ability.

Thermodynamic data on intramolecular hydrogen bonding interactions in RMe_2SiOH (R = $PhCH_2$, $BrCH_2$, $PhCH_2CH_2$, $BrCH_2CH_2$, $PhCH_2Me_2SiO$, $BrCH_2Me_2SiO$, etc.) in hexane solution have been

TABLE I

INFRARED SPECTROSCOPIC DATA FOR SILANOLS AND THEIR COMPLEXES WITH BASES

Silanol	Base	Free O–H stretch[a] (cm^{-1})	$\Delta\nu$ (cm^{-1})	ΔH (kJ mol^{-1})	Refs.
Cl_3SiOH		3680[b]			*12*
Me_3SiOH[c]		3688			*77*
		3690			*182*
		3695			*159*
		3702			*183*
	Me_3SiOH		189		*77*
	EtOAc		146		*183*
	MeCN		140–175[d]		*183*
	dioxane		220		*183*
	Et_2O		238		*12, 159*
	THF		265		*183*
	PhCl		29		*183*
	C_6H_6		40		*183*
	PhMe		59		*183*
	p-xylene		63		*183*
	Me_3Ph		71		*77*
Et_3SiOH		3685			*77*
		3683			*93*
	Et_3SiOH		185		*77*
	dioxane		212		*93*
	Et_2O		230		*77*
	Me_3Ph		62		*77*
Ph_3SiOH		3677			*77*
		3681.4			*157*
		3678			*184*
		3686			*161*

Ph_3SiOH	206		*77*
Et_2O	311		*77*
	319		*154*
	317		*184*
	316		*180*
	308		*161*
$Pr^n{}_2O$	311		*154*
$Bu^n{}_2O$	319.5		*154*
Pr^nOPr^i	326.5		*154*
PhOMe	184.5		*154*
1,4-dioxane	283		*154*
THF	333		*154*
	338		*180*
furan	67		*154*
$MeC(O)CH_2Ph$	185	11.3	*157*
MeC(O)Ph	192	11.4	*156, 157*
MeC(O)Et	195	15.1	*156, 157*
MeC(O)Me	226		*156*
$MeC(O)Bu^i$	237		*156*
$MeC(O)C_6H_{11}$	222	20.1	*156, 157*
$cyclopropyl_2O$	223	17.6	*157*
cyclohexanone	275		*156*
DMSO	411		*163*
	445		*185*
$(CH_2)_4SO$	440		*184*
Me_3Ph	79		*77*

(*continues*)

TABLE I (*Continued*)

Silanol	Base	Free O–H stretch[a] (cm^{-1})	$\Delta\nu$ (cm^{-1})	ΔH (kJ mol^{-1})	Refs.
$(1\text{-naphthyl})_3SiOH$[e]		3670			*186*
	DMSO[e]		150		*186*
	dioxane[e]		130		*186*
	toluene[e]		65		*186*
	o-xylene[e]		60		*186*
	m-xylene[e]		50		*186*
	p-xylene[e]		80		*186*
$Ph_3SiSiPh_2OH$	DMSO		401		*163*
$HO(SiPh_2)_7OH$		3605[f]			*185*
	DMSO		345[g]		*185*
$HO(SiPh_2)_4OH$		3608[f]			*185*
		3415[h]			*185*
$HO(SiPh_2)_5OH$		3605[f]			*185*
	$HO(SiPh_2)_5OH$	3280			*185*
$(HOMe_2Si)_2O$		3693			*187*
	$(HOMe_2Si)_2O$		402[i]		*187*
$(HOMe_2SiO)_2SiMe_2$		3683			*187*
	$(HOMe_2SiO)_2SiMe_2$		403[i]		*187*
	$(HOMe_2SiO)_2SiMe_2$		193[h]		*187*
$(HOPh_2Si)_2O$		3681			*187*
	$(HOPh_2Si)_2O$		284[i]		*187*
$(HOPh_2SiO)_2SiPh_2$		3679, 3670			*187*
		3616[f]			*187*
	$(HOPh_2SiO)_2SiPh_2$		384[i]		*187*
	$(HOPh_2SiO)_2SiPh_2$		201[h]		*187*
$HO(SiPh_2O)_4H$		3680			*188*
		3620[f]			*188*
		3600[j]			*188*

	$HO(SiPh_2O)_4H$		230	*188*
	$HO(SiPh_2O)_4H$		390	*188*
Ph_2SiHOH		3675		*77*
	Ph_2SiHOH		223	*77*
	Et_2O		322	*77*
	Me_3Ph		74	*77*
$(Bu^tO)_2SiOH$	Et_2O	3694.5	290	*158*
$(Pr^iO)_3SiOH$		3695.5	319	*158*
$(EtO)_3SiOH$		3697.5	335	*158*
$(MeO)_3SiOH$		3698	352	*158*
$(PhO)_3SiOH$		3685	420	*158*
$(PhCH_2O)_3SiOH$		3691	368	*158*
$(Me_3SiO)_3SiOH$		3705	300	*158*
$(Bu^tO)_2MeSiOH$		3695.5	263	*158*
$(Me_3SiO)_2MeSiOH$		3700.5	280	*158*
$(Bu^tO)Me_2SiOH$		3695.5	241	*158*
$(Me_3SiO)Me_2SiOH$		3696.5	259	*158*
$(Bu^tO)_2(Me_3SiO)SiOH$		3698.5	294	*158*
$(Bu^tO)(Me_3SiO)_2SiOH$		3702	297	*158*
$PhCH_2Me_2SiOH$		3690	252	*159*
ICH_2Me_2SiOH		3686	276	*159*
$BrCH_2Me_2SiOH$		3684	279	*159*
$ClCH_2Me_2SiOH$		3684	283	*159*
Cl_2CHMe_2SiOH		3677	311	*159*
$(p\text{-}MeC_6H_4)_3SiOH$		3686.5	297	*161*
$(m\text{-}MeC_6H_4)_3SiOH$		3686.5	299	*161*
$(p\text{-}FC_6H_4)_3SiOH$		3684	332	*161*
$(p\text{-}ClC_6H_4)_3SiOH$		3683	347	*161*

(*continues*)

TABLE I (*Continued*)

Silanol	Base	Free O–stretch[a] (cm^{-1})	$\Delta\nu$ (cm^{-1})	ΔH (kJ mol^{-1})	Refs.
$(m\text{-}FC_6H_4)_3SiOH$		3682.5	354		*161*
$(m\text{-}ClC_6H_4)_3SiOH$		3682	356		*161*
$(p\text{-}CF_3C_6H_4)_3SiOH$		3680.5	372		*161*
$Me_2Si(OH)_2$		3683			*93*
		3693			*187*
	dioxane		239		*93*
$(CH_2{=}CH)MeSi(OH)_2$		3685			*187*
$Et_2Si(OH)_2$		3682			*93*
	dioxane		237		*93*
	Et_2O		270		*93*
$Bu_2Si(OH)_2$		3680			*93*
	dioxane		235		*93*
	Et_2O		263		*93*
$EtMeSi(OH)_2$		3679			*93*
	dioxane		256		*93*
$PhMeSi(OH)_2$		3676			*93*
		3686			*187*
	dioxane		265		*93*
	Et_2O		294		*93*
$Ph_2Si(OH)_2$		3670			*93*
		3681			*187*
	dioxane		285		*93*
	Et_2O		322		*93*

$ClCH_2MeSi(OH)_2$		3673		*93*
	dioxane		278	*93*
	Et_2O		314	*93*
$BrCH_2MeSi(OH)_2$		3673		*93*
	dioxane		278	*93*
$ICH_2MeSi(OH)_2$		3673		*93*
	dioxane		276	*93*
	Et_2O		313	*93*
$Cl_2CH_2MeSi(OH)_2$		3669		*93*
	dioxane		317	*93*
	Et_2O		353	*93*
$HOMe_2SiCCo_3(CO)_9$		3660[k]		*55*
$(HO)_2MeSiCCo_3(CO)_9$		3650[k]		*55*
$(HO)_3SiCCo_3(CO)_9$		3640[k]		*55*

[a] Data are for CCl_4 solutions of the silanol containing the proton acceptor, unless otherwise stated.

[b] In $SiCl_4$ solution.

[c] For values of Δv O–H for Me_3SiOH in various aromatic hydrocarbons, esters, ketones, ethers, etc., see Ref. *189*.

[d] The Δv O–H varies as the MeCN concentration is varied.

[e] It is unclear under what conditions these spectra were recorded, but it is likely that they were for solids and not for CCl_4 solutions, and so direct comparison with other spectra in the table should not be attempted.

[f] Intramolecular OH···π interaction.

[g] Difference between OH···π stretch and DMSO complex.

[h] Intramolecular OH···O interaction.

[i] Intermolecular OH···O interaction.

[j] Spectrum recorded as a thin film. This band was not originally thought to be due to an intramolecular OH···π interaction, but in the light of other recent results, this now seems likely.

[k] Value is for a nujol mull, not a CCl_4 solution.

TABLE II

INFRARED SPECTROSCOPIC DATA FOR SILANOLS IN VARIOUS SOLVENTS

Silanol	Free OH in $CHCl_3$ (cm^{-1})	Free OH in CS_2 (cm^{-1})	Free OH in CCl_4 (cm^{-1})	Free OH in C_6H_{12} (cm^{-1})	Refs.
Ph_3SiOH	3667	3670	3686	3691	*162*
$Ph_2MeSiOH$	3665	3675	3689	3695	*162*
$PhMe_2SiOH$	3669	3679	3693	3699	*162*
Me_3SiOH[a]	3675	3685	3697	3706	*162*
Et_3SiOH	3672	3684	3696	3703	*162*
$Pr^n{}_3SiOH$	3673	3683	3695	3702	*162*
$Bu^n{}_3SiOH$	3671	3683	3695	3702	*162*

[a] Values of free O–H stretches for Me_3SiOH in $CHCl_3$, C_6H_6, EtOAc, MeCN, Et_2O, dioxane, and THF are 3668, 3642, 3540, 3524, 3464, 3466, and 3430 cm^{-1}, respectively (*182*).

obtained. Enthalpies of formation of these intramolecular interactions (which presumably arise between the OH group and either the aromatic ring or the halogen) are, for example, −3.31, −5.40, and −12.7 $kJmol^{-1}$ for RMe_2SiOH, R = $PhCH_2$, $PhCH_2CH_2$, and $PhCH_2Me_2SiO$, respectively, and −1.70, −3.01, and −4.70 $kJmol^{-1}$ for RMe_2SiOH, R = $BrCH_2$, $BrCH_2CH_2$, and $BrCH_2Me_2SiO$, respectively. The size of the ring formed by intramolecular hydrogen bond formation seems to be the dominant factor in each case (*164*).

The relative acidities of a variety of substituted arylsilanols ($X\text{-}C_6H_4)_3SiOH$ (X = *p*-NH_2, *p*-Me, *m*-Me, H, *m*-OMe, *p*-F, *p*-Cl, *m*-F, *m*-Cl, and *p*-CF_3) have been measured by determination of the half-neutralization potentials in pyridine, $Bu^n{}_4NOH$/pyridine, or pyridine/Pr^iOH solution. The relative acidities correlate well with the σ° constants of the substituents, the most electron-withdrawing substituents giving the more acidic silanols (*161, 165*). Triphenylsilanol has been found to be a slightly weaker protonic acid (the half neutralization potentials for phenol, *p*-methoxyphenol, Ph_3SiOH, and *p*-nitroaniline are 0.68, 0.73, 0.80, and 0.90 V, respectively) in pyridine solution than phenol, but stronger than *p*-nitroaniline. It is a stronger acid than trialkylsilanols and trialkylcarbinols, which cannot be titrated in this way (*166*). The pK_a of Et_3SiOH in aqueous solution determined by a method using the distribution of the silanol between CCl_4 and aqueous $NaClO_4$ solution has been found to be 13.63 ± 0.07 (*167*), i.e., it is somewhat more acidic than Me_3COH, which has a pK_a of 19 (*120, 168*). Titration methods give pK_a's of 16.57–16.63 for Ph_3SiOH (*163*). The

silanols RMe_2SiOH have been estimated to have high acidities in water with pK_a's of about 11 and 9.8 for R = *m*-ClC_6H_4 and PhC≡C, respectively (*169*).

The gas phase acidities of a variety of silanols have been determined to give data that are unavailable for solutions because of unwanted condensation reactions. As might be expected, H_3SiOH has a higher acidity than H_3COH, and phenyl, methoxy, fluoro, and chloro substituents enhance the acidity, resulting in the following sequence of acidities: $Me_3SiOH < PhH_2SiOH < (MeO)_3SiOH < F_3SiOH < Cl_3SiOH$; the trichloro derivative is of comparable acidity in the gas phase to HNO_3 and HBr (*170*). The experimentally determined (*171*) gas phase acidity of Et_3SiOH has been found to be slightly greater than that of Me_3SiOH, and the calculated (*172*) acidity of EtH_2SiOH to be greater than that of MeH_2SiOH. It is unclear, however, whether polarizability or inductive effects play the more significant role when the alkyl chain is lengthened in this situation.

Proton NMR studies show that there is less shielding of the OH proton in Me_3SiOH than in Me_3COH, thus indicating increased protonic character for the silanol (*173*). There is also a linear correlation between the chemical shift in the ^{29}Si NMR spectra of silanols and the solvent donor ability, with strong donors such as HMPA causing a larger upfield shift than weaker donors (*174*). The effects of donor solvents on the chemical shifts of SiOH protons in ^1H NMR spectra have also been studied (*175–177*). The acidity of the silanol group was shown to correlate well with the chemical shift, δ, in the presence of the coordinating solvent DMSO, although this trend only seems to hold well for closely related series of compounds (*176*). In the case of X-$C_6H_4Si(OH)_3$ species (X = *p*-NMe_2, *p*-OMe, *p*-Me, *m*-OMe, *m*-Cl, *m*-CF_3, etc.), excellent correlation ($r > 0.99$) between the OH proton chemical shift, δ, and the Hammett σ constant was found for various bases, for example $\delta = 6.73 + 0.773\sigma$ for HMPA solutions. A straight-line plot is also obtained by plotting δ OH (ppm) against ν O–H (cm^{-1}), indicating that the factors affecting both δ and ν are the same (*102*). An attempt has been made to estimate the pK_a of silanols using the equation $pK_a = 8.9 + 1.06\tau OH$ (τOH = chemical shift of OH proton in ppm) derived from earlier data. The pK_a values derived in this way for silanols in DMSO are 14.06, 13.46, 13.24, 13.00, 12.64, 12.08, and 12.04 for Et_3SiOH, (*p*-$MeOC_6H_4$)Me_2SiOH, $PhMe_2SiOH$, $(CF_3CH_2CH_2)_3SiOH$, $EtPh_2SiOH$, $Ph_2Si(OH)_2$, and Ph_3SiOH, respectively (*178*). These values show the approximate expected sequence of acidity, and also indicate that the acidities are higher than those of the corresponding carbinols. However, the values do not agree well

with those derived from acid/base titration methods (see earlier discussion). The chemical shift of protons is subject to a variety of factors (not only acidity), and the direct measurements by titration are probably more reliable.

Semiempirical calculations have been carried out on the interaction of silanols and alcohols with ethers and ketones using the silanol or methanol to water and to formaldehyde cases as models. The calculated geometries are shown in Fig. 1 for the triphenyl example. Although it has been shown that the strength of hydrogen bonds is proportional to the change in frequency of the O–H stretch on going from a free to a coordinated situation, the calculations on such systems do not reproduce the agreement. This has been ascribed to the fact that the calculations only take a single isolated pair of molecules into account, whereas in solution, interactions are much more complicated (*179*).

B. Basicity

An IR spectroscopic study of silanols in the presence of phenol shows that the basicity order is alkylcarbinols > alkylsilanols > arylcarbinols ≈ arylsilanols, i.e., the silanols are nearly as basic as the alcohols despite the fact that they are much more acidic. Table III gives data for the change in stretching frequency on hydrogen bond formation between silanols and phenol. It can be seen that the values for $\Delta\nu$ are similar in size to those found on coordination between silanol and a base (see data in Table I), and that the ΔH values for hydrogen bond strength are also similar to those found in the silanol/base cases (see Table I). That the silanols have such basicities (in contrast to alcohols, where there is an inverse relationship between acidity and basicity) has been rationalized by invoking $p\pi$–$d\pi$ bonding between Si and O, which allows the negative charge of an R_3SiO^- ion to be delocalized,

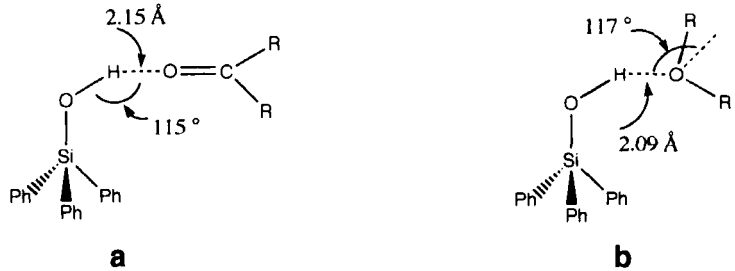

FIG. 1. Calculated geometries for the hydrogen bonding interaction of Ph_3SiOH with (a) ketones and (b) ethers.

TABLE III

INFRARED SPECTROSCOPIC DATA FOR SILANOLS AND THEIR COMPLEXES WITH PHENOL

Silanol	Acid	Free O–H stretch[a] (cm^{-1})	$\Delta\nu$ (cm^{-1})	ΔH ($kJmol^{-1}$)	Refs.
Me_3SiOH	PhOH	3688	216		*77*
Et_3SiOH		3685	228		*77*
Ph_3SiOH		3677	175		*77, 180*
Ph_2SiHOH		3675	194		*77*
$Bu^i_2Si(OH)_2$			208	16.72	*190*
$(PhCH_2)_2Si(OH)_2$			169	13.79	*190*
$(m\text{-tolyl})_2Si(OH)_2$			326		*190*
$(o\text{-tolyl})_2Si(OH)_2$			296		*190*
$(HOMe_2Si)_2O$		3686	268	20.48	*45, 190*
$(HOMe_2SiO)_2SiMe_2$		3686	291	22.15	*45, 190*
$(HOPh_2Si)_2O$		3674	190	15.47	*45, 190*
$(HOPh_2SiO)_2SiPh_2$		3674	243	18.81	*45, 190*

[a] Data are for CCl_4 solutions of the silanol containing the proton acceptor.

thus giving an enhanced acidity. However, there will still be lone pairs on the oxygen atom, and thus the silanol will still have basic properties (*77*). This argument is, however, complicated when one takes into account that Ph_3GeOH is much more basic than the corresponding silanol (*180*). Also, as M in Ph_3MOH becomes more electropositive, the stretching frequency decreases; free O–H stretching frequencies for Ph_3MOH are 3677, 3651, 3647,and 3618 cm^{-1} for M = Si, Ge, Sn, and Pb, respectively, in CCl_4 solution (*181*).

In view of the high acidity and the relatively high basicity of silanols, it is to be expected that they will form strong hydrogen bonds both with themselves and with other suitable species. The association of silanols in solution has been discussed (see refs. *182–189* in Table I; Ref. *190* in Table III), while the following section describes the wide range of hydrogen-bonded structures that have been found in the solid state.

IV. Structural Studies of Silanols

A. INTRODUCTION

The discussion in this section relates to structural studies carried out by calculation, x-ray diffraction, or electron diffraction techniques and will concentrate on how the molecular structures are influenced

by hydrogen bonding to the SiOH group. Further data concerning bond lengths and angles can be found in the various tables, but they will not usually be discussed in detail. Apart from the computational studies, the compounds are arranged in order of increasing numbers of SiOH groups present and from silanols to silanediols to silanetriols. There are now also known to be a range of materials that are well-defined adducts or clathrates of silanols with organic molecules. These are included in the appropriate silanol section rather than being grouped together.

The position and orientation of OH protons is clearly of particular importance in studies of hydrogen-bonded species. Unfortunately, relatively few of the structures determined by x-ray crystallography are of sufficient quality for meaningful discussion of such hydrogens to be made. In the absence of reliable positions for the hydrogens, the O···O, O···N, O···F, or O···π-system distances are commonly used as a basis for the discussion of hydrogen bonding in silanols. The structural data for the hydrogen bonds in silanols, together with a brief summary of their structures, are given later in Tables IV–VII. Data given in the tables that are not found in the original publications have been generated using atomic coordinates deposited at the Cambridge Crystallographic Data Centre, as have many of the figures.

B. Calculations on the Structures of Silanols

The simple silanols $H_nSi(OH)_{4-n}$ ($n = 0, 1, 2,$ or 3) are far too unstable towards condensation reactions to be isolated and structurally characterized, but they have been the subject of several theoretical studies. The calculated geometry of H_3SiOH at the HF/3-21G(*) level is staggered, as are methanol, MeSH, and H_3SiSH. The Si–O–H bond angle of 128.8°, is large but this is common in Si–O–R compounds such as siloxanes and alkoxysilanes, while the Si–O bond length of 1.633 Å is about normal for silanols (*191–194*). The most stable conformation of $H_2Si(OH)_2$ has been calculated to be the *gauche* arrangement with an Si–O distance of 1.642 Å and H–Si–H, O–Si–O, and Si–O–H angles of 110.32, 112.84, and 118.14°, respectively. This geometry has been interpreted in terms of a strong anomeric effect (*195, 196*). The geometry of $HSi(OH)_3$ has been calculated (*191, 194*) at the 3-21G level to be of a near-*gauche* arrangement around all three of the Si–O bonds (Si–O distance 1.625 Å, O–Si–O angle 108.8°), which would be expected if the anomeric effect has a significant role in determining the geometry (*195*).

The structure of $Si(OH)_4$ has been the subject of several computational investigations (for a comparison of the various studies, see Ref. *191*). The lowest-energy geometry is of S_4 (hydrogen staggered) rather than D_{2d} symmetry, the S_4 conformation being calculated as 13.8 (*196*) or 16.05 kJmol^{-1} (*194*) lower in energy. At the 6-31G* level of theory, the Si–O bond length in $(HO)_4Si$ is 1.629 Å and the O–Si–O angles are 115.82 and 106.39° (*197*). Calculations on $(HO)_3SiCN$ and $(HO)_3SiNC$ have been carried out, but details regarding the OH groups in these compounds were not reported (*198*).

Calculations on the geometries of **28** and **29** have been carried out as models for pairs of edge- and face-sharing SiO_4 tetrahedra, respectively, in silicates. The structures are both found to be highly strained, involving 58 and 127 kJ mol^{-1} strain energy for each Si–O bond in the rings (*199*). This result is not surprising, because SiOSiO four-membered rings are not generally found in silicates, and compounds containing such rings have proved very difficult to prepare. However, West and co-workers have found that addition of O_2 to the disilene $mes_2Si{=}Simes_2$ does result in the four-membered ring species **30** (*200*).

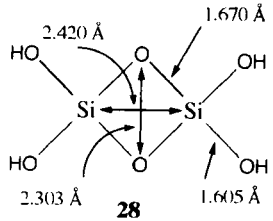

28

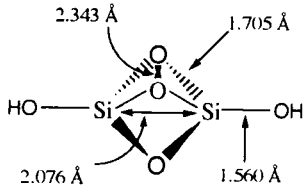

29

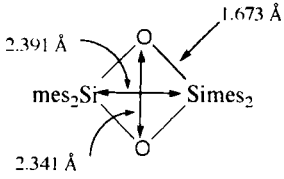

30

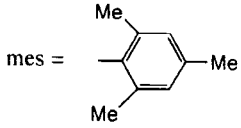

Disilicic acid $[(HO)_3Si]_2O$ has been the subject of numerous investigations (*201, 202*). At the 6-31G** level of theory with polarization functions on the bridging oxygen, the Si–O(bridging) length is 1.617 Å and the Si–O–Si angle 141° (*203*).

The majority of Si–O bond lengths fall in the range 1.64 ± 0.03 Å (*204*), which is somewhat shorter than the expected 1.76 Å estimated

from the corrected sum of the covalent radii for O and Si (using the Stevenson–Schomaker approximation, referred to in Ref. *204*). The shortening and strengthening of bonds between Si and electronegative elements such as O, N, F, and Cl has often been attributed to the involvement of donation of lone pair *p*-electrons on the electronegative element into the vacant *d*-orbitals of the silicon. This relatively simple description has been applied in many circumstances, but in recent years its validity has been questioned (see Ref. *193* for discussion). Various calculations have found that to reproduce accurately the Si–O–Si bond angles in siloxanes, it is important to include polarization functions on the oxygen, and that Si *d*-orbital participation is relatively unimportant. The strength and shortness of these bonds has instead been attributed to the high polarity of the Si–X bond (X = O, N, F, Cl, etc.) (*193, 194, 203*).

C. Compounds Containing One Si–OH Group

1. Highly Sterically Hindered Silanols

There appears to be no hydrogen bonding present in several of the reported structures of compounds containing only one Si–OH group. In **31** (derived from the oxidation of a disilacyclopropane species with trimethylamine-*N*-oxide) (*205*), there appears to be no hydrogen bonding, not even to the aromatic rings (*206*), steric hindrance presumably preventing intermolecular interactions. In **32** (prepared by addition of water to a tetrasilabicylo[1.1.0]butane derivative) (*207*), there are no intermolecular interactions, but recent work (*206*) suggests that there is an intramolecular interaction between the SiOH group and one of the aromatic rings. The oxygen atom lies 2.8 Å from the plane of one of the rings and 3.2 and 3.6 Å from two of the aromatic carbon atoms, which is consistent with the O–H hydrogen atom being close to and above an aromatic C–C bond (*208*). This suggestion is supported by the IR data reported for **32** (*207*), which has a ν SiO–H band at 3600 cm^{-1} in the solid state. This corresponds well with IR absorbtions assigned to similar interactions in silanols containing aromatic substituents—for example, in $HO(SiPh_2)_nOH$ species, for which there are bands at 3608, 3605, and 3605 cm^{-1} for n = 4, 5, and 7, respectively in CCl_4 solution (*184*). The disilane **33** was not reported to show any hydrogen bonding in its structure (*209*). A more recent study has confirmed this and shown that the OH group is surrounded by Pr^i groups, and that it cannot participate in OH···OH or OH···π

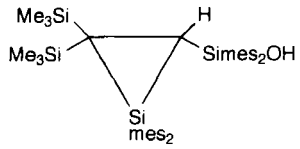

31

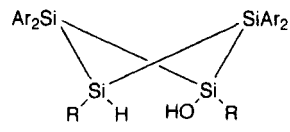

32

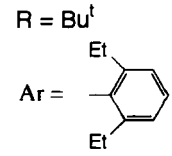

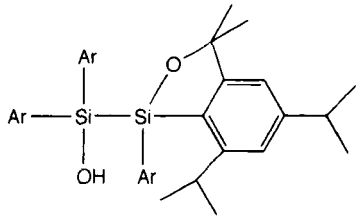

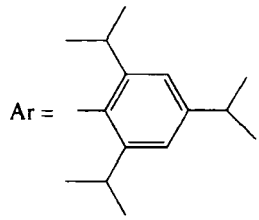

33

interactions because of the steric hindrance provided by the bulky aryl groups (*210*).

The structures of the closely related silanols $(PhMe_2Si)_3CSiMeR(OH)$ [where R = H (*211*) or Me (*212*)] and of $(PhMe_2Si)_3CSiH_2(OH)$ (*79*) show that the molecules have no intermolecular hydrogen bonds, but instead have intramolecular hydrogen bonds involving the π-electron cloud of a phenyl ring. Such OH$\cdots\pi$-electron interaction has also been seen in $HO(SiPh_2)_7OH$ (see Section IV,D,3) and it can also be inferred from IR spectra. For example, $(PhMe_2Si)_3CSiH_2(OH)$ has a band at 3623 cm^{-1} in dilute CCl_4 solution (*210*). The structure of $(PhMe_2Si)_3CSiMeH(OH)$ shown in Fig. 2 shows that one of the rings is twisted towards the OH group such that the hydroxyl proton lies

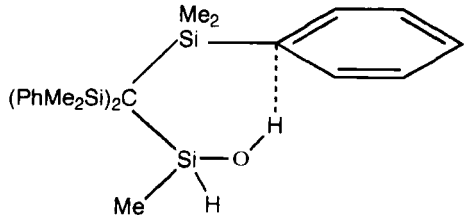

FIG. 2. A schematic representation of the OH$\cdots\pi$ interaction in $(PhMe_2Si)_3CSiMeHOH$.

almost directly above the *ipso* carbon of the ring and about 2.37(6) Å from the carbon. The hydroxyl proton lies about 2.33 Å above the plane of the ring. A similar arrangement is found in $(PhMe_2Si)_3CSiMe_2OH$ (*212*). In $(PhMe_2Si)_3CSiH_2OH$, there are $O\cdots C_{aromatic}$ distances of 2.881 and 3.016 Å (*210*).

The sterically hindered arylsilane $(Me_3Si)_3CSiPhOMeOH$ (*84*) forms a hydrogen-bonded dimer **34.** It was originally thought that the intermolecular OH···OH interaction (O···O distance 2.86 Å, O-H···O angle 158.5°) was the only hydrogen bond present, but more recent work has shown that this compound also possesses an intermolecular OH···π interaction (*206*). The related diphenyl compound $(Me_3Si)_3CSiPh_2OH$ has a structure comprising two types of simple dimer, the molecules within each dimer being linked by a single SiOH···OHSi hydrogen bond with no OH···π interactions present (*213*). The iodohydroxysilane TsiSiPhIOH has also been found not to have a structure involving OH···OH hydrogen bonds (or OH···I bonding). Again, it comprises dimers formed via an intermolecular OH···π interaction (*206*). This interaction can also be inferred from the IR spectra: In the solid state, there is a band at 3585 cm^{-1} which may be attributed to the OH···π·interaction, but in dilute CCl_4 solution a band attributable to free SiO-H at 3656 cm^{-1} is observed (*206*). Infrared spectroscopy can therefore be a useful tool in determining whether OH···π interactions are present in silanols. A band at about 3600–3610 cm^{-1} in dilute solution may indicate an intramolecular interaction, and a band at ca. 3585 cm^{-1} in the solid state that disappears in solution spectra to be replaced by a free SiO–H stretch in the 3650–3680 cm^{-1} range may indicate an intermolecular OH···π· interaction. A change of stretching frequency of this magnitude on going from a situation of OH···π· to free OH might be expected in the light of studies of the spectra of silanols in the presence of aromatic solvents. In one example, a change of 59 cm^{-1} is observed in the stretching frequency for Me_3SiOH between the free compound in CCl_4 solution and in the presence of toluene. (See Table I for this and similar data.)

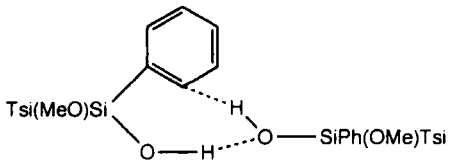

34

2. *Sila Drugs*

A series of silicon analogues of drugs, many of them containing the SiOH group, has been studied by x-ray crystallography. Sila-difenidol, (3-piperidinopropyl)diphenylsilanol, has been prepared both by hydrolysis of the corresponding methoxysilane and by base hydrolysis of the corresponding Si–H species, the methoxysilane route giving a better yield. It shows no intermolecular hydrogen bonds, but has a strong intramolecular OH···N bond with an O···N distance of 2.685 Å and an O–H···N angle of 173.2° (*214*). Sila-pridinol, (2-piperidinoethyl)diphenylsilanol, has been prepared by hydrolysis of the corresponding methoxy- or piperidinosilanes. It forms centrosymmetric dimers, whereas the carbon analogue, pridinol, forms only intramolecular hydrogen bonds. The O···N distance in sila-pridinol is 2.758 Å, and the intermolecular O–H···N angle is 172.5° (*215*). A similar arrangement to that found in sila-pridinol is found in [2-(dimethylamino)ethylthiomethyl]diphenylsilanol, which exhibits anticholinergic activity. Its structure comprises centrosymmetric dimers with an O···N distance of 2.744(6) Å and an O–H···N angle of 161(2)° (*216*).

The hydrogen bonding in (2-morpholinoethyl)diphenylsilanol connects the molecules via intermolecular O–H···N interactions to give an infinite chain structure, Fig. 3, with an O···N distance of 2.776(8) Å and an O–H···N angle of 168(3)° (*217*). A similar chain structure is found in (3-morpholinopropyl)diphenylsilanol, which has an extra CH_2 unit in the alkyl chain, an O···N distance of 2.840(3) Å, and an O–H···N angle of 174(3)° (*218*).

In contrast to its carbon analogue, which forms intramolecular hydrogen bonds, (2-piperidino-ethoxymethyl)diphenylsilanol (prepared by hydrolysis of the corresponding SiH species) forms intermolecular O–H···N hydrogen bonds to give a chain structure similar to that found for (2-morpholinoethyl)diphenylsilanol shown in Fig. 3 (*219*).

Sila-procyclidine, (cyclohexyl)phenyl[2-pyrrolidin-1-yl]silanol, may be prepared by hydrolysis of the corresponding methoxysilane (*220*) and is interesting in that it can form two types of hydrogen-bonded structure depending on whether it is enantiomerically pure or a racemate. In the racemate, the compound forms centrosymmetric dimers of (R)- and (S)-configuration molecules with an O···N distance of 1.791 Å. In the pure (R)-compound, however, the molecules are linked into infinite chains via intermolecular O–H···N hydrogen bonds (O···N distance 2.792 Å) (*221*), again similar to those in (2-morpholinoethyl)diphenylsilanol shown in Fig. 3.

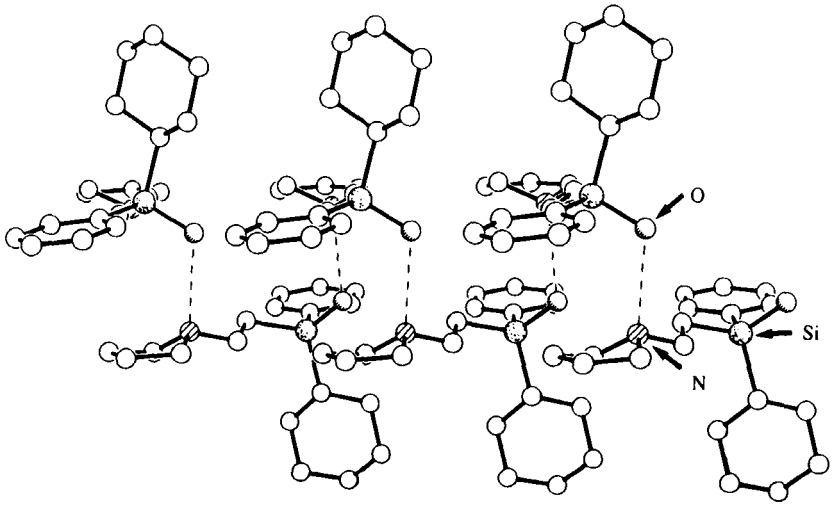

FIG. 3. The hydrogen-bonded chain structure of (2-morpholinoethyl)diphenylsilanol with the hydrogen atoms omitted for clarity. Drawn using coordinates taken from the Cambridge Crystallographic Database.

Sila-biperidin *rac*-(SiRS, C2 SR), **35**, can be prepared by hydrolysis of the corresponding methoxysilane and behaves in a similar way to sila-procyclidine: The *exo* form has centrosymmetric dimers formed via a pair of intermolecular OH···N hydrogen bonds (O···N distance 2.810 Å), while the *endo* form has intermolecular OH···N hydrogen bonds linking the molecules into infinite chains (*222*).

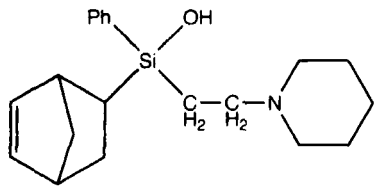

35

3. *Other Aryl Silanols and Their Adducts*

Triphenylsilanol has 16 molecules in the unit cell, arranged as two sets of two independent tetrameric hydrogen-bonded units. These units each have a flattened tetrahedral arrangement of silicon atoms, Fig. 4, and O···O distances varying from 2.637(5) to 2.684(6) Å (*223*). Tri-

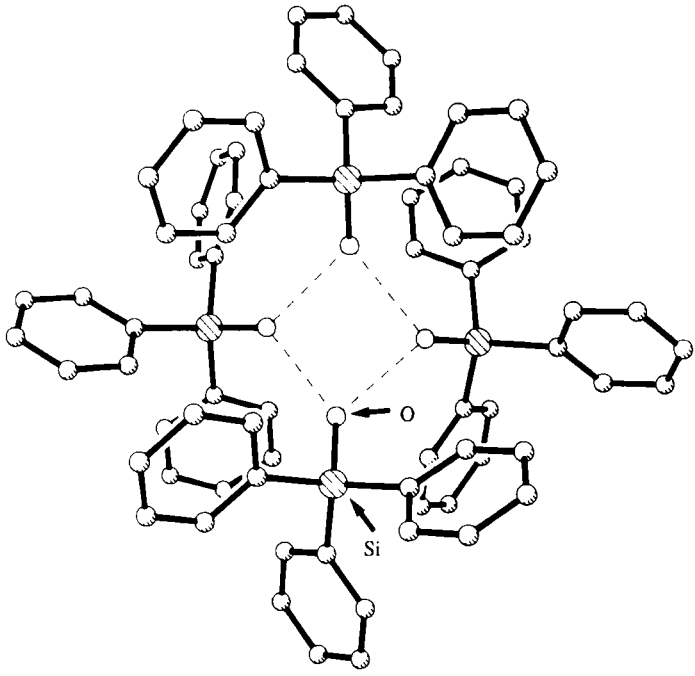

FIG. 4. The flattened tetrahedral structure of Ph_3SiOH with hydrogen atoms omitted for clarity (*304*).

phenylsilanol is unusual as it may be compared with all of the Ph_3MOH analogues in group 14 (M = C, Ge, Sn and Pb). The structure of triphenylmethanol comprises pyramidal hydrogen-bonded tetramers similar to Ph_3SiOH (but not flattened) (*224*). The germanium analogue is isomorphous with Ph_3SiOH and has O···O distances ranging from 2.609(11) to 2.657(11) Å (*225*). The tin and lead analogues are isostructural with each other. They comprise zigzag chains with the OH groups linking planar Ph_3M units to give a trigonal bipyramidal arrangement at each M (*226*). The tetrameric structure is retained in the adduct with ethanol, $[Ph_3SiOH]_4 \cdot EtOH$, which has a cyclic network of hydrogen bonds with O···O distances between 2.60 and 2.79 Å. The silanol is very selective in its adduct formation and forms the clathrate with ethanol in the presence of water, methanol, or propanol (*227*). Triphenylmethanol also forms adducts with MeOH and DMSO selectively in the presence of a variety of other small organic molecules such as EtOH, acetone, or THF (*228*).

Triphenylsilanol also forms simple hydrogen-bonded adducts with ethers. For example, the crown ether 12-crown-4 forms a 2:1 adduct

in which the O···O distance is 2.76 Å (*229*). A host–guest complex between Ph_3SiOH and dioxane can be obtained by slow evaporation of the solvent from a diethylether solution of the two compounds. The structure has a 4 : 1 stoichiometry, $(Ph_3SiOH)_4$·dioxane, in which two pairs of hydrogen-bonded Ph_3SiOH molecules are joined via further hydrogen bonds to the oxygen atoms in the dioxane molecule (*230*).

Tri(1-naphthyl)silanol forms 1 : 1 adducts with toluene, *o*-xylene, and *m*-xylene, and a 1 : 2 adduct with *p*-xylene. The toluene and *o*-xylene adducts have similar structures in which the arene molecules lie in channels (having regular constrictions) in the lattice of the silanol molecules. The *m*-xylene structure is closely related with narrow channels connecting cavities in which the arene guest molecules are found. The 1 : 2 adduct with *p*-xylene is different and contains three crystallographically distinct guest molecules lying in intersecting channels in the lattice (Fig. 5). These adducts seem not to show any OH···O hydro-

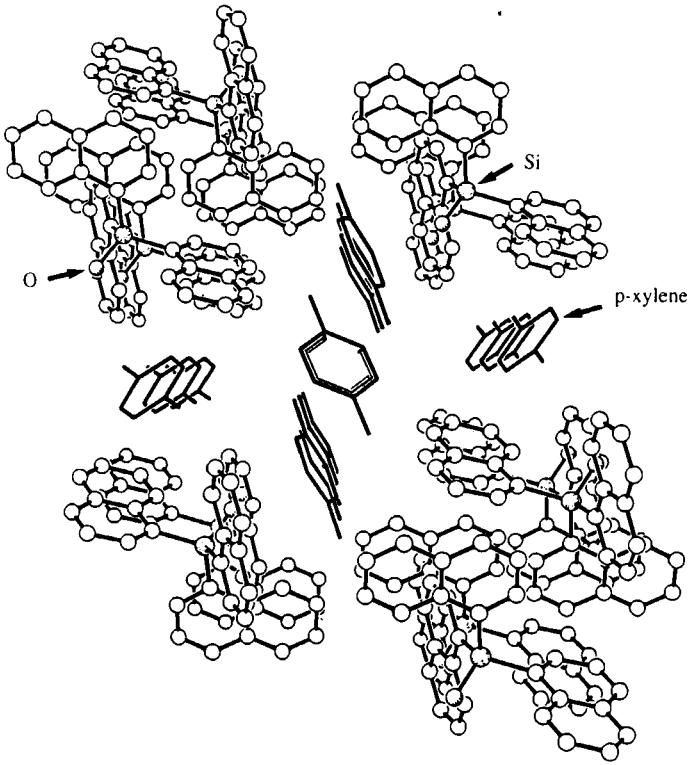

FIG. 5. The 1 : 2 host–guest complex (1-naphthyl)$_3$SiOH·2*p*-xylene with hydrogen atoms omitted. The *p*-xylene molecules are shown drawn with solid lines. Drawn using coordinates taken from the Cambridge Crystallographic Database.

gen bonds, but there do seem to be OH···π interactions indicated by both x-ray crystallography and by IR spectroscopy. The O···ring centroid distances for the adducts range from 3.66 to 3.28 Å for the *m*- and *p*-xylene cases, respectively. The O–H stretching frequency also decreases on adduct formation from 3670 cm^{-1} in the free silanol to between 3590 and 3620 cm^{-1} in the adducts. This again is indicative of an interaction between the OH group and an arene ring (the interaction between Ph_3SiOH and mesitylene causes a similar change from 3677 to 3598 cm^{-1}; see Table I). On heating the toluene adduct, loss of toluene leaves the host framework of molecules intact (*186*). Tris(1-naphthyl)silanol forms a 1:1 host–guest complex with dioxane comprising a single OH···O hydrogen bond (2.736 Å), the second dioxane oxygen being free from hydrogen bonds (*230*).

Each of the rings in Ph_3SiOH may be coordinated by a $Cr(CO)_3$ fragment to give complexes $(Ph_3SiOH)[Cr(CO)_3]_n$ (n = 1–3) on boiling with $Cr(CO)_6$ in $Bu^n{}_2O$. In all three cases, the $Cr(CO)_3$ fragments point towards the SiOH group. Interactions between the SiOH group and the $Cr(CO)_3$ groups are, however, weak. There are no Si(O)···Cr distances less than 4 Å, and the shortest Si(O)···O=C distance is 3.2 Å, which may indicate a weak hydrogen-bonding interaction (*231*).

The arylsilane Ph_2(fluorenyl)SiOH has been prepared in almost quantitative yield by hydrolysis of the corresponding chloride in a boiling aqueous suspension. The lack of HCl-catalyzed condensation or Si–Ar bond cleavage is presumably minimized by the steric hindrance and by HCl being lost rapidly from the boiling solution (*232*). It forms a simple hydrogen-bonded dimer with a pair of hydrogen bonds [O···O distance 2.912(9) Å] linking up the two independent molecules.

The hydrolysis of $[C_6H_4CH_2NMe_2]_2SiCl_2$ in the presence of lithium naphthalenalide gives a complicated lithium siloxide which, after crystallization from *n*-pentane/$CHCl_3$ has been shown to be $\{[C_6H_4CH_2NMe_2]_2Si(OLi)(OH)\}_4 \cdot 2LiCl \cdot 2CHCl_3$ (*233*). The basic unit of the tetramer comprises the structure shown in Fig. 6, in which one NMe_2 group in each molecule is involved in an intramolecular OH···N hydrogen bond and the second is coordinated to the OLi lithium atom. Further intermolecular coordination between the OLi groups and the LiCl present build up the overall structure to form the complicated aggregate.

The salt $[mes_2Si(F)O]_2[H][Et_4N]$ can be isolated in low yield as a hydrolysis product from the reaction between $mesityl_2SiF_2$ and $Et_4NF \cdot 2H_2O$. {This reaction may also yield $mes_2SiF(OH)$, $(mes_2SiF)_2O$, or $[mes_2SiF_3][Et_4N]$, depending on the conditions used (*202*).} The salt has a structure in which the two $[mes_2Si(F)O]^-$ anions appear

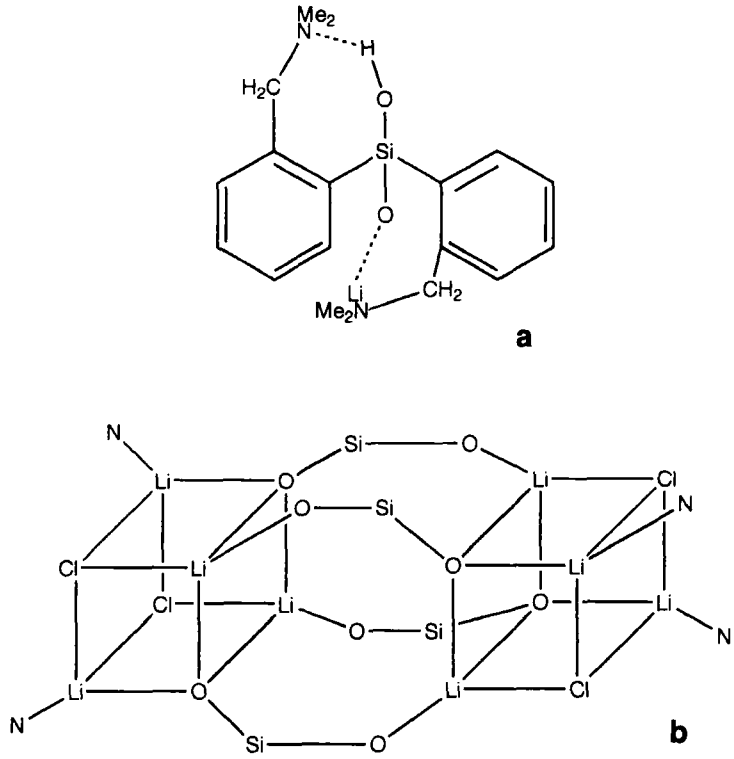

FIG. 6. Two partial views of the structure $\{[C_6H_4CH_2NMe_2]_2Si(OLi)(OH)\}_4 \cdot 2LiCl \cdot 2CHCl_3$. (a) The immediate environment around each Si. (b) A representation of the tetrameric core of the cluster (aromatic substituents omitted for clarity).

to be held together by a single proton in a symmetrical hydrogen bond with a very short O···O distance of 2.434(7) Å.

4. Tert-Butyl Substituted Silanols

The steric hindrance provided by Bu^t groups has been used to good effect in silanol synthesis, and a range of compounds containing unusual functional groupings have been isolated and structurally characterized. Two related silanols form tetrameric structures. One, $Bu^t_2Si(OH)F$ (*234*), has a cyclic arrangement of molecules [O···O distance 2.756(9)Å, O···O···O angles 89.7°] **36** in which, surprisingly, the fluorine plays no part in the hydrogen bonding. [The fluorohydroxysilane $Bu^t_2SiF(OH)$ forms a 1:1 adduct with pyridine-*N*-oxide when the two compounds are heated together in petroleum ether (*235*).] The

O···O distance is 2.630(6) Å, and the fluoro substituent again [as in the case of the free $Bu^t_2SiF(OH)$] does not seem to participate in hydrogen bonding. The second tetramer $Bu^t_2Si(OH)OLi$ [derived from $Bu^t_2Si(OH)_2$, see section IV,G] is held together by Si–O–Li interactions **37,** with the Si–OH groups hydrogen-bonding to the solvent THF molecules, OH···O(THF) distances 2.64–2.78 Å (*236*). The structures of the related tin compounds Bu^t_2SnXOH (X = F, Cl, or Br) are also known. In these compounds, the structure comprises dimeric units formed via bridging OH groups to give Sn_2O_2 rings which are further linked by pairs of OH···X hydrogen bonds to give infinite chains (*237*).

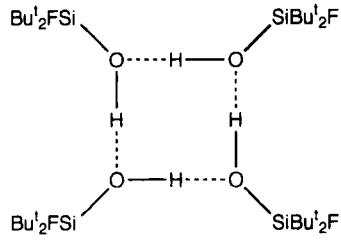

36

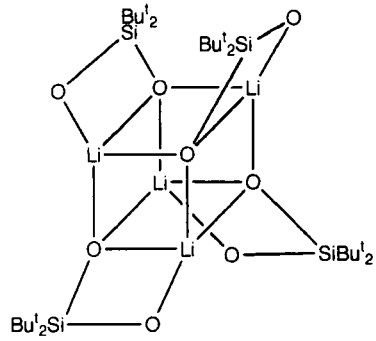

37

The sodium analogue, $Bu^t_2Si(OH)(ONa)$ of the lithium siloxide can be prepared by treatment of $Bu^t_2Si(OH)_2$ with sodium metal in hexane/THF. The compound crystallizes as a hexameric THF solvate, $[Bu^t_2Si(OH)(ONa)\cdot THF]_6$, rather than the tetrameric structure of the lithium compound. The structure is based on a hexagonal prism **38** built up of alternating Na and O atoms, the SiOH groups being hydrogen-bonded to the THF molecules (*238*).

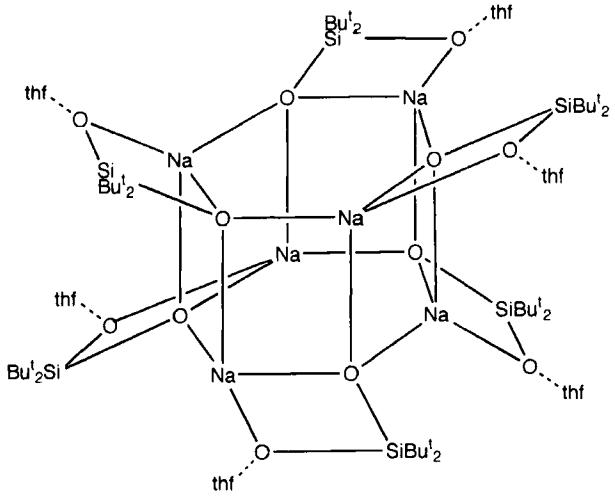

38

If the lithium siloxide $Bu^t_2SiF(OLi)$ is stirred in hexane/THF in the presence of atmospheric moisture, partial hydrolysis occurs to give an aquo complex, $\{[Bu^t_2SiF(OLi)]_3.[Bu^t_2Si(OH)(OLi)].THF.H_2O\}$, in which one Si–F group in the original, tetrameric $Bu^t_2SiF(OLi)$ has been replaced by an Si–OH group. The structure **39** comprises cubic tetramers which are held together in pairs by intercube $F\cdots H_2O$ hydrogen bonds, the SiOH groups being hydrogen-bonded to the THF molecules (*239*).

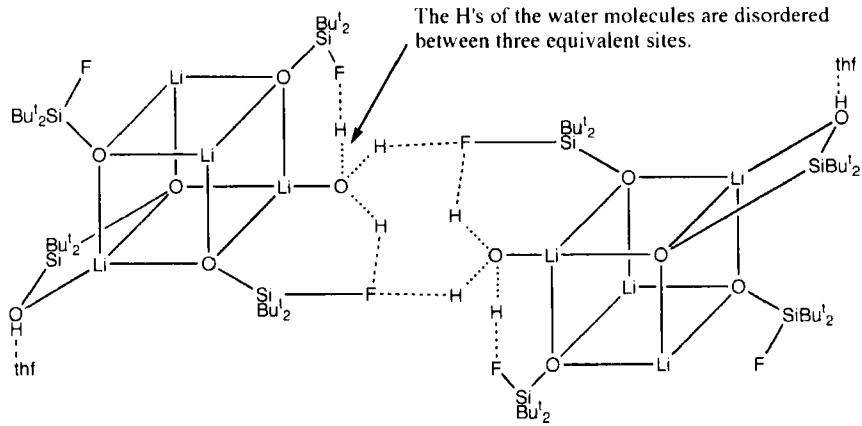

39

An intramolecular O–H···N hydrogen bond similar to those found in the sila drugs (see Section IV,C,2) is also found in the trisiloxane $HOBu^t_2SiOSiMe_2OSiBu^t_2NH_2$ in which the O···N distance is 2.859(4) Å and the O–H···N angle is 151.5(27)°. The bulky Bu^t groups seem to prevent intermolecular hydrogen bonding, the closest intermolecular O···N distance being 3.284 Å (*67*).

The di-*t*-butyl-substituted silanols **40** and **41** result from hydrolysis during column chromatography of the corresponding triflates and have also been structurally characterized (*240*). The adamantyl compound **40** forms centrosymmetric dimers via OH···N(1) hydrogen bonds (*240*) in a manner similar to some of the sila drugs. The pyrazole derivative **41** also comprises such dimers, but in this case the dimers are linked to form chains via NH···O=C hydrogen bonds (*210*).

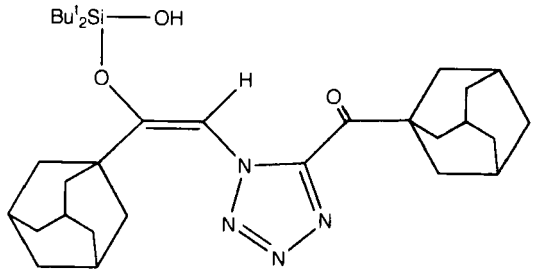

40

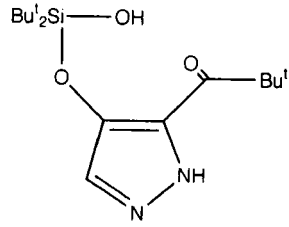

41

The anhydrous silanol Bu^tMe_2SiOH is a liquid, but on exposure to moisture it forms a solid hemihydrate $[Bu^tMe_2SiOH]_2.H_2O$ (*52, 241*) in which hydrogen-bonded chains are formed with the water molecules acting as linkages down the chain (Fig. 7). The carbon analogue

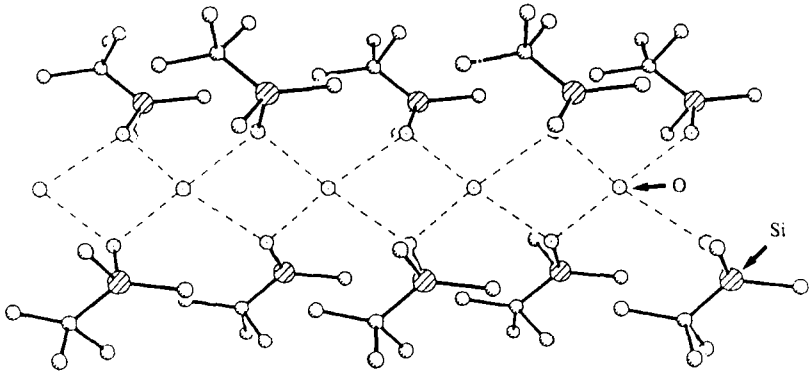

FIG. 7. A view along the *c*-axis showing the hydrogen bonding in $[Bu^tMe_2SiOH]_2.H_2O$. All hydrogen atoms have been omitted (*304*).

Bu^tMe_2COH forms a similar chain structure (*242, 243*), but the related silanols Pr^iMe_2SiOH, *t*-hexylMe_2SiOH, and Ph_2Bu^tSiOH do not appear to form simple hydrates (*241*). A gas-phase electron diffraction study of both the free silanol and its hemihydrate has shown that there is no interaction between water and silanol molecules in the gas phase, and that the material in the gas phase derived from either compound is essentially the same (*244*). The yttrium complex $[\{Y(OSiMe_2Bu^t)_2(HOMe_2SiBu^t)\}\{Y(OSiMe_2Bu^t)_2\}(\mu\text{-}OSiMe_2Bu^t)_2]$ is formed in the reaction between $[Y\{N(SiMe_3)_2\}_3]$ and 3.5 equivalents of Bu^tMe_2SiOH. It contains a single terminal Bu^tMe_2SiOH molecule. There is no intramolecular hydrogen bonding in the complex, but it is unclear whether there is intermolecular hydrogen bonding (*245*).

5. *Transition Metal Silyl and Related Complexes*

The ruthenium phosphine complex **42,** which can be prepared by hydrolysis of the corresponding Si–H compound, has been reported (*246*) to exhibit no intra- or intermolecular interactions with the SiOH group. Again, however, recent work (*206*) has suggested that there may in fact be an intramolecular interaction with one of the phenyl rings. The oxygen lies 2.85 Å from the plane of one of the Ph rings and 3.28 and 3.35 Å from two of the aromatic carbons. This is consistent with the O–H hydrogen being close to and above a C–C bond in the aromatic ring (*206*). A related ruthenium complex **43** can be obtained by treatment of the bridged diruthenium complex $[Ru_2(\mu\text{-}PPh_2CH_2SiMe_2)_2(CO)_6]$ with CF_3CO_2H in CH_2Cl_2 and subsequent crystallization from Et_2O/heptane. In this case, an ether molecule hydrogen bonds to the Si–OH group (*247*).

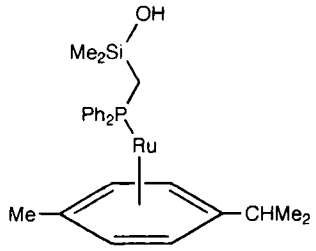

42

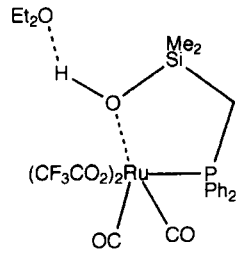

43

The tungsten complex $Cp^*(CO)_2(PMe_3)WSiPh_2OH$ has no HO···HO hydrogen bonds, but it is not clear whether there are OH···CO or OH···aryl interactions (*29*). The iron complex $Cp(CO)_2FeSi(p\text{-tolyl})_2OH$ (*248*) has also been reported to have no intra- or intermolecular hydrogen bonds.

Hydrogen bonding between an SiOH group and fluorine occurs in the platinum complex **44** [prepared by hydrolysis of a bis(alkylidene)-silacyclopropane] in which the SbF_6^- anion hydrogen bonds to the platinum-containing cation (O···F distance 2.77(2) Å) (*249*). The platinum complex **45** is not reported (*250*) to form hydrogen bonds, and a more recent study (*210*) has confirmed that there do not appear to be any OH···OH or OH···π interactions.

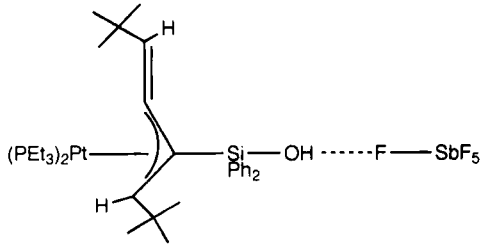

44

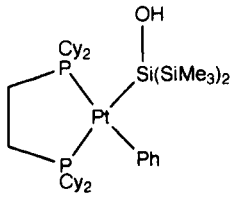

Cy = *cyclo*-C_6H_{11}

45

6. *Other Miscellaneous Silanols*

The structure of $(PhCH_2)_3SiOH$ [prepared by hydrolysis of $(PhCH_2)_3SiCl$ (*251*)], determined by Rietveld refinement of powder x-ray diffraction data, has a shortest O···O distance of 6.07 Å, clearly indicating that there are no intermolecular hydrogen bonds present (*252*). There also appear, perhaps surprisingly in view of other examples discussed earlier, to be no close OH···π interactions. There do seem, however, to be interactions of the edge-to-face type for the aryl rings, each of which interacts with a ring from two neighboring molecules (ring-centroid to ring-centroid distances 5.00–5.20 Å) so as to build up a three-dimensional framework (*210*).

The bicyclic silanol *endo*-3-methyl-*exo*-3-hydroxy-3-silabicyclo-[3.2.1]octane may be prepared by treating the corresponding methoxysilane with silica gel. Although the position of the OH hydrogen atom was found to be disordered (*253*), the intermolecular O···O distances of 2.69 and 2.71 Å suggest that the molecules are joined into zigzag chains as shown in Fig. 8 (*210*).

The related cyclic silanols **46** (*254*) and **47** (*255*) both have single intermolecular hydrogen bonds between the silanol group and a ring oxygen to build up chains. The carbon-centered molecule is formed via a complicated thermal or a base-catalyzed rearrangement of $(HOMe_2Si)_4C$ (for its structure, see Section IV,F), and the nitrogen-centered compound by hydrolysis ($H_2O/Et_2O/Et_3N$) of 1,2-bis(chlorodimethylsilyl)-2,2,4,4-tetramethylcyclodisilazane (*256*).

The racemic acetylsilanol $Bu^t(Me_3SiCH_2)Si(OH)C(O)CH_3$ is formed on hydrolysis of $Bu^t(Me_3SiCH_2)Si(OMe)C(OMe)=CH_2$ and crystallizes to form simple chains linked by hydrogen bonds between the OH and C=O groups of molecules of the same absolute configuration, the O···O distance being 2.757(4) Å. This seems to be another case in which there

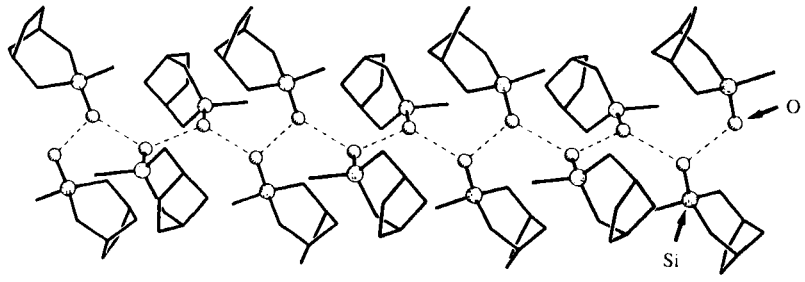

FIG. 8. The hydrogen-bonded chain structure of *endo*-3-methyl-*exo*-3-hydroxy-3-silabicyclo[3.2.1]octane, with hydrogen atoms omitted for clarity. Drawn using coordinates taken from the Cambridge Crystallographic Database.

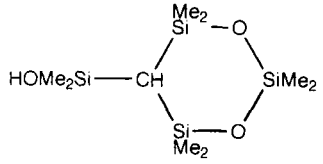

46

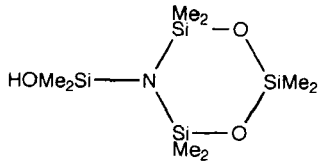

47

is less than maximal hydrogen bonding, as each OH group is involved in only a single interaction with the carbonyl groups (*257*).

The unusual 1-sila-1,2-diol $(CH_2{=}CH)CH(OH)SiPh_2OH$, prepared by hydrolysis of the acylsilane $(CH_2{=}CH)C(O)SiHPh_2$, has a structure comprising hydrogen-bonded double chains as shown in Fig. 9. Only COH···HOSi hydrogen bonds are present, with the bonds between the chains being shorter than those that build up the chain, 2.666 and 2.739 Å, respectively (*131, 210*).

D. Compounds Containing Two Si–OH Groups

1. Disiloxanes

A variety of simple disiloxanes of general formula $(HOR_2Si)_2O$ (where R = Me, Et, Pr^n, Pr^i, c-C_5H_9, or Ph) **48**, a thienyl compound **49**, and the cyclic species **50** have all been structurally investigated. The simplest

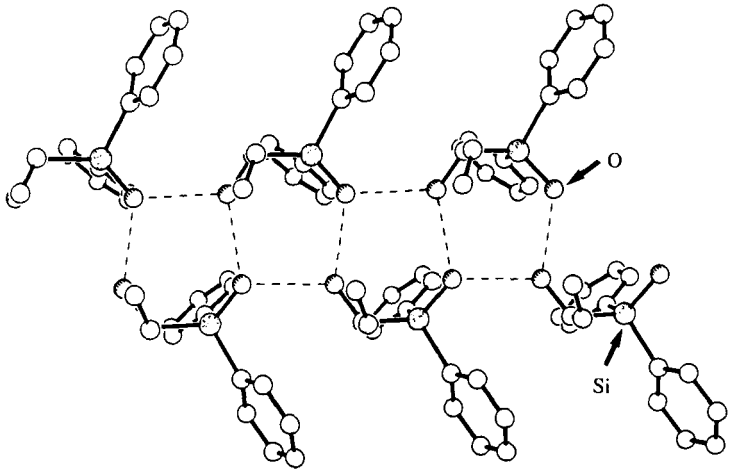

FIG. 9. The hydrogen-bonded double chain structure of $(CH_2{=}CH)CH(OH)SiPh_2OH$ with hydrogen atoms omitted for clarity. Drawn using coordinates taken from the Cambridge Crystallographic Database.

TABLE IV

STRUCTURAL DATA FOR COMPOUNDS CONTAINING ONE Si–OH GROUP

Compound	Si–OH (Å)	OH···X(Å)	O···X (Å)[a]	O-H···X (°)[a]	Structural summary	Refs.
$(PhCH_2)_3SiOH$	1.70(1)		6.07		No hydrogen bonding, edge-to-face aryl ring interactions	*210, 252*
31					No hydrogen bonding	*205, 206*
32					Monomeric, possible OH···π interaction	*207* *206*
33					No hydrogen bonding	*209, 210*
Ph_3SiOH	1.633(5)–1.652(5)		2.637(5)–2.684(6)		Tetrameric, flattened tetrahedra	*223*
$(Ph_3SiOH)_4 \cdot$ dioxane			2.789(2) 2.703(2)	164.7(42) 165.6(26)	4:1 host–guest complex, both OH···OH and OH···dioxane bonds	*230*
$(Ph_3SiOH)_2 \cdot$ 12-crown-4	1.632(2)	1.91(2)	2.76		Simple adduct	*229*
$(Ph_3SiOH)_4 \cdot$ EtOH			2.60–2.79		4:1 clathrate	*227*
$(Ph_3SiOH)[Cr(CO)_3]$					Monomeric, possible OH···OC interaction	*231*

$(Ph_3SiOH)[Cr(CO)_3]_2$					Monomeric, possible OH···OC interaction	*231*
$(Ph_3SiOH)[Cr(CO)_3]_3$					Monomeric, possible OH···OC interaction	*231*
[(1-naphthyl)$_3$SiOH] · dioxane			2.736(3)	169.7(23)	Simple adduct, OH···dioxane bond only	*230*
[(1-naphthyl)$_3$SiOH] · toluene					Host–guest complex with O···π interaction only	*186*
[(1-naphthyl)$_3$SiOH] · *o*-xylene					Host–guest complex with O···π interaction only	*186*
[(1-naphthyl)$_3$SiOH] · *m*-xylene					Host–guest complex with O···π interaction only	*186*
[(1-naphthyl)$_3$SiOH] · (*p*-xylene)$_2$					Host–guest complex with O···π interaction only	*186*
$(Me_3Si)_3CSiPh_2OH$	1.653(14) 1.702(13)		2.85(2) 2.90(1)		Dimeric	*213*
$(Me_3Si)_3CSiPh(OMe)OH$	1.634(2) 1.645(2)	2.17	2.86	158.5	Dimeric, OH···OH and OH···π interactions	*84* *206*

(*continues*)

TABLE IV (*Continued*)

Compound	Si–OH (Å)	OH···X(Å)	O···X (Å)[a]	O-H···X (°)[a]	Structural summary	Refs.
$(Me_3Si)_3CSiPh(I)OH$					Dimeric via OH···π interactions	*206*
$(PhMe_2Si)_3CSiH_2OH$	1.369–1.638				Monomeric, intramolecular OH···π interaction	*310*
$(PhMe_2Si)_3CSiMe_2OH$	1.655(4)				Monomeric, intramolecular OH···π interaction	*208*
$(PhMe_2Si)_3CSiMe(H)OH$					Monomeric, intramolecular OH···π interaction	*211*
Sila-difenidol	1.631(3)	1.665[b]	2.685[b]	173.2[b]	Intramolecular OH···N only	*214*
Sila-pridinol	1.625(2)		2.758[b]	172.5[b]	Dimers, intermolecular OH···N only	*215*
$Me_2NCH_2CH_2SCH_2SiPh_2OH$	1.609(3)		2.744(6)[b]	161(2)[b]	Dimers, intermolecular OH···N only	*216*
(2-morpholino)$SiPh_2OH$	1.625(4)		2.776(8)[b]	168(3)[b]	Chains, intermolecular OH···N only	*217*

(3-morpholino)$SiPh_2OH$	1.635(2)		2.840(3)[b]	174(3)[b]	Chains, intermolecular OH···N only	*218*
$(C_5H_{10}N)(CH_2)_2OCH_2SiPh_2OH$	1.610(1)		2.77		Chains, intermolecular OH···N only	*219*
Sila-procyclidine (racemate)	1.632(2)		2.791		Dimers, intermolecular OH···N only	*221*
(R)-sila-procyclidine	1.635(3)		2.792[b]		Chains, intermolecular OH···N only	*221*
exo-sila-biperidin	1.626(1)	2.03[b]	2.810[b]	176.6[b]	Dimers, intermolecular OH···N only	*222*
endo-sila-biperidin	1.621(3)	1.82	2.745[b]	162.0[b]	Chains, intermolecular OH···N only	*222*
$Bu^t(Me_3SiCH_2)Si(OH)C(O)Me$	1.638(1)		2.757(4)		Chains via OH···O=C interactions	*257*
(fluorenyl)$SiPh_2OH$	1.629(6) 1.648(7)		2.912(9)		Dimeric	*232*
$(CH_2{=}CH)(OH)ChSiPh_2OH$			2.666 2.739		Ladder chains	*131*
$Ar_2Si(OH)(OLi)$[c]	1.65(2)		2.655[b]	160[b]	Complicated tetrameric	*233*
	1.565(5)		2.434		Salt, anions bridged by proton	*202*

(*continues*)

TABLE IV (*Continued*)

Compound	Si–OH (Å)	OH···X(Å)	O···X (Å)[a]	O-H···X (°)[a]	Structural summary	Refs.
Bu^tMe_2SiOH	1.662(3)				Monomeric in gas phase (electron diffraction study)	*244*
$[Bu^tMe_2SiOH]_2 \cdot H_2O$	1.760		2.499, 2.790		Disordered chains, silanol–water bonds only	*210*
Bu^tMe_2SiOH yttrium complex[d]					Coordinated silanol molecule, no apparent H-bonding	*245*
39	1.676(7)	1.702(26) 2.208(39)–2.868(41)[e]			Cubic tetramers linked by OH···F bonds	*239*
$Bu^t_2SiF(OH)$	1.613(7)	2.08	2.756(9)	160	Cyclic tetramers	*234*
$Bu^t_2SiF(OH) \cdot C_5H_5NO$	1.609(2)		2.630		Simple adduct, OH···O=N bond	*235*
$Bu^t_2(H_2N)SiOSiMe_2OSi(Bu^t)_2OH$	1.630(3)	2.036(35)[b]	2.859(4)[b]	151.5(27)[b]	Monomeric, intramolecular OH···N bond	*67*
$[Bu^t_2Si(OLi)(OH)]_4$	1.664(7)–1.683(7)		2.64–2.78		Cubic tetramers	*236*
$[Bu^tSi(OH)(ONa) \cdot THF]_6$	1.672(3) 1.668(3)				Hexameric, OH···THF only	*238*
40	1.664(5)	2.0(1)[b]		162(8)[b]	Dimeric via OH···N interaction	*240*

41	1.617(3)		2.934[b,f]	Chains of dimers, SiOH···N and NH···O=C interactions	*210, 240*
42	1.591(8)			Monomeric, possible intramolecular OH···π interaction	*246* *206*
43	1.692(21)		2.64	Monomeric, OH···O link to Et_2O	*247*
44	1.63(1)		2.77(2)[e]	OH···F bond in SbF_6- anion	*249*
45	1.726(4)			No hydrogen bonding	*250*
$Cp^*(PMe_3)(CO)_2WSiPh_2OH$				Monomeric	*29*
46	1.645(3)	1.80		Chains, $OH\cdots O_{ring}$ interactions	*254*
47	1.59		2.898	Chains, $OH\cdots O_{ring}$ interactions	*210, 255*
Me(OH)Si-bicyclo[3.2.1]octane[g]	1.657(2)		2.69, 2.71	Chains	*210, 253*

[a] X = oxygen unless otherwise stated.
[b] X = N.
[c] $(o\text{-}Me_2NC_6H_4)_2Si(OH)(OLi)_4 \cdot 2LiCl.2CHCl_3$.
[d] $[\{Y(OSiMe_2Bu^t)_2(HOSiMe_2Bu^t)\}\{Y(OSiMe_2Bu^t)_2\}(\mu\text{-}OSiMe_2Bu^t)_2]$.
[e] X = F.
[f] The dimeric units are linked by further NH···O=C hydrogen bonds of length 2.983 Å.
[g] *endo*-3-methyl-*exo*-3-hydroxy-3-silabicyclo[3.2.1]octane.

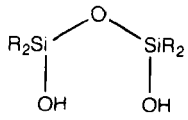

48 R = Me, Et, Pr^n, Pr^i, *cyclo*-C_5H_9 or Ph

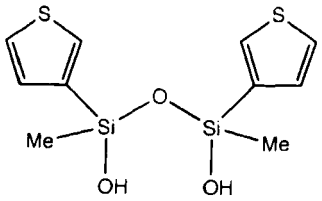

49

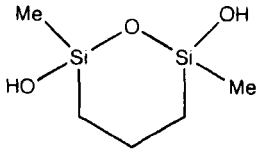

50

example (**48**, R = Me) is one of the basic units from which the polydimethylsiloxanes or silicones are built up.

The hydrogen bonding in the acyclic disiloxanes may take one of several forms, depending on the relative positions of the molecules along the two sides of a double chain, as shown in Fig. 10a–c, while the cyclic compound adopts a more complicated structure, shown in Fig. 10d.

The hydrogen bonding arrangement, Fig. 10a, is adopted by the Me (*258, 259*), Et (*260*), Pr^n (*261*), and Ph compounds (*262, 263*); the arrangement in Fig. 10b, by the Pr^i (*264*) and the *c*-C_5H_9 (*265*) compounds; the arrangement in Fig. 10c by the thienyl compound (*266*); and the arrangement in Fig. 10d by the cyclic compound **50** (*267*). The Et, Pr^n, and Bu^n compounds all form unusual thermotropic mesophases with crystal-to-liquid-crystal phase changes of −36 and 35.0°C, and liquid-crystal-to-isotropic liquid phase changes of 37.0 and 64.0°C, respectively, for the Et and Pr^n compounds (*259, 268–270*). The Bu^n compound $(HOBu^n{}_2Si)_2O$ undergoes a transition between two solid mesophases at 17.7°C (*259*), while the Me, Pr^i, and Ph analogues show no mesogenic behavior (*259*). The mesophase adopted by the siloxanediols has been designated "columnar phases with hydrogen-bonded assemblies" (*259*). The mesophases are attributed to the columns of hydrogen-bonded molecules having aliphatic, hydrophobic exteriors

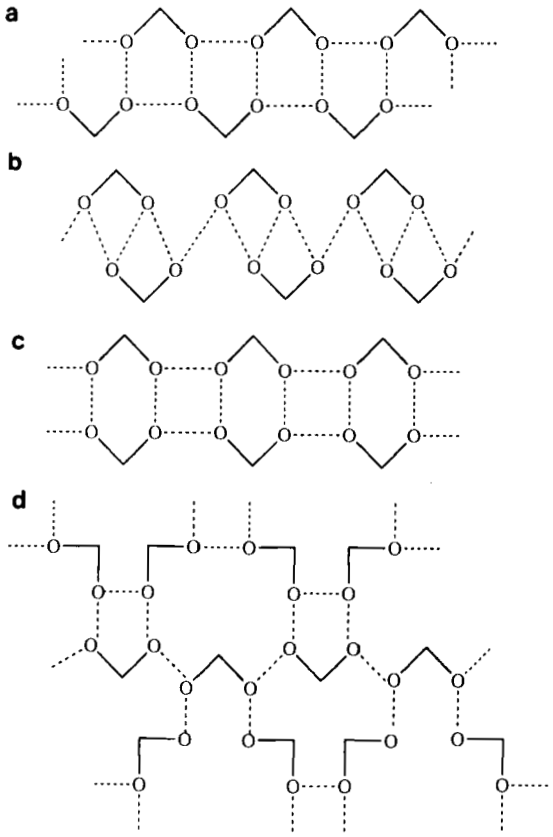

FIG. 10. Hydrogen-bonded networks in disiloxanediols.

that are relatively flexible when compared to the Me and Ph compounds (which show no mesophases), while the Pr^i analogue has a different type of hydrogen-bonded arrangement (*259*). The structure of $(HOMe_2Si)_2O$ has also been the subject of a detailed IR spectroscopic study which concluded, as was later found in the crystallographic studies mentioned earlier, that there is no intramolecular hydrogen bonding present. It gave a similar geometry for the molecule (*271*). The reaction between $Bu^t{}_2Si(OH)_2$ and Cl_4Sn affords, after workup and crystallization from CH_2Cl_2, compound **51** cocrystallized with $(HOBu^t{}_2Si)_2O$ (*272*). The $(HOBu^t{}_2Si)_2O$ molecules do not hydrogen-bond to each other, but act as links via OH···OH hydrogen bonds between columns of compound **51**, as shown in Figs. 11 and 12. The columns of the tin species **51** are built up via OH···Cl hydrogen bonds only, which join the them into pairs. These then stack and are joined by the $(HOBu^t{}_2Si)_2O$ molecules.

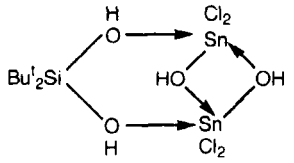

51

As was seen earlier for Ph_3SiOH, the disiloxane $(HOPh_2Si)_2O$ also forms hydrogen-bonded adducts with organic species. For example, addition of pyridazene to $(HOPh_2Si)_2O$ affords a 3:2 adduct $[(HOPh_2Si)_2O]_3.(C_4N_2H_4)_2$ **52** in which there are both OH···OH (2.71 Å) and OH···N (2.75A) hydrogen bonds (*273*). One unusual feature of the structure is that the central siloxane molecule has a linear Si–O–Si angle, while the other two siloxane molecules have a more normal value of 144.5°. A pyridinium hydrochloride adduct, $(HOPh_2Si)_2O.C_5H_5N.HCl$

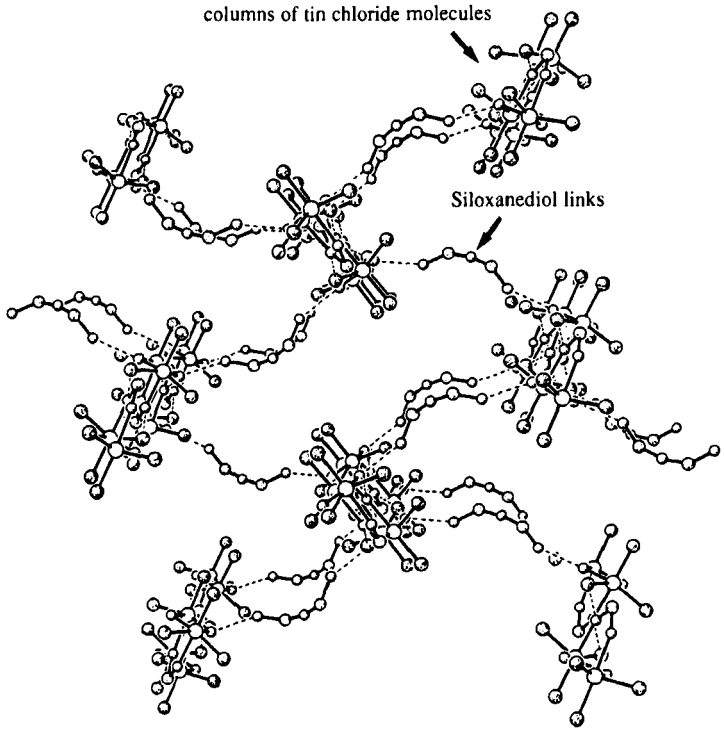

FIG. 11. A view parallel to the columns of hydrogen-bonded $Bu^t_2SiOH_2(SnCl_3OH)_2$ molecules, showing the linking of the columns by the cocrystallized $(Bu^t_2HOSi)_2O$ molecules. All hydrogen atoms and Bu^t groups have been omitted for clarity. Drawn using coordinates taken from the Cambridge Crystallographic Database.

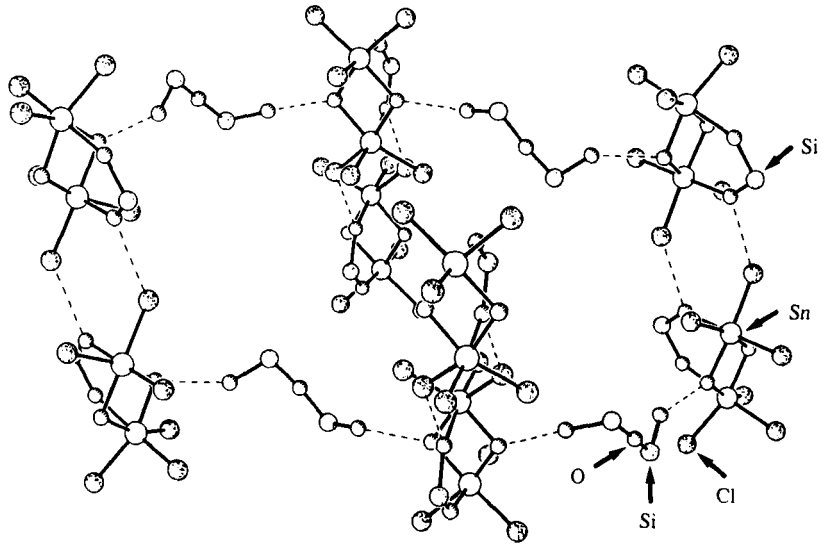

FIG. 12. A view perpendicular to the columns of hydrogen-bonded $[Bu^t_2Si(OH)_2\text{-}(Cl_3SnOH)_2]$ molecules showing the linking of the columns by the cocrystallized $(Bu^t_2\text{-}HOSi)_2O$ molecules. All hydrogen atoms and Bu^t groups have been omitted for clarity. Drawn using coordinates taken from the Cambridge Crystallographic Database.

53, crystallizes from a reaction mixture of the silanol and $TiCl_4$ in the presence of pyridine (*274*). The Cl^- ion interacts both with the pyridinium proton and the two silanol OH's, and the Si–O–Si angle of 149.6(2) is within the usual range for siloxane linkages.

The disiloxanediol **54,** like several of the sila drugs described in Section IV,C,2, contains intramolecular hydrogen bonds only (O···N distance 2.644 Å) (*233*). This disiloxanediol is thus different from the others in that it forms discrete molecules with no significant intermolecular interactions. It is also unusual in that the Si–O–Si linkage is linear, as in the case of one of the molecules of $(HOPh_2Si)_2O$ in $[(HOPh_2Si)_2O]_3$.2pyridazine **52,** and in $[(HO)_2Bu^tSi]_2O$ (see Section IV,H).

The possibility of hydrogen bonding in the highly sterically hindered siloxane $[(2,6\text{-}Et_2C_6H_3)(2,6\text{-}Et_2\text{-}4\text{-}Bu^tC_6H_2)(OH)Si]_2O$ (prepared by $LiAlH_4$ reduction of a 1,2,4,3,5-trioxadisilolane ring species) was not reported (*275*), but a more recent examination (*210*) using the coordinates deposited at the Cambridge Crystallographic Database has shown that an interesting hydrogen-bonded system is present in the structure as shown in Fig. 13. The structure comprises a pair of disilox-

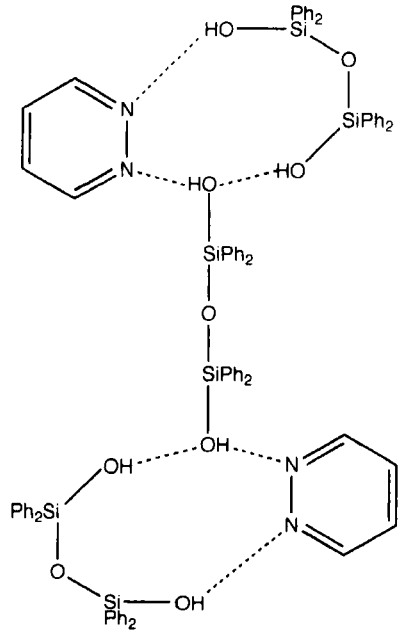
HO
Ph2
Si
O
SiPh2
N
N
HO
HO
SiPh2
O
SiPh2
OH
OH
N
Ph2Si
N
O
Si
Ph2
OH

52

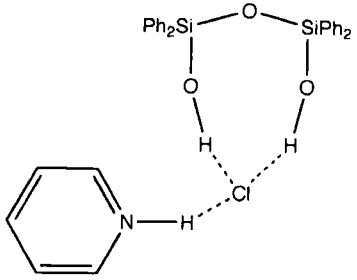
Ph2Si
O
SiPh2
O
O
H
H
Cl
N
H

53

Cl⁻

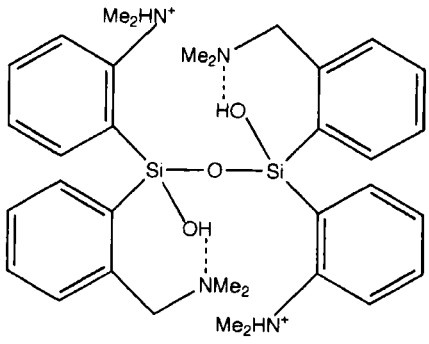
Me2HN+
Me2N
HO
Si
O
Si
OH
NMe2
Me2HN+

54

Cl⁻

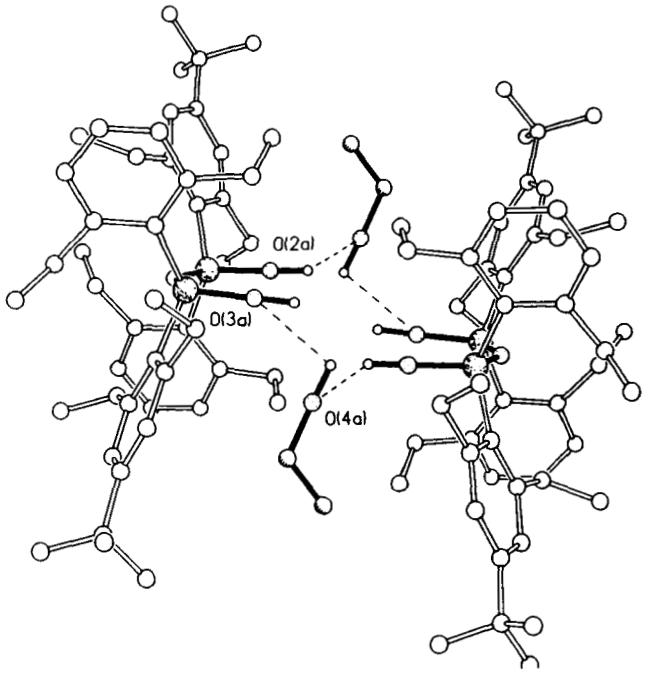

FIG. 13. The hydrogen-bonded dimeric structure of $[(2,6\text{-}Et_2C_6H_3)(2,6\text{-}Et_2\text{-}4\text{-}Bu^tC_6H_2)(OH)Si]_2O$ with EtOH, with the bonds involved in the hydrogen bonded network shown as solid lines. Hydrogen atoms have been omitted for clarity. Drawn using coordinates taken from the Cambridge Crystallographic Database.

ane molecules which, instead of being joined directly to each other like most of the other disiloxanediols, are joined via a pair of ethanol molecules (from the hexane/ethanol solvent mixture used for crystallization) to give a cyclic arrangement. Each SiOH group is involved in only one hydrogen bond, but the COH groups are involved in two. It seems likely that if the compound were crystallised in the absence of ethanol, it would form a simple dimer, as a chain formation of the types shown in Fig. 10 would probably be prevented by the steric effect of the bulky aryl groups. The structure has some similarities with that of $(Me_3Si)_3CSiF(OH)_2$, which forms the aggregate $[(Me_3Si)_3CSiF(OH)_2]_6.2H_2O$ (see Section IV,G) in which two sets of three bulky molecules are joined via hydrogen bonding to the water molecules and further hydrogen bonds are prevented by the bulky and hydrophobic $(Me_3Si)_3C$ groups.

A further disiloxanediol, 1,3-bis(dicyclopentenyl)-1,3-dimethyldihydroxydisiloxane, is obtained by hydrolysis of the product obtained from

the hydrosilylation of dicyclopentadiene with $MeCl_2SiH$ catalyzed by H_2PtCl_6. Unfortunately, no details of bond angles or hydrogen bonding for this compound have been reported (*276*).

2. *Other Siloxanes*

The solid-state structures of two trisiloxanes, $HO(SiPh_2O)_3H$ (*277*) and $(HOBu^t{}_2SiO)_2SiMe_2$ (*278*), have been determined. Both compounds form hydrogen-bonded dimers, but they differ in the detail of the hydrogen bonding. The phenyl compound contains both intra- (2.74 Å) and intermolecular (2.72 Å) hydrogen bonds **55** while in the butyl compound there seems to be no intramolecular hydrogen bonding, but rather a pair of intermolecular hydrogen bonds **56.**

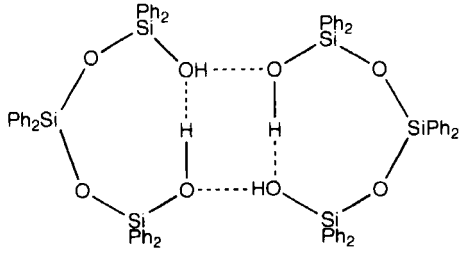

55

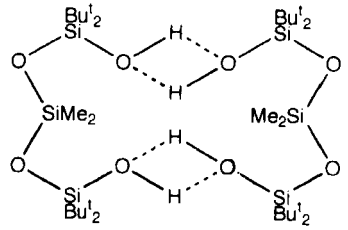

56

The disilanol *cis*-1,5-dihydroxy-1,5-dimethyl-3,3,7,7-tetraphenylcyclotetrasiloxane has a boat conformation for the siloxane ring, but it does not show intramolecular hydrogen bonding, rather, intermolecular hydrogen bonding joins the molecules into chains. The hydrogen-bonded network is similar in arrangement to that shown in Fig. 10b for the disiloxane diols, in which both OH groups from one molecule in the chain interact with a single OH group from an opposite molecule, the other two hydrogen-bonding sites then being used to join up adjacent molecules (*279*).

The crystal structures of both the *cis* and the *trans* isomers of 2,8-dihydroxy-2,4,4,6,6,8,10,10,12,12-decamethylcyclohexasiloxane have been determined. In this case (unlike the cyclotetrasiloxane in Fig. 26), the *cis* isomer does contain an intramolecular hydrogen bond, and intermolecular hydrogen bonds link the molecules into cyclic pairs **57**. The *trans* isomer cannot form intramolecular hydrogen bonds, but forms cyclic tetramers which are further hydrogen-bonded to form infinite sheets **58** (*280*).

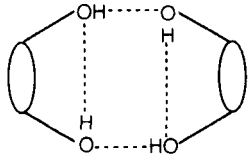

57 *cis* isomer

= 2,8-dihydroxy-2,4,4,6,6,8,10,10,12,12-decamethylcyclohexasiloxane.

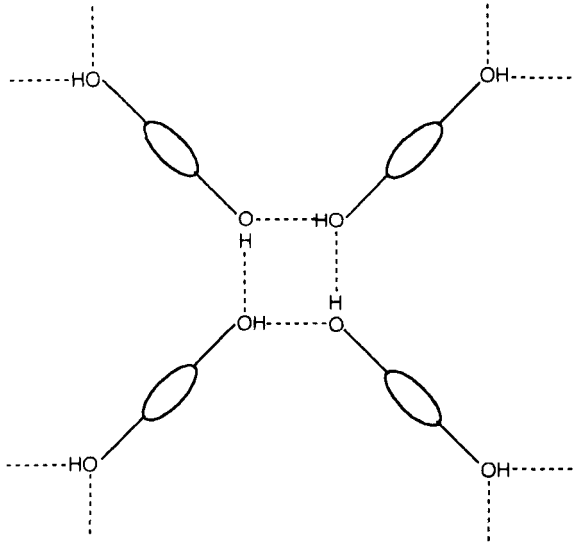

58 *trans* isomer

Silylation of the silsesquioxane $[(C_6H_{11})_7Si_7O_9(OH)_3]$ (see Section IV,E for its structure) leads to disilanols $[(C_6H_{11})_7Si_7O_9(OH)_2SiMe_2R]$ (R = Me or Ph). The structure of the phenyl compound **59** shows the

molecules to be hydrogen-bonded dimers with intramolecular (O···O distance 2.722 Å) as well as intermolecular hydrogen bonding (O···O distance 2.670 Å) (*281*). The $SiMe_3$ analogue is disordered (*282*), but the hydrogen bonding is thought to have the same arrangement as the $SiMe_2Ph$ compound (*283*). The related siloxane **60** has also been investigated by x-ray crystallography, but disorder problems have prevented a detailed structural analysis (*284*). The full structure of its bis Ph_3Sn derivative has, however, been determined (*75*).

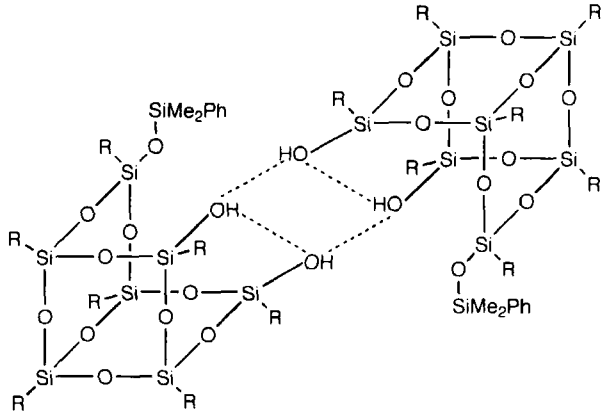

59

R = *cyclo*-C_6H_{11}

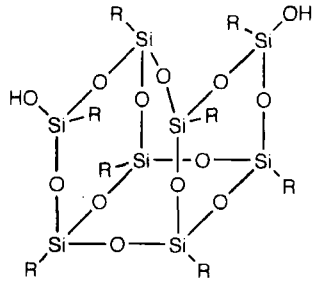

60

3. α, ω-Oligosilanediols

The addition of water to $(Bu^t_2ISi)_2$ causes rapid hydrolysis and the formation of the 1,2-disilanediol $(Bu^t_2HOSi)_2$ (*285*). There is no intramo-

lecular hydrogen bonding, as the OH groups point in opposite directions, but the molecules are linked together by intermolecular hydrogen bonds to form simple chains in which each OH group is involved in only one hydrogen-bonding interaction.

Hydrolysis of the α, ω-dichloro-oligosilanes $Cl(SiPh_2)_nCl$ (n = 4 or 7) affords the corresponding α, ω-dihydroxy-oligosilanes. The structure of the tetrasilane has been determined by two groups with similar but not identical results. Párkányi *et al.* (*286*) reported that there is a single intramolecular hydrogen bond, causing a cyclic arrangement, and that intermolecular hydrogen bonding is prevented by the bulk of the phenyl groups. Ovchinikov *et al.* (*287*) also found a similar intramolecular interaction, but also that there is an intermolecular hydrogen bond linking the molecules into pairs around an inversion center **61.** The reason for this discrepancy in results is unclear. The structure of the heptasilane $HO(SiPh_2)_7OH$ also shows the molecules to have intermolecular hydrogen bonds, this time linking them into chains **62.** There is also an intramolecular interaction between an OH group and the π-system of one of the aryl rings, characterized by an $OH\cdots C_{ipso}$ distance of 2.90 Å and the O and H atoms being 3.2 and 2.52 Å, respectively, from the plane of the ring (*287*).

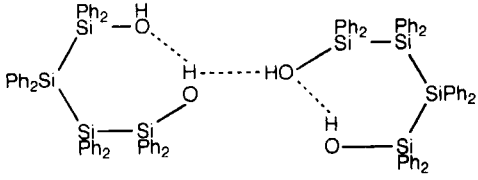

61

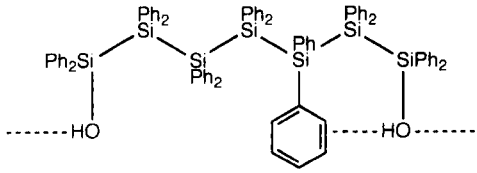

62

The conformation of $HO(SiPh_2)_nOH$ species (n = 4, 5, or 7) has also been investigated in solution by IR spectroscopy. The intramolecular π-interaction in the heptasilane is seen in CCl_4 solution as a relatively narrow band at 3605 cm^{-1}, a shift of 80 cm^{-1} from the approximate

value of 3685 cm^{-1} for free O–H in such a compound (cf. 3685 cm^{-1} for Ph_3SiOH in CCl_4 solution; see Table I). A similar intermolecular H-bond–induced shift is seen in Ph_3SiOH, which has an O–H stretch of 3620 cm^{-1} in benzene solution (*185*). The IR spectrum of $HO(SiPh_2)_5OH$ in dilute solution in CCl_4 is more complicated and shows three types of O–H stretch. Again, there is a band (at 3605 cm^{-1}) attributable to an intramolecular OH$\cdots\pi$ interaction, but there are also bands at 3405 cm^{-1}, attributable to an intramolecular OH$\cdots$OH hydrogen bond, and at about 3660 cm^{-1}, attributable to free O–H stretching. (The relatively low-frequency stretch for the free OH is thought to be due to the fact that the OH group is already involved as an electron donor in an intramolecular hydrogen bond.) For the pentasilane there thus seems to be an equilibrium between molecules having an OH$\cdots\pi$ interaction and cyclic conformations having an intramolecular OH$\cdots$O interaction, with the equilibrium favoring the former species. At increasing concentrations, the 3405 cm^{-1} band in $HO(SiPh_2)_5OH$ broadens and shifts towards a new band, centered at 3300 cm^{-1}, attributable to intermolecular OH$\cdots$O bonding. The tetrasilane $HO(SiPh_2)_4OH$ also has bands at 3608 and 3415 cm^{-1}, attributable to intramolecular OH$\cdots\pi$ and OH$\cdots$O interactions, but in this case the OH$\cdots$O conformation predominates. The conformation of these oligosilanediols seems to be governed by the chain length. If the chain is relatively short, as in the tetra- and pentasilanes, intramolecular OH$\cdots$OH interactions occur, giving cyclic conformations. In the longer-chain heptasilane, however, formation of a 10-membered ring by hydrogen bonding is less favored. The cyclic conformation induced by the conformation also has an effect on the chemistry of the compounds. For example, $HO(SiPh_2)_4OH$ loses water relatively readily to give the cyclic siloxane OSi_4Ph_8 in quantitative yield on heating, while the pentasilane analogue reacts more slowly to give a low yield of OSi_5Ph_{10}, and the cyclic OSi_7Ph_{14} is not formed at all under similar conditions (*185*). Recent work has also shown that for organic compounds, if OH$\cdots$OH interactions are not sterically available, then OH$\cdots\pi$ hydrogen bonds may form (see, for example, Ref. *288*, and references therein). For example, in $Ph_2(PhCH_2)COH$ there are intermolecular O$\cdots C_{aryl}$ and OH$\cdots C_{aryl}$ distances of 3.525 and 2.73 Å, respectively (*288*). The phenyl-substituted siloxanediols show similar IR characteristics (*187*) to the oligosilanes, in that the disiloxane $(HOSiPh_2)_2O$ has only free OH's in dilute solution, but $HO(SiPh_2O)_3H$ has bands corresponding to both intramolecular OH$\cdots\pi$ and OH$\cdots$O hydrogen bonding.

4. *Other Compounds Containing Two SiOH Groups*

The extent of hydrogen bonding in the cyclic silazane 1,3-bis(diphenylhydroxysilyl)-2,2-dimethyl-4,4-diphenylcyclodisilazane was not reported in the original publication (*289*), but a more recent examination (*210*) of the x-ray data reveals that although there do not appear to be any OH···OH or OH···π interactions, there is a short, 2.393 Å, *ortho*-CH···OH distance, indicating a probable CH···OH interaction, and a second relatively short distance, 2.580 Å, between the other *ortho* CH and the second OH group, also indicating a possible weak interaction, as shown in Fig. 14. This appears to be the only silanol exhibiting such interactions, and it is not clear why the compound does not participate in the types of interaction more normally found.

The structure of the disilanol 1,7-bis[hydroxy(dimethyl)silylmethyl]-*m*-carborane has a hydrogen-bonded network reminiscent of the siloxanediol type shown in Fig. 10c, in which pairs of molecules are hydrogen-bonded together and then these pairs are further linked to give a double chain (*290*).

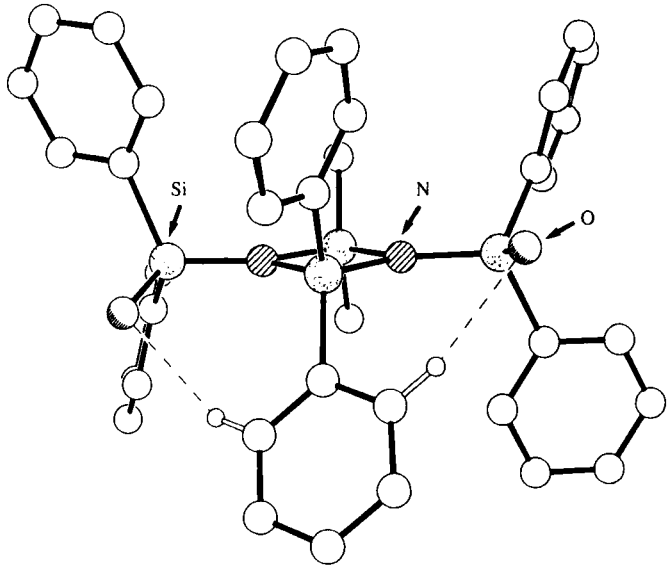

FIG. 14. The molecular structure of 1,3-bis(diphenylhydroxysilyl)-2,2-dimethyl-4,4-diphenylcyclodisilazane, showing the orientation of the *ortho* –CH groups of one of the aromatic rings with respect to the SiO groups. Other hydrogen atoms have been omitted for clarity. Drawn using coordinates taken from the Cambridge Crystallographic Database.

The extremely bulky silanol $[(Me_3Si)_2(HOMe_2Si)C]_2Zn$ is unusual in that diorganozinc compounds are usually highly reactive towards protic species. The steric protection of the reactive C–Zn bonds by the bulky ligands presumably provides the stability. The compound forms cyclic dimers via both intra- and intermolecular hydrogen bonds, which causes the C–Zn–C linkage to deviate slightly from linearity to 175.9(1)° (*291*). A related disilanol $(Me_3Si)_2C(SiMe_2OH)_2$, prepared as described in Section II,C,2,d, also shows alternating intra- and intermolecular hydrogen bonds, but in this case they form a chain structure rather than a cyclic dimer (*292*). Early work reported unit-cell data for $(HOMe_2Si)_2CH_2$, but a detailed analysis of the structure is not available (*293*).

The hydrogen-bonded arrangement in p-$(HOMe_2Si)_2C_6H_4$ is much more complicated than the other simple disilanols described earlier. There are three crystallographically independent types of molecules in the unit cell. Two are joined by hydrogen bonds to form chains, while

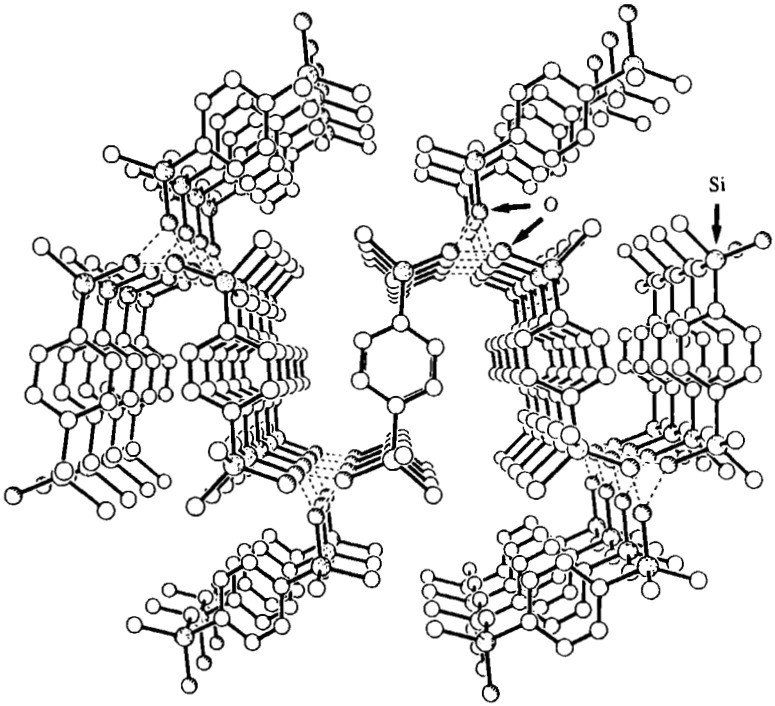

FIG. 15. A view, perpendicular to the aromatic ring, of the three-dimensional hydrogen-bonded network formed by p-$(HOMe_2Si)_2C_6H_4$, with hydrogen atoms omitted for clarity. Drawn using coordinates taken from the Cambridge Crystallographic Database.

the third cross-links between the chains to give a three-dimensional network (Figs. 15 and 16) (*294*).

E. Compounds Containing Three Si–OH Groups

The slow hydrolysis of $C_6H_{11}SiCl_3$ affords the incompletely condensed polyhedral oligosilsesquioxane $[(c\text{-}C_6H_{11})_7Si_7O_9(OH)_3]$ as a hydrogen-bonded dimer **63.** The most likely hydrogen-bonded arrangement for this is thought to be the solely intermolecular network, which has O···O distances of 2.63–2.64 Å (*75*).

F. Compounds Containing Four Si–OH Groups

Three very different compounds containing four SiOH groups have been structurally characterized. The tetrasilanol $(HOSiMe_2)_4C$ may be prepared by treatment of $(IMe_2Si)_4C$ with AgOCN in moist ether (*253*) (presumably via hydrolysis of the highly reactive Si-OCN species formed as intermediates) and has a three-dimensional hydrogen-bonded network. There are four independent molecules A, B, C, and D, in the unit cell, and each contains two intramolecular hydrogen bonds. The four types of molecules are arranged in alternating layers,

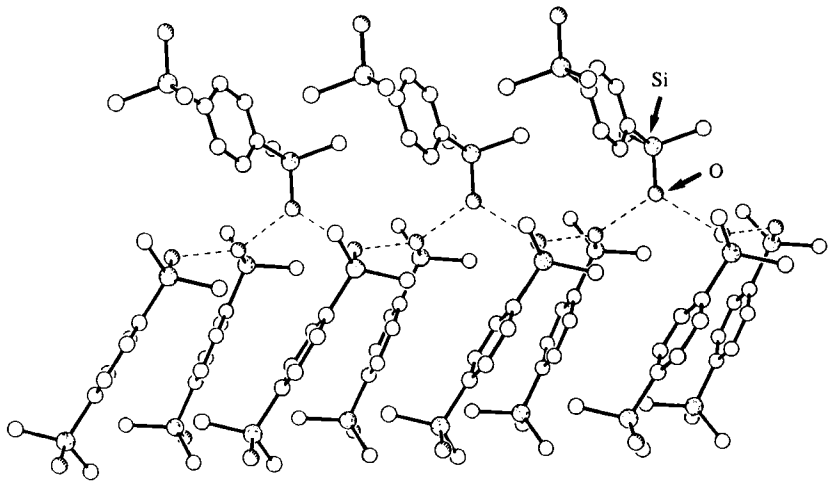

FIG. 16. A view showing one of the chain units that are linked to form the three-dimensional hydrogen-bonded network in p-$(HOMe_2Si)_2C_6H_4$, with hydrogen atoms omitted for clarity. Drawn using coordinates taken from the Cambridge Crystallographic Database.

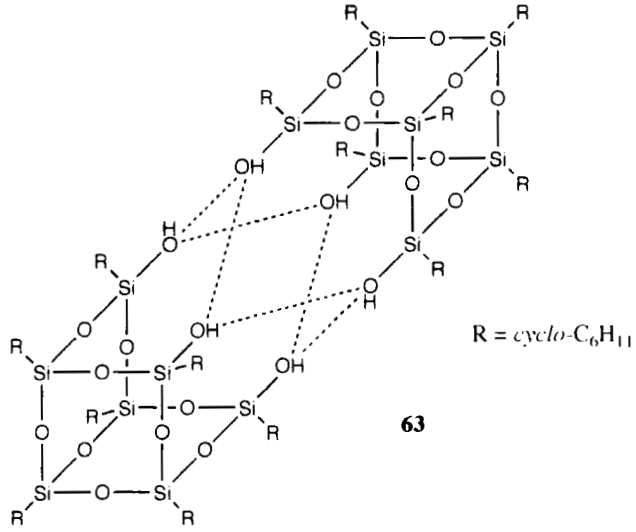

63

with two types of molecules, B and C, in $z = 0$ and $z = \frac{1}{2}$ layers in the cell, and the other two, A and D, at $z = \frac{1}{4}$ and $z = \frac{3}{4}$. Each molecule bonds to neighbors within the plane to give sheets, the two different types of plane having slightly different hydrogen-bonding arrangements. The sheets are also linked together to form a three-dimensional network by the single spare hydrogen-bonding site in each molecule that is not used in forming the sheet structure. The connectivity of all four types of molecule in the (101) plane is shown in Fig. 17 (*295*).

The structure of 1,1,5,5-tetrakis(hydroxydimethylsiloxy)-3,3,7,7-tetraphenylcyclotetrasiloxane contains two crystallographically different molecules in the unit cell. The molecules are joined by intermolecular hydrogen bonds to form sheets, as shown in Fig. 18, which are built up from units of four molecules that are centered on an eight-membered ring, of S_8 crown conformation, of hydrogen-bonded oxygen atoms. All possible hydrogen-bonding sites are used in forming the sheets, and there are no interactions between the sheets (*296*).

The structure of the norbornylsiloxane **64** has been determined, but the x-ray data are of poor quality and do not permit a detailed picture of the hydrogen bonding to be made. However, as all of the hydroxy groups seem to point towards each other and there are broad absorptions at 3403 and 3243 cm^{-1} in the IR spectrum (KBr disk), it seems likely that both intra- and intermolecular hydrogen bonds are present (*297*).

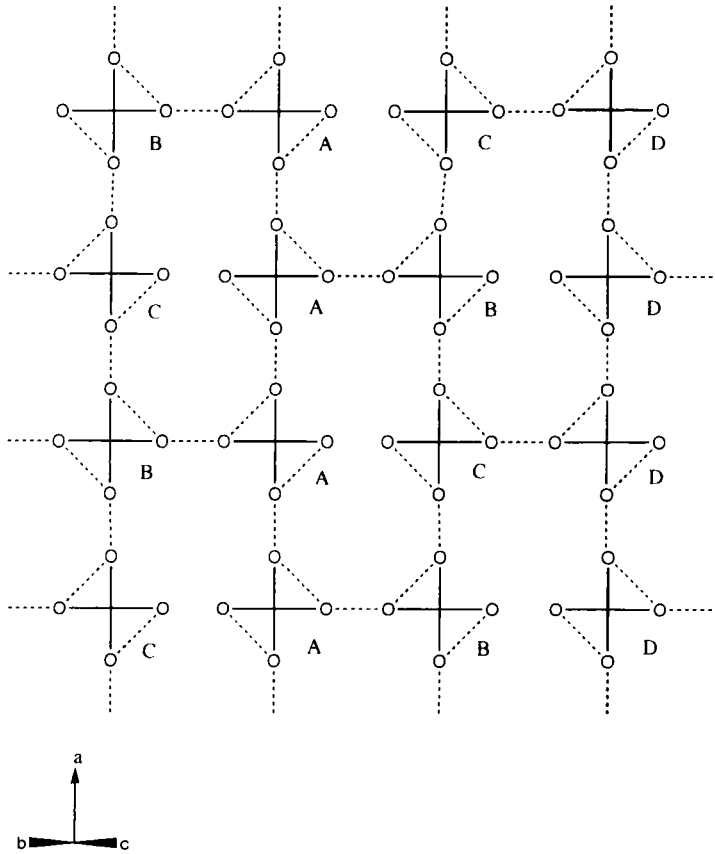

FIG. 17. A representation of the hydrogen bonding in $(HOMe_2Si)_4C$ in the (001) plane, showing all four molecules A, B, C, and D.

G. COMPOUNDS CONTAINING AN $Si(OH)_2$ GROUP, SILANEDIOLS

The isolation of pure silanediols is more difficult than that of silanols because of their tendency to undergo condensation reactions. Most of the compounds characterized by x-ray crystallography therefore contain bulky substituents at silicon. The size of the substituents at silicon plays an important role in determining the hydrogen-bonded structure of the diol. Small substituents allow infinite hydrogen-bonded arrays of molecules to be formed, while larger substituents give simple chains, and very bulky groups lead to the formation of simple tetramers or dimers.

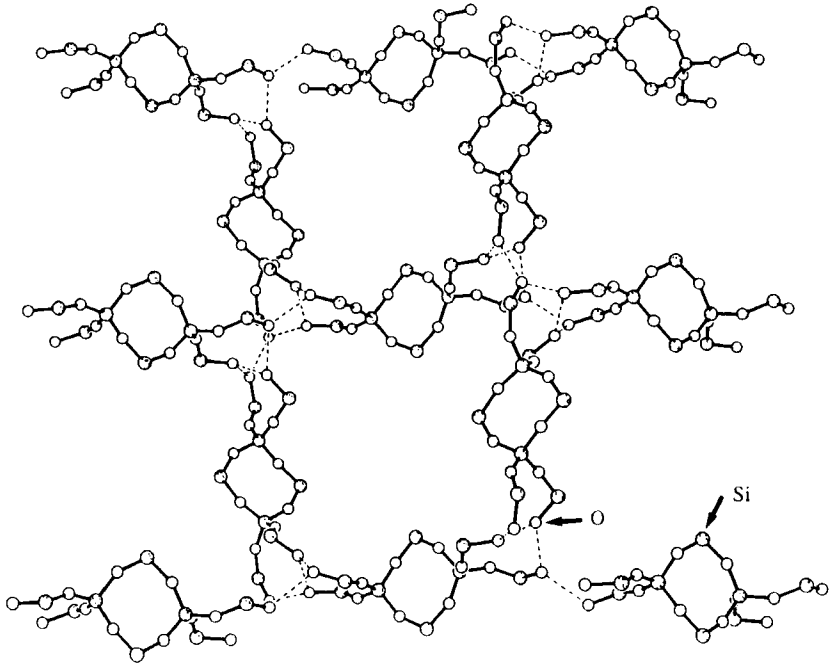

FIG. 18. The hydrogen-bonded sheet structure of 1,1,5,5-tetrakis(hydroxydimethylsiloxy)-3,3,7,7-tetraphenylcyclotetrasiloxane. Note the crown-shaped eight-membered rings of oxygen atoms at the junctions where four of the molecules meet. All hydrogen and carbon atoms have been omitted for clarity. Drawn using coordinates taken from the Cambridge Crystallographic Database.

Early work on $Et_2Si(OH)_2$ and on $allyl_2Si(OH)_2$ (*293, 298, 299*) suggested that the two compounds had similar structures and that these were due not to normal hydrogen bonding, but to a special arrangement involving a type of dipole–dipole interaction on OH···O angles of about

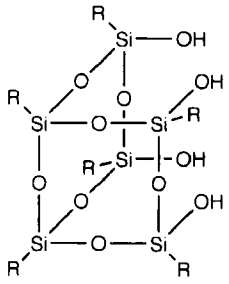

R = norbornyl

64

TABLE V

STRUCTURAL DATA FOR COMPOUNDS CONTAINING TWO, THREE, OR FOUR Si–OH GROUPS

Compound	Si–OH (Å)	OH···X (Å)[a]	O···X (Å)[a]	O-H···X (°)[a]	Structural summary	Refs.
$(Me_2HOSi)_2O$	1.640(5) 1.643(5)		2.656 2.728		Ladder chains, data in table from Ref. *258*	*258, 259*
$(Et_2HOSi)_2O$	1.56(1)–1.72(1)		2.69–2.79		Ladder chains	*260*
$(Pr^n{}_2HOSi)_2O$	1.58(1)–1.63(1)		2.66–2.77		Ladder chains	*261*
$(Pr^i{}_2HOSi)_2O$	1.636(2) 1.644(2)		2.719(5) 2.849(5)		Ladder chains	*264*
$(Bu^t{}_2HOSi)_2O$	1.662 1.668		2.686 2.757		Acts as link between columns of tin complex; see Table VI	*272*
$[Me(thienyl)HOSi]_2O$	1.613(5) 1.614(5) 1.668	2.14(6) 2.14(6)	2.702(7) 2.741(7) 2.757	150(6) 162(6)	Ladder chains	*266*
$(Ph_2HOSi)_2O$	1.620(3)–1.647(3)		2.641(5)–2.798(5)		Ladder chains, data in table from Ref. *263*	*262, 263*
$(Ph_2HOSi)_2O \cdot C_5H_6NCl$	1.618(5) 1.626(5)	2.28[b] 2.42[b]			Simple adduct, OH···Cl interactions	*274*

(*continues*)

TABLE V (*Continued*)

Compound	Si–OH (Å)	OH···X (Å)[a]	O···X (Å)[a]	O-H···X (°)[a]	Structural summary	Refs.
$[(Ph_2HOSi)_2O]_3 \cdot 2C_4H_4N_2$	1.632(9) 1.623(9) 1.62(1)		2.71(1) 2.75(1)[c] 2.75(2)[c]		Discrete 3:2 adduct with OH···OH and OH···N interactions	*273*
50	1.631(2)	1.91–2.18	2.72–2.78	169–178	Sheets	*267*
$[ArAr'(HO)Si]_2O \cdot EtOH$[d]	1.633(5) 1.638(4)		2.685 2.884		Dimeric, joined via hydrogen bonds to ethanol	*275*
$[HOMe(C_{10}H_{13})Si]_2O$[e]	1.62(3) 1.63(3)				Unknown	*276*
54	1.635(1)		2.644[c]	166.6[c]	Monomeric, intramolecular OH···N interactions only	*233*
$1,7\text{-}(HOMe_2SiCH_2)_2C_2B_{10}H_{10}$	1.650(2) 1.659(2)	2.05(3) 2.12(3)		171(4)	Ladder chains	*290*
$(HOBu^t_2SiO)_2SiMe_2$	1.625(4)–1.635(4)		2.773, 2,824[f]		Dimeric, intra- and intermolecular OH···OH bonds	*278*
$(Ph_2HOSi)_2SiPh_2$	1.631(6) 1.651(5)	1.78[g]	2.74[g] 2.72[f]	155.5[g]	Cyclic dimers, intra- and intermolecular OH···OH bonds	*277*

$(Ph_2HOSiN)Me_2Si(Ph_2HOSiN)$-$SiPh_2$	1.629(5) 1.642(5)		3.214[h] 3.444[h]		Monomeric, possible CH···OH interactions	*289*
cis-$[Ph_2SiOSiMe(OH)O]_2$	1.637(9) 1.649(9)		2.686(8)–2.736(8)		Chains	*279*
cis-$(HOMeSiOSiMe_2OSiMe_2O)_2$	1.643(7) 1.663(7)		2.64[f] 2.71[g]		Cyclic dimers, inter- and intramolecular OH···OH bonds	*280*
trans-$(HOMeSiOSiMe_2OSiMe_2O)_2$	1.641(6)		2.68		Sheets	*280*
$(Bu^t_2SiOH)_2$	1.663(2) 1.665(2)		2.775 2.896		Chains	*285*
$HO(SiPh_2)_4OH$	1.643(2) 1.651(2)	2.12	2.816	170.9	Monomeric, intramolecular OH···OH bonds only	*286*
	1.643(3)		2.808(4)[g]	180	Cyclic dimers, intra- and intermolecular OH···OH bonds	*287*
$(Me_3Si)_2C(SiMe_2OH)_2$	1.637(3)–1.652(3)	2.36[g] 2.07[f]		137.1[g] 169.4[f]	Chains, intra- and intermolecular OH···OH bonds	*292*
$(HOMe_2Si)_2CH_2$					Unknown, only unit cell data available	*293*
$[(HOMe_2Si)(Me_3Si)_2C]_2Zn$	1.663(2) 1.658(2)		2.831(3)[f] 2.910(3)[g]	162(3) 156(3)	Cyclic dimers, intra- and intermolecular OH···OH bonds	*291*

(*continues*)

TABLE V (*Continued*)

Compound	Si–OH (Å)	OH···X (Å)[a]	O···X (Å)[a]	O-H···X (°)[a]	Structural summary	Refs.
p-$(HOMe_2Si)_2C_6H_4$	1.643(3)–1.649(3)	1.72(9)–1.99(6)	2.698(4)–2.715(4)	160(5)–175(6)	Three-dimensional network	*294*
[*c*-$C_6H_{11})_7Si_7O_9(OH)_3$]	1.620(3)–1.626(3)		2.63–2.64		Cyclic dimers	*75*
$(HOMe_2Si)_4C$	1.644(6)–1.674(6)				Three-dimensional network	*295*
[(norbornyl)$_6Si_6O_7(OH)_4$]					Unknown	*297*
[$Ph_2SiO(HOMe_2SiO)_2SiO]_2$	1.610–1.657	1.80(2)[f]	2.60(3)–2.71(2)		Sheets	*296*

[a] X = oxygen unless otherwise stated.
[b] X = Cl.
[c] X = N.
[d] $(2,6\text{-}Et_2C_6H_3)(2,6\text{-}Et_2\text{-}4\text{-}Bu^tC_6H_2)(HO)Si)_2O\cdot EtOH$.
[e] 1,3-bis(dicyclopentenyl)-1,3-dimethyl-1,3-dihydroxydisiloxane.
[f] Intermolecular.
[g] Intramolecular.
[h] X = *ortho* carbon in aromatic ring.
[i] Average of five values.

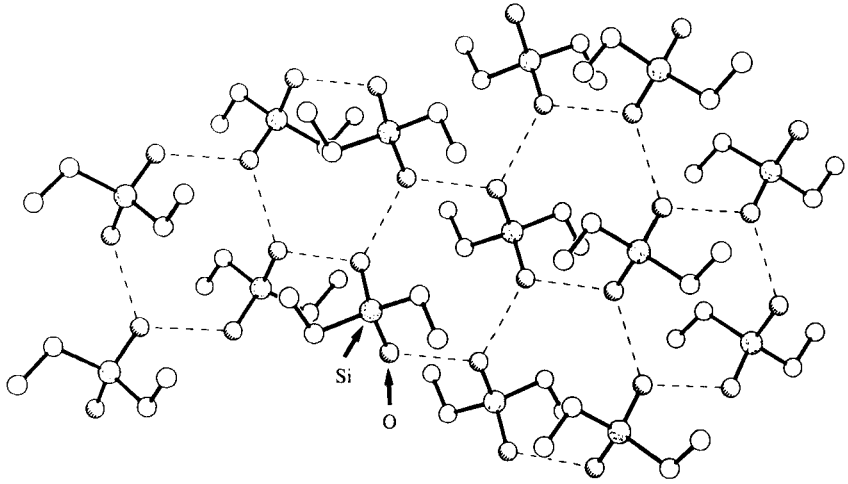

FIG. 19. A view looking onto the plane formed by the hydrogen bonding in $Et_2Si(OH)_2$, with hydrogen atoms omitted for clarity. Drawn using coordinates taken from the Cambridge Crystallographic Database.

90° within intramolecular hydrogen bonds. Later it was found that the diallyl compound actually comprised sheets (*300*). More recently, the structure of $Et_2Si(OH)_2$ has been reexamined (*301*) and has been found not to require unusual types of hydrogen bonding to describe it, but rather to consist solely of intermolecular hydrogen bonds to form infinite sheets (Figs. 19 and 20) that are similar in structure to those proposed for $(allyl)_2Si(OH)_2$.

The structure of the more hindered $Ph_2Si(OH)_2$ has been determined by several groups (*302–304*). The structure comprises columns

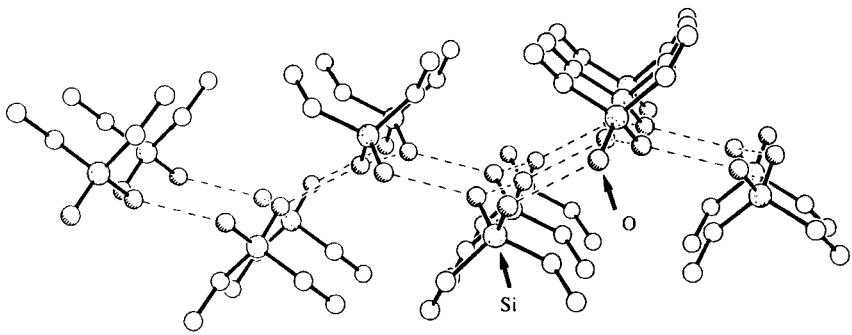

FIG. 20. A view looking parallel to the sheet formed by the hydrogen bonding in $Et_2Si(OH)_2$, showing the hydrophilic interior of the sheet and the hydrophobic exterior, with hydrogen atoms omitted for clarity. Drawn using coordinates taken from the Cambridge Crystallographic Database.

of hydrogen-bonded molecules (Fig. 21). There are six molecules in the unit cell, comprising two pairs of three independent molecules related by a center of symmetry. The six molecules form a chair-shaped hydrogen-bonded ring of oxygens with alternating short, medium, and long O···O distances (2.670, 2.688, and 2.698 Å), and further hydrogen bonding links the hexameric groups both above and below so as to form a column. The OH groups all point towards the center of the column, and the phenyl groups away from the center, so that there is no hydrogen bonding between the columns. There also appears to be no hydrogen bonding to the aromatic rings. These columns are reminiscent of those formed by the $(HOR_2Si)_2O$ species (R = Et, Pr^n, or Bu^n, Section IV,D,I) but $Ph_2Si(OH)_2$ has not been reported to show similar liquid-crystalline behavior.

The simple diols $R_2Si(OH)_2$ (R = Pr^i, Bu^t, *c*-C_6H_{11}, and *o*-tolyl) form similar, but not identical, hydrogen-bonded chains. The structures of the Pr^i (*305*), Bu^t (*40, 278*), and *c*-C_6H_{11} (*292*) compounds are very similar in that they comprise ladder chains of the general type **65,** in which pairs of molecules are linked to form dimers and then further hydrogen bonds link the dimers to form the chains. [It has also been

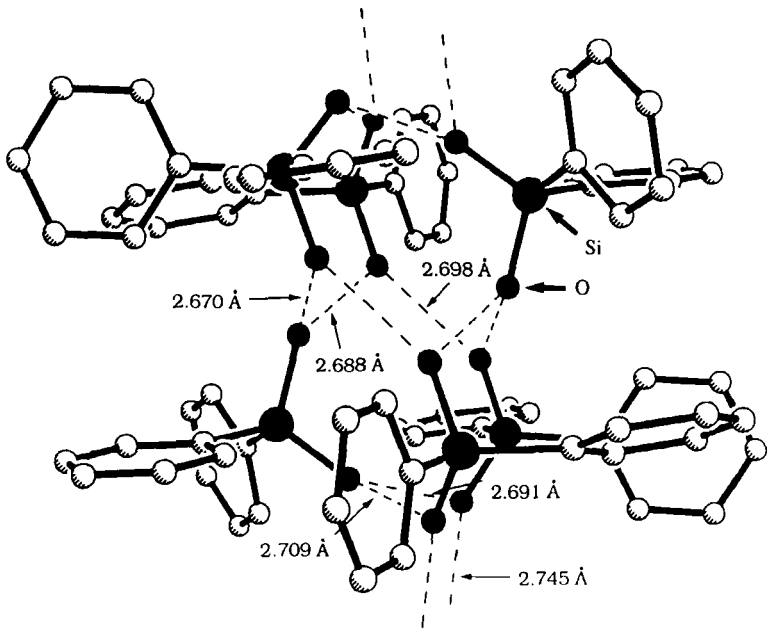

FIG. 21. The hydrogen-bonded hexameric unit that builds up the columnar structure of $Ph_2Si(OH)_2$, with hydrogen atoms omitted for clarity (*304*).

found that $Bu^t_2Ge(OH)_2$ forms similar hydrogen bonded ladder chains (*306*).] A small difference between the structure of the Bu^t compound and that of the Pr^i and $c\text{-}C_6H_{11}$ compounds exists: In the butyl compound, the chair-shaped Si_2O_4 six-membered rings of each hydrogen bonded dimer are inverted with respect to their neighbors in the chain, but in the propyl and the cyclohexyl species, the chair-shaped rings are related simply by unit translation to their neighbors. The structure of $(o\text{-tolyl})_2Si(OH)_2$ is also built up from chains of pairs of molecules, but in this case opposing pairs of molecules are not linked together; rather, they are bonded to the neighbors of the molecule opposite, as shown in **66** (*307*). The diol $Bu^tPhSi(OH)_2$, bearing both a Bu^t and a Ph substituent, has a structure similar to that of $(o\text{-tolyl})_2Si(OH)_2$, rather than that of the related di-*t*-butyl or the diphenyl species (*304*). The iron complex $Cp(CO)_2FeSiPr^i(OH)_2$ has also been reported to have a structure comprising ladder chains, but the chains twist to give a helical arrangement (*248*). The structural type **65** is similar to that of the thienyldisiloxanediol **49** shown in Fig. 10c. The reasons for the differences in structure between quite closely related $R_2Si(OH)_2$ com-

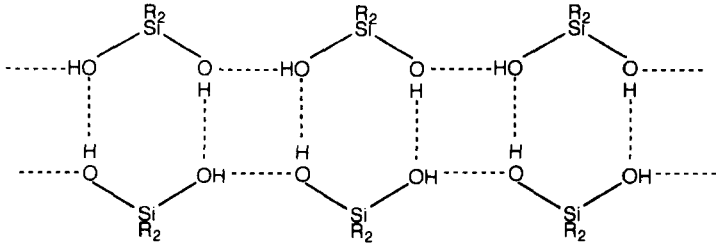

65

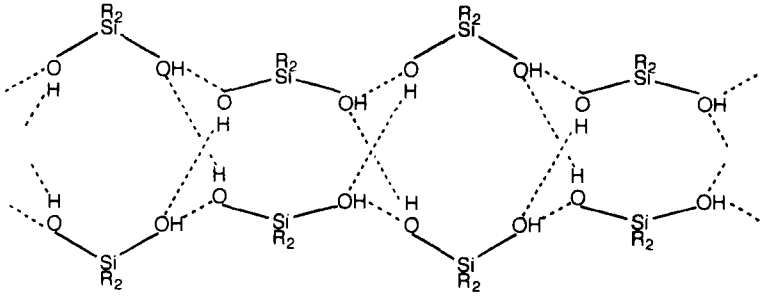

66

pounds is unclear, but the precise steric requirements of the substituents at silicon seem to play a crucial role.

The interest in the structures of simple $R_2Si(OH)_2$ compounds lies in the fact that one of them, $Bu^i_2Si(OH)_2$, forms a discotic liquid crystalline phase (*308, 309*). Despite many attempts, it has not proved possible to obtain crystals of $Bu^i_2Si(OH)_2$ suitable for a crystallographic study, the material obtained from various solvents usually being of a fine fibrous nature. The discotic phase of $Bu^i_2Si(OH)_2$ has been proposed (*309*) to be due to the formation of dimeric "disks" of molecules which remain on breaking the interdimer hydrogen bonds in a structure of type **65** at the transition between crystal and mesophase. As has been described, structure type **65** is found for several diols similar to $Bu^i_2Si(OH)_2$, and it is thus quite likely that $Bu^i_2Si(OH)_2$ does indeed have the proposed structure.

The reaction between $Bu^t_2Si(OH)_2$ and Cl_4Sn affords, after workup and crystallization from CH_2Cl_2, the tin complex **51** containing a bridging $Bu^t_2Si(OH)_2$ molecule, which is cocrystallized with $(HOBu^t_2Si)_2O$, the structure of which is described in Section IV,D,1 (*272*).

Silanediols containing very bulky groups on silicon do not form extended hydrogen-bonded arrays, but rather discrete hexamers, tetramers, or dimers. The structure of the fluorosilanediol TsiSiF(OH)$_2$ (for preparation, see Scheme 4) is found in the solid state to comprise $[TsiSiF(OH)_2]_6.2H_2O$ hydrogen-bonded hexamers, as shown in Fig. 22. The hexamer contains two sets of three molecules related by an inversion center which are hydrogen-bonded together via the two water molecules (*310*). This hexameric cluster of molecules is closely related to those of the triols $(Me_3Si)_3MSi(OH)_3$ (M = C or Si) described in Section IV,I. The cluster contains both OH···OH and OH···F hydrogen bonds, which might be expected despite the fact that other structures such as that of $Bu^tSiF(OH)$, described in Section IV,C,4, do not have OH···F bonding.

The structure of $(\eta^1\text{-}C_5Me_5)_2Si(OH)_2$ (obtained by treatment of the divalent silicon species $(\eta^5\text{-}C_5Me_5)_2Si$ with moist pyridine-*N*-oxide) provides an interesting progression away from the chain structures of the diols discussed earlier, e.g., $Pr^i_2Si(OH)_2$ towards discrete hydrogen-bonded units. The unit cell contains 12 molecules arranged as three tetrameric units. One of the tetramers lies on an inversion center and contains two independent molecules, while in the other two tetramers (which are related by the inversion center), all four of the molecules are different, giving a total of six independent molecules. The hydrogen bonding network in each tetramer is the same: A pair of opposing molecules are connected as in structure **65,** but instead of these being

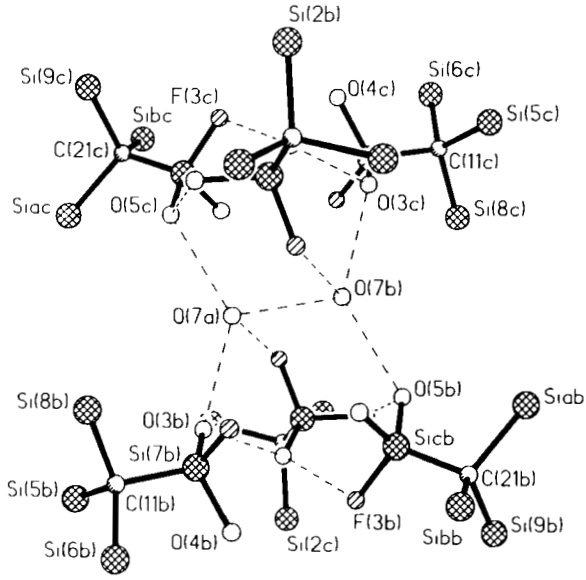

FIG. 22. The hydrogen-bonded structure of $(Me_3Si)_3CSiF(OH)_2$, showing the hexameric unit containing two water molecules, $[(Me_3Si)_3CSiF(OH)_2]_6 \cdot 2H_2O$, with hydrogen atoms and methyl groups omitted for clarity (*310*).

linked into chains, they are bridged by "terminal" silanediol molecules **67.** This arrangement leaves free hydrogen-bonding sites at the terminal molecules which do not link the tetramers, presumably because of steric hindrance by the α-Me groups on the rings (*311*).

The bulky silanediol $TsiSi(OH)_2O_2CCF_3$ also forms tetrameric units **68,** but in this case there are potential hydrogen bonding sites both to OH groups and to CO and C–F groups. Only the OH and C=O groups are used in hydrogen bonding; as in the case of $Bu^t_2Si(OH)F$ (see Section IV,C,4), the fluorine atoms do not take part in the hydrogen bonding. The tetramer may be viewed as a more complicated version of the (η^1-

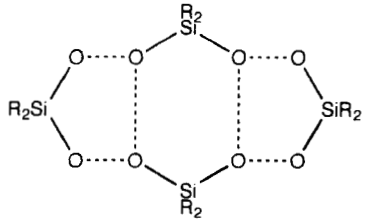

R = η^1–pentamethylcyclopentadienyl

67

$C_5Me_5)_2Si(OH)_2$ tetramers **67.** Again there are opposing molecules, this time joined by OH···O=C interactions, the "terminal" molecules bridging via both OH···OH and OH···O=C hydrogen bonds (*312*).

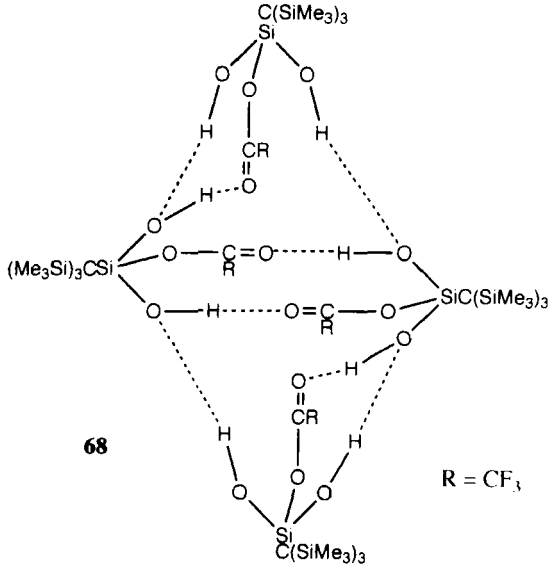

68 R = CF_3

The extremely bulky TsiSiPh$(OH)_2$ (see Scheme 5 for its preparation) has an even more restricted hydrogen-bonding scheme comprising simple dimers only, in which further hydrogen bonding to build up larger units is hindered by the steric effect of the Ph and Tsi groups (*84*).

The hydrolysis of SiI_4.2bipy affords, after an aqueous workup, *cis*-bis(2,2′-bipyridine)dihydroxysilicondiiodidedihydrate, in which each of the SiOH groups is hydrogen-bonded to a water molecule only **69** (*313*).

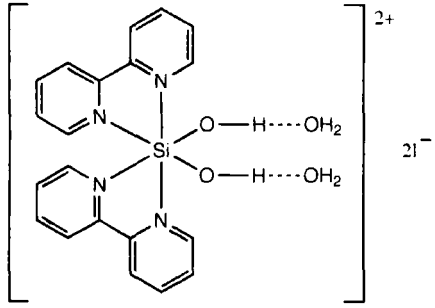

69

Although not strictly comparable to the four-coordinate organosilanols described earlier, this molecule is included as it is probably the only silanediol not to form intermolecular hydrogen bonds to itself. It is also a further example of a silanol molecule forming an adduct via hydrogen bonding. It would be of interest to see if it did form a hydrogen-bonded network itself if the water molecules were removed.

H. Compounds Containing Two $Si(OH)_2$ Groups

It is perhaps not surprising that, given the often ready condensation reactions of silanediols, few compounds containing two silanediol groups have been isolated, and only three crystallographic studies have been reported. The controlled hydrolysis (H_2O/MeOH/KOH) of Bu^tSiCl_3 affords the disiloxane $[Bu^t(OH)_2Si]_2O$ (see Section IV,I for the hydrolysis of Bu^tSiCl_3 to give other products) in which the Si–O–Si angle is linear. Only intermolecular hydrogen bonding occurs to give chains of molecules which are further connected to give sheets. Within a particular chain of molecules, the Bu^t groups alternate above and below the sheet, thus giving a hydrophobic region between the sheets, Fig. 23 (*314*). The sheet formation may be viewed as being built up from a combination of units of the type shown in Fig. 10a and 10c for siloxanediols.

The tetrahydroxydisiloxane $[OsCl(CO)(PPh_3)_2Si(OH)_2]_2O$ is produced in 70% yield from the reaction between $Os(SiCl_3)Cl(CO)(PPh_3)_2$ and $Os[Si(OH)_3]Cl(CO)(PPh_3)_2$ in wet CH_2Cl_2, and in less than 10% yield by the direct hydrolysis of $Os(SiCl_3)Cl(CO)(PPh_3)_2$. Unlike $[Bu^t(OH)_2Si]_2O$, the Si–O–Si angle is not linear but has the more usual value of 137.9(7)°. There appear to be no intermolecular hydrogen bonds, but there is a weak intramolecular OH···Cl interaction, O···Cl distance 3.17 Å, and there are short intramolecular distances to ring carbons O···C of 3.04 and 3.20 Å which may indicate OH···π hydrogen bonding (*315*).

The cyclotetrasiloxane 1,1,5,5-tetraphenyl-3,3,7,7-tetrahydroxycyclotetrasiloxane forms a stable complex with two pyridine molecules *trans* to each other across the siloxane ring (*316*). The adduct may be prepared by the addition of an excess of pyridine to the free silanol {the isomeric silanol $[Ph(OH)SiO]_4$ does not form an adduct with pyridine} (*317*). As well as hydrogen-bonding to the pyridine molecules, each of the two crystallographically independent molecules in the unit cell hydrogen-bonds to others of the same type to form two independent infinite chains (Fig. 24). Branching to form sheets by joining the chains, as in $[Bu^t(OH)_2Si]_2O$, is partially blocked by the interactions with the

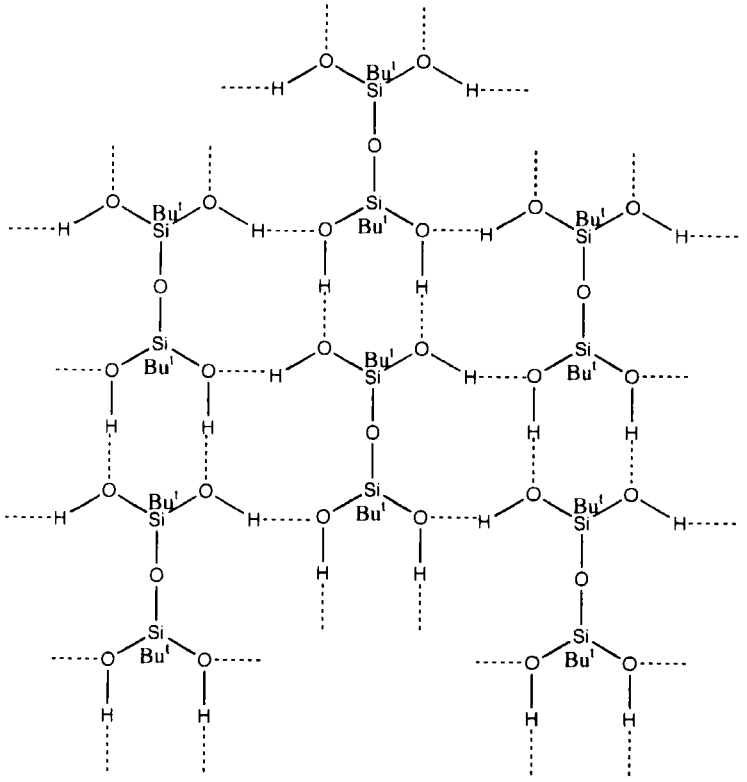

FIG. 23. A diagrammatic representation of the hydrogen bonding in $[Bu^t(OH)_2Si]_2O$, viewed perpendicular to the plane of the hydrogen bonding.

pyridine molecules, but free hydrogen bonding sites are still available. Further interactions between the molecules are presumably stopped by the steric effects of the phenyl rings which point above and below the siloxane ring.

I. COMPOUNDS CONTAINING AN $Si(OH)_3$ GROUP, SILANETRIOLS

The increasing tendency of silanols to condense as the number of OH groups on a particular silicon increases means that relatively few silanetriols have been isolated and even fewer structurally characterized. A wide range of substituted arylsilanetriols have been prepared (*102*), but none have been studied by x-ray crystallography. The first silanetriol to be structurally characterized was $c\text{-}C_6H_{11}Si(OH)_3$, which has a sheet structure comprising double layers of molecules joined in a

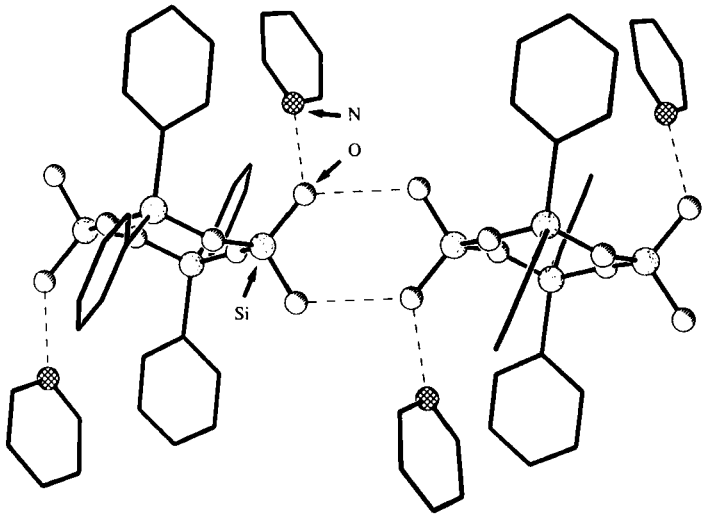

FIG. 24. A portion of the hydrogen-bonded chain formed by the 1:2 complex between 1,1,5,5-tetraphenyl-3,3,7,7-tetrahydroxycyclotetrasiloxane and pyridine. Hydrogen atoms have been omitted for clarity. Drawn using coordinates taken from the Cambridge Crystallographic Database.

head-to-head fashion, giving a highly hydrophobic outer surface which prevents further interaction between the sheets (Figs. 25 and 26) (as in the case of $[Bu^t(OH)_2Si]_2O$, Section IV,H) (*318*).

The careful hydrolysis of Bu^tSiCl_3 in Et_2O/H_2O/aniline affords $Bu^tSi(OH)_3$ (cf. hydrolysis to give $[Bu^t(OH)_2Si]_2O$, Section IV,H) as a stable crystalline solid in 94% yield. Its structure (Figs. 27 and 28) has some similarities to that of $[Bu^t(OH)_2Si]_2O$, in that the molecules are joined by hydrogen bonds into sheets with alternating Bu^t groups above and below the sheet such that they prevent interactions between the sheets by forming strongly hydrophobic regions.Each molecule uses all six of its potential hydrogen-bonding sites (three acceptor and three donor) to interact with four other molecules, two in a pairwise manner (cf. the $R_2Si(OH)_2$ dimer motif **65**) and two forming single hydrogen bonds to the molecule (*319*).

The hydrolysis of $Os(SiCl_3)Cl(CO)(PPh_3)_2$ in $NaOH/H_2O$/THF affords the silanetriol complex $Os[Si(OH)_3]Cl(CO)(PPh_3)_2$ in good yield. Surprisingly the compound shows no hydrogen bonding involving OH···Cl or OH···OH interactions but there is an intramolecular $OH\cdots C_{aromatic}$ distance of 3.17 Å and a band in the IR spectrum at 3616 cm^{-1} also suggests that there is an $OH\cdots\pi$ interaction. Intermolecular interactions are presumably prevented by the bulky PPh_3 ligands (*315*).

TABLE VI

STRUCTURAL DATA FOR COMPOUNDS CONTAINING ONE OR TWO $Si(OH)_2$ GROUPS

Compound	Si–OH (Å)	OH···X (Å)[a]	O···X (Å)[a]	O-H···X (°)[a]	Structural summary	Refs.
$Et_2Si(OH)_2$	1.638(3) 1.636(3)		2.679(6)– 2.727(6)		Sheets	*301*
$(allyl)_2Si(OH)_2$	1.63		2.53		Sheets	*300*
$Pr^i_2Si(OH)_2$	1.655(3), 1.663(4)		2.71. 2.74		Ladder chains	*305*
$Bu^t_2Si(OH)_2$	1.654(9) 1.646(3)		2.69, 2.77 2.785		Ladder chains	*40* *278*[b]
$[Bu^t_2Si(OH)_2(SnCl_3OH)_2]$[c]	1.690(4) 1.702(5)		3.247[d]		Silanediol unit links Cl_3SnOH dimers into columns via H-bonds; see also Table V	*272*
$(c\text{-}C_6H_{11})_2Si(OH)_2$	1.636(1) 1.643(1)	2.08, 2.15	2.733(2), 2.755(1)	169.0 170.3	Ladder chains	*292*
$(C_5Me_5)_2Si(OH)_2$	1.64(2)– 1.69(2)		2.65–2.75		Tetrameric, intermolecular OH···OH interactions only	*311*
$Ph_2Si(OH)_2$	1.636(3)– 1.649(3)	1.68–1.77	2.69–2.77	156.4–169.5	Columns of linked hexamers [data in table from Ref. *303*].	*302–304*
$Bu^tPhSi(OH)_2$					Ladder chains	*304*
$(o\text{-tolyl})_2Si(OH)_2$	1.629(4), 1.633(4)	2.21(3), 2.20(5)	2.82	154(4), 179(6)	Ladder chains	*307*

$[(Me_3Si)_3CSiF(OH)_2]_6 \cdot 2H_2O$	1.598(31)–1.682(25)			2.656–2.789	Hexameric, water molecules link two sets of three silanols	*310*
$(Me_3Si)_3CSi(O_2CCF_3)(OH)_2$	1.616(3)–1.633(3)	2.12(6)–2.18(6)[f] 1.96(5)–2.41(5)[g]	2.833(5)–2.918(5)[f]	158(6)–175(6)[f] 137(6)–161(6)[g]	Tetrameric via OH···OH and OH···O=C interactions	*312*
$(Me_3Si)_3CSiPh(OH)_2$	1.631(3) 1.653(3)	2.29	2.90	166	Dimeric	*84*
$[Si(OH)_2(bipy)_2]I_2 \cdot 2H_2O$	1.643(4)	1.69	2.687(11)		Monomeric, with silanol-to-water hydrogen bonds.	*313*
$Cp(CO)_2FeSiPr^i(OH)_2$					Helical ladder chains	*248*
$[Bu^t(OH)_2Si]_2O$	1.626(2)		2.678–2.690		Sheets	*314*
$[OsCl(CO)(PPh_3)_2Si(OH)_2]_2O$			3.17[d]		Monomeric, intramolecular OH···Cl, and OH···π interactions	*315*
$\{Ph_2SiO[Si(OH)_2]\}_2 \cdot 2C_5H_5N$	1.609(2)–1.616(2)	1.81(3)[h] 1.86(3)[h] 2.03(3) 2.06(3)	2.699(6)[h] 2.681(6)[h] 2.830(5) 2.812(5)	175(3)[h] 177(3)[h] 173.8(3) 175(1)	Chains and OH···N links to pyridine molecules	*316*

[a] X = oxygen unless otherwise stated.
[b] For a note on the reported differenes in the structure of $Bu^t_2Si(OH)_2$, see Ref. *292*.
[c] Compound cocrystallizes with $(Bu^t_2HOSi)_2O$.
[d] X = Cl.
[e] X = F.
[f] OH···OH distances.
[g] OH···O=C interaction.
[h] X = N.

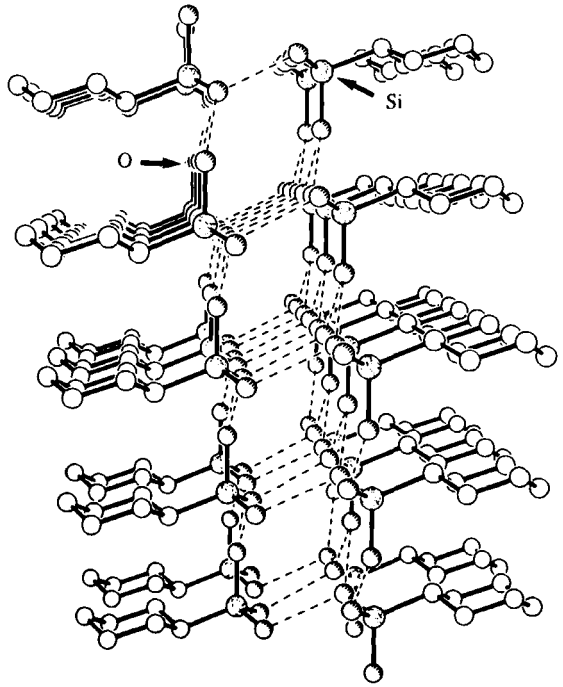

FIG. 25. A view parallel to the double-sheet hydrogen-bonded structure formed by *cyclo*-$C_6H_{11}Si(OH)_3$, showing the hydrophilic interior and the hydrophobic exterior of the sheet. Hydrogen atoms are omitted for clarity. Drawn using coordinates taken from the Cambridge Crystallographic Database.

Three closely related, highly bulky silanetriols, $(Me_3Si)_3CSi(OH)_3$, $(Me_3Si)_3SiSi(OH)_3$, and $(PhMe_2Si)_3CSi(OH)_3$, have been structurally characterized, the first two having very similar structures. The syntheses of the three compounds are, however, very different. Although $(Me_3Si)_3SiSiCl_3$ hydrolyzes readily in a H_2O/Et_2O/aniline mixture to give the triol (*44*), the corresponding trichlorides $(Me_3Si)_3CSiCl_3$ and $(PhMe_2Si)_3CSiCl_3$ are highly resistant towards hydrolysis [even $(Me_3Si)_3CSiBr_3$ may be recovered unchanged from boiling aqueous ethanol (*310*)], and alternative methods are required. Thus, $(Me_3Si)_3CSiH_2I$ may be hydrolyzed readily (the two hydrogen substituents providing less hindrance to attack than two chlorines) to give $(Me_3Si)_3CSiH_2OH$, which reacts with I_2 to give the unusual hydroxyiodosilane $(Me_3Si)_3CSiHIOH$, which may be further hydrolyzed using H_2O/DMSO to give $(Me_3Si)_3CSi(OH)_3$ (see Scheme 4) (*81*). The triphenyl compound may be prepared by hydrolysis of $(PhMe_2Si)_3CSiH_2Cl$ to give

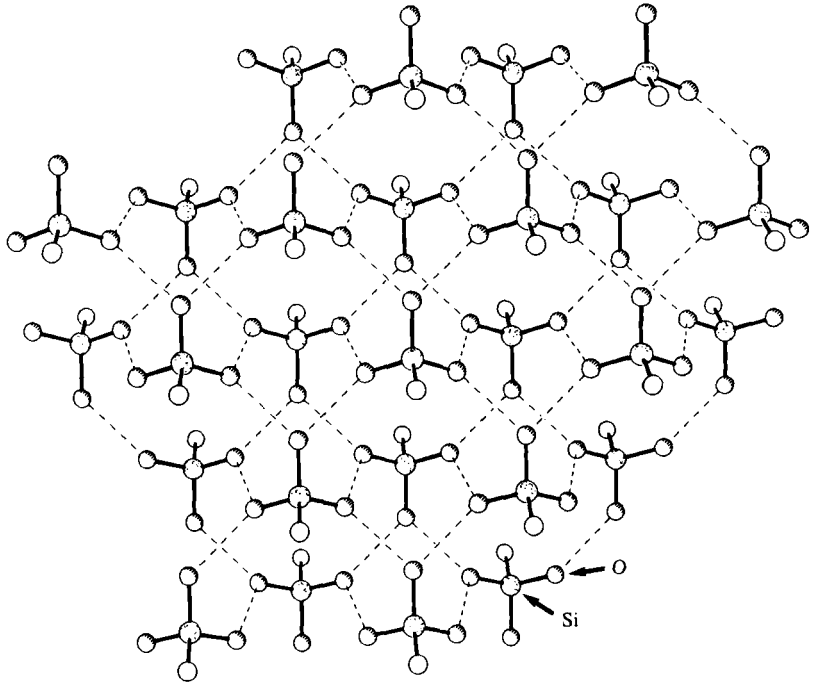

FIG. 26. A view perpendicular to the double sheet, showing the hydrogen-bonded network in *cyclo*-$C_6H_{11}Si(OH)_3$. Hydrogen atoms are omitted for clarity, as are all except the α-carbon atoms of the cyclohexyl rings. Drawn using coordinates taken from the Cambridge Crystallographic Database.

$(PhMe_2Si)_3CSiH_2OH$ and subsequent reaction with two equivalents of dimethyldioxirane to give $(PhMe_2Si)_3CSi(OH)_3$ (*310*).

The structures of $(Me_3Si)_3CSi(OH)_3$ and $(Me_3Si)_3SiSi(OH)_3$ are very similar and comprise hexameric cages (shown in Figs. 29 and 30) for the Si-centered compound (*44, 320*). The cage in the carbon-centered compound is slightly shorter and wider than the silicon analogue, the distance between the triangular end faces being 6.7 and 7.2 Å, respectively, and the diameter of the cages is about 6 and 5 Å, respectively.

The phenyl compound $(PhMe_2Si)_3CSi(OH)_3$ forms a tetramer via OH···OH hydrogen bonds as shown in Fig. 31. Some of the potential hydrogen bonding sites are not used in this way, which seems to be due to the presence of OH···π interactions. The structure is similar to that of $(Me_3Si)_3CSi(OH)_2O_2CCF_3$, **68**, in which there are OH···O=C rather than OH···OH interactions across the center of the tetramer. As in compounds **32** and **42**, there are several O···$C_{aromatic}$ distances of

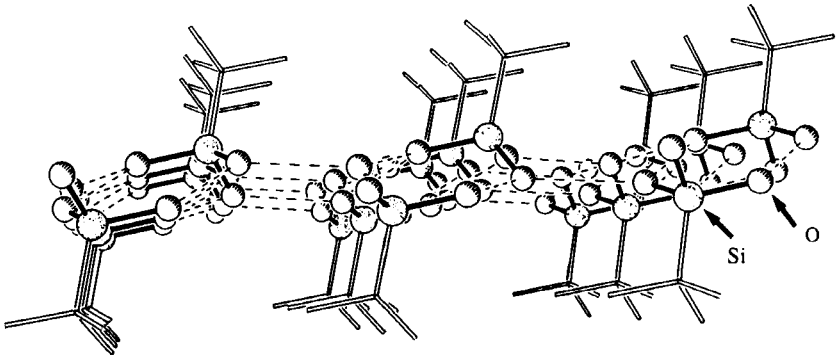

FIG. 27. A view parallel to the double-sheet hydrogen-bonded structure formed by $Bu^tSi(OH)_3$, showing the hydrophilic interior and the hydrophobic exterior of the sheet. Hydrogen atoms are omitted for clarity. Drawn using coordinates taken from the Cambridge Crystallographic Database.

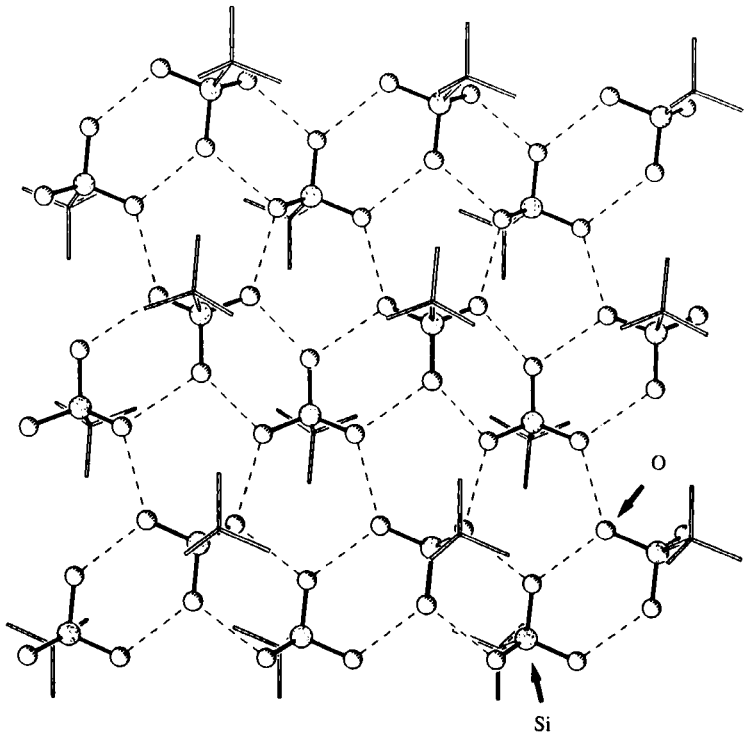

FIG. 28. A view perpendicular to the double sheet, showing the hydrogen-bonded network in $Bu^tSi(OH)_3$. Hydrogen atoms are omitted for clarity. Drawn using coordinates taken from the Cambridge Crystallographic Database.

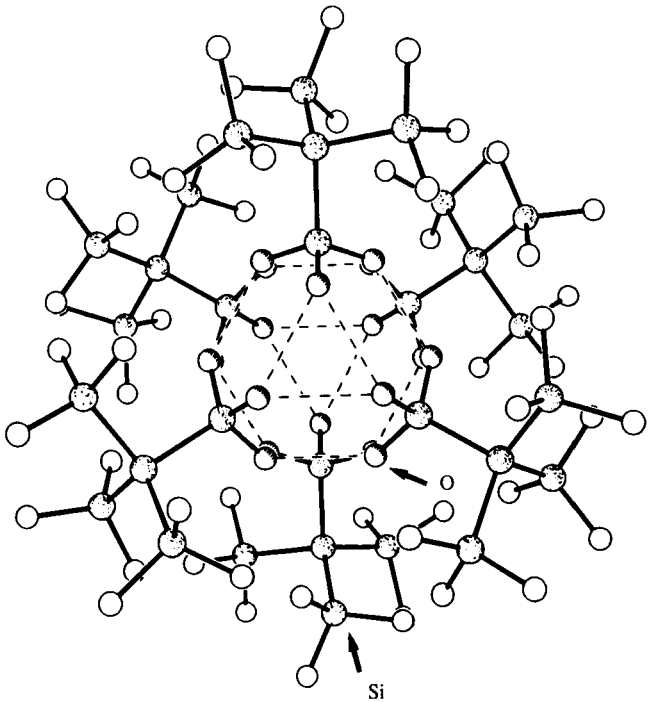

FIG. 29. The hydrogen-bonded hexamer formed by $(Me_3Si)_3SiSi(OH)_3$. Hydrogen atoms are omitted for clarity. Drawn using coordinates taken from the Cambridge Crystallographic Database.

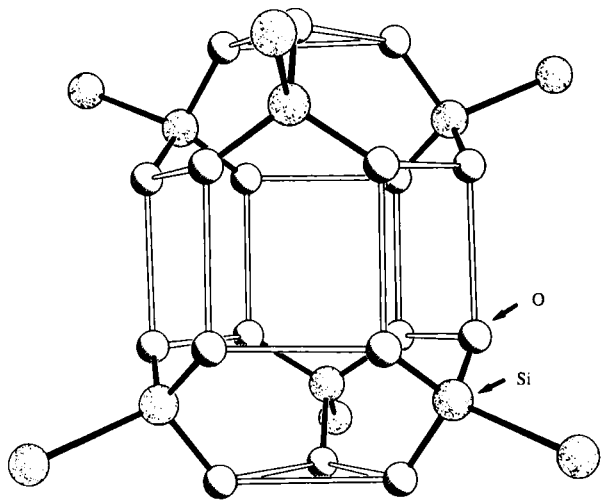

FIG. 30. The cage of oxygen atoms making up the core of the $(Me_3Si)_3SiSi(OH)_3$ hexamer (open bonds denote hydrogen bonds). Hydrogen atoms and Me_3Si groups are omitted for clarity. Drawn using coordinates taken from the Cambridge Crystallographic Database.

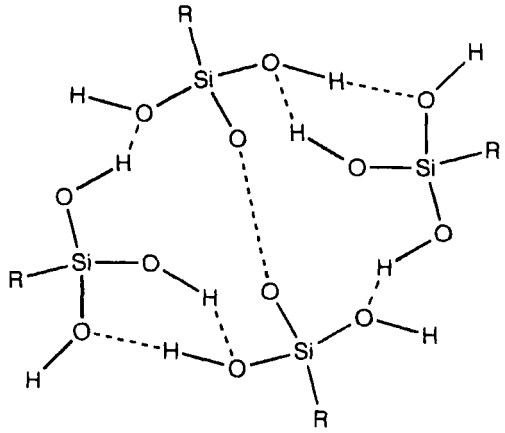

FIG. 31. A diagrammatic representation of the hydrogen-bonding arrangement in $(PhMe_2Si)_3CSi(OH)_3$. Hydrogen atoms on two of the oxygens could not be located (*321*).

less than 3.3 Å, indicative of such interactions, and in dilute CCl_4 solution there is a band at 3624 cm^{-1} in the IR spectrum, which is also consistent with such interactions (*321*).

V. Summary and Conclusions

The wide range of hydrogen-bonded arrangements found in silanols is perhaps not surprising in view of the variety of functional groups, e.g., SiOH, $Si(OH)_2$, $Si(OH)_3$, siloxanediol, that are available to silicon, not all of which are common functions in carbon chemistry. Although there are a variety of structures, many of which seem unrelated to each other, there are some common structural types, and an attempt is made here to categorize and describe their important general features.

As would be expected for highly polar species, most of the structures seen have a strongly hydrophilic region in which the hydrogen bonding occurs, and this is surrounded by hydrophobic alkyl groups, aryl groups, etc. Extended arrays including chains, sheets, and three-dimensional networks are encouraged by increasing the number of SiOH groups present and by reducing the size of the other substituents in the molecule. Many of the compounds with more than one SiOH present (and those containing one SiOH group and a second functional group capable of participating in hydrogen bonding) form a relatively small number of different types of structure, which can be seen as being built up from

TABLE VII

STRUCTURAL DATA FOR COMPOUNDS CONTAINING AN $Si(OH)_3$ GROUP

Compound	Si–OH (Å)	SiOH···X (Å)[a]	O···X (Å)[a]	Structural summary	Refs.
$Bu^tSi(OH)_3$	1.613(4), 1.631(4), 1.634(3)		2.705, 2.704	Sheets	*319*
$c\text{-}C_6H_{11}Si(OH)_3$	1.608(2), 1.637(2)		2.722(3), 2.724(2)	Double sheets	*318*
$Os[Si(OH)_3]Cl(CO)(PPh_3)_2$	1.624(5)–1.649(5)			Intramolecular OH···π interaction, possible intermolecular OH···π interaction	*315*
$(Me_3Si)_3CSi(OH)_3$	1.623(12), 1.666(14), 1.655(11)		2.82 2.93 3.12	Hexameric cages	*44, 320*
$(Me_3Si)_3SiSi(OH)_3$	1.65(2) 1.66(2) 1.69(2)		2.71(2) 2.78(2) 2.95(3)	Hexameric cages	*44*
$(PhMe_2Si)_3CSi(OH)_3$	1.615(3)–1.638(2)		2.818–3.157	Tetrameric	*321*

[a] X = O.

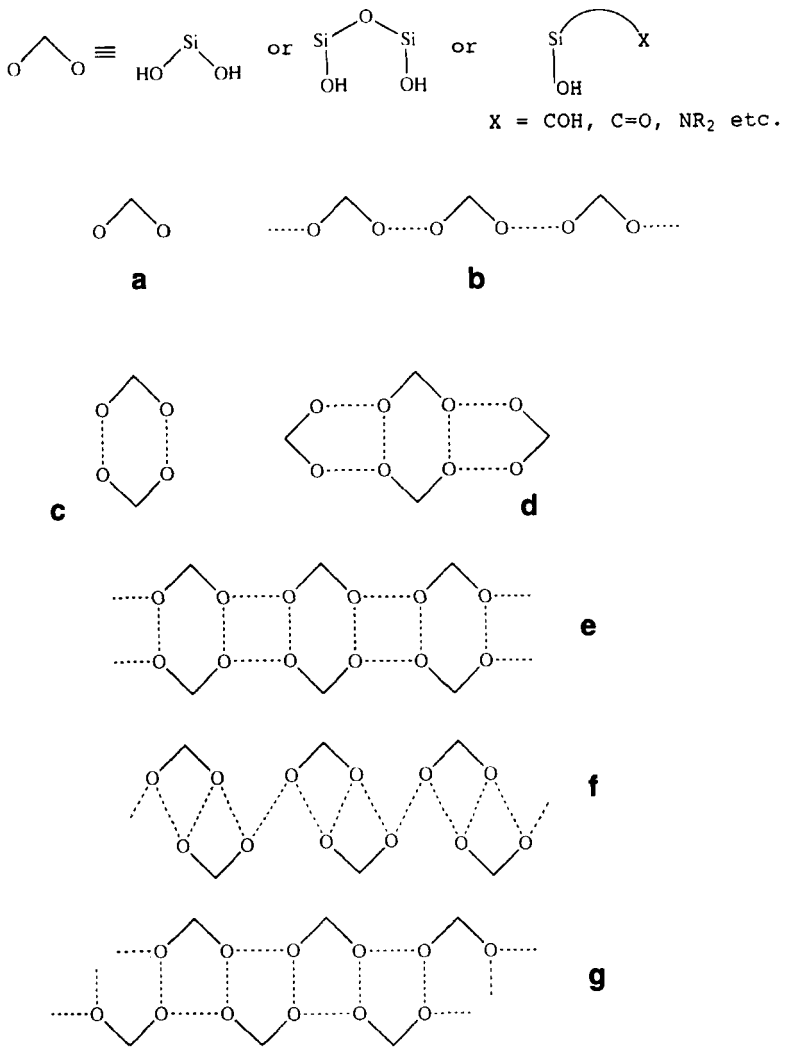

FIG. 32. Structural units found in silanols with two hydrogen-bonding sites.

simple units as shown in Fig. 32. Few, if any silanols have the simple structure (a), although the disiloxane shown in Fig. 13 bonds only to EtOH and not to itself. Large substituents, for example in $(Me_3Si)_3CSiPh(OH)_2$ and in $(C_5Me_5)_2Si(OH)_2$, lead to small discrete units (c) and (d), while compounds containing a single SiOH group together with a COH, C=O, or nitrogen functions tend to form simple chains (b). Smaller substituents allow chains of types (e), (f), and (g)

to be formed, cf. Fig. 10, and silanetriols may form double sheets or small clusters depending on the size of the substituent.

It should be noted that none of the structures {except the cocrystallized mixture of $(Bu^t_2HOSi)_2O$ with $[Bu^t_2Si(OH)_2(Cl_3SnOH)_2]$} described in this article contain a combination of SiOH, $Si(OH)_2$ or $Si(OH)_3$ groups together in same molecule. There would seem to be no synthetic reason why such compounds could not be prepared and structurally characterized, and it is likely that they will also exhibit extended hydrogen-bonded arrays, for example containing interconnected cages. This type of compound, together with further investigations into the selective formation of adducts of silanols, should ensure continued interest in the structural chemistry of silanols.

Furthermore, since this article was originally prepared several important papers have come to our attention. Improved procedures for the preparation of sensitive silanols such as $(HOMe_2Si)_2O$ and $Me_2Si(OH)_2$ from the corresponding chlorosilanes have been developed using either a two phase system or Et_3N as an HCl scavenger in the hydrolysis (*322*). Ab initio calculations have been carried out for the silicon equivalent, $(HSiOOH)_2$, of the formic acid dimer. The calculations show that the dissociation energy for such a hydrogen bonded dimer is much higher for the silicon analog, but that if double bonds to silicon are avoided, then a much lower energy is found for the cyclic dimer containing an Si_2O_2 four-membered ring (*323*). The first isolation of a protonated silanol $Bu^t_3SiOH_2^+$ has been achieved by treatment of the silicocationic species $[Bu^t_3Si]^+[Br_6CB_{11}H_6]^-$ with wet solvent. The stability of the protonated species seems to rely on the presence of the very poorly coordinating $Br_6CB_{11}H_6^-$ anion, and its structure suggests weak hydrogen bonding between the OH_2 group and bromine atoms on the carborane cage. It also has an unusually long Si–O bond of 1.779(9) Å (*324*). The reaction between acylsilanes $(Me_3Si)_3SiC(O)R$ (R = Bu^t, adamantyl or 2,2,2-bicyclooctyl) with $TiCl_4$ followed by an aqueous workup gives disilanols $(Me_3SiMeSiOH)C(SiMe_3)RSiMe_2OH$ (*325*). The structure of the bicyclooctyl compound shows that the hydrogen bonding arrangement is similar to that found in $(Me_3Si)_2C(SiMe_2OH)_2$ (see Section IV,D). The structural characterization of 1,3-$(HOMe_2Si)_2C_6H_4$ shows that the compound is very unlike the 1,4-isomer (see Section IV,D) but forms double chains of the type shown in Fig. 32e (*326*).

ACKNOWLEDGMENTS

The author wishes to thank Professors C. Eaborn and F. J. Feher and Dr. K. C. Molloy for supplying data prior to publication, and Dr. A. White for his patient and careful production of many of the figures found in this article.

References

1. Ladenburg, A., *Chem. Ber.* **4,** 901 (1871).
2. Ladenburg, A., *Ann. Chem. Pharm.* **164,** 300 (1872).
3. Sauer, J., and Hill, J.-R., *Chem. Phys. Lett.* **218,** 333 (1994).
4. Mittal, K. L., ed., "Silanes and Other Coupling Agents." VSP, Utrecht, 1992; Pluddeman, E. P., "Silane Coupling Agents," 1st ed. Plenum, New York, 1982; 2nd ed., 1990.
5. Edelmann, F. T., *Angew. Chem., Int. Ed. Engl.* **31,** 586 (1992); Herrmann, W. A., Anwander, R., Dufaud, V., and Scherer, W., *ibid.* **33,** 1285 (1994); Feher, F. J., and Tajima, T. L., *J. Am. Chem. Soc.* **116,** 2145 (1994).
6. Lebrun, J. J., and Porte, H., *in* "Comprehensive Polymer Science" (G. Allen and J. C. Bevington, eds.), Vol. 5, p. 593. Pergamon, Oxford, 1989; F. O. Stark, J. R. Falender, and A. P. Wright, *in* "Comprehensive Organometallic Chemistry" (G. Wilkinson, F. G. A. Stone, and E. W. Abel, eds.), Vol. 2, p. 305. Pergamon, Oxford, 1982; Clarson, S. J., and Semlyen, J. A., eds., "Siloxane Polymers." Ellis Horwood-PTR Prentice-Hall, Englewood Cliffs, NJ, 1993; Zeigler, J. M., and Fearon, F. W. G., eds., "Silicon Based Polymer Science." Am. Chem. Soc., Washington, DC, 1990.
7. Rubinsztajn, S., Cypryk, M., and Chojnowski, J., *J. Organomet. Chem.* **367,** 27 (1989); Guibergia-Pierron, M., and Sauvet, G., *Eur. Polym. J.* **28,** 29 (1992); Helary, G., and Sauvet, G., *ibid.,* 37; Kazmierski, K., Chojnowski, J., and McVie, J., *ibid.* **30,** 515 (1994).
8. See, for example, the "Proceedings of the Fourth, Fifth, and Sixth International Workshops on Glasses and Ceramics from Gels," published in *J. Non-Cryst. Solids* **100** (1988); **121** (1990); **147/148** (1992).
9. Chojnowski, J., Cypryk, M., Kazmierski, K., and Rózga, K. *J. Non-Cryst. Solids* **125,** 40 (1990).
10. Hench, L. L., and West, J. K., *Chem. Rev.* **90,** 33 (1990); and numerous articles *in* "Better Ceramics Through Chemistry V" (M. J. Hampden-Smith, W. G. Klemperer, and C. J. Brinker, eds.), Mater. Res. Soc., Vol. 271. Materials Research Society, Pittsburgh, 1992.
11. For a discussion, see Eaborn, C., "Organosilicon Compounds," p. 198. Butterworth, London, 1960.
12. Gooden, R., *Inorg. Chem.* **22,** 2272 (1983).
13. Curtice, J., Gilman, H., and Hammond, G. S., *J. Am. Chem. Soc.* **79,** 4754 (1957).
14. Nagai, Y., Honda, K., and Migita, T., *J. Organomet. Chem.* **8,** 372 (1967).
15. Sommer, L. H., Ulland, L. A., and Parker, G. A., *J. Am. Chem. Soc.* **94,** 3469 (1972).
16. Al-Shali, S. A., Eaborn, C., Fatah, F. A., and Najim, S. T., *J. Chem. Soc., Chem. Commun.,* 318 (1984).
17. Ayoko, G. A., and Eaborn, C., *J. Chem. Soc., Perkin Trans. 2,* 1047 (1987).
18. Lickiss, P. D., and Lucas, R., unpublished results.
19. Duffaut, N., Calas, R., and Macé, J., *Bull. Chem. Soc. Fr.,* 1971 (1959).
20. Wiberg, E., and Amberger, E., "Hydrides of the Elements of Main Groups I–IV," p. 523. Elsevier, Amsterdam, 1971.
21. Ouellette, R. J., and Marks, D. L., *J. Organomet. Chem.* **11,** 407 (1968).
22. Spialter, L., Pazdernik, L., Bernstein, S., Swansiger, W. A., Buell, G. R., and Freeburger, M. E., *J. Am. Chem. Soc.* **93,** 5682 (1971).
23. Dexheimer, E. M., and Spialter, L., *J. Organomet. Chem.* **102,** 21 (1975).

24. Corey, E. J., Mehrotra, M. M., and Khan, A. U., *J. Am. Chem. Soc.* **108,** 2472 (1986).
25. Alexandrov, Yu. A., and Taunin, B. I., *Russ. Chem. Rev. (Engl. Transl.)* **46,** 905 (1977).
26. Alexandrov, Yu. A., *J. Organomet. Chem.* **238,** 1 (1982).
27. Adam, W., Mello, R., and Curci, R., *Angew. Chem., Int. Ed. Engl.* **29,** 890 (1990).
28. Adam, W., Azzena, U., Prechtl, F., Hindahl, K., and Malisch, W., *Chem. Ber.* **125,** 1409 (1992).
29. Malisch, W., Schmitzer, S., Kaupp, G., Hindahl, K., Käb, H., and Wachtler, U., *in* "Organosilicon Chemistry from Molecules to Materials" (N. Auner and J. Weis, eds.), p. 185. VCH, Weinheim, 1994.
30. Eaborn, C., "Organosilicon Compounds," p. 200. Butterworth, London, 1960.
31. Wiberg, E., and Amberger, E., "Hydrides of the Elements of Main Groups I–IV," p. 526. Elsevier, Amsterdam, 1971.
32. Sommer, L. H., Korte, W. D., and Frye, C. L., *J. Am. Chem. Soc.* **94,** 3463 (1972).
33. Barnes, G. H., Jr., and Daughenbaugh, N. E., *J. Org. Chem.* **31,** 885 (1966).
34. Pittman, C. U., Jr., Patterson, W. J., and McManus, S. P., *J. Polym. Sci.* **13,** 39 (1975); Patterson, W. J., McManus, S. P., and Pittman, C. U., Jr., *Macromol. Synth.* **6,** 99 (1977); Merker, R. L., and Scott, M. J., *J. Polym. Sci., Part A* **2,** 15 (1964); Pittman, C. U., Jr., Patterson, W. J., and McManus, S. P., *J. Polym. Sci., Polym. Chem. Ed.* **14,** 1715 (1976).
35. Eaborn, C., "Organosilicon Compounds," p. 276. Butterworth, London, 1960.
36. Eaborn, C., "Organosilicon Compounds," p. 233. Butterworth, London, 1960.
37. Van Dyke, C. H., *in* "The Bond to Halogens and Halogenoids" (A. G. MacDiarmid, ed.), p. 167. Dekker, New York, 1972.
38. Sommer, L. H., Pietrusza, E. W., and Whitmore, F. C., *J. Am. Chem. Soc.* **68,** 2282 (1946).
39. Eaborn, C., *J. Chem. Soc.,* 2840 (1952).
40. Buttrus, N. H., Eaborn, C., Hitchcock, P. B., and Saxena, A. K., *J. Organomet. Chem.* **284,** 291 (1985).
41. Schütte, S., Freire-Erdbrügger, C., Klingebiel, U., and Sheldrick, G. M., *Phosphorous, Sulfur Silicon Relat. Elem.* **78,** 75 (1993).
42. Rutz, W., Lange, D., and Kelling, H., *Z. Anorg. Allg. Chem.* **528,** 98 (1985).
43. Takiguchi, T., *J. Am. Chem. Soc.* **81,** 2359 (1959).
44. Al-Juaid, S. S., Buttrus, N. H., Damja, R. I., Derouiche, Y., Eaborn, C., Hitchcock, P. B., and Lickiss, P. D., *J. Organomet. Chem.* **371,** 287 (1989).
45. Harris, G. I., *J. Chem. Soc.,* 5978 (1963).
46. George, P. D., Sommer, L. H., and Whitmore, F. C., *J. Am. Chem. Soc.* **75,** 1585 (1953).
47. Lehnert, R., *in* "Organosilicon Chemistry from Molecules to Materials" (N. Auner and J. Weis, eds.), p. 71. VCH, Weinheim, 1994.
48. Barton, T. J., and Tulley, C. R., *J. Organomet. Chem.* **172,** 11 (1979).
49. Davies, A. G., and Neville, A. G., *J. Organomet. Chem.* **436,** 255 (1992).
50. Graalmann, O., and Klingebiel, U., *J. Organomet. Chem.* **275,** C1 (1984).
51. Graalmann, O., Klingebiel, U., Clegg, W., Haase, M., and Sheldrick, G. M., *Angew. Chem., Int. Ed. Engl.* **23,** 891 (1984).
52. Sommer, L. H., and Tyler, L. J., *J. Am. Chem. Soc.* **76,** 1030 (1954).
53. Weidenbruch, M., Pesel, H., and Hieu, D. V., *Z. Naturforsch, B: Anorg. Chem., Org. Chem.* **35B,** 31 (1980).

54. Klingebiel, U., Schütte, S., and Schmidt-Bäse, D., *in* "The Chemistry of Inorganic Ring Systems" (R. Steudal, ed.), p. 75. Elsevier, Amsterdam, 1992.
55. Seyferth, D., and Nivert, C. L., *J. Am. Chem. Soc.* **99,** 5209 (1977).
56. Eaborn, C., Happer, D. A. R., Safa, K. D., and Walton, D. R. M., *J. Organomet. Chem.* **157,** C50 (1978).
57. Eaborn, C., Happer, D. A. R., and Safa, K. D., *J. Organomet. Chem.* **191,** 355 (1980).
58. Derouiche, Y., and Lickiss, P. D., *J. Organomet. Chem.* **407,** 41 (1991).
59. Eaborn, C., and Reed, D. E., *J. Chem. Soc., Perkin Trans. 2,* 1687 (1985).
60. Damrauer, R., *J. Organomet. Chem.* **216,** C1 (1981).
61. El-Kaddar, Y. Y., Eaborn, C., and Lickiss, P. D., *J. Organomet. Chem.* **460,** 7 (1993).
62. Eaborn, C., and Safa, K. D., *J. Organomet. Chem.* **234,** 7 (1982).
63. Weidenbruch, M., Peter, W., and Pierrard, C., *Angew. Chem., Int. Ed. Engl.* **15,** 43 (1976).
64. Boksányi, L., Liardon, O., and Kováts, E. Sv., *Helv. Chim. Acta* **59,** 717 (1976).
65. Birchall, J. D., Carey, J. G., and Howard, A. J., *Nature (London)* **266,** 154 (1977).
66. Kazoura, S. A., and Weber, W. P., *J. Organomet. Chem.* **243,** 149 (1983).
67. Schmidt-Bäse, D., and Klingebiel, U., *Z. Naturforsch., B: Anorg. Chem., Org. Chem.* **44B,** 395 (1989).
68. Voss, P., Meinicke, C., Popowski, E., and Kelling, H., *J. Prakt. Chem.* **320,** 34 (1978).
69. Schott, G., and Sprung, W. D., *Z. Anorg. Allg. Chem.* **333,** 76 (1964).
70. Popowski, E., Holst, N., and Kelling, H., *Z. Anorg. Allg. Chem.* **494,** 166 (1982).
71. Schott, G., and Kibbel, H. U., *Z. Anorg. Allg. Chem.* **311,** 53 (1961).
72. Holdt, H.-J., Schott, G., Popowski, E., and Kelling, H., *Z. Chem.* **23,** 252 (1983).
73. Chu, H.-K., Cross, R. P., and Crossan, D. I., *J. Organomet. Chem.* **425,** 9 (1992).
74. Brown, J. F., Jr., and Vogt, L. H., Jr., *J. Am. Chem. Soc.* **87,** 4313 (1965).
75. Feher, F. J., Newman, D. A., and Walzer, J. F., *J. Am. Chem. Soc.* **111,** 1741 (1989).
76. Wiberg, E., and Simmler, W., *Z. Anorg. Allg. Chem.* **282,** 330 (1955).
77. West, R., and Baney, R. H., *J. Am. Chem. Soc.* **81,** 6145 (1959).
78. Eaborn, C., Hitchcock, P. B., and Lickiss, P. D., *J. Organomet. Chem.* **252,** 281 (1983).
79. Lickiss, P. D., and Whittaker, S. M., unpublished results (1993).
80. Eaborn, C., and Lickiss, P. D., *J. Organomet. Chem.* **294,** 305 (1985).
81. Damja, R. I., and Eaborn, C., *J. Organomet. Chem.* **290,** 267 (1985).
82. Al-Shali, S. A. I., Eaborn, C., Fattah, F. A., and Najim, S. T., *J. Chem. Soc., Chem. Commun.,* 318 (1984).
83. Eaborn, C., and Fattah, F. A., *J. Organomet. Chem.* **396,** 1 (1990).
84. Aiube, Z. H., Buttrus, N. H., Eaborn, C., Hitchcock, P. B., and Zora, J. A., *J. Organomet. Chem.* **292,** 177 (1985).
85. Aiube, Z. H., and Eaborn, C., *J. Organomet. Chem.* **421,** 159 (1991).
86. Eaborn, C., and Reed, D. E., *J. Chem. Soc., Perkin Trans. 2,* 1695 (1985).
87. Al-Wassil, A. I., Eaborn, C., and Saxena, A. K., *J. Chem. Soc., Chem. Commun.,* 974 (1983).
88. Barton, T. J., and Tulley, C. R., *J. Org. Chem.* **43,** 3649 (1978).
89. Eaborn, C., Hitchcock, P. B., and Safa, K. D., *J. Organomet. Chem.* **222,** 187 (1981).
90. Smith, K. A., *J. Org. Chem.* **51,** 3827 (1986).
91. Osterholz, F. D., and Pohl, E. R., *J. Adhes. Sci. Technol.* **6,** 127 (1992); Oostendorp, D. J., Bertrand, G. L., and Stoffer, J. O., *ibid.,* 171; Arkles, B., Steinmetz, J. R., Zazyczny, J., and Mehta, P., *ibid.,* 193.

92. Hyde, J. F., *J. Am. Chem. Soc.* **75,** 2166 (1953).
93. Chojnowski, J., and Chrzczonowicz, S., *Bull. Acad. Pol. Sci., Ser. Sci. Chim.* **13,** 143 (1965).
94. Sauer, R. O., *J. Am. Chem. Soc.* **66,** 1707 (1944).
95. Sieburth, S. McN., and Mu, W., *J. Org. Chem.* **58,** 7584 (1993).
96. Åkerman, E., *Acta Chem. Scand.* **10,** 298 (1956).
97. Tacke, R., Linoh, H., Zilch, H., Wess, J., Moser, U., Mutschler, E., and Lambrecht, G., *Liebigs Ann. Chem.*, 2223 (1985).
98. Wrobel, D., and Wannagat, U., *Liebigs Ann. Chem.*, 211 (1983).
99. Breed, L. W., and Elliott, R. L., *J. Organomet. Chem.* **9,** 188 (1967).
100. Sorenson, W. R., and Campbell, T. W., "Preparative Methods of Polymer Chemistry," 2nd ed., p. 187. Wiley, New York, 1968.
101. Patterson, W. J., McManus, S. P., and Pittman, C. U., *J. Polym. Sci., Polym. Chem. Ed.* **12,** 837 (1974).
102. Michalska, Z., and Lasocki, Z., *Bull. Acad. Pol. Sci., Ser. Sci. Chim.* **19,** 757 (1971).
103. Andrianov, K. A., and Zhdanov, A. A., *Dokl. Chem. (Engl. Transl.)* **114,** 597 (1957).
104. Doyle, M. P., and West, C. T., *J. Org. Chem.* **40,** 3829 (1975).
105. Voronkov, M. G., Sviridova, N. G., and Borisov, S. N., *J. Gen. Chem. USSR (Engl. Transl.)* **39,** 1959 (1969).
106. Andrianov, K. A., Zhdanov, A. A., and Morgunova, E. F., *J. Gen. Chem. USSR (Engl. Transl.)* **27,** 173 (1957).
107. Shostakovsky, M. F., and Kondratyez, Kh. I., *Bull. Acad. Sci. USSR (Engl. Transl.)*, 985 (1956).
108. Dua, S. S., and Eaborn, C., *J. Organomet. Chem.* **204,** 21 (1981).
109. Damja, R. I., Eaborn, C., and Saxena, A. K., *J. Chem. Soc., Perkin Trans. 2,* 597 (1985).
110. Hudrlik, P. F., and Feasley, R., *Tetrahedron Lett.*, 1781 (1972).
111. Eaborn, C., and Mansour, A. I., *J. Chem. Soc., Perkin Trans. 2,* 729 (1985).
112. Uhlig, W., *Z. Anorg. Allg. Chem.* **618,** 144 (1992).
113. Eaborn, C., and Mahmoud, F. M. S., *J. Chem. Soc., Perkin Trans. 2,* 1309 (1981).
114. Eaborn, C., Lickiss, P. D., and Taylor, A. D., *J. Organomet. Chem.* **340,** 283 (1988).
115. Eaborn, C., El-Kaddar, Y. Y., and Lickiss, P. D., *Inorg. Chim. Acta* **198-200,** 337 (1992).
116. Eaborn, C., El-Kaddar, Y. Y., and Lickiss, P. D., *J. Chem. Soc., Chem. Commun.*, 1450 (1983).
117. Wojnowski, W., and Becker, B., *Z. Anorg. Allg. Chem.* **397,** 91 (1973).
118. Eaborn, C., *J. Chem. Soc.*, 3077 (1950).
119. Ried, W., and Suarez-Rivero, E., *Chem. Ber* **96,** 1475 (1963).
120. Chisholm, M. H., Huffman, J. C., and Wisemann, J. L., *Polyhedron* **10,** 1367 (1991).
121. Miner, C. S., Jr., Bryan, L. A., Holysz, R. P., Jr., and Pedlow, G. W., Jr., *Ind. Eng. Chem.* **39,** 1368 (1947).
122. Bailey, D. L., and Pines, A. N., *Ind. Eng. Chem.* **46,** 2363 (1954).
123. Sommer, L. H., Goldberg, G. M., Dorfman, E., and Whitmore, F. C., *J. Am. Chem. Soc.* **68,** 1083 (1946).
124. Sommer, L. H., and Baughman, G. A., *J. Am. Chem. Soc.* **83,** 3346 (1961).
125. Zimmermann, W., *Chem. Ber* **87,** 887 (1954).
126. Fearon, F. W. G., and Gilman, H., *J. Organomet. Chem.* **6,** 577 (1966).
127. Carilla, J., Fajarí, L., Juliá, L., Riera, J., Lloveras, J., Verdaguer, N., and Fita, I., *J. Organomet. Chem.* **423,** 163 (1992).

128. Morris, P. J., Fearon, F. W. G., and Gilman, H., *J. Organomet. Chem.* **9,** 427 (1967).
129. Brook, A. G., *J. Am. Chem. Soc.* **77,** 4827 (1955).
130. Brook, A. G., *J. Am. Chem. Soc.* **79,** 4373 (1957).
131. Buynak, J. D., Strickland, J. B., Lamb, G. W., Khasnis, D., Modi, S., Williams, D., and Zhang, H., *J. Org. Chem.* **56,** 7076 (1991).
132. Brook, A. G., *Adv. Organomet. Chem.* **7,** 95 (1968).
133. Ricci, A., and Degl'Innocenti, A., *Synthesis,* 647 (1989).
134. Page, P. C. B., Klair, S. S., and Rosenthal, S., *Chem. Soc. Rev.* **19,** 147 (1990).
135. Hengge, E., and Zimmermann, H., *Angew. Chem., Int. Ed. Engl.* **7,** 142 (1968).
136. Wittenberg, D., and Gilman, H., *Q. Rev., Chem. Soc.* **13,** 116 (1959).
137. George, M. V., and Gilman, H., *J. Am. Chem. Soc.* **81,** 3288 (1959).
138. Barton, T. J., and Hoekman, S. K., *J. Am. Chem. Soc.* **102,** 1584 (1980).
139. Wiberg, N., *J. Organomet. Chem.* **273,** 141 (1984).
140. Wiberg, N., Preiner, G., Wagner, G., and Köpf, H., *Z. Naturforsch., B: Chem. Sci.* **42B,** 1062 (1987).
141. Brook, A. G., Nyburg, S. C., Abdesaken, F., Gutekunst, B., Gutekunst, G., Kallury, R. K. M. R., Poon, Y. C., Chang, Y., and Wong-Ng, W., *J. Am. Chem. Soc.* **104,** 5667 (1982).
142. Wiberg, N., and Wagner, G., *Angew. Chem., Int. Ed. Engl.* **22,** 1005 (1983).
143. Wiberg, N., and Wagner, G., *Chem. Ber.* **119,** 1467 (1986).
144. Wiberg, N., and Köpf, H., *J. Organomet. Chem.* **315,** 9 (1986).
145. De Young, D. J., Fink, M. J., West, R., and Michl, J., *Main Group Met. Chem.* **10,** 19 (1987).
146. Masamune, S., Eriyama, Y., and Kawase, T., *Angew. Chem., Int. Ed. Engl.* **26,** 584 (1987).
147. Masamune, S., Murakami, S., and Tobita, H., *Organometallics* **2,** 1464 (1983).
148. Wiberg, N., Schurz, K., Reber, G., and Müller, G., *J. Chem. Soc., Chem. Commun.,* 591 (1986).
149. Bolotov, B. A., Kharitonov, N. P., Batyaev, E. A., and Rumyantseva, E. G., *J. Gen. Chem. USSR (Engl. Transl.)* **37,** 2002 (1967).
150. Pankratova, V. N., Stepovik, L. P., Lomakova, I. V., and Pogodina, L. A., *J. Gen. Chem. USSR (Engl. Transl.)* **42,** 1740 (1972).
151. Sollott, G. P., and Peterson, W. R., Jr., *J. Am. Chem. Soc.* **89,** 6783 (1967).
152. Bassindale, A. R., and Taylor, P. G., *in* "The Chemistry of Organic Silicon Compounds" (S. Patai and Z. Rappoport, eds.), Vol. 1, Chapter 12, p. 809. Wiley, Chichester, 1989.
153. Badger, R. M., and Bauer, S. H., *J. Chem. Phys.* **5,** 839 (1937).
154. Bogunovic, Lj. J., Dragojevic, M. D., Ribnikar, S. V., and Mioc, U. B., *J. Mol. Struct.* **175,** 271 (1988).
155. Salinger, R. M., and West, R., *J. Organomet. Chem.* **11,** 631 (1968).
156. Mioc, U. B., Bogunovic, Lj. J., Ribnikar, S. V., and Dragojevic, M. D., *J. Mol. Struct.* **177,** 379 (1988).
157. Mioc, U. B., Bogunovic, Lj. J., Ribnikar, S. V., and Stankovic, N., *J. Serb. Chem. Soc.* **54,** 541 (1989).
158. Holdt, H. J., Popowski, E., and Kelling, H., *Z. Anorg. Allg. Chem.* **519,** 233 (1984).
159. Voss, P., Elsner, A., Popowski, E., Schott, G., and Kelling, H., *Z. Anorg. Allg. Chem.* **445,** 219 (1978).
160. Drozdov, V. A., Kreshkov, A. P., and Knyzev, V. N., *J. Gen. Chem. USSR (Engl. Transl.)* **38,** 1781 (1968).

161. Popowski, E., Kelling, H., and Schott, G., *Z. Anorg. Allg. Chem.* **391,** 137 (1972).
162. Nillius, O., and Kriegsmann, H., *Spectrochim. Acta, Part A* **26A,** 121 (1970).
163. Steward, O. W., and Fussaro, D. R., *J. Organomet. Chem.* **129,** C28 (1977).
164. Bilda, S., Popowski, E., and Kelling, H., *Z. Chem.* **27,** 223 (1987).
165. Schott, G., and Popowski, E., *Z. Anorg. Allg. Chem.* **380,** 283 (1971).
166. West, R., and Baney, R. H., *J. Inorg. Nucl. Chem. Lett.* **7,** 297 (1958).
167. Arm, H., Hochstrasser, K., and Schindler, P. W., *Chimia* **28,** 237 (1974).
168. McEwen, W. K., *J. Am. Chem. Soc.* **58,** 1124 (1936).
169. Eaborn, C., and Stanczyk, W. A., *J. Chem. Soc., Perkin Trans. 2,* 2099 (1984).
170. Damrauer, R., Simon, R., and Krempp, M., *J. Am. Chem. Soc.* **113,** 4431 (1991).
171. Grimm, D. T., and Bartmess, J. E., *J. Am. Chem. Soc.* **114,** 1227 (1992).
172. Gordon, M. S., Damrauer, R., and Krempp, M., *J. Phys. Chem.* **97,** 7820 (1993).
173. Allred, L., Rochow, E. G., and Stone, F. G. A., *J. Inorg. Nucl. Chem.* **2,** 416 (1956).
174. Williams, E. A., Cargioli, J. D., and Larochelle, R. W., *J. Organomet. Chem.* **108,** 153 (1976).
175. Hampton, J. F., Lacefield, C. W., and Hyde, J. F., *Inorg. Chem.* **4,** 1659 (1965).
176. Brook, A. G., and Pannell, K. H., *J. Organomet. Chem.* **8,** 179 (1967).
177. Peddle, G. J., Woznow, R. J., and McGeachin, S. G., *J. Organomet. Chem.* **17,** 331 (1969).
178. Kreshkov, A. P., Andrianov, V. F., and Drozdov, V. A., *Russ. J. Phys. Chem. (Engl. Transl.)* **46,** 1605 (1972).
179. Reichstat, M. M., Mioc, U. B., Bogunovic, Lj. J., and Ribnikar, S. V., *J. Mol. Struct.* **244,** 283 (1991).
180. West, R., Baney, R. H., and Powell, D. L., *J. Am. Chem. Soc.* **82,** 6269 (1960).
181. West, R., and Baney, R. H., *J. Phys. Chem.* **64,** 822 (1960).
182. Rouvière, J., Monnier, A., and Salvinien, J., *C. R. Seances Acad. Sci., Ser. C* **267,** 1635 (1968).
183. Kagiya, T., Sumida, Y., Watanabe, T., and Tachi, T., *Bull. Chem. Soc. Jpn.* **44,** 923 (1971).
184. Matwiyoff, N. A., and Drago, R. S., *J. Organomet. Chem.* **3,** 393 (1965).
185. Leites, L. A., Yadritseva, T. S., Dement'ev, V. V., Antipova, B. A., Frunze, T. M., and Zhdanov, A. A., *Organomet. Chem. USSR (Engl. Transl.)* **2,** 537 (1989).
186. Bourne, S. A., Nassimbeni, L. R., Weber, E., and Skobridis, K., *J. Org. Chem.* **57,** 2438 (1992).
187. Harris, G. I., *J. Chem. Soc. B,* 488, 492 (1970).
188. Jarvie, A. W., Holt, A., and Thompson, J., *J. Organomet. Chem.* **11,** 623 (1968).
189. Kagiya, T., Sumida, Y., and Tachi, T., *Bull. Chem. Soc. Jpn.* **43,** 3716 (1970).
190. Harris, G. I., *J. Chem. Soc. B,* 2083 (1971).
191. Apeloig, Y., *in* "The Chemistry of Organic Silicon Compounds" (S. Patai and Z. Rappoport, eds.), Part 1, p. 79. Wiley, Chichester, 1989.
192. Ragavachari, K., Chandrasekhar, J., and Frisch, M. J., *J. Am. Chem. Soc.* **104,** 3779 (1982).
193. Luke, B. T., Pople, J. A., Krogh-Jesperson, M.-B., Apeloig, Y., Chandrasekhar, J., and Schleyer, P. von R., *J. Am. Chem. Soc.* **108,** 260 (1986).
194. Reed, A. E., Schade, C., Schleyer, P. von R., Kamath, P. V., and Chandrasekhar, J., *J. Chem. Soc., Chem. Commun.,* 67 (1988).
195. Hargittai, I., and Seip, H. M., *Acta Chem. Scand., Ser. A* **A30,** 153 (1976).
196. Apeloig, Y., and Stanger, A., *J. Organomet. Chem.* **346,** 305 (1988).
197. Hess, A. C., McMillan, P. F., and O'Keeffe, M., *J. Phys. Chem.* **91,** 1395 (1987).

198. Hertler, W. R., Dixon, D. A., Matthews, E. W., Davidson, F., and Kitson, F. G., *J. Am. Chem. Soc.* **109,** 6532 (1987).
199. O'Keeffe, M., and Gibbs, G. V., *J. Chem. Phys.* **81,** 876 (1984).
200. Sohn, H., Tan, R. P., Powell, D. R., and West, R., *Organometallics* **13,** 1390 (1994).
201. Gibbs, G. V., *Am. Mineral.* **67,** 421 (1982).
202. Johnson, S. E., Deiters, J. A., Day, R. O., and Holmes, R. R., *J. Am. Chem. Soc.* **111,** 3250 (1989).
203. O'Keeffe, M., Domengès, B., and Gibbs, G. V., *J. Phys. Chem.* **89,** 2304 (1985).
204. Sheldrick, W. S., *in* "The Chemistry of Organic Silicon Compounds" (S. Patai and Z. Rappoport, eds.), Part 1, p. 227. Wiley, Chichester, 1989.
205. Ishikawa, M., Matsuzawa, S., Sugisawa, H., Yano, F., Kamitori, S., and Higuchi, T., *J. Am. Chem. Soc.* **107,** 7706 (1985).
206. Al-Juaid, S. S., Al-Nasr, A. K. A., Eaborn, C., and Hitchcock, P. B., *J. Organomet. Chem.* **429,** C9 (1992).
207. Masamune, S., Kabe, Y., Collins, S., Williams, D. J., and Jones, R., *J. Am. Chem. Soc.* **107,** 5552 (1985)
208. Eaborn, C., personal communication, 1994.
209. Watanabe, H., Takeuchi, K., Nakajima, K., Nagai, Y., and Goto, M., *Chem. Lett.*, 1343 (1988).
210. Lickiss, P. D., and White, A., unpublished results.
211. Al-Juaid, S. S., Al-Nasr, A. K., Eaborn, C., and Hitchcock, P. B., *J. Chem. Soc., Chem. Commun.*, 1482 (1991).
212. Al-Juaid, S. S., Al-Nasr, A. K., Eaborn, C., and Hitchcock, P. B., unpublished results quoted in Ref. *206.*
213. Al-Mansour, A. I., Al-Juaid, S. S., Eaborn, C., and Hitchcock, P. B., *J. Organomet. Chem.* **480,** 139 (1994).
214. Tacke, R., Strecker, M., Sheldrick, W. S., Heeg, E., Berndt, B., and Knapstein, K. M., *Z. Naturforsch, B: Anorg. Chem., Org. Chem.* **34B,** 1279 (1979).
215. Tacke, R., Strecker, M., Sheldrick, W. S., Ernst, L., Heeg, E., Berndt, B., Knapstein, C.-M., and Niedner, R., *Chem. Ber.* **113,** 1962 (1980).
216. Söderholm, M., *Acta Chem. Scand., Ser. B* **B38,** 303 (1984).
217. Söderholm, M. *Acta Chem. Scand., Ser. B* **B38,** 31 (1984).
218. Söderholm, M., *Acta Chem. Scand., Ser. B* **B38,** 95 (1984).
219. Tacke, R., Lange, H., Sheldrick, W. S., Lambrecht, G., Moser, U., and Mutschler, E., *Z. Naturforsch., B: Anorg. Chem., Org. Chem.* **B38,** 738 (1983).
220. Tacke, R., Strecker, M., Lambrecht, G., Moser, U., and Mutschler, E., *Liebigs Ann. Chem.* 922 (1983).
221. Sheldrick, W. S., Linoh, H., Tacke, R., Lambrecht, G., Moser, U., and Mutschler, E., *J. Chem. Soc., Dalton Trans.*, 1743 (1985).
222. Tacke, R., Pikies, J., Weisenberger, F., Ernst, L., Schomburg, D., Waelbroeck, M., Christophe, J., Lambrecht, G., Gross, J., and Mutschler, E., *J. Organomet. Chem.* **466,** 15 (1994).
223. Puff, H., Braun, K., and Reuter, H., *J. Organomet. Chem.* **409,** 119 (1991).
224. Ferguson, G., Gallagher, J. F., Glidewell, C., Low, J. N., and Scrimgeour, S., *Acta Crystallogr., Sect. C: Cryst. Struct. Commun.* **C48,** 1272 (1992).
225. Ferguson, G., Gallagher, J. F., Murphy, D., Spalding, T. R., Glidewell, C., and Holden, D. H., *Acta Crystallogr., Sect. C: Cryst. Struct. Commun.* **C48,** 1228 (1992).
226. Glidewell, C., and Liles, D. C., *Acta Crystallogr., Sect. B: Struct. Crystallogr. Cryst. Chem.* **B34,** 129 (1978).

227. Bourne, S. A., Nassimbeni, L. R., Skobridis, K., and Weber, E., *J. Chem. Soc., Chem Commun.*, 282 (1991).
228. Weber, E., Skobridis, K., and Goldberg, I., *J. Chem. Soc., Chem. Commun.*, 1195 (1989).
229. Babaian, E. A., Huff, M., Tibbals, F. A., and Hrncir, D. C., *J. Chem. Soc., Chem. Commun.*, 306 (1990).
230. Bourne, S. A., Johnson, L., Marais, C., Nassimbeni, L. R., Weber, E., Skobridis, K., and Toda, F., *J. Chem. Soc., Perkin Trans. 2*, 1707 (1991).
231. Malisza, K. L., Chao, L. C. F., Britten, J. F., Sayer, B. G., Jaouen, G., Top, S., Decken, A., and McGlinchey, M. J., *Organometallics* **12,** 2462 (1993).
232. Rengstl, A., and Schubert, U., *Chem. Ber.* **113,** 278 (1980).
233. Auner, N., Probst, R., Heikenwälder, C.-R., Herdtweck, E., Gamper, S., and Müller, G., *Z. Naturforsch.* **48B,** 1625 (1993).
234. Buttrus, N. H., Eaborn, C., Hitchcock, P. B., and Saxena, A. K., *J. Organomet. Chem.* **287,** 157 (1985).
235. Clegg, W., Sheldrick, G. M., Klingebiel, U., Bentmann, D., Henkel, G., and Krebs, B., *Acta Crystallogr., Sect. C: Cryst. Struct. Commun.* **C40,** 819 (1984).
236. Schmidt-Bäse, D., and Klingebiel, U., *Chem. Ber.* **122,** 815 (1989).
237. Puff, H., Hevendehl, H., Höfer, K., Reuter, H., and Schuh, W., *J. Organomet. Chem.* **287,** 163 (1985).
238. Schütte, S., Klingebiel, U., and Schmidt-Bäse, D., *Z. Naturforsch., B: Anorg. Chem., Org. Chem.* **48B,** 263 (1993).
239. Schütte, S., Pieper, U., Klingebiel, U., and Stalke, D., *J. Organomet. Chem.* **446,** 45 (1993).
240. Fronda, A., Krebs, F., Daucher, B., Werle, T., and Maas, G., *J. Organomet. Chem.* **424,** 253 (1992).
241. Lickiss, P. D., and Stubbs, K. M., *J. Organomet. Chem.* **421,** 171 (1991).
242. Pachler, K., and von Stackelberg, M., *Z. Kristallogr., Kristallgeom., Kristallphys., Kristallchem.* **119,** 15 (1963).
243. Bator, G., Jakubas, R., and Malarski, Z., *in* "Interactions of Water in Ionic and Nonionic Hydrates" (H. Kleeberg, ed.), p. 291. Springer-Verlag, Berlin, 1987.
244. Lickiss, P. D., Clipston, N. L., Rankin, D. W. H., and Robertson, H. E., *J. Mol. Struct.* **344,** 111 (1995).
245. McGeary, M. J., Coan, P. S., Folting, K., Streib, W. S., and Caulton, K. G., *Inorg. Chem.* **30,** 1723 (1991).
246. Brost, R. D., Bruce, G. C., and Stobart, S. R., *J. Chem. Soc., Chem Commun.*, 1580 (1986).
247. Auburn, M. J., Holmes-Smith, R. D., Stobart, S. R., Zaworotko, M. J., Cameron, T. S., and Kumari, A., *J. Chem. Soc., Chem. Commun.*, 1523 (1983).
248. Käb, H., Ries, W., Veith, M., and Malisch, W., *Int. Symp. Organosilicon Chem., 9th,* Edinburgh, *1990,* Abstract for Poster 3.25 (1990).
249. Dema, A. C., Lukehart, C. M., McPhail, A. T., and McPhail, D. R., *J. Am. Chem. Soc.* **112,** 7229 (1990).
250. Chang, L. S., Johnson, M. P., and Fink, M. J., *Organometallics* **10,** 1219 (1991).
251. Dilthey, W., *Chem. Ber.* **38,** 4132 (1905).
252. Lightfoot, P., Glidewell, C., and Bruce, P. G., *J. Organomet. Chem.* **466,** 51 (1994).
253. Haque, M., Horne, W., Cremer, S. E., and Blankenship, C. S., *J. Chem. Soc., Perkin Trans. 2*, 395 (1983).
254. Eaborn, C., Hitchcock, P. B., and Lickiss, P. D., *J. Organomet. Chem.* **264,** 119 (1984).

255. Gusev, A. I., Los', M. G., Varezhkin, Yu. M., Morgunova, M. M., and Zhinkin, D. Ya., *J. Struct. Chem.* (*Engl. Transl.*) **17,** 329 (1976).
256. Varezhkin, Yu. M., Zhinkin, D. Ya., Morgunova, M. M., and Bocharev, V. N., *J. Gen. Chem. USSR* (*Engl. Transl.*) **45,** 2410 (1975).
257. Tacke, R., Hengelsberg, H., Klingner, E., and Henke, H., *Chem. Ber.* **125,** 607 (1992).
258. Lickiss, P. D., Redhouse, A. D., Thompson, R. J., Stanczyk, W. A., and Rózga, K., *J. Organomet. Chem.* **453,** 13 (1993).
259. Polishchuk, A. P., Timofeeva, T. V., Makarova, N. N., Antipin, M. Yu., and Struchkov, Yu. T., *Liq. Cryst.* **9,** 433 (1991).
260. Polishchuk, A. P., Antipin, M. Yu., Timofeeva, T. V., Makarova, N. N., Golovina, N. A., and Struchkov, Yu. T., *Sov. Phys.—Cryst.* (*Engl. Transl.*) **36,** 50 (1991).
261. Polishchuk, A. P., Makarova, N. N., Antipin, M. Yu., Timofeeva, T. V., Kravers, M. A., and Struchkov, Yu. T., *Sov. Phys.—Crystallogr.* (*Engl. Transl.*) **35,** 258 (1990).
262. Hossain, M. A., and Hursthouse, M. B., *J. Crystallogr. Spectrosc. Res.* **18,** 227 (1988).
263. Shklover, V. E., Struchkov, Yu. T., Karpova, I. V., Odinets, V. A., and Zhdanov, A. A., *J. Struct. Khim.* (*Engl. Transl.*) **26,** 251 (1985).
264. Clegg, W., *Acta Crystallogr., Sect. C: Cryst. Struct. Commun.* **C39,** 901 (1983).
265. Lickiss, P. D., Drake, R., and Williams, D. J., unpublished results, 1994.
266. Khananashvili, L. M., Vardosanidze, Ts. N., Griunova, G. V., Shklover, V. E., Struchkov, Yu. T., Markarashvili, E. G., and Tsutsunava, M. Sh., *Izv. Akad. Nauk Gruz. SSR, Ser. Khim.* **10,** 262 (1984).
267. Ovchinikov, Yu. E., Zamaev, I. A., Struchkov, Yu. T., Astapova, T. V., and Zhdanov, A. A., *Organomet. Chem. USSR* (*Engl. Transl.*) **2,** 452 (1989).
268. Polishchuk, A. P., Timofeeva, T. V., Antipin, M. Yu., Makarova, N. N., Golovina, N. A., Struchkov, Yu. T., and Lavrentovich, O. D., *Organomet. Chem. USSR* (*Engl. Transl.*) **4,** 77 (1991).
269. Makarova, N. N., Kuz'min, N. N., Godovskii, Yu. K., and Matukhina, E. V., *Proc. Acad. Sci. USSR* **300,** 151 (1988).
270. Polishchuk, A. P., Makarova, N. N., Timofeeva, T. V., Antipin, M. Yu., Lavrentovich, O. D., Golovina, N. A., Puchkovskaya, G. A., Struchkov, Yu. T., and Godovskii, Yu. K., *Sov. Phys.—Crystallogr.* (*Engl. Transl.*) **35,** 261 (1990).
271. Dobros, S., Mátrai, E., and Castéllucci, E., *J. Mol. Struct.* **43,** 141 (1978).
272. Mazzah, A., Haudi-Mazzah, A., Noltemeyer, M., and Roesky, H. W., *Z. Anorg. Allg. Chem.* **604,** 93 (1991).
273. Ruud, K. A., Sepeda, J. S., Tibbals, F. A., and Hrncir, D. C., *J. Chem. Soc., Chem. Commun.*, 629 (1991).
274. Hossain, M. A., Rahman, M. T., Rasul, G., Hursthouse, M. B., and Hussain, B., *Acta Crystallogr., Sect. C: Cryst. Struct. Commun.* **C44,** 1318 (1988).
275. Ando, W., Kako, M., Akasaka, T., and Nagase, S., *Organometallics* **12,** 1514 (1993).
276. Chogovadze, T. V., Nogaideli, A. I., Khananashvili, L. M., Nakaidze, L. I., Tskhovrebashvili, V. S., Gusev, A. I., and Nesterov, D. U., *Proc. Acad. Sci. USSR* **246,** 281 (1979).
277. Behbehani, H., Brisdon, B. J., Mahon, M. F., Molloy, K. C., and Mazhar, M., *J. Organomet. Chem.* **463,** 41 (1993).
278. Graalmann, O., Klingebiel, U., Clegg, W., Haase, M., and Sheldrick, G. M., *Chem. Ber.* **117,** 2988 (1984).

279. Shklover, V. E., Dubchak, I. L., Struchkov, Yu. T., Mileshkevich, V. P., Nikolaev, G. A., and Tsiganov, Yu. V., *J. Struct. Chem.* (*Engl. Transl.*) **22,** 225 (1981).
280. Furmanova, N. G., Andrianov, V. I., and Makarova, N. N., *J. Struct. Chem.* (*Engl. Transl.*) **28,** 256 (1987).
281. Feher, F. J., and Newman, D. A., *J. Am. Chem. Soc.* **112,** 1931 (1990).
282. Feher, F. J., and Newman, D. A., *J. Am. Chem. Soc.* **112,** footnote 13 (1990).
283. Feher, F. J., personal communication, 1993.
284. Feher, F. J., Newman, D. A., and Walzer, J. F., *J. Am. Chem. Soc.* **111,** footnote 13 (1989).
285. West, R., and Pham, E. K., *J. Organomet. Chem.* **403,** 43 (1991).
286. Párkányi, L., Stüger, H., and Hengge, E., *J. Organomet. Chem.* **333,** 187 (1987).
287. Ovchinikov, Y. E., Shklover, V. E., Struchkov, Yu. T., Dement'ev, V. V., Frunze, T. M., and Antipova, B. A., *J. Organomet. Chem.* **335,** 157 (1987).
288. Ferguson, G., Gallagher, J. F., Glidewell, C., and Zakaria, C. M., *Acta Crystallogr., Sect. C: Cryst. Struct. Commun.* **C50,** 70 (1994).
289. Chen, B., Xie, Z., and Wang, J., *Jiegou Huaxue* **3,** 113 (1984); *Chem. Abstr.* **103,** 62901y.
290. Yanovskii, A. I., Dubchak, I. L., Shklover, V. E., Struchkov, Yu. T., Kalinin, V. N., Izmailov, B. A., Myakushev, V. D., and Zakharin, L. I., *J. Struct. Chem.* (*Engl. Transl.*) **23,** 728 (1982).
291. Aigbirhio, F. I., Al-Juaid, S. S., Eaborn, C., Habtemariam, A., Hitchcock, P. B., and Smith, J. D., *J. Organomet. Chem.* **405,** 149 (1991).
292. Buttrus, N. H., Eaborn, C., Hitchcock, P. B., Lickiss, P. D., and Taylor, A. D., *J. Organomet. Chem.* **309,** 25 (1986).
293. Kakudo, M., Kasai, N., and Watase, T., *J. Chem. Phys.* **21,** 1894 (1953).
294. Alexander, L. E., Northolt, M. G., and Engmann, R., *J. Phys. Chem.* **71,** 4298 (1967).
295. Al-Juaid, S. S., Eaborn, C., Hitchcock, P. B., and Lickiss, P. D., *J. Organomet. Chem.* **353,** 297 (1988).
296. Dubchak, I. L., Shklover, V. E., Struchkov, Yu. T., Khynku, E. S., and Zhdanov, A. A., *J. Struct. Chem.* (*Engl. Transl.*) **22,** 770 (1981).
297. Hambley, T. W., Maschmeyer, T., and Masters, A. F., *Appl. Organomet. Chem.* **6,** 253 (1992).
298. Kakudu, M., and Watase, T., *Technol. Rep. Osaka Univ.* **2,** 247 (1952); *Chem. Abstr.* **47,** 10309e (1953).
299. Kakudo, M., and Watase, T., *J. Chem. Phys.* **21,** 167 (1953).
300. Kasai, N., and Kakudo, M., *Bull. Chem. Soc. Jpn.* **27,** 605 (1954).
301. Tomlins, P. E., Lydon, J. E., Akrigg, D., and Sheldrick, B., *Acta Crystallogr., Sect. C: Cryst. Struct. Commun.* **C41,** 941 (1985).
302. Fawcett, J. K., Camerman, N., and Camerman, A., *Can. J. Chem.* **55,** 3631 (1977).
303. Párkányi, L., and Bocelli, G., *Cryst. Struct. Commun.* **7,** 335 (1978).
304. Kaur, H., Lickiss, P. D., and Redhouse, A. D., unpublished results.
305. Buttrus, N. H., Eaborn, C., Hitchcock, P. B., and Lickiss, P. D., *J. Organomet. Chem.* **302,** 159 (1986).
306. Puff, H., Franken, S., Schuh, W., and Schwab, W., *J. Organomet. Chem.* **254,** 33 (1983).
307. Al-Juaid, S. S., Eaborn, C., Hitchcock, P. B., and Lickiss, P. D., *J. Organomet. Chem.* **362,** 17 (1989).
308. Eaborn, C., and Hartshorne, N. H., *J. Chem. Soc.,* 549 (1955).
309. Bunning, J. E., Lydon, J. E., Eaborn, C., Jackson, P. M., Goodby, J. W., and Gray, G. W., *J. Chem. Soc., Faraday, Trans. 1* **78,** 713 (1982).

310. Whittaker, S. M., Ph.D. Thesis, University of Salford, United Kingdom, (1993).
311. Al-Juaid, S. S., Eaborn, C., Hitchcock, P. B., Lickiss, P. D., Möhrke, A., and Jutzi, P., *J. Organomet. Chem.* **384,** 33 (1990).
312. Al-Juaid, S. S., Eaborn, C., and Hitchcock, P. B., *J. Organomet. Chem.* **423,** 5 (1992).
313. Sawitzki, G., G. von Schnering, H., Kummer, D., and Seshadri, T., *Chem. Ber.* **111,** 3705 (1978).
314. Lickiss, P. D., Litster, S. A., Redhouse, A. D., and Wisener, C. A., *J. Chem. Soc., Chem. Commun.*, 173 (1991).
315. Rickard, C. E. F., Roper, W. R., Salter, D. M., and Wright, L. J., *J. Am. Chem. Soc.* **114,** 9682 (1992).
316. Shklover, V. E., Dubchak, I. L., Struchkov, Yu. T., Khynku, E. S., and Zhdanov, A. A., *J. Struct. Chem.* (*Engl. Transl.*) **22,** 229 (1981).
317. Andrianov, K. A., Zhdanov, A. A., Kurasheva, N. A., and Khynku, E. S., *Dokl. Chem.* (*Engl. Transl.*) **240,** 229 (1978).
318. Ishida, H., Koenig, J. L., and Gardner, K. C., *J. Chem. Phys.* **77,** 5748 (1982).
319. Winkhofer, N., Roesky, H. W., Noltemeyer, M., and Robinson, W. T., *Angew. Chem., Int. Ed. Engl.* **31,** 599 (1992).
320. Buttrus, N. H., Damja, R. I., Eaborn, C., Hitchcock, P. B., and Lickiss, P. D., *J. Chem. Soc., Chem. Commun.*, 1385 (1985).
321. Fronczek, F., Lickiss, P. D., and Whittaker, S. M., unpublished results, 1993.
322. Cella, J. A., and Carpenter, J. C., *J. Organomet. Chem.* **480,** 23 (1994).
323. Seidl, E. T., and Schafer, H. F., III, *J. Amer. Chem. Soc.* **111,** 1569 (1989).
324. Xie, Z., Bau, R., and Reed, C. A., *J. Chem. Soc., Chem. Commun.* 2519 (1994).
325. Brook, A. G., Hesse, M., Baines, K. M., Kumarathasan, R., and Lough, A. J., *Organometallics* **12,** 4259 (1993).
326. Arndt, H.-D., Goodgame, D. M. L., Lickiss, P. D., and Williams, D. J., unpublished results.

ADVANCES IN INORGANIC CHEMISTRY, VOL. 42

STUDIES OF THE SOLUBLE METHANE MONOOXYGENASE PROTEIN SYSTEM: STRUCTURE, COMPONENT INTERACTIONS, AND HYDROXYLATION MECHANISM

KATHERINE E. LIU and STEPHEN J. LIPPARD

Department of Chemistry, Massachusetts Institute of Technology, Cambridge, Massachusetts 02139

I. Introduction
II. Structural Studies of sMMO Hydroxylase
  A. The Oxidized Hydroxylase, H_{ox}
  B. The Mixed-Valent Hydroxylase, H_{mv}
  C. The Reduced Hydroxylase, H_{red}
III. Component Interactions
  A. Catalytic Activity
  B. Reduction Potentials of the Hydroxylase
  C. Product Distributions
  D. Yields and Rate Constants with Single Turnover Reactions
IV. Mechanism of Hydroxylation
  A. Reaction of H_{red} with Dioxygen
  B. Reaction of Q with Substrate
V. Conclusions
  References

I. Introduction

Methanotrophic bacteria have the fascinating ability to use methane as their sole source of carbon and energy (*1*). The organisms play a crucial role in the atmospheric balance of this greenhouse gas and in the overall global carbon cycle by annually consuming billions of tons of methane (*2*, *3*). Because these bacteria are capable of converting methane into methanol at ambient pressure and temperature, methanotrophs have received much attention in the search for alternative methods for methanol synthesis (*4*), which are currently not cost-efficient and require high temperatures and pressures (*5*). In addition to methane, these organisms can metabolize a wide variety of other

Copyright © 1995 by Academic Press, Inc.
All rights of reproduction in any form reserved.

substrates (*6–8*), spurring interest in their bioremedial applications (*9–13*).

Methanotrophs rely on the enzymatic system methane monooxygenase (MMO) to catalyze the first step in the metabolism of methane, shown in Eq. (1) (*1, 14*).

$$CH_4 + O_2 + H^+ + NADH \rightarrow CH_3OH + H_2O + NAD^+ \quad (1)$$

The soluble MMO (sMMO) systems in two organisms, *Methylococcus capsulatus* (Bath) and *Methylosinus trichosporium* OB3b, have been the focus of intense research in recent years. A detailed discussion of the structure determination of the oxidized hydroxylase of sMMO from *M. capsulatus* (Bath) has recently appeared (*15*), as has a review focusing mainly on work with sMMO from *M. trichosporium* OB3b (*16*). In the present article, we cover progress toward understanding the structure of the nonheme iron catalytic center in its various oxidation states, interactions between components of MMO, and the current state of understanding the hydroxylation mechanism. Results for the sMMO systems from both organisms will be compared and contrasted.

In most methanotrophs, two distinct forms of MMO can exist, with the dominant species depending on the bioavailability of copper (*17*). The particulate MMO (pMMO) is a membrane-bound system which has been difficult to study because of its instability outside the cell. Recently, progress has been made in the isolation and characterization of pMMO from *M. capsulatus* (Bath), the activity of which was found to depend on the copper concentration within the membrane (*18, 19*). EPR and magnetic susceptibility studies indicated that pMMO contains an exchange-coupled trinuclear Cu cluster (*19*). Since the EPR signal of the chemically reduced tricopper cluster converted to the signal of the oxidized, or resting, state of the enzyme upon exposure to dioxygen, the cluster is believed to occur at the active site of pMMO (*19*).

Under conditions of copper deficiency, some methanotrophs can express a cytosolic, soluble form of MMO (sMMO) (*20–23*), the properties of which form the focus of the present review. The sMMO system comprises three separate protein components which have all been purified to homogeneity (*24, 25*). The hydroxylase component, a 251 kD protein, contains two copies each of three subunits in an $\alpha_2\beta_2\gamma_2$ configuration. The α subunit of the hydroxylase houses the dinuclear iron center (*26*) responsible for dioxygen activation and for substrate hydroxylation (*27*). The 38.6 kD reductase contains flavin adenine dinucleotide (FAD) and Fe_2S_2 cofactors (*28*), which enable it to relay electrons from reduced nicotinamide adenine dinucleotide (NADH) to the diiron center in the

hydroxylase (*29, 30*). The third component, protein B, contains no cofactors (*31*). This small, 15.5 kD protein interacts with hydroxylase and reductase in several ways, regulating the rate and regioselectivity of substrate hydroxylation as well as the reduction potentials for MMO.

II. Structural Studies of sMMO Hydroxylase

The hydroxylase component of sMMO belongs to a family of proteins which contain a nonheme, carboxylate-bridged, dinuclear iron unit at their active sites (*32–36*). Included in this family are the proteins hemerythrin, ribonucleotide reductase, and purple acid phosphatase, as well as a number of other hydroxylating enzymes. Understanding how the diiron unit in each protein is tuned to exhibit diverse functions, ranging from the reversible binding of dioxygen in hemerythrin to the activation of dioxygen for converting methane to methanol in MMO, is a primary goal of research in this area. Emerging features of the nonheme systems can be compared to related structural and functional information from the analogous heme proteins hemoglobin and cytochrome P-450, which have been studied more extensively.

A. The Oxidized Hydroxylase, H_{ox}

The diiron center in the sMMO hydroxylase has been investigated by a variety of physical techniques. Selected physical properties of the hydroxylase from both *M. capsulatus* (Bath) and *M. trichosporium* OB3b in three oxidation states are listed in Table I. The enzyme is isolated in its native Fe(III)Fe(III) oxidation state (H_{ox}) (*37*). Mössbauer parameters are consistent with the presence of two high-spin iron(III) atoms (*38, 39*) and are slightly perturbed with an increase in pH (*39*). The ground state of H_{ox} is EPR-silent because of antiferromagnetic coupling between the two Fe(III) atoms (*38, 39*). EPR signals at $g = 4.3$ and 2.0, which together account for <5% of total iron, are present in spectra of the enzyme in all oxidation states and are assigned to adventitious Fe(III) and a protein-associated free radical, respectively. The $S = 2$ excited state of H_{ox} displays an integer spin EPR signal at $g = 8$ ($J \approx -8\ cm^{-1}$, where $\mathcal{H} = -2JS_1 \cdot S_2$) (*39*). Since the oxo-bridged diiron(III) units in hemerythrin and the R2 subunit of ribonucleotide reductase exhibit coupling constants of -135 and $-110\ cm^{-1}$, respectively, the small J value suggested that an oxo bridge is not present in H_{ox} (*39*). This hypothesis is in accord with previous EXAFS spectral studies (*38, 40*) in which no short Fe–O distance was found, and with

TABLE I

PHYSICAL PROPERTIES OF MMOH FROM *M. trichosporium* OB3b AND *M. capsulatus* (BATH)

		M. trichosporium OB3b				*M. capsulatus* (Bath)			
		H_{red}	H_{mv}	H_{ox}	Ref.	H_{red}	H_{mv}	H_{ox}	Ref.
Optical	λ_{max}, nm			282	*27*			280	*38*
Magnetics	J, cm^{-1}	0.35	−30	−8	*39*		−32		*38*
Mössbauer	site 1:								
	δ, mm/s	1.3	0.48[a]	0.51	*39*	1.30[c]		0.51	*51*
	ΔE_Q, mm/s	3.10	−1.3[a]	1.16	*39*	2.87		1.12	*51*
	site 2:								
	δ, mm/s	1.3	1.19[a]	0.50	*39*	1.30[c]		0.50	*51*
	ΔE_Q, mm/s	2.4–3.0	2.4[a]	0.87	*39*	2.87		0.79	*51*
EPR	g_x		1.94		*27*		1.92		*38*
	g_y		1.86		*27*		1.86		*38*
	g_z		1.75		*27*		1.71		*38*
	g_{av}	16	1.85	8	*27*	15	1.83		*38*
	g_{av} + protein B		1.75		*66*		1.74		*48*
ENDOR[b]	A, MHz		13–23		*46*		14–30		*42*

[a] Determination was performed in the presence of DMSO at 150 K. All other measurements were at 4.2 K.

[b] Value for hydroxide bridge proton only.

[c] The two sites are unresolved and the apparent values are quoted.

the lack of any electronic spectral bands above 300 nm in any oxidation state (*38*). A 2.2 Å resolution x-ray crystal structure of H_{ox} from *M. capsulatus* (Bath) (*41*) provides further evidence for the occurrence of a bridging hydroxide ligand (vide infra), and the active site structure derived from this analysis is illustrated in Fig. 1. Two additional bridges, a bidentate glutamate and an exogenous bridging ligand, tentatively assigned as acetate ion introduced during crystal growth, have also been identified. The Fe···Fe distance is determined to be 3.4 Å. Each iron atom is ligated by one histidine nitrogen atom. The remaining octahedral coordination sites are occupied by two monodentate glutamate residues on one iron atom, whereas the second iron atom contains one monodentate glutamate and a water ligand in its coordination sphere. Further details are discussed elsewhere (*15, 41*).

B. The Mixed-Valent Hydroxylase, H_{mv}

Hydroxylase in the mixed-valent Fe(II)Fe(III) oxidation state (H_{mv}) is readily accessible by one-electron reduction of the dinuclear center. Mössbauer data indicate the presence of one Fe(III) and one Fe(II) (*39*). H_{mv} has a rhombic EPR signal with $g_{av} = 1.83$ (*27, 37*) and $J \approx -30\ cm^{-1}$ (*38, 39*), properties characteristic of other mixed-valent nonheme carboxylate-bridged diiron centers such as that in semimet hemerythrin ($J \approx -15\ cm^{-1}$) (*32*). ENDOR spectroscopic studies of H_{mv}

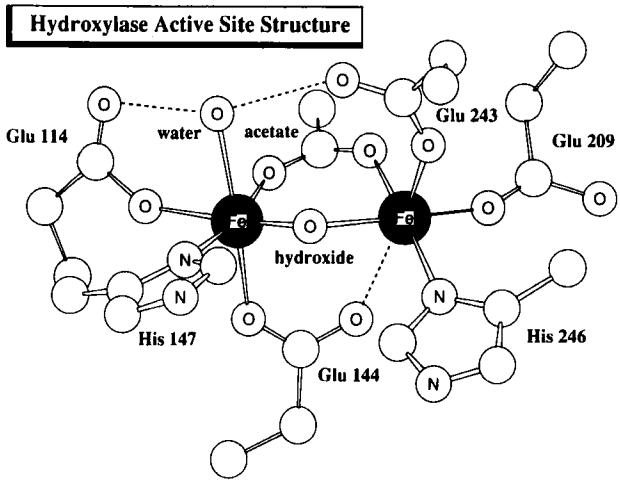

FIG. 1. Structure of the active site of H_{ox} as determined by x-ray crystallography (*41*). Broken lines are used to designate hydrogen bonding of the water molecule to Glu 114 and Glu 243, as well as the semibridging interaction of Glu 144 with the diiron center.

from *M. capsulatus* (Bath) provide good evidence for a hydroxide bridge and a terminal water or hydroxide ligand of the diiron unit (*42*). The hyperfine interaction parameter of the hydroxide proton is highly unusual, displaying an extremely large and anisotropic coupling to the paramagnetic diiron center. Exchange with D_2O demonstrated that the proton is derived from solvent. Spectra of semimetazido hemerythrin displayed a similar feature, confirming the assignment. The mixed-valent dinuclear iron center of this protein was known from a variety of other methods to contain a bridging hydroxide ligand (*43–46*). A pulsed EPR study of H_{mv} from *M. trichosporium* OB3b was consistent with these conclusions (*47*). Extensive ESEEM and ENDOR investigations of H_{mv} have been carried out (*48–50*). These experiments provide further characterization of the diiron core through examination of ^{14}N, ^{15}N, ^{1}H, ^{2}H, ^{13}C, and ^{57}Fe nuclei in H_{mv}. Parallel studies of the protein containing the bound inhibitor DMSO (*50*) afford information about the geometry of the substrate binding site in H_{mv} (*48, 50*). A Mims' pulsed ENDOR analysis of H_{mv} treated with d_6-DMSO suggests that the dimethyl sulfoxide ligand is coordinated through its oxygen atom to the iron(III) center, with the methyl groups asymmetrically disposed such that one is appreciably closer to the diiron center (*48*).

C. The Reduced Hydroxylase, H_{red}

Further reduction of H_{mv} results in the formation of the fully reduced, Fe(II)Fe(II) protein (H_{red}). Mössbauer spectra of H_{red} from both organisms are best interpreted as arising from two unique quadrupole doublets (*39, 51*). For *M. trichosporium* OB3b, the doublets were interpreted as indicating the presence of two distinct Fe(II) sites in each diiron center (*39*). For *M. capsulatus* (Bath), the signal is very broad, owing in part to dinuclear Fe(II) centers in the protein that react with dioxygen in a nonproductive manner (*51*). H_{red} from *M. trichosporium* OB3b and both forms of H_{red} from *M. capsulatus* (Bath) exhibit an EPR feature at $g \approx 15–16$ (*27, 38*) arising from a ferromagnetically coupled, $S = 4$ spin system, with the two lowest spin levels being nearly degenerate (*52*). Identification of nitrogen donor ligands was possible from the pulsed ENDOR and ESEEM spectra of H_{red} from *M. capsulatus* (Bath) (*53*). These studies provide the first advanced EPR studies of a non-Kramers doublet spin system, and they suggest the possibility of investigating similar signals from other proteins in this family. EXAFS spectroscopy does not exhibit Fe···Fe backscattering in H_{red} (*38*). This observation could reflect thermal motion, or it may suggest that, as a consequence of the reduction of H_{ox} to H_{red}, the Fe···Fe distance has

increased significantly. MCD experiments were interpreted in terms of a model in which both iron atoms are five-coordinate and ferromagnetically coupled to one another, with $J \approx 0.3$ to 0.5 cm^{-1} (*54*). Comparisons with deoxyhemerythrin, the diiron center of which contains a hydroxo bridge and antiferromagnetically coupled (J -12 to -36 cm^{-1}) iron atoms (*43, 44, 55, 56*), have led to the hypothesis that the hydroxide bridge present in H_{ox} and H_{mv} is converted to a water bridge in H_{red} (*54*).

III. Component Interactions

Although the structure of the hydroxylase is now reasonably well understood, less is known about the interactions among the three component proteins of MMO. Despite the fact that the physical properties of the *M. capsulatus* (Bath) and *M. trichosporium* OB3b hydroxylases are very similar, preliminary work with the other components indicates that significant differences exist. The manner in which the component proteins interact is quite complex, as manifested by the regulation of electron transfer to the hydroxylase, the product yields and regioselectivity of the hydroxylation reaction, and the detailed kinetic behavior of the systems.

A. Catalytic Activity

In the *M. capsulatus* (Bath) system, all three components are necessary to obtain turnover with NADH as the reductant (*57*). With the *M. trichosporium* OB3b system, protein B is apparently not required (*27*). Instead, in this latter system, protein B increases the initial rates of the catalytic hydroxylation reaction (*27*). Catalysis can be achieved by means of a shunt pathway with hydrogen peroxide and H_{ox} alone from both organisms (*58–60*). The efficiency of the shunt pathway, however, varies significantly. With *M. trichosporium* OB3b, alcohol yields greater than those obtained with the completely reconstituted system have been observed (*58*). Furthermore, upon addition of protein B, the initial rate constants are diminished, in contrast to those observed for the catalytic system (*61*). The reasons for the different effects of protein B on the two reactions with H_{ox} are unknown. With H_{ox} from *M. capsulatus* (Bath), activities of only $\approx$10% of the values observed under optimal catalytic conditions were found with the H_2O_2 shunt pathway, assuming specific activities to be greater than 200 mU/mg (*59*). As a consequence of the poor yields observed, the effect of protein B on the system was not investigated further.

B. Reduction Potentials of the Hydroxylase

Determination of the reduction potentials of the diiron center in the hydroxylase, shown in Eq. (2), and investigation of the effects of the other two MMO components on those potentials, have revealed different behavior for the two organisms (Table II).

$$\underset{H_{ox}}{Fe(III)Fe(III)} \xrightarrow{E_1^\circ} \underset{H_{mv}}{Fe(II)Fe(III)} \xrightarrow{E_2^\circ} \underset{H_{red}}{Fe(II)Fe(II)} \qquad (2)$$

For *M. capsulatus* (Bath), values of +350 and −25 mV, for E_1° and E_2°, respectively, vs NHE were obtained from redox titrations by measuring the appearance and disappearance of the EPR signal of H_{mv} (*37*). Problems were encountered in producing high yields of H_{mv} from this organism for use in physical studies, despite the large difference between E_1° and E_2°, and so the potentials were remeasured. In the latter experiments, two sets of electron-transfer mediators were used,

TABLE II

Reduction Potentials (mV vs NHE, pH 7.0) of the MMO Hydroxylase from *M. capsulatus* (Bath) and *M. trichosporium* OB3b

Component(s)	Conditions[b]	E_1°	E_2°
	M. capsulatus (Bath)		
H	1	48 ± 5	−135 ± 5
	2, 3	100 ± 15	−100 ± 15
H, protein B	2, 3	50 ± 15	−170 ± 15
H, propylene	1	30 ± 5	−156 ± 5
H, protein B, R	1	*a*	*a*
H, protein B, R, propylene	1	<100 ± 25	≈100 ± 25
	M. trichosporium OB3b		
H	4	76 ± 15	21 ± 15
H, protein B	4	−52 ± 15	−115 ± 15
H, protein B, R	4	>76 ± 15	>21 ± 15
H, R	4	>76 ± 15	>21 ± 15
H, protein B, R, propylene	4	>76 ± 15	>21 ± 15

Adapted from Refs. (*62–64*).

[a] No reduction was observed under these conditions.

[b] See text and appropriate references for specific experimental conditions, which differ mainly in the number and choice of mediators employed in the redox titrations.

the first of which matched those employed in the original study (*37*), and yielded potentials of +48 and −135 mV vs NHE (*62*). The second set omitted two mediators that were suggested to bind to the *M. trichosporium* OB3b hydroxylase (*63*), and both reduction potentials shifted to slightly more positive values of +100 and −100 mV, although the difference between them remained approximately the same (*64*). In one sense this difference is more important than the absolute values of the potentials, because it determines thermodynamically the amount of H_{mv} that can be obtained theoretically. Substrate had little effect on these potentials, whereas addition of protein B altered them to values of +50 and −170 mV for $E_1°$ and $E_2°$, respectively. In the presence of a mixture containing both protein B and reductase, no EPR signals associated with H_{mv} or H_{red} were detected at potentials as negative as −200 mV (*62*). When the titration of the three components was carried out in the presence of substrate, however, only H_{red} was detected, but at potentials as high as 100 mV. No EPR signal indicative of H_{mv} was observed. These results indicate that, with the complete reconstituted system including substrate, a two-electron transfer occurs; reduction of H_{ox} directly to H_{red} without formation of H_{mv} reveals an $E_2°$ which has shifted to a value greater then $E_1°$. The redox experiments therefore provide important evidence that H_{mv} is not likely to be of physiological significance. The inability to reduce the hydroxylase in the presence of a mixture containing protein B and reductase was consistent with kinetic work in which component B prevents NADH oxidation by the MMO system in the absence of substrate (*65*). Addition of substrate similarly led to efficient electron transfer to the hydroxylase, as measured by the consumption of NADH. Thus, control of electron transfer to the hydroxylase is regulated by the binding of substrate and the other two proteins in the system, assuring that reducing equivalents are not wasted and that the protein is protected from oxidative damage (vide infra) in the absence of substrate.

$E_1°$ and $E_2°$ values of +76 and +21 mV, respectively, have been measured for H_{ox} from *M. trichosporium* OB3b by similar methods (*63*). These values are more closely spaced and imply that H_{mv} from this organism is thermodynamically less stable with respect to disproportionation. Addition of protein B lowered the potentials to −52 mV and −115 mV, respectively. The regulation of electron transfer to the hydroxylase with protein B and reductase observed with the *M. capsulatus* (Bath) MMO was not seen with this system. Instead, it was reported that the potentials of H_{ox} and of H_{ox} with added protein B are shifted slightly to more positive values in the presence of reductase (Table II), and the reduction was not substrate-dependent.

As indicated by the negative shifts in the reduction potentials of H_{ox}, protein B can interact with the diiron center in H_{mv} from both MMO systems (*63, 64*). Consistent with this interpretation are EPR studies of H_{mv} from both organisms which indicate that, in the presence of protein B, the EPR signal moves from $g_{av} \approx 1.83$ to $g_{av} \approx 1.75$ (*48, 66*).

C. Product Distributions

The distribution of products formed by hydroxylation of nitrobenzene and isopentane with MMO from *M. trichosporium* OB3b were investigated (*58, 61*), and the results for nitrobenzene are listed in Table III. Protein B had a dramatic effect on the regioselectivity of hydroxylation (*61*). This behavior was attributed to changes in the hydroxylase structure upon complexation with protein B, causing the substrate molecule to interact differently at the active site of the enzyme. Similar studies of the substrate nitrobenzene with the *M. capsulatus* (Bath) system were carried out (*51*), and the results are included in Table III. Very different regioselectivity is observed for the native reconstituted system, with product distributions that curiously match those obtained by the hydrogen peroxide shunt pathway with *M. trichosporium* OB3b. With the *M. capsulatus* (Bath) system, addition of protein B in single turnover reactions (see next section) for chemically reduced H_{red} has no effect on the regioselectivity of the reaction. This result implies that it is the reductase/protein B combination, and not protein B alone,

TABLE III

Product Distributions from Reactions of MMO with Nitrobenzene[a]

Organism	Components	Reductant	4-Nitrophenol	3-Nitrophenol
M. trichosporium OB3b[b]	H_{ox}, protein B, reductase	NADH	89%	11%
	H_{ox}, reductase	NADH	<10%	>90%
	H_{ox}	H_2O_2	38%	59%
	H_{ox}, protein B	H_2O_2	59%	41%
M. capsulatus (Bath)[c]	H_{ox} ± protein B	chemical[d]	>95%	—
	H_{ox}, protein B, reductase	NADH	57%	43%

[a] In all cases, very little 2-nitrophenol was detected.
[b] See Refs. (*58* and *61*).
[c] See Ref. (*51*).
[d] H_{red} was prepared with mediated reduction by sodium dithionite.

which can significantly affect the distribution of products from the hydroxylation reaction. Of interest are the K_M values measured for nitrobenzene hydroxylation in the various systems. A K_M value of $\approx$5 mM was obtained with both the catalytic system from *M. capsulatus* (Bath) (*51*) and the H_2O_2 shunt pathway with *M. trichosporium* OB3b (*58*). As indicated earlier, these two systems display similar product distributions in the hydroxylation reaction. The catalytic system from *M. trichosporium* OB3b yields a K_M value of $\approx$100 μM (*58*), however, and the regioselectivity differs from that observed with the other two systems. Further work is required to understand the reasons for these differences.

D. Yields and Rate Constants with Single Turnover Reactions

Single turnover experiments can be carried out by addition of substrate and dioxygen to chemically reduced MMO hydroxylase, monitoring either the formation of colored products such as *p*-nitrophenol or the uptake of dioxygen by a Clark electrode. Yields of single turnover reactions with H_{red} from *M. trichosporium* OB3b are not sensitive to the presence of the other two components (*27*). From these and other studies with this system, it was concluded that protein B does not affect the reactivity of the hydroxylase with dioxygen, and that it has little effect on the hydroxylation reaction once H_{red} is formed (*66*). In contrast to this work, experiments with MMO from *M. capsulatus* (Bath) indicate that total yield from single turnover reactions of chemically reduced H_{red} are significantly affected by the other components of the system (*51*). Maximal yields occur when greater than 1.5 equivalents of protein B are added, either prior to or following reduction of H_{ox} to H_{red}. Combining both protein B and reductase with H_{red} results in slightly diminished yields, and adding protein B and reductase to H_{ox} prior to reduction afforded very little hydroxylation. This latter finding is consistent with the redox studies in which, even at quite negative potentials, H_{red} was not detected by EPR spectroscopy in the presence of both protein B and reductase (*62*). Adding reductase alone to H_{ox} or H_{red} did not have a substantial effect on the product yields, which were quite low because protein B is absent.

Protein B from *M. capsulatus* (Bath) not only increases the product yields, but also influences the rate constant for the single turnover reaction of H_{red} with nitrobenzene (*51, 67*). The pseudo–first-order rate constant increases up to 33-fold when H_{red} is titrated with protein B. Neither addition of reductase to H_{ox} or H_{red}, nor addition of protein B and reductase to H_{red}, could similarly affect the rate constant. These

observations again imply either that protein B alone activates the hydroxylase, or that protein B and reductase do not significantly affect H_{red}.

Thus, protein B from *M. capsulatus* (Bath) affects the single turnover hydroxylation reaction efficiency by increasing both the rate constants and product yields. Presumably, protein B in some manner activates the H_{red} species formed by chemical reduction of H_{ox}. The activation could be at least partially thermodynamic in origin, since the reduction potentials become more negative in the presence of this protein component. Addition of protein B and reductase to H_{red}, however, may not produce the same reactive species as that formed when H_{ox} is reduced in the presence of protein B and reductase. The inability to reduce H_{ox} to H_{red} chemically in the absence of substrate and protein B (*62*) makes it difficult to obtain definitive information about this possibility through single turnover experiments. Structural alterations in the coordination spheres of the iron atoms accompanying the change in oxidation state from H_{ox} to H_{red} could be facilitated by the other two components, altering the kinetics of the ensuing hydroxylation steps from those observed with protein B alone (*51*). Such a change in active-site geometry could account for the increased reduction potentials observed for H_{ox} upon addition of the other two components and substrate (*62*).

Complex formation among the three protein components of the *M. trichosporium* OB3b MMO has been demonstrated (*66*). In this work, it was hypothesized that protein B binds tightly to H_{ox} to form an activated complex but that, after formation of H_{red}, the binding affinity is diminished (*63, 66*). Results reported for *M. capsulatus* (Bath) are consistent with initial binding of H_{ox} to protein B to form an activated complex (*51*), because increased yields and rate constants are seen when protein B is added to H_{red}. If the H_{red}–protein B complex of *M. capsulatus* (Bath) is the species influencing reactivity, then there should be a direct relationship between equivalents of added B and the rate constant, at which point the B-specific binding sites would be saturated. Since H is a dimer ($\alpha_2\beta_2\gamma_2$), two equivalents of protein B and reductase are likely to bind per molecule, probably in the canyon formed at the interface of the α and β subunits (*41*). Amounts of protein B greater than two equivalents per H_{red} may diminish the rate constant of the reaction by binding nonspecifically and sterically hindering substrate access to H_{red}. The total product yield could still remain high, because nearly all of the H_{red} is in the active, protein B-bound form. If there are a finite number of nonspecific binding sites for additional molecules of protein B beyond two equivalents, excess protein B would have little effect once all of these extra sites were fully occupied, except

possibly to block the reductase binding site. Similar reasoning was also invoked in work with *M. trichosporium* OB3b to explain the titration curve describing the effect of protein B on the initial rate constants for the catalytic system with H_{ox} and reductase (*66*).

The *M. capsulatus* (Bath) reductase alters the distribution of products formed in the reaction of H_{red} and dioxygen with nitrobenzene (*51*), but protein B has a more diverse role in this fully reconstituted MMO system. As mentioned earlier, it regulates electron transfer from the reductase to the hydroxylase so that it occurs only in the presence of substrate (*62, 65*); it shifts the reduction potentials of the substrate/reductase/hydroxylase complex (*62*); and it affects k_{obs} and yields in single turnover reactions of H_{red} (*51*). Protein B from *M. trichosporium* OB3b changes product distributions with H_{red} (*61*), increases the initial velocity of the complete reconstituted system (*66*), but reduces the initial velocity with the H_2O_2 shunt system (*66*). Reductase plays no major role in the regioselectivity of the hydroxylation reaction in this case (*61*). With hydroxylase from both organisms, protein B perturbs the EPR signal of H_{mv} (*48, 66*) and lowers the reduction potentials (*63, 64*). A unifying explanation for these observed functions has yet to be found. Some of the differences may arise from variations in the proteins themselves. For example, appreciable differences in protein B from the two systems are reflected by the inability of antibodies raised toward one protein B to bind the other (*68*). More structural work on component interactions is essential for a full understanding of the fundamental reasons for the observed effects, and to reconcile differences between the two MMO systems.

IV. Mechanism of Hydroxylation

A. Reaction of H_{red} with Dioxygen

H_{red} is the form of hydroxylase which reacts with dioxygen (*27*). Recently, intermediates were detected in this reaction (*51, 69–72*). In all cases, dioxygen was mixed with H_{red} in the presence of two equivalents of protein B under pseudo–first-order conditions in dioxygen. Reactions were carried out at 4°C in the absence of substrate in order to allow detectable quantities of the intermediates to build up. Spectroscopic parameters and kinetic constants for two intermediates, originally designated L and Q, are listed in Table IV. The proposed reaction sequence is summarized in Eq. (3). Magnetic Mössbauer (*51, 69*) and EPR spectroscopic results (*51, 70*) indicated that both intermediates are diamagnetic. In the *M. trichosporium* OB3b MMO system, rapid

TABLE IV

SPECTROSCOPIC AND KINETIC PARAMETERS FOR INTERMEDIATES IN THE REACTION OF H_{red} WITH DIOXYGEN

		M. trichosporium[a]	*M. capsulatus* (Bath)[b]	
		Q	H_{peroxo}	Q
Optical	λ_{max}, nm	330 430	≈600–650	350 420
	k_{form}, s^{-1}	1	22	0.5
	k_{decay}, s^{-1}	0.05	—	0.07
Mössbauer	site 1:			
	δ, mm/s	0.17	0.66	0.21
	ΔE_Q, mm/s	0.53	1.51	0.68
	site 2:			
	δ, mm/s	—	—	0.14
	ΔE_Q, mm/s	—	—	0.55
	k_{form}, s^{-1}		28	0.3
	k_{decay}, s^{-1}		0.3	0.03
Raman ν_{O-O}	cm^{-1}		905	

[a] See Refs. (*69* and *70*).
[b] See Refs. (*51, 71, 72*).

$$H_{red} \xrightarrow{k_1} H_{peroxo} \xrightarrow{k_2} Q \xrightarrow{k_3} H_{ox} \quad (3)$$

freeze-quench EPR studies revealed that the $g = 16$ EPR signal of H_{red} decays with a first-order rate constant of $\approx 22 \pm 5\ s^{-1}$ upon exposure to dioxygen (*70*). Based on this observation, a proposed intermediate named "P" was suggested as the immediate precursor to Q (vide infra). Mössbauer analysis of rapid freeze-quench samples prepared from the *M. capsulatus* (Bath) system identified such an intermediate (*71*), but this compound was designated "L" because it was unknown at that time whether it corresponded to the immediate precursor to Q. Subsequent kinetic Mössbauer data for L from *M. capsulatus* (Bath) indicated that L forms, concomitantly with the decay of H_{red}, with a first-order rate constant of $\approx 28\ s^{-1}$ (*51*). The minimal mechanism therefore dictates that intermediate L represents the initial species formed in the reaction of H_{red} with dioxygen.

The Mössbauer spectrum of L consists of a symmetric doublet which was fitted with parameters $\delta = 0.66 \pm 0.02$ mm/s and $\Delta E_Q = 1.51 \pm 0.03$ mm/s (*71*). The isomer shift is larger than values (0.45–0.55 mm/s) generally seen for carboxylate-bridged diiron(III) clusters,

but significantly smaller than isomer shift values for diiron(II) clusters (1.1–1.3 mm/s) (*32–34*). Although parameters matching the values of L have not been observed in model compounds, the magnitude of the isomer shift is close to parameters seen for diiron(III) clusters, and L was accordingly proposed to be a diiron(III) peroxide complex (*71*). Such species have been assigned to products formed in reactions of several diiron(II) model complexes with dioxygen and result from transfer of two electrons from the Fe atoms to the dioxygen ligand (*35*). The optical absorption at λ = 600–650 nm ($\varepsilon_{625} \approx 1500\ M^{-1}\ cm^{-1}$) reported for L (*51, 73*) resembles published electronic spectral features for several diiron(III) peroxide model complexes (*74–76*). Similarly, the resonance Raman spectrum of L with excitation at 647 nm displays an isotope-sensitive band at 905 cm^{-1} (*72*), which matches ν(O–O) values reported for several nonheme diiron(III) peroxide model compounds (*74–76*). The Raman spectrum the intermediate generated with $^{16}O-^{18}O$ contains a single O–O stretch, ruling out structures in which the O–O bond has cleaved and suggesting that the peroxide ion is coordinated to iron through both of its oxygen atoms (*72*). We shall therefore refer hereafter to L as the peroxo intermediate or species, H_{peroxo}.

From the sharp, symmetrical shape of the Mössbauer signal, the iron atoms were interpreted as being in nearly equivalent coordination environments (*71*). To account for the high isomer shift value of 0.66 mm/s for the peroxo intermediate, six-coordinate iron atoms with substantial peroxide-to-iron charge transfer or seven-coordinate iron atoms were invoked (*71*). Such structures can be readily envisaged from the known crystal structure of H_{ox} (Fig. 1), in which a peroxide ligand replaces the bridging acetate. The two resulting Fe(III) atoms may bind the peroxide ligand either in a μ-η^1:η^1, or μ-η^2:η^2 fashion. The latter binding mode has been observed for oxyhemocyanin (*77*) and in a dicopper(II) peroxide complex (*78*). Figure 2 illustrates structures for the peroxo intermediate which are most compatible with its spectroscopic parameters, as well as another, less likely, possibility (*51*).

The time-dependent, rapid freeze-quench Mössbauer experiments with *M. capsulatus* (Bath) (*51*) indicate that decay of the peroxo species proceeds with the concomitant formation of another intermediate, named compound "Q." This intermediate, observed in both the *M. trichosporium* OB3b (*69, 70*) and *M. capsulatus* (Bath) (*51, 71*) MMO systems by Mössbauer and optical spectroscopy, decays faster in the presence of substrates. Such behavior indicates that this intermediate is probably on the kinetic reaction pathway for hydroxylation (*51, 70*).

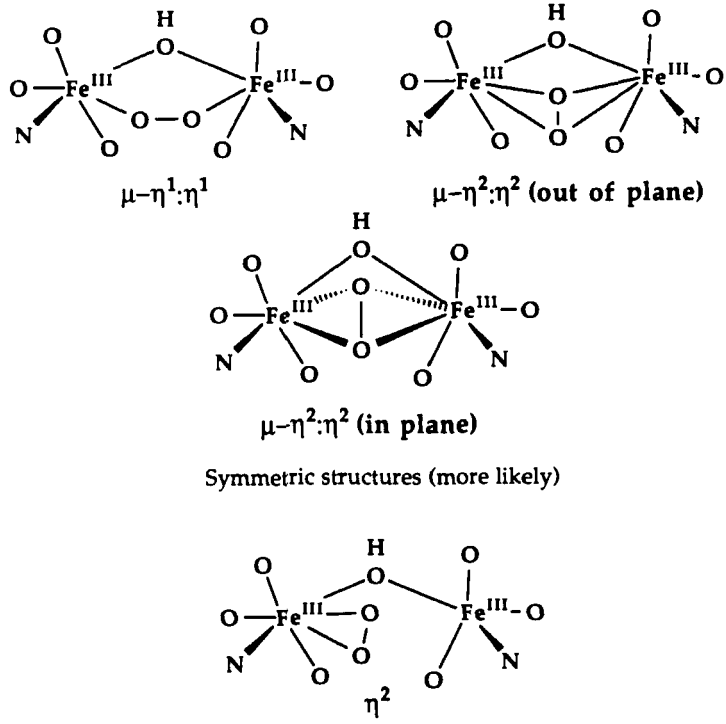

FIG. 2. Possible structures for a diiron(III) peroxide unit in the peroxo intermediate consistent with available Raman and Mössbauer spectroscopic data. The symbols N and O designate nitrogen and oxygen donor atoms of histidine and glutamate residues, respectively. Some of the latter must be bidentate to fill the coordination spheres.

The Mössbauer spectrum of Q from *M. trichosporium* OB3b contained a doublet with $\delta = 0.17$ mm/s and $\Delta E_Q = 0.53$ mm/s (*69*). This signal is reported to be symmetrical, and the iron atoms are assumed to have equivalent coordination environments. In the *M. capsulatus* (Bath) system, two unresolved doublets of equal intensity were distinguished and fitted to the following parameters: $\delta = 0.21 \pm 0.02$ mm/s and $\Delta E_Q = 0.68 \pm 0.03$ mm/s for doublet 1, and $\delta = 0.14 \pm 0.02$ mm/s and $\Delta E_Q = 0.55 \pm 0.03$ mm/s for doublet 2 (*71*). The average isomer shift and quadrupole splitting of the two doublets, 0.18 mm/s and 0.62 mm/s, respectively, agree with parameters obtained from the corresponding spectrum of Q from the *M. trichosporium* OB3b organism. In the *M. capsulatus* (Bath) system, however, the presence of two distinct signals for Q indicates that the iron atoms are in inequivalent sites.

From the low isomer shift value, it was suggested that Q is an

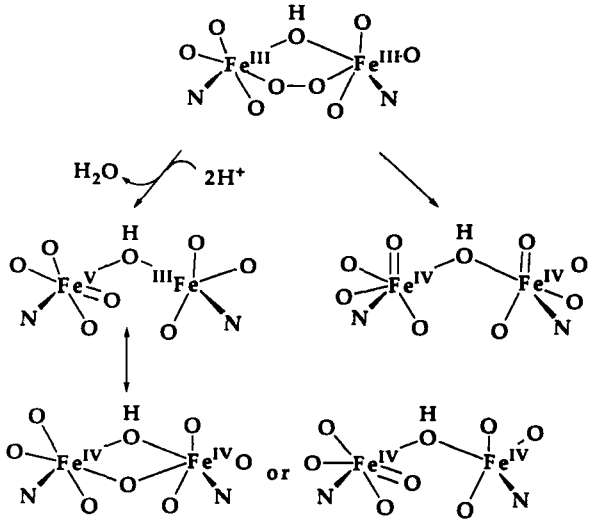

Intermediate Q

FIG. 3. Proposed routes for conversion of the peroxo intermediate to intermediate Q, one involving loss of water (left-hand side) and one not (right-hand side). In the former case the resulting diiron(IV) oxo species could bind an oxygen atom with one iron, or the oxygen could be bound symmetrically by both iron atoms. Although written as an iron(IV) oxo species, Q can also be formulated as an iron(III) oxyl radical complex (*35,51*).

iron(IV) oxo species (*69*). Figure 3 illustrates possible structures for Q. In *M. capsulatus* (Bath), the inequivalent Fe sites could arise from rearrangement of the protein ligands in Q compared to their positions as revealed in the x-ray crystal structure of H_{ox} (*41*). Alternatively, the oxo ligand in the proposed Fe(IV) species may not be bound symmetrically between the Fe atoms. Equivalent iron sites in the *M. trichosporium* OB3b system could arise from symmetrical bridging of the oxygen atoms between the two Fe(IV) atoms or terminal coordination on both Fe(IV) atoms (*51*).

Cleavage of the O–O bond in the peroxo species, possibly accompanied by release of H_2O, most likely results in the formation of Q (*51*). The second iron atom in the MMO hydroxylase active site can stabilize this unit through redox charge delocalization (Fig. 3) in a manner similar to that proposed for the stabilization of a high-valent iron oxo species in cytochrome P-450 by oxidation of the porphyrin ring to a π-cation radical (*79*). A large change in entropy ($\Delta S^{\ddagger} \approx 147$ J mole^{-1}K^{-1}) has been reported for the conversion of peroxo to Q, consistent with O–O bond cleavage and possibly the release of water during this step

(*51*). The rate constant for growth of Q is independent of dioxygen concentration (*51, 70*). Since formation of the peroxo intermediate is rapid and irreversible and formation of Q is the slow step, the rate constant for Q is not expected to depend on dioxygen concentration under experimentally practical conditions. Conversion of the diiron(III) peroxide species to Q, a putative diiron(IV) oxo species, would require proton transfer within the active site if a molecule of water were produced from the second oxygen atom of the peroxide. The lack of a pH dependence or a significant kinetic deuterium isotope effect on the rate constant for this process, however, suggests that proton transfer is not overall rate-determining in the conversion (*51*). Perhaps Q is a diferryl species, $(Fe^{IV}{=}O)_2$ (see Fig. 3).

The widely accepted hydroxylation mechanism for the heme protein cytochrome P-450 invokes an Fe(IV) oxo species which abstracts a hydrogen atom from the substrate molecule (*79*). Since cytochrome P-450 cannot hydroxylate methane, a similar Fe(IV) oxo intermediate in MMO is presumed to be significantly more reactive. Very recently, Fe(IV) intermediates have been ruled out in the mechanism for generating the tyrosyl radical in the R2 subunit of ribonucleotide reductase (*80–82*). Instead, a diiron(III) oxygen radical species was invoked as the species which causes the oxidation and deprotonation of the tyrosyl residue. A similar formulation has been considered for Q (*35,51*). In addition, the O–H bond of tyrosine is significantly weaker than the C–H bond in methane, and the active abstracting species in R2 may not be strong enough to break the C–H bond in methane. It has been speculated that a cysteinyl radical may help to homolyze this bond (*35*). If such a species were to couple magnetically with the oxyl radical in Q, it could account for the observed diamagnetism. The diferryl unit depicted in Fig. 3, or a magnetically coupled bis(oxyl radical) diiron(III) complex, are attractive alternatives.

In the *M. trichosporium* OB3b system, a third intermediate, T, with λ_{max} at 325 nm (ε = 6000 $M^{-1}cm^{-1}$) was observed in the presence of the substrate nitrobenzene (*70*). This species was assigned as the product, 4-nitrophenol, bound to the dinuclear iron site, and its absorption was attributed primarily to the 4-nitrophenol moiety. No analogous intermediate was found with the *M. capsulatus* (Bath) system in the presence of nitrobenzene. For both systems, addition of methane accelerated the rate of disappearance of the optical spectrum of Q ($k > 0.065\ s^{-1}$) without appreciatively affecting its formation rate constant (*51, 70*). In the absence of substrate, Q decayed slowly ($k \approx 0.065\ s^{-1}$). This decay may be accompanied by oxidation of a protein side chain.

A proposed cycle (*51*) for hydroxylation by MMO is illustrated in

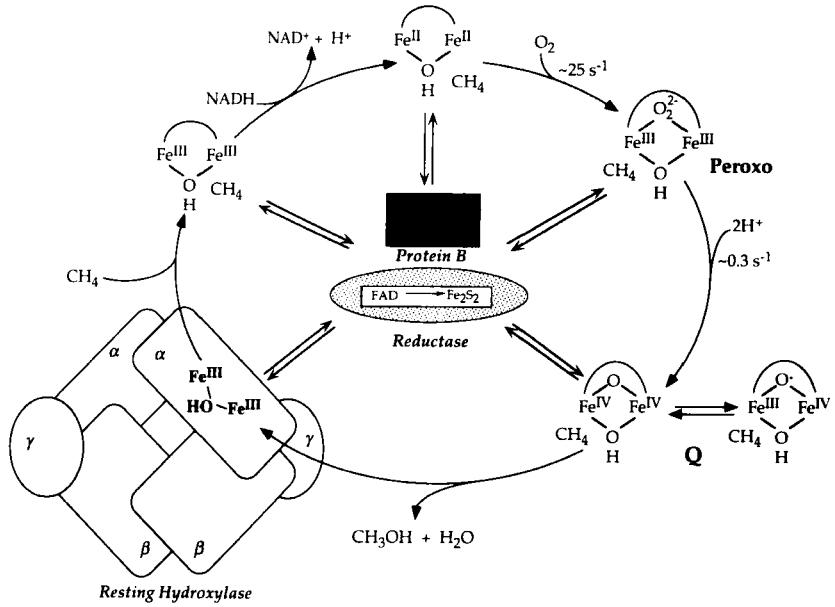

FIG. 4. Proposed catalytic cycle for the hydroxylation of methane by MMO. The reductase and B components may interact with the hydroxylase in one or more steps of the cycle. Protons are shown in the step in which intermediate Q is generated, but other possibilities exist (see Fig. 3 and the text). The curved line represents a bridging glutamate carboxylate ligand.

Fig. 4. Substrate first binds to the complete system containing all three protein components. Addition of NADH next effects two-electron reduction of the hydroxylase from the oxidized Fe(III)Fe(III) to the fully reduced Fe(II)Fe(II) form, bypassing the inactive Fe(II)Fe(III) state. The fully reduced hydroxylase then reacts with dioxygen in a two-electron step to form the first known intermediate, a diiron(III) peroxo complex. The possibility that this species itself is sufficiently activated to carry out the hydroxylation reaction for some substrates cannot be ruled out. The peroxo intermediate is then converted to Q as shown in Fig. 3. Substrate reacts with Q, and product is released with concomitant formation of the diiron(III) form of the hydroxylase, which enters another cycle in the catalysis.

B. Reaction of Q with Substrate

Figure 5 presents some possible mechanisms for substrate hydroxylation by intermediate Q; additional possibilities are discussed elsewhere (*59*). Mechanisms **A–C** assume that this species is a diiron(IV) oxo

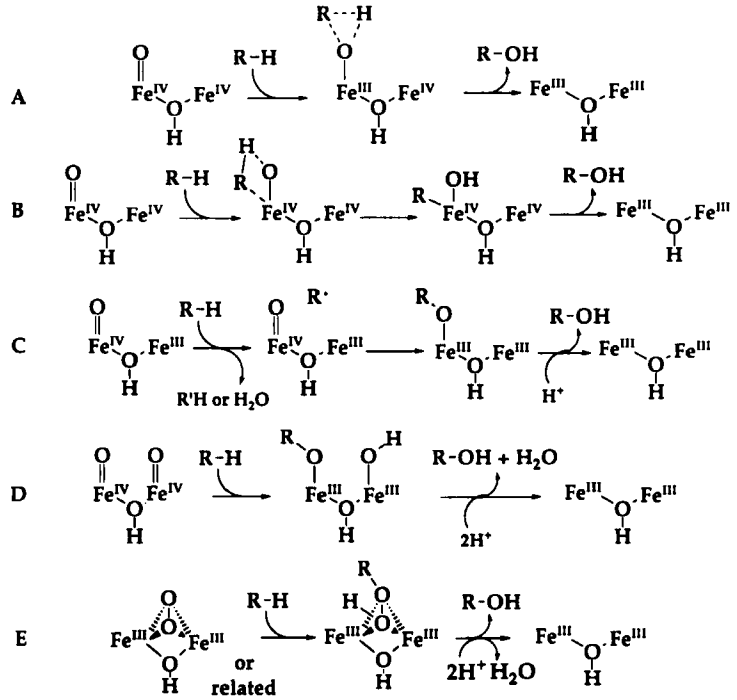

FIG. 5. Possible mechanisms for the MMO hydroxylation step. Pathway **A:** insertion of the oxygen atom of Q into the C–H bond; **B:** concerted addition of the C–H bond to Q followed by reductive elimination; **C, D:** homolytic attack of Q on the C–H bond; **E:** reaction of the peroxo species with substrate.

complex formed by heterolytic cleavage of the O–O bond with loss of water. In mechanism **A,** direct insertion of the oxygen atom of Q into a C–H bond occurs. Concerted 2 + 2 cycloaddition of the C–H bond to Q to form a metal–carbon bond, followed by reductive elimination of the alcohol, is outlined in mechanism **B,** whereas **C** involves homolysis of the C–H bond by Q, followed by return of the hydroxyl group from iron to the alkyl radical. This last process is analogous to the oxygen rebound step in the postulated hydroxylation mechanism of cytochrome P-450 (*8, 58, 83*). In mechanism **D,** the O–O bond has been cleaved homolytically with no loss of water to form a diferryl species, $(Fe^{IV}{=}O)_2$. This unit can then attack the hydrocarbon in a concerted or stepwise fashion; subsequent protonation releases the products. An alternative mechanism, in which the peroxo species reacts in a con-

certed fashion with substrate via electrophilic attack to form a carbon–oxygen bond followed by release of product, is outlined in mechanism **E**. In **E**, the O–O bond does not cleave before the C–H bond.

Evidence for the presence of substrate radical intermediates in cytochrome P-450 includes studies with radical clock substrate probes from which the rebound rate constant was calculated to be $\approx 2 \times 10^{10}$ s^{-1} (*84, 85*). Such substrates rearrange rapidly upon the abstraction of a hydrogen atom in the enzyme active site, affording skeletally modified hydroxylation products (*59, 85–87*). The presence of such rearranged products is taken as evidence that a substrate radical intermediate participates in the mechanism. Studies of MMO from *M. capsulatus* (Bath) and *M. trichosporium* OB3b were carried out by using several radical clock substrate probes, including two much faster probes than those reported previously for experiments with cytochrome P-450 (*59*). For *M. capsulatus* (Bath) MMO, no products consistent with the formation of a substrate radical were detected. This result implies that reactions of these substrates do not generate substrate radical or carbocation intermediates. Alternatively, any rebound reaction occurring would have a rate constant $> 10^{13}$ s^{-1}.

By using an identical radical clock substrate probe which did not rearrange upon hydroxylation with *M. capsulatus* (Bath), rearranged product was detected with MMO from *M. trichosporium* OB3b (*59*). From the ratio of unrearranged to rearranged products, a rebound rate constant was calculated to be $\approx 6 \times 10^{12}$ s^{-1} at 30°C for this system. A separate study with another radical clock substrate probe with MMO from *M. trichosporium* OB3b reported products consistent with both radical and cationic substrate intermediates (*88*).

Evidence in support of radical intermediates with MMO from both *M. capsulatus* (Bath) and *M. trichosporium* OB3b was reported from experiments in which substrate radicals were trapped during turnover (*89, 90*). The amount of trapped radical, however, was not quantified in these experiments. In other reports, no diffusable radical species were detected in reactions with MMO from *M. trichosporium* OB3b (*61*).

With *M. trichosporium* OB3b, epimerization with *exo, exo, exo, exo*-2,3,5,6-d_4-norbornane upon hydroxylation occurs (*83*), which parallels results for cytochrome P-450 hydroxylation with this substrate (*91*). The extent of epimerization with MMO, however, was significantly lower, being 2% following hydrogen atom abstraction from the *endo* position compared to 18% with cytochrome P-450, and 5% after abstraction at the *exo* position as compared to 14% with cytochrome P-450

(*92*). Allylic rearrangements with 3,3,6,6-d_4-cyclohexene occurred in 20% of the MMO hydroxylation products compared to 33% for cytochrome P-450. These two experiments suggest that, with *M. trichosporium* OB3b, a rebound reaction must occur with a greater rate constant than with cytochrome P-450, in accord with the radical clock substrate work.

Since work with the radical clock substrate probes indicated important differences in the hydroxylation mechanisms for *M. capsulatus* (Bath) and *M. trichosporium* OB3b, work with (R) and (S)-[1-^{2}H,1-^{3}H]ethane with both enzymes was carried out (*93, 94*). With *M. trichosporium* OB3b, approximately 65% of the product displays retention of stereochemistry (*93*). A rebound rate constant of $2 - 6 \times 10^{12}$ s^{-1} was calculated, assuming a free energy change of 0.5 kcal $mole^{-1}$ for rotation about the C–C bond (*94*). This estimate approaches the value obtained from the radical clock substrate probe analysis (*59*).

Kinetic isotope effects in the hydroxylation reaction have been measured for MMO from both organisms. With both systems, no significant intermolecular kinetic isotope effect was found for most substrates (*59, 95, 96*), although a value of $k_H/k_D \approx 12$ was reported with CH_4 vs CD_4 (*65*). Substantial intramolecular isotope effects ($k_H/k_D \approx 5$) with *M. capsulatus* (Bath) were found with several substrates (*59, 95*). Studies with *M. trichosporium* OB3b have revealed intramolecular isotope effects of $k_H/k_D \approx 4$ to 5 (*83, 93*). These results indicate that C–H bond breaking is not the rate-determining step in the overall enzymatic reaction. The intramolecular isotope effect, however, is consistent with the assertion that the actual hydroxylation step involves a substantial C–H bond-breaking component. The magnitude of the intramolecular isotope effects for both MMOs can be compared to values of $k_H/k_D \approx 7$–14 seen with cytochrome P-450 hydroxylations (*79, 97*).

Some fundamental differences between MMO and cytochrome P-450 have emerged. The ability of high concentrations of hydrogen peroxide to effect a shunt pathway for the *M. trichosporium* OB3b MMO has been cited as evidence for a hydroxylation mechanism paralleling that of cytochrome P-450 (*58*). It is noteworthy, however, that oxo transfer reagents such as iodosylbenzene, which support catalysis with cytochrome P-450, cannot effect turnover with MMO. In addition, the mechanism for olefin epoxidation by MMO from *M. trichosporium* OB3b (*83*) differs from the proposed mechanism for cytochrome P-450 (*98*). With cytochrome P-450, the 1-*trans*-proton of propylene exchanges with solvent protons during turnover, from which an epoxidation mechanism involving oxametallocycles and iron carbene intermediates was pro-

posed. In the reaction of propylene with MMO, however, no such exchange occurred.

In summary, mechanistic studies have revealed intriguing differences between MMO from *M. capsulatus* (Bath) and MMO from *M. trichosporium* OB3b. With *M. capsulatus* (Bath), radical clock substrate probes indicated either that a substrate radical is not produced or that it reacts with a rate constant $> 10^{13}$ s^{-1}. With MMO from *M. trichosporium* OB3b, radical involvement was suggested from several experiments, and a rebound rate constant of 6×10^{12} s^{-1} was calculated for this system.

The different behavior between the two MMO systems has several implications. For each case, two reaction pathways may operate in parallel, one involving a substrate radical (Fig. 5**C** or **D**), and one not (Fig. 5**A**, **B**, **D**, or **E**). The degree to which the radical vs nonradical mechanism is followed may be imposed by the steric requirements of the substrate in the active site. Alternatively, abstraction of a hydrogen atom to form a substrate radical may occur in both cases, but the rate constants for rebound may differ between the two organisms. For example, in the *M. capsulatus* (Bath) system, the rebound rate constant may be so large that only an extremely small amount of the substrate radical has a sufficient lifetime for rotation about the C–C bond to occur before recombination with the bound hydroxyl group. The physical meaning of rate constants approaching or exceeding 10^{13} s^{-1} is unclear.

V. Conclusions

Physical studies of the hydroxylase have established the structural nature of the diiron core in its three oxidation states, H_{ox}, H_{mv}, and H_{red}. Although the active site structures of hydroxylase from *M. trichosporium* OB3b and *M. capsulatus* (Bath) are similar, some important differences are observed for other features of the two MMO systems. The interactions with the other components, protein B and reductase, vary substantially. More structural information is necessary to understand how each of the components affects the others with respect to its physical properties and role in the hydroxylation mechanism and to reconcile the different properties seen in the two MMO systems. The kinetic behavior of intermediates in the hydroxylation reaction cycle and the physical parameters of intermediate Q appear similar. The reaction of Q with substrate, however, varies. The participation of radical intermediates is better established with the *M. trichosporium*

OB3b system, although it certainly is not ruled out for the *M. capsulatus* (Bath) enzyme. In comparison to the cytochrome P-450 system, the hydroxylation mechanism for both MMO systems either has a rebound rate constant which is much larger and/or it takes place by an alternative pathway to classical radical rebound.

ACKNOWLEDGMENTS

This work was supported by grants from the National Institutes of Health. We thank D. Coufal, S. Komar-Panicucci, A. Salifoglou, and A. Valentine for helpful comments on the manuscript, and S. Komar-Panicucci for assistance in preparing Fig. 4.

REFERENCES

1. Hanson, R. S., *Adv. Appl. Microbiol.* **26,** 3 (1980).
2. Enhalt, D. H., *in* "Microbial Production and Utilization of Gases" (H. G. Schlegel, G. Gottschalk, and N. Pfennig, eds.), p. 13. Goltze Publishers, Göttingen, 1976.
3. Enhalt, D., and Schmidt, U., *Pure Appl. Geophys.* **116,** 452 (1978).
4. Dalton, H., and Leak, D. J., *in* "Gas Enzymology" (H. Degn, ed.), p. 169. Reidel, London, 1985.
5. Burch, R., Squire, G. D., and Tsang, S. C., *J. Chem. Soc., Faraday Trans. 1* **85,** 3561 (1989).
6. Colby, J., Stirling, D. I., and Dalton, H., *Biochem. J.* **165,** 395 (1977).
7. Dalton, H., *Adv. Appl. Microbiol.* **26,** 71 (1980).
8. Green, J., and Dalton, H., *J. Biol. Chem.* **264,** 17698 (1989).
9. Adriaens, P., *Appl. Environ. Microbiol.* **60,** 1658 (1994).
10. Jahng, D., and Wood, T. K., *Appl. Environ. Microbiol.* **60,** 2473 (1994).
11. Fox, B. G., Borneman, J. G., Wackett, L. P., and Lipscomb, J. D., *Biochemistry* **29,** 6419 (1990).
12. Lindstrom, J. E., Prince, R. C., Clark, J. C., Grossman, M. J., Yeager, T. R., Braddock, J. F., and Brown, E., *Appl. Environ. Microbiol.* **57,** 2514 (1991).
13. Pritchard, P. H., and Costa, C. F., *Environ. Sci. Tehnol.* **25,** 372 (1991).
14. Anthony, C., "The Biochemistry of Methylotrophs," p. 296. Academic Press, New York, 1982.
15. Rosenzweig, A. C., and Lippard, S. J., *Acc. Chem. Res.* **27,** 229 (1994).
16. Lipscomb, J. D., *Annu. Rev. Microbiol.* **48,** 371 (1994).
17. Bedard, C., and Knowles, R., *Microbiol. Rev.* **53,** 68 (1989).
18. Akent'eva, N. F., and Gvozdev, R. I., *Biokhimiya* **53,** 91 (1988).
19. Nguyen, H. T., Shiemke, A. K., Jacobs, S. J., Hales, B. J., Lidstrom, M. E., and Chan, S. I., *J. Biol. Chem.* **269,** 14995 (1994).
20. Stainthorpe, A. C., Salmond, G. P., Dalton, H., and Murrell, J. C., *FEMS Microbiol. Lett.* **70,** 211 (1991).
21. Stainthorpe, A. C., Lees, V., Salmond, G. P. C., Dalton, H., and Murrell, J. C., *Gene* **91,** 27 (1990).

22. Nakajima, T., Uchiyama, H., Yagi, O., and Nakahara, T., *Biosci. Biotechnol. Biochem.* **56,** 736 (1992).
23. Koh, S.-C., Baumeen, J. P., and Sayler, G. S., *Appl. Environ. Microbiol.* **59,** 960 (1993).
24. Pilkington, S. J., and Dalton, H., *in* "Methods in Enzymology" (M. Lidstrom, ed.), Vol. 188, p. 181. Academic Press, San Diego, CA, 1990.
25. Fox, B. G., Froland, W. A., Jollie, D. R., and Lipscomb, J. D., *in* "Methods In Enzymology" (M. Lidstrom, ed.), Vol. 188, p. 191. Academic Press, San Diego, CA, 1990.
26. Prior, S. D., and Dalton, H., *FEMS Microbiol. Lett.* **29,** 105 (1985).
27. Fox, B. G., Froland, W. A., Dege, J. E., and Lipscomb, J. D., *J. Biol. Chem.* **264,** 10023 (1989).
28. Colby, J., and Dalton, H., *Biochem. J.* **177,** 903 (1979).
29. Lund, J., Woodland, M. P., and Dalton, H., *Eur. J. Biochem.* **147,** 297 (1985).
30. Lund, J., and Dalton, H., *Eur. J. Biochem.* **147,** 291 (1985).
31. Green, J., and Dalton, H., *J. Biol. Chem.* **260,** 15795 (1985).
32. Que, L., Jr., and True, A. E., *Prog. Inorg. Chem.* **38,** 97 (1990).
33. Kurtz, D. M., *Chem. Rev.* **90,** 585 (1990).
34. Wilkins, R. G., *Chem. Soc. Rev.,* 171 (1992).
35. Feig, A. L., and Lippard, S. J., *Chem. Rev.* **94,** 759 (1994).
36. Shanklin, J., Whittle, E., and Fox, B. G., *Biochemistry* **33,** 12787 (1994).
37. Woodland, M. P., Patil, D. S., Cammack, R., and Dalton, H., *Biochim. Biophys. Acta* **873,** 237 (1986).
38. DeWitt, J. G., Bentsen, J. G., Rosenzweig, A. C., Hedman, B., Green, J., Pilkington, S., Papaefthymiou, G. C., Dalton, H., Hodgson, K. O., and Lippard, S. J., *J. Am. Chem. Soc.* **113,** 9219 (1991).
39. Fox, B. G., Hendrich, M. P., Surerus, K. K., Andersson, K. K., Froland, W. A., Lipscomb, J. D., and Münck, E., *J. Am. Chem. Soc.* **115,** 3688 (1993).
40. Prince, R. C., George, G. N., Savas, J. C., Cramer, S. P., and Patel, R. N., *Biochim. Biophys. Acta* **952,** 220 (1988).
41. Rosenzweig, A. C., Frederick, C. A., Lippard, S. J., and Nordlund, P., *Nature (London)* **366,** 537 (1993).
42. DeRose, V. J., Liu, K. E., Kurtz, D. M., Jr., Hoffman, B. M., and Lippard, S. J., *J. Am. Chem. Soc.* **115,** 6440 (1993).
43. Maroney, M., Kurtz, D. M., Jr., Nocek, J. M., Pearce, L. L., and Que, L., Jr., *J. Am. Chem. Soc.* **108,** 6871 (1986).
44. Pearce, L. L., Kurtz, D. M., Jr., Xia, Y.-M., and Debrunner, P. G., *J. Am. Chem. Soc.* **109,** 7286 (1987).
45. Scarrow, R. C., Maroney, M. J., Palmer, S. M., Que, L., Jr., Roe, A. L., Salowe, S. P., and Stubbe, J., *J. Am. Chem. Soc.* **109,** 7857 (1987).
46. McCormick, J. M., Reem, R. C., and Solomon, E. I., *J. Am. Chem. Soc.* **113,** 9066 (1991).
47. Thomann, H., Bernardo, M., McCormick, J. M., Pulver, S., Andersson, K. K., Lipscomb, J. D., and Solomon, E. I., *J. Am. Chem. Soc.* **115,** 8881 (1993).
48. DeRose, V. J., Liu, K. E., Lippard, S. J., and Hoffman, B. M., submitted.
49. Bender, C. J., Rosenzweig, A. C., Lippard, S. J., and Peisach, J., *J. Biol. Chem.* **269,** 15993 (1994).
50. Hendrich, M. P., Fox, B. G., Andersson, K. K., Debrunner, P. G., and Lipscomb, J. D., *J. Biol. Chem.* **267,** 261 (1992).
51. Liu, K. E., Wang, D., Valentine, A. M., Huynh, B. H., Edmondson, D. E., Salifoglou, T., and Lippard, S. J., in preparation.

52. Hendrich, M. P., Münck, E., Fox, B. G., and Lipscomb, J. D., *J. Am. Chem. Soc.* **112,** 5861 (1990).
53. Hoffman, B. M., Sturgeon, B. E., Doan, P. E., DeRose, V. J., Liu, K. E., and Lippard, S. J., *J. Am. Chem. Soc.* **116,** 6023 (1994).
54. Pulver, S., Froland, W. A., Fox, B. G., Lipscomb, J. D., and Solomon, E. I., *J. Am. Chem. Soc.* **115,** 12409 (1993).
55. Reem, R. C., and Solomon, E. I., *J. Am. Chem. Soc.* **106,** 8323 (1984).
56. Reem, R. C., and Solomon, E. I., *J. Am. Chem. Soc.* **109,** 1216 (1987).
57. Colby, J., and Dalton, H., *Biochem. J.* **171,** 461 (1978).
58. Andersson, K. K., Froland, W. A., Lee, S.-K., and Lipscomb, J. D., *New J. Chem.* **15,** 411 (1991).
59. Liu, K. E., Johnson, C. C., Newcomb, M., and Lippard, S. J., *J. Am. Chem. Soc.* **115,** 939 (1993).
60. Jiang, Y., Wilkins, P. C., and Dalton, H., *Biochim. Biophys. Acta* **1163,** 105 (1993).
61. Froland, W. A., Andersson, K. K., Lee, S.-K., Liu, Y., and Lipscomb, J. D., *J. Biol. Chem.* **267,** 17588 (1992).
62. Liu, K. E., and Lippard, S. J., *J. Biol. Chem.* **266,** 12836, 24859 (1991).
63. Paulsen, K. E., Liu, Y., Fox, B. G., Lipscomb, J. D., Münck, E., and Stankovich, M. T., *Biochemistry* **33,** 713 (1994).
64. Liu, K. E., and Lippard, S. J., unpublished results.
65. Green, J., and Dalton, H., *Biochem. J.* **259,** 167 (1989).
66. Fox, B. G., Liu, Y., Dege, J., and Lipscomb, J. D., *J. Biol. Chem.* **266,** 540 (1991).
67. Liu, K. E., Feig, A. L., Goldberg, D. P., Watton, S. P., and Lippard, S. J., *in* "The Activation of Dioxygen and Homogeneous Catalytic Oxidation" (D. H. R. Barton, A. E. Martell, and D. T. Sawyer, eds.), p. 301. Plenum, New York, 1993.
68. Tsien, H.-C., and Hanson, R. S., *Appl. Environ, Microbiol.* **58,** 953 (1992).
69. Lee, S.-K., Fox, B. G., Froland, W. A., Lipscomb, J. D., and Münck, E., *J. Am. Chem. Soc.* **115,** 6450 (1993).
70. Lee, S.-K., Nesheim, J. C., and Lipscomb, J. D., *J. Biol. Chem.* **268,** 21569 (1993).
71. Liu, K. E., Wang, D., Huynh, B. H., Edmondson, D. E., Salifoglou, A., and Lippard, S. J., *J. Am. Chem. Soc.* **116,** 7465 (1994).
72. Liu, K. E., Valentine, A. M., Qiu, D., Edmondson, D. E., Appelman, E. H., Spiro, T. G., and Lippard, S. J., *J. Am. Chem. Soc.* **117,** 4997 (1995).
73. This absorption was detected by using monochromatic methods at 15 nm resolution. The 625 nm value may therefore not reflect a true absorbance maximum for L.
74. Brennan, B. A., Chen, Q., Juarez-Garcia, C., True, A. E., O'Connor, C. J., and Que, L., Jr., *Inorg. Chem.* **30,** 1937 (1991).
75. Nishida, Y., Takeuchi, M., Shimo, H., and Kida, S., *Inorg. Chim. Acta* **96,** 115 (1984).
76. Nishida, Y., and Takeuchi, M., *Z. Naturforsch., B: Chem. Sci.* **42B,** 52 (1987).
77. Magnus, K. A., Hazes, B., Ton-That, H., Bonaventura, C., Bonaventura, J., and Hol, W. G. J., *Proteins: Sruct., Funct., Genet.* **19,** 302 (1994).
78. Kitajima, N., Fujisawa, K., Fujimoto, C., Moro-oka, Y., Hashimoto, S., Kitagawa, T., Toriumi, K., Tatsumi, K., and Nakamura, A., *J. Am. Chem. Soc.* **114,** 1277 (1992).
79. Ortiz de Montellano, P. R., *in* "Cytochrome P-450 Structure, Mechanism, and Biochemistry" (P. R. Ortiz de Montellano, ed.), p. 217. Plenum, New York, 1986.
80. Bollinger, J. M., Jr., Tong, W. H., Ravi, N., Huynh, B. H., Edmondson, D. E., and Stubbe, J., *J. Am. Chem. Soc.* **116,** 8015 (1994).
81. Bollinger, J. M., Jr., Tong, W. H., Ravi, N., Huynh, B. H., Edmondson, D. E., and Stubbe, J., *J. Am. Chem. Soc.* **116,** 8024 (1994).

82. Ravi, N., Bollinger, J. M., Jr., Huynh, B. H., Edmondson, D., and Stubbe, J., *J. Am. Chem. Soc.* **116,** 8007 (1994).
83. Rataj, M. J., Kauth, J. E., and Donnelly, M. I., *J. Biol. Chem.* **266,** 18684 (1991).
84. Bowry, V. W., Lusztyk, J., and Ingold, K. U., *J. Am. Chem. Soc.* **111,** 1927 (1989).
85. Bowry, V. W., and Ingold, K. U., *J. Am. Chem. Soc.* **113,** 5699 (1991).
86. Bowry, V. W., Lusztyk, J., and Ingold, K. U., *J. Am. Chem. Soc.* **113,** 5687 (1991).
87. Ortiz de Montellano, P. R., and Stearns, R. A., *J. Am. Chem. Soc.* **109,** 3415 (1987).
88. Ruzicka, F., Huang, D.-S., Donnelly, M. I., and Frey, P. A., *Biochemistry* **29,** 1696 (1990).
89. Wilkins, P. C., Dalton, H., Podmore, I. D., Deighton, N., and Symons, C. R., *Eur. J. Biochem.* **210,** 67 (1992).
90. Dalton, H., Wilkins, P. C., Deighton, N., Podmore, I. D., and Symons, M. C. R., *Faraday Discuss. Chem. Soc.* **93,** 163 (1992).
91. Groves, J. T., and McClusky, G. A., *Biochem. Biophys. Res. Commun.* **81,** 154 (1978).
92. Groves, J. T., and Subramanian, D. V., *J. Am. Chem. Soc.* **106,** 2177 (1984).
93. Priestley, N. D., Floss, H. G., Froland, W. A., Lipscomb, J. D., Williams, P. G., and Morimoto, H., *J. Am. Chem. Soc.* **114,** 7461 (1992).
94. Wilkinson, B., Liu, K. E., Valentine, A. M., Morimoto, H., Williams, P. G., Lippard, S. J., and Floss, H., unpublished results.
95. Choi, S.-Y., Eaton, P. E., Hollenberg, P. F., Liu, K. E., Lippard, S. J., Newcomb, M., Put, D. A., and Upadhyaya, S. P., in preparation.
96. Shimoda, M., and Okura, I., *J. Mol. Catal.* **72,** 263 (1992).
97. Atkinson, J. K., Hollenberg, P. F., Ingold, K. U., Johnson, C. C., Le Tadic, M.-H., Newcomb, M., and Putt, D. A., *Biochemistry* **33,** 10630 (1994).
98. Groves, J. T., Avaria-Neisser, G. E., Fish, K. M., Imachi, M., and Kuczkowski, R. L., *J. Am. Chem. Soc.* **108,** 3837 (1986).

ADVANCES IN INORGANIC CHEMISTRY, VOL. 42

ALKYL, HYDRIDE, AND HYDROXIDE DERIVATIVES OF THE *s*- AND *p*-BLOCK ELEMENTS SUPPORTED BY POLY(PYRAZOLYL)BORATO LIGATION: MODELS FOR CARBONIC ANHYDRASE, RECEPTORS FOR ANIONS, AND THE STUDY OF CONTROLLED CRYSTALLOGRAPHIC DISORDER

GERARD PARKIN

Department of Chemistry, Columbia University, New York, New York 10027

I. Introduction
II. Syntheses, Structures, and Steric Properties of Poly(pyrazolyl)hydroborato Ligands
  A. Abbreviations
  B. Syntheses
  C. Structures of M[$Bp^{RR'}$] and M[$RTp^{RR'}$] Derivatives
  D. Steric Properties
  E. Electronic Properties
III. Terminal Alkyl Derivatives of the *s*- and *p*-Block Metals Supported by Poly(pyrazolyl)borato Ligation
  A. Poly(pyrazolyl)borato Alkyl Derivatives of the Group 2 Elements
  B. Poly(pyrazolyl)borato Alkyl Derivatives of the Group 11 Elements
  C. Poly(pyrazolyl)borato Alkyl Derivatives of the Group 12 Elements
  D. Poly(pyrazolyl)borato Alkyl Derivatives of the Group 13 Elements
  E. Poly(pyrazolyl)borato Alkyl Derivatives of the Group 14 Elements
IV. Terminal Hydride Derivatives of the *s*- and *p*-Block Metals Supported by Poly(pyrazolyl)borato Ligation
  A. [Tp^{But}]BeH
  B. [Tp^{But}]ZnH
  C. [Tp^{But}]CdH
V. Terminal Hydroxide Derivatives of the *s*- and *p*-Block Metals Supported by Poly(pyrazolyl)borato Ligation
  A. Hydroxide Derivatives of Beryllium and Magnesium
  B. Hydroxide Derivatives of Zinc and Cadmium
VI. Anion Coordination by Protonated Tris(pyrazolyl)hydroborato Derivatives

Copyright © 1995 by Academic Press, Inc.
All rights of reproduction in any form reserved.

VII. Controlled Crystallographic Disorder in [$Tp^{RR'}$]MX Complexes: Bond Length Artifacts as Determined by Single Crystal X-Ray Diffraction
A. Introduction
B. Disorder between Structurally Similar Groups
C. Disorder between Structurally Disparate Groups
VIII. Summary
References

I. Introduction

In 1966 Trofimenko first reported the synthesis of a class of molecule that would become a valuable ligand system in modern coordination chemistry (*1–2*). Specifically, the system that Trofimenko developed is that of the poly(pyrazolyl)borato ligand. The three fundamental types of poly(pyrazolyl)borato ligands that are presently utilized may be classified according to the degree of pyrazolyl substitution at boron, namely the bis, tris, and tetrakis pyrazolyl derivatives $[X_{4-n}B(RR'pz)_n]^-$ (e.g., X = H, alkyl, aryl, NR_2, SAr; RR'pz = substituted pyrazolyl group; n = 2, 3, 4), shown in Fig. 1 (*3*). As is evident from the formulation of $[X_{4-n}B(pz)_n]^-$, the poly(pyrazolyl)borato ligand system constitutes a very large number of potential ligands, especially when one considers that each of the pyrazolyl groups and X groups need not necessarily be identical in a given ligand (*4*). Poly(pyrazolyl)borato ligands, therefore, constitute a highly versatile ligand system, which may be both electronically and sterically tuned to modify a metal center in a desired fashion.

Poly(pyrazolyl)borato ligands offer a variety of coordination modes according to their degree of substitution. Bis and tris(pyrazolyl)hydroborato derivatives tend to adopt bidentate and tridentate coordination modes almost exclusively (*5*), while the tetrakis(pyrazolyl)borato ligand

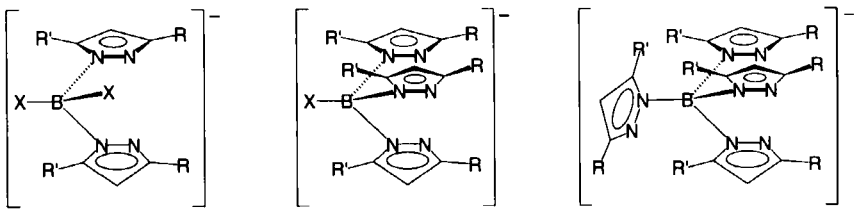

FIG. 1. Bis-, tris- and tetrakis(pyrazolyl)borato ligands.

frequently adopts both bidentate and tridentate coordination modes, depending upon the specific system. Furthermore, depending upon the nature of the X substituents, bis(pyrazolyl)borato ligands may offer tridentate coordination to a metal center via a B–X–M interaction. The principal coordination modes that are adopted by poly(pyrazolyl)borato ligands are summarized in Fig. 2. At the outset, it should be emphasized that the particular choice of poly(pyrazolyl)borato ligand is often crucial to obtaining the desired results, whether it be stabilizing a particular coordination geometry, or promoting a certain kind of reactivity. Of the poly(pyrazolyl)borato derivatives illustrated in Fig. 2, the highlighted tridentate coordination of the tris(pyrazolyl)hydroborato ligand is perhaps the most commonly encountered and forms the major component of the studies to be described in this review. In particular, the scope of this review will be mainly limited to the use of sterically demanding bis and tris(pyrazolyl)hydroborato derivatives to support monomeric alkyl, hydride, hydroxide and related derivatives of the *s*- and *p*-block metals.

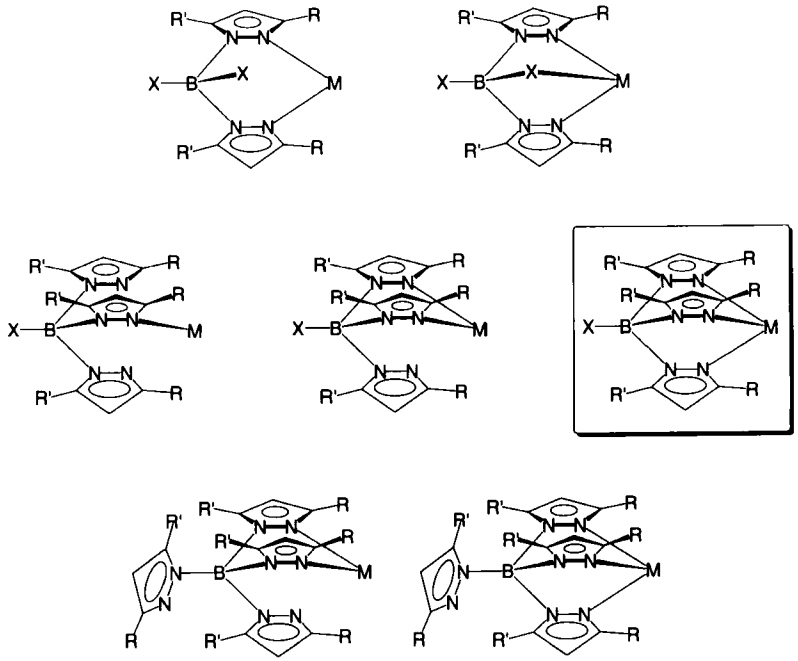

FIG. 2. Coordination modes adopted by poly(pyrazolyl)borato ligands.

II. Syntheses, Structures, and Steric Properties of Poly(pyrazolyl)hydroborato Ligands

A. ABBREVIATIONS

Given the large variety of poly(pyrazolyl)borato ligands which exist, a system of nomenclature is desirable. The system which is adopted here is based on that described by Trofimenko (*2a*). Thus, the tris(pyrazolyl)hydroborato ligands are represented by the abbreviation [Tp], with the 3- and 5-alkyl substituents (see Fig. 3 to identify the 3- and 5-positions) listed respectively as superscripts, e.g., [Tp^{But}], [$Tp^{But,Me}$], and [Tp^{Me2}] (*6, 7*). If the fourth substituent on boron is anything other than hydrogen, the substituent is listed as a prefix, e.g., [pzTp] and [RTp]. Similarly, the bis(pyrazolyl)hydroborato ligands will be represented by the abbreviation [Bp] with appropriate prefixes and superscripts. For convenience, the abbreviations [$Tp^{RR'}$] and [$Bp^{RR'}$] will be used to refer to a general ligand type, and the prefixes η^1- and η^2- will be used to specify if the [$Tp^{RR'}$] ligand is not tridentate. Some of the

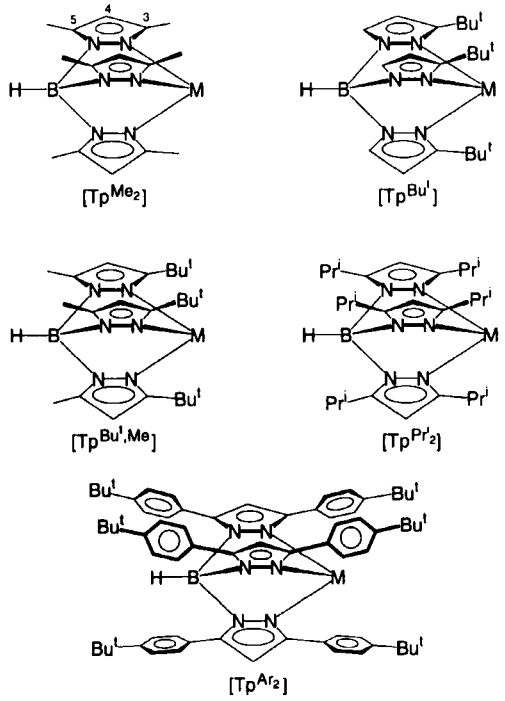

FIG. 3. A selection of tris(pyrazolyl)hydroborato ligands.

poly(pyrazolyl)borato ligands that are featured in this review, such as $[Tp^{Me2}]$ (*8*), $[Tp^{But}]$ (*9*), $[Tp^{But,Me}]$ (*10*), $[Tp^{Pri2}]$ (*11*), and $[Tp^{Ar2}]$ (Ar = *p*-$C_6H_4Bu^t$) (*12*), are summarized in Fig. 3.

B. SYNTHESES

Bis and tris(pyrazolyl)hydroborato ligands are generally prepared as the potassium derivatives by the direct reaction of KBH_4 with the appropriate pyrazole (RR'pzH), as illustrated in Scheme 1 for the parent system (*13*). The reaction is extremely general and has been applied to a number of different derivatives, which have included the incorporation of chiral (*14, 15*) and tethered (*16*) substituents. However, if the alkyl substituents of the pyrazole are inequivalent (i.e., R ≠ R'), a potential problem may be encountered with the formation of isomeric products, in which either of the R and R' substituents may occupy the 3-position of the poly(pyrazolyl)borato ligand. Nevertheless, if the difference in steric demands of R and R' is large, there is a strong

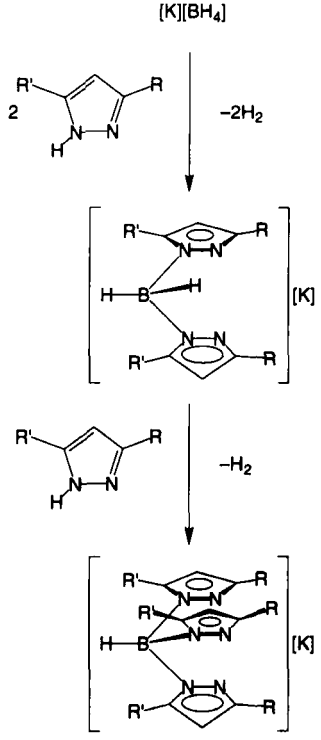

SCHEME 1. Synthesis of $K[Bp^{RR'}]$ and $K[Tp^{RR'}]$ derivatives.

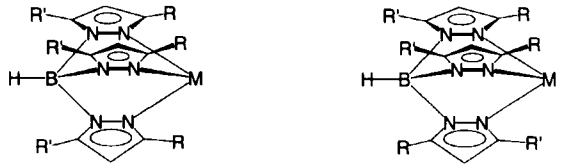

C_3-symmetric C_s-symmetric

FIG. 4. Possible isomers for [$Tp^{RR'}$] derivatives if R and R′ have similar steric demands.

tendency for each of the larger alkyl substituents to occupy the 3-positions of the poly(pyrazolyl)borato ligand (since this reduces the steric interactions that would result around boron if they occupied the 5-positions), and a single isomer is obtained. One such example is observed for R = Bu^t and R′ = H, which results in the formation of a C_3-symmetric tris(pyrazolyl)hydroborato derivative, [Tp^{But}]. In contrast, if R and R′ have similar steric demands, so that there is not a strong preference for either one of the substituents to occupy the 3-position, then derivatives with only C_s symmetry may be obtained in addition to the C_3-symmetric [$Tp^{RR'}$] derivative (Fig. 4) (*17, 18*). The use of symmetric pyrazole derivatives (R = R′) naturally eliminates such a problem.

The potassium derivatives obtained from the reaction mixture are typically not isolated in pure form, and the crude products are often converted directly to the thallium complexes by metathesis with either thallium nitrate or thallium acetate [Eqs. (1) and (2)].

$$K[Bp^{RR'}] + TlX \longrightarrow Tl[Bp^{RR'}] + KX \quad (1)$$

$$K[Tp^{RR'}] + TlX \longrightarrow Tl[Tp^{RR'}] + KX \quad (2)$$

$M[Tp^{RR'}]$ complexes (M = Li, Na, Cs, R_4N^+) may also be obtained by the reactions of the monoprotonated derivative $H[Tp^{RR'}]$ with MOH (*1b*). Both the $M[Tp^{RR'}]$ and $M[Bp^{RR'}]$ complexes are useful starting materials for the preparation of poly(pyrazolyl)borato complexes of both the transition and main group metals.

C. STRUCTURES OF $M[Bp^{RR'}]$ AND $M[RTp^{RR'}]$ DERIVATIVES

As far as bis(pyrazolyl)hydroborato derivatives of monovalent ions are concerned, only the structure of $Tl[Bp^{But,Me}]$ has been determined by x-ray diffraction (*19*). The structure consists of a monomer in which

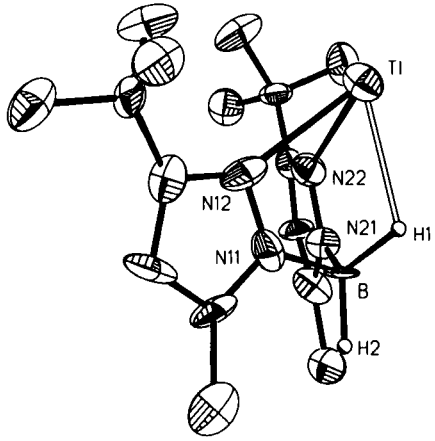

FIG. 5. ORTEP drawing of $Tl[Bp^{Bu^t,Me}]$.

coordination via the pyrazolyl groups is supplemented by interaction with one of the B-H groups [$d(Tl\cdots H)$ = 2.4(1) Å], as shown in Figs. 5 and 6 (*20*). Although only one $Tl[Bp^{RR'}]$ derivative has been structurally characterized by x-ray diffraction, the structures of several $Tl[Tp^{RR'}]$ derivatives have been determined. Specific examples include $Tl[Tp^{Bu^t}]$ (*21*), $Tl[Tp^{Bu^t,Me}]$ (*22*), $Tl[Tp^{Bu^t_2}]$ (*23*), $Tl[Tp^{p\text{-}Tol}]$ (*24*), $Tl[Tp^{Ar_2}]$ (Ar = p-$C_6H_4Bu^t$) (*12*), $Tl[Tp^{Ant}]$ (Ant = 9-anthryl) (*25*), $Tl[Tp^{Menth}]$ (Menthpz = 7(*R*)-isopropyl-4(*R*)-methyl-4,5,6,7-tetrahydroindazolyl)

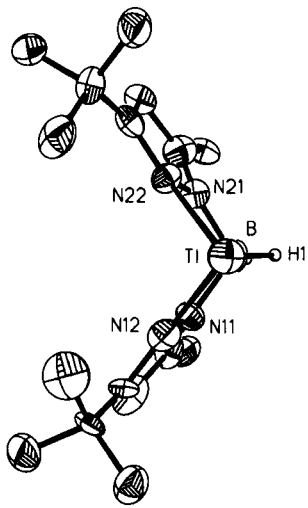

FIG. 6. View of $Tl[Bp^{Bu^t,Me}]$ down Tl···B vector.

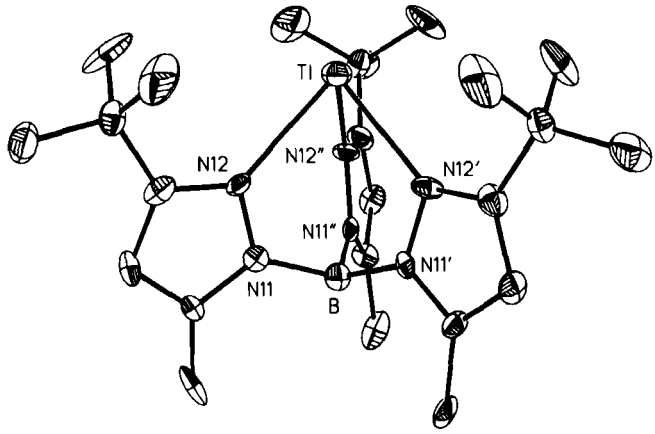

FIG. 7. ORTEP drawing of Tl[Tp$^{Bu^t,Me}$]. Reprinted from *Polyhedron, 14*, Yoon, K., and Parkin, G., p. 811, © copyright 1995, with kind permission from Elsevier Science Ltd, The Boulevard, Langford Lane, Kidlington 0X5 1GB, UK.

(*15*), and Tl[Tp^{Mementh}] (Mementhpz = 7(*S*)-*t*-butyl-4(*R*)-methyl-4,5,6,7-tetrahydroindazolyl) (*15*). For comparison with Tl[Bp$^{Bu^t,Me}$], the structure of Tl[Tp$^{Bu^t,Me}$] is shown in Figs. 7 and 8. In each of the complexes Tl[Tp$^{RR'}$], the tris(pyrazolyl)hydroborato ligand is coordinated to thallium in a tridentate fashion. With the exception of Tl[Tp^{Ant}], for which the structure is not of high accuracy due to compositional dis-

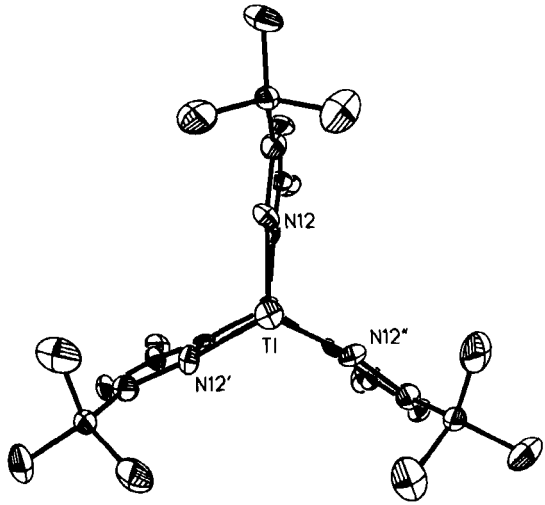

FIG. 8. View of Tl[Tp$^{Bu^t,Me}$] down Tl · · · B vector. Reprinted from *Polyhedron, 14*, Yoon, K., and Parkin, G., p. 811, © copyright 1995, with kind permission from Elsevier Science Ltd, The Boulevard, Langford Lane, Kidlington 0X5 1GB, UK.

TABLE I

SELECTED METRICAL DATA FOR Tl[$Bp^{RR'}$] AND Tl[$Tp^{RR'}$] DERIVATIVES

	d(Tl–N_{av})/Å	N–Tl–N_{av}/°	Ref.[d]
Tl[$Bp^{Bu^t,Me}$]	2.59(3)	74(1)	1
Tl[Tp^{Bu^t}]	2.59(1)	78(3)	2
Tl[$Tp^{Bu^t,Me}$]	2.50(2)	78(1)	3
Tl[$Tp^{Bu^t_2}$]	2.57(3)	78(3)	4
Tl[Tp^{Menth}]	2.55(2)	76(4)	5
Tl[$Tp^{Mementh}$]	2.56(4)	77(3)	5
Tl[$Tp^{p\text{-}Tol}$]	2.58(1)	77(2)	6
Tl[Tp^{In}][a]	2.53(2)	76(4)	7
Tl[Tp^{Ar_2}][b]	2.61(5)	77(2)	8
Tl[Tp^{Ant}]	2.68(3)[c]	66(1)[c]	9

[a] [Tp^{In}] = tris(1,4-dihydroindeno[1,2-*c*]pyrazol-1-yl)borato.

[b] Ar = *p*-$C_6H_4Bu^t$.

[c] The structure was performed on a compositionally disordered crystal, so that the derived metrical data is of limited accuracy.

[d] (1) Dowling, C., and Parkin, G., unpublished results (1995); (2) Cowley, A. H., Geerts, R. L., Nunn, C. M., and Trofimenko, S., *J. Organomet. Chem.* **365,** 19 (1989); (3) Yoon, K., and Parkin, G., *Polyhedron* **14,** 811 (1995); (4) Dowling, C., Leslie, D., Chisholm, M. H., and Parkin, G., *Main Group Chemistry,* in press; (5) LeCloux, D. D., Tokar, C. J., Osawa, M., Houser, R. P., Keyes, M. C., and Tolman, W. B., *Organometallics* **13,** 2855 (1994); (6) Ferguson, G., Jennings, M. C., Lalor, F. J., and Shanahan, C., *Acta Crystallogr., Sect. C: Cryst. Struct. Commun.* **C47,** 2079 (1991); (7) Rheingold, A. L., Ostrander, R. L., Haggerty, B. S., and Trofimenko, S., *Inorg. Chem.* **33,** 3666 (1994); (8) Libertini, E., Yoon, K., and Parkin, G., *Polyhedron* **12,** 2539 (1993); (9) Han, R., Parkin, G., and Trofimenko, S., *Polyhedron* **14,** 387 (1995).

order (*25*), the average Tl–N bond lengths fall in the range 2.50–2.61 Å, while the average N–Tl–N bond angles are in the range 77–78° (Table I). The Tl–N bond lengths are longer than the sum of the covalent radii (2.31 Å), presumably because the bonding between Tl and the tris(pyrazolyl)hydroborato ligand comprises one normal covalent and two dative covalent interactions (*26*).

Another feature to be noted about the structures of Tl[$Tp^{RR'}$] is concerned with the structural influence of the 5-alkyl substituent. For example, whereas the 5-methyl derivative Tl[$Tp^{Bu^t,Me}$] exhibits approximate C_{3v} symmetry (Fig. 8), the 5-*t*-butyl derivative Tl[$Tp^{Bu^t_2}$] displays a pronounced distortion such that the molecule possesses only C_3 symmetry (Figs. 9 and 10) (*27*).

The structure of K[$Tp^{Bu^t_2}$] has also been determined by x-ray diffraction thereby providing a rare example of a potassium complex in which the primary coordination number is three, with an average K–N bond

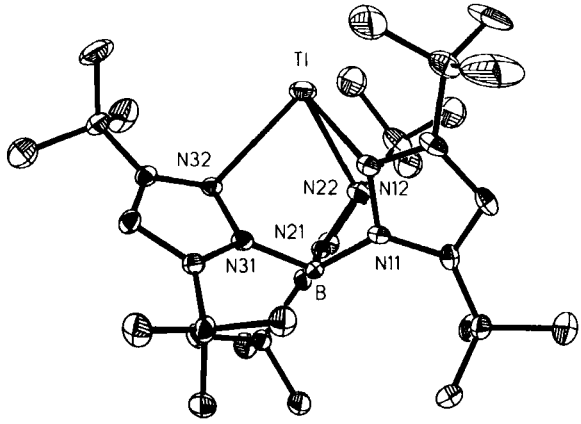

FIG. 9. ORTEP drawing of $Tl[Tp^{But2}]$.

length of 2.73[2] Å (*28*). Interestingly, the potassium also exhibits a weak association with a molecule of benzene in the solid state (Figs. 11 and 12), with K···C separations in the range 3.44–3.82 Å (*29*). The structure of the cesium derivative $Cs[Tp^{But2}]$, with an average Cs–N bond length of 3.01[1] Å, is similar to that of the potassium derivative in that it also exhibits a pronounced distortion from C_{3v} symmetry (Fig. 13) (*23*). However, in contrast to the potassium derivative, there is no association between Cs and benzene, even though benzene is a component of the crystal lattice.

The structures of the hydrated sodium and potassium derivatives

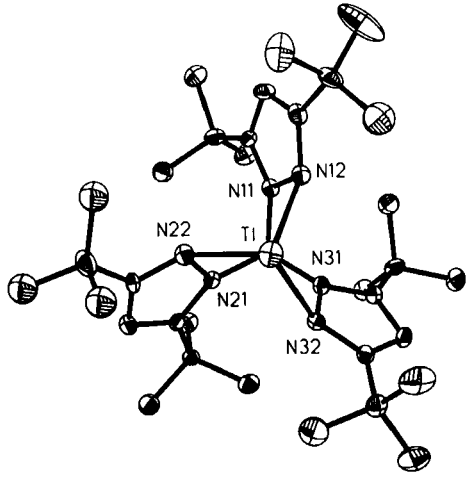

FIG. 10. View of $Tl[Tp^{But2}]$ down Tl···B vector.

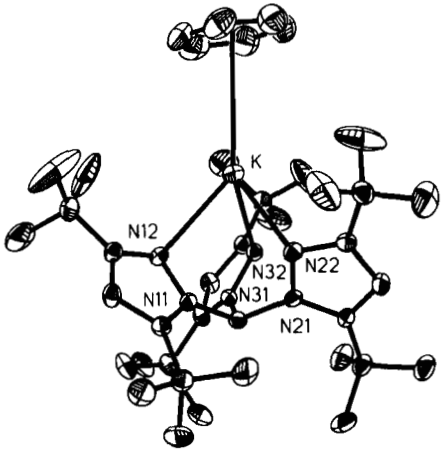

FIG. 11. ORTEP drawing of $K[Tp^{But2}](C_6H_6)$.

$M[pzTp](H_2O)$ (M = Na, K) have been determined by x-ray diffraction (*30*). In contrast to the discrete monomeric structures of the tris (pyrazolyl)hydroborato complexes $Tl[Tp^{RR'}]$, $K[Tp^{But2}]$, and $Cs[Tp^{But2}]$ described earlier, the hydrated tetrakis(pyrazolyl)borato complexes $M[PzTp](H_2O)$ (M = Na, K) exhibit an interesting polymeric-type structure, a portion of which is illustrated in Fig. 14. In each case, the cations occupy two different crystallographic sites, and the cation in one of the sites is coordinated to two pyrazolyl groups in a π-type fashion.

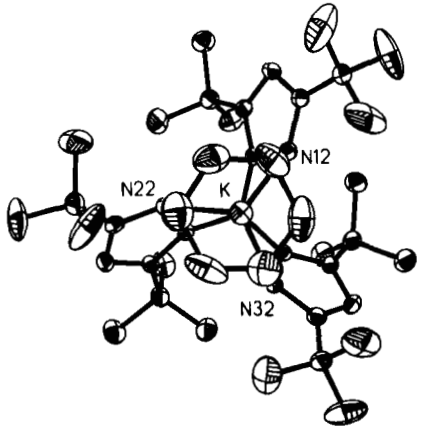

FIG. 12. View of $K[Tp^{But2}](C_6H_6)$ down K···B vector.

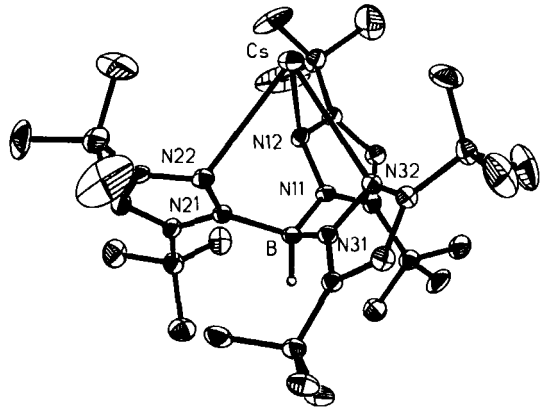

FIG. 13. ORTEP drawing of Cs[Tp^{But2}].

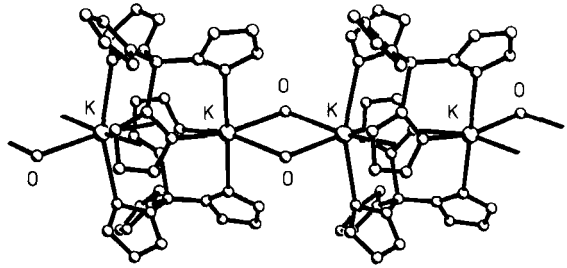

FIG. 14. Part of the polymeric structure of K[pzTp](H$_2$O).

D. STERIC PROPERTIES

1. Substitution at the 3-Position

The emphasis of the studies to be described in this review is principally concerned with poly(pyrazolyl)borato ligands that have been modified to create a sterically demanding environment about a metal center. Such modification may be readily achieved by appropriate substitution at the 3-position of the pyrazolyl group. The steric demands of a [Tp$^{RR'}$] ligand may be defined by a cone angle (θ) (*31*) and a wedge angle (ω), (*16b*) as illustrated in Fig. 15. The cone angle provides a measure of the overall encapsulation of the metal center, while the wedge angle provides an indication of the open space available between the planes of the substituted pyrazolyl groups (Table II). The data demonstrate that the cone angle increases substantially across the series [Tp] (199°) < [Tp^{Me2}] (236°) < [Tp^{Pri4Br}] (262°) < [Tp^{But}] (244°) (*9, 16b*) while

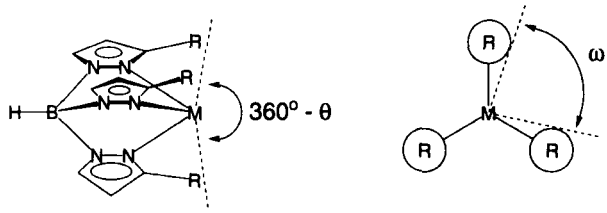

FIG. 15. Cone angles (θ) and wedge angles (ω) of tris(pyrazolyl)hydroborato ligands.

the wedge angle decreases. Although the [Tp^{Ms}] ligand (Ms = mesityl), with a cone angle of 281° and a wedge angle of only 7°, represents one of the most sterically demanding tris(pyrazolyl)hydroborato derivatives, it is the [Tp^{But}] ligand that has been the most utilized of the sterically demanding ligands. Indeed, the steric demands provided by *t*-butyl substituents in the 3-positions of the pyrazolyl rings result in the [Tp^{But}] ligand providing an environment that strongly stabilizes four-coordination in preference to higher coordination numbers. Consequently, the ligand has been aptly termed a "tetrahedral enforcer," especially with regard to the first-row transition metals and main group metals (*9*). Such a property will be seen to be critical for the studies to be described in this review. Furthermore, in addition to providing a stable coordination environment, the presence of alkyl substituents such as *t*-butyl provides an invaluable spectroscopic handle for monitoring the reactivity of the complexes.

As expected, the related isopropyl ligand systems [Tp^{Pri}] (*32*) and [Tp^{Pri_2}] (*11*) are noticeably less sterically demanding than their *t*-butyl counterparts. Thus, neither ligand prevents the formation of five-coordinate complexes of the types [Tp^{Pri}]M(X)L or [Tp^{Pri_2}]M(X)L

TABLE II

CONE ANGLE AND WEDGE ANGLE DATA FOR SOME [$Tp^{RR'}$] LIGANDS[a]

	Cone angle θ/°	Wedge angle ω/°
[Tp]	199	91
[Tp^{Me_2}]	236	75
[Tp^{Pri_4Br}]	262	36
[Tp^{But}]	265	35
[Tp^{Ms}]	281	7

[a] Data taken from Rheingold, A. L., Ostrander, R. L., Haggerty, B. S., and Trofimenko, S., *Inorg. Chem.* **33**, 3666 (1994).

for certain metals. A further complication that is observed for the [Tp^{Pr^i}] ligand system is that octahedral complexes, e.g., [η^3-HB(3-Pr^ipz)$_2$(5-Pr^ipz)]$_2$Co may result as a consequence of ligand rearrangement.

The formation of six-coordinate sandwich complexes is even more prevalent with less sterically demanding ligands such as [Tp^{Me2}], [Tp^{Ph}] and [Tp^{Ph2}], e.g., [Tp^{Me2}]$_2$Mg (*27*) and [Tp^{Ph}]$_2$M (M = Mn, Fe) (*33*). Similarly, the neopentyl (Np) derivative [Tp^{Np}] also forms a six-coordinate sandwich complex of nickel, [Tp^{Np}]$_2$Ni (*34*). Moreover, the [Tp^{Np}] ligand is also known to undergo rearrangement analogous to that of the [Tp^{Pr^i}] ligand, e.g., [η^3-HB(3-Nppz)$_2$(5-Nppz)]$_2$M (M = Co, Fe). In view of these ligand rearrangements, the use of a symmetric 3,5-disubstituted pyrazolyl derivative offers the advantage that potential rearrangements are degenerate.

Since the variation of the interplanar angle between the pyrazolyl and aryl groups at the 3-position may also serve to modify the steric environment about a metal center, a number of tris(pyrazolyl)borato ligands have been prepared with a variety of modifications to the 3-aryl substituent. For example, the interaction between the *ortho* methyl groups of the mesityl substituents and the MX moiety in complexes of the type [Tp^{Ms}]MX (Ms = mesityl) promotes noncoplanarity of the pyrazolyl and aryl groups (*18*). Similarly, a 9-anthryl substituent in the 3-position has been used to provide a ligand system [Tp^{Ant}] in which the aryl and pyrazolyl planes are strongly inhibited from adopting a coplanar orientation (*25*). Such a ligand offers potential in providing an environment that is less sterically demanding than that created by the [Tp^{But}] ligand, but it is sufficient to inhibit the formation of six-coordinate sandwich complexes of the type [Tp^{Ant}]$_2$M.

Based on a similar strategy, the *para-t*-butylphenyl ligand [Tp^{Ar2}] (Ar = *p*-$C_6H_4Bu^t$) has been prepared with the notion that the *t*-butyl substituents may be sufficient to inhibit the formation of six-coordinate [Tp^{Ar2}]$_2$M sandwich complexes (*12*). At the same time, however, it is anticipated that the phenyl substituents in the immediate vicinity of the metal center will provide a coordination environment that is less sterically demanding than that of [Tp^{But}]. A related ligand with *para-i*-propylphenyl substituents, K[$Tp^{Ar',Me}$] (Ar' = *p*-$C_6H_4Pr^i$) has also been synthesized by Vahrenkamp (*35*).

Another illustration of the structural changes that may result as a consequence of alkyl substitution at the 3-position of the pyrazolyl group is provided by the structures of the dimeric copper(I) complexes {[Tp]Cu}$_2$ (*36*), {[Tp^{Me2}]Cu}$_2$ (*36*), {[Tp^{Ph2}]Cu}$_2$ (*37*), and {[Tp^{But}]Cu}$_2$ (*37*), which differ in the manner in which the tris(pyrazolyl)hydroborato ligand bridges the two copper centers (Fig. 16).

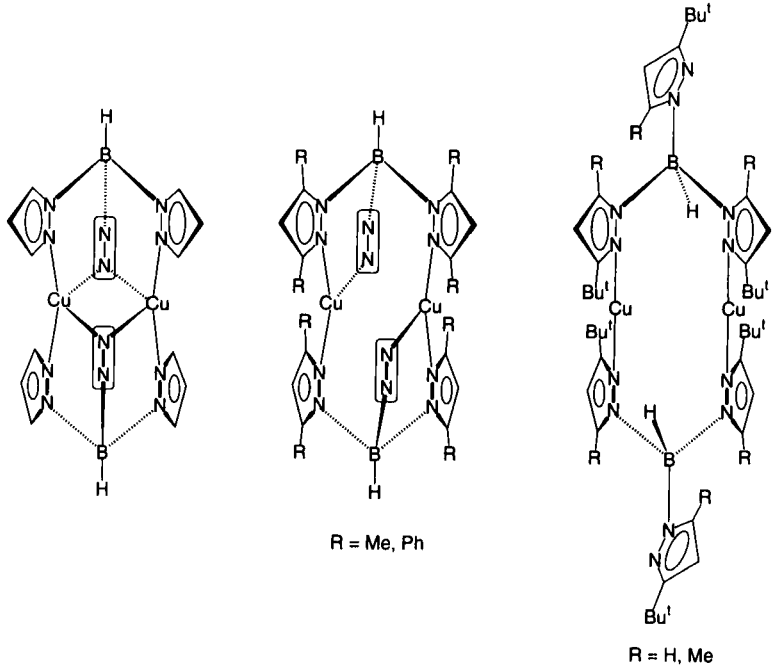

FIG. 16. Structures of $\{[Tp^{RR'}]Cu\}_2$ derivatives.

Thus, the degree of bridging of the tris(pyrazolyl)hydroborato ligand is reduced considerably from that in $\{[Tp]Cu\}_2$, in which the ligand bridges the two copper centers in an approximately symmetric manner, to that in $\{[Tp^{But}]Cu\}_2$, in which one of the pyrazolyl groups of each ligand is uncoordinated. Correspondingly, the coordination number of the copper is reduced from four for $\{[Tp]Cu\}_2$, to three for $\{[Tp^{Me2}]Cu\}_2$ and $\{[Tp^{Ph2}]Cu\}_2$, and to two for $\{[Tp^{But}]Cu\}_2$. The separation between the two copper centers in $\{[Tp^{But}]Cu\}_2$ [3.284(8) Å] is also substantially greater than the separations in $\{[Tp]Cu\}_2$ [2.660(1) Å], $\{[Tp^{Me2}]Cu\}_2$ [2.506(1) Å], and $\{[Tp^{Ph2}]Cu\}_2$ [2.544(2) Å].

2. *Substitution at the 5-Position*

The use of substitution at the 3-position to modify the steric environment about the metal center has been described in Section II,D,1. In a similar vein, substitution at the remote 5-position has been used with the specific goal of providing steric protection for the B–H moiety in attempts to inhibit ligand degradation. Indeed, as will be described, the steric protection that is provided by the methyl groups of the

[$Tp^{But,Me}$] ligand has allowed the syntheses of complexes that were not accessible for the corresponding [Tp^{But}] system.

Compared to substitution at the 3-position, alkyl substitution at the 5-position would not be expected to exert a strong structural influence at the metal center, although increased steric interactions between the 5-substituents would be expected to increase the ligand bite at the metal center (*10*). However, as seen with the structures of the thallium derivatives Tl[$Tp^{RR'}$] described in Section II,C, the structural influence of a 5-alkyl substituent should not be dismissed. Thus, it is possible to observe quite dramatic structural changes upon incorporation of a 5-alkyl substituent, as emphasized by the structure of Tl[Tp^{But2}] (Figs. 9 and 10). Such structural changes are related to the observation that the complexes $[pzTp]_2Pb$ and $[Tp]_2Pb$ exhibit different structures as a result of *intraligand interactions*. As a consequence of these interactions, the potentially tridentate tetrakis(pyrazolyl)borato ligand [pzTp] acts only as a *bidentate* ligand in $[pzTp]_2Pb$, whereas the tris(pyrazolyl)-hydroborato ligands in $[Tp]_2Pb$ are tridentate (*38, 39*).

Structural changes due to the presence of a 5-substituent may also be observed for groups less bulky than *t*-butyl. For example, the structural change that is induced upon incorporation of a 5-methyl substituent is observed by comparison of the two copper centers in [Tp^{But}]CuCl (*40*) and [$Tp^{But,Me}$]CuCl (Fig. 17) (*22*). Thus, from the two orthogonal views of both [$Tp^{But,Me}$]CuCl and [Tp^{But}]CuCl shown in Fig. 17, it is apparent that the two complexes differ substantially in the position of the chloride ligand, even though the Cu–Cl bond lengths ([$Tp^{But,Me}$]CuCl [2.168(1) Å] and [Tp^{But}]CuCl [2.143(2) Å]) are very similar. Specifically, the Cl–Cu–N(32) bond angle of 113.2(1)° in [Tp^{But}]CuCl expands considerably to 142.8(1)° for Cl–Cu–N(12) in [$Tp^{But,Me}$]CuCl, a change that is accompanied by an increased separation of the pyrazolyl groups on either side of the mirror plane, from 92.0(1)° for N(12)–Cu–N(22) in [Tp^{But}]CuCl, to 102.9(1)° for N(22)–Cu–N(22′) in [$Tp^{But,Me}$]CuCl.

However, despite the rather dramatic change in coordination geometry that is observed upon comparing [$Tp^{But,Me}$]CuCl and [Tp^{But}]CuCl (*41*), only rather minor perturbations are observed in comparing the structures of the Cu(I) dimers $\{[Tp^{But}]Cu\}_2$ (*37*) and $\{[Tp^{But,Me}]Cu\}_2$ (*22*). Thus, both the average Cu–N bond lengths and also the Cu···Cu separations in $\{[Tp^{But,Me}]Cu\}_2$ and $\{[Tp^{But}]Cu\}_2$ are very similar. Nevertheless, although the coordination environment about each copper center is similar, the 5-methyl substituent does influence the fluxional nature of the molecule in solution. Thus, whereas $\{[Tp^{But}]Cu\}_2$ is fluxional on the NMR time scale at room temperature, with a static structure that is only observed at −56°C, $\{[Tp^{But,Me}]Cu\}_2$ exhibits a static ^1H NMR spectrum at room temperature. Furthermore, a static spectrum for

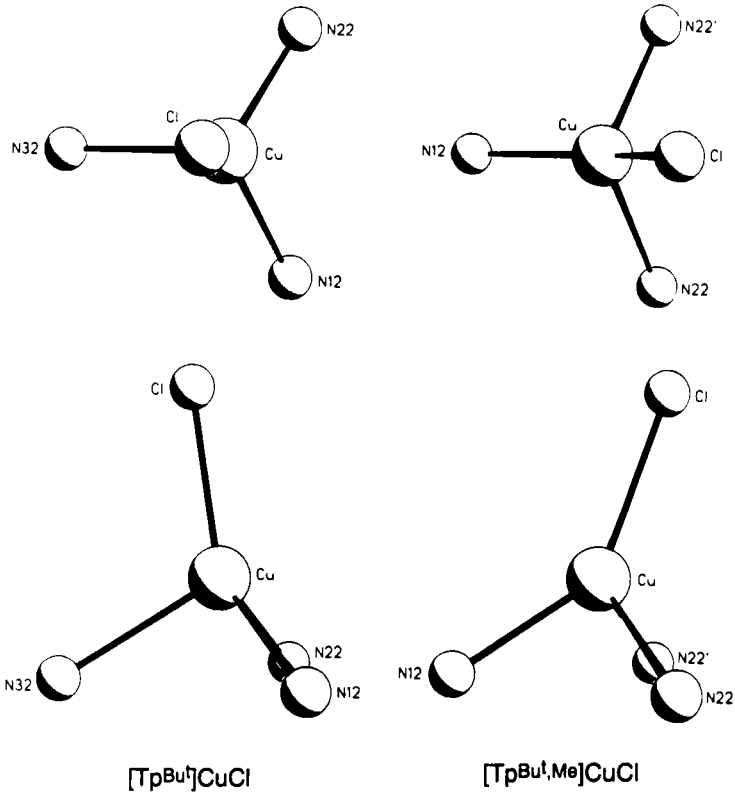

FIG. 17. Comparison of the copper coordination environments in $[Tp^{Bu^t}CuCl$ and $[Tp^{Bu^t,Me}]CuCl$. Reprinted from *Polyhedron, 14,* Yoon, K., and Parkin, G., p. 811, © copyright 1995, with kind permission from Elsevier Science Ltd, The Boulevard, Langford Lane, Kidlington 0X5 1GB, UK.

$\{[Tp^{Bu^t,Me}]Cu\}_2$ is also observed at temperatures up to 90°C! It is possible that marked difference in fluxionality of $\{[Tp^{Bu^t}]Cu\}_2$ and $\{[Tp^{Bu^t,Me}]Cu\}_2$ is a consequence of increased steric interactions between the 5-methyl substituents that would result in a structure for a transition state (or intermediate) in which all three pyrazolyl groups are coordinated to the dicopper moiety in a similar fashion to that of $\{[Tp^{Me2}]Cu\}_2$ (Fig. 16).

E. ELECTRONIC PROPERTIES

Kitajima and Tolman have provided estimates of the relative electron-donating properties of poly(pyrazolyl)borato ligands based upon comparisons of the observed ν(CO) stretching frequencies of sev-

eral series of transition metal carbonyl complexes $[Tp^{RR'}]M(CO)_n$ (*2j*). The electron donating abilities of the $[Tp^{RR'}]$ ligands were suggested to decrease according to the following series:

$$[Tp^{RR'}] > [Tp^{But}] \approx [Tp^{Pri}] \approx [Tp^{Me}] \approx [Tp^{Ms}] > [Tp] > [Tp^{Ph2}] \approx [Tp^{Ph}] > [Tp^{Pri,4Br}] > [Tp^{CF3,Me}]$$

Other noteworthy features include: (i) the electron-donating ability of the $[Tp^{RR'}]$ ligand increases with the degree of alkyl substitution, (ii) a 4-Br substituent exhibits a pronounced effect in reducing the electron-donating ability to less than that for $[Tp^{Ph}]$, and (iii) the $[\eta^3\text{-}Tp^{RR'}]$ ligand is more electron-donating than its $[\eta^2\text{-}Tp^{RR'}]$ counterpart.

III. Terminal Alkyl Derivatives of the *s*- and *p*-Block Metals Supported by Poly(pyrazolyl)borato Ligation

Alkyl derivatives of the *s*- and *p*-block metals are useful reagents in both organic and organometallic syntheses, with each reagent offering valuable differences with regard to both reactivity and selectivity (*42*). The structures of these alkyl derivatives are highly variable and depend upon the nature of both the metal and the alkyl substituent. For example, R_2Zn derivatives exist as monomeric two-coordinate linear molecules, whereas the magnesium derivatives typically exhibit four-coordination, both in the solid state and as solvated complexes in solution. Furthermore, a Grignard reagent solution comprises a complex distribution of magnesium alkyl derivatives, which in its simplest form may be described by the well-known Schlenk equilibrium [Eq. (3)], but is further complicated by solvation and oligomerization (*43–45*).

$$2\,RMgX \rightleftharpoons R_2Mg + MgX_2 \qquad (3)$$

For example, the species that crystallize from solution include (i) 4- and 5-coordinate solvated monomers, e.g., $RMgBr(OEt_2)_2$ [R = Et (*46*) Ph (*47*)] and $MeMgBr(THF)_3$ (*48*); (ii) halogen bridged dimers, e.g., $[EtMgBr(OPr^i_2)]_2$ (*49*) and $[EtMgBr(NEt_3)]_2$ (*50*), and (iii) the tetranuclear complex $[EtMg_2Cl_3(THF)_3]_2$(*51*). In view of the wide variety of structural types, and the general synthetic importance of alkyl derivatives of the *s*- and *p*-block metals, it is of some interest to determine and compare their reactivity in a well-defined common coordination environment. Poly(pyrazolyl)hydroborato ligation has, therefore, been utilized to provide series of alkyl complexes of the types $[Tp^{RR'}]MR_n$

and $[Bp^{RR'}]MR_n$. In cases where these complexes are isostructural, e.g., $[Tp^{RR'}]MgR$ and $[Tp^{RR'}]ZnR$, studies have allowed the intrinsic reactivities of the respective M–R bonds to be assessed. For example, as will be discussed in the following sections, the Mg–C bond in $[Tp^{But}]MgR$ is typically much more reactive than the Zn–C bond in isostructural $[Tp^{But}]ZnR$.

A. Poly(pyrazolyl)borato Alkyl Derivatives of the Group 2 Elements

Alkyl derivatives of the Group 2 metals (Be, Mg, Ca, Sr, Ba) supported by poly(pyrazolyl)borato ligation have only been isolated for the lighter congeners, beryllium and magnesium.

1. Alkyl Derivatives of Beryllium

a. Syntheses. Only one poly(pyrazolyl)borato beryllium alkyl complex, namely $[Tp^{But}]BeMe$, has been synthesized and fully characterized. $[Tp^{But}]BeMe$ is prepared by the reaction of Me_2Be with $Tl[Tp^{But}]$ [Eq. (4)] (*52*), by a similar method to that used for the magnesium analogues (Section III,A,2).

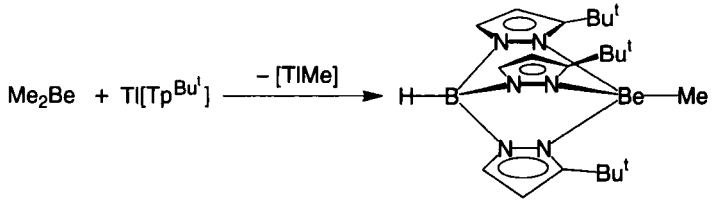

(4)

As with the magnesium derivatives, the reaction between Me_2Be and $Tl[Tp^{But}]$ is accompanied by the deposition of Tl metal because the decomposition of the by-product [TlR], thereby providing an efficient driving force (*53, 54*). In this regard, it is noteworthy that $[Tp^{But}]BeMe$ was not isolated from the reactions of $[Tp^{But}]BeX$ (X = Cl, Br) with MeLi (*52*).

b. Structures and Spectroscopic Properties. The molecular structure of $[Tp^{But}]BeMe$ (*52*) has been determined by single crystal x-ray diffraction (Fig. 18), confirming a monomeric structure with η^3-coordination of the $[Tp^{But}]$ ligand. It is noteworthy that the tris(pyrazolyl)hydroborato ligand in $[Tp^{But}]BeMe$ adopts an η^3-coordination mode, because the derivatives $[\eta^2\text{-pzTp}]_2Be$ and $\{[\eta^2\text{-Tp}]Be(\mu\text{-OH})\}_3$

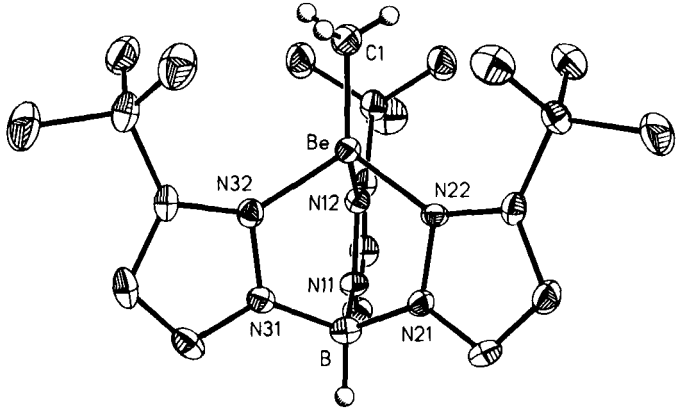

FIG. 18. ORTEP drawing of Tp^{But}]BeMe. Reprinted with permission from Ref. (*52*). © Copyright 1993 American Chemical Society.

adopt only an η^2-coordination mode (*39c, 55*). The trigonally distorted tetrahedral coordination environment about beryllium in [Tp^{But}]BeMe is, however, similar to those in the derivatives [Tp^{But}]BeH and [Tp^{But}]-BeBr (*56*).

The Be–Me bond length in [Tp^{But}]BeMe [1.708(6) Å] is similar to the sum of the covalent radii of Be and C (1.66 Å) (*57*), and also compares well with those of CpBeMe [1.706(3) Å] (*58*), Me_2Be [1.698(5) Å] (*59*), and But_2Be [1.699(3) Å] (*60*), measured in the gas phase by electron diffraction. However, the Be–C bond lengths in [Tp^{But}]BeMe and CpBeMe are substantially shorter than those in (i) "ate" derivatives, such as Li_2BeMe_4 [1.84(10) Å] (*61*), and (ii) bridging methyl derivatives, such as solid $[Me_2Be]_n$ [1.93(2) Å] (*62*).

[Tp^{But}]BeMe is characterized by well-defined ^1H and ^{13}C NMR spectra. For example, the ^1H NMR resonance of the beryllium methyl group of [Tp^{But}]BeMe is observed as a relatively sharp singlet at δ 0.57 ppm, as shown in Fig. 19. The ^{13}C NMR resonance of the Be–CH_3 moiety, however, is only observed as a relatively broad peak at δ 4.7 ppm, as a result of quadrupolar relaxation by the beryllium nucleus (Fig. 20). [Tp^{But}]BeMe is also characterized by a broad signal at δ 5.2 ppm (relative to $[Be(H_2O)_4]^{2+}$) in the ^9Be NMR spectrum, close to the range δ 1–4 ppm observed for other four-coordinate [Tp^{But}]BeX complexes (X = H, Cl, Br, I, SH) (*52, 56*), but substantially different from that for the cyclopentadienyl derivative CpBeMe (δ −20.4 ppm) (*63*).

c. Reactivity. The reactivity of the beryllium methyl complex [Tp^{But}]BeMe has only been studied to a limited extent. For example, the Be–C bond is cleaved by H_2S to give the hydrosulfido deriva-

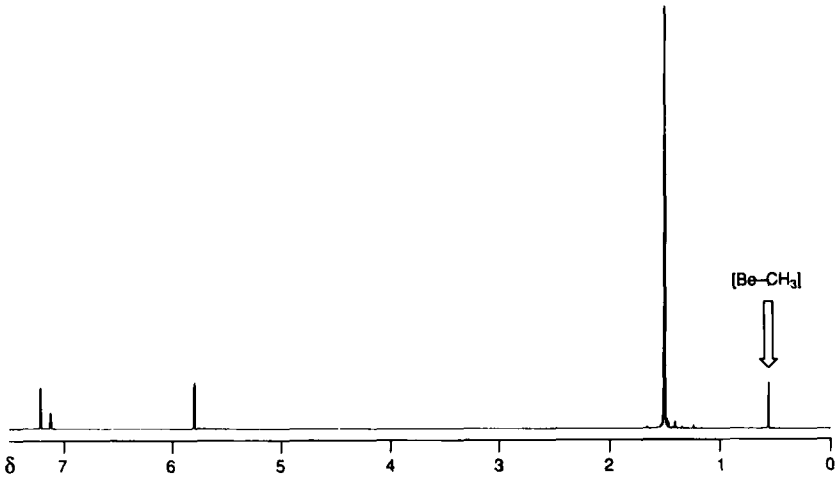

FIG. 19. ^{1}H NMR spectrum of [Tp$^{Bu^t}$]BeMe. Reprinted with permission from Ref. (*52*). © Copyright 1993 American Chemical Society.

tive [Tp^{But}]BeSH and CH_4, and by I_2 to give [Tp^{But}]BeI and MeI (Scheme 2).

2. *Alkyl Derivatives of Magnesium*

a. Syntheses. The first application of tris(pyrazolyl)hydroborato ligands to stabilize monomeric four-coordinate alkyl derivatives of the type [Tp$^{RR'}$]MR was reported for magnesium. Specifically, monomeric

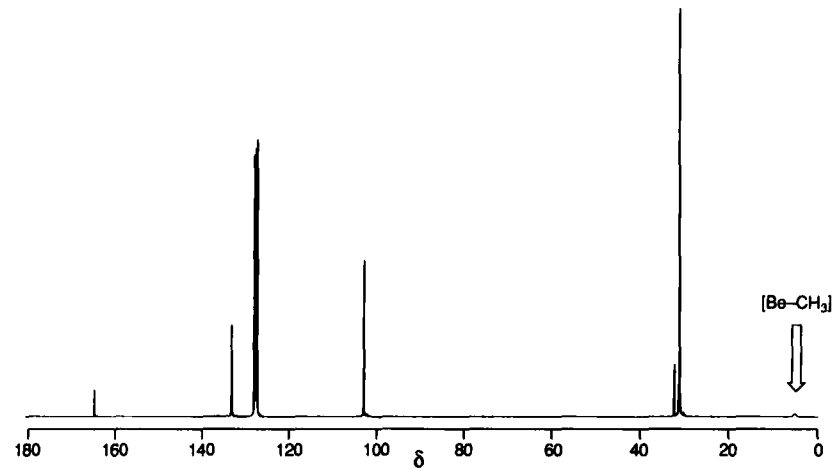

FIG. 20. ^{13}C{^{1}H} NMR spectrum of [Tp$^{Bu^t}$]BeMe. Reprinted with permission from Ref. (*52*). © Copyright 1993 American Chemical Society.

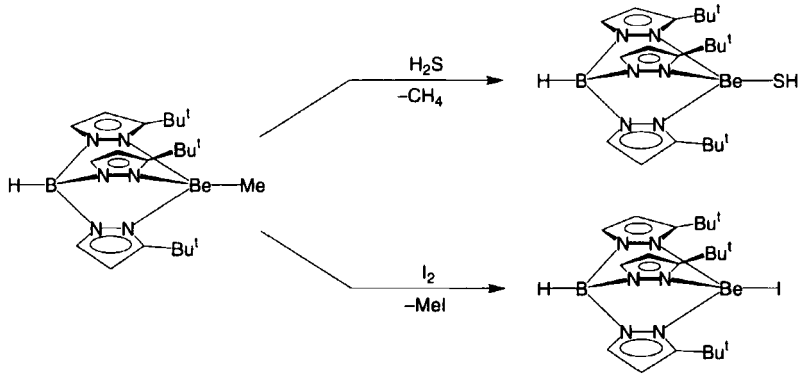

SCHEME 2. Reactivity of [Tp$^{Bu^t}$]BeMe.

magnesium alkyl complexes supported by tris(pyrazolyl)hydroborato ligation [Tp$^{RR'}$]MgR are readily obtained by the reaction of the appropriate dialkylmagnesium with either the potassium or thallium derivatives [M][Tp$^{RR'}$] (M = K, Tl) [Eq. (5)] (*64*).

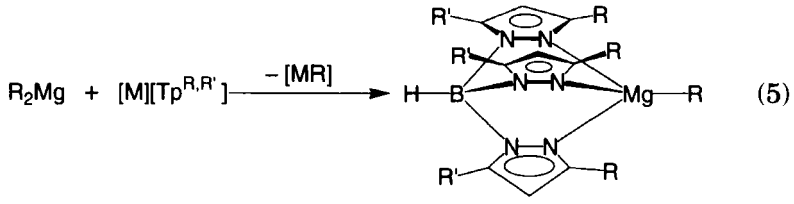

(5)

This synthetic method has been shown to be very general, and a series of primary, secondary, tertiary, vinyl, and phenyl derivatives has been obtained. For example, the tris(3-t-butylpyrazolyl)hydroborato ligand has permitted the isolation of the alkyl derivatives [Tp$^{Bu^t}$]MgR (R = Me, Et, Bu^n, Pr^i, Bu^t, CH_2SiMe_3, $CH{=}CH_2$, Ph). Other [Tp$^{RR'}$] ligands have also been used to prepare magnesium alkyl derivatives, e.g., [Tp^{Me2}]MgR (*64*), [Tp^{But,Me}]MgR (*65*), [Tp^{But2}]MgR (*66*), and [Tp^{Ar2}]MgR (Ar = *p*-$C_6H_4Bu^t$) (*65*), although not necessarily for all of the alkyl groups shown earlier. Each of these magnesium alkyl complexes [Tp$^{RR'}$]MgR is a white crystalline solid that is soluble in hydrocarbon solvents such as benzene.

The reactions between R_2Mg and Tl[Tp$^{RR'}$] are also accompanied by the deposition of Tl metal due to the decomposition of [TlR] (*53, 54*). The deposition of Tl thereby provides a very effective driving force for the reaction. However, for reactions involving less sterically demanding [Tp$^{RR'}$] ligands, the driving force achieved by deposition of Tl may be such that disubstitution occurs, with the resulting formation of the 6-

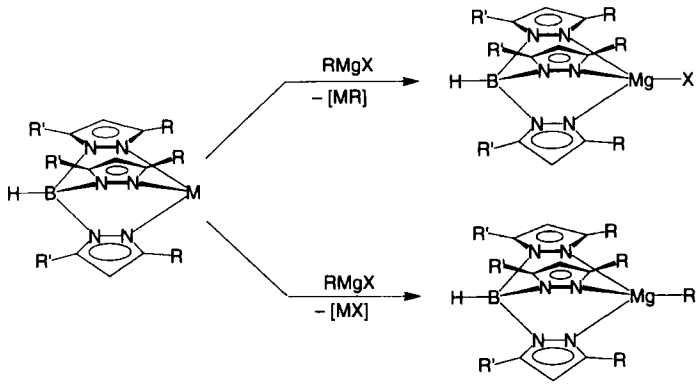

SCHEME 3. Competition between Mg–X and Mg–R bond metathesis in the reactions of M[$Tp^{RR'}$] with Grignard reagents.

coordinate magnesium derivatives $[Tp^{RR'}]_2Mg$. In such instances, the potassium derivative [K][$Tp^{RR'}$] may be the preferred choice of reagent, as, for example, in the syntheses of [Tp^{Me_2}]MgR.

Although the syntheses of [$Tp^{RR'}$]MgR described earlier appear to be rather general, it is worth noting that alternative approaches have not been particularly successful. For example, the syntheses of [$Tp^{RR'}$]MgR complexes by the reactions of Grignard reagents RMgX with [M][$Tp^{RR'}$] are complicated by the formations of the corresponding magnesium halide derivatives [$Tp^{RR'}$]MgX, resulting from competition between Mg–X and Mg–R bond metathesis (Scheme 3) (*64*). The products obtained, [$Tp^{RR'}$]MgR vs [$Tp^{RR'}$]MgX, depend critically upon the choice of Grignard reagent and reactant ratio, and for this reason the use of R_2Mg, rather than RMgX, as the reagent is highly recommended for the syntheses of [$Tp^{RR'}$]MgR.

b. Structures and Spectroscopic Properties. The molecular structures of several [$Tp^{RR'}$]MgR (*64*) derivatives have been determined by single crystal x-ray diffraction, as illustrated in Figs. 21 and 22. In each case the molecules are solvent-free monomers and the tris(pyrazolyl)hydroborato ligand is η^3-coordinated to the metal, with a coordination environment about the metal which may be described as trigonally distorted tetrahedral. Selected bond lengths are presented in Table III. The Mg–C bond lengths in [$Tp^{RR'}$]MgMe are in the range 2.08(1) Å to 2.182(8) Å, comparable to the sum of the covalent radii, 2.13 Å (*57*). For reference, other 4-coordinate monomeric magnesium alkyl complexes of the type $RMgX(L)_2$ have Mg–C bond lengths in the range 2.15 Å to 2.34 Å (*67*).

The alkyl complexes [$Tp^{RR'}$]MgR are characterized by well-resolved

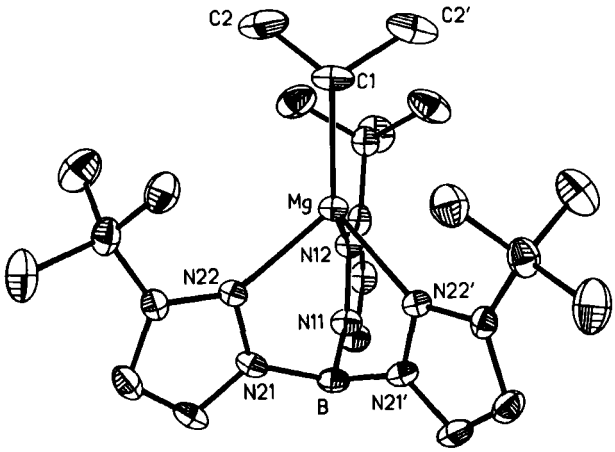

FIG. 21. ORTEP drawing of [Tp^{Bu^t}]MgPr^i. Reprinted with permission from Ref. (*64c*). © Copyright 1991 American Chemical Society.

^1H and ^{13}C NMR spectra, analogous to the beryllium derivative [Tp^{Bu^t}]BeMe. For example, the ^1H NMR signals of the Mg–CH_3 groups of [Tp^{Bu^t}]MgMe, [Tp^{Ar2}]MgMe, and [Tp^{Me2}]MgMe are observed at δ −0.05, −0.58, and −0.25 ppm, respectively (*64–65*). The corresponding ^{13}C NMR signals are observed at −5.2 ppm, −9.5, and −17.1 ppm, respectively, each with a $^1J_{C-H}$ coupling constant of 109 Hz. It is also noteworthy that each of these ^{13}C NMR signals is sharp, in contrast to that of the Be–CH_3 moiety in [Tp^{Bu^t}]BeMe, which is observed as a

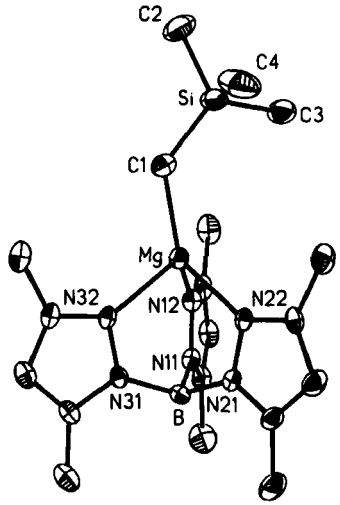

FIG. 22. ORTEP drawing of [Tp^{Me_2}]$MgCH_2SiMe_3$. Reprinted with permission from Ref. (*64c*). © Copyright 1991 American Chemical Society.

TABLE III

SELECTED BOND LENGTHS (Å) FOR [Tp^{But}]BeMe AND [$Tp^{RR'}$]MgR COMPLEXES

	d(M–C)/Å	*d*(M–N_{av})/Å	Ref.[a]
[Tp^{But}]BeMe	1.708(6)	1.87(1)	1
[Tp^{But}]MgMe	2.12(1)	2.14(1)	2
[$Tp^{But,Me}$]MgMe	2.08(1)	2.13(1)	3
[Tp^{But}]MgPr^i	2.182(8)	2.17(1)	2
[Tp^{Me2}]$MgCH_2SiMe_3$	2.096(9)	2.08(7)	2

[a] (1) Han, R., and Parkin, G., *Inorg. Chem.* **32,** 4968 (1993); (2) Han, R., and Parkin, G., *Organometallics* **10,** 1010 (1991); (3) Ghosh, P., and Parkin, G., unpublished results (1995).

relatively broad peak because of quadrupolar relaxation by the beryllium nucleus (Fig. 20).

In addition to the ^1H NMR resonances of [$Tp^{RR'}$]MgR attributable to the metal–alkyl moieties, the ^1H NMR resonances associated with the [$Tp^{RR'}$] ligands also provide a valuable spectroscopic handle for monitoring reactivity. For example, each of the complexes [Tp^{But}]MgR exhibits a single characteristic resonance in the range δ 1.34–1.44 attributable to the *t*-butyl substituents of the [Tp^{But}] ligand.

c. Reactivity. In contrast to the rather limited reactivity study of the beryllium complex [Tp^{But}]BeMe, the reactions of the magnesium derivatives [$Tp^{RR'}$]MgR have been studied quite extensively. Such studies have been important both in terms of determining the reactivity of the Mg–C bond in a well-defined coordination environment, and in terms of providing a comparison with the reactivities of other derivatives such as [$Tp^{RR'}$]ZnR (vide infra). The reactivities of [$Tp^{RR'}$]MgR are typically lower than those of Grignard reagents, and in some cases the reactions do not parallel those of the corresponding Grignard reagent.

Solutions of the alkyl derivatives [Tp^{Me2}]MgR are generally stable at room temperature. However, heating to 80–120°C results in ligand redistribution, analogous to the Schlenk equilibrium, and the formation of [Tp^{Me2}]$_2$Mg [Eq. (6)] (*64*).

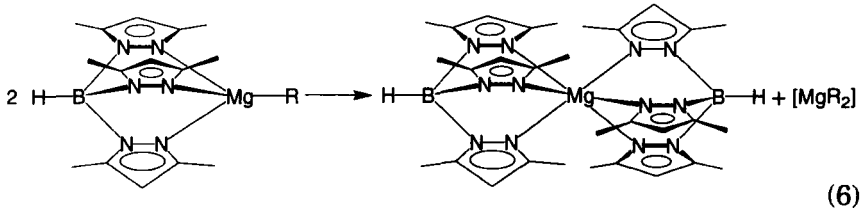

(6)

In contrast, the more sterically demanding [Tp^{But}]MgR derivatives of the "tetrahedral enforcer" system are stable to such redistributions, presumably due to the inability to form the corresponding [Tp^{But}]$_2$Mg complex. For this reason, the reactivity of the [Tp^{But}]MgR complexes has been studied more extensively than that of the less sterically demanding [Tp^{Me2}]MgR system.

The magnesium alkyl derivatives [Tp^{But}]MgR exhibit reactivity that is both similar to and different from that of Grignard reagents. For example, [Tp^{But}]MgR reacts with CO_2 to give the acetate derivative [Tp^{But}]Mg(η^1-O_2CMe), a transformation analogous to that of a Grignard reagent (Scheme 4). In contrast, the reaction of [Tp^{But}]MgMe with acetone is atypical of Grignard reactivity. Thus, the reaction between [Tp^{But}]MgMe and Me_2CO gives the enolate complex [Tp^{But}]Mg{η^1-OC(=CH_2)Me} (Scheme 4), rather than the alkoxide derivative [Tp^{But}]MgOBu^t. Magnesium enolate complexes are rare (*68*), and the formation of [Tp^{But}]Mg{η^1-OC(=CH_2)Me} represents an interesting example of a magnesium enolate derived from acetone. The formation of enolate complexes from methyl ketones appears to be general, since MeC(O)Bu^t also reacts with [Tp^{But}]MgMe to give [Tp^{But}]Mg{η^1-OC(=CH_2)(Bu^t)}.

The alkyl complexes [Tp^{But}]MgR (R = Me, Et, Pr^i, Bu^t) react with excess O_2 at room temperature to give alkylperoxo complexes [Tp^{But}]-MgOOR (Scheme 5), which have been characterized by ^{17}O NMR spectroscopy. Each complex exhibits two ^{17}O NMR resonances in the ranges δ 102–183 and δ 323–427 for the two distinct oxygen atoms of the alkylperoxo (Mg–O–O–R) moiety (Table IV). Organometallic derivatives generally react with oxygen to produce complex mixtures (*69*,

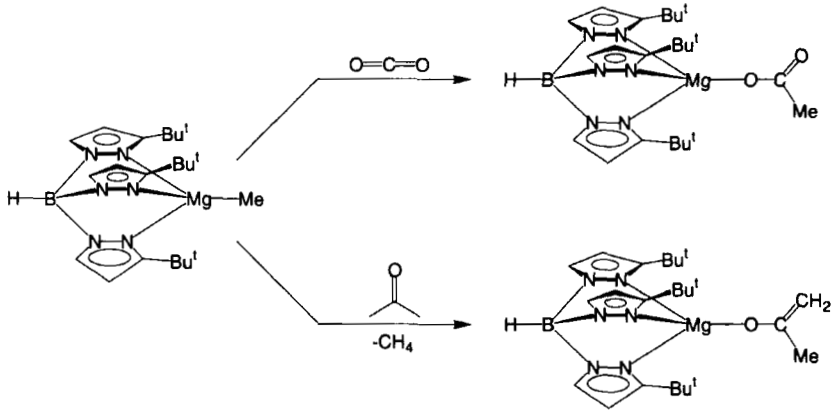

SCHEME 4. Reactions of [Tp^{But}]MgMe with CO_2 and Me_2CO.

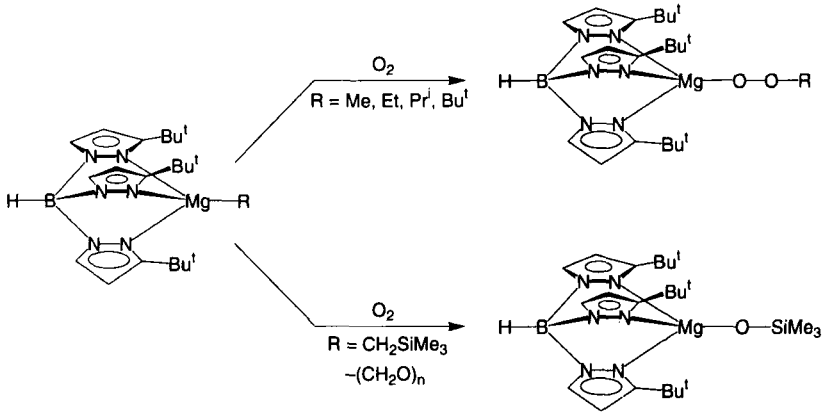

SCHEME 5. Reactions of $[Tp^{But}]MgR$ with O_2.

70). Furthermore, the isolated products of these reactions are commonly alkoxo derivatives, $[L_nMOR]$, rather than alkylperoxo complexes, $[L_nMOOR]$ (*71*). The ability to isolate the magnesium alkylperoxo complexes $[Tp^{But}]MgOOR$ from the reactions of $[Tp^{But}]MgR$ with O_2 has been proposed to be a consequence of the sterically demanding environment created by the $[Tp^{But}]$ ligand. However, in contrast to the alkyl derivatives $[Tp^{But}]MgR$, the analogous reaction of the trimethylsilylmethyl derivative $[Tp^{But}]MgCH_2SiMe_3$ with O_2 is accompanied by Si–C bond cleavage and the formation of the trimethylsiloxide derivative, $[Tp^{But}]MgOSiMe_3$ (Scheme 5) (*64*). The formation of a siloxide derivative bears some analogy with the reaction of the Grignard reagent Me_3SiCH_2MgCl with O_2, which gives significant quantities of Me_3SiOH, $(Me_3Si)_2O$, and $(CH_2O)_n$ after hydrolysis (*72*).

The reactions of oxygen with metal–alkyl derivatives typically involve radical intermediates (*73, 74*), and a likely mechanism for the reactions of $[Tp^{But}]MgR$ with O_2 is illustrated in Scheme 6. Specific

TABLE IV

^{17}O NMR DATA (ppm) FOR $[Tp^{But}]MgOOR$ (RELATIVE TO $H_2{}^{17}O$)

	δ(MgOOR)	δ(MgOOR)
$[Tp^{But}]MgOOMe$	427	102
$[Tp^{But}]MgOOEt$	407	130
$[Tp^{But}]MgOOPr^i$	373	159
$[Tp^{But}]MgOOBu^t$	323	183

(1) Initiation

$$L_nM\text{-}R + {}^3O_2 \longrightarrow [L_nMR\bullet]^+ + [O_2\bullet]^-$$

$$[L_nMR\bullet]^+ \longrightarrow [L_nM]^+ + R\bullet$$

(2) Radical chain

$$R\bullet + O_2 \longrightarrow ROO\bullet$$

$$L_nM\text{-}R + ROO\bullet \longrightarrow L_nMOOR + R\bullet$$

(3) Termination

$$[L_nM]^+ + [O_2\bullet]^- \longrightarrow L_nMOO\bullet$$

$$L_nMOO\bullet + R\bullet \longrightarrow L_nMOOR$$

SCHEME 6. Possible mechanism for the reactions of the reactions of $[Tp^{Bu^t}]MgR$ with O_2.

evidence for radical intermediates in the reactions of $[Tp^{Bu^t}]MgR$ with O_2 is provided by the observations that (i) the reaction of $[Tp^{Bu^t}]MgMe$ with O_2 is inhibited by small quantities of the radical trap galvinoxyl, and (ii) crossover products are formed in the presence of two different tris(pyrazolyl)hydroborato ligands, e.g., $[Tp^{Bu^t}]MgMe$ and $[Tp^{Me_2}]$-$MgBu^t$. The formation of the trimethylsiloxide product $[Tp^{Bu^t}]MgOSiMe_3$ in the reaction of $[Tp^{Bu^t}]MgCH_2SiMe_3$ with O_2 is also proposed to occur via a radical process. Specifically, elimination of formaldehyde from the radical intermediate $Me_3SiCH_2O_2\cdot$ [Eq. (7)] would generate the trimethylsiloxide radical $Me_3SiO\cdot$, a rearrangement that would be expected to be promoted by the formation of a strong Si–O bond.

$$Me_3Si\text{—}CH_2\text{—}O\text{—}O^{\bullet} \longrightarrow Me_3Si\text{—}O^{\bullet} + CH_2{=}O \qquad (7)$$

The alkylperoxo derivatives $[Tp^{Bu^t}]MgOOR$ are capable of transferring an oxygen atom to certain substrates, with the concomitant formation of the magnesium alkoxide complex $[Tp^{Bu^t}]MgOR$. For example, $[Tp^{Bu^t}]MgOOR$ transfers an oxygen atom to PPh_3 at room temperature to give $[Tp^{Bu^t}]MgOR$ and Ph_3PO [Eq. (8)].

$$[Tp^{Bu^t}]MgOOR + PPh_3 \longrightarrow [Tp^{Bu^t}]MgOR + Ph_3PO \quad (8)$$

Similarly, $[Tp^{Bu^t}]MgOOPr^i$ transfers an oxygen atom to the alkyl derivative $[Tp^{Bu^t}]MgPr^i$ at 80°C to give $[Tp^{Bu^t}]MgOPr^i$ [Eq. (9)].

$$[Tp^{Bu^t}]MgOOR + [Tp^{Bu^t}]MgR \longrightarrow 2[Tp^{Bu^t}]MgOR \quad (9)$$

The magnesium–alkyl bonds in $[Tp^{Bu^t}]MgR$ are very susceptible toward reactions with protic reagents HX, as illustrated by the formation of novel enolate derivatives from methyl ketones described earlier. Other examples of such protonolysis reactions are summarized in Scheme 7. Nonprotic reagents, e.g., Me_2S_2, RX, Me_3SiX, and X_2, also react with $[Tp^{Bu^t}]MgR$, as illustrated in Scheme 8. The reactions between $[Tp^{Bu^t}]MgR$ and RX have been proposed to involve a radical mechanism. For example, for the reactions with MeI, EtI, Pr^iI, and Bu^tI, the increasing order of reactivity is primary < secondary < tertiary, and for the benzyl halides $PhCH_2X$, the order of reactivity is chloride < bromide ≈ iodide. Finally, it is notable that the reaction between $[Tp^{Bu^t}]MgCH_3$ and labeled $^{13}CH_3I$ demonstrates that, in addition to alkylation (to give $[Tp^{Bu^t}]MgI$ and $^{13}CH_3CH_3$), there is also a competitive metathesis process involving alkyl exchange (to give $[Tp^{Bu^t}]Mg^{13}CH_3$ and CH_3I), as shown in Scheme 9. The exchange of

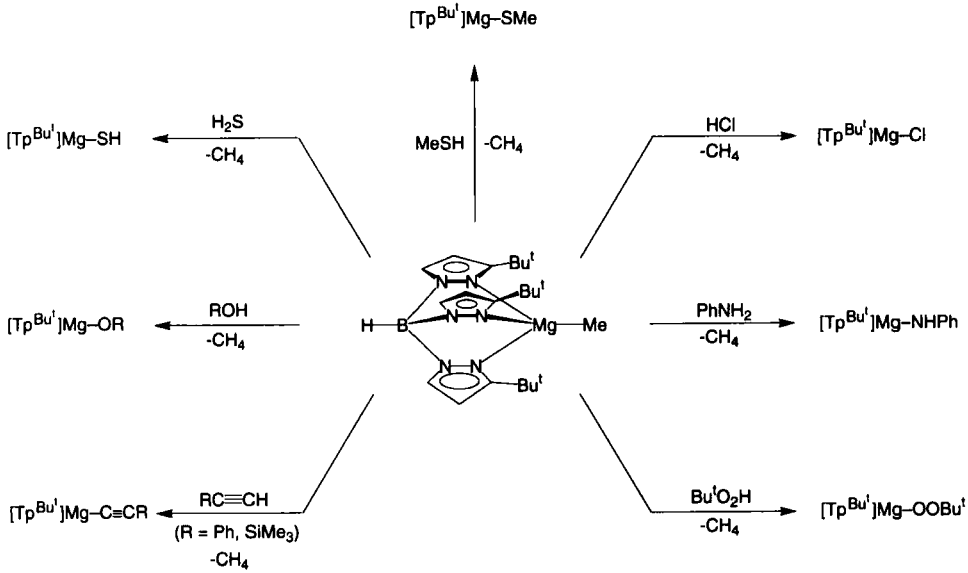

SCHEME 7. Reactivity of $[Tp^{Bu^t}]MgMe$ toward HX.

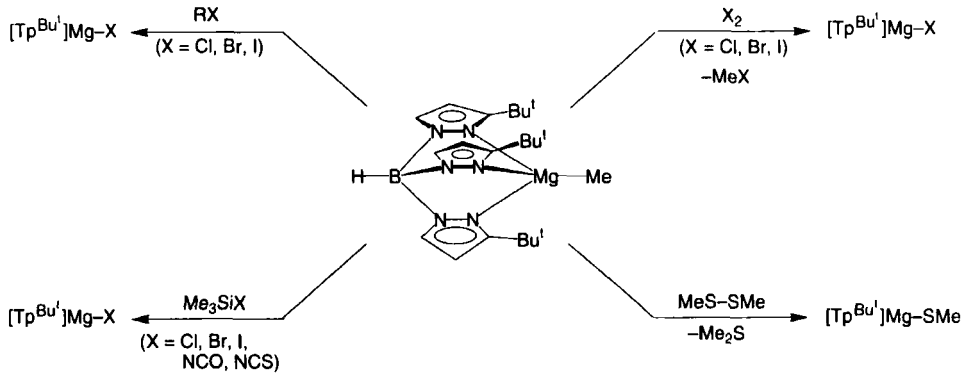

SCHEME 8. Reactivity of $[Tp^{Bu^t}]MgMe$ toward XY.

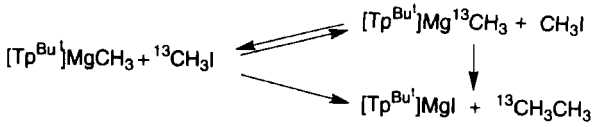

SCHEME 9. Competitive alkyl exchange and coupling in the reaction of $[Tp^{Bu^t}]MgMe$ with $^{13}CH_3I$.

alkyl groups between Grignard reagents and simple alkyl halides is not well documented, although indirect evidence has been presented (*75, 76*).

B. Poly(pyrazolyl)borato Alkyl Derivatives of the Group 11 Elements

Stable alkyl derivatives of the Group 11 metals (Cu, Ag, Au) supported by poly(pyrazolyl)borato ligation have only been isolated for gold.

1. Alkyl Derivatives of Gold

The gold alkyl derivatives $[Tp]AuMe_2$ and $[pzTp]AuMe_2$ have been prepared by the reaction of aqueous solutions of $Me_2Au(NO_3)$ with $K[Tp^{RR'}]$ [Eq. (10)] (*77, 78*).

$$Me_2Au(NO_3) + K[Tp^{RR'}] \longrightarrow [Tp^{RR'}]AuMe_2 + KNO_3 \qquad (10)$$

The structures of both $[Tp]AuMe_2$ and $[pzTp]AuMe_2$ have been determined by x-ray diffraction. In each case the $[Tp^{RR'}]$ ligands are biden-

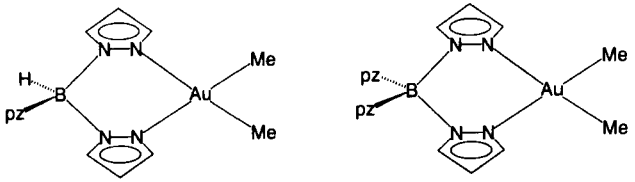

FIG. 23. Square-planar $[Tp^{RR'}]AuMe_2$ complexes.

tate, with square planar coordination at gold and average Au–C bond lengths of 2.05(3) Å and 2.04(2) Å, respectively (Fig. 23). $[Tp]AuMe_2$ and $[pzTp]AuMe_2$ are fluxional on the NMR time scale at room temperature, but cooling to −90°C allows a static structure analogous to the solid-state structure to be observed.

The gold alkyl derivatives $[Tp]AuMe_2$ and $[pzTp]AuMe_2$ are protonated by dilute HCl to give $\{[TpH]AuMe_2\}^+$ and $\{[pzTpH]AuMe_2\}^+$, in which the proton resides on one of the nitrogen atoms of the pyrazolyl groups.

C. POLY(PYRAZOLYL)BORATO ALKYL DERIVATIVES OF THE GROUP 12 ELEMENTS

1. Alkyl Derivatives of Zinc

a. Syntheses. Monomeric four-coordinate zinc alkyl derivatives $[Tp^{RR'}]ZnR$ have been prepared by metathesis of R_2Zn with $Tl[Tp^{RR'}]$ (Scheme 10), an analogous procedure to that described for the syntheses

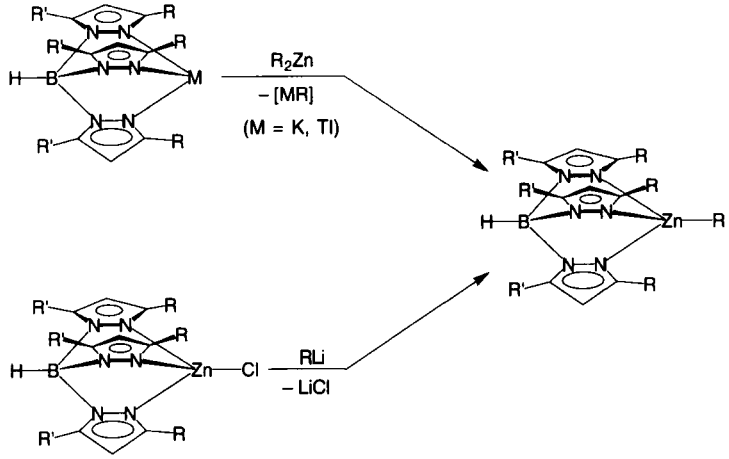

SCHEME 10. Syntheses of $[Tp^{RR'}]ZnR$.

of the beryllium and magnesium derivatives discussed in Section III,A. Moreover, Vahrenkamp has also prepared zinc alkyl derivatives by metathesis of $[Tp^{RR'}]ZnCl$ with LiR. Some specific complexes that have been synthesized include $[Tp^{But}]ZnR$ (R = Me, Et) (*79*, *80*), $[Tp^{Me_2}]ZnMe$ (*80*), $[Tp^{But_2}]ZnMe$ (*66*), $[Tp^{Ph_2}]ZnEt$ (*81*), and $[Tp^{Ph}]ZnR$ (R = Me, Et, Bu^t, Ph) (*81*). In addition to four-coordinate $[Tp^{RR'}]ZnR$, the three-coordinate zinc alkyl derivatives $[Bp^{But}]ZnR$ (R = Me, Et, Bu^t) are readily prepared by metathesis of R_2Zn with the thallium derivative $Tl[Bp^{But}]$ [Eq. (11)] (*80*, *82*).

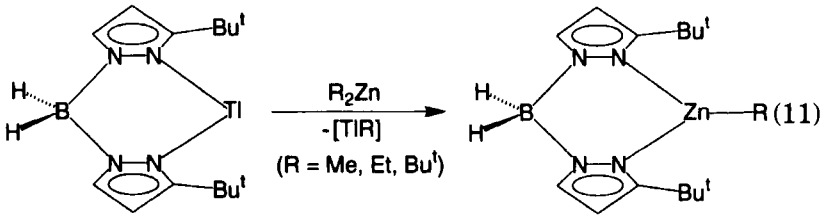

(11)

b. Structures and Spectroscopic Properties. The molecular structures of the zinc methyl derivatives $[Tp^{But}]ZnMe$ (*83*), $[Tp^{Me_2}]ZnMe$ (*80*), $[Tp^{But_2}]ZnMe$ (*66*), and $[Tp^{Ph}]ZnMe$ (*81*) have been determined by x-ray diffraction, confirming the η^3-coordination mode of the tris(pyrazolyl)hydroborato ligands. ORTEP drawings for $[Tp^{Me_2}]ZnMe$ and $[Tp^{But_2}]$-ZnMe are shown in Figs. 24 and 25, respectively. The zinc centers of each of these complexes may be described as trigonally distorted

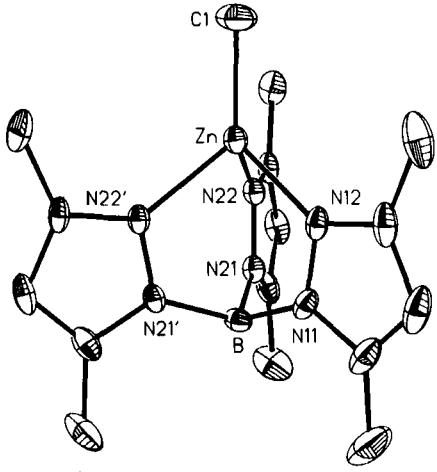

FIG. 24. ORTEP drawing of $[Tp^{Me_2}]ZnMe$. Reprinted with permission from Ref. (*80*).
© Copyright 1995 American Chemical Society.

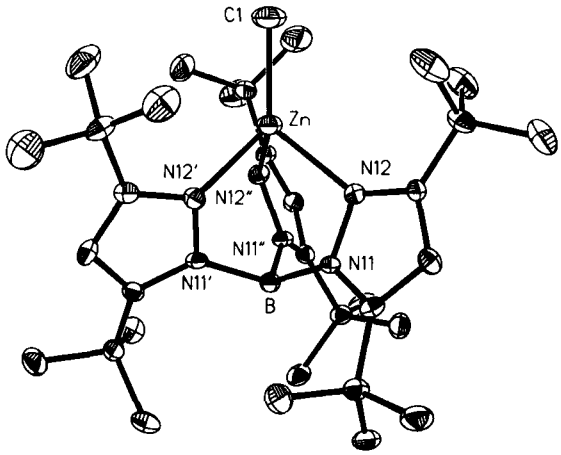

FIG. 25. ORTEP drawing of [Tp^{But2}]ZnMe.

tetrahedral, with average C–Zn–N and N–Zn–N bond angles of ca. 125° and 90°, respectively. Selected bond lengths and angles for [$Tp^{RR'}$]ZnMe derivatives are given in Table V. The Zn–C bond lengths for [$Tp^{RR'}$]ZnMe (1.95–1.98 Å) are close to, but slightly less than, the sum of the covalent radii of Zn and C [2.02 Å] (*57*), and are in the range of other known Zn–C bond lengths (1.9–2.0 Å). It is also worth noting that the Zn–C bond length of [Tp^{But}]ZnMe [1.971(4) Å] is longer than the value cited in the original report [1.890(10) Å], and it is believed that the shorter value may be an artifact due to compositional disorder with an impurity (possibly [Tp^{But}]ZnOH), as described in Section VII. The Zn–C bond length in [Tp^{But}]ZnMe [1.971(4) Å] may also be compared with the Mg–C bond length [2.118(11) Å] in the isostructural magnesium derivative, [Tp^{But}]MgMe (*64*). As expected on the basis of

TABLE V

COMPARISON OF BOND LENGTHS AND ANGLES FOR [$Tp^{R,R'}$]ZnMe COMPLEXES

	d(M–C)/Å	*d*(M–N)/Å[a]	N–M–C/°	Ref.[a]
[Tp^{Me2}]ZnMe	1.981(8)	2.053[10]	125[2]	1
[Tp^{Ph}]ZnMe	1.950(4)	2.108[30]	126[2]	2
[Tp^{But}]ZnMe	1.971(4)	2.109[10]	125[2]	3
[Tp^{But2}]ZnMe	1.98(2)	2.118(6)	125.0(2)	4

[a] (1) Looney, A., Han, R., Correll, I. B., Cornebise, M., Yoon, K., Parkin, G., and Rheingold, A. L., *Organometallics* **14,** 274 (1995); (2) Alsfasser, R., Powell, A. K., Trofimenko, S., and Vahrenkamp, H., *Chem. Ber.* **126,** 685 (1993); (3) Yoon, K., and Parkin, G., *J. Am. Chem. Soc.* **113,** 8414 (1991); (4) Dowling, C., and Parkin, G., unpublished results (1995).

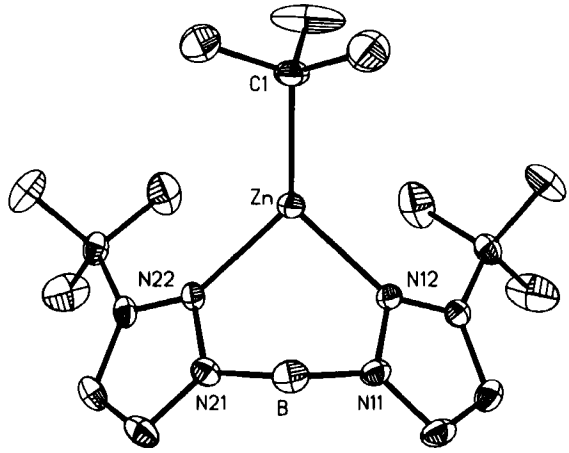

FIG. 26. ORTEP drawing of [Bp^{Bu^t}]ZnBu^t. Reprinted with permission from Ref. (*80*). © Copyright 1995 American Chemical Society.

the respective covalent radii, the Zn–C bond is slightly shorter than the Mg–C bond.

The molecular structure of the *t*-butyl derivative [Bp^{Bu^t}]ZnBu^t has been determined by an x-ray diffraction study, which confirms a distorted trigonal planar coordination environment for zinc, as shown by the two views in Figs. 26 and 27 (*80*). In comparison to tetrahedral coordination, three-coordinate zinc alkyl complexes are rare (*84*).

As with their beryllium and magnesium counterparts, the zinc alkyl derivatives [$Tp^{RR'}$]ZnR and [Bp^{Bu^t}]ZnR are soluble in hydrocarbon

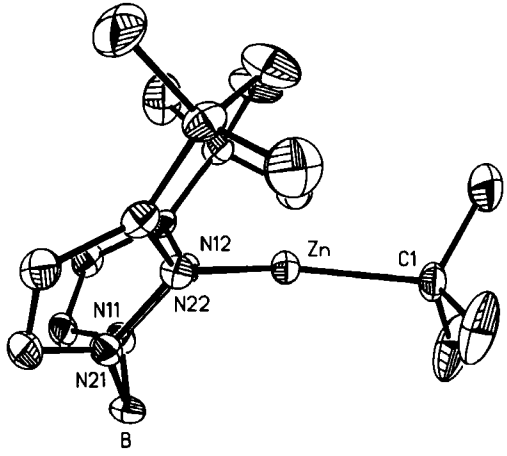

FIG. 27. Orthogonal view of [Bp^{Bu^t}]ZnBu^t. Reprinted with permission from Ref. (*80*). © Copyright 1995 American Chemical Society.

solvents and are characterized in solution by well-defined ^1H and ^{13}C NMR spectra. For example, the complex [Tp^{But}]ZnMe is characterized by resonances attributable to the Zn–Me group at δ 0.54 ppm in the ^1H NMR spectrum and at δ −2.8 [*q*, $^1J_{C-H}$ = 118 Hz] in the ^{13}C NMR spectrum. Similarly, three coordinate [Bp^{But}]ZnMe exhibits resonances attributable to the Zn-Me group at δ 1.41 and 30.7 [*q*, $^1J_{C-H}$ = 126 Hz] in the ^1H and ^{13}C NMR spectra, respectively.

c. Reactivity. The reactivity of [Tp^{But}]ZnR towards a number of reagents is summarized in Scheme 11. Halogens (X_2) rapidly cleave the Zn–C bond to eliminate RX and give the halide complex [Tp^{But}]ZnX (X = Cl, Br, I). Protic reagents (HX) also readily cleave the Zn–R bond in [Tp^{But}]ZnR to eliminate RH, with the concomitant formation of the corresponding [Tp^{But}]ZnX derivative. For example, [Tp^{But}]ZnR reacts with hydrogen chloride, acetic acid, and phenylacetylene to give [Tp^{But}]ZnCl, [Tp^{But}]Zn(η^1-O_2CMe), and [Tp^{But}]ZnCCPh, respectively, while [Tp^{Ph}]ZnBu^t reacts with EtSH to give the monomeric thiolate derivative [Tp^{Ph}]ZnSEt (*81*). Moreover, HX (X = Br, I, CN, N_3, NCS), generated in situ by the treatment of Me_3SiX with H_2O, also reacts with [Tp^{But}]ZnR to give [Tp^{But}]ZnX. Some of the complexes [Tp^{But}]ZnX (X = Cl, Br, I, CN, O_2CMe, N_3, NCS) have also been synthesized by metathesis of ZnX_2 with either K[Tp^{But}] or Tl[Tp^{But}] [Eq. (12)] (*9, 80*).

$$M[Tp^{Bu^t}] + ZnX_2 \longrightarrow [Tp^{Bu^t}]ZnX + MX \qquad (12)$$

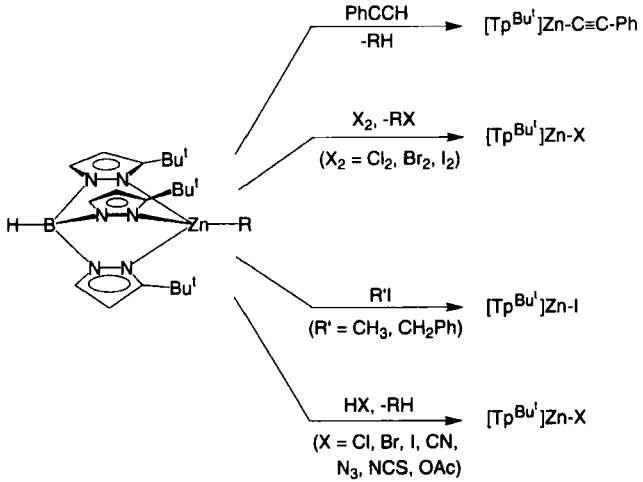

SCHEME 11. Reactivity of [Tp^{But}]ZnR.

Furthermore, Vahrenkamp and Kläui have also used related methods for the syntheses of $[Tp^{Ph2}]ZnX$ and $[Tp^{Ar}]ZnX$ derivatives (*81, 85*).

The molecular structures of several $[Tp^{But}]ZnX$ derivatives have been determined by x-ray diffraction. For example, x-ray diffraction studies confirm that the acetate ligand in $[Tp^{But}]Zn(\eta^1\text{-}O_2CMe)$ is bound to zinc in a unidentate mode, similar to that proposed for $[Tp^{But}]Mg(\eta^1\text{-}O_2CMe)$, but in contrast to the bidentate coordination proposed for the copper analogue $[Tp^{But}]Cu(\eta^2\text{-}O_2CMe)$ (*86, 87*). Such a change in coordination mode for copper and zinc derivatives is to be anticipated on the basis of structural studies on the nitrate derivatives $[Tp^{But}]M(NO_3)$ (M = Co, Ni, Cu, Zn), as described in Section V,B,2,e. The thioacetate $[Tp^{Ph}]Zn\{\eta^1\text{-}SC(O)Me\}$ (*81*), and cyanoacetate $[Tp^{Ph}]Zn(\eta^1\text{-}O_2CCH_2CN)$ (*88*) derivatives also exhibit unidentate coordination.

The reactivity of the zinc alkyl derivatives $[Tp^{But}]ZnR$ is typically lower than that of the corresponding magnesium derivatives (Section III,A,2,c.). For example, whereas $[Tp^{But}]MgMe$ undergoes insertion of CO_2 into the Mg–C bond at room temperature, no reaction is observed between $[Tp^{But}]ZnMe$ and CO_2 at 140°C. Similarly, whereas the magnesium alkyl derivatives $[Tp^{But}]MgR$ (R = Me, Et, Pr^i, Bu^t) react immediately with O_2 at room temperature to give alkylperoxo derivatives $[Tp^{But}]MgOOR$, solutions of the zinc derivative $[Tp^{But}]ZnEt$ are stable in the presence of O_2 at 100°C.

The less sterically demanding alkyl derivative $[Tp^{Me2}]ZnMe$ is more reactive than $[Tp^{But}]ZnMe$ towards a number of reagents, e.g., Br_2, I_2, MeOH, PhOH, Bu^tOOH, MeI, BrCN, and HCl. However, as a result of ligand redistribution, in each case the major product of the reaction is the six-coordinate sandwich complex $[Tp^{Me2}]_2Zn$ [Eq. (13)] (*80, 89*).

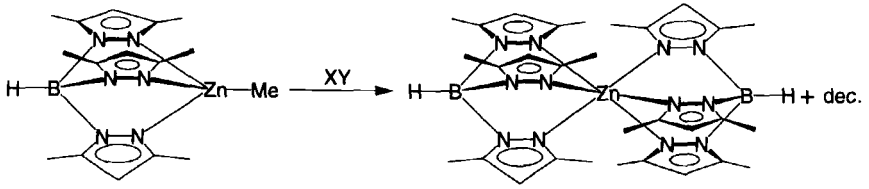

(XY = Br_2, I_2, MeOH, PhOH, Bu^tO_2H, MeI, BrCN, HCl) (13)

Moreover, the sandwich complexes $[Tp^{Ph}]_2Zn$ and $[Tp^{Ar2}]_2Zn$ have also been observed to be products of the reactions of $[Tp^{RR'}]ZnX$ derivatives (*81, 85*).

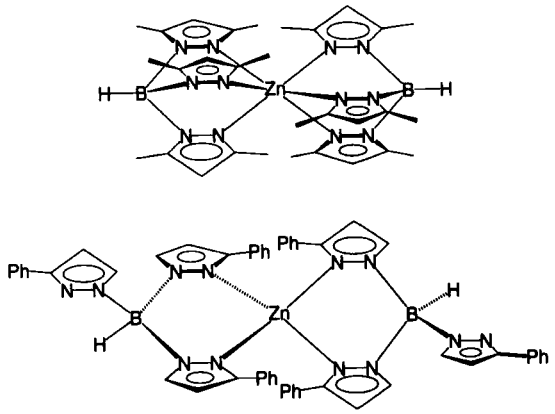

FIG. 28. Structures of $[Tp^{RR'}]_2Zn$ derivatives.

The structures of $[Tp^{Me2}]_2Zn$ (*80*) and $[Tp^{Ph}]_2Zn$ (*85*) have been determined by x-ray diffraction (Fig. 28). Interestingly, $[Tp^{Me2}]_2Zn$ and $[Tp^{Ph}]_2Zn$ do not possess similar structures. Specifically, whereas the zinc center in $[Tp^{Me2}]_2Zn$ is six-coordinate and octahedral, the zinc center in $[Tp^{Ph}]_2Zn$ is only four-coordinate and tetrahedral. Thus, the potentially tridentate $[Tp^{Ph}]$ ligand acts only as a bidentate ligand in $[\eta^2\text{-}Tp^{Ph}]_2Zn$. However, it should be noted that the Fe in the related complex $[Tp^{Ph}]_2Fe$ is octahedrally coordinated (*90*).

The reactivity of three-coordinate $[Bp^{Bu^t}]ZnR$ is summarized in Scheme 12. The Zn–C bonds of $[Bp^{Bu^t}]ZnR$ are readily cleaved by H_2O and $MeCO_2H$ to give the hydroxo and acetato complexes $\{[Bp^{Bu^t}]Zn(\mu\text{-}OH)\}_3$ and $[Bp^{Bu^t}]Zn(\eta^2\text{-}O_2CMe)$, respectively. The structure of $\{[Bp^{Bu^t}]Zn(\mu\text{-}OH)\}_3$, determined by x-ray diffraction, is a cyclic trimer, with Zn–OH bond lengths in the range 1.89–1.99 Å (Fig. 29). The

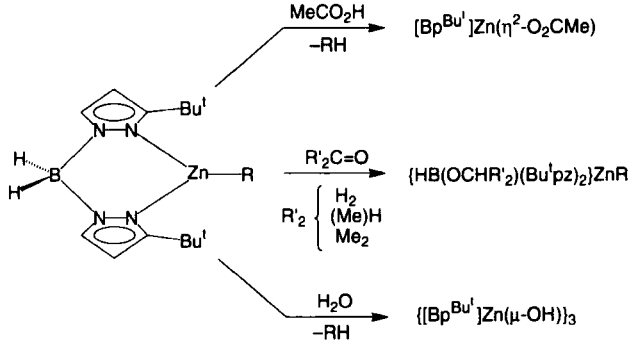

SCHEME 12. Reactivity of $[Bp^{Bu^t}]ZnR$.

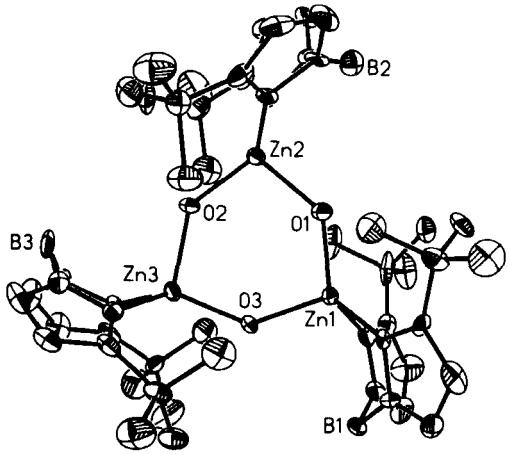

FIG. 29. ORTEP drawing of $\{[Bp^{Bu^t}]Zn(\mu\text{-}OH)\}_3$. Reprinted with permission from Ref. (*80*). © Copyright 1995 American Chemical Society.

$[Zn(\mu\text{-}OH)]_3$ moiety is also characterized by an absorption at 3611 cm^{-1} in the IR spectrum and a signal at 2.25 ppm in the ^1H NMR spectrum.

In addition to reactions at the Zn–C bond, the complexes $[Bp^{Bu^t}]ZnR$ also exhibit reactivity at the B–H bond. Thus, $[Bp^{Bu^t}]ZnR$ reacts with aldehydes and ketones, $(CH_2O)_n$, MeCHO, and Me_2CO, to give $\{HB(OR')(3\text{-}Bu^tpz)_2\}ZnR$ (R′ = Me, Et, Pr^i), as a result of insertion into the B–H bond. In contrast, the tris(pyrazolyl)hydroborato complexes $[Tp^{Bu^t}]ZnR$ are inert towards B–H insertion under similar conditions.

2. *Alkyl Derivatives of Cadmium*

a. Syntheses. The cadmium analogues $[Tp^{Bu^t,Me}]CdMe$ (*91*) and $[Tp^{Me_2}]CdR$ (R = Me, Et, Pr, Pr^i, Bu, Bu^i, Bu^s, Bu^t, Ph) (*92*) have been recently prepared by reaction of R_2Cd with $Tl[Tp^{RR'}]$ [Eq. (14)].

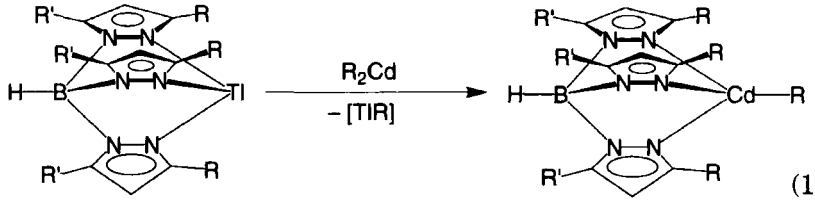

(14)

b. Structures and Spectroscopic Properties. The structure of the cadmium complex $[Tp^{Bu^t,Me}]CdMe$ has been determined by x-ray diffraction, thereby confirming the presence of a trigonally distorted tetrahe-

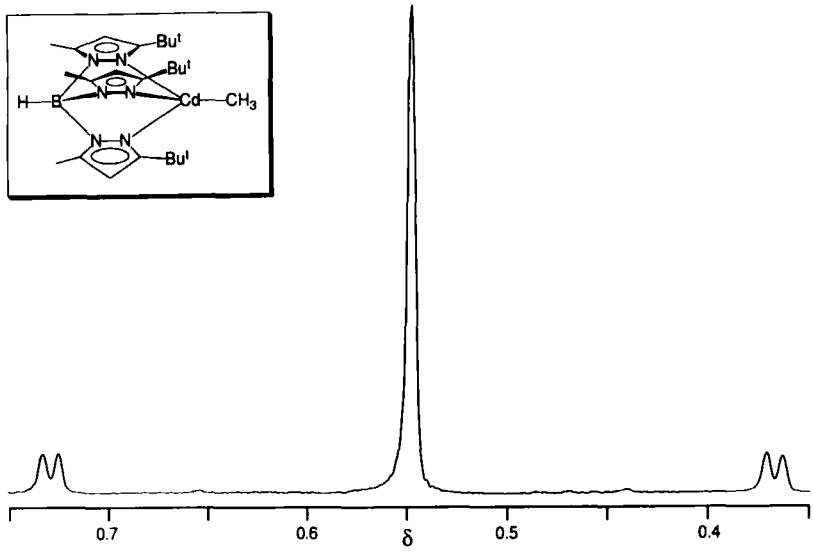

FIG. 30. ^{1}H NMR spectrum of the Cd–CH_3 moiety of [$Tp^{Bu^t,Me}$]CdMe. Reprinted with permission from Ref. (*91*). © Copyright 1994 American Chemical Society.

dral cadmium center, with a Cd–CH_3 bond length of 2.07(2) Å, close to the established range for other Cd–CH_3 bond lengths (2.09–2.11 Å).

The Cd–CH_3 groups of the cadmium derivative [$Tp^{Bu^t,Me}$]CdMe is characterized by the observation of both ^{111}Cd ($^2J_{Cd\text{-}H}$ = 71 Hz) and ^{113}Cd ($^2J_{Cd\text{-}H}$ = 74 Hz) satellites in the ^{1}H NMR spectrum, as shown in Fig. 30. Similarly, $^2J_{Cd\text{-}H}$ coupling constants for [Tp^{Me2}]CdR are observed in the range ca. 78–84 Hz, although these values were incorrectly reported in the literature as half their true values (*92, 93*). For comparison, the values of $^2J_{Cd\text{-}H}$ for two-coordinate alkyls R_2Cd are in the range 50–53 Hz (*94*), while tetrameric alkoxides $[(RO)CdCH_3]_4$ are in the range 80–90 Hz (*95*). The ^{13}C NMR signal of the Cd–CH_3 groups of [$Tp^{Bu^t,Me}$]CdMe and [Tp^{Me2}]CdMe are observed at δ −6.1 and −18.0 ppm, respectively, and each with a $^1J_{C\text{-}H}$ coupling constant of 126 Hz. [Tp^{Me2}]CdMe is also characterized by a $^1J_{Cd\text{-}C}$ coupling constant of 982 Hz (*92, 93*). The ^{13}C NMR data for the complexes [Tp^{Me2}]CdR were also analyzed in order to determine the effect of the [Tp^{Me2}]Cd moiety on the chemical shifts of the alkyl carbon atoms (*92, 96, 97*).

c. Reactivity. The [Tp^{Me2}]CdR derivatives have been reported to undergo ligand redistribution reactions analogous to those of the magnesium derivatives [cf. Eq. (6)] (*92*). Furthermore, the alkyl ligands of

[Tp^{Me2}]CdR have been reported to exchange with the alkyl groups of R'_2Cd, while alkyl exchange was also observed between [Tp^{Me2}]CdEt and [$MepzTp^{Me}$]CdMe. However, since exchange was likewise observed between [Tp^{Me2}]CdMe and [$MepzTp^{Me}$]$_2$Cd (to give [$MepzTp^{Me}$]CdMe), it was pointed out that the aforementioned exchange reactions do not necessarily have to be viewed as "alkyl" exchange reactions because the poly(pyrazolyl)borato ligands themselves may partake in exchange reactions.

In contrast to the chemistry of the zinc complexes [$Tp^{RR'}$]ZnR, the cadmium alkyl derivatives have not been used to prepare an extensive series of half-sandwich [$Tp^{RR'}$]CdX complexes. However, several [$Tp^{RR'}$]CdX complexes supported by sterically demanding tris(pyrazolyl)hydroborato ligands, e.g., [Tp^{But}]CdCl (*98*), [Tp^{But}]CdI (*91*), [Tp^{Pri2}]CdI (*91*), and [$Tp^{But,Me}$]Cd(η^2-O_2NO) (*91*), have been synthesized by metathesis between CdX_2 and either K[$Tp^{RR'}$] or Tl[$Tp^{RR'}$] [Eq. (15)].

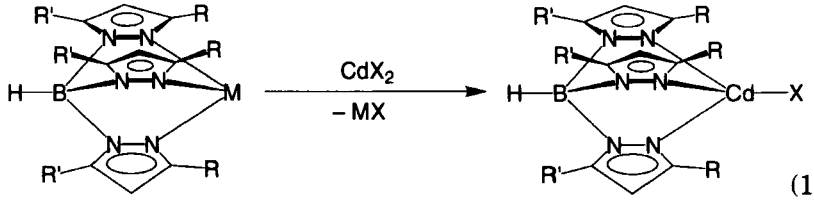

(15)

However, less sterically demanding derivatives, such as [Tp^{Me2}]CdX (X = Cl, I), have been prepared with only limited success because of contamination with the six-coordinate sandwich complex [Tp^{Me2}]$_2$Cd (*89*). The molecular structures of [Tp^{Pri2}]CdI (*91*), [Tp^{But}]CdCl (*99*), [Tp^{But}]CdI (*91*), and [$Tp^{But,Me}$]Cd(η^2-O_2NO) (*91*) have been determined by x-ray diffraction. Each of these complexes exhibits similar coordination of the tris(pyrazolyl)hydroborato ligands, as evidenced by the similar average Cd–N bond lengths and N–Cd–N bond angles: [Tp^{Pri2}]CdI [2.22 Å, 86.0°], [Tp^{But}]CdCl [2.24 Å, 88.3°], [Tp^{But}]CdI [2.25 Å, 88.5°], and [$Tp^{But,Me}$]Cd(η^2-O_2NO) [2.24 Å, 89.8°]. The Cd–N bond lengths in these complexes are shorter than those in the six-coordinate sandwich complexes [Tp^{Me2}]$_2$Cd [2.36 Å and 2.43 Å (*89*); 2.35 Å (*97*)], [pzTp]$_2$Cd [2.33 Å], and [$MepzTp^{Me}$]$_2$Cd [2.35 Å] (*97*).

3. *Alkyl Derivatives of Mercury*

a. Syntheses. The mercury derivatives [TP]HgMe (*100*) and [Tp^{Me2}]HgR (R = Me, Et, Pr^i, Bu^t, CH_2Ph, $CH_2CH{=}CHMe$, Ph, *p*-

C_6H_4Me, $CpFeC_5H_4$) (*89, 101*) have been prepared by the reactions of $K[Tp^{RR'}]$ with $MeHg(NO_3)$ and with RHgCl [Eqs. (16) and (17)].

$$MeHg(NO_3) + K[Tp] \longrightarrow [Tp]HgMe + KNO_3 \quad (16)$$

$$RHgCl + K[Tp^{Me_2}] \longrightarrow [Tp^{Me_2}]HgR + KCl \quad (17)$$

b. Structures and Spectroscopic Properties. In contrast to $[Tp^{RR'}]ZnR$ and $[Tp^{RR'}]CdR$, the $[Tp^{Me2}]$ ligand of $[Tp^{Me2}]HgR$ has been proposed to coordinate to mercury via only one of its pyrazolyl groups so that the mercury center is two-coordinate and linear. The basis of this suggestion is the lack of observed Hg–H or Hg–C coupling to the pyrazolyl rings. However, this proposal has not been confirmed by an x-ray structure determination. Nevertheless, the structure of [pzTp]HgMe has been determined by x-ray diffraction, demonstrating that only two of the pyrazolyl groups were coordinated to Hg. Moreover, the coordinated pyrazolyl groups are bound in an asymmetric manner, with Hg–N bond lengths of 2.07(4) Å and 2.65(4) Å (Fig. 31) (*102*). The coordination geometry about Hg may be described as "T-shaped," with C–Hg–N bond angles of 169(2)° and 112(1)°and a Hg–CH_3 bond length of 2.05(4) Å. In solution, the pyrazolyl groups of [η^2-pzTp]HgMe and [η^2-Tp]HgMe are fluxional, and a structure corresponding to that in the solid state is not frozen out at −90°C. Such behavior is in contrast to the bidentate gold derivatives [η^2-pzTp]$AuMe_2$ and [η^2-Tp]$AuMe_2$, for which the fluxionality is frozen out at −90°C (*77, 78*).

The resonances associated with the Hg–R groups of $[Tp^{Me2}]HgR$ show coupling to ^{199}Hg in their ^1H NMR spectra. For example, $[Tp^{Me2}]HgMe$ exhibits $^2J_{Hg\text{-}H}$ = 225 Hz. The complexes $[Tp^{Me2}]HgR$ are also characterized by ^{199}Hg resonances in the range −576 to −1098 ppm (*101*). The ^{199}Hg NMR spectrum of the phenyl derivative $[Tp^{Me2}]HgPh$ has been reported as both (i) a signal at −925 ppm (*101, 103*) and (ii) two signals at 816 and 614 ppm at 5°C (relative to aqueous $HgCl_2$) for a material of composition $[Tp^{Me2}]HgPh \cdot 0.5KCl$ (*89*). In the latter case, the sharp

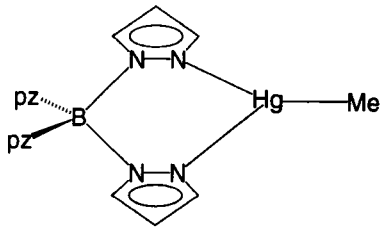

FIG. 31. Structure of [η^2-pzTp]HgMe.

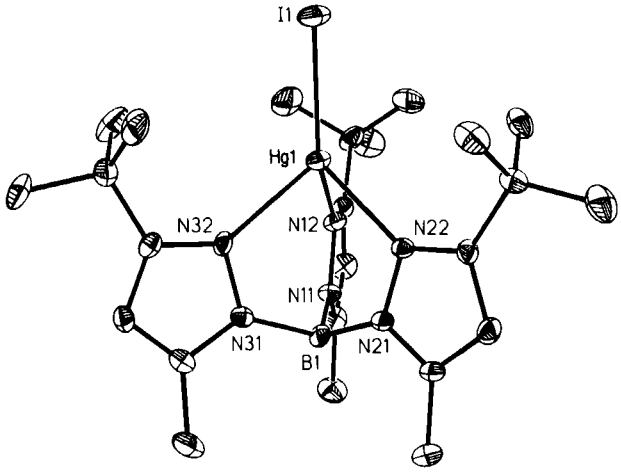

FIG. 32. ORTEP drawing of $[Tp^{But,Me}]HgI$.

resonance at 816 ppm dominates, but at −60°C it is the broad resonance which shifts to 662 ppm that is dominant, and it was proposed that an equilibrium existed between the two species $[Tp^{Me2}]HgPh$ (δ 614 ppm) and $[HgPh]^+$ (δ 816 ppm) in order to account for the data.

$$[Tp^{Me2}]HgPh \rightleftarrows [Tp^{Me2}]^- + [HgPh]^+$$

c. Reactivity. As with $[Tp^{RR'}]CdR$, the reactivity of the mercury alkyl complexes $[Tp^{RR'}]HgR$ has not been studied in significant detail. However, a number of $[Tp^{Me2}]HgX$ complexes have been prepared by the reaction of HgX_2 with $K[Tp^{Me2}]$. Specific complexes include $[Tp^{Me2}]_2Hg$, $[Tp^{Me2}]HgX$ (X = Cl, Br, I, CNS, CO_2CH_3), and the novel mercury(I) derivative $[Tp^{Me2}]_2Hg_2$ (*104*). The structure of $[Tp^{But,Me}]HgI$ has been determined by x-ray diffraction (Figure 32) (*105*), confirming a pseudo-tetrahedral coordination environment, in contrast to the lower coordinate structures proposed for the alkyl derivatives.

D. POLY(PYRAZOLYL)BORATO ALKYL DERIVATIVES OF THE GROUP 13 ELEMENTS

Poly(pyrazolyl)borato alkyl derivatives of the Group 13 elements (Al, Ga, In, Tl) have been synthesized for all members with the exception of thallium.

1. Alkyl Derivatives of Aluminum

The tris(pyrazolyl)hydroborato aluminum methyl derivatives $[Tp^{Me2}]AlMe_2$ and $[Tp^{But}]AlMe_2$ may be prepared by metathesis of Me_3Al with $K[Tp^{Me2}]$ and $Tl[Tp^{But}]$, respectively (Scheme 13) (*106*). $[Tp^{But}]AlMe_2$ has been characterized by NMR spectroscopy as a four-coordinate complex with a bidentate tris(pyrazolyl)hydroborato ligand. For example, the ^1H NMR spectrum at room temperature shows two sets of *t*-butylpyrazolyl groups in the ratio 2:1, and two inequivalent Al–Me groups in the ratio 1:1.

In contrast to $[Tp^{But}]AlMe_2$, $[Tp^{Me2}]AlMe_2$ shows only one type of pyrazolyl and Al–Me group in the NMR spectrum at $-90°C$, consistent with either a five-coordinate structure or a highly fluxional four-coordinate structure. A precedent for tridentate coordination of the $[Tp^{Me2}]$ ligand to aluminum is provided by the six-coordinate complex $\{[Tp^{Me2}]_2Al\}[AlCl_4]$ (*107*).

The bis(3-t-butylpyrazolyl)hydroborato complex, $[Bp^{But}]AlMe_2$, has been synthesized by the reactions of either Me_3Al or Me_2AlCl with $K[Bp^{But}]$ (Scheme 14). Similarly, $[Et_2Bp]AlEt_2$ has been prepared by the reaction of Et_2AlCl with $K[Et_2Bp]$ (*108*).

The methyl complex $[Bp^{But}]AlMe_2$ undergoes rearrangement upon heating at ca. 100°C to give the more stable isomer, $[\eta^2\text{-}H_2B(3\text{-}Bu^tpz)(5\text{-}Bu^tpz)]AlMe_2$, as shown in Eq. (18).

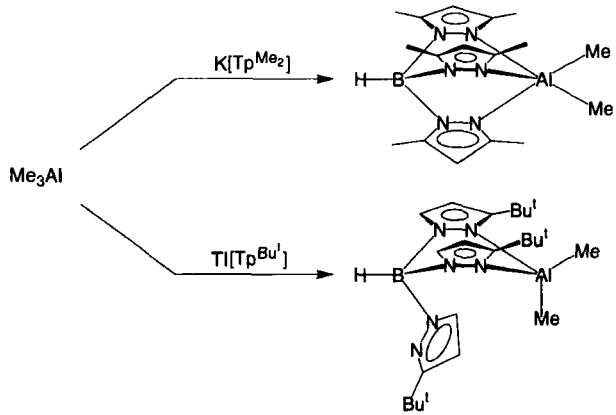

SCHEME 13. Syntheses of $[Tp^{RR'}]AlMe_2$ derivatives.

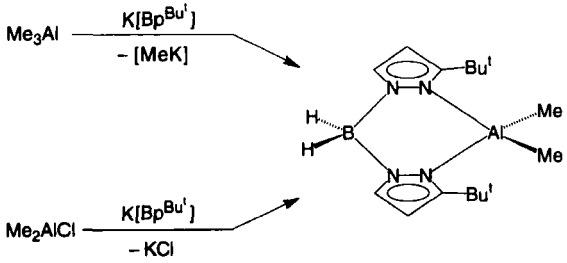

SCHEME 14. Syntheses of $[Bp^{Bu^t}]AlMe_2$.

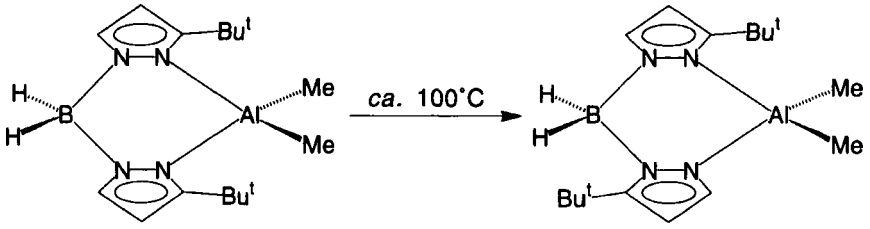

(18)

Kinetics studies have demonstrated that the isomerization is a first-order process, characterized by the activation parameters $\Delta H‡$ = 34.5(8) kcal mol^{-1} and $\Delta S‡$ = 6(2) e.u. Such rearrangements of poly(pyrazolyl)borato ligands are not uncommon, and have also been observed for Cu and Co complexes of the tris(3-isopropylpyrazolyl)hydroborato ligand system, i.e., $[\eta^3\text{-HB(3-Pr}^i\text{pz)}_3]M \rightarrow [\eta^3\text{-HB(3-Pr}^i\text{pz)}_2(5\text{-Pr}^i\text{pz})]M$ (*32*).

2. *Alkyl Derivatives of Gallium*

The first gallium alkyl derivatives to be stabilized by poly(pyrazolyl)borato ligation were the four-coordinate complexes $[Bp]GaMe_2$ and $[Me_2Bp]GaMe_2$, obtained by the reactions of $Me_2GaCl \cdot OEt_2$ with K[Bp] and $K[Me_2Bp]$, respectively [Eq. (19)] (*109, 110*).

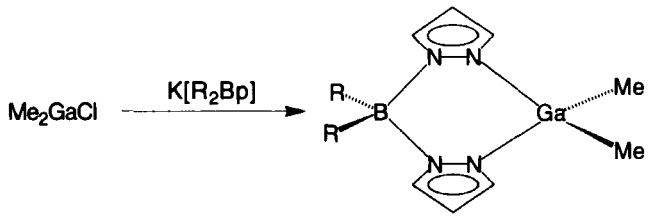

(19)

The gallium ethyl derivatives $[R_2Bp]GaEt_2$ (R = Et, Ph, pz) have likewise been synthesized (*108*).

The structure of $[Me_2Bp]GaMe_2$ has been obtained by x-ray diffraction, and the Ga–Me bond lengths have been determined to be 1.962(7) Å and 1.971(8) Å (*109*). However, the first crystal structure determination of $[Me_2Bp]GaMe_2$ resulted in the derivation of an anomalously small equivalent isotropic thermal parameter for the carbon atom of one of the gallium methyl groups. It was concluded that the specific "methyl" group in question was in fact a hydroxy group, i.e., that the crystal was in fact the hydroxy complex $[Me_2Bp]GaMe(OH)$. Refinement of the anomalous atom as oxygen resulted in a lower *R* value and a more reasonable thermal parameter (*109*). However, the derived Ga–C [1.957(8) Å] and Ga–O [2.033(5) Å] bond lengths are not consistent with the formulation $[Me_2Bp]GaMe(OH)$. Specifically, since the covalent radius of oxygen is smaller than that of carbon, a Ga–OH bond that is longer than a $Ga–CH_3$ bond is unexpected. An alternative explanation that accounts for both (i) an anomalous thermal parameter and (ii) a bond that is longer than that of $Ga–CH_3$ is that the dialkyl $[Me_2Bp]GaMe_2$ is contaminated with a small amount of the chloride derivative $[Me_2Bp]GaMe(Cl)$. Because it is likely that $[Me_2Bp]GaMe_2$ and $[Me_2Bp]GaMe(Cl)$ would be isostructural, it would not be unexpected for the two complexes to cocrystallize and thereby result in an artificially elongated "Ga–C" bond (see Section VII).

One of the Ga–Me bonds in the dimethyl derivative $[Bp]GaMe_2$ is cleaved by $MeCO_2H$ to give the monoalkyl complex $[Bp]GaMe(O_2CMe)$ (*110*). Other monoalkyl complexes of gallium include [Bp]GaMe(Cl) and $[Bp]_2GaMe$, which have been obtained by the reactions of $MeGaCl_2$ with one and two equivalents of K[Bp], respectively (Scheme 15) (*110, 111*). Related tris(pyrazolyl)hydroborato derivatives $[Tp^{RR'}]GaMe(Cl)$ and $[Tp^{RR'}]GaMe_2$ have also been synthesized by the reactions of $K[Tp^{RR'}]$ with $MeGaCl_2$ and Me_2GaCl, respectively [Eq. (20)].

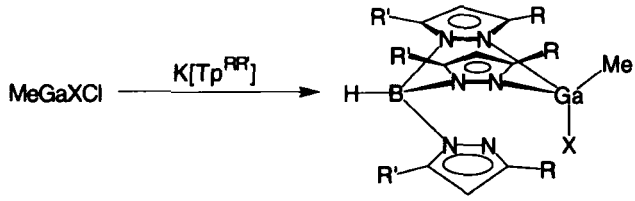

(X = Cl, Me) (20)

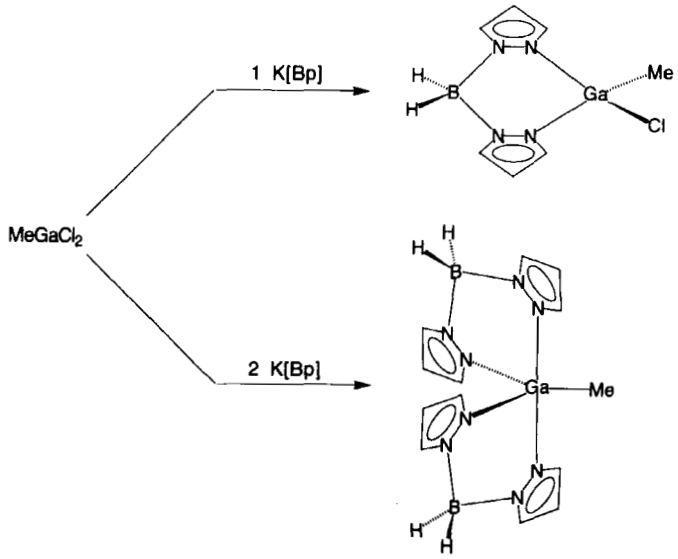

SCHEME 15. Syntheses of [Bp]GaMe(X).

The structures of $[Tp^{Me2}]GaMe(Cl)$ and $[Tp^{Me2}]GaMe_2$ have been determined by x-ray diffraction (*112*). In the solid state, both $[Tp^{Me2}]GaMe(Cl)$ and $[Tp^{Me2}]GaMe_2$ exhibit bidentate coordination of the tris(pyrazolyl)hydroborato ligand, so that the gallium center adopts a distorted tetrahedral coordination environment. In solution, however, the complexes are fluxional, exhibiting only one set of pyrazolyl resonances in the ^1H NMR spectrum at room temperature. The less sterically demanding K[Tp] and K[pzTp] derivatives (two equivalents), however, react further with $MeGaCl_2$ to give complexes of compositions $[Tp]_2GaMe$ and $[pzTp]_2GaMe$ [Eq. (21)] (*112*).

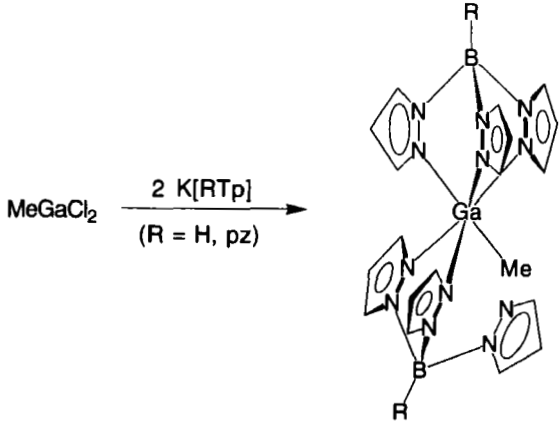

(21)

The structure of $[pzTp]_2GaMe$, determined by x-ray diffraction, demonstrates that the [pzTp] ligands adopt both bidentate and tridentate coordination. However, in solution, the complexes $[Tp]_2GaMe$ and $[pzTp]_2GaMe$ are fluxional on the NMR time scale at room temperature, exhibiting a single set of resonances for the pyrazolyl groups.

3. *Alkyl Derivatives of Indium*

Bis(pyrazolyl)hydroborato indium alkyl derivatives with both one and two [Bp] ligands, e.g., [Bp]InMe(Cl) and $[Bp]_2InMe$, have been prepared by the reactions of $MeInCl_2$ with one and two equivalents of K[Bp], respectively (Scheme 16) (*113*). Likewise, the dimethyl derivative $[Bp]InMe_2$ is prepared by the reaction of Me_2InCl with K[Bp] [Eq. (22)].

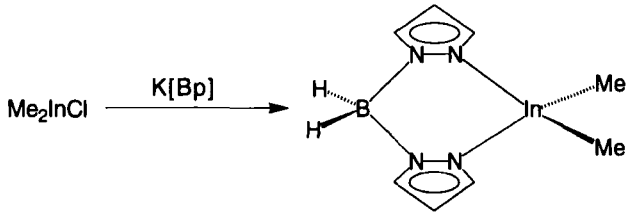

(22)

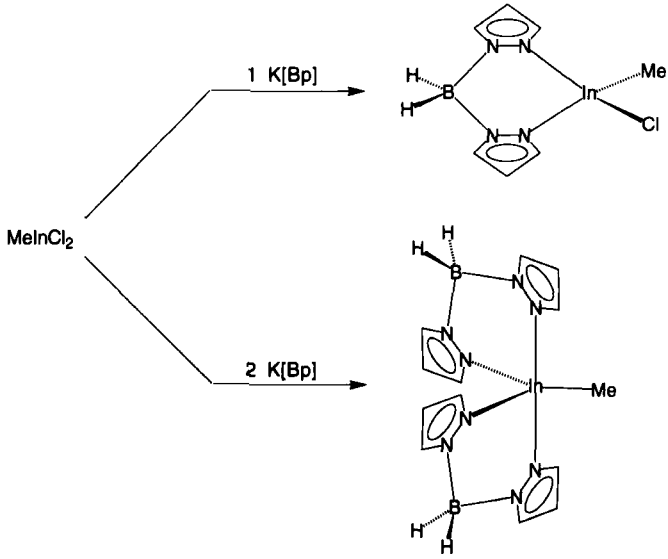

SCHEME 16. Syntheses of [Bp]InMe(X).

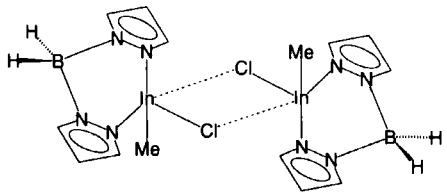

FIG. 33. Structure of $\{[\eta^2\text{-pzTp}]\text{In(Me)Cl}\}_2$.

The x-ray structure of $[Bp]InMe_2$ confirms that the complex is monomeric with a distorted tetrahedral geometry at indium and with In–Me bond lengths of 2.133(5) Å and 2.138(6) Å. In contrast, the chloride derivative [Bp]InMe(Cl) exists as a weak dimer, with asymmetrically bridged chloride ligands (Fig. 33). The In–Cl bond lengths are 2.410(1) Å and 3.203(1) Å, while the In–Me bond length is 2.091(5) Å. Indium alkyl derivatives with one and two [pzTp] coligands have been prepared similarly. Thus, Me_2InCl reacts with K[pzTp] to give $[pzTp]InMe_2$ [Eq. (23)] while $MeInCl_2$ reacts with two equivalents of K[pzTp] to give $[pzTp]_2InMe$ [Eq. (24)] (*114*).

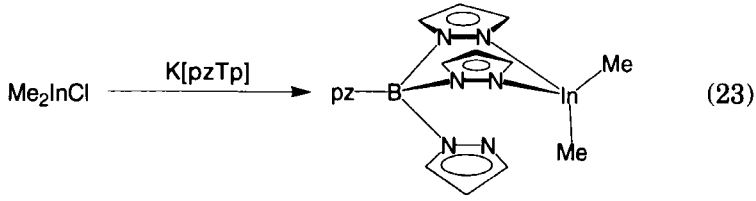

(23)

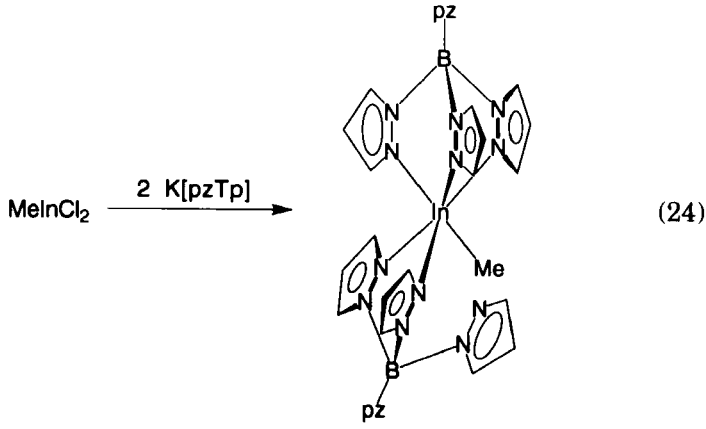

(24)

$[pzTp]InMe_2$ has been proposed to possess a four-coordinate structure with a bidentate [pzTp] ligand, while $[pzTp]_2InMe$ exhibits an octahe-

dral structure in which the [pzTp] ligands adopt both bidentate and tridentate coordination (*114*).

E. Poly(pyrazolyl)borato Alkyl Derivatives of the Group 14 Elements

Of the group 14 elements (Si, Ge, Sn and Pb), only tin is known to form a variety of poly(pyrazolyl)borato alkyl derivatives. For example, the reactions between K[pzTp] and the silicon derivatives Me_nSiCl_{4-n} (n = 1–3) have not given tractable products (*115*). Similarly, the reaction between K[pzTp] and Me_2GeCl_2 gives a complex that has been spectroscopically characterized as $[pzTp]_2GeMe_2$, but which readily decomposes.

1. Alkyl Derivatives of Tin

In contrast to the scarcity of stable poly(pyrazolyl)borato alkyl complexes of Si, Ge, and Pb, such derivatives are common for tin. The first poly(pyrazolyl)borato tin alkyl derivatives to be prepared were the parent derivatives, namely five-coordinate $[Bp]SnMe_nCl_{3-n}$ and six-coordinate $[Tp]SnMe_nCl_{3-n}$ (n = 0–3), obtained by the reactions of Me_nSnCl_{4-n} with K[Bp] and K[Tp], respectively [Eqs. (25) and (26)] (*116*).

$$Me_nSnCl_{4-n} + K[Bp] \longrightarrow [Bp]SnMe_nCl_{3-n} + KCl \qquad (25)$$

$$Me_nSnCl_{4-n} + K[Tp] \longrightarrow [Tp]SnMe_nCl_{3-n} + KCl \qquad (26)$$

The five-coordinate $[Bp]SnMe_nCl_{3-n}$ complexes adopt a trigonal bipyramid geometry, with the [Bp] ligand occupying axial and equatorial coordination sites, while the six-coordinate $[Tp]SnMe_nCl_{3-n}$ complexes adopt an octahedral geometry (Fig. 34). In solution, however, the com-

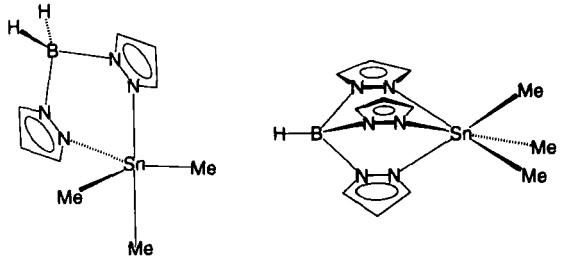

FIG. 34. Structures of $[Bp]SnMe_3$ and $[Tp]SnMe_3$.

plexes $[Tp]SnMeCl_2$ and $[Tp]SnMe_2Cl$ show only one type of pyrazolyl group in the ^1H NMR spectrum, indicative of a fluxional octahedral structure. Similarly, only one type of pyrazolyl group is observed in the ^1H NMR spectrum for the five-coordinate complexes $[Bp]SnMe_nCl_{3-n}$.

Other $[Bp^{RR'}]SnR_nX_{3-n}$ and $[Tp^{RR'}]SnR_nX_{3-n}$ complexes have also been synthesized by an analogous method. Specific examples include $[Bp]SnCl(CH_2CH_2COOMe)_2$ (*117*), $[Tp]SnR_nX_{3-n}$ (R = Me, Et, Bu, Ph; X = Cl, Br; n = 0–2) (*118*), $[Tp]SnX_2(CH_2CH_2COOMe)$ (X = Cl, NCS) (*119*), $[Tp^{Me2}]SnR_nX_{3-n}$ (R = Me, Et, Bu, Ph; X = Cl, Br; n = 0–2) (*120*), and $[pzTp]SnR_nX_{3-n}$ (R = Me, Et, Bu, Ph; X = Cl, Br; n = 0–2) (*121, 122*).

The six-coordinate $[RTp]SnR_nCl_{3-n}$ derivatives are typically characterized by ^{119}Sn NMR signals in the range −195 to −670 ppm (relative to Me_4Sn) (*115, 118, 120, 121*), while five-coordinate $[RBp]SnR_nCl_{3-n}$ complexes exhibit shifts to lower field in the range −103 to −182 ppm (*115*). For $[Tp^{RR'}]SnR_nX_{3-n}$ derivatives, the ^{119}Sn chemical shift was also determined to be a linear function of n (*120*).

In addition to tin alkyl derivatives with one poly(pyrazolyl)borato ligand, bis[(poly)pyrazolylborato] complexes of the types $[Tp]_2SnR_2$ and $[R_2Bp]_2SnR_2$ have also been prepared (*123, 124*).

IV. Terminal Hydride Derivatives of the *s*- and *p*-Block Metals Supported by Poly(pyrazolyl)borato Ligation

By analogy with the alkyl derivatives described earlier, poly(pyrazolyl)hydroborato ligation may also be utilized to support monomeric terminal hydride derivatives $[Tp^{RR'}]MH_n$. However, at present, the chemistry of such complexes is effectively restricted to that of four-coordinate derivatives of the type $[Tp^{But}]MH$.

A. $[Tp^{But}]BeH$

1. Synthesis

The beryllium hydride derivative $[Tp^{But}]BeH$ is obtained by metathesis of either $[Tp^{But}]BeCl$ or $[Tp^{But}]BeBr$ with $LiAlH_4$ in Et_2O at room temperature [Eq. (27)] (*56*).

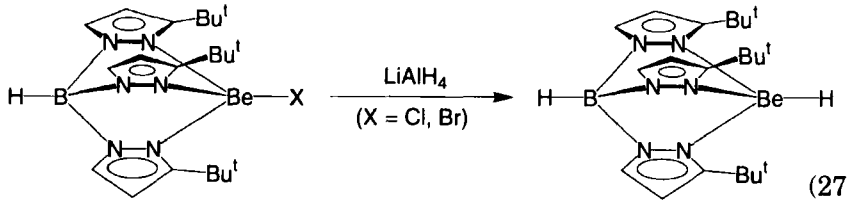

(27)

$[Tp^{But}]BeH$ is a well-defined example of a monomeric complex containing a terminal beryllium hydride ligand. In this regard, other than the cyclopentadienyl compounds $(C_5H_5)BeH$ (*9*) and $(C_5Me_5)BeH$ (*125*), beryllium hydride complexes, e.g., $[MeBe(OEt_2)]_2(\mu\text{-}H)_2$ (*126*), $[PhBe(NMe_3)]_2(\mu\text{-}H)_2$ (*127*), and $[(Et_2O)NaHBeEt_2]_n$ (*128*), are typically oligomeric with bridging hydride ligands (*129*). A notable exception, however, is $[(\mu\text{-}\eta^2\text{-}Me_2NCH_2CH_2NMe)BeH]_2$, the first terminal beryllium hydride complex to be studied by x-ray diffraction (*130*).

2. *Structure and Spectroscopic Properties*

The structure of $[Tp^{But}]BeH$ has been determined by x-ray diffraction (Fig. 35). The Be–H bond length was found to be 1.23(7) Å, close to the sum of the covalent radii (1.19 Å) (*57*), but shorter than those observed for $[(\mu\text{-}\eta^2\text{-}Me_2NCH_2CH_2NMe)BeH]_2$ [1.39(2) Å] (*130*) and $(C_5H_5)BeH$ [d(Be-H) = 1.32(1) Å] (*131, 132*). Theoretical calculations on a series of hypothetical beryllium hydride derivatives have estimated terminal Be–H bond lengths to be in the range 1.25–1.29 Å (*133*).

The terminal Be–H moiety in $[Tp^{But}]BeH$ is observed as a quadrupolar-broadened peak at δ 5.0 ppm in the ^1H NMR spectrum at room temperature, close to that for the B–H group at δ 4.5 ppm. At higher temperatures, however, quadrupolar relaxation is reduced and a 1 : 1 : 1 : 1 quartet structure is observed for both the Be–H and B–H resonances (Fig. 36) (*134*), with $^1J_{^9Be\text{-}H}$ and $^1J_{^{11}B\text{-}H}$ coupling constants of 28 Hz and 113 Hz, respectively (*135*). For comparison, the hydride ligands in $(C_5H_5)Be(\eta^2\text{-}H_2BH_2)$, which are fluxional at $-80°C$, exhibit smaller coupling constants $J_{^9Be\text{-}H}$ = 10.2 Hz and $J_{^{11}B\text{-}H}$ = 84 Hz ($J_{^{10}B\text{-}H}$ =

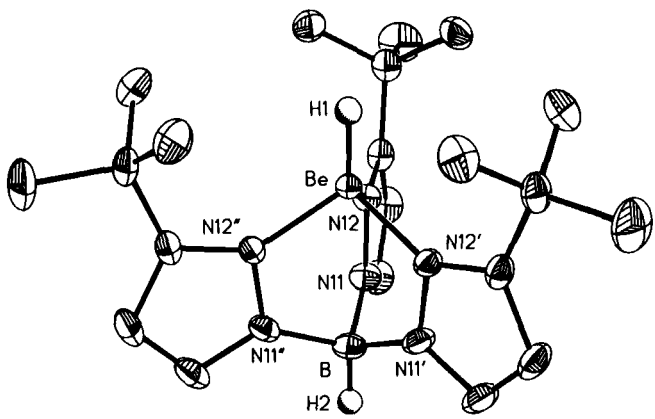

FIG. 35. ORTEP drawing of $[Tp^{But}]BeH$. Reprinted with permission from Ref. (*56*).
© Copyright 1992 American Chemical Society.

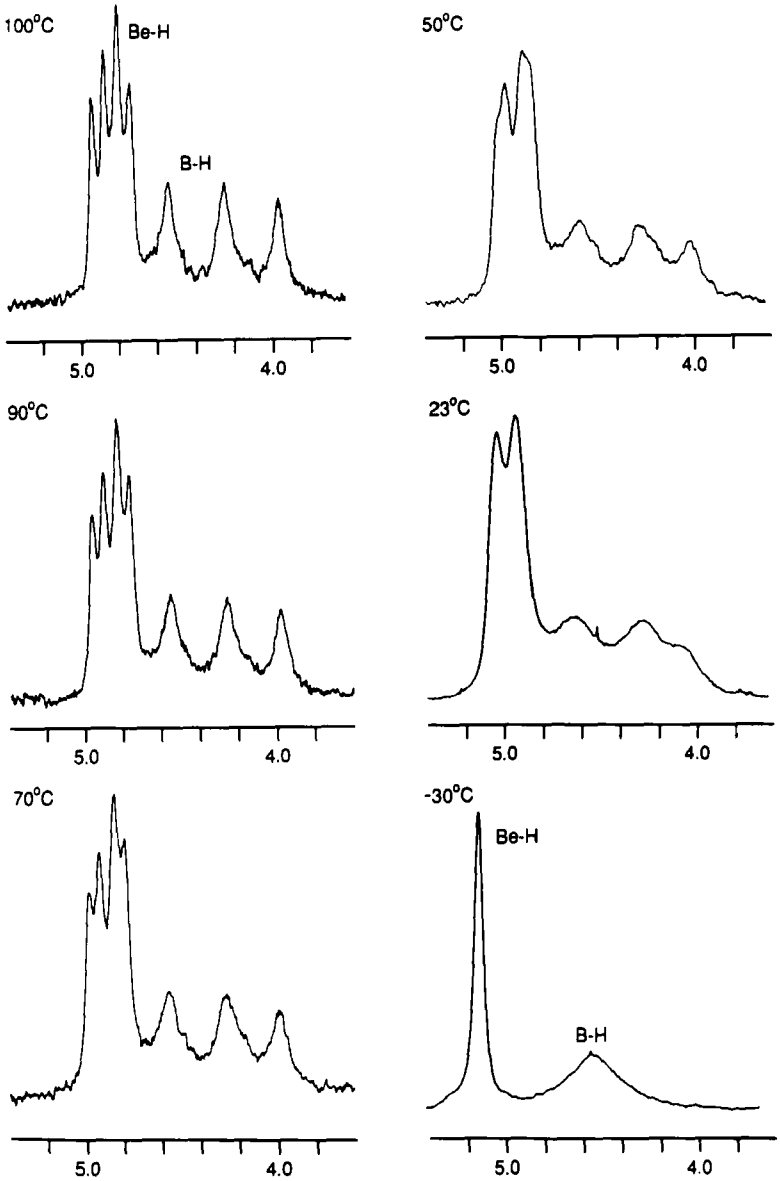

FIG. 36. Variable-temperature ^{1}H NMR spectra of [Tp$^{Bu^t}$]BeH. Reprinted with permission from Ref. (*56*). © Copyright 1992 American Chemical Society.

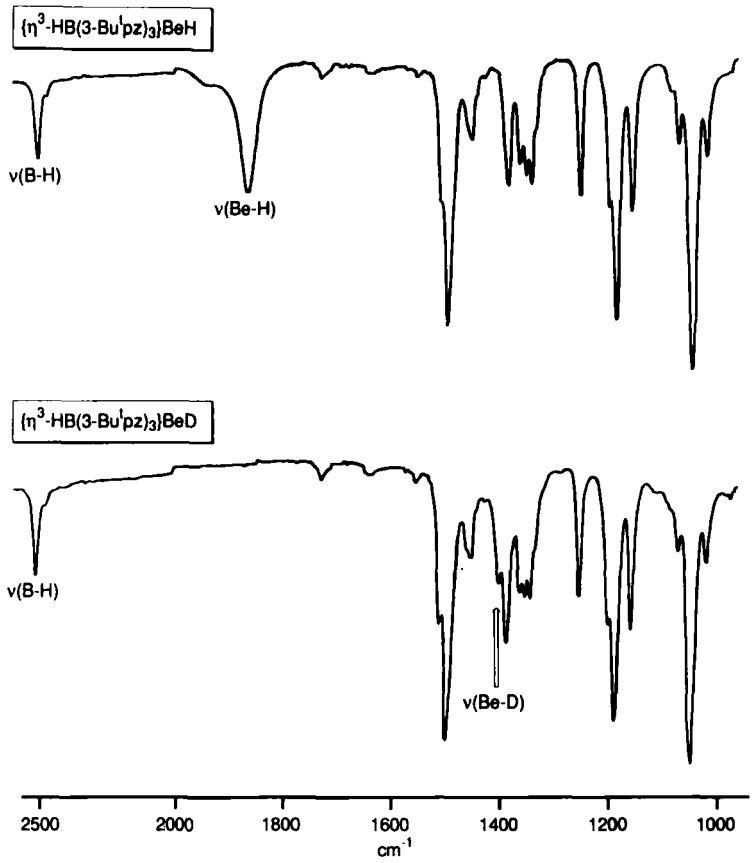

FIG. 37. IR spectra of [Tp$^{Bu^t}$]BeH and [Tp$^{Bu^t}$]BeD. Reprinted with permission from Ref. (*56*). © Copyright 1992 American Chemical Society.

28 Hz) (*135, 136*). [Tp$^{Bu^t}$]BeH is also characterized by a broad resonance ($W_{1/2}$ = 61 Hz) at δ 2.7 ppm in the ^{9}Be NMR spectrum.

The IR spectra of [Tp$^{Bu^t}$]BeH and [Tp$^{Bu^t}$]BeD demonstrate that ν(Be–H) is observed at 1865 cm^{-1}, shifting to 1410 cm^{-1} (ν_H/ν_D = 1.32) upon deuterium substitution (Fig. 37). For comparison, ν(Be–H) of (C_5H_5)BeH is observed at 2030 cm^{-1} in the gas phase, with ν(Be–D) = 1535 cm^{-1} (ν_H/ν_D = 1.32). However, in the solid state the absorptions were observed at lower frequencies, with ν(Be–H) = 1720 cm^{-1} and ν(Be–D) = 1275 cm^{-1} (ν_H/ν_D = 1.35), indicative of some degree of intermolecular association (*137*).

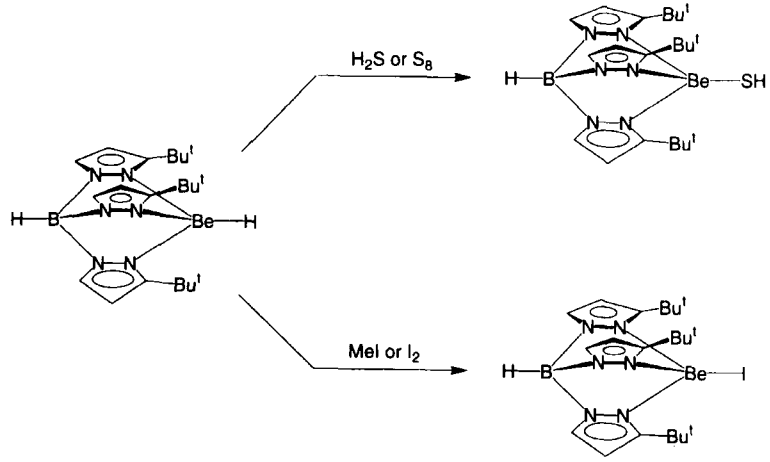

SCHEME 17. Reactivity of [Tp^{But}]BeH.

3. *Reactivity*

The reactivity of [Tp^{But}]BeH is summarized in Scheme 17. The Be–H moiety is cleaved by both MeI and I_2 to give [Tp^{But}]BeI, and by H_2S to give [Tp^{But}]BeSH. Furthermore, [Tp^{But}]BeSH is also obtained by the direct insertion of elemental sulfur into the Be–H bond.

B. [Tp^{But}]ZnH

1. *Synthesis*

The zinc hydride complex [Tp^{But}]ZnH, the first metal hydride derivative of the type [Tp$^{RR'}$]MH to be prepared, is readily synthesized by metathesis of ZnH_2 with Tl[Tp^{But}] [Eq. (28)] (*80, 138*).

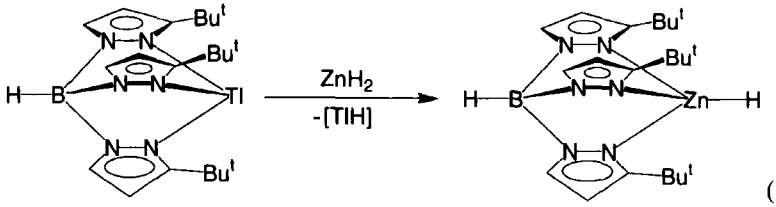

(28)

As with the reactions between MR_n and Tl[Tp^{But}] described earlier, the decomposition of putative [TlH] provides an effective driving force

for the reaction. Similar to beryllium hydride complexes, zinc hydride derivatives are rare and typically oligomeric (*139*). For example, some dimeric, trimeric, and tetrameric zinc hydride derivatives include $[HZnN(Me)CH_2CH_2NMe_2]_2$ (*140*), $[HZnO(CH_2)_2NMe_2]_2$ (*141*), $[RZnH(NC_5H_5)]_3$ (R = Et, Ph) (*142*), and $[HZnOBu^t]_4$ (*143*), of which only $[HZnN(Me)CH_2CH_2NMe_2]_2$ has been structurally characterized by x-ray diffraction.

2. *Structure and Spectroscopic Properties*

The structure of $[Tp^{But}]ZnH$ has been determined by x-ray diffraction, although the hydride ligand was not located (Fig. 38). However, definitive evidence for the presence of the hydride ligand is provided by NMR and IR spectroscopies. Specifically, the hydride resonance is observed at δ 5.36 ppm in the ^1H NMR spectrum, and ν(Zn–H) is observed as a strong absorption at 1770 cm^{-1} in the IR spectrum, which shifts to 1270 cm^{-1} (ν_H/ν_D = 1.39) upon deuterium substitution (Fig. 39).

3. *Reactivity*

The reactivity of the zinc hydride moiety in $[Tp^{But}]ZnH$ is illustrated in Scheme 18. Protic reagents (HX = H_2S, Me_3SiOH, $MeCO_2H$, $PhC{\equiv}CH$) react with the Zn–H bond to give $[Tp^{But}]ZnX$ and H_2. Metathesis reactions are also observed with RI (R = Me, $PhCH_2$), MeCOCl, Me_3SiX (X = Cl, I), and I_2 to give $[Tp^{But}]ZnX$ (X = Cl, I). Insertion of CO_2 into the Zn–H bond is observed at 50°C to give the formato complex, $[Tp^{But}]Zn(\eta^1\text{-}O_2CH)$, characterized as an η^1- rather than η^2-formato derivative on the basis of the observed $\nu_{asym}(CO_2)$ [1655 cm^{-1}]

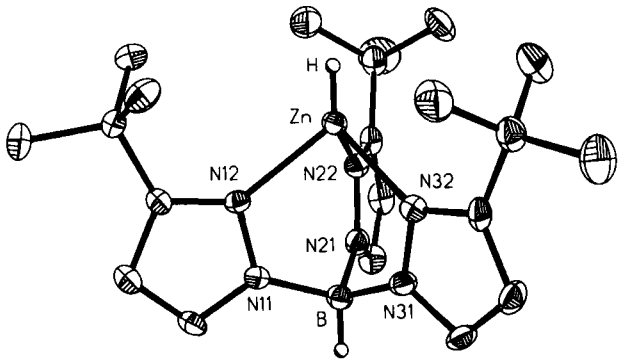

FIG. 38. ORTEP drawing of $[Tp^{But}]ZnH$ (the zinc hydride ligand was not located, but is illustrated in the expected axial position). Reprinted with permission from Ref. (*80*). © Copyright 1995 American Chemical Society.

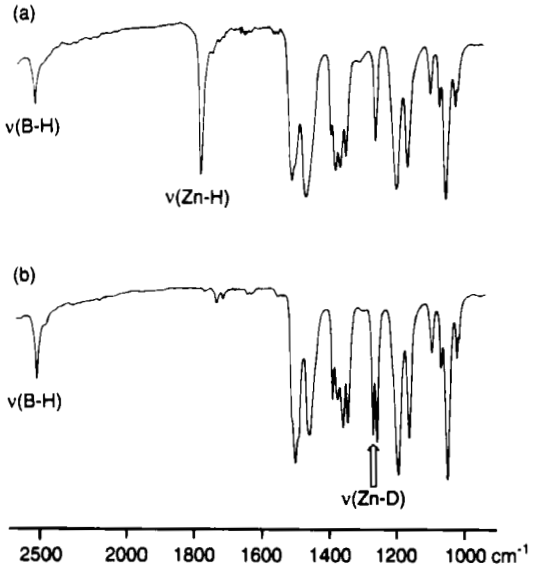

FIG. 39. IR spectra of (a) [Tp$^{Bu^t}$]ZnH and (b) [Tp$^{Bu^t}$]ZnD. Reprinted with permission from Ref. (*80*). © Copyright 1995 American Chemical Society.

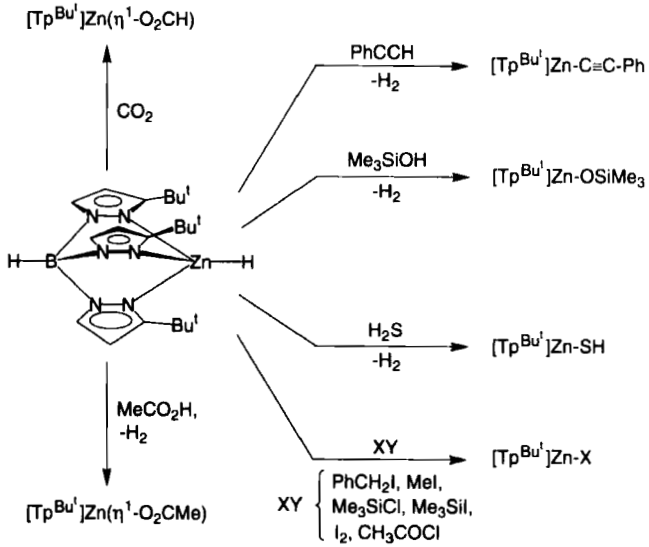

SCHEME 18. Reactivity of [Tp$^{Bu^t}$]ZnH.

and $\nu_{sym}(CO_2)$ [1290 cm^{-1}] absorptions in the IR spectrum (*144*). The reactivity of the Zn–H bond of [Tp^{But}]ZnH towards CO_2 contrasts with the inertness of the alkyl derivatives [Tp^{But}]ZnR towards CO_2.

C. [Tp^{But}]CdH

The cadmium hydride analogue [Tp^{But}]CdH of the aforementioned beryllium and zinc hydride derivatives has been synthesized by the reaction of $CdCl_2$ with KBH_4 (or $LiEt_3BH$), followed by addition of Tl[Tp^{But}] (Scheme 19) (*145*). The Cd–H moiety in [Tp^{But}]CdH is characterized by resonance at δ 6.30 ppm in the ^1H NMR spectrum, with both ^{111}Cd ($^1J_{Cd\text{-}H}$ = 2411 Hz) and ^{113}Cd ($^1J_{Cd\text{-}H}$ = 2522 Hz) satellites. Correspondingly, the ^{113}Cd NMR signal is also observed as a doublet.

In contrast to the formation of a cadmium hydride derivative, the related reaction of the less sterically demanding reagent Tl[Tp^{Me2}] with [$CdCl_2$/$LiEt_3BH$] gives the novel Cd–Cd bonded dimer {[Tp^{Me2}]Cd}$_2$ (Scheme 19), characterized by a ^{111}Cd–^{113}Cd coupling constant of 20,646 Hz. Interestingly, the corresponding reaction using KBH_4 rather than $LiEt_3BH$ affords the η^2-borohydride complex [Tp^{Me2}]Cd(η^2-H_2BH_2) rather than either the dimer {[Tp^{Me2}]Cd}$_2$ or the terminal hydride derivative [Tp^{Me2}]CdH (*145*).

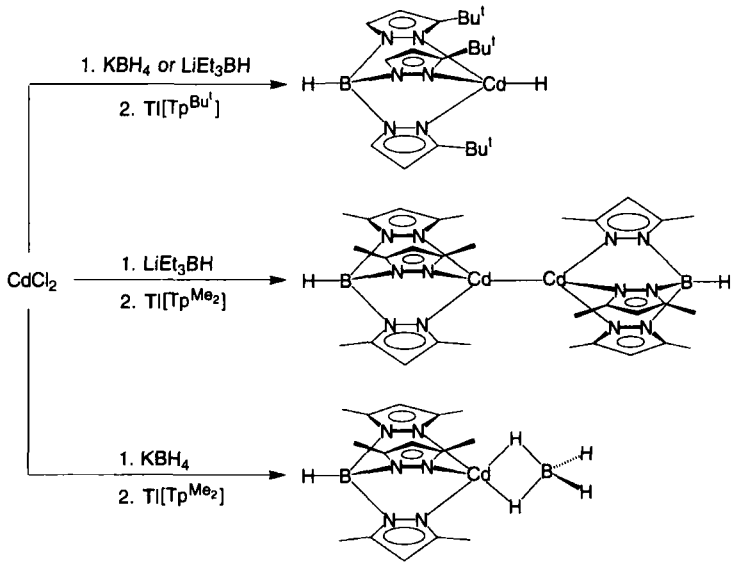

SCHEME 19. Synthesis of [Tp^{But}]CdH and related derivatives.

V. Terminal Hydroxide Derivatives of the *s*- and *p*-Block Metals Supported by Poly(pyrazolyl)borato Ligation

A. Hydroxide Derivatives of Beryllium and Magnesium

Addition of NaOH to a mixture of aqueous K[Tp^{Me2}] and Be^{2+} in hydrochloric acid results in precipitation of [Tp^{Me2}]BeOH, which has been proposed to be monomeric. However, x-ray diffraction studies on crystals obtained from Et_2O indicate a trimeric structure, {[η^2-Tp^{Me2}]Be(μ-OH)}$_3$, in which the [Tp^{Me2}] ligands are bidentate (Scheme 20) (*146*). The cyclic structure is similar to that observed in the zinc complex {[Bp^{But}]Zn(μ-OH)}$_3$ (*80*). The analogue {[η^2-Tp]Be(μ-OH)}$_3$, prepared by a similar method involving extraction of an acidic solution of $BeCl_2$ and K[Tp] into dichloroethane, has also been structurally

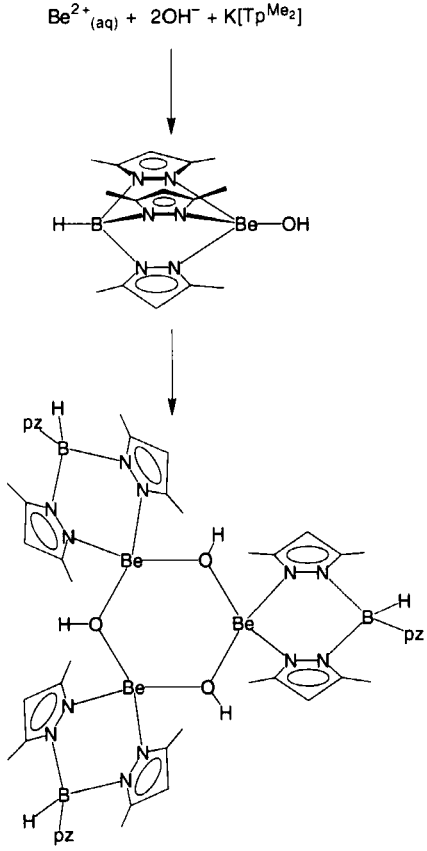

SCHEME 20. Syntheses of beryllium hydroxide derivatives.

characterized by x-ray diffraction (*39c, 55, 147*). The [Be(μ-OH)] moieties of $\{[\eta^2\text{-Tp}]\text{Be}(\mu\text{-OH})\}_3$ and $\{[\eta^2\text{-Tp}^{Me2}]\text{Be}(\mu\text{-OH})\}_3$ are characterized by signals in the ^{1}H NMR spectra at δ 7.72 and 9.30 ppm, respectively, and OH–N hydrogen bonds have been proposed to be present between the hydroxide ligand and the uncoordinated pyrazolyl group.

The magnesium hydroxide complex $[\text{Tp}^{Ar2}]\text{MgOH}$ (Ar = p-$C_6H_4Bu^t$) has been obtained by the reaction of the methyl derivative $[\text{Tp}^{Ar2}]\text{MgMe}$ with H_2O [Eq. (29)], although it has not been confirmed that the product is monomeric, and a dimeric structure is possible (*148*).

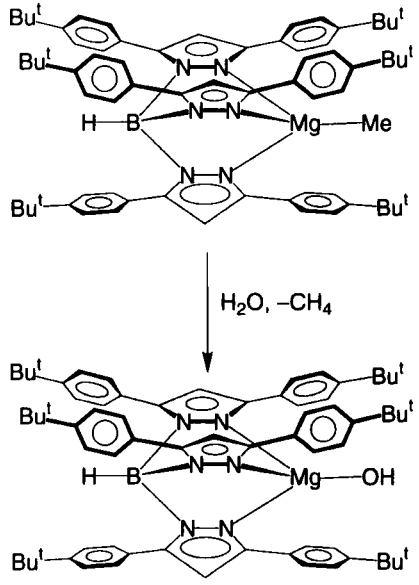

(29)

The Mg–OH moiety has been characterized by IR and NMR spectroscopies. For example, $\nu_{(OH)}$ is observed at 3735 cm^{-1}, shifting to 2747 cm^{-1} for the isotopically substituted derivative $[\text{Tp}^{Ar2}]\text{MgOD}$.

Related to terminal hydroxide complexes, hydrosulfido complexes of beryllium and magnesium have also been synthesized. Thus, the beryllium hydrosulfido complex $[\text{Tp}^{But}]\text{BeSH}$ has been prepared by the reactions of $[\text{Tp}^{But}]\text{BeH}$ and $[\text{Tp}^{But}]\text{BeMe}$ with H_2S (*52, 56*), while the magnesium derivative $[\text{Tp}^{But}]\text{MgSH}$ has been prepared by the reaction of $[\text{Tp}^{But}]\text{MgMe}$ with H_2S (*64*). The M–SH moieties of $[\text{Tp}^{But}]\text{BeSH}$ and $[\text{Tp}^{But}]\text{MgSH}$ are characterized by ^{1}H NMR signals at δ -0.10 and -1.02 ppm, respectively. The reactivity of the beryllium and magnesium hydrosulfido complexes $[\text{Tp}^{RR'}]\text{MSH}$ (M = Be, Mg) has not been extensively studied.

B. Hydroxide Derivatives of Zinc and Cadmium

1. Syntheses, Structures, and Spectroscopic Properties

$[Tp^{But,Me}]ZnOH$, the first monomeric terminal zinc hydroxide complex to be isolated, was prepared by the direct reaction between equimolar amounts of $Zn(ClO_4)_2 \cdot 6H_2O$, $K[Tp^{But,Me}]$, and KOH in methanol (Scheme 21) (*149, 150*). The derivative $[Tp^{Ar',Me}]ZnOH$ (Ar' = *p*-$C_6H_4Pr^i$) has also been prepared by a similar procedure (*35*). In addition to this method, $[Tp^{RR'}]ZnOH$ complexes have been prepared by the metathesis of $[Tp^{RR'}]ZnX$ with a hydroxide reagent [M]OH (Scheme 21). For example, (i) $[Tp^{But,Me}]ZnOH$ has also been prepared by the reaction of $[Tp^{But,Me}]ZnI$ with $Bu^n{}_4NOH$ (*151*), analogous to the synthesis of the cobalt derivative $[Tp^{But,Me}]CoOH$ (*152*), (ii) $[Tp^{Pri2}]ZnOH$ has been synthesized by reactions of both $[Tp^{Pri2}]Zn(NO_3)$ or $[Tp^{Pri2}]Zn(O_2CMe)$ with $NaOH_{(aq)}$ (*151, 153*); and (iii) $[Tp^{Ar2}]ZnOH$ (Ar = *p*-$C_6H_4Bu^t$) has been prepared by the reaction of $[Tp^{Ar2}]ZnI$ with $NaOH_{(aq)}$ and $Bu^n{}_4NOH$ (*154*).

The structure of $[Tp^{But,Me}]ZnOH$ has been determined by x-ray diffraction, confirming the presence of a terminal zinc hydroxide functionality, with a Zn–OH bond length of 1.850(8) Å (Fig. 40). The Zn–OH moiety has also been characterized by a variety of spectroscopic techniques, including IR, ^1H, ^2H, and ^{17}O NMR spectroscopies, as summarized in Table VI. For example, the ^1H NMR spectrum of $[Tp^{But,Me}]ZnOH$, shown in Fig. 41, illustrates that the [Zn–OH] moiety is observed as a sharp signal at δ −0.07 ppm in C_6D_6. The importance of using a sterically

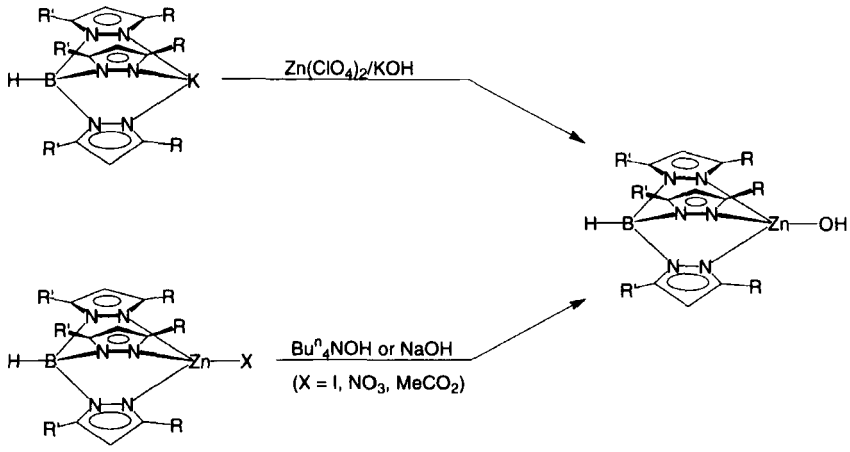

Scheme 21. Syntheses of $[Tp^{RR'}]ZnOH$.

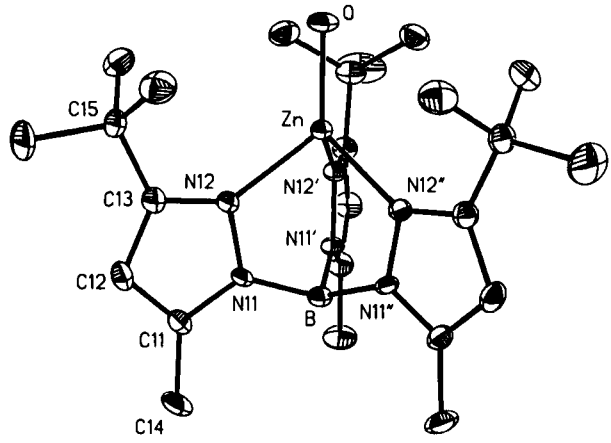

FIG. 40. ORTEP drawing of $[Tp^{Bu^t,Me}]ZnOH$. Reprinted with permission from Ref. (*149*). © Copyright 1991 American Chemical Society.

demanding tris(pyrazolyl)hydroborato ligand to stabilize a monomeric zinc hydroxide functionality can be appreciated when one considers that the related $\{[Bp^{Bu^t}]Zn(\mu\text{-}OH)\}_3$ exists as a cyclic trimer (Section III,C,1,c).

A cadmium hydroxide complex of composition "$[Tp^{Me2}]CdOH \cdot H_2O$," obtained as an intractable material from the reactions of both $(Et_2NCH_2CH_2NEt_2)CdCl_2$ and $(Ph_3P)_2CdCl_2$ with $K[Tp^{Me2}]$ in acetone, has been reported (*89*). However, the complex is not well characterized.

TABLE VI

SPECTROSCOPIC DATA FOR $[Tp^{RR'}]ZnOH$ COMPLEXES

	ν(O–H)/cm^{-1}	^{1}H/ppm	^{17}O/ppm	Refs.[d]
$[Tp^{Bu^t,Me}]ZnOH$	3676	−0.07[a]	−8	1, 2
$[Tp^{Pr^i_2}]ZnOH$	3668	−0.29[a]	−36	2, 3
$[Tp^{Ar2}]ZnOH$[b]	3558			4
$[Tp^{Ar',Me}]ZnOH$[c]	3647			5

[a] Confirmed by ^{2}H NMR spectroscopy on the deuterated complexes $[Tp^{RR'}]ZnOD$.

[b] Ar = *p*-$C_6H_4Bu^t$.

[c] Ar′ = *p*-$C_6H_4Pr^i$.

[d] (1) Alsfasser, R., Trofimenko, S., Looney, A., Parkin, G., and Vahrenkamp, H., *Inorg. Chem.* **30,** 4098 (1991); (2) Looney, A., Han, R., McNeill, K., and Parkin, G., *J. Am. Chem. Soc.* **115,** 4690 (1993); (3) Kitajima, N., Hikichi, S., Tanaka, M., and Moro-oka, Y., *J. Am. Chem. Soc.* **115,** 5496 (1993); (4) Yoon, K., Ghosh, P., Dowling, C., and Parkin, G., unpublished results (1995); (5) Ruf, M., Weis, K., and Vahrenkamp, H., *J. Chem. Soc., Chem. Commun.,* 135 (1994).

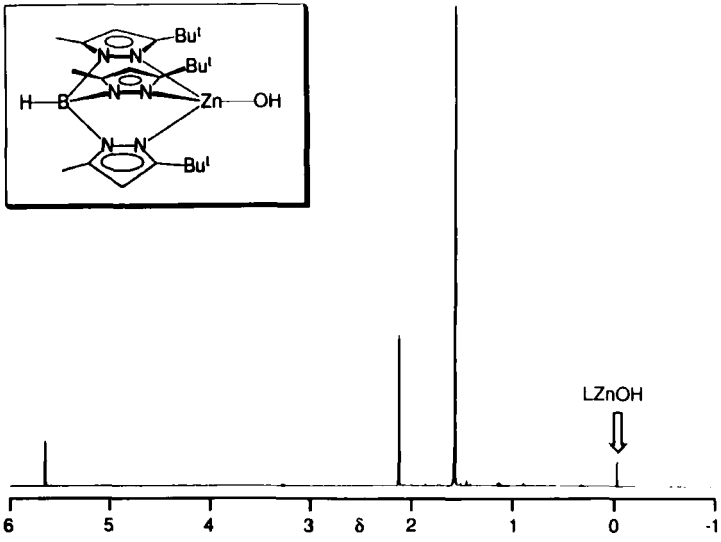

FIG. 41. ^{1}H NMR spectrum of Tp$^{Bu^t,Me}$]ZnOH. Reprinted with permission from Ref. (*151*). © Copyright 1993 American Chemical Society.

Related to the zinc hydroxide complexes [Tp$^{RR'}$]ZnOH, the hydrosulfido complex [Tp$^{Bu^t}$]ZnSH has been synthesized by the reaction of [Tp$^{Bu^t}$]ZnH with H_2S (*80*). However, the corresponding hydrosulfido complex [Tp^{Ph}]ZnSH was not isolated from the reaction of the less sterically demanding derivative [Tp^{Ph}]ZnBu^t with H_2S, which gave preferentially the sandwich complex [Tp^{Ph}]$_2$Zn because of ligand redistribution (*81b*).

2. *[Tp$^{RR'}$]ZnOH Complexes as Models for Carbonic Anhydrase*

a. Introduction. Carbonic anhydrase is a ubiquitous zinc enzyme which catalyzes the reversible hydration of carbon dioxide [Eq. (30)] (*155*).

$$CO_2 + H_2O \rightleftharpoons HCO_3^- + H^+ \qquad (30)$$

X-ray diffraction studies on several forms of the enzyme have demonstrated that the active site is composed of a pseudo-tetrahedral zinc center coordinated to three histidine imidazole groups and either a water molecule $[(His)_3Zn{-}OH_2]^{2+}$ (His = histidine), or a hydroxide anion $[(His)_3Zn{-}OH]^+$, depending upon pH (*156, 157*). On the basis of mechanistic studies, a number of details of the catalytic cycle for carbonic anhydrase have been elucidated, as summarized in Scheme 22

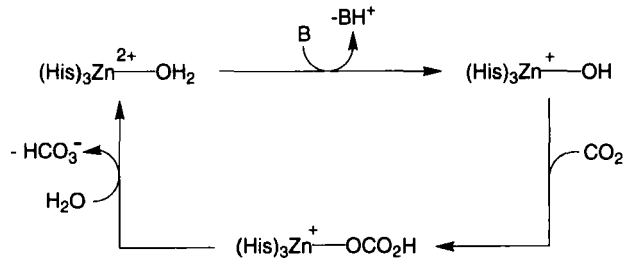

SCHEME 22. Proposed catalytic cycle for carbonic anhydrase.

(*158*). As with other enzymes, insight into the mechanism of action can be obtained by studying simplified structural and functional models of the enzyme. In this regard, the three nitrogen atom donors of the tris(pyrazolyl)hydroborato ligand bind to the zinc center of $[Tp^{RR'}]ZnOH$ in a manner closely analogous to that of the histidine imidazole groups in carbonic anhydrase (Fig. 42). Indeed, the active site of carbonic anhydrase has also been modeled by a variety of other ligand systems (*159*). A notable recent example is the hydroxide complex $\{[12]aneN_3Zn(OH)\}(ClO_4)$ described by Kimura (*160, 161*). Although this complex is a hydrogen-bonded trimer in the solid state, associated with a molecule of perchloric acid, i.e., $\{[12]aneN_3Zn(OH)\}_3(ClO_4)_3 \cdot (HClO_4)$, it is water-soluble and an excellent functional model.

The value of the tris(pyrazolyl)hydroborato complexes $[Tp^{RR'}]ZnOH$ is that they are rare examples of monomeric four-coordinate zinc complexes with a terminal hydroxide funtionality. Indeed, $[Tp^{But}]ZnOH$ is the first structurally characterized monomeric terminal hydroxide complex of zinc (*149*). As such, the monomeric zinc hydroxide complexes $[Tp^{RR'}]ZnOH$ may be expected to play valuable roles as both structural and functional models for the active site of carbonic anhydrase. Although a limitation of the $[Tp^{RR'}]ZnOH$ system resides with their poor solubility in water, studies on these complexes in organic solvents

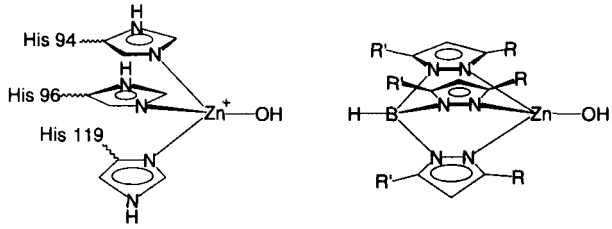

FIG. 42. Comparison of the coordination environment about zinc in the active site of carbonic anhydrase in its deprotonated form with that of $[Tp^{RR'}]ZnOH$. Reprinted with permission from Ref. (*151*). © Copyright 1993 American Chemical Society.

have allowed the reactivity of the terminal Zn–OH functionality to be defined in an environment closely related to that in carbonic anhydrase.

b. The Reactions of [Tp$^{RR'}$]ZnOH with CO_2: Evidence for Bicarbonate Complexes. One of the most important proposed steps of the carbonic anhydrase catalytic cycle (Scheme 22) involves the reaction of a nucleophilic zinc hydroxide group with carbon dioxide to give a bicarbonate intermediate. The reactions of [Tp$^{RR'}$]ZnOH with CO_2 provide excellent precedents for this reaction. In particular, the zinc hydroxide complex [Tp^{But,Me}]ZnOH reacts rapidly with CO_2 to give the bicarbonate derivative [Tp^{But,Me}]Zn(OCO_2H) (Scheme 23). Evidence for the formation of [Tp^{But,Me}]Zn(OCO_2H) is provided by IR studies, which show two bands at 1675 and 1302 cm^{-1} that are assigned to the bicarbonate ligand. It is also proposed that, on the basis of the positions of these bands, and also the magnitude of their difference ($\Delta\nu$ = 373 cm^{-1}) (*162*), the bicarbonate ligand is coordinated in a unidentate fashion. Structurally authenticated bicarbonate complexes are rare, but some examples include (i) bidentate $RhH_2(PPr^i_3)_2(\eta^2\text{-}O_2COH)$ [1587 and 1338 cm^{-1}; $\Delta\nu$ = 249 cm^{-1}] (*163*), and (ii) unidentate *trans*-$Pd(CH_3)(PEt_3)_2(\eta^1\text{-}OCO_2H)$ [1634 and 1353 cm^{-1}; $\Delta\nu$ = 281 cm^{-1}] (*164*), *cis*-$Pd(dppe)(\eta^1\text{-}OCO_2H)_2$ [1700, 1630, 1410, 1300 & 850 cm^{-1}] (*165*), and $Rh(PPh_3)_2(CO)(\eta^1\text{-}OCO_2H)$ [1600, 1500, and 1350 cm^{-1}] (*166–168*). Additional support for the proposed identity of [Tp^{But,Me}]Zn(OCO_2H) as a unidentate bicarbonate complex is also provided by Vahrenkamp's

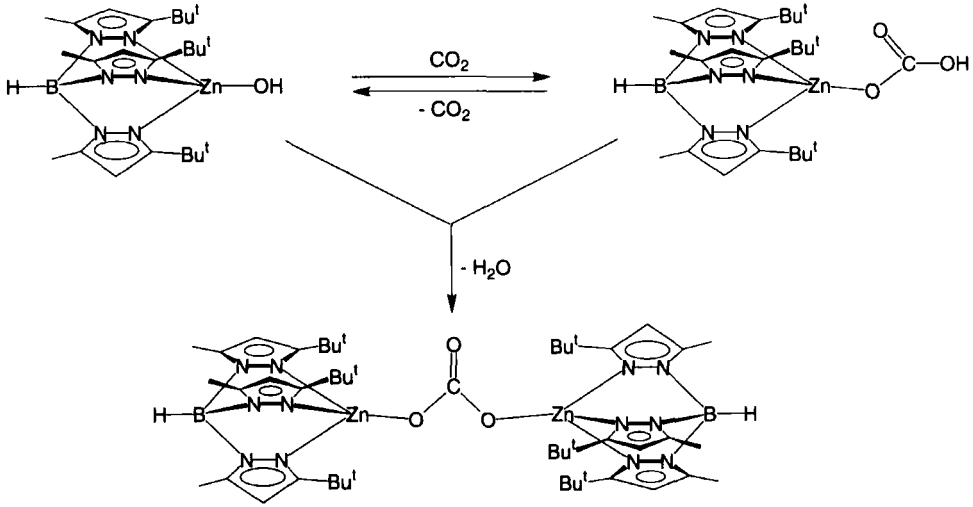

SCHEME 23. Reaction of [Tp^{But,Me}]ZnOH with CO_2.

synthesis of the unidentate methylcarbonate derivative [$Tp^{But,Me}$]Zn(O-CO_2Me) by the reaction of [$Tp^{But,Me}$]ZnOH with $O(CO_2Me)_2$ [Eq. (31)] (*150*).

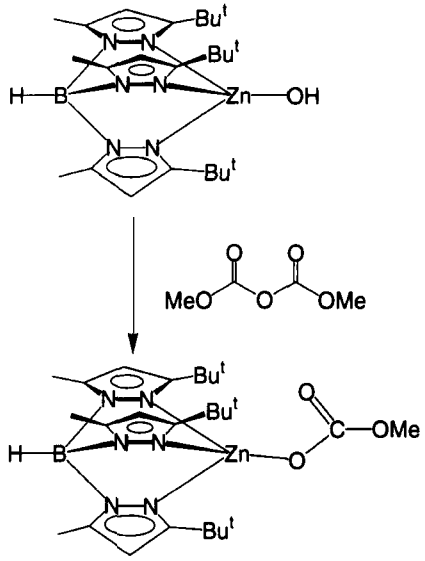

(31)

As expected, [$Tp^{But,Me}$]Zn(η^1-OCO_2Me) [1689 and 1280 cm^{-1}] and [$Tp^{But,Me}$]Zn(η^1-OCO_2H) [1675 and 1302 cm^{-1}] exhibit similar ν(CO) stretching frequencies, indicative of similar binding modes for the (OCO_2H) and (OCO_2Me) ligands.

Although the bicarbonate complex [$Tp^{But,Me}$]Zn(OCO_2H) has been characterized spectroscopically, it has not been isolated because its formation is readily reversible, and removal of the CO_2 atmosphere results in regeneration of the hydroxide [$Tp^{But,Me}$]ZnOH. Indeed, ^1H NMR spectroscopy demonstrates that the reversible reaction betweeen [$Tp^{But,Me}$]ZnOH and CO_2 is rapid on the NMR time scale. Specifically, the sharp resonance at -0.06 ppm that is assigned to the hydroxy functionality of [$Tp^{But,Me}$]ZnOH is both shifted and broadened substantially (into the base line) upon addition of CO_2, accompanied by small shifts of the resonances associated with the tris(pyrazolyl)hydroborato ligand. Significantly, upon the incremental removal of the CO_2 atmosphere, the hydroxy resonance becomes sharper and eventually returns to the sharp resonance of [$Tp^{But,Me}$]ZnOH, as shown in Fig. 43. Evidently, the reversible reaction between [$Tp^{But,Me}$]ZnOH and CO_2 is rapid on the NMR time scale at room temperature. Indeed, because the interconversion between [$Tp^{But,Me}$]Zn(OCO_2H) and [$Tp^{But,Me}$]ZnOH is facile,

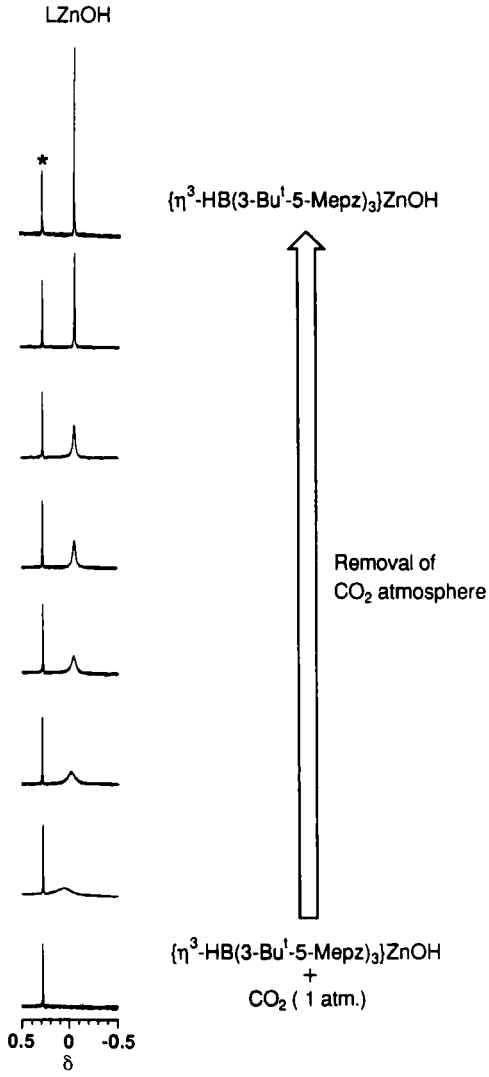

FIG. 43. ^{1}H NMR evidence that the reversible reaction between $[Tp^{Bu^t,Me}]ZnOH$ and CO_2 is rapid on the NMR time scale (* = internal standard). Reprinted with permission from Ref. (*151*). © Copyright 1993 American Chemical Society.

complete NMR characterization of $[Tp^{But,Me}]Zn(OCO_2H)$ has proved difficult, and reliable ^{13}C and ^{17}O NMR data for the bicarbonate moiety have not been obtained (*169*). It has also not yet proven possible to isolate $[Tp^{But,Me}]Zn(OCO_2H)$ in a pure crystalline form. For example, it is the bridging carbonate complex $\{[Tp^{But,Me}]Zn\}_2(\mu$-

η^1,η^1-CO_3), rather than the bicarbonate derivative, that was crystallized from a solution of $[Tp^{But,Me}]ZnOH$ under an atmosphere of CO_2 (Scheme 23) (*170*). Conceptually, the bridging carbonate complex $\{[Tp^{But,Me}]Zn\}_2(\mu\text{-}\eta^1,\eta^1\text{-}CO_3)$ may be regarded as a product of the condensation of $[Tp^{But,Me}]Zn(OCO_2H)$ and $[Tp^{But,Me}]ZnOH$. It is likely that the preferential crystallization of $\{[Tp^{But,Me}]Zn\}_2(\mu\text{-}\eta^1,\eta^1\text{-}CO_3)$ is a consequence of its lower solubility: Once isolated, it reacts instantaneously with water to regenerate $[Tp^{But,Me}]ZnOH$ [Eq. (32)].

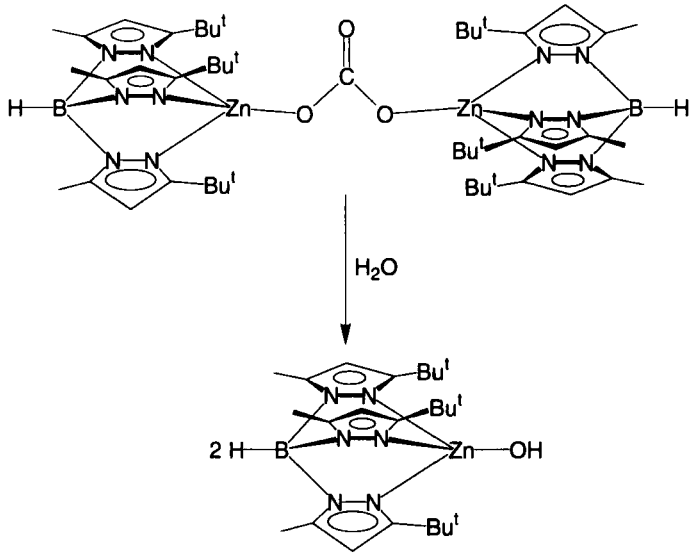

(32)

X-ray diffraction studies on $\{[Tp^{But,Me}]Zn\}_2(\mu\text{-}\eta^1,\eta^1\text{-}CO_3)$ have identified that the bridging carbonate ligand is coordinated to each zinc center in a *unidentate* fashion (*171, 172*), which thereby provides additional support for the presence of a unidentate, rather than bidentate, bicarbonate ligand in $[Tp^{But,Me}]Zn(OCO_2H)$. The carbonate complex $\{[Tp^{But,Me}]Zn\}_2(\mu\text{-}\eta^1,\eta^1\text{-}CO_3)$ is also characterized by ν(CO) absorptions at 1587 and 1311 cm^{-1} in the IR spectrum (*173*), and a ^{13}C NMR signal at δ 164 ppm (in C_6D_6).

The course of the reaction of $[Tp^{RR'}]ZnOH$ with CO_2 is strongly influenced by the presence of different substituents on the pyrazolyl groups, and the reaction between $[Tp^{Pri_2}]ZnOH$ and CO_2 presents some interesting differences from that of the $[Tp^{But,Me}]$ system.

Firstly, the reaction between $[Tp^{Pri_2}]ZnOH$ and CO_2 rapidly gives the dinuclear bridging carbonate complex $\{[Tp^{Pri_2}]Zn\}_2(\mu\text{-}\eta^1,\eta^2\text{-}CO_3)$ (Scheme 24) (*153*), so that the postulated bicarbonate complex

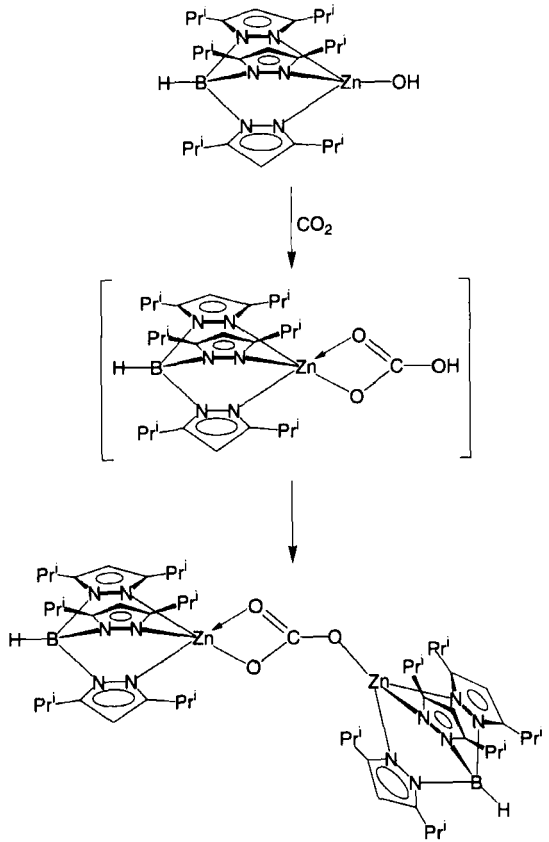

SCHEME 24. Reaction of $[Tp^{Pri_2}]ZnOH$ with CO_2.

$[Tp^{Pri_2}]Zn(OCO_2H)$ system must have only a fleeting existence. In contrast, for the $[Tp^{But,Me}]$ system, the bicarbonate complex $[Tp^{But,Me}]Zn(OCO_2H)$ was sufficiently stable to be spectroscopically identified.

Secondly, the molecular structure of $\{[Tp^{Pri_2}]Zn\}_2(\mu\text{-}\eta^1,\eta^2\text{-}CO_3)$, as determined by x-ray diffraction (*151, 153*), reveals that the carbonate ligand is coordinated in an asymmetric manner, with unidentate coordination to one zinc center and bidentate coordination to the other zinc center, i.e., $\mu\text{-}\eta^1,\eta^2\text{-}CO_3$ (Scheme 24). Such coordination is noticeably distinct from that of $\{[Tp^{But,Me}]Zn\}_2(\mu\text{-}\eta^1,\eta^1\text{-}CO_3)$, in which the carbonate ligand bridges in a symmetric unidentate mode.

Thirdly, it is significant that the difference in coordination modes of the bridging carbonate ligands of $\{[Tp^{Pri_2}]Zn\}_2(\mu\text{-}\eta^1,\eta^2\text{-}CO_3)$ and $\{[Tp^{But,Me}]Zn\}_2(\mu\text{-}\eta^1,\eta^1\text{-}CO_3)$ is manifested in their reactivity. Thus, whereas $\{[Tp^{But,Me}]Zn\}_2(\mu\text{-}\eta^1,\eta^1\text{-}CO_3)$ reacts instantaneously with H_2O

to give $[Tp^{But,Me}]ZnOH$, $\{[Tp^{Pri2}]Zn\}_2(\mu\text{-}\eta^1,\eta^2\text{-}CO_3)$ is stable to H_2O at room temperature. It has been suggested that the increased thermodynamic stability of $\{[Tp^{Pri2}]Zn\}_2(\mu\text{-}\eta^1,\eta^2\text{-}CO_3)$ towards H_2O may be due to additional ground-state stabilization imparted by bidentate coordination of the carbonate ligand at one of the zinc centers (*151*).

c. Substitution Reactions of $[Tp^{But,Me}]ZnOH$. Methanol solutions of the zinc hydroxide complex $[Tp^{But,Me}]ZnOH$ react with a variety of anions, including Cl^-, CN^-, and N_3^-, to give the corresponding $[Tp^{But,Me}]ZnX$ ($X = Cl, CN, N_3$) derivatives (*150*). The relevance of these transformations derives from the observation that such anions are known to be inhibitors of carbonic anhydrase.

d. The Functional Equivalence of $[Tp^{But,Me}]ZnOH$. Evidence that $[Tp^{But,Me}]ZnOH$ is a functional model for carbonic anhydrase has been provided by using ^{17}O NMR spectroscopy to demonstrate the ability of $[Tp^{But,Me}]ZnOH$ to catalyze oxygen atom transfer between CO_2 and $H_2{}^{17}O$ [Eq. (33)] (*174*).

$$CO_2 + H_2{}^{17}O \rightleftharpoons CO^{17}O + H_2O \qquad (33)$$

Thus, in the presence of $[Tp^{But,Me}]ZnOH$, addition of excess CO_2 to a solution of $H_2{}^{17}O$ in benzene results in rapid exchange and the formation of ^{17}O-enriched $CO^{17}O$, as illustrated in Fig. 44. It is important to emphasize that in the absence of the $[Tp^{But,Me}]ZnOH$, samples prepared under similar conditions take several days to proceed to completion (*175*), thereby clearly demonstrating the catalytic efficiency of $[Tp^{But,Me}]ZnOH$.

e. Metal-Substituted Carbonic Anhydrases: The Consequences of Unidentate vs Bidentate Coordination. In addition to studies on the native zinc enzyme, metal-substituted (e.g., Mn, Co, Ni, Cu, Cd, Hg) carbonic anhydrases have also been actively investigated (*176, 177*). Such studies, which are in part a consequence of the lack of suitable spectroscopic probes for the diamagnetic d^{10} Zn(II) center of the native enzyme (*178*), have been pursued in order to provide information concerned with both enzyme structure and activity. For example, cadmium-substituted carbonic anhydrase has been studied by ^{113}Cd NMR spectroscopy (*179, 180*). However, of these metal-substituted carbonic anhydrases, it is only the cobalt derivative which exhibits comparable activity (ca. 50%) to that of the zinc enzyme, and the order of activity decreases across the series $Zn > Co \gg Ni, Cu, Cd$ (*155, 181–183*).

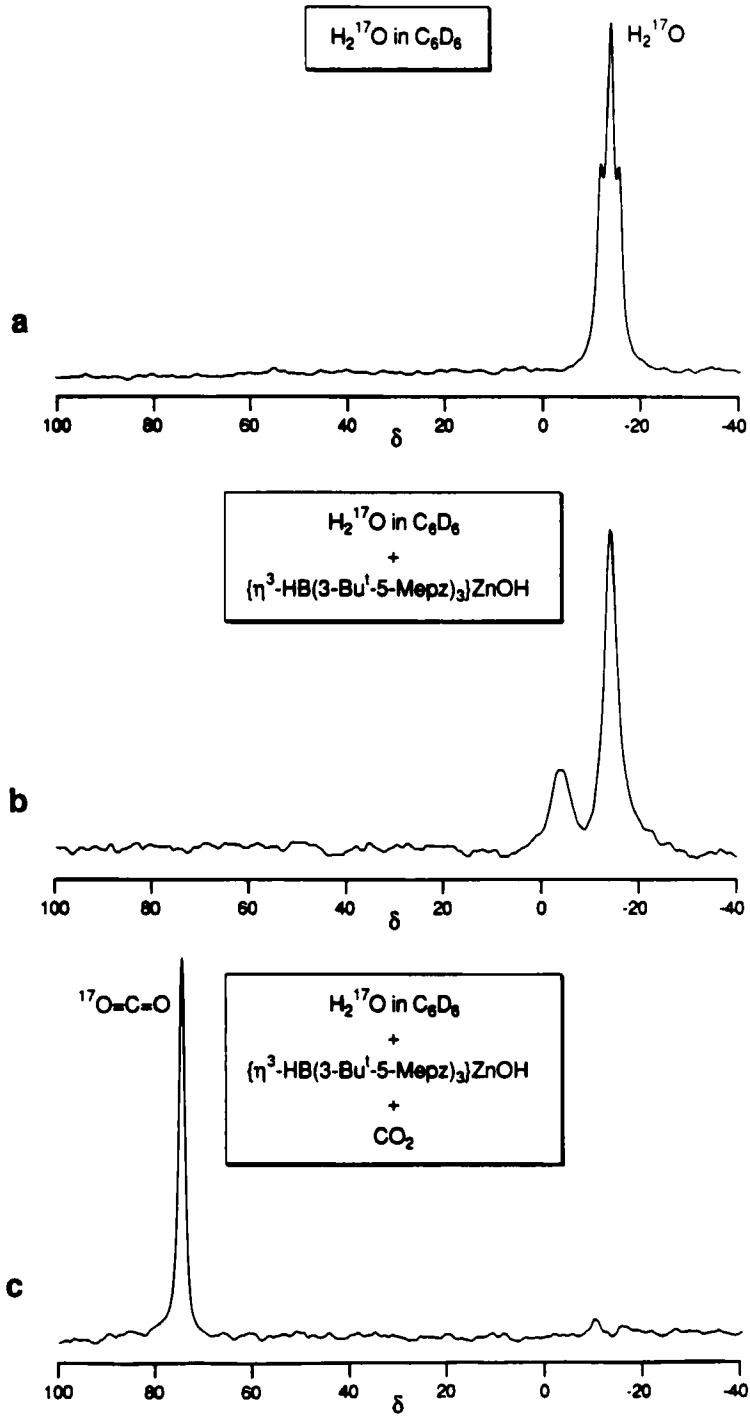
H2 17O in C6D6
H2 17O
a
100
80
60
40
20
0
-20
-40
δ
H2 17O in C6D6
+
{η3-HB(3-But-5-Mepz)3}ZnOH
b
100
80
60
40
20
0
-20
-40
δ
17O=C=O
H2 17O in C6D6
+
{η3-HB(3-But-5-Mepz)3}ZnOH
+
CO2
c
100
80
60
40
20
0
-20
-40
δ

Many factors (e.g., the pK_a of the coordinated water and different coordination geometries) are undoubtedly responsible for the observed metal-substituted carbonic anhydrase activity series. One of the requirements for an efficient catalytic cycle for carbonic anhydrase (Scheme 22) is the rapid displacement of bicarbonate by water. The preceding studies on the carbonate complexes $\{[Tp^{Pr^i_2}]Zn\}_2(\mu\text{-}\eta^1,\eta^2\text{-}CO_3)$ and $\{[Tp^{Bu^t,Me}]Zn\}_2(\mu\text{-}\eta^1,\eta^1\text{-}CO_3)$ demonstrate that the reactivity of a carbonate ligand may be dramatically influenced by its coordination mode. On the basis of this observation, it was suggested that if the same reasoning were to be applied to the corresponding bicarbonate derivatives, then the formation of a bidentate bicarbonate intermediate could inhibit a catalytic cycle. It was, therefore, of interest to determine how the coordination of a bicarbonate ligand would vary (i.e., unidentate vs bidentate) as a function of the metal in a related series of complexes, such as $[Tp^{RR'}]M(OCO_2H)$. However, as a result of the general instability of bicarbonate complexes, a series of complexes of the type $L_nM(OCO_2H)$ is not known. In view of the lack of such bicarbonate complexes, it was suggested that structural changes of the bicarbonate ligand across a series $[Tp^{RR'}]M(OCO_2H)$ could be gleaned by observing the corresponding changes for the related isoelectronic nitrate derivatives $[Tp^{RR'}]M(NO_3)$ (*184*). It is important to note that this argument does not imply a direct correlation between the coordination mode of a nitrate ligand and that of a bicarbonate ligand to a given metal center (*185*), but is rather intended to indicate the trend as a function of the metal. Before analyzing the structures of the complexes $[Tp^{RR'}]M(NO_3)$, it is worthwhile first to discuss the coordination modes that the nitrate ligand is known to adopt. The discussion is restricted to a single metal center. The nitrate ligand is known to bind by three different coordination modes, namely (i) symmetric bidentate, (ii) anisobidentate (or asymmetric bidentate), and (iii) unidentate (*186, 187*). These different coordination modes may be identified by some simple geometrical criteria, as illustrated in Fig. 45 and Table VII (*186, 187*). Specifically, complexes in which (i) the difference in M–O bond lengths $(d_2 - d_1)$ is greater than 0.6 Å, and (ii) the difference in bond angles

FIG. 44. ^{17}O NMR evidence for the $[Tp^{Bu^t,Me}]ZnOH$-catalyzed exchange of oxygen atoms between CO_2 and $H_2{}^{17}O$ in benzene. (a) ^{17}O NMR spectrum of $H_2{}^{17}O$ in benzene. (b) ^{17}O NMR spectrum of solution in (a) to which $[Tp^{Bu^t,Me}]ZnOH$ has been added. Two resonances are observed, one due to $H_2{}^{17}O$ and one due to $[Tp^{Bu^t,Me}]Zn^{17}OH$ produced by an exchange process. (c) ^{17}O NMR spectrum of solution in (b) to which excess CO_2 has been added. The ^{17}O label has been completely transferred from $H_2{}^{17}O$ to CO_2 within a period of minutes at room temperature. Reprinted with permission from Ref. (*151*). © Copyright 1993 American Chemical Society.

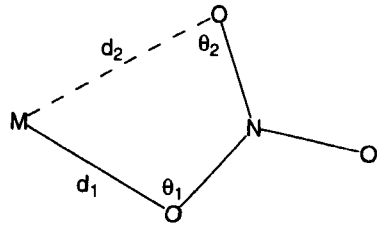

FIG. 45. Criteria for distinguishing nitrate coordination modes.

at oxygen ($\theta_1 - \theta_2$) is greater than 28°, are classified as unidentate. Correspondingly, complexes with (i) $d_2 - d_1$ in the range 0.3 to 0.6 Å, and (ii) $\theta_1 - \theta_2$ in the range 14–28°, are classified as anisobidentate. Complexes for which $d_2 - d_1 < 0.3$ Å and $\theta_1 - \theta_2 < 14°$ are referred to as bidentate, and symmetric bidentate when $d_2 = d_1$ and $\theta_1 = \theta_2$ (*186, 187*).

The coordination modes of the nitrate ligand in the complexes $[Tp^{But}]M(NO_3)$ (M = Cu, Ni, Co, Zn) are summarized in Fig. 46. (*171, 184*). Evidently, the coordination mode varies from unidentate for Zn to symmetric bidentate for Ni and Cu, with the cobalt derivative exhibiting an anisobidentate coordination mode. Moreover, the related cadmium derivative $[Tp^{But,Me}]Cd(NO_3)$ also exhibits bidentate coordination of the nitrate ligand, with Cd–O bond lengths of 2.272(6) Å and 2.295(7) Å (*91*). Such symmetric bidentate coordination contrasts with the significantly different Zn–O interactions [1.978(3) Å and 2.581(3) Å] in unidentate $[Tp^{But}]Zn(NO_3)$. The coordination modes for a variety of $[Tp^{RR'}]M(NO_3)$ complexes are summarized in Table VIII.

The structural variations observed for $[Tp^{RR'}]M(NO_3)$ (M = Co, Ni, Cu, Zn Cd) reveal that, for a given $[Tp^{RR'}]$ ligand, the preference for bidentate coordination increases across the series Zn < Co ≪ Cu, Ni, and Cd. Significantly, these structural preferences of the nitrate ligand correlate with the activity of the metal-substituted enzymes: Zinc, the metal with the greatest tendency to exhibit unidentate coordination of the nitrate ligand, is the most active, while nickel, copper, and

TABLE VII

CRITERIA FOR DISTINGUISHING NITRATE COORDINATION MODES

	Unidentate	Anisobidentate	Bidentate
$d_2 - d_1$ (Å)	>0.6	0.3–0.6	<0.3
$\theta_1 - \theta_2$ (°)	>28	14–28	<14

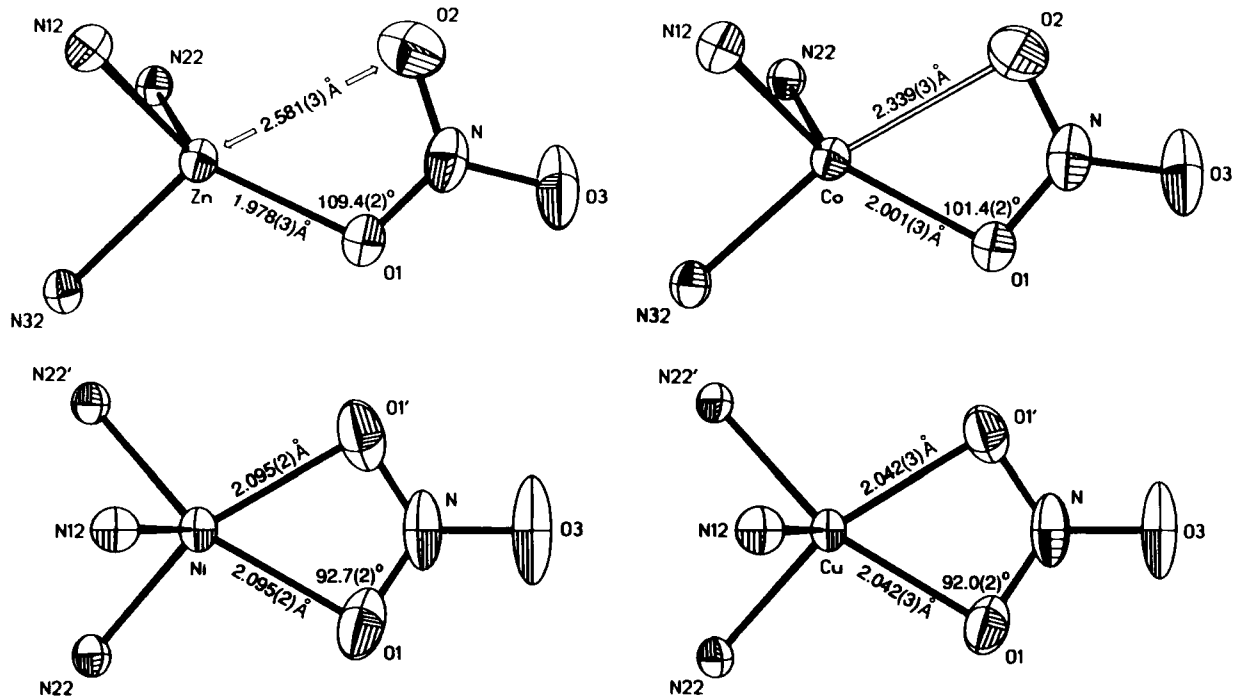

FIG 46. Variation of nitrate coordination mode for the complexes $[Tp^{Bu^t}]M(NO_3)$ (M = Co, Ni, Cu, Zn). Reprinted with permission from Ref. (*184*). © Copyright 1991 American Chemical Society.

TABLE VIII

NITRATE COORDINATION MODES IN $[Tp^{RR'}]M(NO_3)$ COMPLEXES

	$d_2 - d_1$ (Å)	$\theta_1 - \theta_2$ (°)	Coordination mode	Ref.[a]
$[Tp]Zn(NO_3)$	0.42	18.7	anisobidentate	1
$[Tp^{Ph}]Zn(NO_3)$	0.53	—	anisobidentate	2
$[Tp^{Bu^t}]Zn(NO_3)$	0.60	29.6	unidentate	3
$[Tp^{Bu^t}]Co(NO_3)$	0.34	15.8	anisobidentate	3
$[Tp^{Bu^t}]Ni(NO_3)$	0	0	bidentate	3
$[Tp^{Bu^t}]Cu(NO_3)$	0	0	bidentate	3
$[Tp^{Bu^t,Me}]Cd(NO_3)$	0.02	1.8	bidentate	4

[a] (1) Looney, A., and Parkin, G., *Inorg. Chem.* **33,** 1234 (1994); (2) Alsfasser, R., Powell, A. K., Trofimenko, S., and Vahrenkamp, H., *Chem. Ber.* **126,** 685 (1993); (3) Han, R., Looney, A., McNeill, K., Parkin, G., Rheingold, A. L., and Haggerty, B. S., *J. Inorg. Biochem.* **49,** 105 (1993); (4) Looney, A., Saleh, A., Zhang, Y., and Parkin, G., *Inorg. Chem.* **33,** 1158 (1994).

cadmium, the metals with the greatest tendency to exhibit bidentate coordination of the nitrate ligands, are least active.

The ability of cobalt(II), nickel(II), and copper(II) to exhibit a greater tendency than Zn(II) towards bidentate coordination is further illustrated by structural comparisons within a series of bridging carbonate complexes (*188*). For example, of the complexes $\{[Tp^{Pri_2}]M\}_2(\mu\text{-}CO_3)$ (M = Mn, Fe, Co, Ni, Cu, Zn), only the zinc derivative does not exhibit bidentate coordination at both metal centers (*151, 153*). Furthermore, the carbonate ligand in the complexes $\{[Tp^{Pri_2}]M\}_2(\mu\text{-}CO_3)$ (M = Mn, Fe, Co, Ni, Cu) also exhibits varying degrees of asymmetry that closely parallel the series of nitrate complexes described earlier (Fig. 47 and Table IX).

The correlation of coordination mode of nitrate and carbonate ligands with the activity of metal-substituted carbonic anhydrases suggests that such structural changes may provide an indication of the relative preferences for unidentate vs bidentate coordination for the bicarbonate intermediates in the catalytic cycles of metal-substituted carbonic anhydrases (*151, 184*). Thus, a progressive ground-state stabilization of the bicarbonate ligand would be expected for the sequence Zn < Co < Cu, Ni, and Cd (*189*). Indeed, the x-ray structure of the nitrate derivative of human carbonic anhydrase II has shown that the nitrate ligand is coordinated to the zinc center via only one of its oxygen atoms (*190*). Stronger binding of the bicarbonate ligand across the series Zn < Co < Cu, Ni, and Cd may result in slower displacement of the bicarbonate ligand by H_2O, and thereby prevent a catalytic cycle

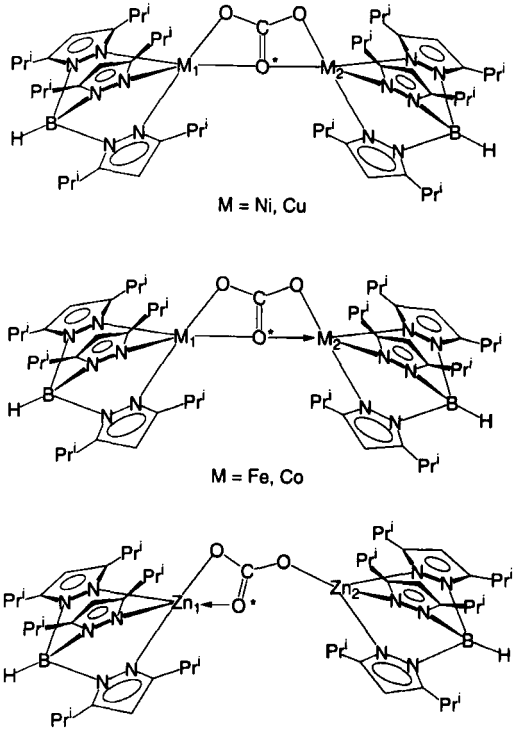

FIG. 47. Variation of carbonate coordination mode for the complexes $\{[Tp^{Pr^i_2}]M\}_2(\mu\text{-}CO_3)$ (M = Mn, Fe, Co, Ni, Cu).

TABLE IX

METRICAL DATA FOR THE BRIDGING CARBONATE MOIETIES IN $\{[Tp^{Pr^i_2}]M\}_2(\mu\text{-}CO_3)$[a]

$\{[Tp^{Pr^i_2}]M\}_2(\mu\text{-}CO_3)$	$d(M_1\text{–}O^*)$/Å	$d(M_2\text{–}O^*)$/Å
Ni	2.047(2)	2.050(2)
Cu	2.019(4)	2.028(4)
Fe	2.085(5)	2.270(5)
Co	2.055(4)	2.271(4)
Zn	1.979(9) [1.957(9)][b]	2.618(9) [2.625(9)][b]

[a] Data taken from Kitajima, N., Hikichi, S., Tanaka, M., and Moro-oka, Y., *J. Am. Chem. Soc.* **115**, 5496 (1993).

[b] Data for two independent molecules in asymmetric unit.

operating for Cu and Ni derivatives, as a result of product inhibition. Therefore, a critical requirement for carbonic anhydrase activity may be the accessibility of a unidentate, rather than a bidentate, bicarbonate intermediate (*191*). Recent kinetic studies by van Eldik have demonstrated that $[\{[12]aneN_4\}ZnOH]^+$ is a more active catalyst than $[\{[12]aneN_3\}ZnOH]^+$ for the hydration of CO_2, a result that has also been attributed to the greater tendency of the former to form a unidentate, rather than bidentate, bicarbonate intermediate (*192*).

The preceding studies demonstrate the manner in which the coordination mode of a nitrate or bicarbonate ligand may be altered by the electronic configuration of a metal center. It is also likely that the coordination mode would be influenced by steric factors, such that a less sterically demanding ligand would promote bidentate coordination. For example, the carbonate ligand in $[[Tp^{But,Me}]Zn]_2(\mu\text{-}\eta^1, \eta^1\text{-}CO_3)$ bridges in a symmetric unidentate fashion, whereas in the less sterically demanding derivative $\{[Tp^{Pri_2}]Zn\}_2(\mu\text{-}\eta^1, \eta^2\text{-}CO_3)$, the carbonate ligand exhibits unidentate coordination to one zinc center and bidentate to the other. In order to address the importance of steric effects in influencing unidentate vs bidentate coordination to a zinc center, the structure of the unsubstituted tris(pyrazolyl)hydroborato derivative $[Tp]Zn(NO_3)$ was compared with that of $[Tp^{But}]Zn(NO_3)$ (*193*). Application of the coordination criteria described earlier to $[Tp]Zn(NO_3)$ indicates that the nitrate ligand in $[Tp]Zn(NO_3)$ is best described as anisobidentate, in contrast to the unidentate coordination in $[Tp^{But}]Zn(NO_3)$ (see Table VIII). Thus, the secondary Zn···O interaction in $[Tp]Zn(NO_3)$ [2.399(3) Å] is much shorter than that in the more sterically demanding derivative $[Tp^{But}]Zn(NO_3)$ [2.581(3) Å]. Furthermore, the nitrate coordination mode in $[Tp^{Ph}]Zn(NO_3)$ (*194*) is intermediate between those in $[Tp^{But}]Zn(NO_3)$ and those in $[Tp]Zn(NO_3)$, so that the degree of interaction of the nitrate ligand with the zinc center in these complexes clearly correlates with the steric demands of the substituent ($H < Ph < Bu^t$) at the 3-position of the tris(pyrazolyl)hydroborato ligand.

Theoretical calculations designed specifically to compare the ligating abilities of nitrate and bicarbonate have been carried out on $[Tp^{RR'}]Zn(NO_3)$ and $[Tp^{RR'}]Zn(OCO_2H)$ derivatives (*195*). Although there was general agreement between the theoretical and experimental structures, the structure of $[Tp]Zn(NO_3)$ obtained by theoretical calculations differs from the experimentally determined structure by its inability to reflect the fact that the coordination mode is not unidentate. For example, the theoretical values of (i) $d_2 - d_1 = 1.25$ Å and (ii) $\theta_1 - \theta_2 = 58°$ very strongly indicate a unidentate coordination mode, whereas the true coordination mode is anisobidentate according to the criteria described earlier.

f. Spectroscopic Models. The existence of a series of well-defined and structurally characterized $[Tp^{RR'}]MX$ complexes is of interest for providing spectroscopic models that would allow comparisons to be made with metal-substituted carbonic anhydrases. Moreover, tailoring the steric environment, while still maintaining a common N_3-ligation mode of the tris(pyrazolyl)hydroborato ligand, allows the effects of subtle changes in coordination on the electronic spectra to be studied. Thus, spectroscopic studies on these complexes may provide useful data for the assignment of the coordination environments of the active sites of metalloenzymes. Specifically, the electronic spectra of four-, five-, and six-coordinate tris(pyrazolyl)hydroborato complexes have been studied with regard to metal-substituted carbonic anhydrases.

For example, the electronic spectrum of the blue four-coordinate chloride derivative $[Tp^{But}]CoCl$ exhibits a band in the range 547–659 nm with an absorption coefficient $\varepsilon = 496\ M^{-1}\ cm^{-1}$ (*171*), consistent with the proposal that the high pH form of cobalt(II)-carbonic anhydrase ($\lambda = 553$ nm, $\varepsilon > 300\ M^{-1}\ cm^{-1}$) exhibits a pseudo-tetrahedral coordination geometry. Similarly, comparison of the electronic spectra of the four-, five-, and six- coordinate nickel complexes, purple $[Tp^{But}]NiCl$, yellow $[Tp^{But}]Ni(\eta^2\text{-}O_2NO)$, and green $[Tp^{Me2}]Ni(\eta^2\text{-}O_2NO)(THF)$, with the electronic spectrum of nickel(II) carbonic anhydrase supports the notion that nickel is six-coordinate in the enzyme at neutral pH. Finally, copper(II) carbonic anhydrase has been proposed to contain either a pseudo-tetrahedral or five-coordinate Cu(II) center. However, comparison of the electronic spectrum of Cu(II)-carbonic anhydrase with those of the four- and five-coordinate complexes $[Tp^{But}]CuCl$ and $[Tp^{But}]Cu(\eta^2\text{-}O_2NO)$ indicates a greater similarity to the five-coordinate structure.

g. $[Tp^{RR'}]ZnOH$ Complexes of Relevance to Esterase, Peptidase, and Phosphatase Activity. In addition to modeling the function of carbonic anhydrase, mononuclear $[Tp^{RR'}]ZnOH$ complexes have also been shown to have relevance to other hydrolytic transformations that are catalyzed by divalent metal ions, such as ester, amide, and phosphate hydrolyses (*196*). For example, Kitajima has reported a sequence of stoichiometric reactions between $[Tp^{Pri2}]ZnOH$ and the phosphate esters $(RO)_x(HO)_{3-x}P(O)$ ($x = 1, 2, 3$; $R = p\text{-}C_6H_4NO_2$) (*197*). Several products are observed during the course of the reaction between excess $[Tp^{Pri2}]ZnOH$ and tris(*p*-nitrophenyl)phosphate $(RO)_3P(O)$ and may be rationalized according to Scheme 25. Thus, the reaction between an excess of $[Tp^{Pri2}]ZnOH$ (5 equiv.) and $(RO)_3P(O)$ gives initially the phenoxy derivative $[Tp^{Pri2}]ZnOR$, releasing bis(*p*-nitrophenyl)phosphate $(RO)_2(HO)P(O)$. Subsequent reaction between the liberated

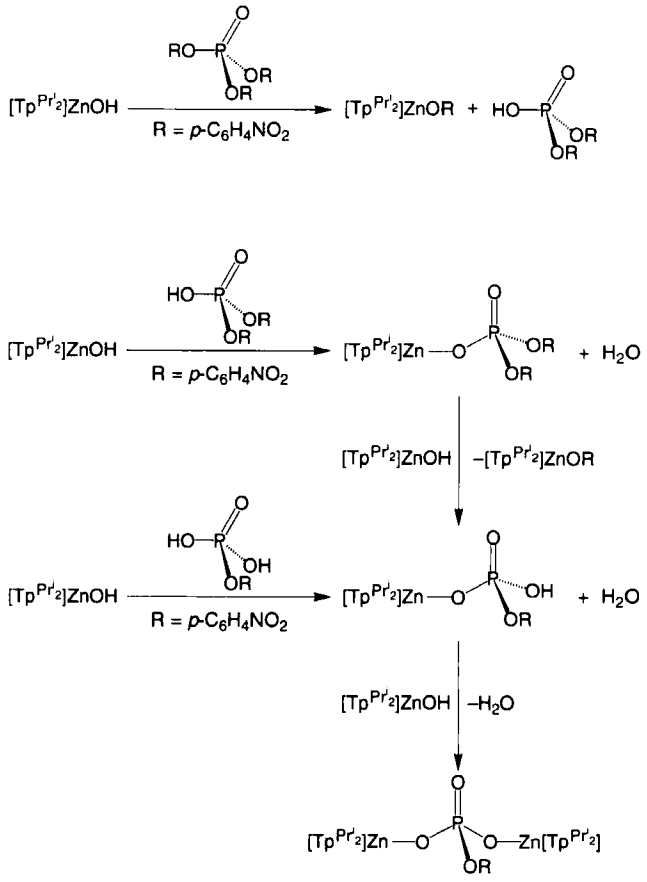

SCHEME 25. Reactions of $[Tp^{Pr^i_2}]ZnOH$ with the phosphate esters $(RO)_x(HO)_{3-x}P(O)$ (x = 1, 2, 3; R = p-$C_6H_4NO_2$).

$(RO)_2(HO)P(O)$ and excess $[Tp^{Pr^i_2}]ZnOH$ gives $[Tp^{Pr^i_2}]ZnOP(O)(OR)_2$ and H_2O. The zinc phosphate derivative $[Tp^{Pr^i_2}]ZnOP(O)(OR)_2$ reacts further with excess $[Tp^{Pr^i_2}]ZnOH$ to give $[Tp^{Pr^i_2}]ZnOP(O)(OR)(OH)$ and $[Tp^{Pr^i_2}]ZnOR$. Finally, reaction between $[Tp^{Pr^i_2}]ZnOP(O)(OR)(OH)$ and $[Tp^{Pr^i_2}]ZnOH$ releases water to give the phosphate-bridged dinuclear complex $\{[Tp^{Pr^i_2}]ZnO\}_2P)O)(OR)$. As expected from such a scheme, the phosphate-bridged complex $\{[Tp^{Pr^i_2}]ZnO\}_2P(O)(OR)$ may be also directly obtained by the reaction of $[Tp^{Pr^i_2}]ZnOH$ with 0.5 equiv. of mono(p-nitrophenyl)phosphate.

Vahrenkamp has also reported that $[Tp^{Ar',Me}]ZnOH$ (Ar' = p-$C_6H_4Pr^i$) reacts with the less reactive aliphatic phosphate $H(MeO)_2P(O)$ and diphosphates $[(RO)_2P(O)]_2O$ (R = Et, Ph) to give $[Tp^{Ar',Me}]ZnO$-

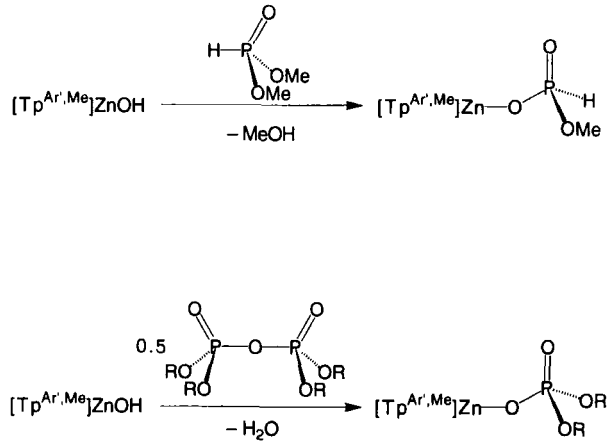

SCHEME 26. Reactions of $[Tp^{Ar',Me}]ZnOH$ (Ar' = p-$C_6H_4Pr^i$) with $H(MeO)_2P(O)$ and $[(RO)_2P(O)]_2O$ (R = Et, Ph).

P(O)(OMe)H and $[Tp^{Ar',Me}]ZnOP(O)(OR)_2$, respectively (Scheme 26) (*35*). In addition, $[Tp^{Ar',Me}]ZnOH$ also cleaves activated esters and amides in a stoichiometric fashion, as illustrated in Scheme 27. Kitajima has described a similar amide cleavage reaction between the copper and nickel hydroxide complexes $\{[Tp^{Pr^i2}]M(OH)\}_2$ (M = Ni, Cu) and p-nitroacetanilide to give $[Tp^{Pr^i2}]M\{\eta^2\text{-}MeC(O)NC_6H_4NO_2\}$ [Eq. (34)] (*198*).

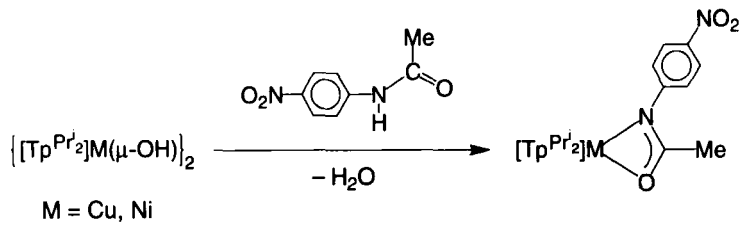

(34)

However, the corresponding zinc, cobalt, and manganese hydroxo complexes were unreactive towards p-nitroacetanilide, an inertness that was proposed to be associated with a different coordination mode for the $[MeC(O)NC_6H_4NO_2]$ ligand. Specifically, it was suggested that since copper and nickel exhibit a greater tendency than zinc, cobalt, and manganese to coordinate ligands in a bidentate fashion, then the formation of strongly bound bidentate complexes for the nickel and copper systems $[Tp^{Pr^i2}]M\{\eta^2\text{-}MeC(O)NC_6H_4NO_2\}$ (M = Ni, Cu) would promote the specific reaction for these derivatives.

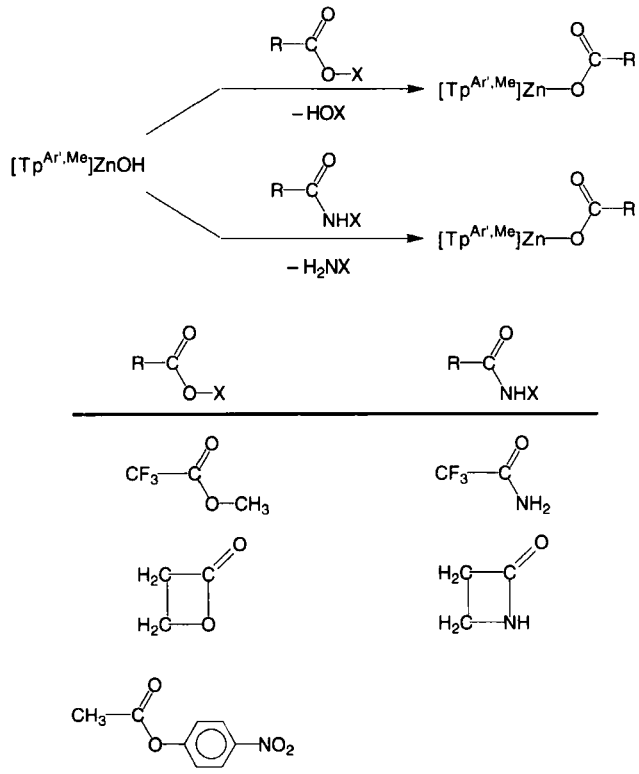

SCHEME 27. Reactions of $[Tp^{Ar',Me}]ZnOH$ (Ar' = p-$C_6H_4Pr^i$) with RCO_2X and RCONHX.

VI. Anion Coordination by Protonated Tris(pyrazolyl)hydroborato Derivatives

As illustrated in the previous sections, the uninegative poly(pyrazolyl)borato ligands provide a versatile system for coordination to cationic centers. However, in their triprotonated form, such ligands offer potential for acting as receptors for anions (Scheme 28). Indeed, since the coordination chemistry of anions (*199*) is significantly less developed than that of cations, protonated poly(pyrazolyl)borato ligands offer potential for exploring the chemistry of such systems.

It has long been recognized that anionic poly(pyrazolyl)borato derivatives may be readily monoprotonated to give the neutral acids (*1b*). For example, [pzTp]H, [Tp]H, and [Bp]H derivatives can be obtained by acidification of the appropriate potassium derivative with glacial acetic acid. (*1b, 123, 200*). Similarly, [Bp]H has also been obtained by acidification of K[Bp] with $HCl_{(aq)}$. The structures of $[(Me_2pz)Tp^{Me2}]H$ (*201*) and [Bp]H (*117*) have been determined by x-ray diffraction. Mono-

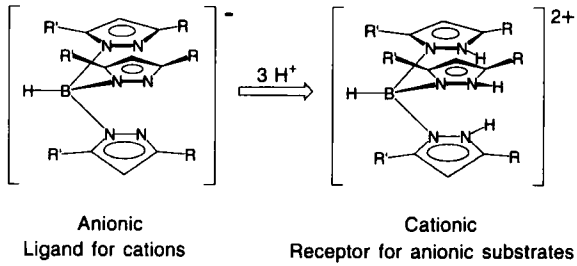

SCHEME 28. Modification of a tris(pyrazolyl)hydroborato ligand to a receptor for binding anions.

protonated poly(pyrazolyl)borato derivatives are also known to coordinate to metal centers, e.g., $[Tp^{Cy}H]CuCl_2$, (*202*), $\{[TpH]AuMe_2\}^+$ and $\{[pzTpH]AuMe_2\}^+$ (*78, 100*). Diprotonated bis(pyrazolyl)hydroborato derivatives, e.g., $\{[Bp^{Me2}]H_2\}^+$, have also been prepared as the I^- derivative, but the nature of the interaction has not been described (*203*).

The first report of a structurally characterized triprotonated poly(pyrazolyl)borato complex was that of the host–guest complex $\{[Tp^{But}H_3]Cl\}^+$, in which a chloride anion substrate was bound to a triprotonated tris(3-t-butylpyrazolyl)hydroborato receptor (*204*). Thus, the cation $\{[Tp^{But}H_3]Cl\}^+$ is readily obtained from the reaction of $Tl[Tp^{But}]$ with $HCl_{(aq)}$ and may be isolated as the $[AlCl_4]^-$ derivative $\{[Tp^{But}H_3]Cl\}\{AlCl_4\}$ upon addition of $AlCl_3$ [Eq. (35)].

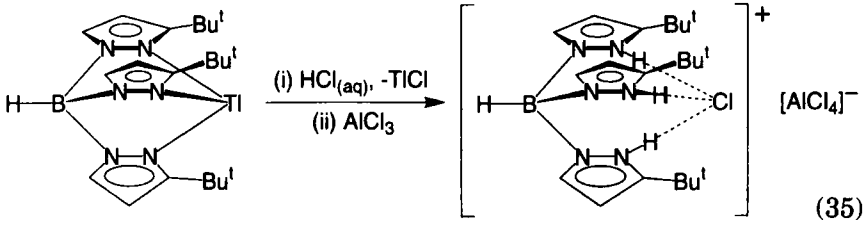

(35)

The molecular structure of $\{[Tp^{But}H_3]Cl\}\{AlCl_4\}$ has been determined by x-ray diffraction, demonstrating that the chloride anion substrate is bound to the N–H groups of the $[Tp^{But}H_3]^{2+}$ receptor by three almost linear (173–175°) hydrogen bonds (Figure 48). The distances between Cl and N for each of the three N-H···Cl interactions [3.07–3.09 Å] are significantly less than the sum of the N and Cl van der Waals radii (3.30Å), so that each N-H···Cl interaction represents a strong hydrogen bond (*205*). Furthermore, one of the most interesting features of the triprotonated tris(3-t-butylpyrazolyl)hydroborato receptor is that it is only capable of binding to one face of the chloride substrate, in contrast

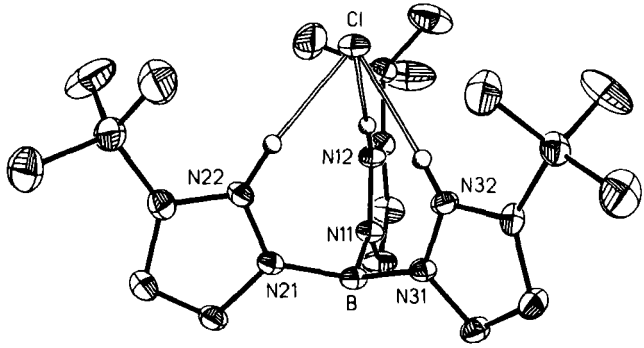

FIG. 48. ORTEP drawing of the cation $\{[Tp^{Bu^t}H_3]Cl\}^+$. Reprinted with permission from Ref. (*204*). © Copyright 1991 American Chemical Society.

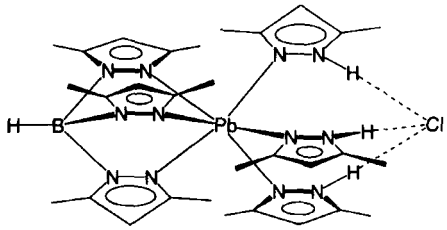

FIG. 49. Structure of $[Tp^{Me_2}]Pb(3,5\text{-}Me_2pzH)_3Cl$.

to other receptor molecules, which effectively encapsulate the bound anions (*206*). It is, however, interesting to note that a similar structural motif has recently been observed for the complex $[Tp^{Me_2}]Pb(3,5\text{-}Me_2pzH)_3Cl$ (Fig. 49), which has been obtained in low yield as a decomposition product in the reaction of $Pb(NO_3)_2$, $P(O)(3,5\text{-}Me_2pz)_3$, and $K[Tp^{Me_2}]$ in the presence of HCl (*207*). The hydrogen-bonded N···Cl distance in $[Tp^{Me_2}]Pb(3,5\text{-}Me_2pzH)_3Cl$ is 3.16 Å, with a N–H···Cl bond angle of 163(5)°, comparable to the values observed for $\{[Tp^{Bu^t}H_3]Cl\}^+$.

VII. Controlled Crystallographic Disorder in $[Tp^{RR'}]MX$ Complexes: Bond Length Artifacts as Determined by Single Crystal X-Ray Diffraction

A. INTRODUCTION

Single crystal x-ray diffraction is, without doubt, one of the most important techniques for the determination of molecular structures in the solid state. The technique is also pivotal to the determination of accurate bond lengths in molecules. However, the analysis of x-ray

diffraction data does not always provide definitive answers with regard to either molecular structure or bond length (*208*). In particular, crystallographic disorder in which a site is occupied by different atoms can result in the incorrect determination of both bond lengths and molecular structures. For example, because of disorder between ethylidyne and methyl ligands, the molecular structure of the ethylidyne complex $W(PMe_3)_4(CH_3)(CCH_3)$ was originally incorrectly assigned as the dimethyl derivative $W(PMe_3)_4(CH_3)_2$ (*209*). A more common occurrence involves disorder of groups that have similar steric requirements, such as pairs of atoms. Disorder of this type is frequently a result of cocrystallization of structurally related, but different, molecules. Such compositional disorder may be extremely deceptive, as illustrated by the original reports of "distortional" or "bond-stretch" isomerism (*210, 211*). Specifically, the observation of blue and green "isomers" of *cis-mer*-$MoOCl_2(PMe_2Ph)_3$, whose significant difference resided only in the lengths of the Mo=O bonds, was demonstrated to be a result of cocrystallization of the blue oxo complex with small quantities of the isostructural yellow trichloride complex *mer*-$MoCl_3(PMe_2Ph)_3$ (*212*). Partial occupancy of the oxo site by a chloride ligand resulted in an apparent increase of the "Mo=O" bond length, since the disordered chloride ligand is located at a much greater distance from the molybdenum center.

One of the most common examples of crystallographic disorder is derived from packing equivalent molecules in different orientations in the crystal. Although it is not possible to control such disorder in a defined manner, it is possible to control disorder at a crystallographic site by doping a crystal with structurally similar molecules, i.e., compositional disorder. The tris(pyrazolyl)hydroborato system $[Tp^{But}]ZnX$ has been shown to be excellent for allowing controlled crystallographic disorder in a series of solid solutions of pairs of the structurally related complexes, namely $[Tp^{But}]ZnX$ (X = Cl, Br, I, CH_3, CN) (*213*). Such a series of structurally related complexes has provided a well-defined system that has allowed the effect of impurities upon observed apparent bond lengths to be quantified.

B. Disorder between Structurally Similar Groups

In order to study the effect of disorder between two atoms, single crystals composed of pairs of the complexes $[Tp^{But}]ZnCl$, $[Tp^{But}]ZnI$, and $[Tp^{But}]ZnMe$, over a range of compositions, were studied. In each case, only a single "atom" was observed at the disordered site, and the Zn–X bond length that was measured corresponded to a composite for the

pair of complexes concerned. The relationships between the observed apparent bond length and composition are illustrated in Fig. 50, which indicates that the relationships are not linear, but are weighted by the relative scattering powers of the disordered groups. Because heavy atoms scatter x-rays strongly, small quantities of such impurities, e.g., I, have a profound effect on observed apparent bond lengths.

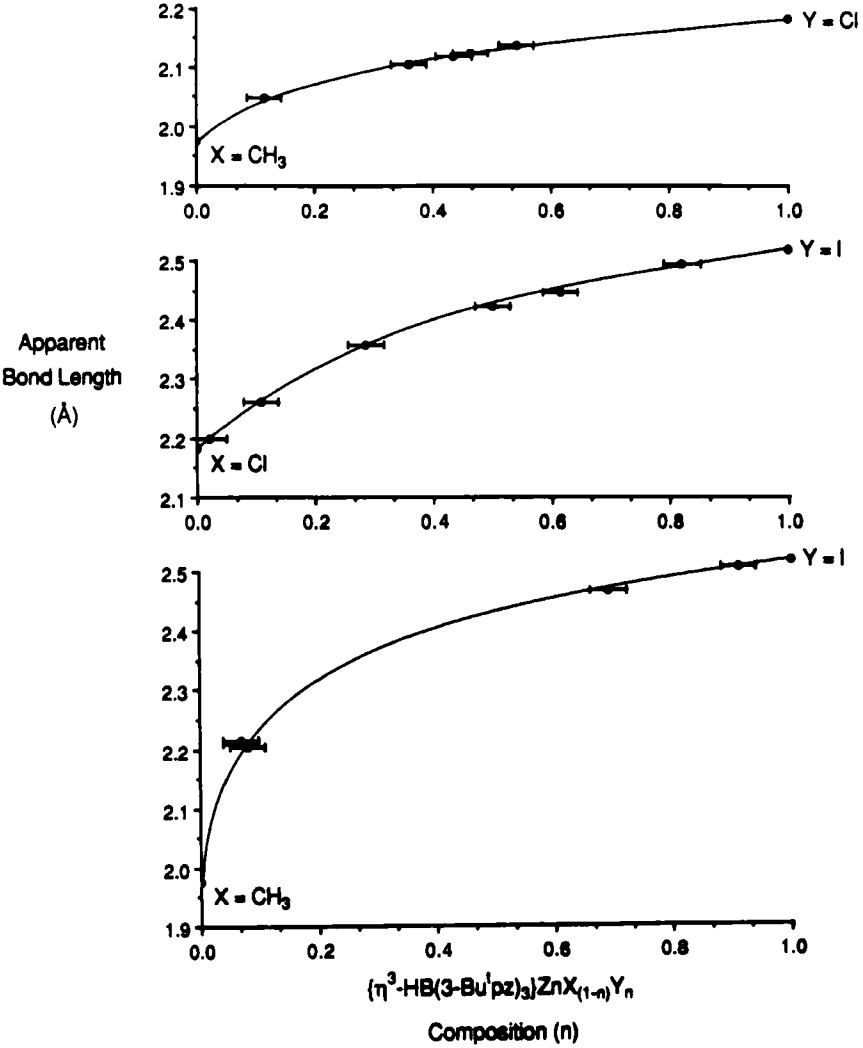

FIG. 50. Variation in apparent bond lengths for [Tp$^{Bu^t}$]ZnX complexes as a function of composition. Reprinted with permission from Ref. (*83*). © Copyright 1991 American Chemical Society.

Although the presence of impurities in a single crystal is often signaled by the observation of abnormal temperature factors, it was noted that reasonable thermal parameters can be observed at impurity levels that are sufficient to result in a significant apparent change in the true bond length. For example, the thermal parameters derived for the series of complexes $[Tp^{But}]ZnCl_{1-n}I_n$, when the disordered site is refined as (i) Cl only, (ii) I only, and (iii) a composite atom ($L = Cl_{1-n}I_n$), are shown in Fig. 51. For reference, the thermal parameters for pure $[Tp^{But}]ZnCl$ and $[Tp^{But}]ZnI$ are also included. Examination of Fig. 51 reveals the expected shrinking of the thermal ellipsoid when the disordered site is refined as Cl and the iodide content at the disordered site increases. Conversely, refining the disordered site as I results in the expected expansion of the thermal ellipsoid as the iodide content decreases. It is evident that unacceptable thermal parameters are obtained at the extremes of these refinement procedures, i.e., when either (i) the composition is iodide-rich and the site is refined as Cl, or (ii) the composition is chloride-rich and the site is refined as I. However, it is also evident that reasonable thermal parameters can be observed at impurity levels that are low. Furthermore, although the impurity level may be sufficiently low so that reasonable thermal parameters may be obtained for such structures, it may be significant enough to result in deviation of the apparent bond length from the true bond length. Thus, the observation of "normal" thermal parameters is not necessarily a good indicator that the crystal is pure, and consequently that the observed bond length is correct, even though it may be determined with high precision and apparently high accuracy. Moreover, it was also noted that expansion of the thermal ellipsoid along the bond vector was not observed for the $[Tp^{But}]ZnCl_{1-n}I_n$ system. Since such expansion may have been expected because the disordered atoms are located at different positions along this vector, this observation further emphasizes that the observation of "normal" thermal parameters is not necessarily a good indicator that an observed bond length is correct. A good illustration is provided by refining the disordered site of the crystal of composition $[Tp^{But}]ZnCl_{0.5}I_{0.5}$ as bromine (Fig. 52), from which it is evident that a perfectly plausible structure can be obtained for the complex $[Tp^{But}]ZnBr$, even though the crystal studied contained no bromine. For reference purposes, Fig. 52 also includes the ORTEP drawing for authentic $[Tp^{But}]ZnBr$, indicating the extremely close similarity with the "artificial" bromide $[Tp^{But}]ZnCl_{0.5}I_{0.5}$. Indeed, without prior knowledge, it would be difficult to distinguish which one of the structures shown in Fig. 52 actually corresponds to the authentic compound $[Tp^{But}]ZnBr$.

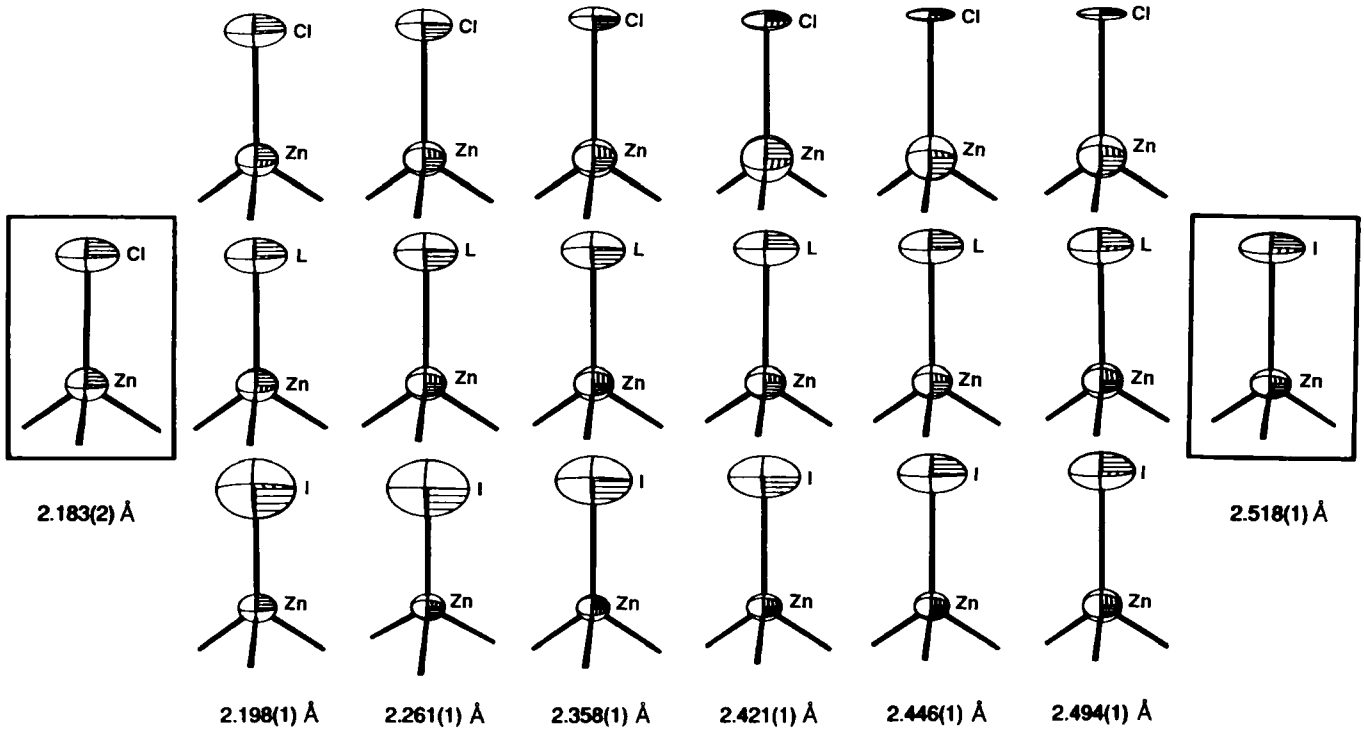

FIG 51. Thermal ellipsoids for the series $[Tp^{Bu^t}]ZnCl_{1-n}I_n$ as the result of refining as (i) Cl (upper row), (ii) I (lower row), and (iii) a composite atom (middle row). Reprinted with permission from Ref. (*83*). © Copyright 1991 American Chemical Society.

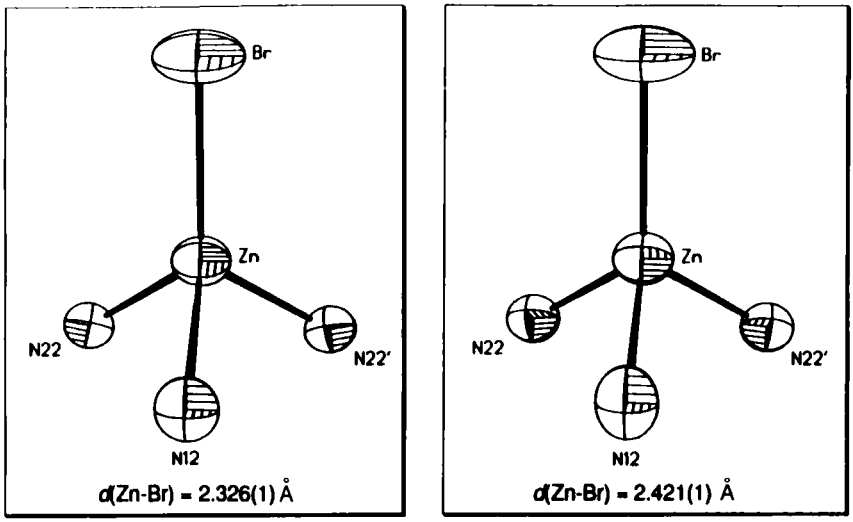

FIG. 52. Comparison of thermal parameters of the disordered structure $[Tp^{Bu^t}]ZnCl_{0.5}I_{0.5}$ when refined as $[Tp^{Bu^t}]ZnBr$, with that of authentic $[Tp^{Bu^t}]ZnBr$. Reprinted with permission from Ref. (*83*). © Copyright 1991 American Chemical Society.

C. DISORDER BETWEEN STRUCTURALLY DISPARATE GROUPS

In addition to disorder between pairs of atoms, disorder between groups that are not isostructural is also common. Examples of such disorder have been observed between (i) CO and other ligands (e.g., halide) (*214*), (ii) N_2 and Cl (*215*), and (iii) C≡CH and CH_3 (*209*). The tris(pyrazolyl)hydroborato ligand system has also been used to study disorder between structurally inequivalent groups. In particular, the effect of partial occupancy by a halide ligand (X = Cl, Br, I) on the structure of the cyanide derivative $[Tp^{But}]ZnCN$ has been studied. Importantly, the location of the disordered atom with respect to the C≡N group could be varied by changing the halide ligand from chloride to bromide to iodide.

For crystals of composition $[Tp^{But}]Zn(CN)_{0.8}Cl_{0.2}$ and $[Tp^{But}]Zn(CN)_{0.95}Br_{0.05}$, disorder between the halide and cyanide groups was not resolved. The partial ORTEP drawings shown in Figs. 53 and 54 illustrate the results of performing two different refinement procedures on both $[Tp^{But}]Zn(CN)_{0.8}Cl_{0.2}$ and $[Tp^{But}]Zn(CN)_{0.95}Br_{0.05}$. The drawings on the left-hand sides of Figs. 53 and 54 illustrate the results of refinement procedure assuming the crystal to be pure $[Tp^{But}]Zn(CN)$, while the

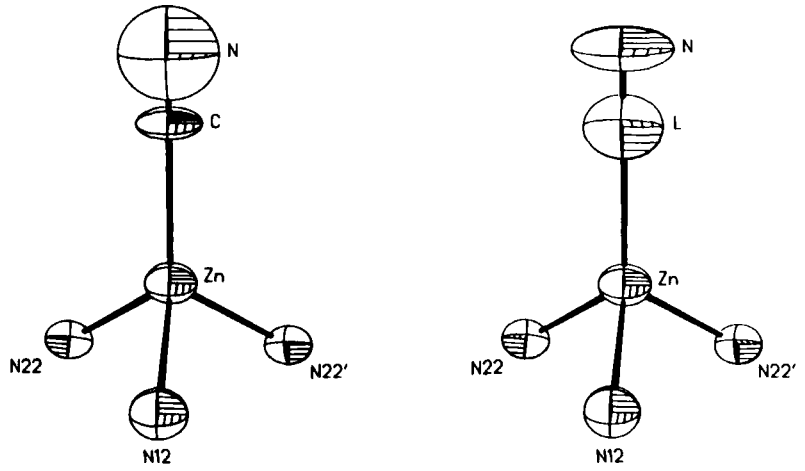

FIG. 53. Partial ORTEP drawings for $[Tp^{Bu^t}]Zn(CN)_{0.8}Cl_{0.2}$. Left: disordered site refined as CN only. Right: disordered site refined as $(CN)_{0.76(1)}Cl_{0.24(1)}$, where L = $C_{0.76(1)}Cl_{0.24(1)}$ and N = $N_{0.76(1)}$. Reprinted with permission from Ref. (*213*). © Copyright 1992 American Chemical Society.

drawings on the right-hand sides correspond to a refinement procedure in which the disordered site was modeled as a composite of CN and X (X = Cl, Br). For reference, the ORTEP drawing of pure $[Tp^{Bu^t}]ZnCN$ is shown in Fig. 55. Although it is evident that the ORTEP drawing for $[Tp^{Bu^t}]Zn(CN)_{0.8}Cl_{0.2}$, in the absence of a disorder model, is

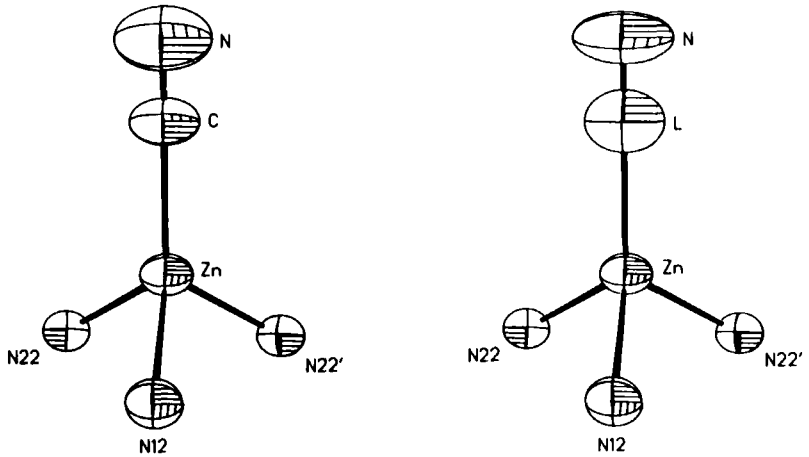

FIG. 54. Partial ORTEP drawings for $[Tp^{Bu^t}]Zn(CN)_{0.95}Br_{0.05}$. Left: disordered site refined as CN only. Right: disordered site refined as $(CN)_{0.96(1)}Br_{0.04(1)}$, where L = $C_{0.96(1)}Br_{0.04(1)}$ and N = $N_{0.96(1)}$. Reprinted with permission from Ref. (*213*). © Copyright 1992 American Chemical Society.

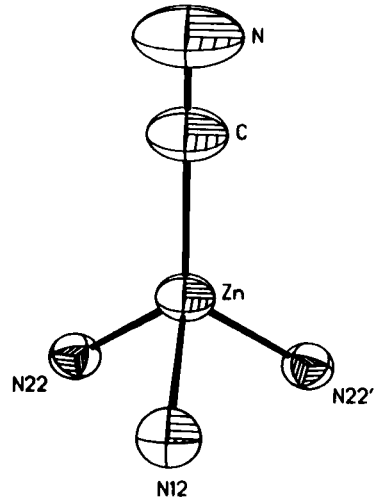

FIG. 55. Partial ORTEP drawing for [Tp^{But}]ZnCN. Reprinted with permission from Ref. (*213*). © Copyright 1992 American Chemical Society.

not particularly satisfactory, the corresponding ORTEP drawing for [Tp^{But}]$Zn(CN)_{0.95}Br_{0.05}$ is reasonable. However, even though the ORTEP drawing appears to be reasonable, the bond lengths associated with the CN ligand are incorrect, with a long Zn–C bond length [2.018(5) Å] and a short C≡N bond length [1.040(8) Å], compared to the values of 1.962(6) Å and 1.117(9) Å, respectively, for the pure compound.

In contrast to the difficulty in resolving the disorder present in the chloride- and bromide-doped crystals [Tp^{But}]$Zn(CN)_{0.8}Cl_{0.2}$ and [Tp^{But}]$Zn(CN)_{0.95}Br_{0.05}$, the disorder between CN and I in [Tp^{But}]$Zn(CN)_{0.9}I_{0.1}$ was readily apparent, and the individual groups could be refined (Fig. 56). However, despite this apparent success, the bond lengths obtained from the disordered structure were also observed to be incorrect, as judged by comparison with data for the pure structures. Thus, the Zn–I bond length of 2.469(8) Å for the disordered structure is slightly shorter than that observed for pure [Tp^{But}]ZnI [2.518(1) Å]; the C–N bond length of 1.178(15) Å is longer than that in [Tp^{But}]ZnCN [1.117(9) Å]; and the Zn–C bond length of 1.932(12) Å is slightly shorter than that in [Tp^{But}]ZnCN [1.962(6) Å].

Finally, the tris(pyrazolyl)hydroborato ligand system has also provided an interesting example in which a crystallographic site is disordered between a vacancy and a chain of three atoms. Thus, the x-ray structure of the cobalt complex [Tp^{Ant}]CoNCS (Ant = 9-anthryl) revealed the presence of the cocrystallized thallium derivative

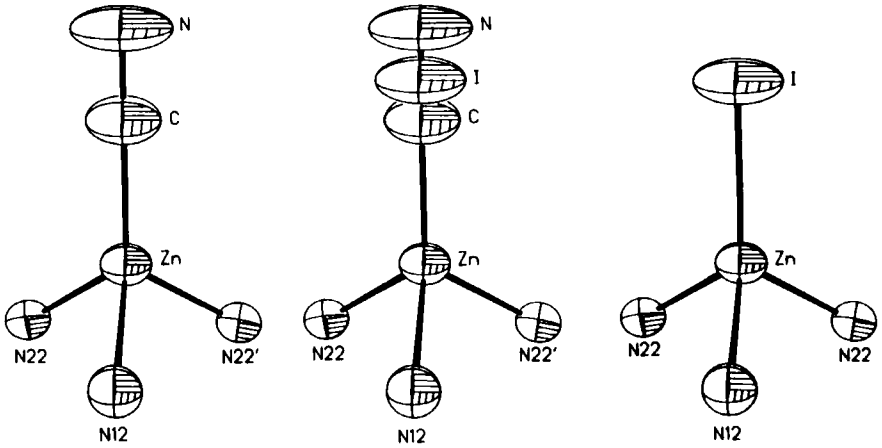

FIG. 56. Partial ORTEP drawings for $[Tp^{Bu^t}]Zn(CN)_{0.9}I_{0.1}$ with disordered site refined as $(CN)_{0.906(4)}I_{0.094(4)}$. Center: superposition of CN and I groups at the disordered site. Left and right: disordered site separated into composite molecules. Reprinted with permission from Ref. (*213*). © Copyright 1992 American Chemical Society.

$[Tp^{Ant}]Tl$, and that the composition of the crystal studied was approximately $[Tp^{Ant}](CoNCS)_{0.94}Tl_{0.06}$. As a consequence of the cocrystallization, the crystallographic "site" occupied by the CoNCS moiety was disordered with a thallium atom (Fig. 57). The ability of $[Tp^{Ant}]CoNCS$ and $[Tp^{Ant}]Tl$, which differ substantially in the number of atoms at the disordered site, to cocrystallize is presumably due to the fact that the disordered site is enclosed within the pocket that is provided by the tris(pyrazolyl)hydroborato ligand.

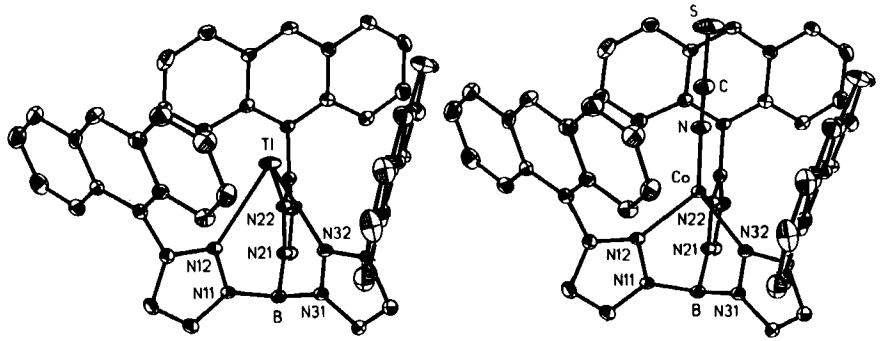

FIG. 57. Cocrystallized $[Tp^{Ant}]CoNCS$ and $[Tp^{Ant}]Tl$. Reprinted from *Polyhedron, 14,* Han, R., Parkin, G., and Trofimenko, S., The tris[3-(9-anthryl)pyrazol-1-yl]hydroborato ligand, $[Tp^{Ant}]$: Compositional disorder between a vacancy and a chain of three atoms, p. 387, © copyright 1995, with kind permission from Elsevier Science Ltd, The Boulevard, Langford Lane, Kidlington 0X5 1GB, UK.

In summary, tris(pyrazolyl)hydroborato complexes have provided a well-defined system that has allowed crystallographic disorder to be studied in a controlled manner. The results of this study serve to emphasize the importance of crystal purity in the determination of correct bond lengths, and also provide further examples which indicate the generality of the phenomenon. Furthermore, although satisfactory refinement of a disordered structure may be taken as good evidence for the nature of the disorder, and therefore a good indication of the molecular structure, attempts to extract the true bond lengths from such a structure must be treated with caution.

VIII. Summary

The thrust of this review has been to describe the role of poly(pyrazolyl)borato ligation in supporting well-defined monomeric terminal alkyl, hydride and hydroxide derivatives $[Tp^{RR'}]MX$ (X = H, R, OH) of the *s*- and *p*-block elements. Specific emphasis has been given to the use of sterically demanding tris(pyrazolyl)hydroborato ligands, such as the "tetrahedral enforcer" ligand $[Tp^{But}]$. However, it is important to emphasize that the structures, stabilities, and reactivities of these complexes are all a sensitive function of the alkyl substituents in both the 3- and the 5-positions, and it is therefore anticipated that the application of tailored $[Tp^{RR'}]$ and $[Bp^{RR'}]$ ligands will generate new and interesting chemistry for other systems.

ACKNOWLEDGMENTS

I sincerely thank the students and postdoctoral researchers who carried out portions of the research described in this article, which was supported by the National Science Foundation (CHE 93-00398), the National Institutes of Health (Grant GM46502), and the Kanagawa Academy of Science and Technology. The numerous conversations with Dr. S. Trofimenko during the course of our research in this area are highly valued, as is the collaboration with Professor Vahrenkamp on carbonic anhydrase models, and the assistance of Professor Arnold Rheingold with crystallography problems. Professors William Tolman, Nobumasa Kitajima, and Daniel Reger are thanked for copies of their reviews prior to publication. I am also grateful to the students and postdoctoral researchers who provided critical comments during the preparation of this article.

REFERENCES

1. (a) Trofimenko, S. *J. Am. Chem. Soc.* **1966,** *88,* 1842.
   (b) Trofimenko, S. *J. Am. Chem. Soc.* **1967,** *89,* 3170.
2. For reviews of this area, see:
   (a) Trofimenko, S. *Chem. Rev.* **1993,** *93,* 943.
   (b) Shaver, A. In "Comprehensive Coordination Chemistry", Wilkinson, G.; Gillard,

R. D.; McCleverty, J. A., Eds., Pergamon Press: Oxford, **1987;** Vol. 2, 245–259.
(c) Trofimenko, S. *Prog. Inorg. Chem.* **1986,** *34,* 115.
(d) Niedenzu, K.; Trofimenko, S. *Top. Curr. Chem.* **1986,** *131,* 1–37.
(e) Shaver, A. *J. Organomet. Chem. Libr.* **1977,** *3,* 157.
(f) Trofimenko, S. *Chem. Rev.* **1972,** *72,* 497.
(g) Trofimenko, S. *Acc. Chem. Res.* **1971,** *4,* 17.
(h) Byers, P. K.; Canty, A. J.; Honeyman, R. T. *Adv. Organomet. Chem.* **1992,** *34,* 1.
(i) Reger, D. L. *Coord. Chem. Rev.*, in press.
(j) Kitajima, N.; Tolman, W. B. *Prog. Inorg. Chem.*, in press.

3. Mono(pyrazoly)hydroborato ligands have not been used significantly to date.
4. For syntheses of unsymmetrical poly(pyrazolyl)borato ligands, see:
(a) Agrifoglio, G. *Inorg. Chim. Acta.* **1992,** *197,* 159.
(b) Frauendorfer, E.; Agrifoglio, G. *Inorg. Chem.* **1982,** *21,* 4122.
5. Tris(pyrazolyl)hydroborato ligands are also known to adopt bidentate and unidentate coordination to a lesser degree. For example, a rare example of unidentate coordination is provided by $[\eta^1\text{-Tp}^{Bu^t}]Ni(PMe_3)_2(p\text{-}C_6H_4X)$ (X = H, Me, OMe). See Gutiérrez, E.; Hudson, S. A.; Monge, A.; Nicasio, M. C.; Paneque, M.; Carmona, E. *J. Chem. Soc., Dalton Trans.* **1992,** 2651.
6. The $[Tp^{Me_2}]$ ligand has also been abbreviated as [Tp*].
7. For derivatives in which there is a 4-alkyl substituent (which are much less common than the 3- and 5-substituents), the superscript is indicated as 4R.
8. Trofimenko, S. J. *Am. Chem. Soc.* **1967,** *89,* 6288.
9. Trofimenko, S.; Calabrese, J. C.; Thompson, J. S. *Inorg. Chem.* **1987,** *26,* 1507.
10. Trofimenko, S.; Calabrese, J. C.; Kochi, J. K.; Wolowiec, S.; Hulsbergen, F. B.; Reedijk, *J. Inorg. Chem.* **1992,** *31,* 3943.
11. (a) Kitajima, N.; Fujisawa, K.; Fujimoto, C.; Moro-oka, Y. *Chem. Lett.* **1989,** 421.
(b) Kitajima, N.; Fujisawa, K.; Fujimoto, C.; Moro-oka, S.; Hashimoto, T.; Toriumi, K.; Tatsumi, K.; Nakamura, A. *J. Am. Chem. Soc.* **1992,** *114,* 1277.
12. Libertini, E.; Yoon, K.; Parkin, G. *Polyhedron* **1993,** *12, 2539.*
13. Trofimenko, S. *Inorg. Synth.* **1970,** *12,* 99.
14. Brunner, H.; Singh, U. P.; Boeck, T.; Altmann, S.; Scheck, T.; Wrackmeyer, B. *J. Organomet. Chem.* **1993,** *443,* C16.
15. (a) LeCloux, D. D.; Tokar, C. J.; Osawa, M.; Houser, R. P.; Keyes, M. C.; Tolman, W. B. *Organometallics* **1994,** *13,* 2855.
(b) LeCloux, D. D.; Tolman, W. B. *J. Am. Chem. Soc.* **1993,** *115,* 1153.
16. In some recently discovered tris(pyrazolyl)hydroborato ligands, the 3-phenyl substituent is tethered to the 4-position of the pyrazolyl ring, e.g., tris(2*H*-benz[G]indazol-2-yl)hydroborato. See
(a) Rheingold, A. L.; Haggerty, B. S.; Trofimenko, S. *J. Chem. Soc., Chem. Commun.* **1994,** 1973.
(b) Rheingold, A. L.; Ostrander, R. L.; Haggerty, B. S.; Trofimenko, S. *Inorg. Chem.* **1994,** *33,* 3666.
17. (a) Cano, M.; Heras, J. V.; Jones, C. J.; McCleverty, J. A.; Trofimenko, S. *Polyhedron* **1990,** *9,* 619.
(b) Cano, M.; Heras, J. V.; Trofimenko, S.; Monge, A.; Gutierrez, E.; Jones, C. J.; McCleverty, J. A. *J. Chem. Soc., Dalton Trans.* **1990,** 3577.
18. A. L. Rheingold, C. B. White and S. Trofimenko, *Inorg. Chem.* **1993,** *32,* 3471.
19. Dowling, C.; Parkin, G., unpublished results, **1995.**
20. M-H-B interactions have been observed previously for transition metal complexes (see Ref. 2).

21. Cowley, A. H.; Geerts, R. L.; Nunn, C. M.; Trofimenko, S. *J. Organomet. Chem.* **1989,** *365,* 19.
22. Yoon, K.; Parkin, G. *Polyhedron* **1995,** *14,* 811.
23. Dowling, C.; Leslie, D.; Chisholm, M. H.; Parkin, G. *Main Group Chemistry,* in press.
24. Ferguson, G.; Jennings, M. C.; Lalor, F. J.; Shanahan, C. *Acta. Cryst.* **1991,** *C47,* 2079.
25. Han, R.; Parkin, G.; Trofimenko, S. *Polyhedron* **1995,** *14,* 387.
26. Haaland, A. *Angew. Chem. Int. Ed. Engl.* **1989,** *28,* 992.
27. Smaller degrees of non-coplanarity are not uncommon in poly(pyrazolyl)borato complexes, e.g., $[Tp^{Me_2}]_2Mg$.
    (a) Han, R.; Parkin, G. *J. Organomet. Chem.* **1990,** *393,* C43.
    (b) Churchill, M. R.; Gold, K.; Maw, C. E., Jr. *Inorg. Chem.* **1970,** *9,* 1597.
    (c) Churchill, M. R.; DeBoer, B. G.; Rotella, F. J.; Abu Salah, O. M.; Bruce, M. I. *Inorg. Chem.* **1975,** *14,* 2051.
28. For other examples of 3-coordinate potassium see:
    (a) Chisholm, M. H.; Drake, S. R.; Naiini, A. A.; Streib, W. E. *Polyhedron* **1991,** *10,* 337.
    (b) Meyer, H.; Schmidt-Lukasch, G.; Baum, G.; Massa, W.; Berndt, A. *Z. Naturforsch., B: Chem Sci.* **1988,** *43B,* 801.
    (c) Veith, M.; Böhnlein, J. *Chem. Ber.* **1989,** *122,* 603.
29. For other complexes with interactions between K and C_6H_6, see:
    (a) Atwood, J. L.; Newberry, III, W. R. *J. Organomet. Chem.* **1974,** *66,* 15.
    (b) Atwood, J. L.; Crissinger, K. D.; Rogers, R. D. *J. Organomet. Chem.* **1978,** *155,* 1.
    (c) Atwood, J. L.; Hrncir, D. C.; Rogers, R. D. *J. Incl. Phenomena* **1983,** *1,* 199.
    (d) Purdy, A. P.; George, C. F. *Organometallics* **1992,** *11,* 1955.
30. Lopez, C.; Claramunt, R. M.; Sanz, D.; Foces-Foces, C.; Cano, F. H.; Faure, R.; Cayon, E.; Elguero, J. *Inorg. Chim. Acta.* **1990,** *176,* 195.
31. (a) Tolman, C. A.; Seidel, W. C.; Gosser; L. W. *J. Am. Chem. Soc.* **1974,** *96,* 53.
    (b) Manser, L. E.; Tolman, C. A. *J. Am. Chem. Soc.* **1975,** *97,* 1955.
32. Trofimenko, S.; Calabrese, J. C.; Domaille, P. J.; Thompson, J. S. *Inorg. Chem.* **1989,** *28,* 1091.
33. Eichhorn, D. M., and Armstrong, W. H. *Inorg. Chem.* **1990,** *29,* 3607.
34. Calabrese, J. C.; Trofimenko, S. *Inorg. Chem.* **1992,** *31,* 4810.
35. Ruf, M.; Weis, K.; Vahrenkamp, H. *J. Chem. Soc., Chem. Commun.* **1994,** 135.
36. Mealli, C.; Arcus, C. S.; Wilkinson, J. L.; Marks, T. J.; Ibers, J. A. *J. Am. Chem. Soc.* **1976,** *98,* 711.
37. (a) Carrier, S. M.; Ruggiero, C. E.; Houser, R. P.; Tolman, W. B. *Inorg. Chem.* **1993,** *32,* 4889.
    (b) Carrier, S. M.; Ruggiero, C. E.; Tolman, W. B. *J. Am. Chem. Soc.* **1992,** *114,* 4407.
38. Reger, D. L.; Huff, M. F.; Rheingold, A. L.; Haggerty, B. S. *J. Am. Chem. Soc.* **1992,** *114,* 579.
39. For some related effects, see:
    (a) Cowley, A. H.; Geerts, R. L.; Nunn, C. M.; Carrano, C. J. *J. Organomet. Chem.* **1988,** *341,* C27.
    (b) Reger, D. L.; Knox, S. J.; Huff, M. F.; Rheingold, A. L.; Haggerty, B. S. *Inorg. Chem.* **1991,** *30,* 1754.
    (c) Sohrin, Y.; Kokusen, H.; Kihara, S.; Matsui, M.; Kushi, Y.; Shiro, M. *J. Am. Chem. Soc.* **1993,** *115,* 4128.
40. Han, R.; Looney, A.; McNeill, K.; Parkin, G.; Rheingold, A. L.; Haggerty, B. S. *J. Inorg. Biochem.* **1993,** *49,* 105.

41. It should be noted that four-coordinate Cu(II) complexes do not typically favor tetrahedral coordination, so that distortions for this metal center may be more pronounced upon substitution at the 5-position. See: Cotton, F. A.; Wilkinson, G. "Advanced Inorganic Chemistry" (5th Ed.); Wiley–Interscience: New York, 1988.

42. (a) Boersma, J. In "Comprehensive Organometallic Chemistry," Wilkinson, G.; Stone, F. G. A.; Abel, E. W., Eds.; Pergamon Press: Oxford, 1982; Vol. 2, 823–862.
(b) Coates, G. E.; Green, M. L. H.; Wade, K. "Organometallic Compounds. Volume I: The Main Group Elements" (3rd Ed.); Methuen: London, 1967.
(c) Elschenbroich, C.; Salzer, A. "Organometallics: A Concise Introduction" (2nd Ed.); VCH: New York, 1992.
(d) Miginiac, L. In "The Chemistry of the Metal-Carbon Bond," Hartley, F. R.; Patai, S., Eds.; Wiley: New York, 1985; Vol. 3, Chapter 2.
(e) Furukawa, J.; Kawabata, N. *Adv. Organomet. Chem.* **1974,** *12,* 83.
(f) Erdik, E. *Tetrahedron* **1992,** *48,* 9577.
(g) Wardell, J. L., Ed. "Organometallic Compounds of Zinc, Cadmium and Mercury"; Chapman and Hall: London; 1985.
(h) Kharasch, M. S.; Reinmuth, O. "Grignard Reactions of Nonmetallic Substances"; Prentice–Hall: New York, 1954.

43. Bickelhaupt, F. J. *Organomet. Chem.* **1994,** *475,* 1.

44. (a) Ashby, E. C. *Pure Appl. Chem.* **1980,** *52,* 545.
(b) Ashby, E. C. *Q. Rev., Chem. Soc.* **1967,** 259.
(c) Ashby, E. C.; Laemmle, J.; Neumann, H. M. *Acc. Chem. Res.* **1974,** *7,* 272.

45. Silverman, G.; Rakipa, P. Eds. "The Handbook of Grignard Reagents," Marcel-Dekker, in press.

46. Guggenberger, L. J.; Rundle, R. E. *J. Am. Chem. Soc.* **1968,** *90,* 5375.

47. Stucky, G.; Rundle, R. E. *J. Am. Chem. Soc.* **1964,** *86,* 4825.

48. Vallino, M. *J. Organomet. Chem.* **1969,** *20,* 1.

49. Spek, A. L.; Voorbergen, P.; Schat, G.; Blomberg, C.; Bickelhaupt, F. *J. Organomet. Chem.* **1974,** *77,* 147.

50. Toney, J.; Stucky, G. D. *J. Chem. Soc., Chem. Commun.* **1967,** 1168.

51. Toney, J.; Stucky, G. D. *J. Organomet. Chem.* **1971,** *28,* 5.

52. Han, R.; Parkin, G. *Inorg. Chem.* **1993,** *32,* 4968.

53. Gilman, H.; Jones, R. G. *J. Amer. Chem. Soc.* **1946,** *68,* 517.

54. Calculations have estimated that decomposition of [TlMe] by either disproportionation to Tl and $TlMe_3$ or by reductive coupling to give Tl and C_2H_6 are thermodynamically favored. See:
Schwerdtfeger, P.; Boyd, P. D. W.; Bowmaker, G. A.; Mack, H. G.; Oberhammer, H. *J. Amer. Chem. Soc.,* **1989,** *111,* 15.

55. Sohrin, Y.; Kokusen, H.; Kihara, S.; Matsui, M.; Kushi, Y.; Shiro, M. *Chem. Lett.* **1992,** 1461.

56. Han, R.; Parkin, G. *Inorg. Chem.* **1992,** *31,* 983.

57. r_{cov}(Be) = 0.89 Å, r_{cov}(Mg) = 1.36 Å, r_{cov}(Zn) = 1.25 Å, r_{cov}(Cd) = 1.41 Å, r_{cov}(H) = 0.30 Å, r_{cov}(C) = 0.77 Å. Pauling, L. "The Nature of The Chemical Bond," 3rd Ed.; Cornell University Press: Ithaca, 1960; pp. 228 and 256.

58. Drew, D. A.; Haaland, A. *Acta Chem. Scand.* **1972,** *26,* 3079.

59. Almenningen, A.; Haaland, A.; Morgan, G. L. *Acta Chem. Scand.* **1969,** *23,* 2921.

60. Almenningen, A.; Haaland, A.; Nilsson, J. E. *Acta Chem. Scand.* **1968,** *22,* 972.

61. Weiss, E.; Wolfrum, R. *J. Organomet. Chem.* **1968,** *12,* 257.

62. Snow, A. I.; Rundle, R. E. *Acta Crystallogr.* **1951,** *4,* 348.
63. (a) Gaines, D. F.; Coleson, K. M.; Hillenbrand, D. F. *J. Magn. Reson.* **1981,** *44,* 84.
(b) Kovar, R. A.; Morgan, G. L. *J. Am. Chem. Soc.* **1970,** *92,* 5067.
64. (a) Han, R.; Looney, A.; Parkin, G. *J. Am. Chem. Soc.* **1989,** *111,* 7276.
(b) Han, R.; Parkin, G. *J. Am. Chem. Soc.* **1990,** *112,* 3662.
(c) Han, R.; Parkin, G. *Organometallics* **1991,** *10,* 1010.
(d) Han, R.; Parkin, G. *J. Am. Chem. Soc.* **1992,** *114,* 748.
65. Ghosh, P.; Yoon, K.; Parkin, G., unpublished results, 1995.
66. Dowling, C.; Parkin, G., unpublished results, 1995.
67. Markies, P. R.; Akkerman, O. S.; Bickelhaupt, F.; Smeets, W. J. J.; Spek, A. L. *Adv. Organomet. Chem.,* **1991,** *32,* 147.
68. For some magnesium enolate derivatives, see:
(a) Williard, P. G.; Salvino, J. M. *J. Chem. Soc., Chem. Commun.* **1986,** 153.
(b) Pinkus, A. G.; Lindberg, J. G.; Wu, A.-B. *Chem. Commun.* **1969,** 1350.
69. (a) Brilkina, T. G.; Shushunov, V. A. "Reactions of Organometallic Compounds with Oxygen and Peroxide," Illiffe Books Ltd.: London, 1969.
(b) Davies, A. G. "Organic peroxides" Swern, D., Ed.; Wiley-Interscience: New York, 1972; Vol. 2, 337–354.
70. Kaim, W. *Top. Curr. Chem.* **1994,** *169,* 231.
71. (a) Fontaine, C.; Duong, K. N. V.; Merienne, C.; Gaudemer, A.; Giannotti, C. *J. Organomet. Chem.* **1972,** *38,* 167.
(b) Chiaroni, A.; Pascard-Billy, C. *Bull. Soc. Chim. Fr.* **1973,** 781.
(c) Jensen, F. R.; Kiskis, R. C. *J. Organomet. Chem.* **1973,** *49,* C46.
(d) Cleaver, W. M.; Barron, A. R. *J. Amer. Chem. Soc.* **1989,** *111,* 8966.
(e) Barron, A. R. *Chem. Soc. Rev.* **1993,** *22,* 93.
72. Eisch, J. J.; Husk, G. R. *J. Org. Chem.* **1964,** *29,* 254.
73. Davies, A. G.; Roberts, B. P. *Acc. Chem. Res.* **1972,** *5,* 387.
74. Kaim, W. *Top. Curr. Chem.* **1994,** *169,* 231.
75. Gilman, H.; Jones, H. L. *J. Am. Chem. Soc.* **1929,** *51,* 2840.
76. For example, examination of the *organic* products after quenching a reaction with CO_2 has provided evidence for alkyl group exchange between RMgX and R'X.
(a) Kharasch, M. S.; Fuchs, C. F. *J. Org. Chem.* **1945,** *10,* 292.
(b) Kharasch, M. S.; Lambert, F. L.; Urry, W. H. *J. Org. Chem.* **1945,** *10,* 298.
77. Canty, A. J.; Minchin, N. J.; Patrick, J. M.; White, A. H. *Aust. J. Chem.* **1983,** *36,* 1107.
78. Byers, P. K.; Canty, A. J.; Minchin, N. J.; Patrick, J. M.; Skelton, B. W.; White, A. H. *J. Chem. Soc., Dalton Trans.* **1985,** 1183.
79. Gorrell, I. B.; Looney, A.; Parkin, G. *J. Chem. Soc., Chem. Commun.* **1990,** 220–222.
80. Looney, A.; Han, R.; Gorrell, I. B.; Cornebise, M.; Yoon, K.; Parkin, G.; Rheingold, A. L. *Organometallics* **1995,** *14,* 274.
81. (a) Alsfasser, R.; Powell, A. K.; Vahrenkamp, H. *Angew. Chem., Int. Ed. Engl.* **1990,** *29,* 898.
(b) Alsfasser, R.; Powell, A. K.; Trofimenko, S.; Vahrenkamp, H. *Chem. Ber.* **1993,** *126,* 685.
82. Gorrell, I. B.; Looney, A.; Parkin, G.; Rheingold, A. L. *J. Am. Chem. Soc.* **1990,** *112,* 4068.
83. Yoon, K.; Parkin, G. *J. Am. Chem. Soc.* **1991,** *113,* 8414.
84. For other examples of three-coordinate organozinc complexes, see:
(a) Chernega, A. N.; Antipin, M. Y.; Struchkov, Y. T.; Romanenko, V. D. *Koord. Chim.* **1989,** *15,* 894.

(b) Purdy, A. P.; George, C. F. *Organometallics* **1992,** *11,* 1955.
(c) Westerhausen, M.; Rademacher, B.; Schwarz, W. *Z. Anorg. Allg. Chem.* **1993,** *619,* 675.
(d) Olmstead, M. M.; Power, P. P.; Shoner, S. C. *J. Am. Chem. Soc.* **1991,** *113,* 3379.
(e) Bell, N. A.; Shearer, H. M. M.; Spencer, C. B. *Acta Crystallogr.* **1983,** *C39,* 1182.
(f) Budzelaar, P. H. M.; Alberts-Jansen, H. J.; Mollema, K.; Boersma, J.; van der Kerk, G. J. M.; Spek, A. L.; Duisenberg, A. J. M. *J. Organomet. Chem.* **1983,** *243,* 137.
(g) Al-Juaid, S. S.; Buttrus, N. H.; Eaborn, C.; Hitchcock, P. B.; Roberts, A. T. L.; Smith, J. D. S.; Sullivan, A. C. *J. Chem. Soc., Chem. Commun.* **1986,** 908.
(h) Gais, H.-J.; Bülow, G.; Raabe, G. *J. Am. Chem. Soc.* **1993,** *115,* 7215.
(i) Parvez, M.; BergStresser, G. L.; Richey, H. G., Jr. *Acta Crystallogr., Sect. C: Cryst. Struct. Commun.* **1992,** *C48,* 641.

85. Hartmann, F.; Kläui, W.; Kremer-Aach, A.; Mootz, D.; Strerath, A.; Wunderlich, H. *Z. Anorg. Allg. Chem.,* **1993,** *619,* 2071.
86. Tolman, W. B. *Inorg. Chem.* **1991,** *30,* 4877.
87. Moreover, the related derivative $[Tp^{Pr^i_2}]Cu(\eta^2\text{-}O_2CC_6H_4Cl)$ has been structurally characterized by x-ray diffraction. Kitajima, N.; Fujisawa, K.; Mor-oka, Y. *J. Am. Chem. Soc.* **1990,** *29,* 357.
88. Darensbourg, D. J.; Holtcamp, M. W.; Longridge, E. M.; Khandelwal, B.; Klausmeyer, K. K.; Reibenspies, J. H. *J. Am. Chem. Soc.* **1995,** *117,* 318.
89. McWhinnie, W. R.; Monsef-Mirzal, Z.; Perry, M. C.; Shaikh, N.; Hamor, T. A. *Polyhedron* **1993,** *12,* 1193.
90. Eichorn, D. M; Armstrong, W. H. *Inorg. Chem.* **1990,** *29,* 3607.
91. Looney, A.; Saleh, A.; Zhang, Y.; Parkin, G. *Inorg. Chem.* **1994,** *33,* 1158.
92. Reger, D. L.; Mason, S. S. *Organometallics* **1993,** *12,* 2600.
93. Both $^2J_{Cd\text{-}H}$ and $^1J_{Cd\text{-}C}$ coupling constants for $[Tp^{Me_2}]Cd$ were inadvertently reported as half their true values. Reger, D. L. personal communication, 1995.
94. Turner, C. J.; White, R. F. M. *J. Magn. Reson.* **1977,** *26,* 1.
95. Kennedy, J. D.; McFarlane, W. *J. Chem. Soc., Perkin Trans. 2,* **1977,** 1187.
96. Reger, D. L.; Mason, S. S. *Polyhedron* **1994,** *13,* 3059.
97. For ^{113}Cd NMR studies on poly(pyrazolyl)borato cadmium complexes, see:
(a) Reger, D. L.; Mason, S. S.; Rheingold, A. L.; Ostrander, R. L. *Inorg. Chem.* **1993,** *32,* 5216.
(b) Lipton, A. S.; Mason, S. S.; Reger, D. L.; Ellis, P. D. *J. Am. Chem. Soc.* **1994,** *116,* 10182.
98. Reger, D. L.; Mason, S. S.; Takats, J.; Zhang, X. W.; Rheingold, A. L.; Haggerty, B. S. *Inorg. Chem.* **1993,** *32,* 4345.
99. Reger, D. L.; Mason, S. S.; Takats, J.; Zhang, X. W.; Rheingold, A. L; Haggerty, B. S. *Inorg. Chem.* **1993,** *32,* 4345.
100. Canty, A. J.; Minchin, N. J.; Patrick, J. M.; White, A. H. *Aust. J. Chem.* **1983,** *36,* 1107.
101. Lobbia, G. G.; Cecchi, P.; Bonati, F.; Rafaiani, G. *Synth. React. Inorg. Met.-Org. Chem.* **1992,** *22,* 775.
102. Canty, A. J.; Skelton, B. W.; White, A. H. *Aust. J. Chem.* **1987,** *40,* 1609.
103. The reference was not specified but is possibly relative to Me_2Hg.
104. Lobbia, G. G.; Bonati, F.; Cecchi, P.; Pettinari, C. *Gazz. Chim. Ital.* **1991,** *121,* 355.
105. Yoon, K.; Parkin, G. unpublished results, 1994.
106. Looney, A.; Parkin, G. *Polyhedron* **1990,** *9,* 265.
107. Cowley, A. H ; Carrano, C. J.; Geerts, R. L.; Jones, R. A.; Nunn, C. M. *Angew. Chem., Int. Ed. Engl.* **1988,** *27,* 277.

108. Dungan, C. H.; Maringgele, W.; Meller, A.; Niedenzu, K.; Nöth, H.; Serwatowska, J.; Serwatowski, J. *Inorg. Chem.* **1991,** *30,* 4799.
109. Rettig, S. J.; Sandercock, M.; Storr, A.; Trotter, J. *Can. J. Chem.* **1990,** *68,* 59.
110. Reger, D. L.; Knox, S. J.; Lebioda, L. *Organometallics* **1990,** *9,* 2218.
111. For the structure of the chloride derivative $[Bp]_2GaCl$, see:
(a) Reger, D. L.; Knox, S. J.; Lebioda, L. *Inorg. Chem.* **1989,** *28,* 3092.
(b) Marsh, R. E. *Inorg. Chem.* **1990,** *29,* 1449.
112. Reger, D. L.; Ding, Y. *Organometallics* **1993,** *12,* 4485.
113. Reger, D. L.; Knox, S. J.; Rheingold, A. L.; Haggerty, B. S. *Organometallics* **1990,** *9,* 2581.
114. Reger, D. L.; Mason, S. S.; Rheingold, A. L.; Ostrander, R. L. *Inorg. Chem.* **1994,** *33,* 1803.
115. Dungan, C. H.; Maringgele, W.; Meller, A.; Niedenzu, K.; Nöth, H.; Serwatowska, J.; Serwatowski, J. *Inorg. Chem.* **1991,** *30,* 4799.
116. (a) Nicholson, B. K. *J. Organomet. Chem.* **1984,** *265,* 153.
(b) Lee, S. K.; Nicholson, B. K. *J. Organomet. Chem.* **1986,** *309,* 257.
117. Jung, O.-S.; Jeong, J. H.; Sohn, Y. S. *Organometallics* **1991,** *10,* 2217.
118. Lobbia, G. G.; Bonati, F.; Cecchi, P.; Cingolani, A.; Lorenzotti, A. *J. Organomet. Chem.* **1989,** *378,* 139.
119. Jung, O.-S.; Jeong, J. H.; Sohn, Y. S. *J. Organomet. Chem.* **1990,** *399,* 235.
120. Lobbia, G. G.; Bonati, F.; Cecchi, P.; Lorenzotti, A.; Pettinari, C. *J. Organomet. Chem.* **1991,** *403,* 317.
121. Lobbia, G. G.; Bonati, F.; Cecchi, P.; Leonesi, D. *J. Organomet. Chem.* **1990,** *391,* 155.
122. Tetrakis(nitroindazolyl)borato complexes of tin, [B(5- and 6-nitroindazolyl)]SnR_3 (R = Me, Bu, Ph), have also been reported. See: Zaidi, S. A. A.; Shaheer, S. A.; Zaidi, S. R. A.; Shakir, M. *Indian J. Chem., Sect. A* **1986,** *25A,* 863–864.
123. Niedenzu, K.; Nöth, H.; Serwatowska, J.; Serwatowski, J. *Inorg. Chem.* **1991,** *30,* 3249.
124. Zaidi, S. A. A.; Hashmi, A. A.; Siddiqui, K. S.; *J. Chem. Res., Synop.* **1988,** 410.
125. Andersen, R. A. personal communication, 1992.
126. Bell, N. A.; Coates, G. E. *J. Chem. Soc. A* **1966,** 1069.
127. Coates, G. E.; Tranah, M. *J. Chem. Soc. A* **1967,** 615.
128. Adamson, G. W.; Shearer, H. M. M. *J. Chem. Soc., Chem. Commun.* **1965,** 240.
129. BeH_2 (*129a*) and M_2BeH_4 (M = Li, Na) (*129b*) are polymeric materials.
(a) Brendel, G. J.; Marlett, E. M.; Niebylski, L. M. *Inorg. Chem.* **1978,** *17,* 3589.
(b) Bell, N. A.; Coates, G. E. *J. Chem. Soc. A* **1968,** 628.
130. (a) Bell, N. A.; Coates, G. E.; Schneider, M. L.; Shearer, H. M. M. *J. Chem. Soc., Chem. Commun.* **1983,** 828.
(b) Bell, N. A.; Coates, G. E.; Schneider, M. L.; Shearer, H. M. M. *Acta. Crystallogr., Sect. C; Cryst. Struct. Commun.* **1984,** *C40,* 608.
131. Bartke, T. C.; Bjørseth, A.; Haaland, A.; Marstokk, K.-M.; Møllendal, H. *J. Organomet. Chem.* **1975,** *85,* 271.
132. These terminal Be-H bond lengths are also shorter than the Be-H bridging interaction in $[(Et_2O)NaHBeEt_2]_n$ (1.4 Å). Adamson, G. W.; Shearer, H. M. M. *J. Chem. Soc., Chem. Commun.* **1965,** 240.
133. Glidewell, C. *J. Organomet. Chem.* **1981,** *217,* 273.
134. (a) Bacon, J.; Gillespie, R. J.; Quail, J. W. *Can. J. Chem.* **1963,** *41,* 3063.
(b) Suzuki, M.; Kubo, R. *Mol. Phys.* **1963–64,** *7,* 201.
135. For reference, terminal boron-hydrogen bonds normally exhibit $^1J11_{B\text{-}H}$ in the range 100–190 Hz, whereas when a hydrogen bridge is involved $^1J11_{B\text{-}H}$ is usually less

than 80 Hz. Harris, R. K.; Mann, B. E. "NMR and the Periodic Table" Academic Press: New York, 1978.
136. Gaines, D. F.; Coleson, K. M.; Hillenbrand, D. F. *J. Magn. Reson.* **1981,** *44,* 84.
137. For comparison, the bridging Be-H-B absorptions in $(C_5H_5)Be(\eta^2\text{-}H_2BH_2)$ are observed at much lower values, 1477 and 1470 cm^{-1}. Coe, D. A.; Nibler, J. W.; Cook, T. H., Drew, D.; Morgan, G. L. *J. Chem. Phys.* **1975,** *63,* 4842.
138. Han, R.; Gorrell, I. B.; Looney, A. G.; Parkin, G. *J. Chem. Soc., Chem. Commun.* **1991,** 717.
139. (a) De Koning, A. J.; Boersma, J.; van der Kerk; G. J. M. *J. Organomet. Chem.* **1980,** *195,* 1.
(b) Ashby, E. C.; Goel, A. B. *Inorg. Chem.* **1981,** *20,* 1096.
(c) De Koning, A. J.; Boersma, J.; van der Kerk, G. J. M. *Tetrahedron Lett.* **1977,** 2547.
140. (a) Bell, N. A.; Coates, G. E. *J. Chem. Soc. A,* **1968,** 823.
(b) Bell, N. A.; Moseley, P. T.; Shearer, H. M. M.; Spencer, C. B. *J. Chem. Soc., Chem. Commun.* **1980,** 359.
(c) Bell, N. A.; Moseley, P. T.; Shearer, H. M. M.; Spencer, C. B. *Acta Crystallogr., Sect. B: Struct. Crystallogr. Cryst. Chem.* **1980,** *B36,* 2950.
141. Goeden, G. V.; Caulton, K. G. *J. Am. Chem. Soc.* **1981,** *103,* 7354.
142. De Koning, A. J.; Boersma, J.; van der Kerk, G. J. M. *J. Organomet. Chem.* **1978,** *155,* C5.
143. Neils, T. L.; Burlitch, J. M. *Inorg. Chem.* **1989,** *28,* 1607.
144. Monomeric carboxylato complexes with $\Delta\nu$ values greater than 200 cm^{-1} invariably have unidentate coordination. Deacon, G. B.; Phillips, R. J. *Coord. Chem. Rev.* **1980,** *33,* 227.
145. (a) Reger, D. L.; Mason, S. S.; Rheingold, A. L. *J. Am. Chem. Soc.* **1993,** *115,* 10406.
(b) Reger, D. L.; Mason, S. S.; Rheingold, A. L. *J. Am. Chem. Soc.* **1994,** *116,* 2233.
146. Sohrin, Y.; Matsui, M.; Hata, Y.; Hasegawa, H.; Kokusen, H. *Inorg. Chem.* **1994,** *33,* 4376.
147. (a) Sohrin, Y.; Kokusen, H.; Kihara, S.; Matsui, M.; Kushi, Y.; Shiro, M. *Chem. Lett.* **1992,** 1461.
(b) Sohrin, Y.; Kokusen, H.; Kihara, S.; Matsui, M.; Kushi, Y.; Shiro, M. *J. Am. Chem. Soc.* **1993,** *115,* 4128.
148. Ghosh, P.; Yoon, K.; Parkin, G. unpublished results, 1995.
149. Alsfasser, R.; Trofimenko, S.; Looney, A.; Parkin, G.; Vahrenkamp, H. *Inorg. Chem.* **1991,** *30,* 4098.
150. Alsfasser, R.; Ruf, M.; Trofimenko, S.; Vahrenkamp, H. *Chem. Ber.* **1993,** *126,* 703.
151. Looney, A.; Han, R.; McNeill, K.; Parkin, G. *J. Am. Chem. Soc.* **1993,** *115,* 4690.
152. Egan, J. W., Jr.; Haggerty, B. S.; Rheingold, A. L.; Sendlinger, S. C.; Theopold, K. H. *J. Am. Chem. Soc.* **1990,** *112,* 2445.
153. Kitajima, N.; Hikichi, S.; Tanaka, M.; Moro-oka, Y. *J. Am. Chem. Soc.* **1993,** *115,* 5496.
154. Parkin, G.; Yoon, K. unpublished results, 1994.
155. (a) Silverman, D. N.; Lindskog, S. *Acc. Chem. Res.* **1988,** *21,* 30.
(b) Banci, L.; Bertini, I.; Luchinat, C.; Donaire, A.; Martínez, M.-J.; Moratal Mascarell, J. M. *Comments Inorg. Chem.* **1990,** *9,* 245.
(c) Wooley, P. *Nature (London)* **1975,** *258,* 677.
(d) Bertini, I.; Luchinat, C.; Scozzafava, A. *Struct. Bonding (Berlin)* **1981,** *48,* 45.
(e) Lindskog, S. In "Zinc Enzymes," Spiro, T. G., Ed.; Wiley: New York, 1983; 77–122.
(f) Sigel, H., Ed., "Metal Ions in Biological Systems, Vol. 15, Zinc and its Role in Biology and Nutrition," Marcel-Dekker: New York, 1983.

(g) Botre, F.; Gros, G.; Storey, B. T., Eds., "Carbonic Anhydrase," VCH: New York, 1991.
(h) Khalifah, R. G.; Silverman, D. N. "The Carbonic Anhydrases," Dodgson, S. J.; Tashian, R. E.; Gros, G.; Carter, N. D., Eds.; Plenum: New York, 1991; 49–70.
(i) Lindskog, S. *Adv. Inorg. Biochem.* **1982,** *4,* 115.
(j) Coleman, J. E. *Ann. N. Y. Acad. Sci.* **1984,** *429,* 26.

156. Eriksson, A. E.; Jones, T. A.; Liljas, A. *Proteins: Struct., Funct., Genet.* **1988,** *4,* 274.

157. Nair, S. K.; Christianson, D. W. *J. Am. Chem. Soc.* **1991,** *113,* 9455.

158. Coleman, J. E. *Ann. N. Y. Acad. Sci.* **1984,** *429,* 26.

159. (a) Wooley, P. J. *J. Chem. Soc., Perkin Trans. 2* **1977,** 318.
(b) Tang, C. C.; Davalian, D., Huang, P.; Breslow, R. *J. Am. Chem. Soc.* **1978,** *100,* 3918.
(c) Curtis, N. J.; Brown, R. S. *J. Org. Chem.* **1980,** *45,* 4038; Read, R. J.; James, M. N. G. *J. Am. Chem. Soc.* **1981,** *103,* 6947.
(d) Brown, R. S., Curtis, N. J.; Kusuma, S.; Salmon, D. *J. Am. Chem. Soc.* **1982,** *104,* 3188.

160. (a) Kimura, E.; Shiota, T.; Koike, T.; Shiro, M.; Kodama, M. *J. Am. Chem. Soc.* **1990,** *112,* 5805.
(b) Kimura, E.; Kurogi, Y.; Shionoya, M.; Dhiro, M. *Inorg. Chem.* **1991,** *30,* 452.
(c) Koike, T.; Kimura, E.; Nakamura, I.; Hashimoto, Y.; Shiro, M. *J. Am. Chem. Soc.* **1992,** *114,* 7338.

161. Kimura, E. *Prog. Inorg. Chem.,* **1994,** *41,* 443.

162. IR spectroscopy is often used for distinguishing between unidentate and bidentate coordination of carboxylate (O_2CR) ligands. For monomeric carboxylate derivatives the separation between the symmetric and asymmetric CO_2 stretching bands, $\Delta\nu = [\nu_{asym}(CO_2) - \nu_{sym}(CO_2)]$, provides a useful indication of the coordination mode: complexes which exhibit values of $\Delta\nu$ greater than 200 cm^{-1} invariably possess unidentate coordination. Deacon, G. B.; Phillips, R. J. *Coord. Chem. Rev.* **1980,** *33,* 227.

163. Yoshida, T.; Thorn, D. L.; Okano, T.; Ibers, J. A.; Otsuka, S. *J. Am. Chem. Soc.* **1979,** *101,* 4212.

164. Crutchley, R. J.; Powell, J.; Faggiani, R.; Lock, C. J. L. *Inorg. Chim. Acta.* **1977,** *24,* L15.

165. Ganguly, S.; Mague, J. T.; Roundhill, D. M. *Inorg. Chem.* **1992,** *31,* 3831.

166. Hossain, S. F.; Nicholas, K. M.; Teas, C. L.; Davis, R. E. *J. Chem. Soc., Chem. Commun.* **1981,** 268.

167. For some other examples of bicarbonate complexes that have not been structurally characterized by x-ray diffraction see:
(a) Jackson, W. G.; Sargeson, A. M. *Inorg. Chem.* **1978,** *17,* 1348.
(b) Tsuda, T.; Chuji, Y.; Saegusa, T. *J. Am. Chem. Soc.* **1980,** *102,* 431.
(c) Baylis, B. K. W.; Bailar, J. C., Jr. *Inorg. Chem.* **1970,** *9,* 641.

168. Bicarbonate complexes that have been structurally characterized, but for which no IR data are reported, include unidentate Cu(STTP)(η^1-OCO_2H) (*168a*) and bidentate Ru(CO)[η^1-$MeO_2CC{=}CHCO_2ME$](PPh_3)(η^2-O_2COH) (*168b*).
(a) Latos-Grazynski, L.; Lisowski, J.; Olmstead, M. M.; Balch, A. L. *J. Am. Chem. Soc.* **1987,** *109,* 4428.
(b) Romero, A.; Santos, A.; Vegas, A. *Organometallics* **1988,** *7,* 1988.

169. A value of 157.9 ppm has been reported for the bicarbonate resonance of [$Tp^{Bu^t,Me}$]Zn(OCO_2H) in $CDCl_3$ (Ref. *150*). However, we have been unable to assign with confidence a resonance that is a singlet in the proton-coupled ^{13}C NMR spectrum at this position.

170. For more information on metal carbonates see:

(a) Palmer, D. A.; van Eldik, R. *Chem. Rev.* **1983,** *83,* 651.
(b) Alvarez, R.; Atwood, J. L.; Carmona, E.; Pérez, P. J.; Poveda, M. L.; Rogers, R. D. *Inorg. Chem.* **1991,** *30,* 1493.

171. Han, R.; Looney, A.; McNeill, K.; Parkin, G.; Rheingold, A. L.; Haggerty, B. S. *J. Inorg. Biochem.* **1993,** *49,* 105.

172. Symmetric bis(unidentate) coordination of bridging carbonate ligands has been observed previously. See:
(a) Tyeklar, Z.; Paul, P. P.; Jacobson, R. R.; Farooq, A.; Karlin, K. D.; Zubieta, J. *Inorg. Chem.* **1989,** *111,* 388.
(b) Churchill, M. R.; Lashewycz, R. A.; Koshy, K.; Dasgupta, T. P. *Inorg. Chem.* **1981,** *20,* 376.
(c) Cotton, F. A.; Felthouse, T. R. *Inorg. Chem.* **1980,** *19,* 320.
(d) Cotton, F. A.; Rice, G. W. *Inorg. Chem.* **1978,** *17,* 2004.
(e) Wieghardt, K.; Schmidt, W.; van Eldik, R.; Nuber, B.; Weiss, J. *Inorg. Chem.* **1980,** *19,* 2922.
(f) Barclay, G. A.; Hoskins, B. F. *J. Chem. Soc.* **1963,** 2807.

173. For IR data on carbonates see:
(a) Nakamoto, K. "Infrared and Raman Spectra of Inorganic and Coordination Compounds" (4th Ed.), Wiley–Interscience: New York, 1986.
(b) Nakamoto, K.; Fujita, J., Tanaka, S.; Kobayashi, M. *J. Am. Chem. Soc.* **1957,** *79,* 4904.
(c) Gatehouse, B. M.; Livingstone, S. E.; Nyholm, R. S. *J. Am. Chem. Soc.* **1958,** *80,* 3137.
(d) Fujita, J.; Martell, A. E.; Nakamoto, K. *J. Chem. Phys.* **1962,** *36,* 339.
(e) Jolivet, J. P.; Thomas, Y.; Taravel, B.; Lorenzelli, V. *J. Mol. Struct.* **1980,** *60,* 93.

174. Similar studies utilizing ^{18}O exchange have been used for measuring the rate of hydration of CO_2 (and dehydration of HCO_3^-) in aqueous solution. See:
(a) Mills, G. A.; Urey, H. C. *J. Am. Chem. Soc.* **1940,** *62,* 1019.
(b) Silverman, D. N. In "Methods in Enzymology," Purich, D., Ed.; Academic Press: San Diego, 1992; Vol. 87, 732–752.

175. Note that the exchange process in benzene solution is significantly slower than in water, which greatly facilitates rate measurements by ^{17}O NMR spectroscopy.

176. Bertini, I.; Luchinat, C. In "Bioinorganic Chemistry," Bertini, I.; Gray, H. B.; Lippard, S.; Valentine, J. Eds.; University Science Books: Mill Valley, CA, 1994; Chapter 2, and references therein.

177. Solo, M.; Mestres, J.; Duran, M.; Carbó, R. *J. Chem. Inf. Comput. Sci.* **1994,** *34,* 1047.

178. For example, neither electronic, ESR or ^{67}Zn NMR spectroscopies are useful for studying the native carbonic anhydrase.

179. (a) Jonsson, N. B.-H.; Tibell, L. A. E.; Evelhoch, J. L.; Bell, S. J.; Sudmeier, J. L. *Proc. Natl. Acad. Sci. U.S.A.* **1980,** *77,* 3269.
(b) Armitage, I. H.; Pajer, R. T.; Schoot Uiterkamp, A. J. M.; Chlebowski, J. F.; Coleman, J. E. *J. Am. Chem. Soc.* **1976,** *98,* 5710.
(c) Armitage, I. H.; Schoot Uiterkamp, A. J. M.; Chlebowski, J. F.; Coleman, J. E. *J. Magn. Reson.* **1977,** *29,* 375.
(d) Sudmeier, J. L.; Bell, S. J. *J. Am. Chem. Soc.* **1977,** *99,* 4499.
(e) Evelhoch, J. L.; Bocian, D. F.; Sudmeier, J. L. *Biochemistry* **1981,** *20,* 4951.

180. For ^{113}Cd NMR in other systems see:
(a) Summers, M. *Coord. Chem. Rev.* **1988,** *86,* 43.
(b) Rivera, E.; Kennedy, Ellis, P. D. *Adv. Magn. Reson.* **1989,** *13,* 257.
(c) Kennedy, M. A.; Ellis, P. D. *J. Am. Chem. Soc.* **1989,** *111,* 3195.

(d) Ellis, P. D. *J. Biol. Chem.* **1989,** *264,* 3108.
(e) Munakata, M.; Kitagawa, S.; Yagi, F. *Inorg. Chem.* **1986,** *25,* 964.

181. (a) Bertini, I.; Luchinat, C. *Ann. N. Y. Acad. Sci.* **1984,** *429,* 89.
(b) Bertini, I.; Canti, G.; Luchinat, C.; Scozzafava, A. *J. Chem. Soc., Dalton Trans.* **1978,** 1269.
(c) Moratal, J. M.; Martínez-Ferrer, M.-J.; Donaire, A.; Castells, J.; Salgado, J.; Jiménez, H. R. *J. Chem. Soc., Dalton Trans.* **1991,** 3393.

182. (a) Lindskog, S.; Malmström, B. G. *J. Biol. Chem.* **1962,** *237,* 1129.
(b) Coleman, J. E. *Nature (London)* **1967,** *214,* 193.
(c) Thorslund, A.; Lindskog, S. *Eur. J. Biochem.* **1967,** *3,* 117.
(d) Williams, R. J. P. *J. Mol. Catal.* **1985,** *30,* 1.

183. It should be noted that activity of cadmium-substituted carbonic anhydrase may be enhanced at higher pH values (ca. pH 9). See Ref. (*182b*) and Bauer, R.; Limkilde, P.; Johansen, J. T. *Biochemistry* **1976,** *15,* 334.

184. Han, R.; Parkin, G. *J. Am. Chem. Soc.* **1991,** *113,* 9707.

185. Indeed, nitrate and bicarbonate do not bind in an identical fashion to the zinc center of carbonic anhydrase. Thus, the bicarbonate ligand is coordinated to the zinc center of a *mutant* of carbonic anhydrase (Thr-200 → His human CA II) with Zn-O bond lengths of 2.2 Å and 2.5 Å (*185a*) whereas the nitrate ligand is coordinated to the zinc center of human carbonic anhydrase II via only one oxygen atom with a Zn-O distance is 2.8 Å (a water molecule also remains coordinated to zinc in this derivative). (*185b*) However, it must be recognized that two different forms of carbonic anhydrase are being compared in the above examples, and that no electron density corresponding to a bicarbonate ligand was detected upon crystallizing native human carbonic anhydrase II in the presence of bicarbonate. (*185c*)
(a) Xue, Y.; Vidgren, J.; Svensson, L. A.; Liljas, A.; Jonsson, B.-H.; Lindskog, S. *Proteins* **1993,** *15,* 80.
(b) Mangani, S.; Håkansson, K. *Eur. J. Biochem.* **1992,** *210,* 867.
(c) Håkansson, K.; Wehnert, A. *J. Mol. Biol.* **1992,** *228,* 1212.

186. Kleywegt, G. J.; Wiesmeijer, W. G. R.; Van Driel, G. J.; Driessen, W. L.; Reedijk, J.; Noordik, J. H. *J. Chem. Soc., Dalton Trans.* **1985,** 2177.

187. Addison, C. C.; Logan, N.; Wallwork, S. C.; Garner, C. D. *Q. Rev. Chem. Soc.* **1971,** *25,* 289.

188. For some additional studies on acetate, formate, nitrite, and nitrate coordination modes in zinc and copper $[M(phen)_2]$ and $[M(bipy)_2]$ derivatives, see:
(a) Simmons, C. J. *Struct. Chemistry* **1992,** *3,* 37.
(b) Simmons, C. J.; Hathaway, B. J.; Amornjarusiri, K.; Santarsiero, B. D.; Clearfield, A. *J. Am. Chem. Soc.* **1987,** *109,* 1947.

189. Mn(II)-substituted carbonic anhydrase, which is less active than the zinc enzyme, has also been postulated to exhibit bidentate bicarbonate coordination.
(a) Led, J. J.; Neesgaard, E. *Biochemistry* **1987,** *26,* 183.
(b) Led, J. J.; Neesgaard, E.; Johansen, J. T. *FEBS Lett.* **1982,** *147,* 74.

190. The Zn-O distance is 2.8 Å, indicating a relatively weak association. Moreover, the nitrate ligand does not displace the coordinated water from the zinc center. See: Mangani, S.; Håkansson, K. *Eur. J. Biochem.* **1992,** *210,* 867.

191. This suggestion is not necessarily intended to imply that the bicarbonate intermediate of the carbonic anhydrase cycle must exhibit unidentate coordination in the ground state. Rather, it is intended to imply that a unidentate species should be readily accessible. Moreover, it is not intended to suggest that this factor alone is responsible for influencing the activity of metal-substituted carbonic anhydrases,

and other factors, such as the coordination environment and the pK_a of the coordinated water, must naturally also be considered. See: Garmer, D. R.; Krauss, M. *J. Am. Chem. Soc.* **1992,** *114,* 6487.

192. Zhang, X.; van Eldik, R. submitted for publication, 1995.

193. Looney, A.; Parkin, G. *Inorg. Chem.* **1994,** *33,* 1234.

194. (a) Alsfasser, R.; Powell, A. K.; Vahrenkamp, H. *Angew. Chem., Int. Ed. Engl.* **1990,** *29,* 898.
(b) Alsfasser, R.; Powell, A. K.; Trofimenko, S.; Vahrenkamp, H. *Chem. Ber.* **1993,** *126,* 685.

195. Kumar, P. N. V.; Marynick, D. S. *Inorg. Chem.* **1993,** *32,* 1857.

196. (a) Karlin, K. D. *Science,* **1993,** *261,* 701.
(b) Christianson, D. W.; Lipscomb, W. N. *Acc. Chem. Res.* **1989,** *22,* 62.
(c) Reichwein, A. M.; Verboon, W.; Reinhoudt, D. N. *Recl. Trav. Chim. Pays-Bas* **1994,** *113,* 343–349.

197. Hikichi, S.; Tanaka, M.; Moro-oka, Y.; Kitajima, N. *J. Chem. Soc., Chem. Commun.* **1992,** 814–815.

198. Hikichi, S.; Tanaka, M.; Moro-oka, Y.; Kitajima, N. *J. Chem. Soc., Chem. Commun.* **1994,** 1737–1738.

199. (a) Lehn, J.-M. *Angew. Chem., Int. Ed. Engl.* **1988,** *27,* 89.
(b) Schmidtchen, F. P. *Top. Curr. Chem.* **1986,** *132,* 101.
(c) Franke, J.; Vogtle, F. *Top. Curr. Chem.* **1986,** *132,* 135.
(d) Kimura, E. *Top. Curr. Chem.* **1985,** *128,* 113.
(e) Pierre, J. L.; Baret, P. *Bull. Soc. Chim. Fr.* **1983,** *2,* 367.
(f) Vogtle, F.; Sieger, H.; Muller, W. M. *Top. Curr. Chem.* **1981,** *98,* 107.
(g) Katz, H. E. *Organometallics* **1987,** *6,* 1134.
(h) Newcomb, M.; Madonik, A. M.; Blanda, M. T.; Judice, J. K. *Organometallics* **1987,** *6,* 145.
(i) Beauchamp, A. L.; Oliver, M. J.; Wuest, J. P.; Zacharie, B. *J. Am. Chem. Soc.* **1986,** *108,* 73.
(k) Tamao, K.; Hayashi, T.; Ito, Y.; Shiro, M. *J. Am. Chem. Soc.* **1990,** *112,* 2422.
(l) Schmidtchen, F. P.; Gleich, A.; Schummer, A. *Pure Appl. Chem.* **1989,** *61,* 1535.
(m) Kaufmann, D. E.; Otten, A. *Angew. Chem., Int. Ed. Engl.* **1994,** *33,* 1832.
(n) Stang, P. J.; Zhdankin, V. V. *J. Am. Chem. Soc.* **1993,** *115,* 9808.
(o) Jacobson, S.; Pizer, R. *J. Am. Chem. Soc.* **1993,** *115,* 11216.
(p) Worm, K.; Schmidtchen, F. P.; Schier, A.; Schäfer, A.; Hesse, M. *Angew. Chem., Int. Ed. Engl.* **1994,** *33,* 327.
(q) Dietrich, B. *Pure Appl. Chem.* **1993,** *65,* 1457.

200. Some other monoprotonated derivatives include $[Me_2NTp]H$, obtained by the reaction of $B(NMe_2)_3$ with pzH, (*200a*) and $[R_2B(3\text{-ferrocenylpz})_2]H$. (*200b*)
(a) Niedenzu, K.; Trofimenko, S. *Inorg. Chem.* **1985,** *24,* 4222.
(b) Niedenzu, K.; Serwatowski, J.; Trofimenko, S. *Inorg. Chem.* **1991,** *30,* 524.

201. Bradley, D. C.; Hursthouse, M. B.; Newton, J.; Walker, N. P. C. *J. Chem. Soc., Chem. Commun.* **1984,** 188.

202. Rheingold, A. L.; Haggerty, B. S.; Trofimenko, S. *Angew. Chem., Int. Ed. Engl.* **1994,** *33,* 1983.

203. Agriofoglio, G. *Inorg. Chim. Acta.* **1992,** *197,* 159.

204. Looney, A.; Parkin, G.; Rheingold, A. L. *Inorg. Chem.* **1991,** *30,* 3099.

205. Emsley, J. *Chem. Soc. Rev.* **1980,** *9,* 91.

206. For other structurally-characterized anion coordination complexes, see:
(a) Bell, R. A.; Christoph, G. G.; Fronczek, F. R.; Marsh, R. E. *Science* **1975,** *190,* 151.

(b) Metz, B.; Rosalky, J. M.; Weiss, R. *J. Chem. Soc., Chem. Commun.* **1976,** 533.
(c) Dietrich, B.; Guilhem, J.; Lehn, J.-M.; Pascard, C.; Sonveaux, E. *Helv. Chim. Acta.* **1984,** *67,* 91.
(d) Schmidtchen, F. P.; Muller, G. *J. Chem. Soc., Chem. Commun.* **1984,** 1115.
207. Reger, D. L.; Ding, Y.; Rheingold, A. L.; Ostrander, R. L. *Inorg. Chem.* **1994,** *33,* 4226.
208. (a) Parkin, G. *Acc. Chem. Res.* **1992,** *25,* 455.
(b) Parkin, G. *Chem. Rev.* **1993,** *93,* 887.
209. (a) Jones, R. A.; Wilkinson, G.; Galas, A. M. R.; Hursthouse, M. B. *J. Chem. Soc., Chem. Commun.* **1979,** 926.
(b) Chiu, K. W.; Jones, R. A.; Wilkinson, G.; Galas, A. M. R.; Hursthouse, M. B.; Malik, K. M. A. *J. Chem. Soc., Dalton Trans.* **1981,** 1204.
210. (a) Chatt, J.; Manojlovic-Muir, L.; Muir, K. W. *Chem. Comm.* **1971,** 655.
(b) Manojlovic-Muir, L. *J. Chem. Soc. (A)* **1971,** 2796.
(c) Manojlovic-Muir, L.; Muir, K. W. *J. Chem. Soc., Dalton Trans.* **1972,** 686.
(d) Haymore, B. L.; Goddard, W. A., III; Allison, J. N. *Proc. Int. Conf. Coord. Chem., 23rd* **1984,** 535.
211. (a) Jean, Y.; Lledos, A.; Burdett, J. K.; Hoffmann, R. *J. Am. Chem. Soc.* **1988,** *110,* 4506.
(b) Jean, Y.; Lledos, A.; Burdett, J. K.; Hoffmann, R. *J. Chem. Soc., Chem. Commun.* **1988,** 140.
212. (a) Yoon, K.; Parkin, G.; Rheingold, A. L. *J. Am. Chem. Soc.* **1991,** *113,* 1437.
(b) Yoon, K.; Parkin, G.; Rheingold, A. L. *J. Am. Chem. Soc.* **1992,** *114,* 2210.
213. Yoon, K.; Parkin, G. *Inorg. Chem.* **1992,** *31,* 1662.
214. (a) Churchill, M. R.; Fettinger, J. C.; Buttrey, L. A.; Barkan, M. D.; Thompson, J. S. *J. Organomet. Chem.* **1988,** *340,* 257.
(b) Del Pra, A.; Zanotti, G.; Segula, P. *Cryst. Struct. Commun.* **1979,** *8,* 959.
(c) Rheingold, A. L.; Geib, S. J. *Acta. Crystallogr., Sect. C: Cryst. Struct. Commun.* **1987,** *C43,* 784.
(d) Brady, R.; De Camp, W. H.; Flynn, B. R.; Schneider, M. L.; Scott, J. D.; Vaska, L.; Werneke, M. F. *Inorg. Chem.* **1975,** *14,* 2669.
(e) Rees, W. M.; Churchill, M. R.; Li, Y.-J.; Atwood, J. D. *Organometallics* **1985,** *4,* 1162.
(f) Fettinger, J. C.; Churchill, M. R.; Bernard, K. A.; Atwood, J. D. *J. Organomet. Chem.* **1988,** *340,* 377.
(g) McGinnety, J. A.; Doedens, R. J.; Ibers, J. A. *Inorg. Chem.* **1967,** *6,* 2243.
(h) La Placa, S. J.; Ibers, J. A. *J. Am. Chem. Soc.* **1965,** *87,* 2581.
215. (a) Carmona, E.; Marin, J. M.; Poveda, M. L.; Atwood, J. L.; Rogers, R. D. *Polyhedron* **1983,** *2,* 185.
(b) Salt, J. E.; Girolami, G. S.; Wilkinson, G.; Motevalli, M.; Thornton-Pett, M.; Hursthouse, M. B. *J. Chem. Soc., Dalton Trans.* **1985,** 685.
(c) Davis, B. R.; Ibers, J. A. *Inorg. Chem.* **1971,** *10,* 578.

INDEX

A

Acidity, silanol group, 176–186
Aconitase, crystal structure, 116–118
Acylsilane, hydrolysis, 173
Ag^+ complexes, log K_1 values, 95–96, 98
Al(III) citrate complex, 116, 118
$[Al(H_2O)_6]^{3+}$, ligand substitution studies, 24
Alkoxysilanes, hydrolysis, 151, 166–170
Aluminum
  poly(pyrazolyl)borato alkyl derivatives, 333–334
  solvent exchange and ligand substitution, 22–25
Annexin, calcium binding sites, 113–114
Aquapentammine complexes, transition metal, solvent exchange and ligand substitution, 43–47
Aryldisilanols, synthesis, 168
Arylsilanetriols, synthesis, 168–169
Arylsilanols, substituted, acidity, 184

B

Bacteria, methanotrophic, 263–264
  copper deficiency, 264
Basicity, silanol group, 186–187
$[Be(H_2O)_4]^{2+}$
  ligand substitution, volumes of activation, 17, 20
  SO_4^{2-}, 15–16
  water exchange, 16
Beryllium
  hydroxide derivatives, 348–349
  poly(pyrazolyl)borato alkyl derivatives, 309–312
  solvent exchange and ligand substitution, 14–21
Bi^{3+} complexes
  citrate complex, 116, 118
  log K_1 values, 95–96, 99
2,2′-Bipyridine, 74
cis-Bis(2,2′-bipyridine)dihydroxysilicon-diiodidedihydrate, 238
Bis[copper(II) tris-pyrazolyl borane] dioxygen complex, 107–108, 110
1,3-Bis(dicyclopentenyl)-1,3-dimethyldihydroxydisiloxane, 217–218
1,3-Bis(diphenylhydroxysilyl)-2,2-dimethyl-4,4-diphenylcyclodisilazane, 223
1,7-Bis[hydroxy(dimethyl)silylmethyl]-*m*-carborane, 223
Bis(pyrazolyl)borato ligands, 292
$[Bp^{Bu^t}]AlMe_2$, 333–334
$[Bp^{Bu^t}]ZnBu^t$, 324
$\{[Bp^{Bu^t}]Zn(\mu\text{-}OH)\}_3$, 327–328
$[Bp^{Bu^t}]ZnR$, reactivity, 327–328
[Bp]GaMe(X), 335–336
[Bp]InMe(X), 337
$[Bp]SnMe_3$, 339
Bromosilanes, hydrolysis, 162–163
$Bu^iPhSi(OH)_2$, 235
$Bu^t(Me_3SiCH_2)Si(OH)C(O)CH_3$, 204
Bu^tMe_2SiOH, 201–202
$[Bu^t(OH)_2Si]_2O$, 239–240
tert-Butoxy silanes, hydrolysis, 161
$Bu^t_2SiF(OLi)$, 200
$Bu^t_2Si(OH)_2$, hydrolysis, 157–158
$[Bu^t_2Si(OH)_2(Cl_3SnOH)_2]$, 215
$Bu^t_2Si(OH)F$, 198–199
$Bu^t_2Si(OH)OLi$, 199
$Bu^t_2Si(OH)(ONa)$, 199–200

C

Cadmium, *see also* Poly(pyrazolyl)borato ligation, hydroxide derivatives
  poly(pyrazolyl)borato alkyl derivatives, 328–329
Calcium, binding sites, 113–114
Calmodulin, calcium binding sites, 113–114

Carbonate
coordination mode, 364–366
moieties, bridging, 364–365
Carbon dioxide, reactions with
[Tp^{But}]MgMe, 316
[$Tp^{RR'}$]ZnOH complexes, 354–359
Carbonic anhydrase
coordination environment about zinc, 353
metal-substituted, 359, 361–366
proposed catalytic cycle, 352–353
$(CH_2{=}CH)CH(OH)SiPh_2OH$, 205
$\{[C_6H_4CH_2NMe_2]_2Si(OLi)(OH)\}_4{\cdot}2LiCl{\cdot}2CHCl_3$, 197–198
Chlorosilanes, hydrolysis, 156–122
$(c\text{-}C_6H_{11})_3SiOc\text{-}C_6H_{11})$, hydrolysis, 167
$c\text{-}C_6H_{11}Si(OH)_3$, 240–241, 244–245
$[(C_6H_{11})_7Si_7O_9(OH)_3]$, 219, 225–226
$(\varepsilon^1\text{-}C_5Me_5)_2Si(OH)_2$, 236–238
Compressibility coefficient of activation, 9
$[Co(NH_3)_5H_2O]^{3+}$, solvent exchange and ligand substitution, 44–45
Coordination mode
carbonate, 364–366
nitrate, 361–364
poly(pyrazolyl)borato ligation, 293
$[Cr(H_2O)_6]^{3+}$, ligand substitution, 46
$[Cr(NH_3)_5H_2O]^{3+}$, ligand substitution, 45–46
18-Crown-6, conformers, 126, 128
Cryptands, 122–124
Cs[Tp^{But2}], structure, 300, 302
$[Cu(H_2O)_6]^{2+}$, solvent exchange, 29–30
$Cu_2(OH)$(O-BISTREN), 141–142
$[Cu(tetb)H_2O]^{2+}$, 105–106
(Cyclohexyl)phenyl[2-pyrrolidin-1-yl]silanol, 193

D

β-Desferriferrioxamine-B, complex stability, 131–133
1,2-Diaminoethane, 76
1,2-Diaminoethane-*N*,*N*,*N*′,*N*′-tetraacetate, 76
α,ω-Dichloro-oligosilane, 221
N,*N*-Diethylacetamide,74
Diethylenetriamine, 74
Diethylenetriamine-*N*,*N*,*N*′,*N*″,*N*‴-pentaacetate, 75
2,8-Dihydroxy-2,4,4,6,6,8,10,10,12,12-decamethylcyclohexasiloxane, 219
cis-1,5-Dihydroxy-1,5-dimethyl-3,3,7,7-tetraphenylcyclotetrasiloxane, 218
α,o-Dihydroxy-oligosilanes, 221
Diiron(III) peroxide, 277–278
Dimethylformamide solution, trivalent lanthides, solution exchange, 61–63
Dimethylsulfoxide, 76
Dimethypropyleneurea, 75
Dioxouranium(VI), solvent exchange and ligand substitution, 64–66
Disilenes, reactions with water, 175
Disilicic acid, 189
Disiloxanediol, 215–216
hydrogen-bonded networks, 212–213
Disiloxanes, structure, 205, 212–218
Dual basicity equation, 96

E

Eigen–Wilkins mechanism, 5
Enniatin-B, 119–120
Esterase, activity, [$Tp^{RR'}$]ZnOH complexes, relevance, 367–370
$[(2,6\text{-}Et_2C_6H_3)(2,6\text{-}Et_2\text{-}4\text{-}Bu^t)(OH)Si]_2O$, 215, 217
Ethylsilanetriol, monosodium salts, 169
$Et_2Si(OH)_2$, 228, 233

F

Fe_4S_4 cluster, electron shift within, 117
Fluorosilanes, hydrolysis, 156

G

$[Ga(H_2O)_6]^{3+}$, ligand substitution studies, 25
Gallium, poly(pyrazolyl)borato alkyl derivatives, 334–337
Gallium(III), solvent exchange and ligand substitution, 22–25
Gold, poly(pyrazolyl)borato alkyl derivatives, 320–321

H

Halosilanes, hydrolysis, 156–166
Heats of protonation, gas phase of bases, 92, 95
Hexaaquaruthenium(II), solvent exchange and ligand substitution, 34–37
Hexamethylphosphoramide, 77
$(HOMe_2Si)_4C$, hydrogen bonding, 226–227
p-$(HOMe_2Si)_2C_6H_4$, 224–225
$(HOPh_2Si)_2O$, 214
$(HOPh_2Si)_2O{\cdot}C_5H_5N{\cdot}HCl$, 214, 216
$[(HOPh_2Si)_2O]_3{\cdot}(C_4N_2H_4)_2$, 214, 216
$(HOSiMe_2)_4C$, 225
$HO(SiPh_2)_nOH$, 221–222
$HO(SiPh_2)_5OH$, 222
Hydrolysis
  alkoxysilanes, 151, 166–170
  alkyl, alkenyl, and aryl compounds, 172–173
  bromosilanes, 162–163
  $Bu^t_2Si(OH)_2$, 157–158
  chlorosilanes, 156–122
  fluorosilanes, 156
  halosilanes, 156–166
  iodosilanes, 163–166
  Me_2SiCl_2, 157
  methylchlorosilanes, 157
  organosilanols, from Si–H compounds, 155
  siloxy silanes, 166–170
  silyl carboxylic acids and acylsilanes, 173
  silyl cyanates, 171
  silyl perchlorates, 170–171
  silyl sulfates, 171
  silyl triflates, 170
Hydroxydisiloxanes, unsymmetrical, synthesis, 160

I

Imidazole, complex stability, 134–135
Indium
  poly(pyrazolyl)borato alkyl derivatives, 337–339
  solvent exchange and ligand substitution, 22–25
Iodosilanes, hydrolysis, 163–166
Ionicity parameter, 97–98, 100
Iron, in aconitase, 116–117
4-Isopropyltropolone, 76

K

$KMnO_4$, oxidation of sterically hindered silanes by, 152–153
$K[pzTp](H_2O)$, structure, 300–302
$K[Tp^{Bu^t_2}](C_6H_6)$, structure, 299–301

L

Lability, nonleaving ligand, effect, 32–34
Lanthanides, *see* Metal ions
Lewis acid–base interactions, 89–143
  change of HSAB behavior, 104
  chelate ring size and metal ion selectivity, 109–118
    ax–ax–ax structure, 114–116
    complex stability and ring size, 109, 112, 114–115
    coordination number and small rings, 111, 113
    ring geometry, 109–110, 112
  entatic state, 107–108
  gas phase, 90–95
  negative oxygen donor, 131–133
  neutral oxygen donor, 119–131
    complex stability, 121–123
    crown ethers, 124–126
    destabilized complexes, 123–124
    potassium ion channel permeability to univalent metal ions, 129–130
    selectivity, 119, 121
    strain energy variation with M–O bond length, 126–127, 129
  nitrogen donor, 133–137
  sulfur donors, 137–139
  systems containing more than one metal ion, 140–143
Lewis acids
  in aqueous solution and gas phase, 95–102
  dual basicity equation, 96
  E_A/C_A ratio, 99–100
  ionicity parameter, 97–98, 100

Pearson's hardness parameter, 101–102
soft, zinc-containing metalloenzymes, 103
softness and coordination site steric situation, 104–105
Lewis bases
in aqueous solution and gas phase, 95–102
E_B/C_B ratio, 99, 101
I_B, E_B, C_B, and D_B parameters, 97–98, 101
Lithium(I)
complex formation energies, gas phase, 91–92
enthalpies of complexation, 92–93
formation, 94, 97
$[Ln(DMF)_8]^{3+}$, solution exchange, 62
$[Ln(H_2O)_8]^{3+}$, water exchange, 58–60
$[Ln(H_2O)_n]^{3+}$, solution exchange, 57–58

M

Macrocycles, 122
Magnesium
hydroxide derivatives, 348–349
poly(pyrazolyl)borato alkyl derivatives, 311–320
competition between Mg—X and Mg—R bond metathesis, 313
competitive alkyl exchange and coupling, 319–320
Mg—C bond lengths, 313, 315
reactions with
CO_2 and Me_2CO, 316
O_2, 316–318
reactivity, 315–320
toward HX, 319
toward XY, 319–320
structures and spectroscopic properties, 313–315
syntheses, 311–313
solvent exchange and ligand substitution, 18–19, 21
$[Me_2Bp]GaMe_2$, 335
Me_2CO, reactions with $[Tp^{But}]MgMe$, 316
Mercaptoethanol, formation constants, 137–138
Mercury, poly(pyrazolyl)borato alkyl derivatives, 330–332
Me_2SiCl_2, hydrolysis, 157
$(Me_3Si)_3CSiF(OH)_2$, 236–237
$(Me_3Si)_3CSiH_2I$, hydrolysis, 164
$(Me_3Si)_3CSiMe_2OSiMe_3$, hydrolysis, 169
$(Me_3Si_3CSiMe_2X$, hydrolysis, 159
$(Me_3Si)_3CSi(OH)_3$, 244–245
$(Me_3Si)_3CSiPhHI$, hydrolysis, 164–165
$(Me_3Si)_3CSiPh_2I$, hydrolysis, 165–166
$(Me_3Si)_3CSiPhOMeOH$, 192
$[(Me_3Si)_2(HOMe_2Si)C]_2Zn$, 224
$(Me_3Si)_3SiSi(OH)_3$, 244–245, 247
$[mes_2Si(F)O]_2[H][Et_4N]$, 197–198
Metal complexes, formation, 4–6
Metal ions
classification of mechanisms, 6–8
dioxouranium(VI), 64–66
formation of complexes, 4–6
interaction with a simple unidentate ligand, 90
ligand exchange processes, 10–11
main group metal, 14–25
Al^{3+}, Ga^{3+}, In^{3+}, and Sc^{3+}, 22–25
beryllium(II), 14–21
characteristics, 14
magnesium(II), 18–19, 21
main group metal ions, 2–3
molybdenum and tungsten cluster complexes, 66–72
outer-sphere complexes, 7
solvated, 1–78
solvent molecule exchange rate constant, 15
transition metal, 3–4, 25–56
aquapentammine complexes, 43–47
characteristics, 25–27
divalent square-planar, 49–56
hexaaquaruthenium(II) and related complexes, 34–37
ligand substitution, 30–32
nonleaving ligand effect of lability, 32–34
octahedral trivalent, 37–42
oxometal ions, 47–49
solvent exchange, 27–30
trivalent lanthanides, 4, 56–64
aqueous solution, 56–60
dimethylformamide, 61–63
lower coordination number species, 63–64

polyaminocarboxylate ligand effect on water exchange, 60–61
volume of activation, 9–14
water exchange, 2–3, 10
Metalloenzymes, zinc-containing, hard and soft acid–base behavior, 103–109
Metallothioneins, 137–139
Methane monooxygenase, 264
component interactions, 269–275
catalytic activity, 269
product distributions, 272–273
reduction potentials of hydroxylase, 270–272
yields and rate constants, single turnover reactions, 273–275
hydroxylase
mixed-valent, 267–268
oxidized, 265–267
physical properties, 266
reduced, 268–269
reduction potentials, 270–272
reactions with nitrobenzene, 272
Methylchlorosilanes, hydrolysis, 149–150, 157
endo-3-Methyl-*exo*-3-hydroxy-3-silabicyclo-[3·2·1]octane, 204
Methyl methylphenylphospinate, 77
$[M(H_2O)_6]^{2+}$, volumes of activation for water exchange, 12–13
$[Mn(H_2O)_6]^{2+}$, ligand substitution, 31
Molybdenum, solvent exchange and ligand substitution, 66–72
Monensin, 119–120
$[Mo_3O_4(H_2O)_9]^{4+}$, solution exchange and ligand substitution, 67–70
(2-Morpholinoethyl)diphenylsilanol, 193–194

N

(1-Naphthyl)$_3$Si*OH*·2*p*-xylene, 196–197
Nickel(II) complexes, lability of coordinated water, 32–33
$NiCp^+$ complexes, complex formation enthalpies, 94, 96
Nitrate coordination modes, 361–364
Nitrobenzene, reactions with methane monooxygenase, 272
Nitrogen donor, 133–137
^{17}O NMR, [Tp^{But}]MgOOR, 316–317
Norbornylsiloxane, 226, 228

O

O-BISTREN complex, 140–142
α,ω-Oligosilanediols, 220–222
Organosilanols, 147–251; *see also* Silanols
intramolecular hydrogen bonding interactions, 177, 184
polysiloxanes, 149–150
silica surfaces, 148–149
sol–gel processes, 151
synthesis, 151–187
addition of water to Si multiple bonds, 174–175
from alkoxy and siloxy silanes, 166–170
hydrolysis of halosilanes, 156–166
hydrolysis of Si–C bonds, 172–173
hydrolysis of Si–N functions, 171–172
miscellaneous methods, 175–176
from Si–H compounds, 152–155
hydrolysis, 155
oxidation, 152–154
from silanethiols and silyl sulfides, 171
from silyl cyanates, 171
from silyl–metal compounds, 173
from silyl perchlorates, 170–171
from silyl sulfates, 171
from silyl triflates, 170
types, 147–148
$[OsCl(CO)(PPh_3)_2Si(OH)_2]_2O$, 239
$Os[Si(OH)_3]Cl(CO)(PPh_3)_2$, 241
Oxidation, organosilanols, from Si–H compounds, 152–154
Oxotitanium(IV), solvent exchange and ligand substitution, 47–48
Oxovandium(IV), solvent exchange and ligand substitution, 47–49
Oxygen, reactions with [Tp^{But}]MgR, 316–318
Oxygen donor
negative, 131–133
neutral, 119–131
buckled, half-buckled, and planar forms, 126, 128

complex stability, 121–123
crown ethers, 124–126
destabilized complexes, 123–124
potassium ion channel permeability to univalent metal ions, 129–130
selectivity, 119, 121
strain energy variation with M–O bond length, 126–127, 129

P

Paladium(III), solvent exchange and ligand substitution, 49–54
Parvalbumin, calcium binding sites, 113–114
Pearson's hardness parameter, 101–102
N,N,N′,N″,N″-Pentaethyldiethylenetriamine, 76
ε^1-Pentamethylcyclopentadienyl, 236–237
N,N,N′,N″,N″-Pentamethyldiethylenetriamine, 77
Peptidase, activity, [$Tp^{RR'}$]ZnOH complexes, relevance, 367–370
Ph_3COH, interaction with ketones, 176–177
Phenylmethylsilanediol, synthesis, 155
Phenylsilanetriol, monosodium salts, 169
Ph_2(fluorenyl)SiOH, 197
$(PhMe_2Si)_3CSiH_2OH$, 244–245, 248
$(PhMe_2Si)_3CSiMeH(OH)$, 191
Phosphatase, activity, [$Tp^{RR'}$]ZnOH complexes, relevance, 367–370
$Ph_2Si(OH)_2$, 233–234
Ph_3SiOH
  interaction with ketones, 176–177
  structure, 194–197
(3-Piperidinopropyl)diphenylsilanol, 193
Platinum(III), solvent exchange and ligand substitution, 49–54
Polyaminocarboxylate ligands, effect on water exchange, trivalent lanthides, 60–61
Polydentate ligands, with negative oxygen donors, 131–132
Poly(pyrazolyl)borato ligation, 291–381
  alkyl derivatives, 309–340
    aluminum, 333–334
    beryllium, 309–312
    cadmium, 328–329
    gallium, 334–337
    gold, 320–321
    indium, 337–339
    magnesium, 311–320
      reactivity, 315–320
      structures and spectroscopic properties, 313–315
      syntheses, 311–313
    mercury, 330–332
    tin, 339–340
    zinc, 321–328
      reactivity, 325–328
      structures and spectroscopic properties, 322–325
      syntheses, 321–322
  coordination modes, 293
  hydroxide derivatives
    beryllium and magnesium, 348–349
    zinc and cadmium, 350–370
      functional equivalence of [$Tp^{Bu^t,Me}$]ZnOH, 359–360
      metal-substituted carbonic anhydrases, 359, 361–366
      spectroscopic models, 367
      substitution reactions of [$Tp^{Bu^t,Me}$]ZnOH, 359
      synthesis, structures, and spectroscopic properties, 350–352
      [$Tp^{RR'}$]ZnOH complexes, relevance to esterase, peptidase, and phosphatase activity, 367–370
      [$Tp^{RR'}$]ZnOH reactions with CO_2, 354–359
  [Tp^{Bu^t}]BeH, 340–344
  [Tp^{Bu^t}]CdH, 347
  [Tp^{Bu^t}]ZnH, 344–347
Poly(pyrazolyl)hydroborato ligands, 294–308
  abbreviations, 294–295
  bond angles and lengths, 298–299
  copper coordination environments, 306–307
  electronic properties, 307–308
  intraligand interactions, 306
  M[$Bp^{RR'}$] and M[$RTp^{RR'}$] derivatives, structures, 296–302
  steric demands of R and R′, 295–296
  substitution
    3-position, 302–305
    5-position, 305–307
  syntheses, 295–296

Polysiloxanes, 149–150
Porphyrin
  complex stability, 135–137
  ruffling, metal ion size effect, 136
Potassium ion channels, permeability to univalent metal ions, 129–130
1,3-Propylenediaminetetraacetate, 78
Protonation constants, methyl-substituted amines and phosphines, 93–94
trans-Pyridine-2-azo(*p*-dimethylaniline), 77
$\{[\varepsilon\text{-pzTp}]In(Me)Cl\}_2$, 338

R

Reduction potentials, methane monooxygenase hydroxylase, 270–272
Reverse chelate effect, 140–143
$R_2Si(OH)_2$, 234–236
$[Ru(H_2O)_6]^{2+}$, solvent exchange and ligand substitution, 34–37
$[Ru(H_2O)_6]^{3+}$, solvent exchange, 39
Ruthenium(II) complexes, solvent exchange, 34–35

S

Scandium(III), solvent exchange and ligand substitution, 22–25
Schlenk equilibrium, 308
Si–C bonds, hydrolysis, 172–173
Sila drugs, structure, 193–194
Silanethiols, hydrolysis, 171
Silanetriols, 240–241, 244–249
Silanols, 148–149
  acidity, 176–186
  basicity, 186–187
  benzylic, synthesis, 160–161
  containing $(Me_3Si)_3C$ group, synthesis, 164
  di-*t*-butyl-substituted, 201
  gas phase acidities, 185
  infrared spectroscopic data
    complexes with bases, 177–183
    complexes with phenol, 186–187
    in various solvents, 177, 184
  sterically hindered, synthesis, 165
  structural studies, 187–249
    aryl silanols and adducts, 194–198
    calculations, 188–190
    compounds containing
      four Si–OH groups, 225–232
      one Si–OH group, 205–225
      three Si–OH groups, 225–226, 229–232
      two Si–OH groups, 205, 212–225, 229–232
      two $Si(OH)_2$ groups, 239–243
    disiloxanes, 205, 212–218
    highly sterically hindered, 190–192
    α,ω-oligosilanediols, 220–222
    sila drugs, 193–194
    silanediols, 227–228, 233–239, 242–243
    silanetriols, 240–241, 244–249
    Si–O, bond lengths, 189–190
    tert-butyl substituted, 198–202
    transition metal silyl, 202–203
    trisiloxanes, 218
  with two hydrogen-bonding sites, structural units, 249–250
Silica surfaces, 148–149
Silicones, *see* Polysiloxanes
Siloxy silanes, hydrolysis, 166–170
Siloxysilanols, synthesis, 161
Silsesquioxane, silylation, 219–220
Silyl bromides, hydrolysis, 162–163
Silyl carboxylic acids, hydrolysis, 173
Silyl cyanates, hydrolysis, 171
Silyl iodide, hydrolysis, 163–165
Silyl–metal compounds, organosilanols synthesis, 173
Silyl perchlorates, hydrolysis, 170–171
Silyl sulfates, hydrolysis, 171
Silyl sulfides, hydrolysis, 171
Silyl triflates, hydrolysis, 170
Si–N bond, hydrolysis, organosilanols synthesis, 171–172
Si–O, bond lengths, 189–190
Sol–gel processes, 151
Soluble methane monooxygenase protein system, 263–286
  hydroxylation
    catalytic cycle, 281
    diiron(III) peroxide, 277–278
    Hred reaction with dioxygen, 275–281
    mechanisms, 281–282

Mössbauer spectrum, 276–277
O—O bond cleavage, 279–280
Q reaction with substrate, 281–285
spectroscopic and kinetic parameters, 276
Solvent exchange equation, 15
Strain energy, variation with M–O bond length, 126–127
Sulfur donors, 137–139

T

α-Terpineol, silicon derivative, 167–168
2,2′,2″-Terpyridine, 78
1,4,7,10-Tetraazacyclododecane, 74
1,4,7,10-Tetraazacyclododecane-*N*,*N*′,*N*″,*N*‴-tetraacetate, 75
1,4,8,11-Tetraazacyclotetradecane, 77
1,1,5,5-Tetrakis(hydroxydimethylsiloxy)-3,3,7,7-tetraphenylcyclotetrasiloxane, 226, 228
Tetrakis(pyrazolyl)borato ligands, 292
1,1,5,5-Tetraphenyl-3,3,7,7-tetrahydroxycyclotetrasiloxane, 239, 241
Tetrasilylmethanes, hydrolysis, 163
Tetrasulfophenylporphyrin, stability, 135
$[Ti(H_2O)_6]^{3+}$, ligand substitution, 40
Tin, poly(pyrazolyl)borato alkyl derivatives, 339–340
Tl[$Bp^{Bu^t,Me}$], structure, 296–298
Tl[Tp^{Bu^t2}], structure, 299–300
[Tp^{Ant}]CoNCS, 379–380
[Tp^{Ant}]Tl, 380
[Tp^{Bu^t}]BeH, 340–344
reactivity, 344
structure and spectroscopic properties, 341–343
synthesis, 340–341
[Tp^{Bu^t}]BeMe, 309–311, 310–312
[Tp^{Bu^t}]CdH, 347
[Tp^{Bu^t}]CuCl, 306–307
{[$Tp^{Bu^t}H_3$]Cl}$^+$, 371–372
[$Tp^{Bu^t,Me}$]CuCl, 306–307
[$Tp^{Bu^t,Me}$]HgI, 332
{[$Tp^{Bu^t,Me}$]Zn}$_2$(μ-ε^1,ε^1-CO_3), 356–358, 361, 366
[$Tp^{Bu^t,Me}$]Zn(OCO_2H), 355–357
[$Tp^{Bu^t,Me}$]ZnOH, 350–352
[Tp^{Bu^t}]MgMe, reactivity, 319–320
[Tp^{Bu^t}]MgPr^i, 313–314
[Tp^{Bu^t}]ZnBr, thermal parameters, 375, 377
[Tp^{Bu^t}]$ZnCl_{1-n}I_n$, thermal parameters, 375–376
[Tp^{Bu^t}]ZnCN, 378–379
[Tp^{Bu^t}]$Zn(CN)_{0.95}Br_{0.05}$, 377–378
[Tp^{Bu^t}]$Zn(CN)_{0.8}Cl_{0.2}$, 377–378
[Tp^{Bu^t}]$Zn(CN)_{0.9}I_{0.1}$, 379–380
[Tp^{Bu^t}]ZnH, 344–347
[Tp^{Bu^t2}]ZnMe, 322–323
[Tp^{Bu^t}]ZnX complexes, bond length variation, 374–375
[Tp^{Me2}]$MgCH_2SiMe_3$, 313–314
[Tp^{Me2}]Pb(3,5-$Me_2pzH)_3Cl$, 372
[$Tp^{RR'}$]$AlMe_2$, 333
[$Tp^{RR'}$]$AuMe_2$, 321
{[$Tp^{RR'}$]Cu}$_2$ derivatives, structures, 304–305
[$Tp^{RR'}$]M(NO_3) complexes, nitrate coordination modes, 361–364
[$Tp^{RR'}$]ZnOH complexes, 352
coordination modes, 361–364
functional equivalence, 359–360
reactions with CO_2, 354–359
relevance to esterase, peptidase, and phosphatase activity, 367–370
spectroscopic data, 350–351
spectroscopic models, 367
substitution reactions, 359
[Tp]$SnMe_3$, 339
Transition metal ions, *see* Metal ions
Transition oxometal ions, solvent exchange and ligand substitution, 47–49
2,2′,2″-Triaminotriethylamine, 78
Triethylenetetraamine, 78
Trimethylphosphate, 78
Tri(1-naphthyl)silanol, 196
2,2′,2″-Tri(*N*,*N*-dimethylamino)triethylamine, 77
Triphenylsilanol, 195–196
Tris(pyrazolyl)borato ligands, 292, 294
Tris(pyrazolyl)hydroborato derivatives, protonated, anion coordination, 370–381
disorder between structurally disparate groups, 377–381
similar groups, 373–377
Tris(pyrazolyl)hydroborato ligand, modification, receptor for binding anions, 370–371

Tris(pyrazolyl)hydroborato ligands, cone and wedge angles, 302–303
$TsiSi(OH)_2O_2CCF_3$, 237–238
$TsiSiPh(OH)_2$, 238
Tungsten cluster complexes, solvent exchange and ligand substitution, 66–72

V

Valinomycin, 120–121
$[V(H_2O)_6]^{2+}$, ligand substitution, 31
Volume of activation, 9–14
  bond-making and -breaking contributions, 12–13

W

Water
  addition to Si multiple bonds, 174–175
  lifetime in first coordination sphere of metal ions, 2–3

Z

Zinc, *see also* Poly(pyrazolyl)borato ligation, hydroxide derivatives
  coordination environment, carbonic anhydrase active site, 353
  poly(pyrazolyl)borato alkyl derivatives, 321–328
    bond lengths and angles, 323
    reactivity, 325–328
    structures and spectroscopic properties, 322–325
    syntheses, 321–322
Zinc(II), Lewis acidity, entatic state, 107–108